

A Thesis Submitted for the Degree of PhD at the University of Warwick

Permanent WRAP URL:

<http://wrap.warwick.ac.uk/98014>

Copyright and reuse:

This thesis is made available online and is protected by original copyright.

Please scroll down to view the document itself.

Please refer to the repository record for this item for information to help you to cite it.

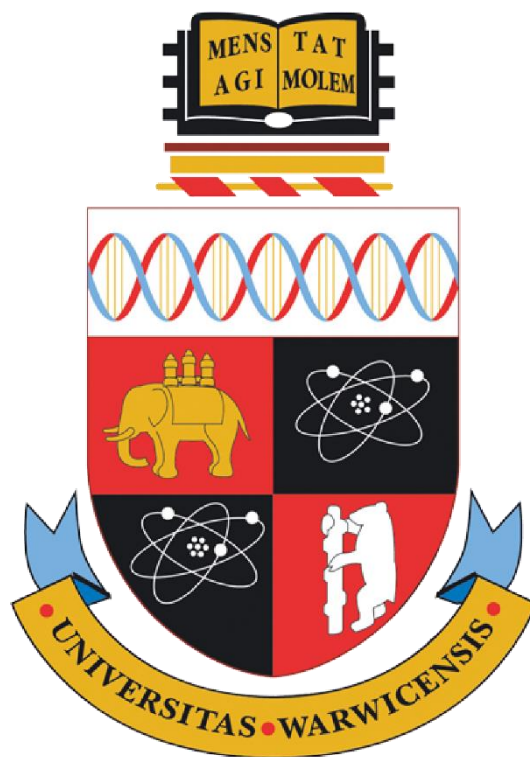
Our policy information is available from the repository home page.

For more information, please contact the WRAP Team at: wrap@warwick.ac.uk

Novel tools for the capture of intermediates of iterative polyketide catalysis

Samantha L. Kilgour

Thesis submitted in partial fulfilment of the requirements for the Degree of
Doctor of Philosophy in Chemistry



University of Warwick
Department of Chemistry
October 2017

Contents

Declaration	xii
Acknowledgements.....	xiii
List of Figures.....	xiv
List of Schemes	xxiv
List of Tables.....	xxvii
Abbreviations and Definitions.....	xxviii
Abstract	xxxiii

1. Introduction	2
1.1. Polyketide natural products and their biosynthesis	2
1.1.1. Fundamentals of polyketide biosynthesis	3
1.2. Type II polyketides and their biosynthesis	7
1.2.1. Biosynthesis of type II polyketides.....	8
<i>1.2.1.1. Ketosynthase-chain length factor – structure-function relationship ...</i>	<i>10</i>
<i>1.2.1.2. Acyl carrier proteins: structure-function relationship.....</i>	<i>12</i>
<i>1.2.1.3. Ketoreductases.....</i>	<i>14</i>
<i>1.2.1.4. Cyclases and aromatases</i>	<i>14</i>
<i>1.2.1.5. Methyltransferases</i>	<i>15</i>
<i>1.2.1.6. Oxygenases</i>	<i>15</i>
<i>1.2.1.7. Glycosyltransferases</i>	<i>17</i>
<i>1.2.1.8. The future of type II PKS engineering</i>	<i>18</i>
1.3. Biosynthesis of actinorhodin	18
1.3.1. Biosynthesis of an octaketide chain by the actinorhodin minimal system....	20
1.3.2. Tailoring steps towards the biosynthesis of actinorhodin	24
1.4. The role of carrier proteins in type II polyketide biosynthesis	27

1.4.1.	Engineering of carrier proteins	30
<i>1.4.1.1.</i>	<i>Modifications to the phosphopantetheinyl arm of carrier proteins</i>	<i>31</i>
1.5.	Methods of investigation of modular and iterative biocatalysis.....	33
1.5.1.	Labelling techniques	34
1.5.2.	Enzyme engineering	36
<i>1.5.2.1.</i>	<i>In vivo.....</i>	<i>36</i>
<i>1.5.2.1.1.</i>	<i>Gene deletions</i>	<i>37</i>
<i>1.5.2.1.2.</i>	<i>Mutagenesis</i>	<i>37</i>
<i>1.5.2.1.3.</i>	<i>Hybrid PKSs</i>	<i>38</i>
<i>1.5.2.1.4.</i>	<i>Heterologous expression</i>	<i>39</i>
<i>1.5.2.1.5.</i>	<i>Modifications to the phosphopantetheinyl arm of carrier proteins</i>	<i>39</i>
<i>1.5.2.2.</i>	<i>In vitro.....</i>	<i>40</i>
1.5.3.	Chemical probes: N-acetylcysteamine thioester (SNAC) substrate analogues.....	41
<i>1.5.3.1.</i>	<i>Chemical synthesis of SNAC analogues.....</i>	<i>42</i>
1.5.4.	Chain termination probes as new tools for the investigation of polyketide biosynthesis	43
<i>1.5.4.1.</i>	<i>Nonhydrolysable NAC chain termination probes.....</i>	<i>46</i>
1.5.5.	The application of proteomics and metabolomics to the investigation of biocatalysis.....	49
1.6.	Mass spectrometry.....	49
1.6.1.	Key ionisation techniques	49
1.6.2.	Key mass analysers.....	50
<i>1.6.2.1.</i>	<i>Time-of-flight (TOF) analysers</i>	<i>52</i>
<i>1.6.2.2.</i>	<i>Ion trap analysers.....</i>	<i>52</i>
<i>1.6.2.3.</i>	<i>Fourier Transform Mass Spectrometers (FT-MS)</i>	<i>52</i>
<i>1.6.2.4.</i>	<i>Ion mobility analysers</i>	<i>53</i>
1.6.3.	Fragmentation techniques in mass spectrometry.....	54

1.6.3.1.	<i>Collisionally activated dissociation (CAD)</i>	55
1.6.3.2.	<i>Infrared multiphoton dissociation (IRMPD)</i>	55
1.6.3.3.	<i>Electron capture dissociation (ECD)</i>	56
1.6.3.4.	<i>Electron transfer dissociation (ETD)</i>	56
1.6.3.5.	<i>Electron impact dissociation (EID)</i>	57
1.6.4.	Analysis of proteins by mass spectrometry	57
1.6.5.	Mass spectrometry for the investigation of natural product biosynthesis	58
1.6.5.1.	<i>The use of isotope labelling in mass spectrometry</i>	58
1.6.5.2.	<i>Fragmentation techniques for natural product research</i>	59
1.6.5.2.1.	<i>Fragmentation of the phosphopantetheinyl (PPant) arm of carrier proteins</i>	59
1.6.5.2.2.	<i>Proteomics based approaches to detect and characterise PKSs</i>	60
1.7.	Photolysis as a tool for investigating biological systems	62
1.7.1.	Desirable traits of photolabile groups for biological applications	62
1.7.2.	Photo-irradiation as a tool for the investigation of biosynthetic pathways	63
1.8.	Research aims and objectives	64
1.8.1.	Primary research aim	64
1.8.2.	Secondary research aim	66
1.8.3.	Tertiary research aim	67
2.	Synthesis of a nonhydrolysable photolabile malonyl <i>N</i>-acetyl cysteamine probe	69
2.1.	Probe design	69
2.2.	Photolabile protecting groups for carboxylic acids	70
2.2.1.	Multicyclic groups	71

2.2.1.1.	<i>Diisopropylsilyl groups</i>	71
2.2.1.2.	<i>Thiochrome groups</i>	71
2.2.1.3.	<i>Polycyclic aromatic hydrocarbons groups</i>	71
2.2.1.4.	<i>Coumarin-4-ylmethyl (CM) groups</i>	72
2.2.2.	Monocyclic aromatic groups	73
2.2.3.	Nitrobenzyl (NB) groups	75
2.2.3.1.	<i>The 4,5-dimethoxy-2-nitrobenzyl (DMNB) group</i>	78
2.2.3.1.1.	<i>Applications for the 4,5-dimethoxy-2-nitrobenzyl (DMNB) photolabile protecting group</i>	80
2.2.4.	Choice of photolabile group for the NAC analogue and the ACP analogue	81
2.3.	Probe synthesis	83
2.4.	Preliminary photolysis experiments	86
3.	Chemoenzymatic preparation of a carrier protein probe 63 for the capture of polyketide intermediates	93
3.1.	Probe rationale and design	93
3.2.	Preparation of a carrier protein probe	95
3.2.1.	Synthesis of the 4,5-dimethoxy-2-nitrobenzyl malonyl carba(dethia) pantetheine	96
3.2.1.1.	<i>Synthesis via acetyl protection of the pantetheine diol moiety</i>	96
3.2.1.2.	<i>Synthesis via di-tert-butylsilyl protection of the pantetheine 41 diol moiety</i>	98
3.2.2.	Enzymatic preparation of a 4,5-dimethoxy-2-nitrobenzyl malonyl carba(dethia) acyl carrier protein	105

4. Trapping of polyketide intermediates <i>in vivo</i> and <i>in vitro</i> with the aid of a photolabile malonyl <i>N</i>-acetyl cysteamine analogue	111
4.1. <i>In vitro</i> trapping of intermediates from the actinorhodin minimal system with the nonhydrolysable photolabile NAC probe	111
4.1.1. Analysis by LC-MS	111
4.1.2. Effect of delayed addition of active NAC probe to the actinorhodin minimal system on SEK4/4b production	115
4.1.3. Analysis by UV-Vis spectroscopy	117
4.2. <i>In vivo</i> trapping of intermediates from the actinorhodin biosynthetic pathway in <i>Streptomyces coelicolor</i> with the nonhydrolysable photolabile NAC probe	119
4.2.1. Photolysis experiments	122
4.3. <i>In vivo</i> trapping of intermediates from the lasalocid biosynthetic pathway in <i>Streptomyces lasaliensis</i> with the nonhydrolysable photolabile NAC probe 126	
5. Capture of polyketide intermediates with the aid of a nonhydrolysable malonyl acyl carrier protein analogue	145
5.1. Photolysis of the carrier protein	145
5.1.1. Rate of photolysis of the nonhydrolysable photoactivatable malonyl acyl carrier protein analogue	145
5.1.2. Incubation of Ketosynthase-Chain Length Factor (KS-CLF) with malonyl and acetyl acyl carrier proteins (ACPs) and the protein probe	146
5.1.2.1. Incubation of KS-CLF with malonyl-ACP 7 and acetyl-ACP	147
5.1.2.2. The impact of KS-CLF on photolysis of the ACP analogue	150

5.2. <i>In vitro</i> trapping of intermediates from the actinorhodin minimal system with the nonhydrolysable photoactivatable malonyl acyl carrier protein analogue	154
5.2.1. Experimental set up	154
5.2.2. Analysis of chain termination assays with protein probe by FTICR-MS	155
5.2.2.1. Detection of a putative captured diketide intermediate	158
5.2.2.2. Detection of a putative captured tetraketide intermediate	160
5.2.2.3. Detection of a putative captured pentaketide intermediate and dehydrated/cyclised pentaketides	162
5.2.2.4. Detection of a putative captured hexaketide intermediate and dehydrated species	167
5.2.2.5. Summary of off-loaded intermediates	172
5.2.2.6. Autocorrelation of low intensity isotopic distributions for detecting trapped polyketide intermediates	173
5.2.2.7. Tryptic digestion of the acyl carrier protein from the actinorhodin minimal system	177
5.2.3. UV-Vis spectroscopy analyses of SEK4/SEK4b production	178
5.2.4. Effect of delayed addition of active ACP probe on SEK4/4b production	179
5.3. <i>In vivo</i> labelling of the acyl carrier protein of the actinorhodin minimal system in <i>E. coli</i>	181
5.4. Conclusions and future work	184
6. Improving molecular structural determination by combining the results of alkali metal adduction assisted tandem mass spectrometry	189

6.1. The use of alkali metal assisted tandem mass spectrometry for structural determination.....	189
6.2. Alkali metal adduction assisted CAD and EID of the nonhydrolysable photolabile malonyl carba(dethia) pantetheine analogue	194
6.3. The effect of alkali metal adduction assisted CAD of modified acyl carrier proteins on the generation of phosphopantetheinyl (PPant) ejection ions	205
6.3.1. Background and aim	205
6.3.2. Generation of lithium and caesium adducted ACP species	206
6.3.3. The effect of alkali metal adduction on generation of a pantetheinyl ion by CAD of the nonhydrolysable photolabile malonyl carba(dethia) ACP	209
6.3.4. The effect of alkali metal adduction on generation of a pantetheinyl ion by CAD of acetyl-ACP.....	211
6.3.5. The effect of alkali metal adduction on generation of a pantetheinyl ion by CAD of malonyl-ACP	213
6.3.6. The effect of alkali metal adduction on CAD of acetoacetyl-ACP..	214
6.3.7. The effect of alkali metal adduction on generation of a pantetheinyl ion by CAD of myristoyl-ACP.....	216
6.3.8. CAD of caesium adducted ACP species.....	219
6.3.9. Summary and conclusions	220
6.4. The effect of alkali metal adduction to acyl carrier proteins (ACPs) on the production of peptides by CAD, and the application to post-translational modification mapping.....	221
6.4.1. The effect of alkali metal adduction to modified ACPs from the actinorhodin minimal system from <i>S. coelicolor</i> on the production of peptide ions by CAD.....	222
6.4.1.1. <i>Acetyl-ACP</i>	223
6.4.1.2. <i>Malonyl-ACP</i>	225
6.4.1.3. <i>Acetoacetyl-ACP</i>	226

6.4.1.4.	<i>Myristoyl-ACP</i>	228
6.4.1.5.	<i>Nonhydrolysable photolabile malonyl carba(dethia) ACP analogue</i>	229
6.4.2.	The effect of alkali metal adduction to ACPs on the production of phospho-peptide ions for post-translational modification mapping	230
6.4.2.1.	<i>Acetyl-ACP</i>	230
6.4.2.2.	<i>Malonyl-ACP</i>	231
6.4.2.3.	<i>Acetoacetyl-ACP</i>	232
6.4.2.4.	<i>Myristoyl-ACP</i>	233
6.4.2.5.	<i>Nonhydrolysable photolabile malonyl carba(dethia) ACP analogue</i>	234
6.4.3.	The effect of alkali metal adduction to ACPs on the production of peptide ions bearing the phosphopantetheinyl arm for post-translational modification mapping	235
6.4.3.1.	<i>Acetyl-ACP</i>	236
6.4.3.2.	<i>Malonyl-ACP</i>	237
6.4.3.3.	<i>Acetoacetyl-ACP</i>	237
6.4.3.4.	<i>Myristoyl-ACP</i>	238
6.4.3.5.	<i>Nonhydrolysable photolabile malonyl carba(dethia) ACP analogue</i>	239
6.4.4.	Summary and conclusions: The application of alkali metal adduction to acyl carrier proteins (ACPs) on the production of peptides by CAD, and the application to post-translational modification mapping	240
6.5.	Summary and conclusions: Alkali metal adduction assisted tandem mass spectrometry for molecular structural determination	243

7. Conclusions and future work	247
7.1. Probing the biosynthesis of an iterative polyketide PKS with a photoactivatable nonhydrolysable malonyl acyl carrier protein probe and future work	248
7.2. Capture of intermediates by the small molecule NAC probe and future work	252
7.3. Alkali metal assisted tandem MS and future work	255
8. Experimental	257
8.1. General methods for synthetic chemistry	257
8.2. Irradiation procedures	257
8.2.1. <i>In vitro</i>	257
8.2.2. <i>In vivo</i>	258
8.3. Expression and purification of Histidine-tagged proteins in <i>E. coli</i> – <i>act apoACP 44</i> , Sfp, PanK, PPAT, and DPCK	258
8.4. SDS-PAGE analysis	259
8.5. Expression and purification of <i>act</i> KS-CLF in <i>S. coelicolor</i>	260
8.6. Trypsin digestion of acyl carrier proteins	261
8.7. Thrombin cleavage of the Histidine-tag from <i>act</i> ACP	262
8.8. Phosphopantetheinylation of <i>act apo-ACPs 44 in vitro</i>	262
8.9. Loading of <i>act</i> KS-CLF	263
8.10. Reconstitution of enzymatic activity for the <i>act</i> PKS minimal system	263
8.11. Trapping of intermediates from the <i>act</i> minimal system with the protein probe	263
8.12. Trapping of intermediates from the <i>act</i> minimal system with the small molecule probe	264

8.13.	Feeding of DMNB NAC probe to <i>S. lasaliensis</i> and preparation for LC-MS analysis.....	265
8.14.	Feeding to <i>S. coelicolor</i> and preparation for LC-MS analysis.....	266
8.15.	Enzyme assay extraction	267
8.16.	LC-MS analysis	267
8.16.1.	HPLC analysis of NAC probe photolysis experiments	267
8.16.2.	UPLC-MS analysis of proteins (not including <i>act</i> ACPs)	268
8.16.3.	UPLC-MS analysis of <i>act</i> ACPs.....	268
8.16.4.	UPLC-MS analysis of cell and enzyme reaction extracts	269
8.16.5.	UPLC-MS analysis of trypsin digested <i>act</i> ACPs.....	270
8.17.	FTICR-MS analyses.....	271
8.18.	Synthetic procedures.....	271

Declaration

The experimental work reported in this thesis is original research carried out by the author, unless otherwise stated, in the Department of Chemistry, University of Warwick between September 2011 and April 2015. No material has been submitted for any other degree, or at any other institution.

Results from other authors are referenced in the usual manner throughout the text.

Date: _____

Samantha L. Kilgour

Acknowledgements

I would firstly like to thank my supervisor, Manuela Tosin, for giving me the opportunity to work in such an amazing field, and on this great project. Getting to work in synthetic chemistry, molecular biology, enzymology, analytical science and photochemistry, to name a few, has made my time in the lab(s) very exciting. Also, thanks go to my co-supervisor, Peter O'Connor, for letting me loose on his multimillion pound instrument.

Members of the lab have made my time at Warwick especially enjoyable, both through practical help and friendship. In no particular order: James, Withall, Sidda, Orestis, Lona, Lauren, Paulina, Elena, Judith, Ina, Nicolas, Piera, Naj, Chloe, Candace, Pan, Pamela, Chidi, Sarah, Vincent, Zdenek, Lauren, Matt, Kathryn, Arupen, Emanuel, Pete, Dhadchi, Maria T, Maria R, Charles, Shanshan, Maartje, Federico, Chris, Juan, Andy, Terry, Huilin, and many, many other wonderful people.

Special thanks go to Greg and Christophe for their advice and teaching during group meetings, and for letting me use their lab equipment. Rod Wesson for building the bespoke light box. The Sadler and Stavros groups for letting me trial their photolysis equipment. Also, to the amazing technical staff: in particular, Lijiang, Phil, and Ivan.

Lastly, thank you to my fabulous and supportive husband and daddy to the best little boy I could ever imagine.

List of Figures

Figure 1 Examples of polyketides from bacteria (Lasalocid A 1 , Actinorhodin 2 , and Phloroglucinol 3), plants (Resveratrol 4) and fungi (Lovastatin 5).....	2
Figure 2 Examples of polyketides biosynthesised by type II iterative polyketide synthases.	8
Figure 3 Exemplary type II ketosynthase crystal structures.....	11
Figure 4 Exemplary structures of acyl carrier proteins (ACPs) from type II polyketide synthases (PKSs).	13
Figure 5 The chemical structure of actinorhodin 2 (left) and <i>S. coelicolor</i> M510 ⁷¹ , Δ redD mutant lacking the pathway-specific activator of Red synthesis, plated on solid medium, showing the intense blue colour caused by production of actinorhodin 2 (right).....	20
Figure 6 Protein sequences of ketosynthase (KS) and chain length factor (CLF), from the actinorhodin minimal system.	21
Figure 7 Solution NMR structure of the <i>apo</i> acyl carrier protein 44 from the actinorhodin minimal system, clearly indicating the four helices.	24
Figure 8 Solution NMR structures of <i>apo</i> -ACP 44 (PDB: 2K0Y) (A and C) and <i>holo</i> -ACP 43 (PDB: 2K0X) (B and D).	28
Figure 9 Solution NMR structures of malonyl-ACP 7 (PDB: 2KG8) and octanoyl ACP 47 (PDB: 2KGC) showing the growing cavity between helices II and III with the size of the polyketide chain. ⁹⁴	29
Figure 10 Structures of acetyl-ACP 40 and the <i>N</i> -acetylcysteamine (NAC) ester derivative 53 showing the priming of a ketosynthase with the acetyl groups from both 40 and 53	41
Figure 11 Malonyl-coenzyme A (CoA) 15 and nonhydrolysable malonyl-CoA analogues 55-57 used for probing the biosynthesis of polyketides from type III PKSs.	44
Figure 12 Small molecule chain termination probes used for the probing of PKS biosynthetic pathways, in particular in <i>S. lasaliensis</i> to generate a library of complex analogues. ^{155, 156}	48
Figure 13 Common fragmentation pathways of proteins and peptides. ¹⁷⁹	55
Figure 14 A comparison between the ‘natural’ 4’-phosphopantetheinyl arm and its carba(dethia) mimic. 7 is the 4’-phosphopantetheinyl arm of ‘malonyl’ acyl	

carrier protein. 66 is the ‘active’ malonyl carba(dethia) N-acetyl cysteamine probe..	69
Figure 15 Multicyclic photocleavable protecting groups for carboxylic acids..	73
Figure 16 Simple aromatic photolabile protecting groups for carboxylic acids	74
Figure 17 A selection of nitrobenzyl type photolabile groups to protect carboxylates.	76
Figure 18 A comparison of the two probes synthesised in this work.	82
Figure 19 UV/Vis spectrum for the nonhydrolysable photolabile malonyl N-acetyl cysteamine probe.....	86
Figure 20 Irradiation of the nonhydrolysable photolabile NAC analogue 65 with 365 nm, 1000 W from 0 to 4 hours (A to E, hourly), showing the generation of decarboxylated product.....	89
Figure 21 Irradiation of the nonhydrolysable photolabile NAC analogue 65 with 365 nm, 1000 W for 0 (A and C) and 1 (B and D) hours, at two different concentrations (0.1 mM (A and B) and 1 mM (C and D)), showing the increased photolysis yield of the decarboxylated product 129 at higher concentrations ..	90
Figure 22 SDS-PAGE results showing expression of the Pantothenate Kinase (PanK or CoaA), the phosphopantetheine adenylyltransferase (PPAT or CoaD) and the dephosphocoenzyme A kinase (DPCK or CoaE) from <i>E. coli</i>	103
Figure 23 SDS-PAGE analyses showing expression of the apo acyl carrier protein 44 (~11 kDa) from the actinorhodin minimal system, and the phosphopantetheinyl transferase, Sfp, (~28 kDa) from <i>B. subtilis</i>	106
Figure 24 A: (Parent) mass spectrum of (hexahistidine-tagged) holo-acyl carrier protein (ACP) 43 from the actinorhodin minimal system. B: Collisionally activated dissociation (CAD) of the 12+ parent ion of holo-ACP 43, generating a singly charged, characteristic, pantetheine ion 80. C: (Parent) mass spectrum of 4,5-dimethoxy-2-nitrobenzyl (DMNB) malonyl carba(dethia) ACP analogue. ACP is from the actinorhodin minimal system. D: CAD of the 12+ parent ion of DMNB malonyl carba(dethia) ACP analogue, generating a singly charged, characteristic, pantetheine ion 81.	108
Figure 25 LC-MS chromatogram showing the protonated and sodiated EIC for the isomers SEK4 41 and SEK4b 42 produced by the actinorhodin minimal system.	111

Figure 26	LC-MS chromatograms showing the photolysis of the DMNB NAC analogue 65 to 129 in the absence (A) and in the presence of the ketosynthase and chain length factor from the actinorhodin minimal system (B) with 365 nm, 1000W for 4 hours.....	112
Figure 27	Irradiation of the nonhydrolysable photolabile NAC analogue 65 with 365 nm, 1000 W for 0 mins (A), 10 mins (B), 30 mins (C), 1 hour (D), 2 hours (E) and 5 hours (F), showing the release of the active probe 66 after just 10 mins, and its stability after 5 hours.	113
Figure 28	The effect of delayed addition of active probe 66 to the actinorhodin 2 minimal system on the production of SEK4 41 and SEK4b 42.	116
Figure 29	SEK4/4b 41/42 production in the actinorhodin minimal system monitored by absorbance at 293 nm.	118
Figure 30	EIC from LC-MS analyses of the DMNB NAC analogue 65 hydrolysing and subsequent decarboxylating to 129 after ethyl acetate extraction of the media in the presence (A to D) and in the absence (E) of <i>S. lasaliensis</i> ACP12, with a comparison of the different supplementation strategies.....	120
Figure 31	EIC from LC-MS analyses of the extracts from feeding experiments with the DMNB NAC analogue 65 to <i>S. lasaliensis</i> ACP12 mutant. Traces shown are the protonated and sodiated ions of compound 131, a ‘trapped’ intermediate from lasalocid A 1 biosynthetic pathway, off-loaded from ACP10 and further reduced by KR11.	121
Figure 32	EIC from LC-MS analyses of the extracts from feeding experiments with the DMNB NAC analogue 65 to <i>S. lasaliensis</i> ACP12 mutant. Trace shown is compound 132, a ‘trapped’ intermediate from lasalocid A 1 biosynthetic pathway, offloaded from ACP11.	122
Figure 33	EIC from LC-MS analyses of the extracts from feeding experiments with the DMNB NAC analogue 65 to <i>S. lasaliensis</i> ACP12 mutant. Trace shown is the doubly charged ion of echinomycin 52, a natural product produced by a non-ribosomal peptide synthetase (NRPS) in <i>S. lasaliensis</i>	123
Figure 34	EIC from LC-MS analyses of the DMNB NAC analogue 65 showing its hydrolysis and subsequent decarboxylation to 129 after ethyl acetate extraction of liquid media in the presence of <i>S. lasaliensis</i> ACP12.	124
Figure 35	EIC from LC-MS analyses of the extracts from feeding experiments with the DMNB NAC analogue 65 to <i>S. lasaliensis</i> ACP12 mutant in liquid media.	

Trace shown is compound **131**, a ‘trapped’ intermediate from lasalocid A **1** biosynthetic pathway, off-loaded from ACP10 and further reduced by KR11. .125

Figure 36 EIC from LC-MS analyses of the extracts from feeding experiments with the DMNB NAC analogue **65** to *S. lasaliensis* ACP12 mutant in liquid media. Trace shown is compound **132**, a ‘trapped’ intermediate from lasalocid A **1** biosynthetic pathway, off-loaded from ACP11. 128

Figure 37 EIC from LC-MS and MS/MS analyses of the extracts from feeding experiments with the DMNB NAC analogue **65** to *S. lasaliensis* ACP12 mutant in liquid media. Trace shown and MS/MS is compound **135**, a ‘trapped’ intermediate from lasalocid A **1** biosynthetic pathway, off-loaded from ACP8 with subsequent epoxidation and cyclisation. 130

Figure 38 EIC from LC-MS and MS/MS analyses of the extracts from feeding experiments with the DMNB NAC analogue **65** to *S. lasaliensis* ACP12 mutant in liquid media. Trace shown and MS/MS is compound **136**, a ‘trapped’ intermediate from lasalocid A **1** biosynthetic pathway, off-loaded from ACP8, with subsequent epoxidation, cyclisation and oxidation. 131

Figure 39 *S. coelicolor* M510 after 5 days growth supplemented with 1 mM, 5 mM and 10 mM nonhydrolysable photolabile NAC probe **65** showing growth inhibition with increasing concentration. 133

Figure 40 EIC from LC-MS analyses of the DMNB NAC analogue **65** showing its hydrolysis and subsequent decarboxylation to **129** after ethyl acetate extraction at the end of (A) day 2, (B) day 3, (C) day 4 and (D) day 5 of growth on solid media in the presence of *S. coelicolor* M510..... 135

Figure 41 EIC from LC-MS analyses of shunt products of the actinorhodin minimal system, SEK4/4b **41/42**, (shown underneath) produced by *S. coelicolor* M510 in the presence of DMNB NAC analogue **65** extracted on (A) day 2, (B) day 3, (C) day 4, (D) day 5 and absence of DMNB NAC analogue **65** extracted on (E) day 2, (F) day 3, (G) day 4 and (H) day 5. 136

Figure 42 EIC from LC-MS analyses of the DMNB NAC analogue **65** showing its hydrolysis and subsequent decarboxylation to **129** after ethyl acetate extraction on day 5 of growth on solid media in the presence of *S. coelicolor* M510 with (A) no irradiation, (B) 1 hour, (C) 2 hours, (D) 3 hours of irradiation on day 3 and (E) 1 hour, (F) 2 hours, (G) 3 hours of irradiation on day 4..... 138

Figure 43 EIC from LC-MS analyses of shunt products of the actinorhodin minimal system, SEK4/4b 41/42 , (shown underneath) produced by <i>S. coelicolor</i> M510 in the presence (A-G) and absence (H-N) of DMNB NAC analogue 65 , extracted on day 5, following (A and H) no irradiation, (B and I) 1 hour, (C and J) 2 hours, (D and K) 3 hours of irradiation on day 3, and (E and L) 1 hour, (F and M) 2 hours, and (G and N) 3 hours of irradiation on day 4.	140
Figure 44 A sample of potential intermediates off-loaded from the actinorhodin 2 biosynthetic pathway by the DMNB NAC analogue 65	141
Figure 45 Irradiation of the photolabile acyl carrier protein (ACP) analogue 63 in TrisCl (50 mM), KCl (20 mM), MgCl ₂ (10 mM) at pH 8, with 365 nm, 1000 W for 0 (A), 2 (B), and 4 (C) hours, showing the synthesis of the decarboxylated product 144 by TOF-MS.	146
Figure 46 Comparison of the ratio of acetyl 40 to <i>holo</i> 43 (not hexahistadine-tagged) acyl carrier protein (ACP) from the actinorhodin minimal system following 2 hours of incubation (A) with and (B) without the actinohorhodin ketosynthase-chain length factor (KS-CLF).	148
Figure 47 Comparison of the ratios of malonyl 7 , acetyl 40 and <i>holo</i> 43 acyl carrier proteins (ACPs) from the actinorhodin minimal system following 2 hours of incubation (A) with and (B) without the actinorhodin 2 ketosynthase-chain length factor (KS-CLF).	149
Figure 48 FTICR-MS analyses showing the irradiation of the nonhydrolysable photolabile acyl carrier protein (ACP) analogue 63 with 365 nm, 1000 W, without the ketosynthase chain length factor (KS-CLF), analysed immediately after 0 (A), 2 (B), and 4 (C) hours, showing the synthesis of the deprotected malonyl product 64 and limited decarboxylated product 144	151
Figure 49 FTICR-MS analyses showing the irradiation of the nonhydrolysable photolabile acyl carrier protein (ACP) analogue 63 with 365 nm, 1000 W, in the presence of the ketosynthase chain length factor (KS-CLF), analysed immediately after 0 (A), 2 (B), and 4 (C) hours.....	152
Figure 50 FTICR-MS time-dependant analysis showing a readily uncaged sample of photolabile carrier protein 63 , in the absence, (A and B) and in the presence (C and D), of KS-CLF.	153

Figure 51 FTICR-MS analysis of active acyl carrier protein (ACP) probe 64 incubated in the actinorhodin minimal system (1:1 ratio, protected ACP probe 63 to malonyl-ACP 7) showing an off-loaded diketide 145	159
Figure 52 FTICR-MS analysis of active acyl carrier protein (ACP) probe 64 incubated in the actinorhodin minimal system (1:10 ratio, protected ACP probe 63 to labelled malonyl-ACP 7b) showing an off-loaded labelled tetraketide 147 .	161
Figure 53 FTICR-MS analysis of ACP probe 64 incubated in the actinorhodin minimal system (1:4 protected ACP probe 63 to labelled malonyl-ACP 7b), showing a captured labelled linear pentaketide 148	164
Figure 54 FTICR-MS analysis of the ACP probe 64 incubated in the actinorhodin minimal system (5:1 protected ACP probe 63 to malonyl-ACP 7) showing a captured putative cyclised pentaketide 154	165
Figure 55 FTICR-MS analysis of the ACP probe 64 incubated in the actinorhodin minimal system (5:1 protected ACP probe 63 to labelled malonyl-ACP 7b), showing a captured putative cyclised dehydrated pentaketide 155	166
Figure 56 FTICR-MS analysis of ACP probe 64 incubated in the actinorhodin minimal system (1:4 protected ACP probe 63 to malonyl-ACP 7), showing a captured linear hexaketide 149	169
Figure 57 FTICR-MS analysis of ACP probe 64 incubated in the actinorhodin minimal system (5:1 protected ACP probe 63 to malonyl-ACP 7), showing a captured cyclised hexaketide 156	170
Figure 58 FTICR-MS analysis of ACP probe 64 incubated in the actinorhodin minimal system (1:1 protected ACP probe 63 to malonyl-ACP 7), showing a captured cyclised dehydrated hexaketide 157	171
Figure 59 Example of a region of a spectrum with a very intense peak (protected ACP probe 63 at charge state 8^+) with the inset showing the auto-correlation of the region indicated, confirming the 8^+ charge state.	174
Figure 60 A blank region of a spectrum with the inset showing the auto-correlation of the region indicated, confirming that no isotopic distributions were detected, and this region of the spectrum is, indeed, noise.	175
Figure 61 Spectrum of a detected cyclised hexaketide 156 of charge state 8^+ with inset showing autocorrelation of region indicated confirming an 8^+ charge state.	176

Figure 62 EIC of the peptide containing the active site serine generated by trypsin digestion of the <i>apo</i> and <i>holo</i> acyl carrier proteins 44 and 45 from the actinorhodin minimal system.	177
Figure 63 LC-MS chromatogram showing the EIC for the isomers SEK4 41 and SEK4b 42 produced by the actinorhodin minimal system. The (A and C) unlabelled and (B and D) ¹³ C labelled actinorhodin minimal system was activated by the addition of final enzyme, <i>holo</i> -ACP 43 , then (A and B) 30 seconds and (C and D) 5 minutes later ‘active’ ACP probe 64 , irradiated for 4 hours in the home built UVA light source, was added.	180
Figure 64 LC-MS chromatograms showing EIC of <i>holo</i> -ACP 43 (red trace) and DMNB protected carba(dethia) malonyl-ACP analogue 63 (blue trace) expressed in <i>E. coli</i> BAP1 cells by supplementing with (A and C) 1 mM and (B and D) 10 mM DMNB protected carba(dethia) malonyl pantetheine analogue 61 (shown) at the same time as induction with Isopropyl β-D-1-thiogalactopyranoside (IPTG) at optical densities 600 nm of (A and B) 0.6 and (C and D) 0.3.	183
Figure 65 Structures of lasalocid A 1 and iso-lasalocid A.	191
Figure 66 Structure of the nonhydrolysable photolabile carba(dethia) pantetheine 61	193
Figure 67 Example peak displaying the increased resolving power before (top) and after (bottom) phasing.	195
Figure 68 A) Mass spectrum of collisionally activated dissociation (CAD) of [M+Na] ⁺ parent ion 61 . B) Mass spectrum of CAD of [M+Li] ⁺ parent ion 61 . Inset: assigned fragmentation diagram.	197
Figure 69 Mass spectra of: A) electron induced dissociation (EID) of [M+Na] ⁺ parent ion 61 ; B) EID of [M+Li] ⁺ parent ion 61 ; C) EID of [M+Cs] ⁺ parent ion 61	198
Figure 70 Fragmentation diagrams showing all the assigned fragments for 61	203
Figure 71 Adduction of lithium to the nonhydrolysable photolabile malonyl carba(dethia) acyl carrier protein (ACP) analogue 63 demonstrated on the 8 ⁺ ion. A) ACP 63 without the addition of LiCl to the sample. B) Simulated isotopic pattern for ACP 63 8 ⁺ ion. C) ACP 63 with the addition of 1 mM LiCl.	207

Figure 72 (A, D, G) Mass spectra showing caesium adduction to the nonhydrolysable photolabile malonyl carba(dethia) acyl carrier protein (ACP) 63 by sample preparation with 1 mM Cs ₂ CO ₃	208
Figure 73 The effect of adduction of lithium to the nonhydrolysable photolabile malonyl carba(dethia) acyl carrier protein (ACP) 63 on the yield of cleaved pantetheine analogue 81 (<i>m/z</i> 524.2239) and the phosphopantetheine analogue 169 (<i>m/z</i> 622.2008) via bond cleavage under collisionally activated dissociation (CAD)	210
Figure 74 Adduction of lithium to acetyl acyl carrier protein (ACP) 40 shows improved yield of cleaved acetylated pantetheine 171 (<i>m/z</i> 303.1373) via phosphodiester bond cleavage under collisionally activated dissociation (CAD).	212
Figure 75 The effect of adduction of lithium to malonyl acyl carrier protein (ACP) 7 on the yield of cleaved malonyl pantetheine 173 (<i>m/z</i> 347.1271) via phosphodiester bond cleavage under collisionally activated dissociation (CAD).	213
Figure 76 The effect of adduction of lithium or caesium to acetoacetyl-ACP 167 , on the yield of cleaved acetoacetyl pantetheine 175 (<i>m/z</i> 345.1479) via phosphodiester bond cleavage under collisionally activated dissociation (CAD).	215
Figure 77 The effect of lithium adduction to myristoyl-ACP 168 on the yield of cleaved myristoyl pantetheine 177 (<i>m/z</i> 471.32511) via phosphodiester bond cleavage under collisionally activated dissociation (CAD).	217
Figure 78 The effect of lithium adduction to myristoyl-ACP 168 on the yield of cleaved myristoyl phosphopantetheine 178 (<i>m/z</i> 569.3020) via phosphodiester bond cleavage under collisionally activated dissociation (CAD).	218
Figure 79 The effect of caesium adduction to four different ACPs 63 , 40 , 167 , and 7 on fragmentation pathways with collisionally activated dissociation (CAD).	219
Figure 80 Cleavage coverage maps showing b and y ions resulting from collisionally activated dissociation (25V) of acetyl-ACP 40 with (A, red) and without (B, blue) lithium adduction.	224

Figure 81	Example spectrum showing b (top) and y (bottom) ions resulting from collisionally activated dissociation (25V) of acetyl-ACP 40 with lithium adduction.	225
Figure 82	Cleavage coverage maps showing b and y ions resulting from collisionally activated dissociation (35V) of malonyl-ACP 7 with lithium (A, red), with caesium (C, green) and without alkali (B, blue) adduction.	226
Figure 83	Cleavage coverage maps showing b and y ions resulting from collisionally activated dissociation (30V) of acetoacetyl-ACP 167 with lithium (A, red), with caesium (C, green) and without alkali (B, blue) adduction.	227
Figure 84	Cleavage coverage maps showing b and y ions resulting from collisionally activated dissociation (25V) of myristoyl-ACP 168 with (A, red) and without (B, blue) lithium adduction.	228
Figure 85	Cleavage coverage maps showing b and y ions resulting from collisionally activated dissociation (28V and 18V) of nonhydrolysable photolabile malonyl carba(dethia) ACP analogue 63 with lithium (A, red), with caesium (C, green) and without alkali (B, blue) adduction.	229
Figure 86	Cleavage coverage maps only showing phosphorylated b and y ions resulting from collisionally activated dissociation (25V) of acetyl-ACP 40 with (A, red) and without (B, blue) lithium adduction.	231
Figure 87	Cleavage coverage maps only showing phosphorylated b and y ions resulting from collisionally activated dissociation (35V) of malonyl-ACP 7 with lithium (A, red), with caesium (C, green) (Note: none detected) and without alkali (B, blue) adduction.	232
Figure 88	Cleavage coverage maps only showing phosphorylated b and y ions resulting from collisionally activated dissociation (30V) of acetoacetyl-ACP 167 with lithium (A, red), with caesium (C, green) and without alkali (B, blue) adduction.	233
Figure 89	Cleavage coverage maps only showing phosphorylated b and y ions resulting from collisionally activated dissociation (25V) of myristoyl-ACP 168 with (A, red) and without (B, blue) lithium adduction.	234
Figure 90	Cleavage coverage maps only showing phosphorylated b and y ions resulting from collisionally activated dissociation (28V and 18V) of nonhydrolysable photolabile malonyl carba(dethia) ACP analogue 63 with	

lithium (A, red), with caesium (C, green) (Note: none detected) and without alkali (B, blue) adduction.	235
Figure 91 Cleavage coverage maps only showing ‘b’ and ‘y’ ions with the acetyl-phosphopantetheinyl arm bound, resulting from collisionally activated dissociation (25V) of acetyl-ACP 40 with (A, red) and without (B, blue) lithium adduction.	236
Figure 92 Cleavage coverage maps only showing ‘b’ and ‘y’ ions with the malonyl-phosphopantetheinyl arm bound, resulting from collisionally activated dissociation (35V) of malonyl-ACP 7 with lithium (A, red), with caesium (C, green) (Note: none detected) and without alkali (B, blue) adduction.	237
Figure 93 Cleavage coverage maps only showing ‘b’ and ‘y’ ions with the acetoacetyl-phosphopantetheinyl arm bound, resulting from collisionally activated dissociation (30V) of acetoacetyl-ACP 167 with lithium (A, red), with caesium (C, green) and without alkali (B, blue) adduction.	238
Figure 94 Cleavage coverage maps only showing ‘b’ and ‘y’ ions with the myristoyl-phosphopantetheinyl arm bound, resulting from collisionally activated dissociation (25V) of myristoyl-ACP 168 with (A, red) and without (B, blue) lithium adduction.	239
Figure 95 Cleavage coverage maps only showing ‘b’ and ‘y’ ions with the nonhydrolysable photolabile malonyl carba(dethia)-phosphopantetheinyl arm bound, resulting from collisionally activated dissociation (28V and 18V) of nonhydrolysable photolabile malonyl carba(dethia) ACP analogue 63 with lithium (A, red), with caesium (C, green) (Note: none detected) and without alkali (B, blue) adduction.	240
Figure 96 Potential next generation photolabile NAC analogues for off-loading of biosynthetic intermediates.	254

List of Schemes

Scheme 1 Illustration of different polyketide synthases (PKSs)	4
Scheme 2 Polyketide chain extension mechanism for the actinorhodin 2 type II minimal system.....	5
Scheme 3 Examples of common oxygenases found in type II polyketides synthases.	16
Scheme 4 Biosynthesis of actinorhodin 2 from acetyl 17 and malonyl-coenzyme A 15	19
Scheme 5 Biosynthesis of shunt products, SEK4/4b 41 and 42 and mutactin 45 , from the actinorhodin 2 biosynthetic pathway.....	25
Scheme 6 Conversion of apo-ACP 44 to holo-ACP 43 with Coenzyme A 46 and a phosphopantetheinyl transferase.	27
Scheme 7 Enzymatic preparation of Coenzyme A analogues via corresponding pantetheine analogues with the aid of enzymes that biosynthesise Coenzyme A 46 in <i>E. coli</i>	32
Scheme 8 Chemical degradation of ¹⁴ C labelled 6-methylsalicylic acid (6-MSA) 50 demonstrating the incorporation of four acetates. ^{4, 130}	34
Scheme 9 General synthesis of N-acetylcysteamine β-ketothioester (SNAC) analogues via coupling to carbonyldiimidazole (CDI).....	42
Scheme 10 In vivo off-loading of polyketide intermediates from the model system, 6-deoxyerythronolide B 51 synthase, with synthetic chain terminators. T	45
Scheme 11 Off-loading of intermediates from the lasalocid A 1 synthase, with synthetic chain terminators from feeding experiments in <i>S. lasaliensis</i> . ^{22, 155, 156}	47
Scheme 12 Generation of a pantetheine (Pant) ejection ion 58 or a phospho-Pant ejection ion 59 from the corresponding ACP by CAD or IRMPD.	60
Scheme 13 Primary project aim	65
Scheme 14 Secondary project aim	67
Scheme 15 Mechanism of photolysis of the 4,5-dimethoxy-2-nitrobenzyl (DMNB) group 107 protecting a carboxylic acid group.	79
Scheme 16 Synthesis of a nonhydrolysable photolabile malonyl N-acetyl cysteamine analogue 65	83
Scheme 17 ‘Protected’ 4,5-dimethoxy-2-nitrobenzyl malonyl carba(dethia) ACP analogue 63 and its product after irradiation to the ‘active’ malonyl carba(dethia) ACP analogue 64	94

Scheme 18	Products of the actinorhodin minimal system, SEK4 41 and SEK4b 42 , via the synthesis of an octaketide chain.....	94
Scheme 19	Overview of the planned chemoenzymatic synthesis of a nonhydrolysable photolabile malonyl acyl carrier protein 63 from pantothenic acid 60	96
Scheme 20	Previous preparation of a nonhydrolysable malonyl carba(dethia) coenzyme A analogue 71 by Tosin and co-workers.....	97
Scheme 21	Synthesis of a nonhydrolysable 4,5-dimethoxy-2-nitrobenzyl malonyl carba(dethia) pantetheine analogue with acetyl protection of the diol 73	98
Scheme 22	Final synthesis of a nonhydrolysable 4,5-dimethoxy-2-nitrobenzyl malonyl carba(dethia) pantetheine analogue 61	99
Scheme 23	Enzymatic synthesis of a nonhydrolysable 4,5-dimethoxy-2-nitrobenzyl malonyl carba(dethia) coenzyme A analogue 62 from a corresponding, chemically synthesised, pantetheine analogue 61	104
Scheme 24	Enzymatic preparation of a nonhydrolysable 4,5-dimethoxy-2-nitrobenzyl malonyl carba(dethia) acyl carrier protein analogue 63 from the corresponding chemoenzymatically synthesised coenzyme A analogue 62	107
Scheme 25	A) In vivo generation of the active probe 66 from the methyl ester protected probe 130 . ¹⁵⁵ B) In vivo generation of the active probe 66 , via endogenous esterases, or photolysis, from the 4,5-Dimethoxy-2-Nitrobenzyl (DMNB) protected probe 65	127
Scheme 26	Lasalocid A 1 biosynthetic pathway from <i>S. lasaliensis</i> showing previously ‘trapped’ intermediates generated by the incubation with NAC analogues.	129
Scheme 27	Lasalocid A 1 biosynthetic pathway from <i>S. lasaliensis</i> showing newly putative ‘trapped’ intermediates 135 and 136 generated by the incubation with DMNB NAC analogue 65 in an ACP12 deletion mutant following UV irradiation.	142
Scheme 28	Investigation of the actinorhodin minimal type II polyketide synthase by means of a protein probe 63	155
Scheme 29	Capture of putative pentaketide intermediates from the actinorhodin minimal system.....	162
Scheme 30	Capture of putative hexaketide intermediates from the actinorhodin minimal system: predicted linear intermediate	167

Scheme 31 Capture of putative intermediates from the actinorhodin minimal system.	
.....	249

List of Tables

Table 1	Overview of notable fragmentation techniques, the instruments they are typically coupled with and their mode of action.	54
Table 2	Reaction conditions trialled for the synthesis of the nonhydrolysable photolabile malonyl N-acetyl cysteamine analogue 65 from 128 , shown.....	84
Table 3	Conditions tested for the photolysis of a nonhydrolysable photolabile malonyl N-acetyl cysteamine probe 65	87
Table 4	Reaction conditions trialled for the synthesis of 79 from 78 , shown.	100
Table 5	Reaction conditions trialled for the deprotection 79	101
Table 6	Intermediates from the actinorhodin minimal system trapped by the carba(dethia) malonyl-ACP probe 64 were detected by FTICR-MS direct injection.	157
Table 7	Comparison of lithiated and non-lithiated ACP samples.....	244
Table 8	SDS-PAGE recipes.....	260
Table 9	LC-MS gradient for the analysis of the nonhydrolysable photolabile SNAC analogue 65 photolysis experiments.....	268
Table 10	UPLC-MS gradient for the analysis of proteins.....	268
Table 11	UPLC-MS gradient for the analysis of acyl carrier proteins	269
Table 12	UPLC-MS gradient for the analysis of cell and enzyme reaction extracts....	270
Table 13	UPLC-MS gradient for the analysis of trypsin digested acyl carrier proteins.....	270

Abbreviations and Definitions

Abbreviations	Definitions
6Deb	6-deoxyerythronolide B
6-MSA	6-methylsalicylic acid
A(+)	Monoisotopic mass and the following series for that ion
Ac ₂ O	Acetic anhydride
ACP	Acyl carrier protein
AcpH	Acyl carrier protein hydrolase
<i>act</i>	Actinorhodin
A- <i>p</i> HP	3-acetamide- <i>para</i> -hydroxyphenacyl
Aqmoc	Anthroquinon-2-ylmethoxycarbonyl
Arg	Arginine
AT	Acyl transferase
ATP	Adenosine triphosphate
Bhc	6-bromo-7-hydroxycoumarin-4-yl)methyl
BLAST	Basic Local Alignment Search Tool
CAD or CID	Collisionally Activated/Induced Dissociation
cAMP	Cyclic adenosine monophosphate
CDA	Calcium-dependent antibiotic
Chc	(6-chloro-7-hydroxycoumarin-4-yl)methyl
CLF	Chain length factor
CM	Coumarin-4-ylmethyl
CMCM	(7-carboxymethoxycoumarin-4-yl)methyl
CoA	Coenzyme A
C- <i>p</i> HP	3-carboxyl- <i>para</i> -hydroxyphenacyl
Cryo-EM	Cryo-electron microscopy
D(NB)	Di(nitrobenzyl)oxycarbonyl
Da	Daltons
DCM	Dichloromethane
DEBS	6-deoxyerythronolide B synthase

Abbreviations	Definitions
DH	Dehydratase
DHK	Dihydrokalafungin
DIPEA	N,N-Diisopropylethylamine
DMAP	4-Dimethylaminopyridine
DMB	3,5-dimethoxybenzyl
DMDMB	α,α -dimethyl-3,5-dimethoxybenzyl
DMNB	4,5-dimethoxy-2-nitrobenzyl
DMNPE	4,5-dimethoxy 1-(2-nitrophenyl)ethyl
DMNPP	2-(4,5-Dimethoxy-2-nitrophenyl)propyl
DMO- <i>p</i> HP	3,5-dimethoxy- <i>para</i> -hydroxyphenacyl
DNB	2,6-dinitrobenzyl
DNPT	2,4-dinitrophenylthio
DPCK	Dephosphocoenzyme A kinase
ECD	Electron capture dissociation
EDC	1-Ethyl-3-(3-dimethylaminopropyl)carbodiimide
EIC	Extracted ion chromatogram
EID	Electron induced dissociation
ER	Enoyl reductase
ESI	Electrospray ionisation
ETD	Electron transfer dissociation
Ex.	Extracted
FAD	Flavin adenine dinucleoside
FAS	Fatty acid synthase
FID	Free induction decay
FRET	Fluorescence resonance energy transfer
FT	Fourier transform
FTICR	Fourier transform ion cyclotron resonance
FT-MS	Fourier transform-mass spectrometry
FWHM	Full width at half maximum
GABA	γ -Aminobutyric acid

Abbreviations	Definitions
Glu	Glutamine
GT	Glycosyltransferase
HATU	<i>N,N,N',N'</i> -Tetramethyl-O-(7-azabenzotriazol-1-yl)uronium hexafluorophosphate
HCM	(7-hydroxycoumarin-4-yl)methyl
His	Histidine
HNVDS	((2-hydroxy-3-naphthyl)vinyl)-diisopropylsilyl
HOBt	Hydroxybenzotriazole
HPLC	High performance liquid chromatography
HR	High resolution
HSDIS	(hydroxystyryl)diisopropylsilyl
ICR	Ion cyclotron resonance
InsP ₃	1,4,5-triphosphate
IPTG	Isopropyl β-D-1-thiogalactopyranoside
IRMPD	Infrared multiphoton dissociation
KR	Ketoreductase
KS	Ketosynthase
LB	Lysogeny broth
LC	Liquid chromatography
LED	Light emitting diode
Leu	Leucine
<i>m/z</i>	Mass to charge ratio
MALDI	Matrix assisted laser desorption ionisation
MCAT	Malonyl-CoA: <i>holo</i> acyl carrier protein transacylase
MCM	(7-methoxycoumarin-4-yl)methyl
MDNB	4,5-methylenedioxy nitrobenzyl
MeCN	Acetonitrile
MeOH	Methanol
MO- <i>p</i> HP	(3-methoxy- <i>para</i> -hydroxyphenacyl
MS	Mass spectrometry

Abbreviations	Definitions
MS/MS	Tandem mass spectrometry
MT	Methyltransferase
MudPIT	Multidimensional Protein Identification Technology
MW	Molecular weight
NAC	<i>N</i> -acetylcysteamine
NADPH	Nicotinamide adenine dinucleotide
NB	Nitro benzyl
Ni-NTA	Nickel-nitrilotriacetic acid
NMR	Nuclear magnetic resonance
NRPS	Non-ribosomal peptide synthase
NVOC	6-nitroveratroyloxycarbonyl
OASIS	Orthogonal Active Site Identification System
OD _{600nm}	Optical Density at 600 nm
ORF	Open reading frame
PanK	Pantothenate kinase
Pant	Pantetheine
<i>p</i> BB	<i>para</i> -bromobenzyl
PCP	Peptidyl carrier protein
PDB	Protein database
Phe	Phenylalanine
Phmoc	Phenanthren-9-ylmethoxycarbonyl
<i>p</i> HP	<i>para</i> -hydroxyphenacyl
PKS	Polyketide synthase
<i>p</i> MOB	<i>para</i> -methoxybenzyl
Pmoc	Pyren-1-ylmethoxycarbonyl
<i>p</i> NB	<i>Para</i> -nitrobenzyl
PPant	4'-phosphopantetheine
PPAT	Phosphopantetheine adenylyltransferase
ppm	Parts per million
PrISM	Proteomic Investigation of Secondary Metabolism

Abbreviations	Definitions
PTM	Post translational modification
QIT	Quadrupole ion trap
Red	Undecylprodigiosin
RF	Retention factor
RP	Reverse phase
SAM	<i>S</i> -Adenosyl methionine
SDS-PAGE	Sodium dodecyl sulphate polyacrylamide gel electrophoresis
Ser	Serine
SNAC	<i>N</i> -acetylcysteamine β -ketoester
TBAF	Tetra- <i>n</i> -butylammonium fluoride
tBhc	3,6,8-tribromo-7-hydroxycoumarin-4-ylmethyl
TBS	<i>tert</i> -butyldimethylsilyl
TCSSD	Thiochrome <i>S,S</i> -dioxide
TE	Thioesterase
TFA	Trifluoroacetic acid
THF	Tetrahydrofuran
Thr	Threonine
TLC	Thin layer chromatography
TOF	Time of flight
UPLC	Ultra pressure liquid chromatography
UV	Ultra violet
UV/Vis	Ultra violet/Visible
W	Watts

Abstract

Polyketide natural products are a major source of pharmaceutical and agricultural compounds. Their biosynthesis is highly complex and the elucidation of intermediate steps is highly desirable to the scientific community for microorganism engineering purposes.

In this work, novel photoactivatable ‘chain termination’ probes were prepared as tools for the off-loading and capture of biosynthetic intermediates from polyketide synthases (PKSs); novel methods to analyse polyketide biosynthetic intermediates *via* FTICR-MS were also investigated.

The chemical probes herein reported are nonhydrolysable analogues of ACP-bound malonate used in polyketide biosynthesis for carbon chain elongation. This research focused on the preparation of a chemoenzymatically modified acyl carrier protein that, upon activation *via* UV irradiation, should compete with discrete ‘natural’ acyl carrier proteins to capture biosynthetic intermediates from challenging type II polyketide iterative assemblies. Promising preliminary results for the use of this tool *in vitro* were obtained in the form of putative actinorhodin ACP-bound intermediates observed and characterised by FTICR-MS. Moreover, a 4,5-dimethoxy-2-nitrobenzyl group was also prepared and successfully employed for trapping biosynthetic intermediates from the *in vivo* assembly of the antibiotic lasalocid A.

Lastly, mass spectrometric methods involving alkali metal adduct ions were explored in order to improve the characterisation of free and enzyme-bound biosynthetic intermediates. Overall this work contributes further to our current and future understanding of polyketide synthases and related systems.

Chapter 1: Introduction

1. Introduction

1.1. Polyketide natural products and their biosynthesis

Polyketides are a broad family of pharmaceutically and industrially important natural products.¹⁻⁵ They are produced by bacteria, fungi, plants, and other organisms, and display a plethora of chemical structures and functions. Examples include lasalocid **1**, a coccidiostat biosynthesised from the soil bacterium *Streptomyces lasaliensis*⁶; actinorhodin **2**, a complex aromatic antibiotic from *Streptomyces. coelicolor*⁷; phloroglucinol **3**, a small aromatic metabolite from *Pseudomonas fluorescens* that displays a range of activities including antibacterial action⁸; resveratrol **4**, an antioxidant found in grapes commonly reported as being responsible for the so-called ‘French paradox’⁹; and lovastatin **5**, a cholesterol lowering compound, and precursor to the drug simvastatin, biosynthesised by the fungus *Aspergillus terreus*¹⁰ (**Figure 1**). Polyketides also include many anticancer and antitumour agents, insecticides, antifungals and antiviral compounds.

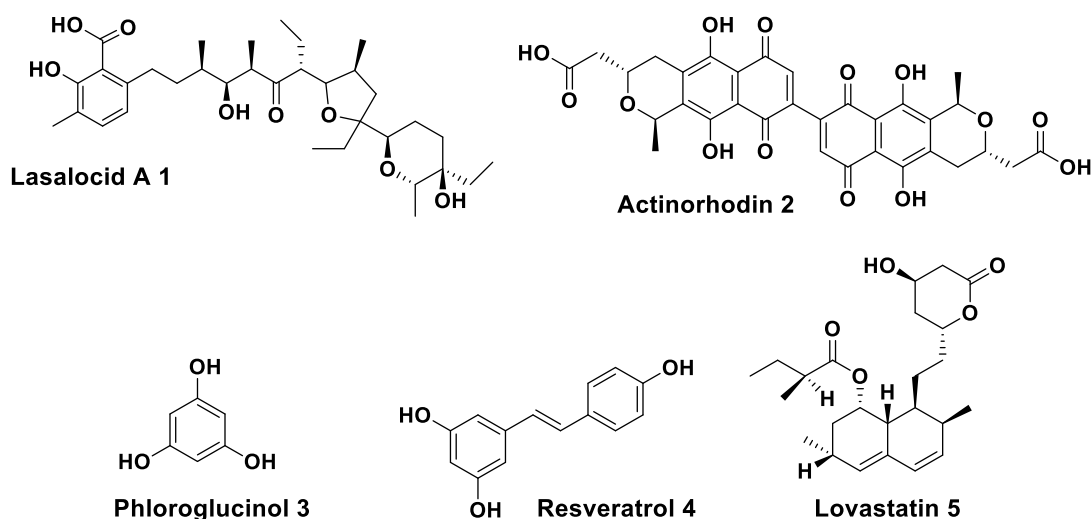


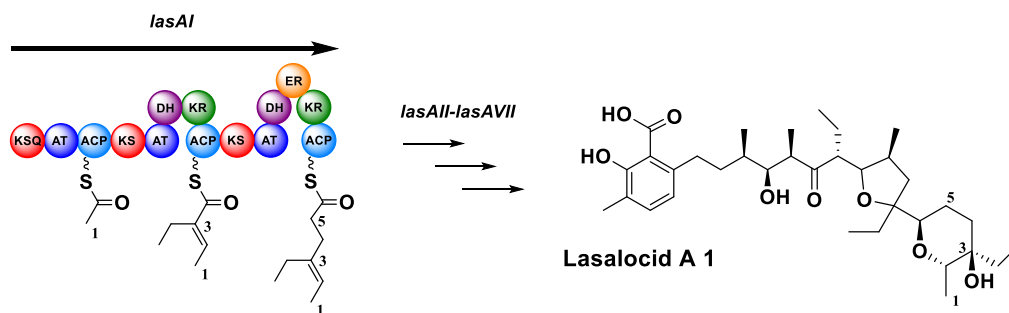
Figure 1 Examples of polyketides from bacteria (Lasalocid A 1, Actinorhodin 2, and Phloroglucinol 3), plants (Resveratrol 4) and fungi (Lovastatin 5).

1.1.1. Fundamentals of polyketide biosynthesis

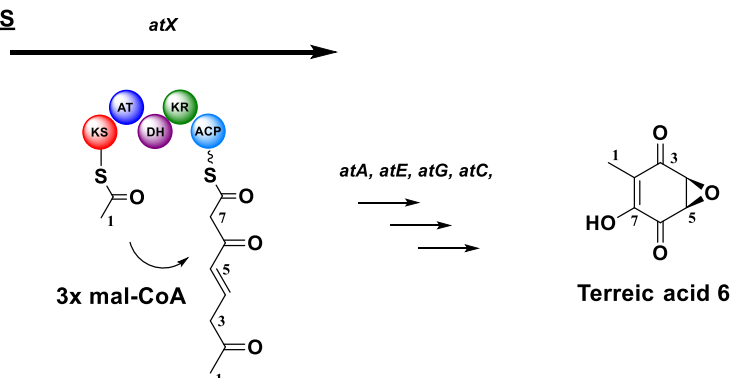
Polyketides are biosynthesised by polyketide synthase (PKS) enzymes. PKSs are roughly categorised into three types per the organisation of their domains and their catalytic activities (**Scheme 1**). While type I and type III PKSs are single proteins comprising multiple domains/catalytic activities, type II PKSs consist of discrete enzymes or domains that act iteratively to produce complex aromatic compounds.¹¹⁻¹³ Type I PKSs can be either ‘modular’ or iterative. Modular PKSs biosynthesise polyketides in a step-wise manner, utilising ‘modules’: these are groups of enzymes or domains which catalyse loading, elongation or termination of the polyketide chain where each domain is used only once. Conversely, iterative type PKSs use each of their domains multiple times. Type III PKSs are always iterative, but differ from type II in that coenzyme A (CoA) is the acyl carrier, whereas an acyl carrier protein (ACP) is used in all other types of PKS.

The common and key step in polyketide biosynthesis is carbon chain formation and elongation by decarboxylative Claisen condensation of malonate units (bound to acyl carrier proteins (ACPs) in type I and II PKSs or to Coenzyme A in type III PKSs) onto acyl groups bound to ketosynthase (KS) domains (**Scheme 1**). Upon new carbon-carbon bond formation, the extended polyketide chain bound to ACPs or CoAs is transferred onto KSs of the same enzyme/module for iterative systems, or to downstream modules in modular systems for further elaboration. This process is repeated a pre-programmed number of times until an ACP bound n-ketide is generated (**Scheme 2**). Starter and extender units include methyl, ethyl or propionyl malonyl.

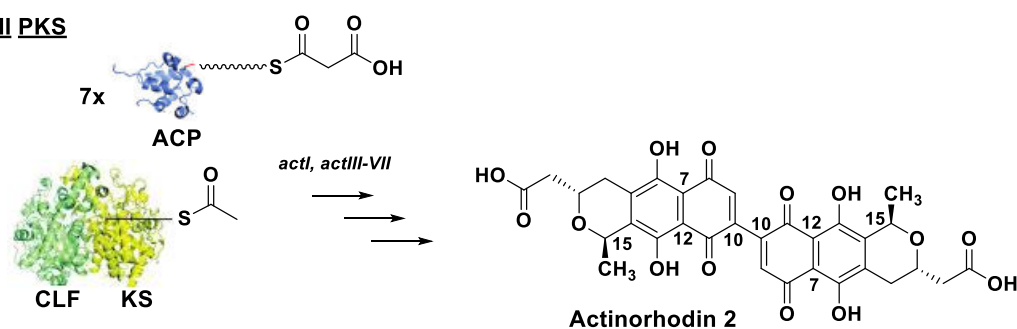
Type I Modular PKS



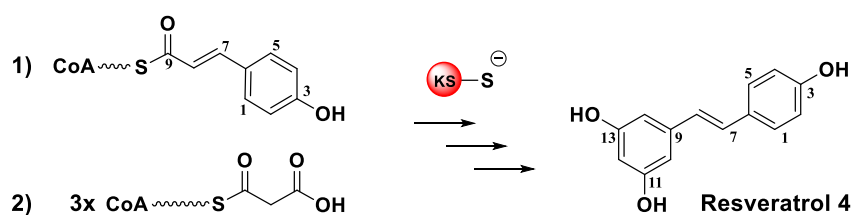
Type I Iterative PKS



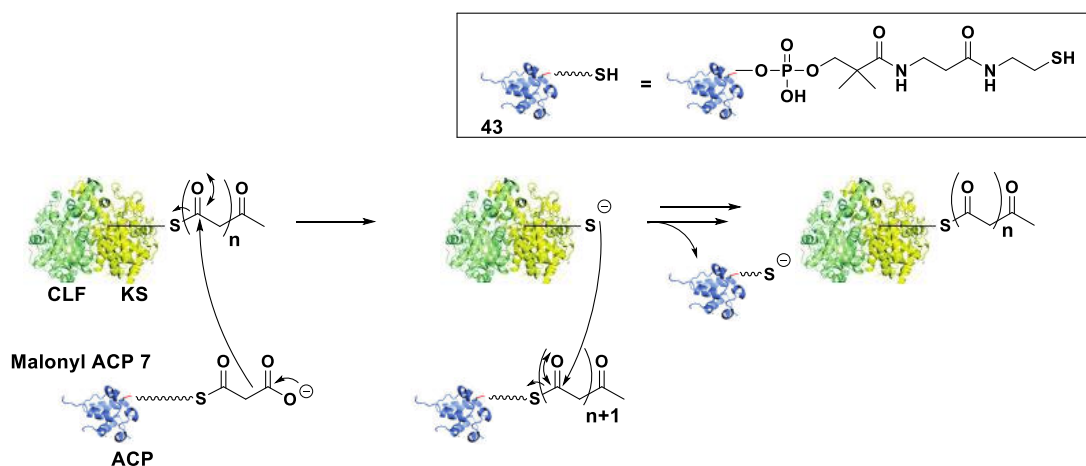
Type II PKS



Type III PKS



Scheme 1 Illustration of different polyketide synthases (PKSs): From top to bottom: Type I modular PKSs use modules for single rounds of chain extension and modification, as exemplified by the first two modules of the lasalocid A PKS which are each responsible for one round of polyketide chain extension. Type I iterative PKSs use their domains iteratively, as shown, for the biosynthesis of Terreic acid 6¹⁴ via the precursor 6-methylsalicylic acid (6-MSA) 50, showing the multiple usage of each domain. Type II PKSs such as that responsible for the biosynthesis of actinorhodin 2. Type III PKSs such as that responsible for the biosynthesis of resveratrol 4, use coenzyme A (CoA) as the acyl carrier. KS = ketosynthase, AT = acyl transferase, ACP = acyl carrier protein, DH = dehydratase, KR = ketoreductase, ER = enoylreductase, and CLF = chain length factor.)



Scheme 2 Polyketide chain extension mechanism for the actinorhodin 2 type II minimal system. ACP = acyl carrier protein, KS = ketosynthase, CLF = chain length factor.

Acyl transferase (AT) domains are present in type I PKSs; they are responsible for selectively loading ACPs with malonyl starter and extender units provided by CoAs. ATs can either be *cis*- or *trans*-. The former are paired with a specific ACP, whereas the latter can transfer extender units to one or more ACPs.¹⁵ The 6-deoxyerythronolide B synthase (DEBS) contains a *cis*-AT, and examples that harbour *trans*-ATs include PKSs that biosynthesise leinamycin¹⁶, bryostatin¹⁷ and disorazole^{15, 18}. However, this domain is not necessary in all PKSs as some ACPs can self-malonate, such as in the biosynthesis of actinorhodin **2**.¹⁹

Further product complexity is achieved by the action of reductive enzymes throughout chain extension. Ketoreductase (KR) domains stereoselectively reduce a β -keto group to a hydroxyl group, using nicotinamide adenine dinucleotide phosphate (NADPH) as a co-factor. Further hydrolysis of the hydroxyl group can be performed by a dehydratase (DH), producing a double bond that can be even further reduced by an enoylreductase (ER).²⁰

The acyl carrier protein (ACP) plays a key role in shuttling the growing polyketide chains to different domains, and provides the starter unit to the ketosynthase (KS) for chain extension to begin (See section 1.2.1 for further detail).

Thioesterase (TE) domains catalyse the hydrolysis or cyclisation of advanced thioester intermediates, releasing the fully biosynthesised polyketide from the PKS. However, TEs are not always present in PKSs as spontaneous hydrolysis or cyclisation can occur to release the compound from the PKS.

‘Tailoring’ enzymes perform further polyketide structural modifications; they are often post-PKS enzymes, and include methyltransferases, cyclases, aromatases and glycosyltransferases, amongst many others. Product tailoring modifications are often crucial to their bioactivity. For example, the glycosylation of erythromycin is essential for its antibiotic action.²¹ The tailoring can also take place on the enzyme bound intermediates such as the epoxidation of the late stage intermediates leading to the polyether rings in lasalocid A **1**.²²

The biosynthesis of polyketides can be very complex, and include numerous stereoselective reactions and tightly regulated steps that, as yet, are not easily attainable by synthetic chemistry. When polyketide generation is achieved by synthetic chemistry, the number of steps becomes far greater than that required within living organisms, and at far greater cost. For example, the optimised chemical synthesis of the lasalocid A **1** requires 29 chemical steps with approximately 0.55% final yield.²³ Therefore, when the compounds are pharmaceutically active it makes economic sense to use microorganism fermentation.

Generating analogues of natural products requires a similar long chemical synthetic process: if it were possible to produce these analogues by bioengineering organisms to introduce the favourable modifications this would cut the time and cost of the process, as well as make them environmentally more acceptable by avoiding the use of industrial chemicals. Currently, bioengineering of PKSs is in its early stages and understanding the fundamentals of how these enzymes function is crucial towards achieving this goal.

1.2. Type II polyketides and their biosynthesis

At this point, gram-positive actinomycetes are the only known organisms that biosynthesise polyketides by type II polyketide synthases.¹² As outlined in section 1.1.1, type II PKSs differ from other PKSs in that the enzymes involved are discrete, and are always iterative enzymes. The products of type II PKSs tend to be highly aromatic due to the facility of the polyketide chain to undergo cyclisation and aromatisation prior to tailoring steps. Actinorhodin **2** (the polyketide of main interest in this thesis), lomaiviticin **8**, doxorubicin **9**, enterocin **10**, jadomycin B **11**, and resistomycin **12** are all examples of polyketides synthesised by type II PKSs (**Figure 2**).

The polyketides made by type II PKSs can be classified by their chemical scaffolds into 7 different types: the aureolic acids, tetracyclines, benzoisochromanequinones, anthracyclines, angucyclines, tetracenomycins and pradimicin-like polyphenols. The compounds from these classes exhibit a wide variety of activities, from cancer chemotherapy agents (e.g. anthracyclines), to antibiotics (e.g. tetracyclines), to antifungal and antiviral activities (pradimicin-like polyphenols).¹²

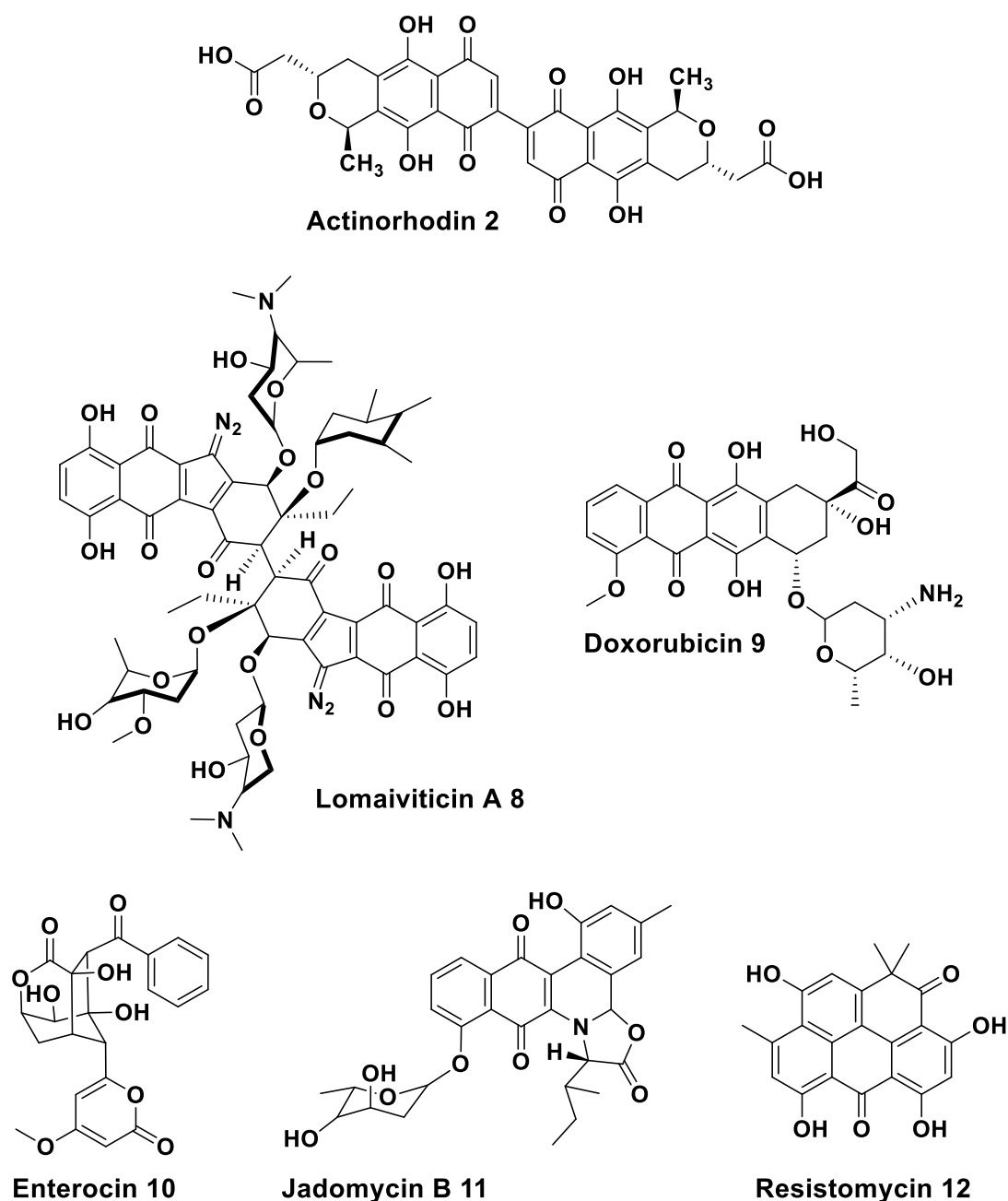


Figure 2 Examples of polyketides biosynthesised by type II iterative polyketide synthases.

1.2.1. Biosynthesis of type II polyketides

Polyketide chain initiation and elongation in type II PKSs is carried out by the ‘minimal system’. This consists of a ketosynthase (KS) and a chain length factor (CLF), also called KS α and KS β , and an acyl carrier protein (ACP) domain.^{4, 24} KS

and CLF co-express as a heterodimer complex. The crystal structure of the KS-CLF from the actinorhodin **2** PKS has been solved, showing the growing polyketide chain located at the heterodimer interface, in an amphipathic tunnel.²⁵ The KS contains an active site cysteine, and mass spectrometry has shown that intermediates are bound to this cysteine, and not elsewhere in the KS-CLF complex.²⁵

The ACP provides the KS with the starter and extender units for polyketide chain formation, and also transports the growing polyketide chain to the KS-CLF, linked via a 4'-phosphopantetheinyl (PPant) arm bound to an active site serine.²⁶ The PPant arm binds all these different substrates as a thioester by employing its terminal thiol moiety (**Scheme 2**).

It is believed that the CLF is crucial for the initial decarboxylation of malonyl-ACP **7** to load an acetyl group onto the KS, and also to initiate the decarboxylative Claisen condensation that begins chain elongation.²⁷ Subsequently, malonyl-ACP **7** is iteratively used for polyketide chain extension as previously described (**Scheme 2**).

The most common starter unit for type II PKSs are acetate units, as those used for example in the biosynthesis of actinorhodin **2**²⁸. However, some PKSs have been found that use other starter units, such as propionate (doxorubicin **9**²⁹ and lomaiviticin **8**³⁰), and benzoate (enterocin **10**³¹). The alternative starter units are synthesised by fatty acid synthases (FASs) or by type I PKSs, as in frenolicin **13**³² and hedamycin **14**³³ biosynthesis, respectively. A third loading mechanism uses an AT domain to directly load starter units from CoA, as has been established for tetracycline biosynthesis.^{12, 34}

As described, malonyl units provide the further extensions of the polyketide chain for all known type II PKSs.¹² The proposed mechanism begins with the loading of

the ACP with a malonyl group. The ACP can either self-malonylate¹⁹ or malonyl-CoA: *holo* acyl carrier protein transacylases (MCATs) can transfer the malonyl group from malonyl-CoA **15** to the ACP. It has been found that MCATs are not essential for polyketide synthesis *in vitro*,¹⁹ however, their importance *in vivo* is unknown. *In vivo* gene knock-outs of MCATs are not possible due to their crucial function in primary metabolism (fatty acid biosynthesis) in the cell.³⁵

1.2.1.1. Ketosynthase-chain length factor – structure-function relationship

The minimal system, alone, is partially able to control the polyketide chain cyclisation by growing the chain within the KS-CLF complex and ‘folding it’ in a specific manner, however, additional cyclisations can occur.^{36, 37} Shunt products are, thus far, the only clues to the mechanisms by which the polyketide chains are synthesised in type II PKSs.

An X-ray crystal structure with the acetate starter unit bound to the KS-CLF of the actinorhodin minimal system has been published.²⁵ They show a 17Å long channel where the 4'-phosphopantetheinyl arm of the ACP would reside once in contact with the KS-CLF, and saw an acetyl group bound to the active site cysteine. The crystal structure of the KS from the R1128 **16** biosynthetic pathway has also been solved with acetyl-CoA **17**, showing a 20Å long channel that places the acetyl group of CoA against the key residues, asparagine, histidine and the active site cysteine that form the catalytic triad (**Figure 3**).³⁸

Chain length is controlled by the KS-CLF complex, and can vary from an octaketide, such as for actinorhodin **2**, to a pentadecaketide, such as for federicamycin. It has been demonstrated, by mutations of the KS-CLF complex of the actinorhodin

minimal system, that the length of the polyketide chain is the controlling factor, and not the number of condensations.²⁵

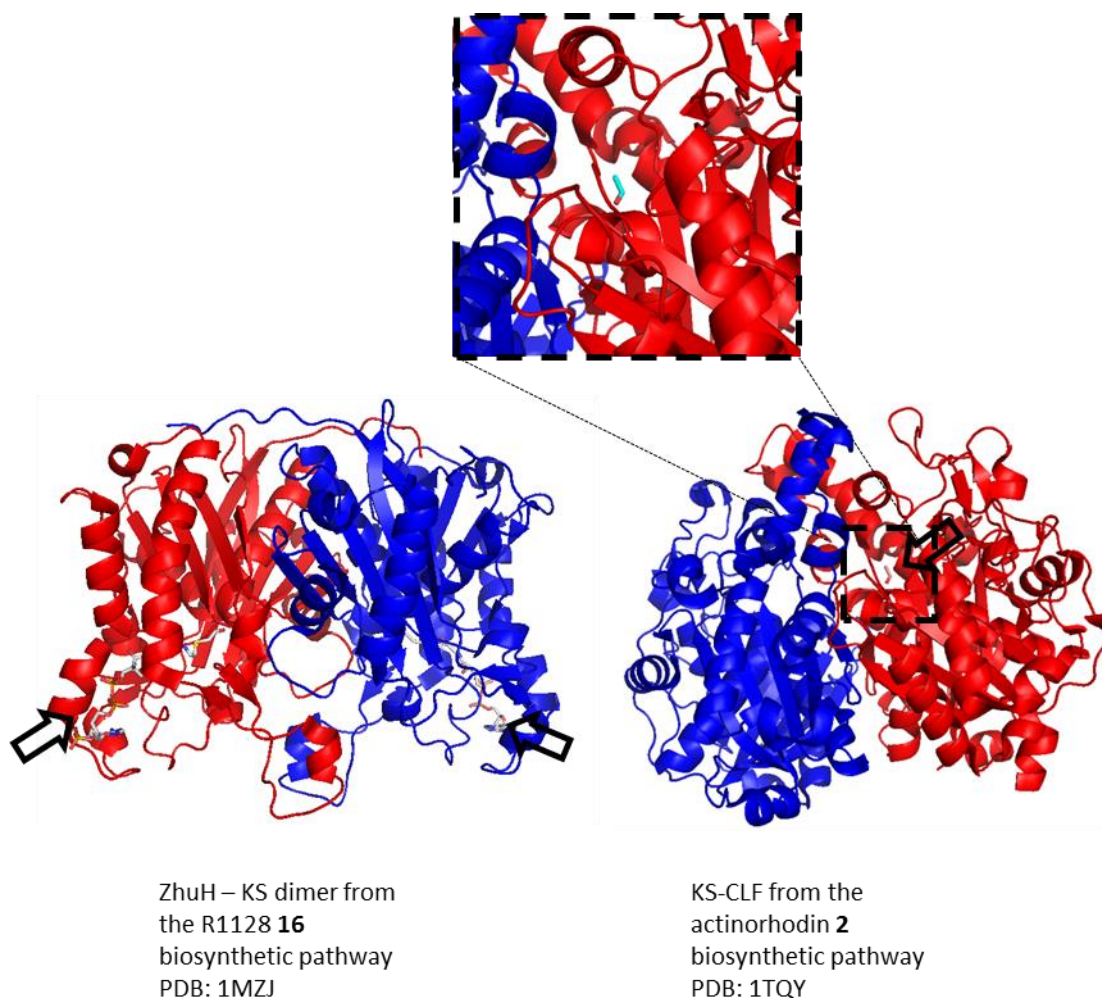


Figure 3 Exemplary type II ketosynthase crystal structures. *Left:* The ketosynthase (KS) dimeric structure from the R1128 **16** biosynthetic pathway, shows the 20Å tunnel where acetyl-Coenzyme A **17** is bound. (PDB: 1MZJ)³⁹ *Right:* The ketosynthase chain length factor (KS-CLF) from the actinorhodin **2** biosynthetic pathway, with acetyl bound to the active site cysteine (Cys169), indicated by an arrow. (PDB: 1TQY)²⁵ *Inset:* magnification of the KS-CLF active site cysteine showing the bound acetyl group and 17Å long channel where the 4'-phosphopantetheinyl cofactor is thought to reside.

Mutations to the channel of the KS-CLF led to the production of longer polyketide chains by mutating key amino acids to smaller ones (see Section 1.3.1). This was

achieved both *in vivo* and *in vitro*, showing promise for further engineering of type II PKSs.⁴⁰ However, the KS-CLF does not appear to be the sole determinant of chain length, on two occasions the presence of the cyclase or aromatase enzymes has been demonstrated to influence the chain length.^{41, 42} This would seem to indicate that a larger PKS complex is formed from the discrete enzymes of type II PKSs, and that the nature of the product is influenced by the interactions taking place amongst the different protein components.

1.2.1.2. Acyl carrier proteins: structure-function relationship

The ACPs of type II PKSs from the actinorhodin **2**⁴³, frenolicin **13**⁴⁴ and oxytetracycline⁴⁵ **19** minimal systems have been extensively characterised by NMR. A three helix bundle fold is common to all acyl carrier proteins, however, ACPs from PKSs are more similar to each other than they are to those from FASs. For example, the PKS ACPs from frenolicin **13** and actinorhodin **2** pathways are 57.5% identical, the FAS ACPs from *E. coli* and *B. subtilis* are 60.5% identical, whereas, the PKS ACP from frenolicin **13** biosynthesis displays only 20.7% of identical residues with each of the FAS ACPs from *E. coli* and *B. subtilis*. A visible difference between the two kinds of ACPs is that Helix I is approximately one turn longer in FAS ACPs than in PKS ACPs (**Figure 4**).⁴⁴

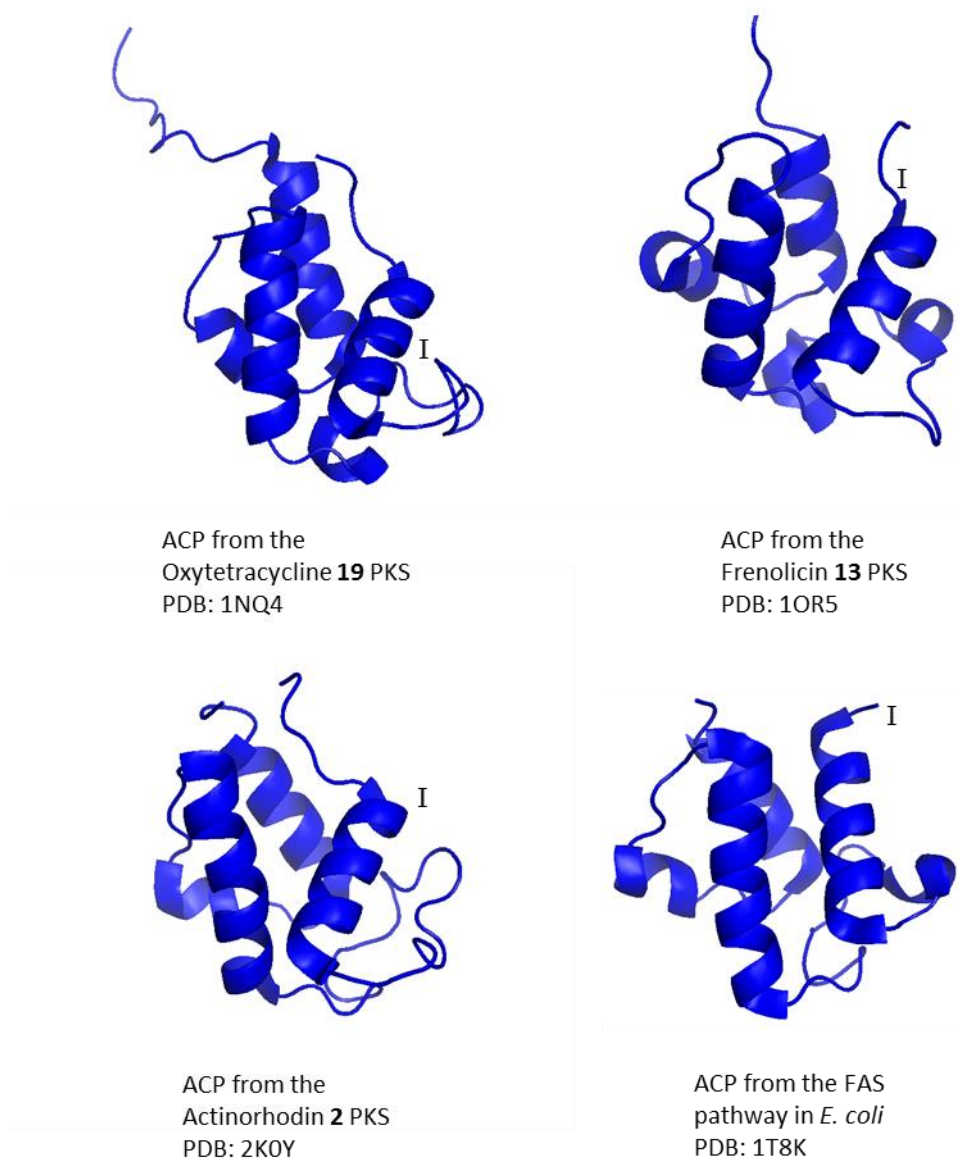


Figure 4 Exemplary structures of acyl carrier proteins (ACPs) from type II polyketide synthases (PKSs). Top left: NMR structure of the ACP from the oxytetracycline **19** PKS. (PDB: 1NQ4)⁴⁵ Top right: NMR structure of the ACP from the Frenolicin **13** PKS. (PDB: 1OR5)⁴⁴ Bottom left: NMR structure of the ACP from the actinorhodin **2** PKS. (PDB: 2K0Y)⁴⁶ Bottom right: Crystal structure of ACP from the fatty acid pathway (FAS) in *E. coli*, containing Zn^{2+} ions and imidazole ions deriving from the crystallisation conditions. (PDB: 1T8K)⁴⁷ Helix I is labelled on each structure. Note the extra turn in Helix I of the FAS ACP.

1.2.1.3. *Ketoreductases*

Ketoreductases in type II PKSs play an important role in controlling when the cyclisation will first occur. KRs stereoselectively reduce a ketone to form a secondary alcohol introduces a 'bend' in the uncyclised chain that will influence that cyclisation. The effect on cyclisation by the KR has been demonstrated in the actinorhodin **2** biosynthetic pathway.³⁶ It is notable to mention that KRs have been shown to be interchangeable within different PKSs and also hybrid PKSs.^{31, 36} Ketoreduction can occur both during and after chain elongation, as in enterocin **10** and actinorhodin **2** biosynthesis, respectively.^{31, 48}

1.2.1.4. *Cyclases and aromatases*

Cyclase domains are necessary to channel polyketide chains into specific arrangements, avoiding incorrect and spontaneous cyclisations to occur. Type II PKS cyclases appear to be highly specific to the PKS system they belong to, and it has not been possible to create hybrid systems by interchanging cyclases.⁴⁹ Utilising recombinant expression of just the minimal *whiE* PKS system in *S. coelicolor*, the Moore group built a library of intermediates that differed in chain length and cyclisation pattern, indicating the importance of cyclase domains within type II PKSs.⁴¹

An aromatase dehydrates alcohols on cyclic structures to create aromatic rings, and they often have bifunctionality towards the goal of aromatisation, such as additional oxidase or ketoreductase activity.^{12, 50, 51}

1.2.1.5. Methyltransferases

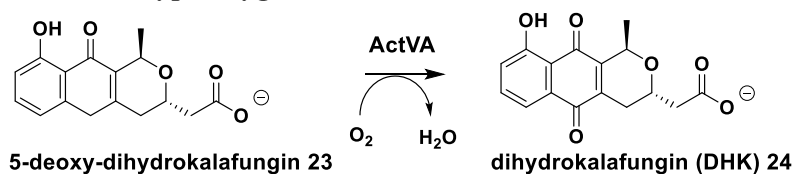
Methyltransferases (MTs) perform important tailoring reactions. They transfer methyl groups *via* the cofactor, *S*-adenosyl-L-methionine (SAM), to nitrogen, carbon or oxygen. Hydroxyl moieties are the most common sites for methylation in polyketides, known specifically as *O*-methyltransferases.¹² In *Streptomyces* there are over 20 genes predicted to function as MTs, including DnrK, a carminomycin 4-*O*-methyltransferase, which methylates the 4-hydroxyl group of daunorubicin **21** in *S. peuceetius*.⁵²

The degree of sequence similarity between MTs of type II PKSs is low, although, a SAM binding site is common to all of the known MTs, and a central β -sheet with surrounding α -helices, known as a chain-fold, is common to most.^{12, 53}

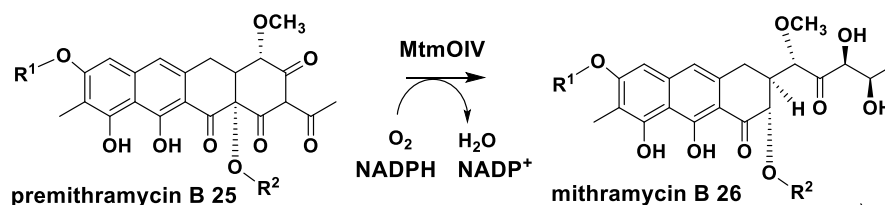
1.2.1.6. Oxygenases

A very important class of tailoring enzymes for type II PKSs are oxygenase enzymes. There are four main types found in type II PKSs: anthrone-type oxygenases, flavin-dependent monooxygenases, Flavin-dependent dioxygenases, and cytochrome-P450 monooxygenases.¹² Anthrone-type oxygenases do not require a co-factor⁵⁴, an example of this type of oxygenase is found in the actinorhodin **2** pathway, ActVA-ORF6 (**Scheme 3**).⁵⁵ It was found that ActVA could be utilised in the tetracenomycin **22** pathway in the place of TcmH, demonstrating a broad substrate specificity of ActVA.⁵⁶

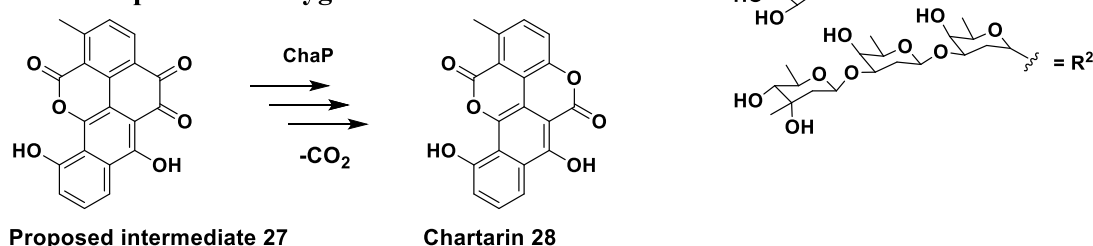
Anthrone-type oxygenase:



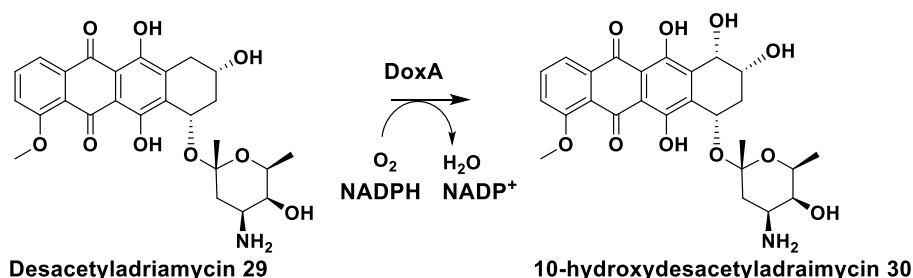
Flavin-dependent monooxygenase:



Flavin-dependent dioxygenase:



Cytochrome-P450 monooxygenase:



Scheme 3 Examples of common oxygenases found in type II polyketides synthases. Anthrone-type oxygenase⁵⁶ in actinorhodin 2 biosynthesis, flavin-dependent monooxygenase⁵⁷ in mithramycin B 26 biosynthesis, flavin-dependent dioxygenase⁵⁸ in chartreusin biosynthesis and cytochrome-P450 monooxygenase^{59, 60} in doxorubicin 9 biosynthesis.

Flavin-dependent oxygenases require flavin adenine dinucleoside (FAD) as a cofactor. The enzymes have two binding sites which are highly conserved among these types of oxygenases, one for the flavin and the other for the adenosine parts of FAD.^{12, 58} Baeyer-Villiger rearrangements, the formation of an ester or lactone from

a ketone or cyclic ketone, respectively, are the most common type of oxygenase reactions in type II PKSs performed by FAD-dependent oxygenases.⁶¹⁻⁶³ As mentioned, there are both mono- and di-oxygenases. Monooxygenases use FAD and NADPH as cofactors to insert molecular oxygen. The oxygenation step in the biosynthesis of mithramycin **26**, by a monooxygenase, is crucial to its biological activity (**Scheme 3**).⁵⁷

The synthesis of chartarin **28**, an intermediate in the biosynthesis of an antitumour agent, chartreusin, is achieved with a flavin-dependent dioxygenase, ChaP by the attack of dioxygen on a dione group within the substrate.⁵⁸ The biosynthesis of the antitumour antibiotics daunorubicin **21** and doxorubicin **9** requires a cytochrome-P450 monooxygenase. These monooxygenases use molecular oxygen and NADPH to oxygenate the substrates (**Scheme 3**).^{59, 60}

1.2.1.7. Glycosyltransferases

Lastly, sugar modifications can be essential to the bioactivity of a polyketide. Jadomycin A, is lacking the sugar, L-digitoxose, moiety that Jadomycin B **11** possesses, does not display anti-yeast activity.⁶⁴ Highly specific glycosyltransferases (GTs) catalyse the addition of sugar moieties to polyketide aglycones. GTs are known as challenging enzymes to purify in active recombinant forms. Only recently a GT from a type II PKS was successfully characterised by X-ray crystallography.⁶⁵ Claesson *et al.* revealed that the GT from the biosynthetic pathway of nogalamycin is a dimer in solution, and that it has a characteristic fold of the GT-B family of GTs. They also established that the GT has two active site histidines that are essential to function.⁶⁵ The GTs involved in the biosynthesis of aclacinomycin, from a type II

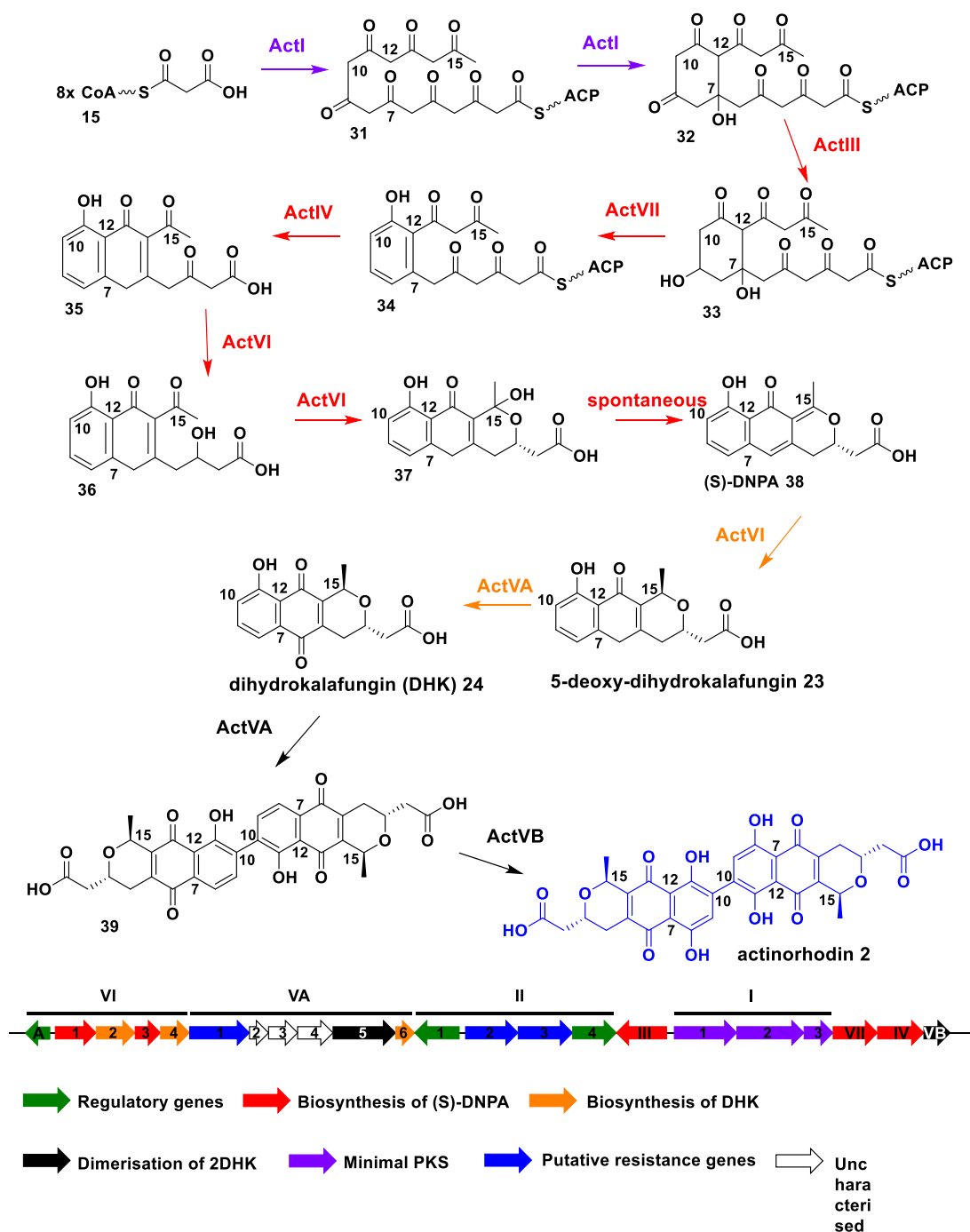
PKS, have been assayed *in vitro* and found to accept a variety of substrates, leading to novel analogues being generated.

1.2.1.8. The future of type II PKS engineering

By utilising type II PKSs as biocatalysts, a variety of chemical structures displaying different bioactivities can be generated. Already, libraries of polyketide analogues have been generated by a combination of mutagenesis and hybrid PKS engineering. For example, by mutagenesis of the KS-CLF of the actinorhodin **2** PKS, longer starter units were able to load onto the KS, generating larger cyclised derivatives.⁶⁶ However, there is still much room for improvement as, thus far, bioengineering has been carried out with a great deal of trial and error.¹²

1.3. Biosynthesis of actinorhodin

Actinorhodin **2** is a benzoisochromanequinone antibiotic produced by a type II PKS in *S. coelicolor* (**Figure 5**). This compound is highly conjugated and can be used as a pH indicator due to its intense blue colour in alkaline conditions and red colour in acidic conditions. This property gave it its original name of ‘blue pigment’ and its host organism the name ‘*coelicolor*’, meaning ‘sky coloured’. It was first named and isolated from *S. coelicolor* in Germany in 1950, and its structure was determined in 1955.⁶⁷⁻⁶⁹ Its gene cluster was first identified in 1976.⁷



Scheme 4 Biosynthesis of actinorhodin 2 from acetyl 17 and malonyl-coenzyme A 15.⁷⁰ The actinorhodin 2 gene cluster is shown underneath.

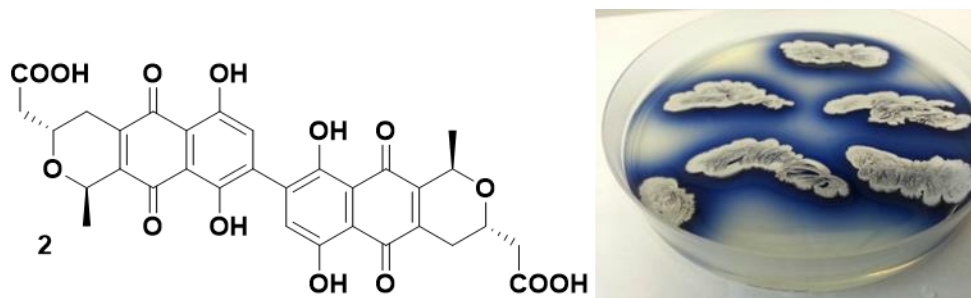


Figure 5 The chemical structure of actinorhodin **2** (left) and *S. coelicolor* M510⁷¹, $\Delta redD$ mutant lacking the pathway-specific activator of Red synthesis, plated on solid medium, showing the intense blue colour caused by production of actinorhodin **2** (right).

1.3.1. Biosynthesis of an octaketide chain by the actinorhodin minimal system

The biosynthetic pathway, eventually leading to actinorhodin **2**, begins with the generation of an octaketide chain **31** by the actinorhodin **2** ‘minimal system’ (the focus of this thesis), via iterative decarboxylative Claisen condensation (section 1.2). The act minimal system comprises three enzymes: the acyl carrier protein (ACP) and two sub-units, ketosynthase (KS) and chain length factor (CLF). KS and CLF express as a homodimer, with close sequence homology (**Figure 6**). The CLF lacks the active site cysteine that gets primed with an acetyl unit, however, the CLF has a glutamine residue in its place that is highly conserved among CLFs of type II PKSs (**Figure 6**). Bisang *et al.* have demonstrated that the glutamine plays an important role in conferring CLF its decarboxylase activity. When the glutamine was mutated to an alanine, the enzyme lost its decarboxylase activity, and, conversely, when the active site cysteine of the KS was mutated to a glutamine, decarboxylase activity was observed.²⁷ The priming unit of the actinorhodin minimal system is acetyl, which is provided by malonyl-ACP **7**. Malonyl-ACP **7** is decarboxylated by the CLF and the resulting acetyl-ACP **40** is used to prime the KS with an acetyl group. In the

acids, which could be utilised *in vivo* to catalyse malonylation of *act holo*-ACP **43**. Unfortunately, due to the necessity of this MCAT for primary metabolism within the cell, this question cannot be answered by enzyme mutagenesis.

The actinorhodin minimal system produces an octaketide chain from the initial priming of the KS with an acetyl group, and then seven subsequent rounds of Claisen condensation. Originally, *in vivo* experiments suggested that the CLF controlled the length of the polyketide chain, at which point that protein was coined ‘chain length factor’.^{72, 73} Burson and Khosla constructed chimeric PKSs *in vivo* in 2000, and their results suggested, by comparison with a KS from *E. coli*, that chain length was controlled by a proposed binding pocket at the KS-CLF interface.⁷⁴ The importance of the residues at the interface of KS and CLF was demonstrated in 2003.⁴⁰ Tang *et al.* used a homology model of the KS-CLF dimer (PDB: 1QXG) to choose certain residues to mutate to attempt to alter the chain length that the mutant minimal system could produce. Comparisons with CLFs from other minimal systems that produced longer chains revealed the importance of residues Phe109 and Phe116 for chain length control. Mutations of Phe109 and Phe116 to smaller amino acids, alanines, converted the minimal system to one which could make a decaketide shunt product.⁴⁰ They also noticed two other amino acids, Thr112 and Phe133, of the *act* CLF of interest. These residues are much smaller in CLFs of minimal systems that produce longer polyketide chains, however mutations of these residues in the *act* CLF did not yield longer chains for this system. Keatinge-Clay *et al.* coined this chain length control a ‘gating mechanism’, and hypothesise that if the ‘gate’ was left ‘open’ it may not be possible to control the length of larger polyketide chains and instead engineer new polymers.²⁵ This hypothesis has not yet been explored.

A simpler experiment demonstrated in a different way how the CLF controls chain length and not the number of Claisen condensations. By utilising a CLF mutant, the conserved glutamine mutated to an alanine, the decarboxylase activity of the KS-CLF complex can be slowed, and allow hexanoyl ACP, β -keto-hexanoyl ACP, butyryl ACP, and β -keto-octanoyl ACP to load the respective starter units onto the KS. Subsequently, the primed system can be incubated with malonyl-CoA **15** and *holo*-ACP **43**, and allowed to produce polyketides. New compounds are produced dependent upon the starter unit provided, however all of these compounds contain no more than 16 carbons, signifying that the KS-CLF controls the chain length and not the number of condensations.⁶⁶

Beltran-Alvarez *et al.* reported that the rate limiting step in the production of the octaketide chain is the reaction between malonyl CoA **15** and *holo*-ACP **43** to produce malonyl-ACP **7**, called the loading step. However, the rate increases from $k_{\text{cat}} = 0.49 \text{ min}^{-1}$ to $k_{\text{cat}} = 2.3 \text{ min}^{-1}$ in the presence of the KS-CLF complex (k_{cat} is the number of molecules an enzyme converts to product per minute). When malonyl-ACP **7** is prepared separately and then incubated with KS-CLF the rate limiting step becomes the decarboxylation of malonyl-ACP **7**, known as chain initiation. The minimal system was supplied with an excess of acetyl-ACP **40** to remove the chain initiation step as a factor in order to decipher which was the rate limiting step in that reaction; it was concluded that, as no ACP-bound intermediates were detected, chain extension must be rate limiting, as the lack of detected intermediates indicates a fast release mechanism.¹³

Later, similar experiments were carried out with point mutated ACPs. The mutations were made at residues on helix II that have been suggested to have important interactions with KS-CLF, based upon NMR results from the type II FAS from *E.*

coli.⁷⁵ In the presence of KS-CLF, the self-malonylation rate increases, mutation of Glu47 caused less of an increase in rate of self-malonylation, and mutation of Glu53 reduced the rate to slower than in the absence of KS-CLF. These results confirmed the involvement of helix II in self-malonylation, however, when Arg72, a residue far from helix II, was mutated, the rate decreased upon addition of KS-CLF, suggesting that more than just helix II is important to the interaction with KS-CLF (**Figure 7**). The rates of decarboxylation were decreased with all mutants barr the Arg72 mutant and similar results were seen for chain extension assays.⁷⁶

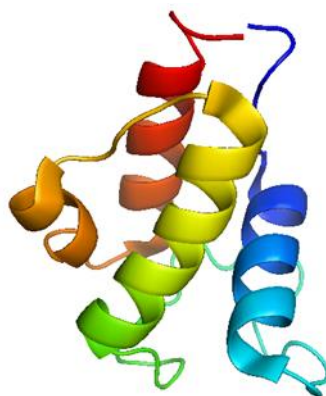
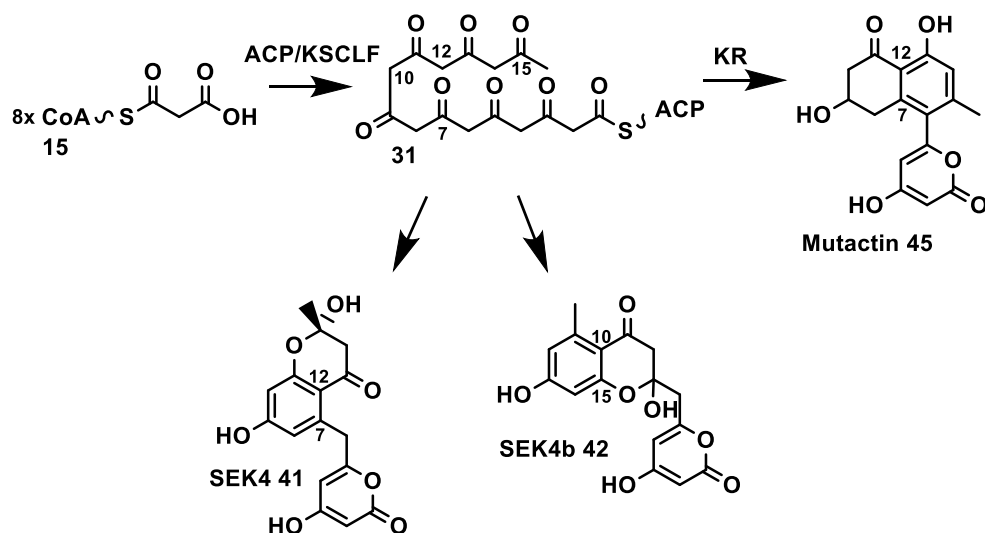


Figure 7 Solution NMR structure of the apo acyl carrier protein **44** from the actinorhodin minimal system, clearly indicating the four helices. Helix I is shown in blue. Helix II is shown in green. Helix III is shown in yellow. Helix IV is shown in red. PDB: 2K0Y.⁴⁶

1.3.2. Tailoring steps towards the biosynthesis of actinorhodin 2

Post-minimal system, a great deal of enzymatic tailoring occurs to produce the final product, actinorhodin **2**, as presented in **Scheme 4**. The *act* minimal system generates shunt products throughout the biosynthetic pathway (**Scheme 5**).



Scheme 5 Biosynthesis of shunt products, SEK4/4b **41** and **42** and mutactin **45**, from the actinorhodin **2** biosynthetic pathway.

The first cyclisation in the biosynthesis of actinorhodin **2**, between C7-C12, is known to be produced by the minimal system, as the shunt product of the minimal system, SEK4 **41**, contains this correct cyclisation (**Scheme 4** and **Scheme 5**). However, SEK4b **42**, the other major product of the minimal system, contains a C10-C15 cyclisation. When the KR, ActIII, is present, however, the shunt product becomes primarily mutactin **45**, with the correct C7-C12 cyclisation. The KR controls the C-9 ketoreduction, **32** to **33**, which would, indeed, introduce the correct ‘bend’, suggesting that the KR controls this first cyclisation (**Scheme 5**).⁷⁷⁻⁸⁰

Following ketoreduction, there is an aromatisation producing **34**, followed by activity of a cyclase, ActIV, which forms the second ring by intramolecular aldol condensation to make **35**.⁸¹

A dehydrogenase, ActVI, performs an enantioselective reduction at C-3 **36**, followed by a cyclisation to form a 6 membered lactone **37**.⁸²⁻⁸⁴ The order of steps was investigated with *N*-acetylcysteamine β -keto thioester (SNAC) derivatives of **36**

which did not possess carbons after C-12 in order to prevent the cyclisation. In each case, the *S* enantiomer was the product of the dehydration.⁸⁴ Spontaneous loss of water from **37** will produce (S)-DNPA **38**, however, it is possible that the reaction is controlled enzymatically, but this has yet to be proven. ActVI-ORF2 and ActVI-ORF4 have high sequence similarity and resemble enoyl reductases. Removal of ORF4, however, did not abolish production of actinorhodin **2**, but deletion of ORF4 did, therefore, ORF4 is thought to assist ORF2 in the reduction of the C-14 to C-15 bond to synthesise 5-deoxy-dihydrokalafungin (5-deoxy-DHK) **23**.^{82, 85}

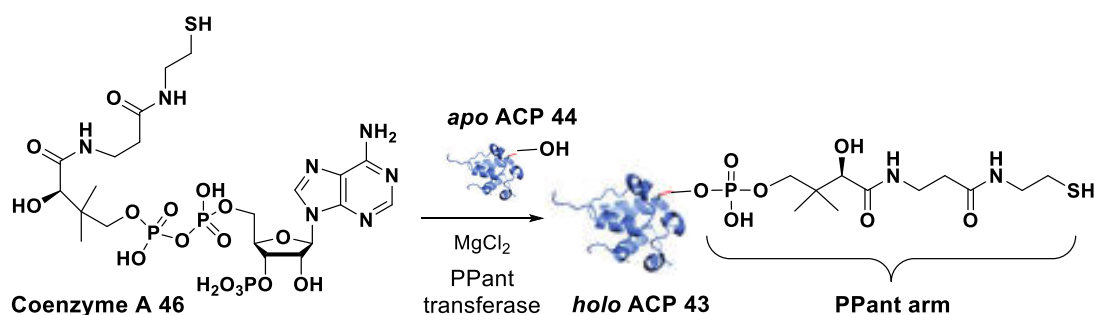
The oxidation of the phenol of **23** to the quinone in DHK **24** is carried out by an anthrone-type monooxygenase, ActVA. This monooxygenase does not require any cofactors or metal ions, and utilises molecular oxygen for the reaction.^{55, 86, 87}

It is not known in which order the last two steps, a dimerisation and an oxygenation, occur.^{88, 89} The oxygenation is carried out by a two-component NADH:flavin-dependent monooxygenase system. ActVB reduces oxidised flavin, which is then bound to ActVA-ORF5 to oxidise substrate **39**.^{88, 90, 91} Interestingly, when ActVA-ORF5 was deleted, a new dimerised, unoxidised, compound was produced, indicating that this protein may be necessary for controlling dimerisation.⁹² However, it is likely that ActVA-ORF4 is the true dimerase as when actVA-ORF4 was deleted, a previously uncharacterised gene, an oxidised DHK compound was produced, undimerised.⁹³ The function of this protein is yet to be confirmed *in vitro*.

The actinorhodin **2** PKS is the most extensively studied type II PKS, and is often referred to as a 'model system'. However, there are still questions regarding several the biosynthetic steps, in particular the chain extension by the minimal system, which is the reason why this system was the chosen subject for this thesis.

1.4. The role of carrier proteins in type II polyketide biosynthesis

All type I and II polyketide synthases (PKSs) contain an acyl carrier protein (ACP). This small, acidic, protein bears a 4'-phosphopantetheinyl (PPant) arm that shuttles polyketide intermediates, bound to the thiol moiety as esters, between the different catalytic sites. The ACP is expressed in its *apo* **44** form, and then, by means of a PPant transferase and coenzyme A **46**, the ACP is converted to its *holo* form **43** (Scheme 6).



Scheme 6 Conversion of apo-ACP **44** to holo-ACP **43** with Coenzyme A **46** and a phosphopantetheinyl transferase. The PPant arm is indicated on the structure of holo-ACP **43**.

The structure of the actinorhodin ACP has been solved by solution NMR.^{43, 46, 94} The ACP has four helices and a large loop between helix I and II. Helix III is much smaller than the other two, and the ACP has a strong hydrophobic core except for two arginine residues, Arg72 and Arg79, which are conserved among PKS ACPs.⁴³

Evan *et al.* compared the structures of *apo* **44** and *holo* **43** ACPs. *Holo*-ACP **43** bears the PPant arm bound to an active site serine, residue 42, which is found on the loop just before helix II begins. The structures revealed that, with the PPant arm

bound, helix III moves closer to helix II. Additionally, Leu43, next to Ser42 on helix II, originally solvent exposed, forms interactions with the PPant arm (**Figure 8**).

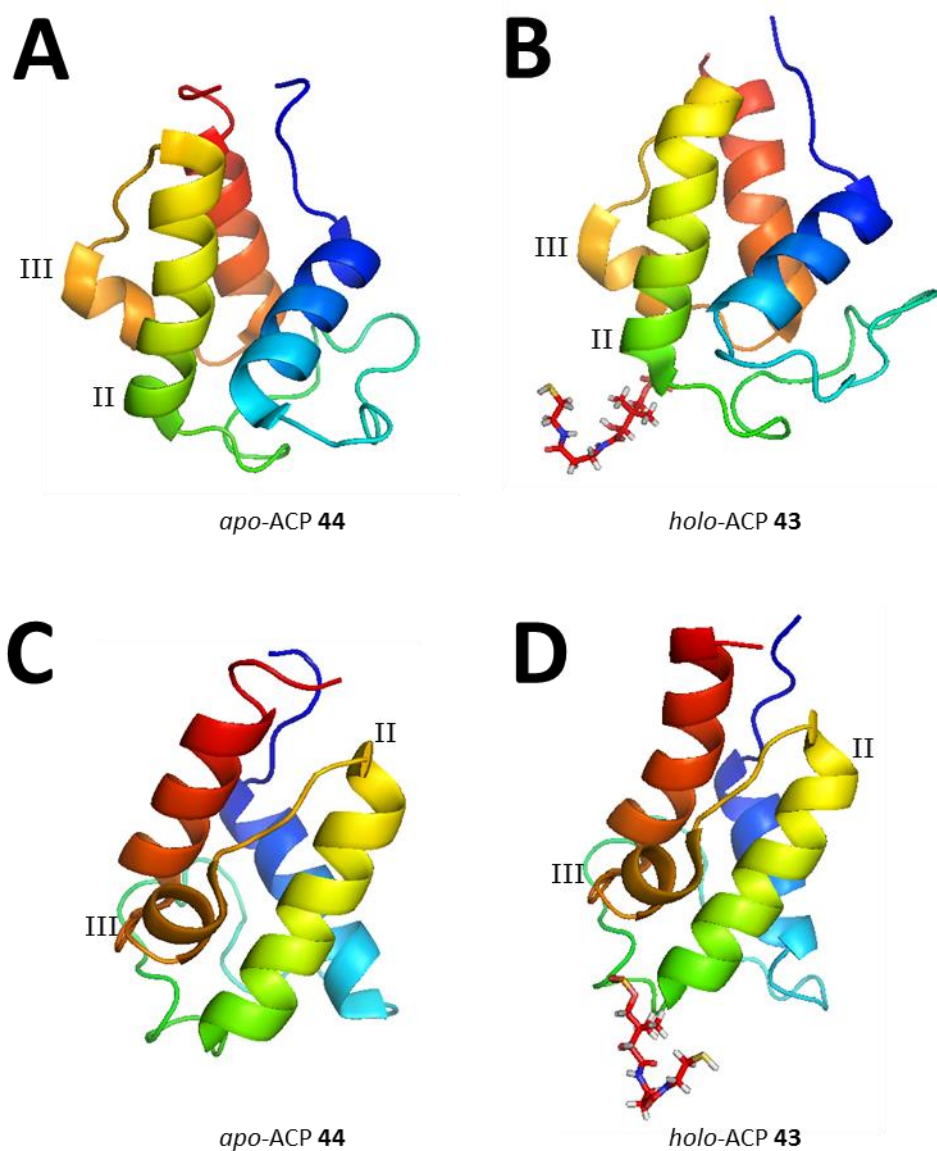


Figure 8 Solution NMR structures of apo-ACP 44 (PDB: 2K0Y) (A and C) and holo-ACP 43 (PDB: 2K0X) (B and D). Presented at two different angles (A and B, C and D) showing the movement of helix III towards helix II upon binding of the phosphopantetheinyl arm. Blue ribbon is helix I, green ribbon is helix II, yellow ribbon is helix III and orange ribbon is helix IV.⁴⁶

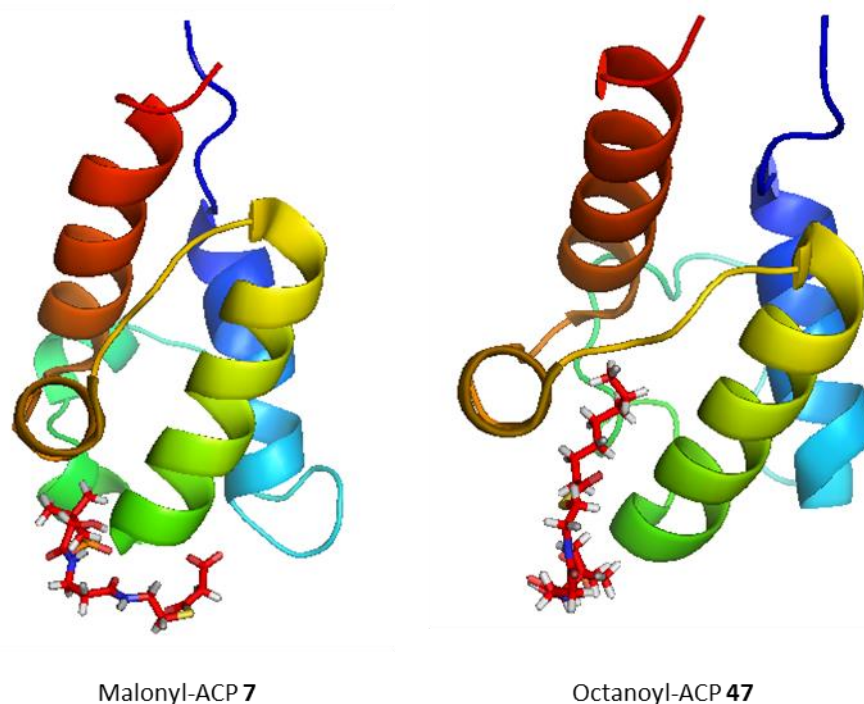


Figure 9 Solution NMR structures of malonyl-ACP **7** (PDB: 2KG8) and octanoyl ACP **47** (PDB: 2KGC) showing the growing cavity between helices II and III with the size of the polyketide chain.⁹⁴

It is thought that the movement of helix III plays a role in the dissociation of the PPant transferase after binding of the PPant arm to the ACP. Mutation of Leu43 to an alanine residue affected the binding to the PPant transferase, ACPS, from FAS in *S. coelicolor*.⁴⁶ The Leu43 residue is part of a motif that is highly conserved among type II PKS ACPs, as well as FAS ACPs and NRPS PCPs, which plays an important role in protein recognition.^{26, 95, 96}

Structural NMR studies of the actinorhodin ACP with bound intermediate and intermediate mimics have been performed. Acetyl **40** and malonyl **7** were the only natural modifications of the ACP used that could be easily reproduced *in vitro*, whereas advanced intermediate mimics were used to investigate the changes to the ACP due to the inability to synthesise advanced intermediates, as well as their

inherent instability. Butyryl and 2-oxo-butyl groups were used as mimics for a diketide, hexanoyl and 2,5-dioxohexyl for a triketide and octanoyl **47** for a tetraketide intermediate mimic. No interaction was found between the acetyl **40**, malonyl **7** and 2-oxo-butyl groups and the ACP. Butyryl, hexanoyl, octanoyl **47** and 3'5-dioxyhexyl groups all caused conformational changes to helices II and III, helix III moving away from helix II, and the cavity volume increasing with the size of the bound mimic (**Figure 9**). The movements of helix II and III may aid dissociation from the KS-CLF once the full polyketide chain has been synthesised. Alternatively, as the octaketide chain is a very unstable molecule, the helices may help to stabilise the polyketide. Compared to similar experiments with FAS ACPs, the actinorhodin ACP showed more structural changes and there is a proposed binding cavity that is larger than in FAS ACPs which may accommodate the bulkier polyketide intermediates.⁹⁴

The structures solved thus far could potentially be non-natural conformations of the ACP. Only mimics of polyketide intermediates were used, and, those intermediates are just putative. Furthermore, the structure of the ACP could be entirely different when it is in complex with the KS-CLF. Advances in NMR, X-ray crystallography and cryo-EM may help to solve these questions in the future.

1.4.1. Engineering of carrier proteins

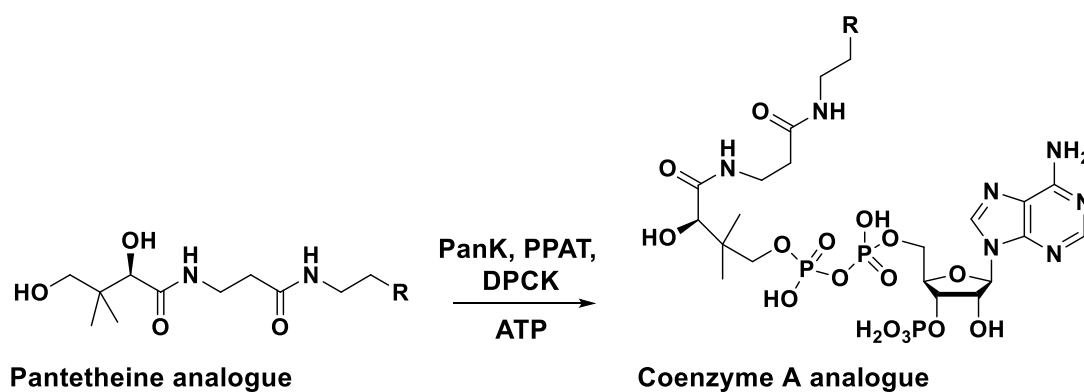
Carrier proteins have been manipulated *in vitro* since, at least, 1964⁹⁷ and, since then, a great deal of manipulation and engineering has been undertaken to probe primary and secondary metabolism.

One key mutation to the actinorhodin acyl carrier protein (ACP) is a cysteine to serine mutation for *in vitro* assays. This mutation is introduced to avoid disulphide bonds forming between the cysteine and the thiol group of the phosphopantetheinyl (PPant) arm, but does not affect the activity of the enzyme.⁹⁸

The ACP can interact with many different partners, and as such it constitutes an attractive target for bioengineering. For example, by making mutations to key residues of ACPs, interactions with different PKS enzymes could be prevented or allowed, leading to the generation of new compounds, or *via* modifications to the PPant arm to act as a tag. The latter has already been proven to be an easier method of bioengineering acyl carrier proteins.

1.4.1.1. Modifications to the phosphopantetheinyl arm of carrier proteins

As previously described, *apo*-ACP **44** can be converted to *holo*-ACP **43** by the action of a PPant transferase which loads the PPant arm from coenzyme A **46** (**Scheme 6**). PPant transferases will accept a wide variety of analogues of coenzyme A **46** and load them onto ACPs. In particular, a transferase from *B. subtilis* of broad substrate specificity, Sfp, is used frequently for generation of ACP analogues.^{99, 100}



Scheme 7 Enzymatic preparation of Coenzyme A analogues via corresponding pantetheine analogues with the aid of enzymes that biosynthesise Coenzyme A **46** in *E. coli*.¹⁰¹

Analogues of Coenzyme A **46** with thioester linkages are relatively simple to synthesise. The two main methods commonly employed are *via* transthioesterification, e.g. by thiolysis of a symmetrical anhydride¹⁰², or by reaction of CoA **46** with a maleimide-reactive precursor. Synthesis of analogues without thioester groups is more challenging. Coenzyme A **46** is biosynthesised from pantetheine **48** with enzymes that are part of primary metabolism, analogues of coenzyme A **46** can also be enzymatically synthesised with that machinery *in vitro* from the corresponding pantetheine analogue (**Scheme 7**).^{11, 101}

The shortest peptide that the PPant transferase Sfp is capable of processing is named the ‘ybbR tag’, as its sequence is derived from *ybbr* ORF in *B. subtilis*. The ‘ybbR tag’ is an 11 residue, helical peptide with the sequence DSLEFIASKLA; essentially, the sequence is helix II of carrier proteins (**Figure 7**). The Ser2 is the active site serine that becomes loaded with the PPant arm. This small sequence can be used to tag *N*- or *C*-terminals of proteins, or inserted in the flexible loop of proteins. The uses for this tag are numerous, for example, a biotin label can be incorporated to the

tag for streptavidin-affinity purification, or for fluorescent labelling for imaging purposes.^{100, 103, 104}

Labelling of carrier proteins through modifications to the PPant arm can be particularly useful for probing the structures and mechanisms of PKSs (see Section 1.5).^{46, 94, 105} The variety of ‘tags’ incorporated so far include fluorescent¹⁰⁶⁻¹⁰⁸, natural polyketide or NRPS intermediates^{46, 109}, unnatural polyketide or NRPS intermediates^{94, 110}, cross-linking¹¹¹⁻¹¹⁴ and affinity¹⁰⁶ tags. *In vivo* labelling of carrier proteins is also possible by supplementing the organism with pantetheine analogues and enabling the endogenous CoA biosynthetic machinery, with the aid of a PPant transferase, to produce labelled ACPs.¹¹⁵⁻¹¹⁸ Aside from the investigation of PKSs, other applications for labelling of carrier proteins include cell surface labelling¹¹⁹, and expanding that to fluorescence resonance energy transfer (FRET) studies¹²⁰⁻¹²², the use of ACPs as fusion tags^{123, 124}, antibiotic activity by inhibition of FAS¹²⁵⁻¹²⁷ and as a scaffold for drug delivery¹²⁸.

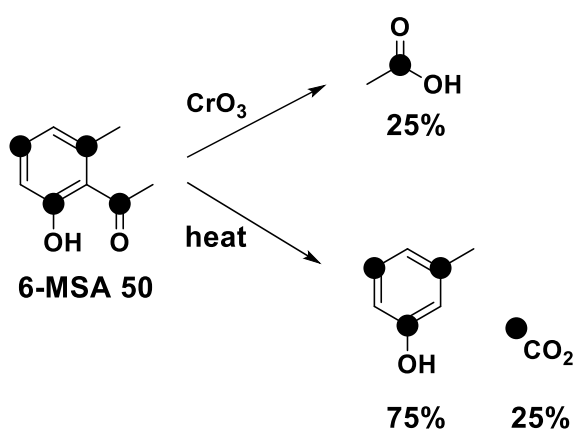
1.5. Methods of investigation of modular and iterative biocatalysis

The investigation of PKSs and their products began over 100 years ago when technology was very limited. Orcinol **49** was the first polyketide structure to be solved, and its biosynthesis to be elucidated. At that time, the techniques used were degradation chemistry, melting point, solubility, and taste to successfully deduce that Orcinol **49** was biosynthesised *via* a polyketone intermediate, and that the synthesis would take place within the cell.^{4, 129} Since then, the techniques utilised for the analysis of natural products and their biosynthesis has vastly improved, making the task today much simpler. As molecular biology has improved, understanding and

manipulation of enzyme catalysis has too, and with the vast improvements in analytical chemistry techniques, such as mass spectrometry, NMR and X-ray crystallography, the detection and analysis of natural products and their biosynthetic machinery has become possible.

1.5.1. Labelling techniques

The biosynthesis of 6-methylsalicylic acid (6-MSA) **50** was one of the first natural products to be studied in any great detail. 6-MSA **50** is an intermediate in the biosynthesis of patulin from *P. patulum*. Its biosynthesis was hypothesised to occur from four acetate units linking to produce a triketo acid. This theory was tested by feeding ^{14}C -labelled acetate to *P. patulum*, and analysing the resulting natural product by degradation chemistry and subsequent radioactivity measurement. The results proved that these types of compounds were, indeed, generated from acetate building blocks (**Scheme 8**).¹³⁰



Scheme 8 Chemical degradation of ^{14}C labelled 6-methylsalicylic acid (6-MSA) **50** demonstrating the incorporation of four acetates.^{4, 130}

After Birch and co-workers published their findings, advances in NMR and commercial availability of ^{13}C labelled compounds meant that feeding experiments and the analysis of the results became simpler and faster. More complex structures and biosynthetic pathways could be probed in this manner, such as the late stage reorganisation of aflatoxin B.¹³¹ Deuterium labelling could also be used as a tool for determining biosynthetic pathways and even specific mechanisms with NMR techniques.^{132, 133} C-H NMR correlations provide even more accurate structural characterisation, and at present, 2D, and even 3D, NMR correlations are available to aid the natural products community.

Acetate labelling was used by Khosla *et al.* to confirm that SEK15b, the product of an engineered strain of *S. coelicolor* from the tetracenomycin **22** pathway, was derived from 10 acetate units.⁷⁹ The structure of SEK4b **42** was also confirmed to contain 8 acetate units by sodium acetate- $^{13}\text{C}_2$ feeding, and the ^{13}C labels also facilitated good quality ^{13}C -NMR assignments for structural characterisation (**Scheme 5**).³⁷

Sodium acetate labelling experiments are still used for distinguishing biosynthetic pathways, however, with the improvements in the field of synthetic chemistry, labelled natural and unnatural precursors can be synthesised and fed *in vivo* or *in vitro* to determine whether the biosynthetic enzymes can uptake these compounds (Also see Section 1.5.3 and Section 1.5.4). Additionally, incubating cultures in $^{18}\text{O}_2$ atmospheres or in H_2^{18}O media can probe the origin of certain oxygen incorporations within natural products, and similarly in D_2O for deuterium labelling.^{134, 135}

1.5.2. Enzyme engineering

Manipulating the enzymatic machinery in PKSs is an effective technique for the investigation of polyketide biosynthesis, thanks to the advances in genetic and enzymatic engineering in recent years. The expression and purification of the enzymes and domains from PKSs has allowed countless *in vitro* experiments to be carried out, from structural biology characterisation of the active sites and interactions with other enzymes or cofactors, to determining the substrate selectivity of the domains and probing the mechanisms. Molecular biological techniques for gene knockouts, mutations or swapping in organisms have supplied knowledge of the importance of those genes and their functionality, and this is opening doors to creating engineered organisms for new and improved synthesis of agriculturally or medicinally relevant compounds.

1.5.2.1. In vivo

The first point of call for tentative assignment of the function of a gene is with bioinformatics analyses. Amongst different tools available from the National Center for Biotechnology Information (NCBI) and other bioinformatics tools providers, the Basic Local Alignment Search Tool, known as BLAST, is the most popular. The tool searches a vast database of known nucleotide and protein sequences to find similarities between the sequence or gene of interest and provide a statistical significance of that match to decipher a function for the gene. When the statistical significance is very high, the likelihood of correct functional assignment is high. Nonetheless, there are examples where the predicted function of a gene or protein is incorrect or not specific enough. This is particularly true for iterative PKSs:

bioinformatics analyses are limited in predicting the nature of the product and the timing of transformation.

1.5.2.1.1. Gene deletions

A common method for deducing the function of a gene is simply to delete that gene and decipher from the natural product produced what that function is, and at what point in the biosynthetic pathway it acts. An example of this method was published by Khosla and co-workers reporting extensive knockouts of the actinorhodin gene cluster in *S. coelicolor* revealing the functions of multiple genes by the shunt products synthesised in each case.³⁷ Unfortunately, you are often relying upon high yield of the product for characterisation. Importantly, deletion of genes that are key to polyketide chain assembly would abolish production entirely.

1.5.2.1.2. Mutagenesis

Genetic mutations can be used to inactivate selected enzymes or to alter the enzyme substrate specificity. For instance, as is demonstrated in a series of *Saccharopolyspora erythraea* (*S. erythraea*) mutants, short intermediates can accumulate along the erythromycin A biosynthetic pathway.¹³⁶ In this way, the full structure of the megasynthase type I PKS is minimally affected.

Gene mutations can also alter the specificity of the enzyme for substrates, allowing new polyketides to be synthesised from minor changes. Mutations to the KS-CLF of the actinorhodin minimal system produced a larger active site for chain elongation,

allowing a decaketide to be produced instead of the natural octaketide, and in doing so created new polyketide structures.⁴⁰

1.5.2.1.3. Hybrid PKSs

Khosla and co-workers combined genes from biosynthetic pathways to create hybrid PKSs, and in doing so they learnt more about the functions of the genes inserted, and their selectivity, alongside engineering new hybrid natural products.^{72, 73, 78, 79}

One of these hybrid PKSs included mutant *S. coelicolor* strains that contained a mixture of KSs, CLFs and ACPs from the actinorhodin **2**, granaticin and tetracenomycin **22** PKSs. Actinorhodin **2** and granaticin are generated from a primary octaketide chain, whereas tetracenomycin **22** is from a decaketide. As expected, the hybrid PKSs provided compounds derived from either an octaketide or a decaketide polyketide chain, indicating the influence of the CLF on the chain length.⁷³

A second heterologous expression system in *S. coelicolor* also combined genes encoding for the three enzymes of the type II minimal system from the actinorhodin **2** and frenolicin **13** PKSs, the latter natural product derives from a nonaketide chain. Again, the compounds that were produced either had 16 or 18 carbon backbones.⁷²

A third example replaced the ACP from the actinorhodin **2** PKS with homologues from granaticin, oxytetracycline **19**, tetracenomycin **22**, and frenolicin **13** biosynthetic pathways. Each hybrid PKS was functional in *S. coelicolor*, but quantitative differences in the shunt products were found.⁷⁸

A final example hybrid PKS focused on combining the *act* KR and/or cyclase with either the actinorhodin **2**, tetracenomycin **22** or frenolicin **13** type II PKS minimal systems. These hybrid PKSs demonstrated that the minimal systems can control, to a degree, the first cyclisation without their respective KRs or cyclases.⁷⁹

1.5.2.1.4. Heterologous expression

Many PKSs are expressed in organisms which are slow growing, or difficult to grow in a laboratory environment. The expression of these PKSs in a faster growing, suitable organism is desirable for biosynthetic investigations, and has been carried out on a number of occasions: for example, the gene clusters encoding for the production of erythromycin A, 6-deoxyerthyronolide B (6dEB) **51** (from the soil bacterium *Saccharopolyspora erythraea*¹³⁷), the quinolone antibiotic echinomycin **52** (from *S. lasaliensis*¹³⁸) and the cytotoxic agents patellamide A and C (from an unculturable obligate symbiont¹³⁹) have all been successfully expressed in *E. coli*.

1.5.2.1.5. Modifications to the phosphopantetheinyl arm of carrier proteins

As mentioned previously, the labelling of acyl carrier proteins *via* their PPant arm.^{105, 112, 116, 117} can be used to investigate polyketide assembly in just its early stages. Also, labelling of ACPs with fluorescent tags have been used to locate and quantify the carrier proteins within cells,¹⁰⁵ and affinity tags, in combination with fluorescent tags, have been exploited for the identification of carrier proteins from organisms that have not yet been sequenced.¹¹⁷ A whole range of pantetheine analogues have been tested to determine their suitability for tagging ACPs,

demonstrating a wide substrate selectivity of both the PPant transferase and the ACP.¹¹⁶

1.5.2.2. *In vitro*

With the advances in the generation of recombinant proteins has come the ability to study the enzyme mechanisms *in vitro*, and to structurally characterise biosynthetic enzymes by NMR, crystallography, and, to some extent, mass spectrometry.

Carrier proteins can be loaded with natural and unnatural starter units to probe the selectivity of other domains or enzymes. An example of such experiment was performed by Oldham and co-workers to probe the selectivity of the initial acylation step of *trans* ATs from the psymberin (Psy) and bacillaene (Bae) PKSs.¹⁴⁰

Kinetic assays can be carried out, for example, to determine the rate limiting steps in reactions, which would not be possible *in vivo*, as was demonstrated in the work by Simpson *et al.* to investigate the interactions between the ACP and KS in the actinorhodin **2** PKS.⁷⁶

X-ray crystallography and NMR can be used to investigate substrate⁹⁴ and co-factor binding, active site characterisation and protein-protein interactions²⁵, to name a few. Recent advances in cryo-EM have allowed the characterisation of a large module of the pikromycin pathway and revealed important structural rearrangements during the biosynthesis.^{141, 142}

There are still several difficulties associated to the expression and purification of components of PKSs. Finding alternative expression hosts, such as yeast and *Pseudomonas* species, is a growing field of research.¹⁴³

1.5.3. Chemical probes: *N*-acetylcysteamine thioester (SNAC) substrate analogues

Chemical methods of probing the mechanism of biosynthetic enzymes are based on the use of synthetic precursors or substrates *in vivo* or *in vitro*. Mimics of PPant arms carrying putative precursors or substrates are widely used, as they have been shown to be uptaken by cells and processed by PKS enzymes (**Figure 10**). These mimics, *N*-acetylcysteamine thioesters (SNACs) were first used in 1968 as an inhibitor of methylmalonyl-CoA mutase, which isomerises methylmalonic acid to succinic acid.¹⁴⁴ The mimics have been used as standard substrates for investigating ACP catalysed reactions since then, due to the relative ease of synthesis compared to preparation of coenzyme A analogues.

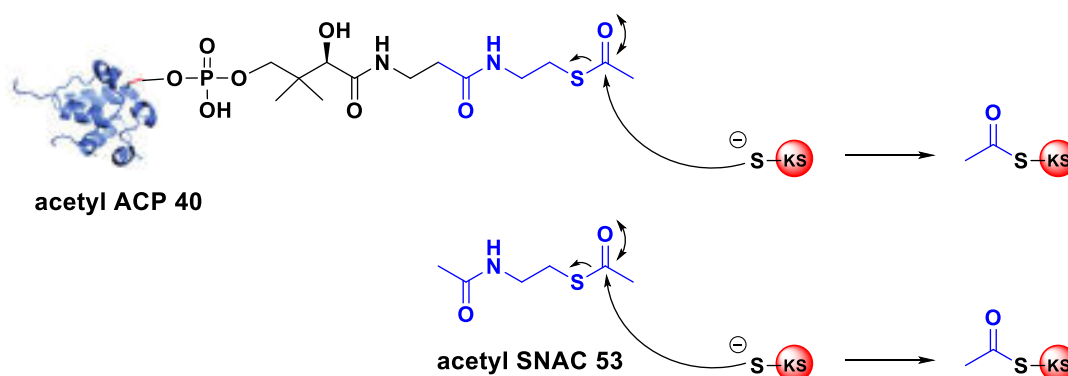


Figure 10 Structures of acetyl-ACP 40 and the *N*-acetylcysteamine (SNAC) ester derivative 53 showing the priming of a ketosynthase with the acetyl groups from both 40 and 53.

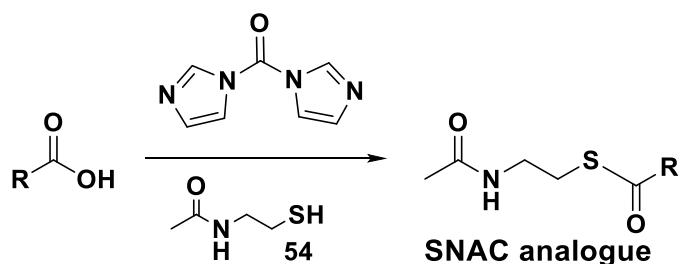
SNAC analogues are often used *in vitro*,^{145, 146} gaining insights into a specific catalytic step, or, due to their hydrophobic nature, it is possible to study their uptake and turn over *in vivo*.¹⁴⁷ SNAC analogues can be used as surrogate starter units, such as hexanoyl SNAC for restoring sterigmatocystin biosynthesis in FAS gene knockouts in *Aspergillus nidulans*¹⁴⁸. They can also provide the extender units, such

as methylmalonyl SNAC incubation with DEBS3, the third module of the 6-deoxyerythronolide B **51** synthase, which was able to act as the extender unit to successfully produce the expected triketide lactone.¹⁴⁵

New natural products can be generated by feeding unnatural substrates bound *via* the thioester linker, and, if they are taken up by the PKS, this unnatural precursor will be incorporated in the final product.^{149, 150}

1.5.3.1. Chemical synthesis of SNAC analogues

The synthesis of SNAC analogues can only require a few steps, dependent upon the complexity of the R group. The reaction of *N*-acetylcysteamine (NAC) **54** with an activated carboxylic acid group, typically by coupling to carbonyldiimidazole, creates the thioester linkage of the (*N*-acetylcysteamine β -ketothioester) SNAC analogues.^{151, 152} The complexity of the synthesis would depend upon the precursor, 'R', being provided by the SNAC analogue (**Scheme 9**).

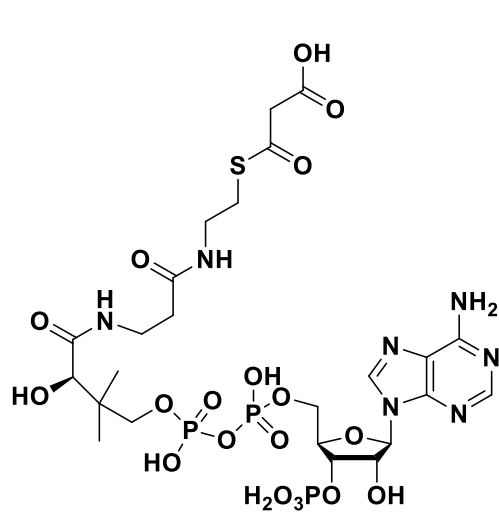


Scheme 9 General synthesis of *N*-acetylcysteamine β -ketothioester (SNAC) analogues via coupling to carbonyldiimidazole (CDI).

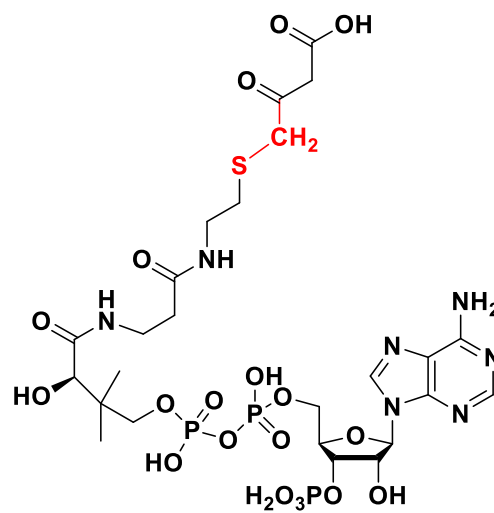
1.5.4. Chain termination probes as new tools for the investigation of polyketide biosynthesis

In 2005, Spiteller and co-workers¹⁵³ reported the preparation of a nonhydrolysable malonyl-CoA mimic **55** bearing an additional methylene group, between the sulphur atom and the malonate group. The compound was shown to be able to capture diketide and triketide intermediates in the biosynthesis of resveratrol **4** by the type III PKS stilbene synthase by mimicking malonyl-CoA **15** in decarboxylative condensation reactions. However steric differences between this compound **55** and malonyl-CoA **15** limited its intermediate capturing ability, leading Tosin and co-workers to prepare carba(dethia) and oxo(dethia) malonyl-CoA derivatives **56** and **57** (**Figure 11**). These analogues presented direct replacements of the sulphur atom with methylene **56** and oxygen **57** moieties respectively (**Figure 11**).^{11, 153}

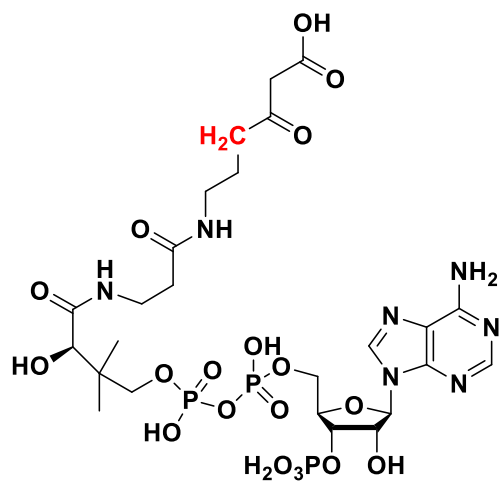
When **56** and **57** were trialled *in vitro* on the type III PKS, stilbene synthase the carba(dethia) analogue **56** proved to be a very efficient probe of the biosynthesis by capturing all the intermediates involved in the assembly, revealing new insights into the mechanism of cyclisation, whereas the oxa(dethia) analogue **57** could undergo just one round of decarboxylation and chain extension. The close steric match to malonyl-CoA **15**, its ability to decarboxylate at faster rates than malonyl-CoA **15** and its robust nonhydrolysable nature have made the malonyl carba(dethia) substrate **56** the perfect starting point for the development of simpler and more sophisticated tools named ‘chain termination’ probes for their ability to sample the biocatalysis by off-loading prematurely truncated intermediates (Section 1.5.4.1, **Scheme 10**).



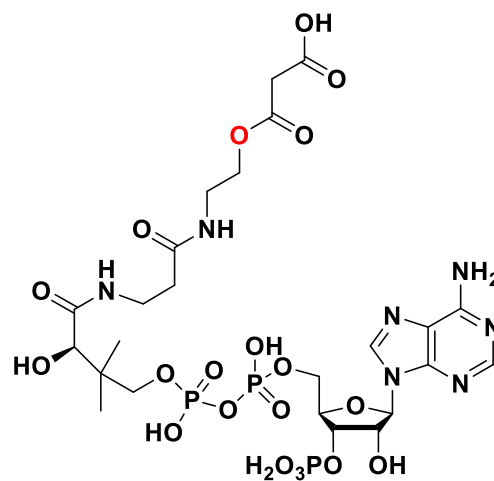
Malonyl CoA 15



Malonyl-CH₂-S-CoA 55

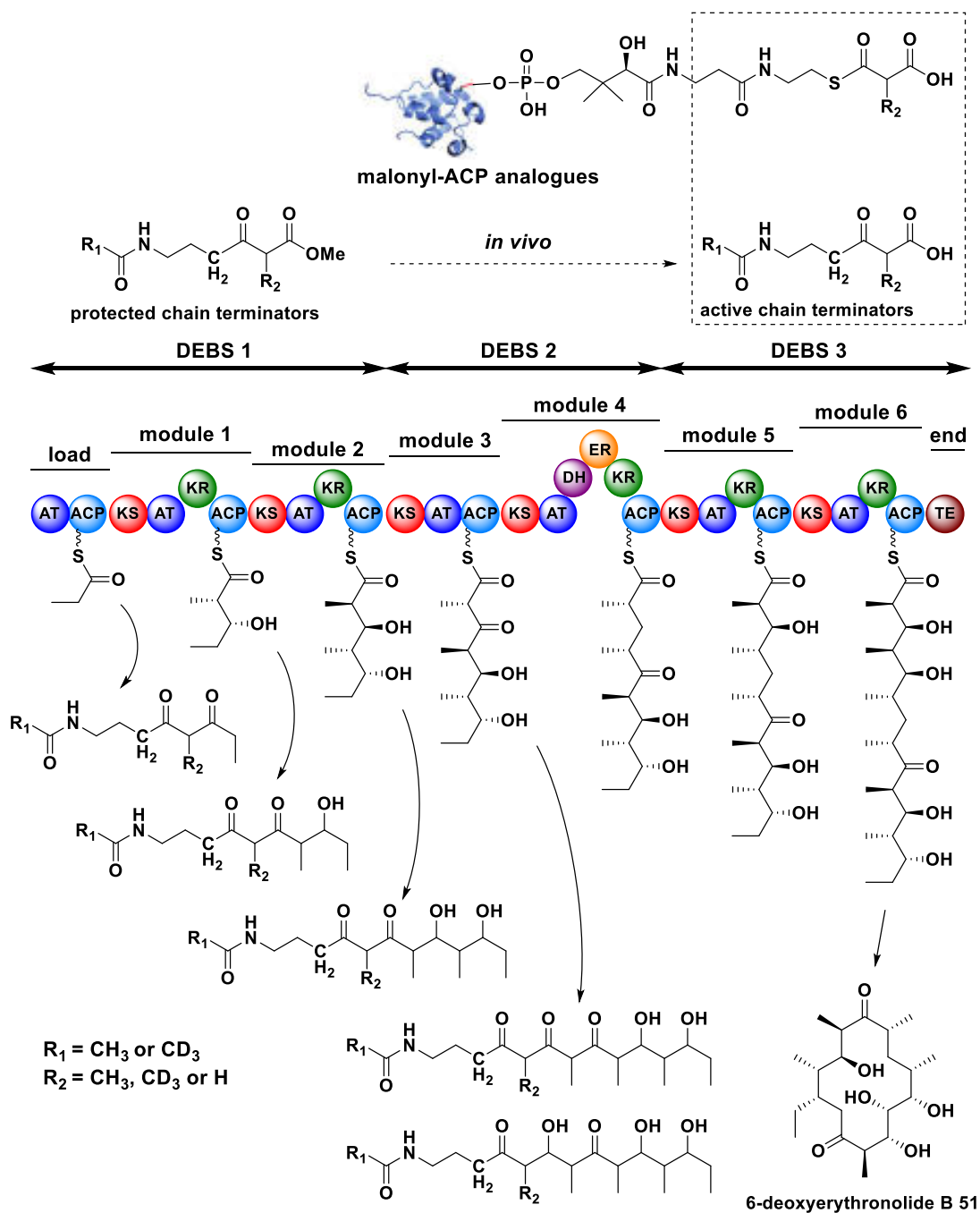


**Malonyl carba(dethia)
CoA 56**



**Malonyl oxa(dethia)
CoA 57**

Figure 11 Malonyl-coenzyme A (CoA) 15 and nonhydrolysable malonyl-CoA analogues 55-57 used for probing the biosynthesis of polyketides from type III PKSs.



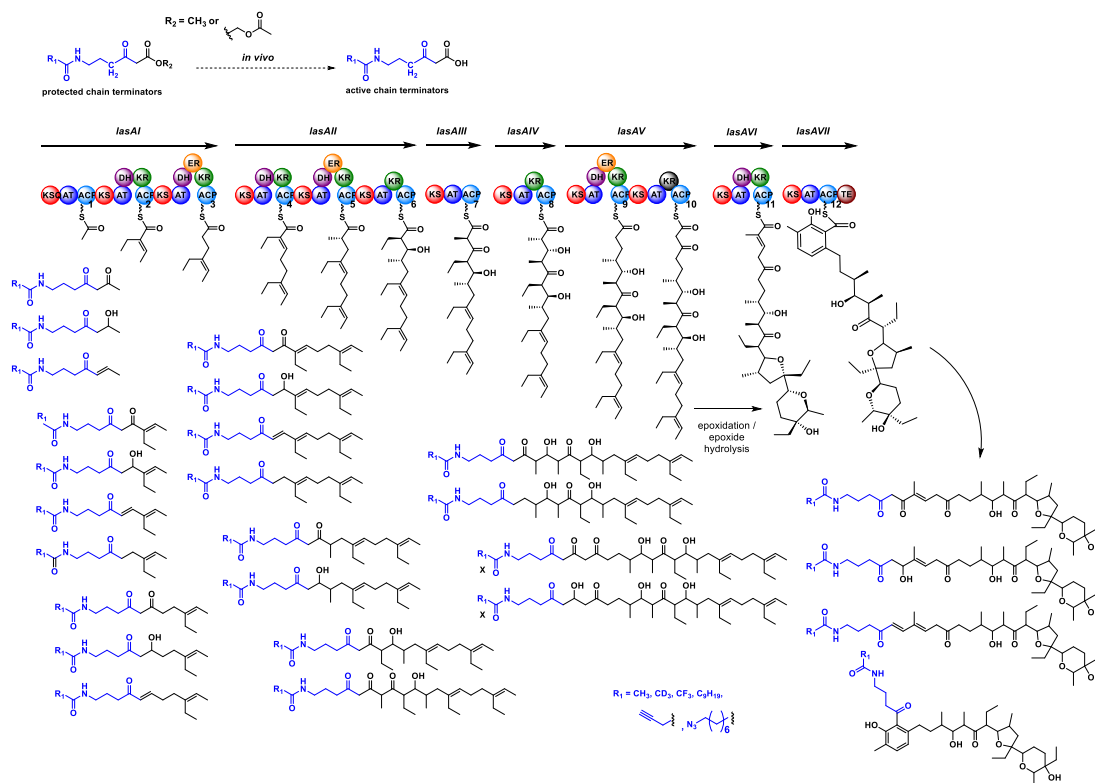
Scheme 10 *In vivo* off-loading of polyketide intermediates from the model system, 6-deoxyerythronolide B 51 synthase, with synthetic chain terminators. Top right box highlights how the synthetic chain terminators mimic the acyl carrier protein phosphopantetheinyl moiety, and the ester hydrolysis *in vivo* to the active chain terminators.^{136, 154}

1.5.4.1. *Nonhydrolysable NAC chain termination probes*

Since the early results obtained using malonyl-CoA analogues **55-57**, the Tosin group has been developing small molecule chemical chain termination probes based on nonhydrolysable NAC analogues. These still efficiently mimic malonyl-ACP **7** and are capable of diffusing into PKS active sites to off-load biosynthetic intermediates from KSs by competitive β -ketoacid decarboxylation and condensation. The obtained captured intermediates cannot undergo transesterification back to the PKS and become available for LC-MS analyses (**Scheme 10**).^{22, 136, 154-156}

The Tosin group has also shown that these probes can be used *in vivo*: once fed to microorganisms as esters, *in situ* esterase hydrolysis generates the active β -ketoacid probe within cells for the direct capture of PKS biosynthetic intermediates (**Scheme 10**).^{11, 22, 136, 153, 154, 156}

The use of small molecule chain termination probes has provided insights into the timing of ring formation in the biosynthesis of the polyether antibiotic lasalocid A **1** in the host producer (*S. lasaliensis*, **Scheme 11**).²²



Scheme 11 Off-loading of intermediates from the lasalocid A **1** synthase, with synthetic chain terminators from feeding experiments in *S. lasaliensis*.^{22, 155, 156} Not shown are the results from feeding with chain terminators with modifications to the malonyl group at α -carbonyl positions.

More recently, the use of functionalised small molecule probes bearing alkyne or azide groups as chemical handles for site-specific modifications¹⁵⁵, and pharmaceutically relevant fluorine atoms, together with engineered *S. lasaliensis* bacteria has allowed the generation of a library of complex polyether analogues for activity testing (**Scheme 11, Figure 12**).

Alternative probe protecting groups with improved bioavailability are being developed within the Tosin group, including a photolabile protecting group reported in this thesis and an acetoxymethyl (AM) ester group.

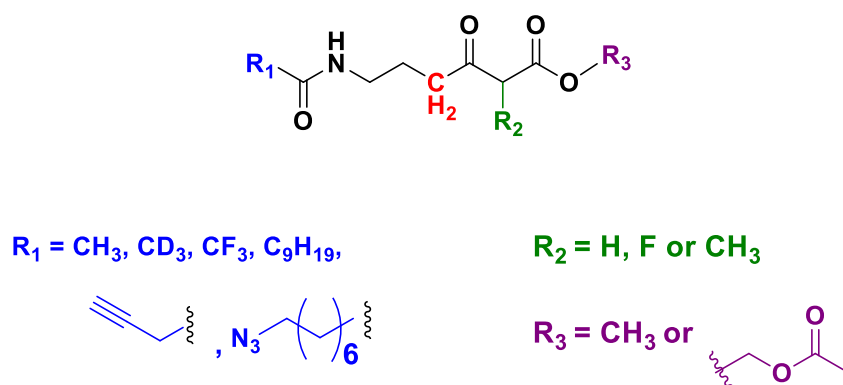


Figure 12 Small molecule chain termination probes used for the probing of PKS biosynthetic pathways, in particular in *S. lasaliensis* to generate a library of complex analogues.^{155, 156}

The small molecule probes have been successfully used to gain insights into polyketide assembly in a number of different systems, both modular and iterative. In particular, the AM ester masking has significantly enhanced the quantity of captured biosynthetic intermediates from the lasalocid A **1** pathway, likely due to the increased bioavailability of this malonyl protection over the simple ester group.¹⁵⁶

The availability of tools makes it possible to obtain mechanistic details that were previously inaccessible. The most challenging systems to investigate remain the iterative PKSs. Developing novel probes to harness iterative polyketide catalysis in conjunction with advanced mass spectrometry analyses was the focus of my research.

1.5.5. The application of proteomics and metabolomics to the investigation of biocatalysis

Mass spectrometry has become the preferred technique for the investigation of natural product biosynthesis *in vitro* and *in vivo* due to its swiftness, sensitivity, accuracy and availability. Mass spectrometry based approaches have been developed in the Kelleher, Bafna and Burkart laboratories.¹⁵⁷⁻¹⁶⁰ Through these methods, described in depth in Section 1.6.5, expressed and functional PKSs can be rapidly identified in conjunction with their associated natural products in complex biological mixtures faster than genome sequencing.

Further details on the use of proteomics will be given in section 1.6.5.2.2.

1.6. Mass spectrometry

Mass spectrometry is a widely used analytical technique, accessible in most modern laboratories. At a basic level, it provides the mass and molecular formulae of compounds, however, an abundance of fragmentation techniques can be used to deduce structure with mass spectrometers. The techniques available depend upon the instrument as well as the expertise of the user.

1.6.1. Key ionisation techniques

Nowadays, the most commonly used ionisation source is electrospray ionisation (ESI) for samples in solution. This soft ionisation source is suitable for a variety of sample types including small molecules and proteins, generating multiply charged ions, and is typically the ionisation source that is coupled to liquid chromatography

(LC). n-ESI, a miniaturised ESI source, is a variation of ESI for lower sample volumes. Charged droplets are produced by the electrospray capillary tip, and solvent evaporation causes the charged droplets to get smaller until they are very small and highly charged. A nitrogen counter current causes vaporisation of solvent and the ions are driven by an electric potential into the heated capillary pathway. Coulombic repulsion drives the ions away from one another. Downstream ion optics transfer the ions into the high-vacuum mass spectrometer, and neutral ions are left behind.^{161, 162}

Matrix assisted laser desorption/ionisation (MALDI) is another soft ionisation source that generates singly charged ions, and is commonly used for polymers and biomolecules. Samples are mixed with a matrix and a pulsed laser irradiates the sample. The irradiation causes ablation and desorption of the matrix and sample, and the sample is ionised by protonation in the hot plume of gases.^{163, 164}

There are many other ionisation sources, out of the scope of this thesis, that are available to analytical scientists. ESI is the only source that was used for this work as it was the most suitable for the samples that were generated.

1.6.2. Key mass analysers

Resolving power, resolution and mass accuracy are important specifications that are used in reporting mass spectral data and in comparing the instruments. Resolving power is the ability of an instrument to separate neighbouring peaks, defined as the ratio of one of the masses of interest (m) to the difference between those masses (Δm). It defines the resolution needed to separate those two peaks. Resolution is calculated from a recorded peak, defined as the ratio of the mass of that peak (m) to

the full width of the peak at half the maximum height of the peak (FWHM).¹⁶⁵ Mass accuracy is how close the experimental mass is to the theoretical mass, often reported in parts per million (ppm).

$$\text{Resolving power} = \frac{m}{\Delta m} \quad \text{Resolution} = \frac{m}{FWHM}$$

Equation 1 Equations for calculation resolving power and resolution in mass spectrometry. m = mass of peak of interest, Δm = difference between masses of neighbouring peaks, $FWHM$ = full width at half maximum height.

Three types of mass analyser herein used were Time-of-Flight (TOF), Ion Trap and Fourier Transform Ion Cyclotron Resonance (FTICR). The instrument used for an application should be carefully chosen to provide the data necessary to answer the question being posed.

In this work, for routine analysis of known small molecules, an ion trap mass analyser was used. An ion trap is a highly sensitive analyser; however, the mass error and resolution are typically limited. For the identification of unknown small molecules a high resolution TOF was used. A TOF can provide accurate mass and high resolution, as well as rapid analysis, however the specifications widely vary for this type of mass analyser. For the analysis of larger peptides and proteins with unknown small modifications, and also for complex fragmentation techniques, an FTICR was utilised. This instrument is not as sensitive as an ion trap or a TOF, however, the mass accuracy and resolution are far superior. FTICRs are often coupled with a range of fragmentation techniques such as CAD, IRMPD and ECD.

1.6.2.1. Time-of-flight (TOF) analysers

A TOF analyser separates pulsed ions of different m/z by their flight time along a field-free drift path. Lighter ions will arrive earlier at a TOF detector than heavier ions. Calibrating with ions of known mass allows the calculation of m/z , the longer the drift path the more accurate the analyser can be.¹⁶⁶

1.6.2.2. Ion trap analysers

An ion trap, or quadrupole ion trap (QIT), creates a three dimensional RF quadrupole field in which to store ions within certain m/z ranges. Unwanted ions are removed when they are unstable and collide with the walls, or when they are resonantly ejected from the trap for detection.

1.6.2.3. Fourier Transform Mass Spectrometers (FT-MS)

FTICR-MS provides the highest resolving power and mass accuracy of all mass analysers. The basic principle of ICRs is that an ion entering a magnetic field perpendicular to its direction will move in a circular path by action of Lorentz force. The cyclotron frequency is unaffected by the ion's initial velocity, instead it is a function of its mass and charge, and of the magnetic field. To detect the ions, an electric field, alternating at their cyclotron frequency, will accelerate the ions and increase the radius of their orbit, inducing an image current each time they pass the detector plates. Lighter ions will reach the same radius as heavier ions with fewer cycles, as they require less energy to accelerate. Scanning all frequencies will excite all ions, for a full mass spectrum, whereas alternating at just a specific frequency will

only excite a particular m/z . The transient free induction decay (FID) is recorded and Fourier transformed (FT) from the time domain to the frequency domain for conversion to m/z data. The longer the FID is recorded, the higher the mass resolution will be and the greater the mass accuracy.¹⁶⁷⁻¹⁶⁹ Additionally, the higher the field strength, the resolving power also increases. As the sample is not destroyed by detection in FTICR-MS, the same ion packet can be recorded repeatedly, generating a cumulative signal, and also the ability to perform numerous MS/MS experiments.^{166, 170-174}

Another category of FT-MS analyser is an Orbitrap, solely manufactured by Thermo Scientific, which radially traps ions about an electrode. Mass to charge ratios are recorded, non-destructively, by measuring the image current generated by ion oscillations.¹⁷⁵ These instruments provide higher resolution and mass accuracy than a TOF instrument, but less so than an FTICR-MS.

1.6.2.4. Ion mobility analysers

Lastly, a mass spectrometry specific separation technique of note is ion mobility MS. These instruments separate gas phase ions based upon their movement through drift tube containing a carrier gas and an electric field. These instruments provide valuable structural information, particularly for proteins, and the ability to often separate isomers.¹⁷⁶

1.6.3. Fragmentation techniques in mass spectrometry

Fragmentation techniques are a powerful method for structural characterisation, also known as tandem MS or MS/MS. The most common method of fragmentation is collisionally activated dissociation (CAD), also known as collisionally induced dissociation (CID). Other modern techniques, particularly for the analysis of biomolecules, include, but are not limited to, infrared multiphoton dissociation (IRMPD), electron transfer dissociation (ETD), electron capture dissociation (ECD) and, covered in this thesis, electron induced dissociation (EID) (**Table 1**).

Fragmentation Technique	Instrument Applicable	Mode of Action
CAD	TOF	Precursor ions collide with inert gas molecules. 1-100 eV energies.
	Ion trap	
ETD	FTICR	Singly charged anions transfer electrons to multiply charged precursors to induce fragmentation.
	Ion trap	
IRMPD	FTICR	Low energy IR laser activates precursor ions by multiphoton absorption causing dissociation.
	Ion trap	
ECD	FTICR	Low energy electrons (< 3 eV) causing electron capture on the precursor, and fragmentation by radical ion chemistry.
EID	FTICR	10-25 eV electrons causing fragmentation of singly charged precursors.

Table 1 Overview of notable fragmentation techniques, the instruments they are typically coupled with and their mode of action.^{177, 178} CAD = Collisionally activated dissociation. ETD = electron transfer dissociation. IRMPD = infrared multiphoton dissociation. ECD = electron capture dissociation. EID = electron impact dissociation. TOF = time-of-flight. FTICR = Fourier transform ion cyclotron resonance.

1.6.3.1. Collisionally activated dissociation (CAD)

CAD fragments are caused by accelerating ions to a high kinetic energy and then allowing collisions with neutral gas molecules, typically helium, nitrogen or argon. Bond breaking is caused by kinetic energy being converted to internal energy and this energy dissociating along an available fragmentation pathway.¹⁶⁶ The amide bond of peptides and proteins is the most common bond cleavage with CAD, generating 'b' and 'y' ions.¹⁷⁹ The method can be useful for sequencing proteins, and locating post-translational modifications (PTMs) (**Figure 13**).

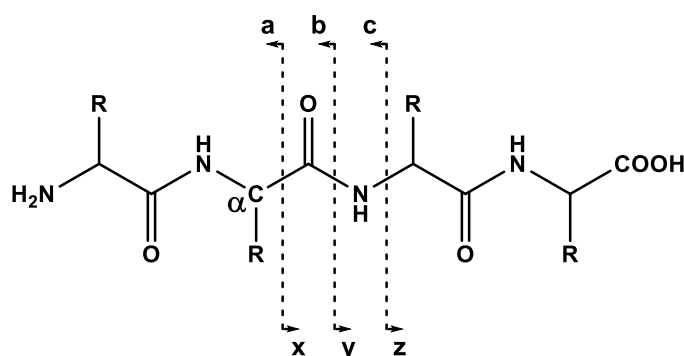


Figure 13 Common fragmentation pathways of proteins and peptides.¹⁷⁹

1.6.3.2. Infrared multiphoton dissociation (IRMPD)

IRMPD fragments trapped ions; typically used in FTICR-MS due to the ability to trap ions for a long period of time. A carbon dioxide laser of wavelength 10.6 μm is focussed into the ICR cell and the amount of energy delivered to the trapped precursor ions is varied by the duration of the irradiation. The energy is received by multiphoton absorption and causes dissociation of the ions.¹⁸⁰ This technique is applicable to a variety of compounds both large and small, and singly and multiply

charged. IRMPD of peptides and proteins causes bond cleavage of the amide bond, as in CAD, generating 'b' and 'y' ions (**Figure 13**).¹⁷⁹

1.6.3.3. Electron capture dissociation (ECD)

ECD is a fragmentation technique that uses low energy electrons to produce fragments in multiply charged precursors, generated by the capture of an electron. It is important to note that the weakest bond will not necessarily break. ECD and other electron based fragmentation techniques need the highest expertise to generate useful information. When fragmenting peptides and proteins, the most common fragmentation point is not the amide bonds, as in CAD, but the N-C α bond, producing 'c' and 'z' type fragments (**Figure 13**). IRMPD can be coupled with ECD, a kind of activated ion ECD, where the irradiation time is much shorter than in a regular IRMPD experiment, and the IR irradiation provides excitation of the precursor before electron capture and fragmentation by ECD, typically generating more backbone coverage than IRMPD or ECD alone.¹⁸¹

1.6.3.4. Electron transfer dissociation (ETD)

ETD requires trapped precursor ions, thus, it is usually carried out in either an ion trap or an ICR cell. Anions, for example fluoranthene, with low electron affinities act as electron donors, and this electron transfer causes the release of a hydrogen radical, inducing radical ion fragmentation similar to ECD.¹⁷⁸

1.6.3.5. *Electron impact dissociation (EID)*

EID is a tandem MS technique for fragmentation of singly charged, positive or negative, ions with electrons of moderate kinetic energies in the range of 10 – 25 eV.¹⁸²⁻¹⁸⁴ The technique has been shown to produce many of the same fragments that are produced by the more common CAD and IRMPD, but also to generate additional unique fragments.¹⁸⁵⁻¹⁸⁸

1.6.4. Analysis of proteins by mass spectrometry

The analysis of proteins can be performed in two main ways: ‘top-down’ or ‘bottom-up’. ‘Top-down’ refers to analysing proteins directly by MS: protein identification is carried out firstly by the accurate mass of the protein, and then by MS/MS fragmentation for sequencing and identifying post-translational modifications (PTMs). Benefits of this technique include limited sample preparation and the analysis of ‘native’ conformations, reducing the risk of altering PTMs by extensive sample preparation. The main disadvantage of the technique is that the detection of large molecules requires more advanced and high resolution instruments, and further characterisation needs experienced instrument users to gather the information needed.¹⁸⁹

The ‘bottom-up’ method of characterising and identifying proteins refers to the use of a protease, typically trypsin, to enzymatically hydrolyse proteins into peptides. The peptides are usually separated by LC before analysis by MS. The peptides are smaller in mass, which is more suitable for lower resolution instruments, and by database searching it is possible to identify proteins. Many PTMs are unaffected by the digestion and sample preparation, however, disulphide bonds will be disrupted,

and information regarding PTMs of unknown proteins and their location is not as reliable. This technique is also not applicable to the identification and sequencing of proteins that are not in databases.

1.6.5. Mass spectrometry for the investigation of natural product biosynthesis

In natural product research, mass spectrometry is a key analytical technique. The rapid identification of both small and large molecules, can be particularly advantageous for high throughput screening. Highly sensitive instruments allow detection of compounds from both low sample volumes and low concentrations, as well as from complex samples. Structural elucidation of compounds can be begun by MS; however, NMR would still be the technique of choice for structural characterisation.

1.6.5.1. The use of isotope labelling in mass spectrometry

Often, labelled precursors, such as ^{13}C sodium acetate, are fed to organisms, and their uptake by PKSs is monitored by MS. High resolution MS instruments can identify molecular formulae of products to a high degree of accuracy, for example, sub ppm accuracy on a FTICR-MS is routine, and with detailed calibration, sub ppb is possible. Detecting mass differences caused by ^{13}C or deuterium labelling is simple for most modern instruments.

1.6.5.2. Fragmentation techniques for natural product research

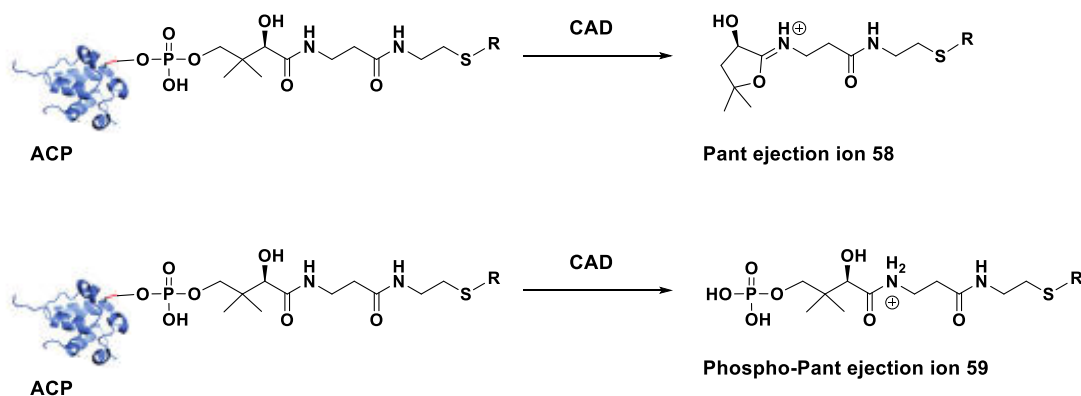
CAD is the most utilised technique for structural characterisation of small molecules and proteins. However, newer modes of fragmentation, such as EID and ECD, can provide structural information where CAD fails. Electron based fragmentation techniques can produce different fragments to those seen with CAD. Håkansson and coworkers have shown that it is possible to determine the location of double bonds in fatty acids by EID, combined with manganese adduction¹⁹⁰, and in the O'Connor group EID was able to differentiate between two isomers, lasalocid A **1** and *iso*-lasalocid A.¹⁹¹

1.6.5.2.1. Fragmentation of the phosphopantetheinyl (PPant) arm of carrier proteins

CAD has proven especially useful in the identification and characterisation of ACPs, and in generating characteristic PPant ejection ions **58**. Upon CAD fragmentation, the phosphodiester bond adjacent to the pantetheinyl moiety is cleaved providing **58**, or alternatively the phosphodiester bond adjacent to the protein is broken, generating the larger phospho-Pant ejection ion **59**. This technique has been used in proteomics for identifying PKSs, but also in off-loading intermediates from ACP-bound species.^{157-159, 192, 193} IRMPD also provides this Pant ion but fewer instruments are equipped with this tool for fragmentation (**Scheme 13**).

A drawback to the “PPant ejection assay” is that it requires a degree of skill by the MS user.¹⁵⁷ The assay has, however, been used effectively on several occasions.^{141, 142, 192, 194} In particular, intermediates from the lovastatin **5** biosynthetic pathway, a non-iterative type I PKS, were trapped by performing a trypsin digest of the 277 kDa

megasynthase once the PKS had been activated *in vitro*, rendering it inactive. The resulting peptides were fragmented, and intermediates, bound to the ejected Pant ion **58/59**, were detected, with additional ^{13}C labelling for confirmation.¹⁹² Similarly, an enzyme bound intermediate was detected with the “PPant ejection assay” from the enediyne C-1027 pathway, and the result aided the understanding of the biosynthetic pathway.¹⁹⁵



Scheme 12 Generation of a pantetheine (Pant) ejection ion **58** or a phospho-Pant ejection ion **59** from the corresponding ACP by CAD or IRMPD.

1.6.5.2.2. Proteomics based approaches to detect and characterise PKSs

Bafna and co-workers developed a proteomics based method that combines enriching the abundance of PKSs in the MS sample by affinity tagging TE domains, followed by tryptic digestion, and then identification of PPant active sites either by MS^3 or by machine learning from the MS^2 spectra. The machine-learning approach allows lower cost instruments to use a proteomics approach to identify PKSs without MS^3 , which is often out of reach for those instruments.¹⁵⁷

A similar method from the Burkart laboratory, called the Orthogonal Active Site Identification System (OASIS), uses active site probes to enrich the carrier protein and thioesterase peptides in complex biological samples. The carrier proteins are

labelled either by incorporation of CoA precursors with azide groups for chemoselective ligation to reporters with alkyne groups or with biotinylated CoA analogues for purification with streptavidin. Thioesterases can be enriched by modification of the active site serine using fluorophosphonate with a biotin linker for pull down. The samples are then analysed by MudPIT^{196, 197} (Multidimensional Protein Identification Technology), which is a 2D LC-MS technology for separating and identifying individual peptides and proteins from complex samples. PKSs and NRPSs are identified by cross-referencing the peptides identified by each probe. Thus far, OASIS has only been demonstrated on a model bacteria, *B. subtilis*, where they successfully detected and identified all of the modular synthases expressed in that organism.¹⁶⁰

Proteomics-based approaches to discovering PKSs have also proven successful in the Kelleher group, combined with the “PPant ejection assay” to find ACPs and identify the PKS from that information. One such platform is the Proteomic Investigation of Secondary Metabolism (PrISM).¹⁵⁹ In this way, only the expressed NRPS/PKSs are detected, avoiding traditional genome mining methods that cannot distinguish between expressed or ‘silent’ gene clusters. Cultures of the bacteria are first screened for the presence of high molecular weight proteins, as those proteins are likely to be NRPSs or PKSs. The bacteria are grown in different conditions, the large proteins (150 kDa or more) are analysed by MS and their peptide fragments from digestion are used to identify the biosynthetic machinery.

Once the carrier protein has been found and its sequence deduced it is possible to design primers to pull down the gene and then identify the full PKS gene, even if the genome sequence of the organism is not known. With that information, it is then possible to search for the natural product produced. Koranimine, a cyclic imine¹⁹⁸,

flavopectins, a class of peptide aldehydes,¹⁹⁹ and gobichelins A and B, siderophores produced by NRPSs,²⁰⁰ were detected for the first time using PrISM.

1.7. Photolysis as a tool for investigating biological systems

Photolysis is the breakdown of a compound by the application of light. It is rapidly becoming a powerful tool of investigation. Photoactivatable compounds are used for a wide range of applications, from chemical synthesis to probing, controlling or tuning biological systems. There are several photolabile groups available to protect different chemical groups and can be selectively removed at specific wavelengths. Protecting groups for carboxylic acids will be further explored in chapter 2 as they are relevant to the probes I have developed in my research.

1.7.1. Desirable traits of photolabile groups for biological applications

Photolabile groups do not require the use of reagents for their cleavage, allowing the mild and selective uncaging of a wide range of molecules in different environments, including complex biological environments.

Photolytic cleavage is the product of absorption of a photon and there are a limited number of pathways by which bond cleavage can occur.²⁰¹

A fast rate of cleavage, selective cleavage pathway, a limited or harmless by-product, high quantum yield (**Equation 2**), and a narrow cleavage wavelength for cleavage are all desirable properties for photolabile groups. A fast cleavage rate is important as long irradiation times may cause heating, and less stable molecules may degrade over time. Additionally, for kinetic studies, being able to denote a starting

point is desirable. The cleavage selectivity of a photolabile group is possibly the most important aspect when choosing the correct group. Ideally, photolysis should yield just two products: the compound of interest and the cleaved photolabile group or by-product. The by-product should be unreactive under the conditions in which it is required, and non-toxic when used for biological applications.

Quantum yield is a measure of how efficiently a photoactivatable group is cleaved, calculated from the number of molecules cleaved per number of photons absorbed. It is used to compare different photolabile groups, a high quantum yield is desirable (**Equation 2**).²⁰² Lastly, the wavelength for cleavage of the protecting group would, ideally, not be within the visible spectrum, as this makes sample handling more challenging. Synthesis and preparation would need to be carried out in the dark, as well causing the time of activation difficult to define.

$$\text{Quantum yield} = \frac{\text{number of cleaved molecules}}{\text{number of photons absorbed}}$$

*Equation 2 Calculation of quantum yield*²⁰²

1.7.2. Photo-irradiation as a tool for the investigation of biosynthetic pathways

There are a few examples of UV irradiation influencing, or causing, important biosynthetic pathways in organisms. A significant example is the light absorption by chlorophyll that induces the electron transport chain in photosynthesis. The absorption can also be released as heat, or re-emitted as fluorescence. Therefore, by measuring the fluorescence, changes in the efficiency of photosynthesis can be monitored.²⁰³

Gene expression has been shown to be controlled to some degree by light irradiation. For example, heme oxygenase 1 following UVA irradiation of mammalian cell lines²⁰⁴, UVB irradiation of peach and nectarine fruits increased gene expression resulting in the synthesis of more phenolic compounds²⁰⁵, and the gene expression profiles of a cyanobacterium, irradiated with UVB or intense white light, showed both up and down regulation of a wide variety of genes, including those involved in secondary metabolite biosynthesis²⁰⁶.

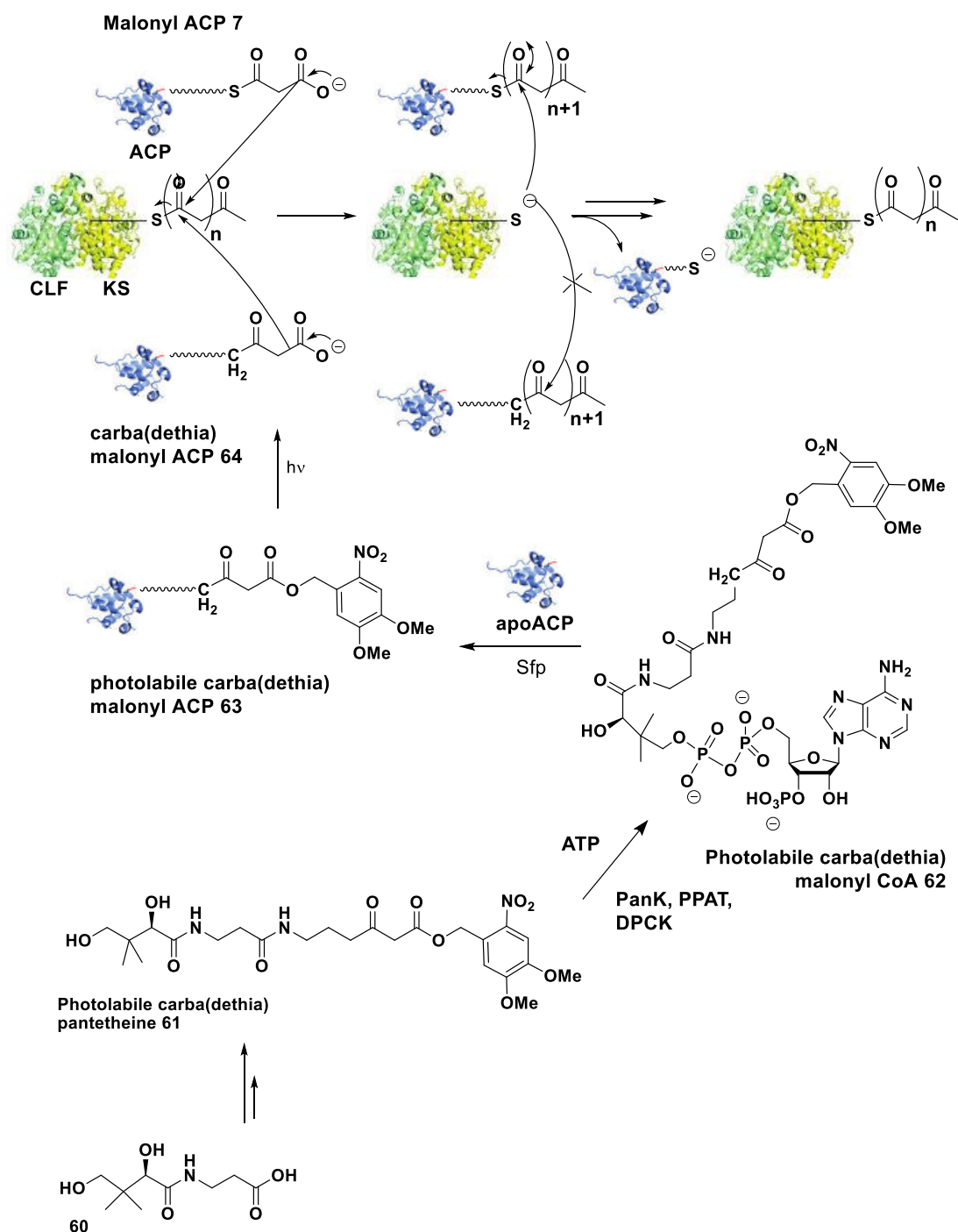
However, to the best of my knowledge, there are no examples of light-activated molecules being used to probe natural product assembly. With the tools available to the community, this is an avenue of research ready to be explored.

1.8. Research aims and objectives

1.8.1. Primary research aim

The principal aim of this PhD project was to develop a new method to probe the biosynthesis of iterative polyketide pathways by means of a photoactivatable nonhydrolysable malonyl acyl carrier protein probe **63**. Intermediates from iterative type II PKSs have never been detected or isolated before. Nonhydrolysable probes of this type have never before been light activated. Light activation negates the need for additional enzymes or reagents and their specific reaction conditions, provides controllable and tunable release of the ‘active’ probe, and is a mild deprotection method.

The proposed method builds from an already established chain terminator methodology within the Tosin group,^{11, 22, 136, 154, 155} with the aim of looking at ACP-bound biosynthetic intermediates otherwise unavailable (**Scheme 13**).



Scheme 13 Primary project aim: chemoenzymatic preparation of a photolabile carba(dethia) malonyl-ACP **63** that, following light irradiation generates a carrier protein 'trap' for type II PKS intermediates from the actinorhodin minimal system.

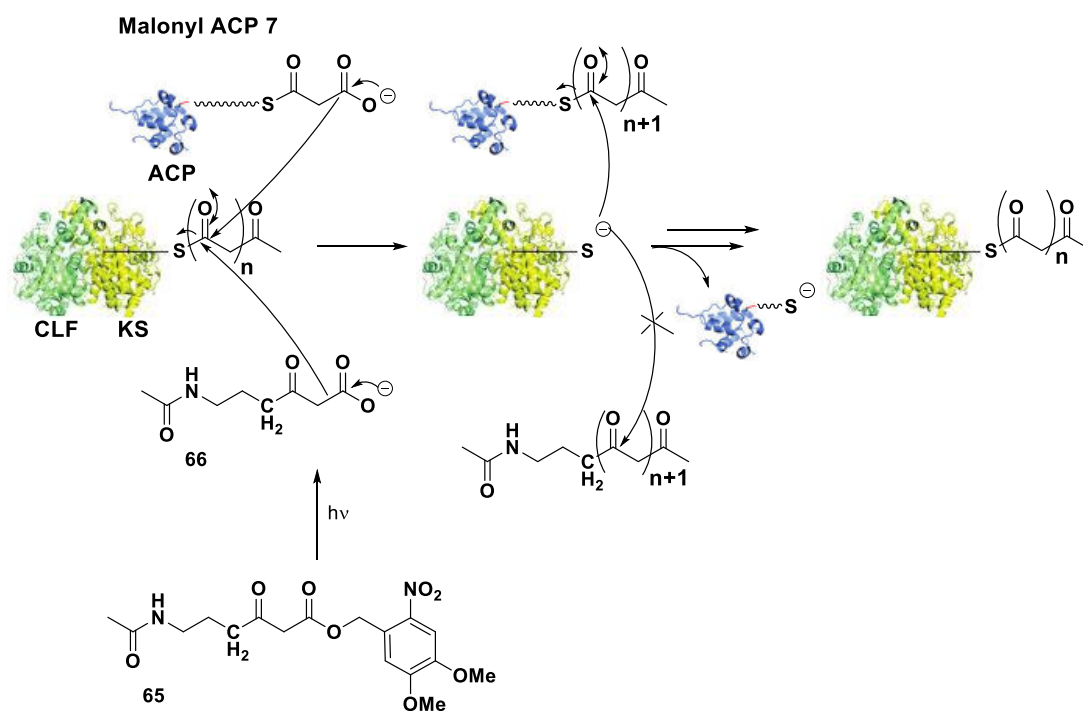
Within this aim, the following objectives were pursued:

- A robust chemoenzymatic preparation of an acyl carrier protein photolabile ‘probe’ **63** (Scheme 13)
- Demonstrate the light activation of a nonhydrolysable malonyl ACP probe
- The investigation of polyketide biosynthesis for the actinorhodin minimal system, chosen as model system for type II PKSs, through the use of the newly devised protein probe **63** *in vitro*
- The analysis of biosynthetic species trapped onto the ACP probe **64** by FTICR-MS.

1.8.2. Secondary research aim

The secondary project aim was to compare the efficiency of intermediate capture by a small molecule photolabile probe **65** with that of the ACP protein probe **64**. For this:

- Demonstrate the photoactivation of a small molecule probe
- A previously established system, the modular lasalocid A **1** biosynthetic pathway from *S. lasaliensis*, investigated with the aid of the synthesised small molecule probe **65**.¹⁵⁵
- The small molecule probe **65** used for the capture of type II PKS intermediates from the reconstituted actinorhodin minimal system *in vitro*, as well as from actinorhodin **2** biosynthesis in *S. coelicolor*.
- Identify and characterise trapped biosynthetic species by LC-HR-MS. (Scheme 14).



Scheme 14 Secondary project aim: Investigation of the actinorhodin minimal type II polyketide synthase by means of a photolabile small molecule chain termination probe **65** *in vitro* and *in vivo*.

1.8.3. Tertiary research aim

Lastly, this research aimed at improving and optimising the characterisation of biosynthetic intermediates in free or protein-bound form. The incorporation of alkali metals to mass spectrometry samples obtained from experiments was explored to establish any influence on fragmentation pathways in collisionally activated dissociation (CAD) and electron impact dissociation (EID). This could prove a new avenue of research for future mass spectrometry analyses of polyketides and proteins, in particular acyl carrier proteins.

Chapter 2: Synthesis of a nonhydrolysable photolabile *N*-acetyl cysteamine probe

2. Synthesis of a nonhydrolysable photolabile malonyl *N*-acetyl cysteamine probe

2.1. Probe design

As mentioned in Chapter 0, mimics of the acyl carrier protein pantetheinyl arm in the form of nonhydrolysable malonyl *N*-acetyl cysteamine analogues (**Figure 14**) have proven successful as tools to chemically ‘trap’ biosynthetic intermediates.^{22, 136, 154,}

¹⁵⁵ It has been shown that carba(dethia) analogues have been the most effective trapping agents, in comparison to oxa(dethia) and amino(dethia).^{11, 154}

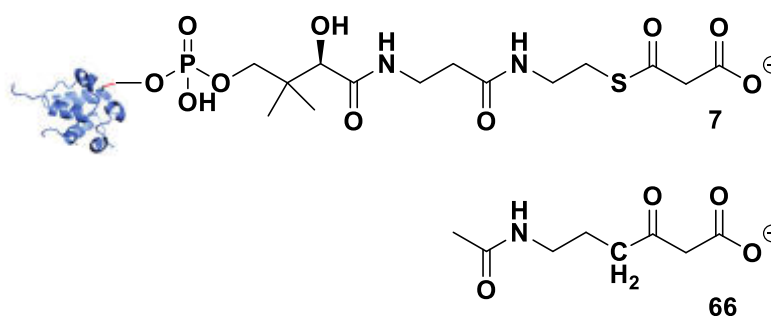


Figure 14 A comparison between the ‘natural’ 4’-phosphopantetheinyl arm and its carba(dethia) mimic. **7** is the 4’-phosphopantetheinyl arm of ‘malonyl’ acyl carrier protein. **66** is the ‘active’ malonyl carba(dethia) *N*-acetyl cysteamine probe.

A photolabile *N*-acetyl cysteamine analogue **65** has been prepared for several motives. The photoactivatable nonhydrolysable malonyl acyl carrier protein analogue (ACP probe **63**) requires a lengthy chemoenzymatic synthesis to prepare, however, the *N*-acetyl cysteamine probes (NAC probes) can be prepared in as little as three steps. Therefore, it was predicted that a larger quantity of probe **65** would be available for preliminary photolysis tests, such as to find the optimum light source and conditions for ‘uncaging’.

In addition to using the NAC probe **65** for optimising photolysis conditions, the comparison of this probe with the ACP probe **63** results *in vitro* would prove important in designing future probes. Lastly, the photolabile NAC probe **65** would be the first photoactivatable probe of its kind, and would be able to be used *in vivo* as well as *in vitro*. Photoactivation allows activation of the probe at different time points for the ‘trapping’ of biosynthetic intermediates. Other generations of NAC probe rely on activation by esterases in the cell, which could occur at an uncontrolled point in the cell growth.^{11, 22, 136, 154}

The following section presents the rationale for choosing the 4,5-dimethoxy-2-nitrobenzyl (DMNB) photolabile protecting group for both probes **63** and **65**.

2.2. Photolabile protecting groups for carboxylic acids

A variety of photolabile protecting groups for the protection of carboxylic acids are described in the literature: these include multicyclic (Section 2.2.1) and monocyclic aromatic (Section 2.2.2) moieties. Those with cleavage wavelengths above approximately 300 nm²²⁶ can be used in biological environments as they are not protein damaging; however additional factors such as quantum yield, by-product interference or toxicity, solubility and bioavailability have to be taken into account in selecting an ideal group. To the best of our knowledge, no malonyl or β -ketoacid photolabile protection has been reported.

2.2.1. Multicyclic groups

2.2.1.1. Diisopropylsilyl groups

There is a class of photoactivatable silyl protecting groups that include (hydroxystyryl)diisopropylsilyl (HSDIS) **85** and ((2-hydroxy-3-naphthyl)vinyl)-diisopropylsilyl (HNVDS) **86** that have been used for chemical synthesis applications, taking advantage of selective deprotection. The HSDIS **85** group cleaves at 254 nm and the HNVDS **86** group at 350 nm, although quantum yields have not yet been reported (**Figure 15**).^{227, 228}

2.2.1.2. Thiochrome groups

A thiochrome protecting group whose activity can be switched on by oxidation, providing thiochrome *S,S*-dioxide (TCSSD) **87**, can also be used as a protecting group for carboxylic acids. With wavelengths over 280 nm, TCSSD **87** will cleave the leaving group and generate a tetracyclic highly fluorescent product that can be used to monitor the deprotection (**Figure 15**).²²⁹

2.2.1.3. Polycyclic aromatic hydrocarbons groups

Also, activated at 350 nm are the polycyclic aromatic hydrocarbons, Phenanthren-9-ylmethoxycarbonyl (Phmoc) **82**, Pyren-1-ylmethoxycarbonyl (Pmoc) **83** and Anthroquinon-2-ylmethoxycarbonyl (Aqmoc) **84**. Aqmoc **84** is the best protecting group for alcohols with a quantum yield of 0.10, followed by Pmoc **83** (quantum yield of 0.003) and least reactive is Phmoc **82** (quantum yield of 0.0009). The highest yields for Aqmoc **84** required THF in the solvent system, which limits its

biological applications. Furthermore, it produces a reactive intermediate that may hinder its application in a number of fields (**Figure 15**).²³⁰

2.2.1.4. *Coumarin-4-ylmethyl (CM) groups*

Interest in coumarins has mainly focused on their fluorescent properties, however coumarin-4-ylmethyl (CM) groups are an entire class of protecting groups. They can present a variety of modifications on the benzopyrone moiety which can affect photolysis quantum yield and rate. Solvent trapped coumarin is the by-product of the photocleavage, and the leaving group is released as an anion.²²⁶ (7-methoxycoumarin-4-yl)methyl ester (MCM) **92** was the first coumarin derivative to be explored as a protecting group for diethylphosphate.²³¹ Later, MCM **92** was used to protect cyclic adenosine monophosphate (cAMP), releasing cAMP with irradiation of 340 nm.²³²

Coumarin-4-ylmethanol (HCM) **88** has an absorption maximum at 310 nm, shifts to longer wavelengths can be made by modifications to the C6 or C7 of the coumarin ring. (6-bromo-7-hydroxycoumarin-4-yl)methyl (Bhc) **89**, for example, the addition of a bromine at the C6 position, shifts the maximum absorption to 375 nm.^{226, 233} Further additions of bromine at the C2 and C8 positions increase the maximum to 397 nm.²³⁴ A chlorine substitution at the C6 position, however, decreased the quantum yield by 40% compared to HCM **88** (**Figure 15**).^{226, 234}

Takaoka and co-workers²³⁵ compared coumarin based protecting groups with a nitrobenzyl (NB) protecting group, 4,5-dimethoxy 1-(2-nitrophenyl)ethyl (DMNPE) **111**, and found MCM **92** and (7-carboxymethoxycoumarin-4-yl)methyl (CMCM) **93** to cleave much faster than DMNPE **111** (**Figure 17** and **Figure 15**).

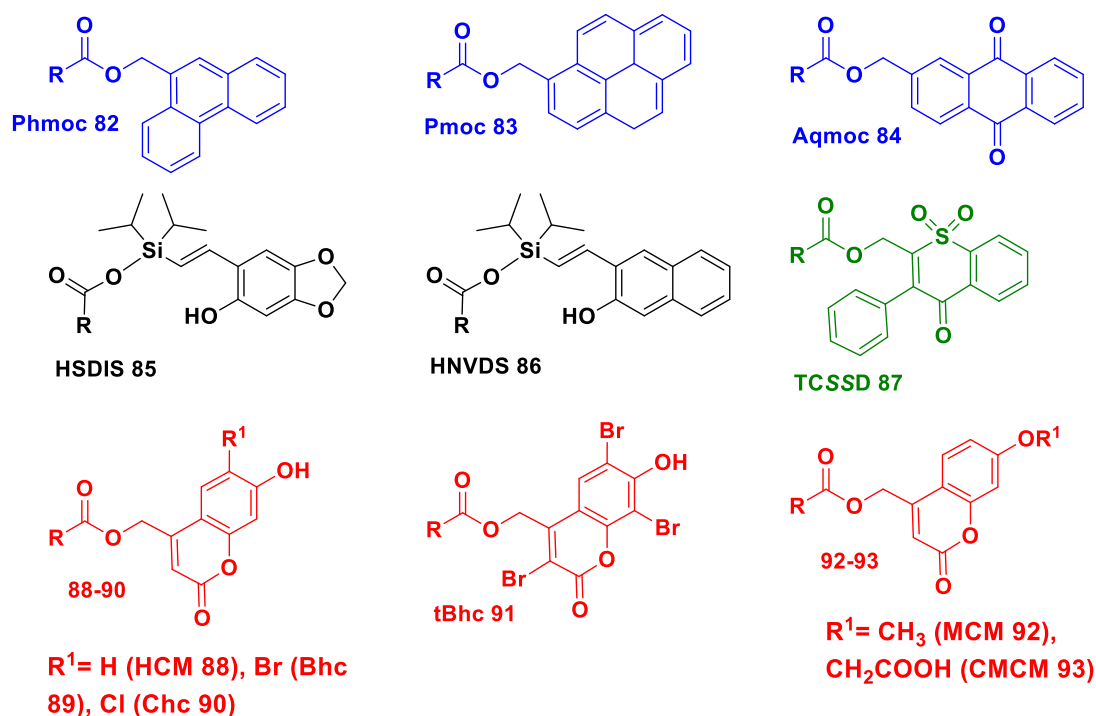


Figure 15 Multicyclic photocleavable protecting groups for carboxylic acids. *Phmoc* = Phenanthren-9-ylmethoxycarbonyl **82**, *Pmoc* = Pyren-1-ylmethoxycarbonyl **83**, *Aqmoc* = Anthroquinon-2-ylmethoxycarbonyl **84**, *HSDIS* = (hydroxystyryl)diisopropylsilyl **85**, *HNVDS* = ((2-hydroxy-3-naphthyl)vinyl)-diisopropylsilyl **86**, *TCSSD* = thiochrome S,S-dioxide **87**, *HCM* = (7-hydroxycoumarin-4-yl)methyl **88**, *Bhc* = (6-bromo-7-hydroxycoumarin-4-yl)methyl **89**, *Chc* = (6-chloro-7-hydroxycoumarin-4-yl)methyl **90**, *tBhc* = 3,6,8-tribromo-7-hydroxycoumarin-4-ylmethyl **91**, *MCM* = (7-methoxycoumarin-4-yl)methyl **92**, *CMCM* = (7-carboxymethoxycoumarin-4-yl)methyl **93**.

2.2.2. Monocyclic aromatic groups

Simple aromatic moieties can also be used as photolabile protecting groups. Barltrop and Schofield, in 1962, demonstrated very simple protecting groups that could be cleaved by irradiation of wavelength 254 nm: benzyl (B) **96**, *para*-nitrobenzyl (*pNB*) **97**, *para*-bromobenzyl (*pBB*) **98** and *para*-methoxybenzyl (*pMOB*) **99** (Figure 16).²³⁶

Two methoxy groups in the *meta* position (DMB) **94** has been shown to increase the photolysis rate, this has been coined the '*meta* effect'.²³⁷⁻²³⁹ The addition of two methyl groups on the α carbon (DMDMB) **95** makes the group even more reactive as it stabilises the positive charge on the benzyl ring, promoting O-C bond cleavage (Figure 16).^{240, 241}

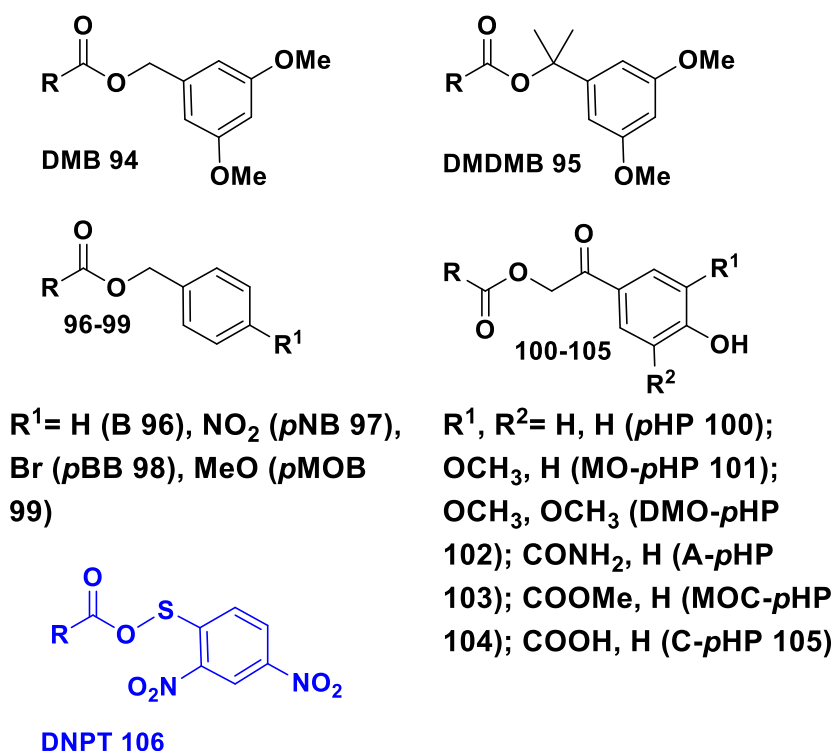


Figure 16 Simple aromatic photolabile protecting groups for carboxylic acids. DMB = 3,5-dimethoxybenzyl **94**. DMDMB = α,α -dimethyl-3,5-dimethoxybenzyl **95**. B = Benzyl **96**. pNB = para-nitrobenzyl **97**. pBB = para-bromobenzyl **98**. pMOB = para-methoxybenzyl **99**. pHP = para-hydroxyphenacyl **100**. MO-pHP = 3-methoxy-para-hydroxyphenacyl **101**. DMO-pHP = 3,5-dimethoxy-para-hydroxyphenacyl **102**. A-pHP = 3-acetamide-para-hydroxyphenacyl **103**. MOC-pHP = 3-methoxycarbonyl-para-hydroxyphenacyl **104**. C-pHP = 3-carboxyl-para-hydroxyphenacyl **105**. DNPT = 2,4-dinitrophenylthio **106**.

A range of photolabile groups based on *para*-hydroxyphenacyl (pHP) **100** with *meta* substitutions can act as protecting groups for carboxylic acids, cleaving at 300 nm. The quantum efficiency of these groups for releasing γ -Aminobutyric acid (GABA)

has been determined and a relationship between the ease of forming the phenoxide anion and the release of the substrate. Of six *meta* substituted protecting groups, the 3-acetamide-*para*-hydroxyphenacyl (A-*p*HP) **103** group had the highest quantum efficiency, whereas the methoxy derivatives **101** and **102** (3-methoxy-*para*-hydroxyphenacyl (MO-*p*HP) **101** and 3,5-dimethoxy-*para*-hydroxyphenacyl (DMO-*p*HP) **102**) had the lowest quantum efficiency (**Figure 16**).^{226, 242}

A 2,4-dinitrophenylthio (DNPT) **106** photolabile group was reported to protect carboxylic acids in the 1960s, however, since then this chemistry has not progressed any further, and applications have not been documented since (**Figure 16**).²⁴³

A subset of monocyclic aromatic protecting groups comprises nitrobenzyl groups which will be discussed in depth in the following section.

2.2.3. Nitrobenzyl (NB) groups

The most common class of photolabile protecting groups are the nitrobenzyl (NB) derivatives (**Figure 17**). A selection of these groups is shown in **Figure 17**. NB protecting groups will cleave in a variety of solvents, and even in solid state, however the rate of photolysis is dependent on the solvent, with acetonitrile being the fastest for deprotection of carboxylates, and the rate is slowest at physiological pH.²⁴⁴⁻²⁴⁸ Most of the NB groups are *ortho*- isomers, however, *para*- and *meta*- NB alcohols have also been synthesised and photoisomerisation has been observed, but not used as photolabile protecting groups.²⁴⁹

Analogues with modifications to the NB **114** have been synthesised on numerous occasions with mixed results. The introduction of an α -methyl group to the NB group (α -CH₃ NB) **118** has been demonstrated to not increase the quantum yield.²⁵⁰

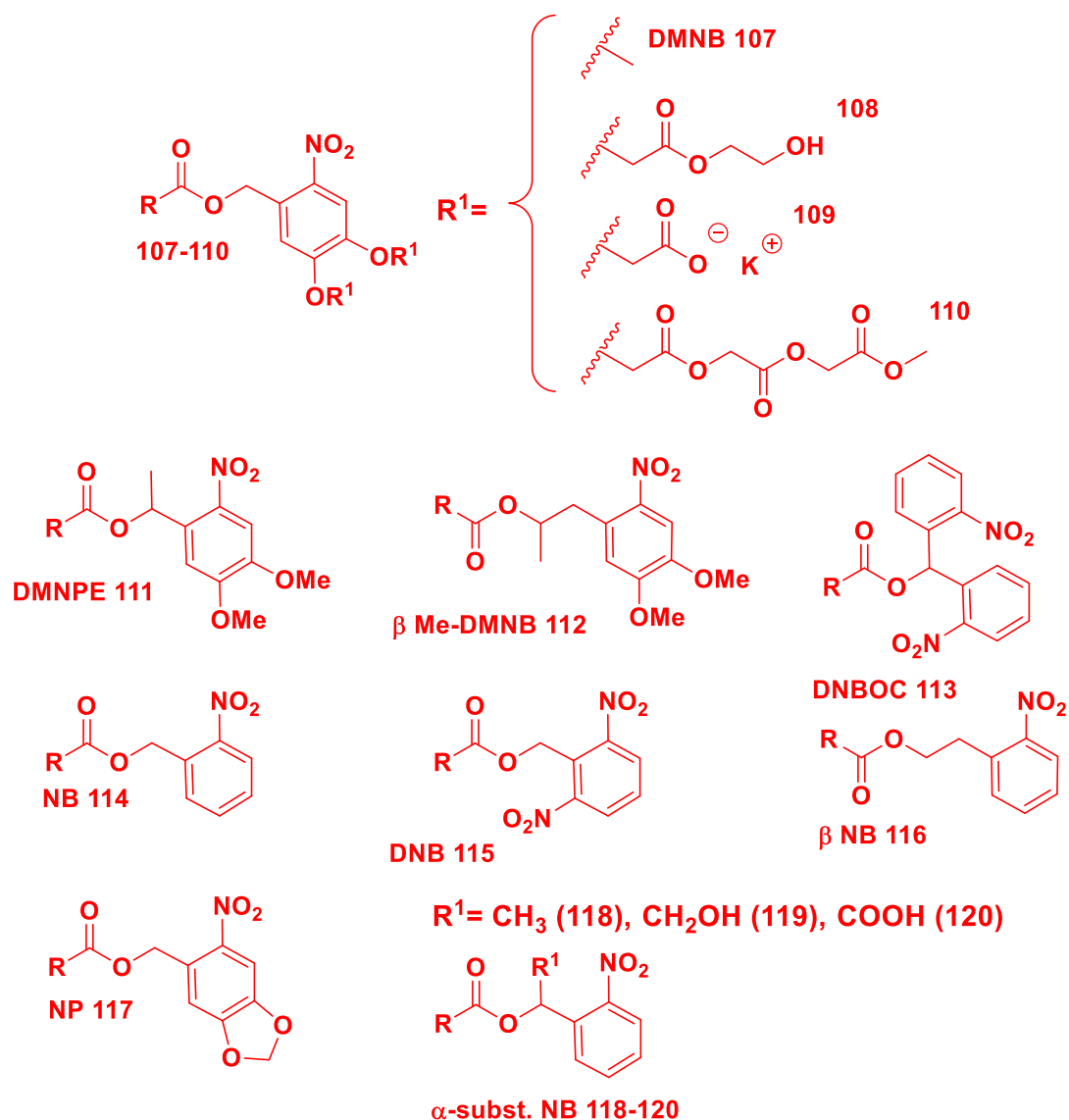


Figure 17 A selection of nitrobenzyl type photolabile groups to protect carboxylates. DMNB = 4,5-dimethoxy-2-nitrobenzyl **107**, DMNPE = 4,5-dimethoxy 1-(2-nitrophenyl)ethyl **111**, DMNPP = 2-(4,5-Dimethoxy-2-nitrophenyl)propyl **112**, D(NB) = di(nitrobenzyl) **113**, NB = nitrobenzyl **114**, DNB = 2,6-dinitrobenzyl **115**, β NB = β nitrobenzyl **116**, MDNB = 4,5-methylenedioxy nitrobenzyl **117**, α -subst. NB = α -substituted (methyl **118**, hydroxymethyl **119** and carboxyl **120**) nitrobenzyl.

A carboxyl group at the α position, α -carboxylated nitrobenzyl (α -COOH NB) **120**, however, does increase the rate of photolysis. An additional *para* carboxylate does not increase the quantum yield, but can make the compound more hydrophilic,

beneficial for some applications.²⁵¹⁻²⁵³ When a hydroxyl group is in the α position (α -hydroxymethyl nitrobenzyl (α -CH₂OH NB) **119**), it is more stable than the α -carboxyl derivative **120**, and the decay kinetics for this analogue were much faster.²⁵⁴

Substitutions at the 4 and 5 positions on the benzene ring (**107** to **110**) do not negatively impact the group's ability to photolyse, and the substitutions do not alter the quantum yield to a great degree.²⁵⁵ Two NB groups (di(nitrobenzyl)oxycarbonyl (D(NB)) **113**) increased the quantum yield compared to a single NB group **114**, but not as greatly as an additional nitro moiety on the other *ortho* position of a single NB ring, 2,6-dinitrobenzyl (DNB) **115**.²⁵⁰ The latter improves the statistical likelihood of producing the *aci*-nitro group, necessary for photolysis to occur (**Figure 17**).²⁴⁰

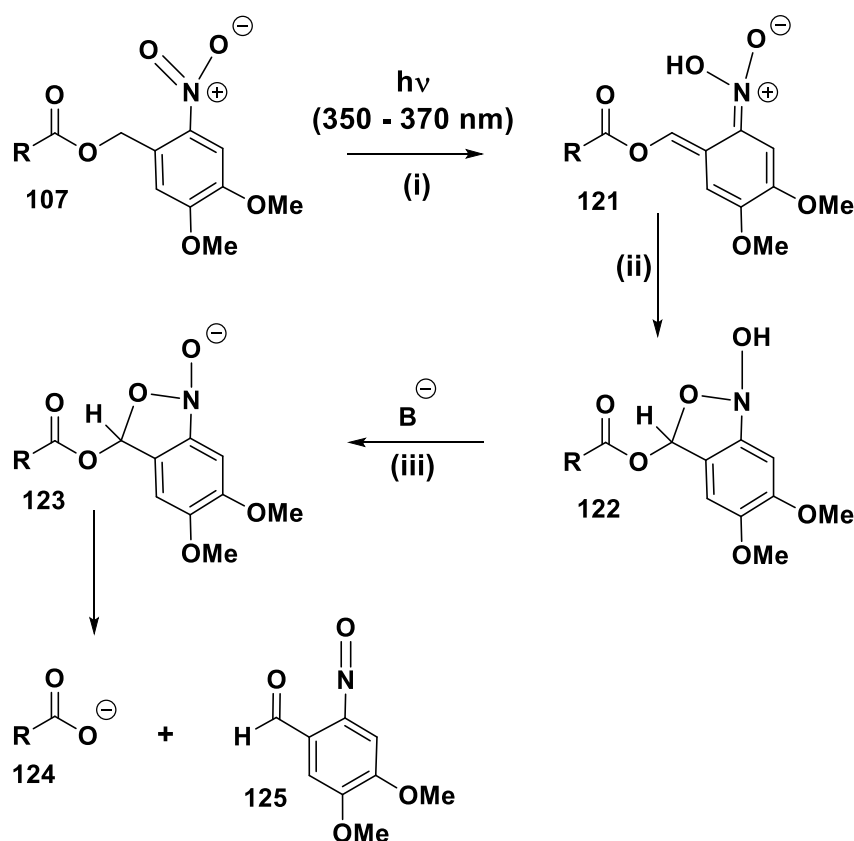
It is also possible to link the NB group **113** at the β position, β nitrobenzyl (β NB) **116** as a photolabile group to protect nucleosides, and increased the photolysis rate compared to at the α position (**Figure 17**).²⁵⁶

The 4,5-dimethoxy-2-nitrobenzyl (DMNB) group **107**, is the most popular NB derivative, and presents two methoxy groups at the *meta* and *para* positions, however a methylenedioxy derivative, 4,5-methylenedioxy nitrobenzyl (MDNB) **117**, is also widespread (**Figure 17**).²⁵⁷ Both substitutions cause an increase in the maximum absorption, producing compounds more suitable for *in vivo* applications.²⁴⁰ Other modifications, as shown in **Figure 17, 118-120**, did little to alter the quantum yield, however, for Makings and Tsien²⁵⁵, hydrophilic or hydrophobic substitutions allowed control over the cell membrane permeability.

2.2.3.1. The 4,5-dimethoxy-2-nitrobenzyl (DMNB) group 107

Modifications to the *para* and *meta* positions on the NB ring have been explored. The most popular protecting group is the 4,5-dimethoxy-2-nitrobenzyl (DMNB) group **107**, also known as the 6-Nitroveratryloxycarbonyl (NVOC) group.²⁴⁰ The group can protect alcohol or carboxylic acid groups as well as amines. A carbamate, carbonate or an ester linkage between the substrate and the protecting group, when photolytically cleaved, yields an aldehyde on the protecting group (by-product) and an amine, carboxylic acid or alcohol group, respectively, on the substrate (product). The methoxy moieties of the DMNB group **107** increase the cleavage wavelength to make the deprotection less toxic in biological systems. In particular, tryptophan, the most sensitive amino acid to light, is not affected by the wavelength required for photolysis of the DMNB group **107**.^{201, 258} In fact, the photolysis can be carried out at a range of wavelengths, 254nm, 350 nm, 365 nm, 380 nm, 400 nm, and 419 nm, which opens up more opportunities for different applications, as well as selective deprotection among other photolabile protecting groups.^{240, 259}

There are three steps towards the photolysis of the DMNB group **107**, and this applies to most *o*-nitrobenzyl alcohol derivatives. To begin with there is photoinduced hydrogen atom transfer to the nitro group that promotes cyclisation involving that nitro group, and then deprotonation of the hydroxyl group leads to cleavage that generates *o*-nitrobenzaldehyde **125** and the desired product **124** (**Scheme 15**). The by-product **125** is likely to undergo side-reactions, such as dimerisation and oxidation.^{245, 258, 260}



Scheme 15 Mechanism of photolysis of the 4,5-dimethoxy-2-nitrobenzyl (DMNB) group **107** protecting a carboxylic acid group. Three key steps are involved in the photolysis: (i) the photoinduced H-atom transfer leading to **121**, (ii) ground state cyclisation of **121** to **122**, (iii) in basic conditions, **122** is deprotonated to **123**, and cleaves irreversibly, releasing the carboxylic acid group **124** and o-nitrobenzaldehyde **125**.²⁶³

Derivatives of DMNB **107** have been synthesised to act as probes with *alpha* substitutions such as an α -methyl group, 4,5-dimethoxy 1-(2-nitrophenyl)ethyl (DMNPE) **111**, which proved to increase the quantum yield from 0.006 to 0.65 when caging glutamate.^{261, 262}

A longer linker between the NB ring and the protected carboxylic acid was explored by Specht and co-workers²⁶⁴, including a *beta* methyl substitution.

The protecting group, 2-(4,5-Dimethoxy-2-nitrophenyl)propyl (DMNPP **112**), when caging glutamate had a quantum yield of 0.36, which is also an improvement on the basic DMNB group **107**. DMNPP **112** has recently been utilised for light-induced protein dimerisation in live cells by caging gibberellic acid.²⁶⁵ Both DMNPE **111** and DMNPP **112** are cleaved with wavelengths of approximately 364 and 350 nm, respectively^{262, 264}, however, it has been reported that DMNPP **112** can be cleaved *via* two-photon uncaging.²⁶⁵ The DMNB alcohol is commercially available, therefore we pursued its straightforward incorporation into our probes as proof of concept.

2.2.3.1.1. Applications for the 4,5-dimethoxy-2-nitrobenzyl (DMNB) photolabile protecting group 107

The following are notable examples of the DMNB **107** group's use *in vivo* and *in vitro*.

DMNB **107** caged lipids have been shown to be able to be assembled into liposomes and upon irradiation, carboxylic acids at the end of each lipid were released, this destabilised the liposome and caused the contents, a fluorescent dye, of the liposomes to escape.^{266, 267}

An α -haemolysin pore has been prepared with DMNB **107** protection on the interior wall *via* an oligo(ethylene glycol) linker. Upon irradiation a carbamic acid is released, which decarboxylates, producing a primary amine. The pH dependence of the reactions was explored by electrical detection at the single-molecule level, revealing rate constants for each step.²⁶⁸

Hydroxy groups on carbohydrates and oligonucleotides have been protected with the DMNB **107** group for the selective deprotection during their complex synthesis.^{269,}
²⁷⁰ Similarly, peptide synthesis has utilised this photolabile protecting group by attaching the DMNB **107** protected amino groups *via* an amino linker to a glass plate, allowing light-directed spatially resolved synthesis.²⁷¹

Kinase activity has been monitored by protecting known phosphorylation sites on Pho4 by genetically encoding DMNB-caged **107** serine on the protein. Once caged, Pho4 could not be exported from the cell, *Saccharomyces cerevisiae*. Additional green fluorescent protein labelling allowed real-time detection of the export of the protein, initiated by photoactivated deprotection and subsequent phosphorylation.²⁷²

Calcium concentrations in cells can be controlled with a DMNB-caged **107** inositol 1,4,5-triphosphate (InsP₃). InsP₃ causes the opening of calcium channels, releasing Ca²⁺ from the intracellular stores into the cytoplasm. The three phosphates of InsP₃ were esterified to allow transport into the cell, then esterases within the cell cleaved the esters. Irradiation of the DMNB-caged **107** InsP₃ released active InsP₃, in a controlled manner, dependent on irradiation time and pulses, causing an increase in Ca²⁺ in the cell.²⁷³

2.2.4. Choice of photolabile group for the NAC analogue 65 and the ACP analogue 64

The 4,5-dimethoxy-2-nitrobenzyl (DMNB) group **107** was chosen for protecting the new chain termination probes (ACP **64** and NAC-based **66**) reported in this thesis. The DMNB group **107** is the most widely studied photolabile group, and has already been used for many biological applications.^{266-268, 272, 273} This group has been

demonstrated in the literature to cleave steadily by irradiation with light of wavelengths between 350 and 370 nm,^{201, 274-279} both *in vitro*²⁷⁶ and *in vivo*.^{264, 280} This wavelength range is not protein damaging, and the by-product, *o*-nitrosobenzaldehyde,²⁶³ is non-toxic at low levels, which has allowed this protecting group to be used in a variety of biological organisms and for a range of purposes, including *in vivo*.

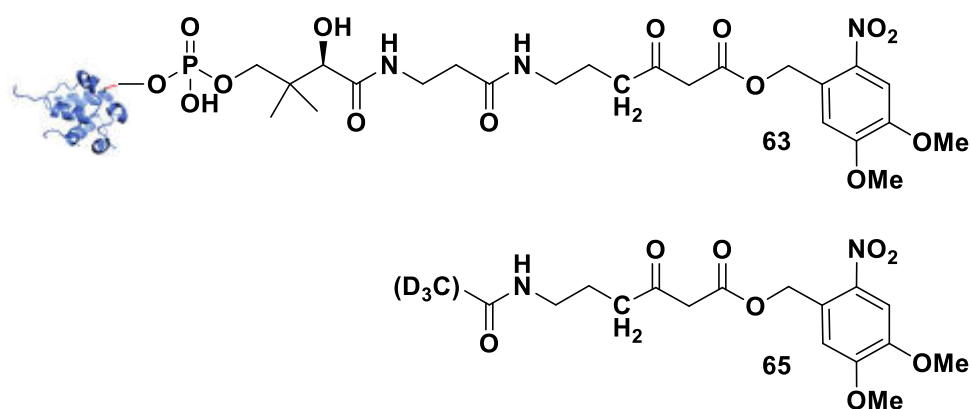
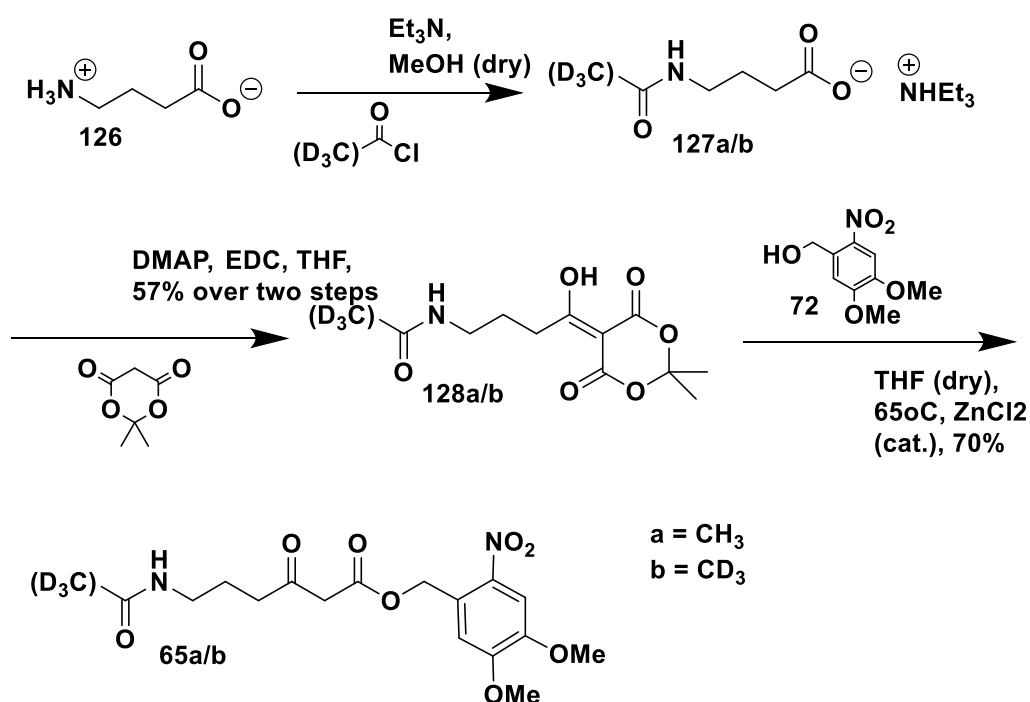


Figure 18 A comparison of the two probes synthesised in this work. **63** is the nonhydrolysable photolabile malonyl acyl carrier protein analogue, and **65** is the nonhydrolysable photolabile malonyl *N*-acetyl cysteamine analogue.

Šolomek, *et al.*, calculated quantum yields a small variety of compounds bearing the same photolabile group but presenting different leaving groups. They showed that esters had the lowest quantum yield compared to ethers and amines, believing the electro-withdrawing substituents on the oxygen reduced the efficiency.²⁶³ Despite this drawback, we envisaged that, amongst all the photolabile group discussed, DMNB **107** would still be the easiest to synthetically introduce in our molecules (Chapters 0 and 0) and also the most compatible with the wide range of experiments in mind. Therefore, it was adopted as a starting point for the generation of novel photolabile probes (**Figure 18**).

2.3. Probe synthesis

The route to synthesising the NAC probe **65** is distinctly shorter than the route to the synthesis of the ACP probe **63**. The synthesis of the *N*-Ac-based photolabile probe **65** was achieved in just three steps, with the first two following synthetic protocols previously established in the Tosin group.⁶ The first step involves the selective *N*-acetylation of GABA **126** with acetyl chloride, followed by the coupling of the resulting carboxylate **127** with Meldrum's acid. This reaction afforded product **128**, which was refluxed at 65°C and reacted with **72** to afford **65** (Scheme 16).

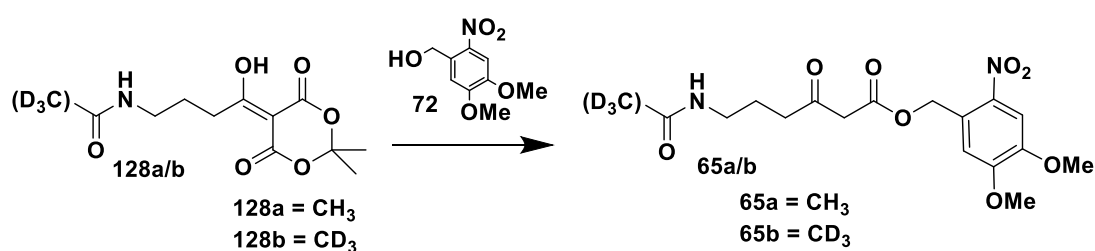


Scheme 16 Synthesis of a nonhydrolysable photolabile malonyl *N*-acetyl cysteamine analogue **65**.

A deuterium labelled probe **65b**, as a control, was also prepared by acetylating GABA **126** with d_3 -acetyl chloride, using the chemistry just described. A deuterium label could be incorporated into **65b** (Figure 18), to further confirm the assignments

of any trapped intermediates. The retention time of these species by HPLC or UPLC analyses is not affected, to a great extent²⁸¹, by this isotope labelling, but a mass shift of 3.018 Da, as well as no effect on the molecule's fragmentation pattern, allows for accurate assignment of intermediates off-loaded by the probes.

The first two steps and purification by flash chromatography did not require further optimising as these steps have been widely utilised for the preparation of a number of other *N*-acetyl cysteamine probes in our group.^{154, 155} However, the thermal degradation of **128** to allow it to react with the alcohol **72** required some optimisation, as it did for the synthesis of pantetheine analogue **61** (Table 2).



Conditions				Yield after purification
Temperature	Solvent	Catalyst	Reaction Time	
65°C	THF	none	3 hrs	41%
40°C	DCM	none	4 hrs	11%
65°C	THF	ZnCl ₂	2.5 hrs	70%

Table 2 Reaction conditions trialled for the synthesis of the nonhydrolysable photolabile malonyl *N*-acetyl cysteamine analogue **65** from **128**, shown. Yield shown is after purification by flash chromatography.

The outcome of this reaction has proven to vary depending on the rest of the molecule. Each reaction was left running until all the starting material had been consumed, and yields were calculated after purification. Refluxing in THF yielded 41% of NAC analogue **65**, but just 29% of pantetheine analogue **61** and required 24 hours refluxing to consume all of the starting material, compared to just 3 hours for

the synthesis of NAC analogue **65**. Reducing the temperature, by refluxing in DCM, decreased the yield of NAC analogue **65** to just 11% and increased the time for consumption of starting material **128**.

The addition of the catalyst, ZnCl_2 ,²⁸² proved beneficial to the synthesis of the NAC analogue **65**, increasing the yield to 70% and decreasing the reaction time by half an hour compared to in the presence of the catalyst. The addition of this catalyst for the synthesis of the pantetheine analogue **61** did dramatically reduce the reaction time, but the product yield dropped to just 5%. Increasing the temperature of reflux, by using toluene as the solvent, improved the yield of pantetheine analogue **61**, as well as reducing the reaction time to 8 hours. The addition of 3Å molecular sieves likely played a part in this increased yield.

There does appear to be a link between reaction time and yield for this reaction. It is likely that difficulty to maintain anhydrous conditions over long reaction times or product instability, may lead to reaction with water rather than the alcohol **72**, and generation of a decarboxylated product. Refluxing in toluene and the addition of 3Å molecular sieves was not tested for the synthesis of NAC analogue **65** as the yield of 70% was sufficient at that time, however, it is hypothesised that this would increase the yield further.

An efficient chemical synthesis of a nonhydrolysable photolabile malonyl *N*-acetyl cysteamine analogue **65** has been devised. The final yield was 40% over 3 steps, with the coupling to meldrum's acid, and the thermal degradation and reaction with the alcohol **72** being the weakest steps. Analogue **65** is the first photoactivatable nonhydrolysable malonyl NAC analogue to be synthesised, with a wide range of applications, beyond the scope of this thesis.

2.4 Preliminary photolysis experiments

The NAC **65**, CoA **62** and ACP **63** analogues bearing the DMNB photolabile group require exposure to light in order to be uncaged in their active forms.

Initially, LED light sources, handheld UVA lamps, and TLC plate viewers (equipped with 365 nm lamps) were employed to cleave the DMNB group, however, only starting material was evident by ESI-MS for these reactions over a variety of times up to six hours. A KiloArc light source was tested, but only up to 45 minutes as it was expected that sufficient photolysis would be achieved within that time for detection by ESI-MS (**Table 3**).

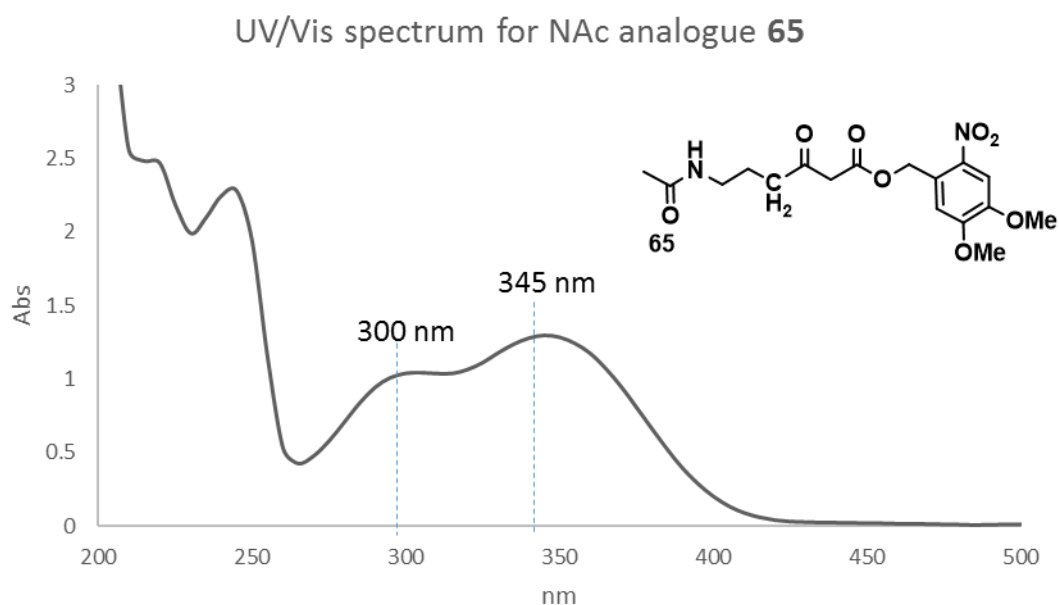
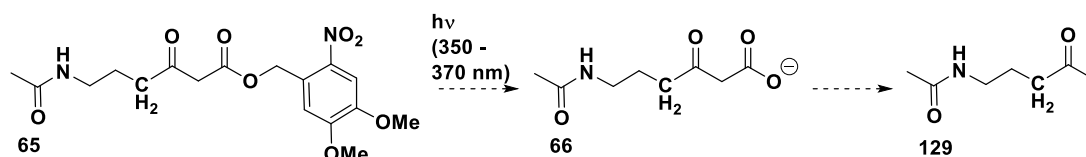


Figure 19 UV/Vis spectrum for the nonhydrolysable photolabile malonyl *N*-acetyl cysteamine probe **65**. Maximum absorptions are shown at 300 nm and 345 nm.



Test conditions for the photolysis of NAC analogue 65

Light Source	Concentration and Solvent/Media	Irradiation Time	Product detected?
UVA LED	73 mM in MeCN/H ₂ O	30 mins - 2hrs	N
Bench UVA lamp within a photoreactor oven	73 mM in MeCN/H ₂ O	30 mins - 2hrs	N
TLC Plate Viewer 365 nm	50 mM in MeCN/H ₂ O	15 mins - 6hrs	N
KiloArc Broadband Arc Lamp 800W, 365 nm	50 mM in MeCN/H ₂ O	15 mins	N
KiloArc Broadband Arc Lamp 1000W, 365 nm	50 mM in MeCN/H ₂ O	45 mins	N
KiloArc Broadband Arc Lamp 1000W, 345 nm	17 mM in MeCN/H ₂ O	5.5 hrs	N
Femtosecond laser 345 nm	17.4 mM in MeCN/H ₂ O	1 hr	N
Femtosecond laser 300 nm	17.4 mM in MeCN/H ₂ O	30 mins	N
Femtosecond laser 345 nm	17.4 mM in MeCN/H ₂ O plus 0.05M NaOH	30 mins	N
KiloArc Broadband Arc Lamp 1000W, 365 nm	17 mM in MeCN/H ₂ O adjusted to pH 10 with NaOH	2 hours	Y
UVA tube lights within a photoreactor oven	1 mM in DMSO	7 hrs	N
Femtosecond laser 365 nm	3 mM in MeCN/H ₂ O	1 hr	N
In-house built light box containing a circular 22W UVA	0.63 mM in MYM media	6 hrs	Y
In-house built light box containing a circular 22W UVA	1.6 mM in H ₂ O	4hrs	Y

Table 3 Conditions tested for the photolysis of a nonhydrolysable photolabile malonyl N-acetyl cysteamine probe **65**. Reaction shows generation of a decarboxylated N-acetyl cysteamine analogue **129**.

A UV/Vis spectrum was recorded for the NAC analogue **65**, showing two maximum absorptions at 300 nm and 345 nm (**Figure 19**). The results from this analysis led on

to trialling 345 nm with the KiloArc light source, however, after a much longer irradiation time of 5.5 hrs, still no product **66** or **129** could be detected.

The Stavros group at the University of Warwick were interested to test their powerful femtosecond pulsed laser to determine if photolysis of this compound could be achieved. 300, 345 and 365 nm wavelengths were tested with no detectable product: it was hypothesised that the femtosecond pulse lengths are too short for the photolysis to occur. The continuous light source, KiloArc™ Broadband Arc Lamp, 1000W, was trialled again for much longer irradiation times than previously, at 365 nm, and this finally provided the decarboxylated product **129** (**Table 3**).

There was little difference in photolysis yield after pH adjustments, however, the extra sodium present in the sample allowed for detection of the sodiated product **129** by MS. The sodiated product **129** appears to ionise more efficiently than the protonated, it is likely that part of the problem with the photolysis trials was the low ionisation efficiency of the protonated product **129** for detection by MS.

Once an adequate light source was found, it was necessary to determine how long to irradiate for to produce sufficient 'active' NAC probe **66**. It was found that the NAC analogue **65** is fully deprotected by 4 hours (**Figure 20**).

The rate of deprotection by photolysis are dependent on concentration; the higher the concentration the more effective the photolysis. This was demonstrated by comparing the relative intensities of NAC analogue **65** and decarboxylated product **129** after one hour of irradiation at 365 nm. The sample at 1 mM after one hour had approximately 50% conversion to the decarboxylated product **129**, whereas the sample at 0.1 mM had approximately 33% conversion (**Figure 21**)

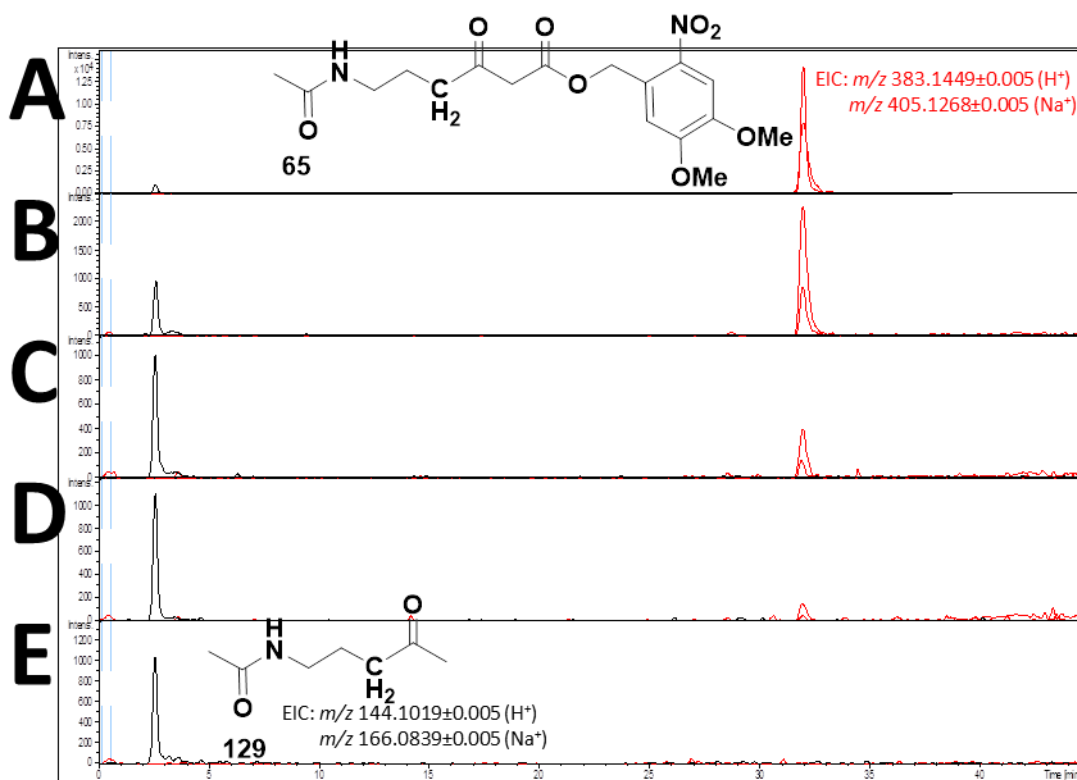


Figure 20 Irradiation of the nonhydrolysable photolabile NAC analogue **65** with 365 nm, 1000 W from 0 to 4 hours (A to E, hourly), showing the generation of decarboxylated product **129**. After 4 hours, no more NAC analogue **65** could be detected.

This rough estimate assumes identical ionisation efficiencies of the two compounds **65** and **129**, however the difference is sufficient to conclude that photolysis is faster at higher concentrations. This behaviour has previously been reported in the photolysis of polycyclic aromatic hydrocarbons^{283, 284} and can be explained by Beer-lambert law (**Equation 3**). For photolysis to occur, the compound needs to absorb light, and, as stated by Beer-lambert law, absorbance increases with concentration, thus more product would be generated at higher concentrations.

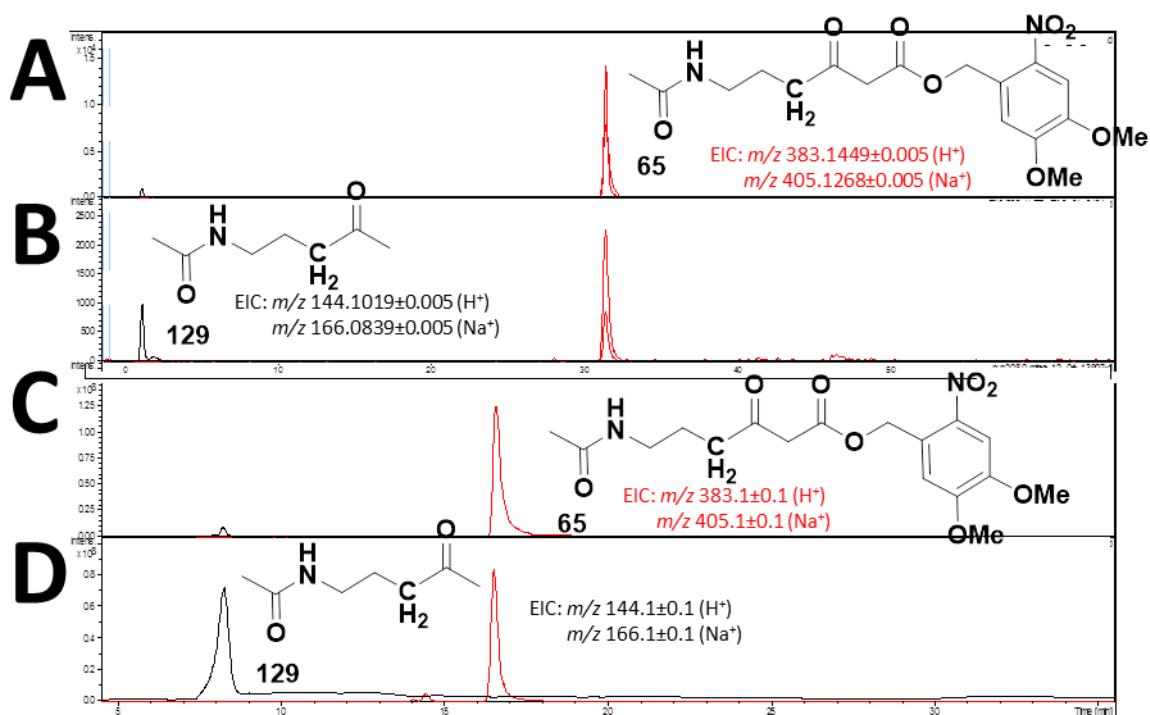


Figure 21 Irradiation of the nonhydrolysable photolabile NAC analogue **65** with 365 nm, 1000 W for 0 (A and C) and 1 (B and D) hours, at two different concentrations (0.1 mM (A and B) and 1 mM (C and D)), showing the increased photolysis yield of the decarboxylated product **129** at higher concentrations. Analyses A and B were analysed by UPLC-MS, and C and D were analysed by HPLC-MS, resulting in the different retention times.

$$A = \epsilon cl$$

Equation 3 Beer-lambert law. A is absorbance (no units). ϵ is molar extinction coefficient ($M^{-1} cm^{-1}$). c is concentration (M). l is path length (cm).

The KiloArc lamp was not a suitable light source for *in vivo* assays, due mainly to the larger sample volume required for such experiments, therefore a light source capable of holding larger volumes, and able to be placed within an Innova incubator was built in-house. The light source contained a circular UVA lamp, with an attachment in the centre of the lamp for either a 5 mL petri dish, or a 50 mL

Erlenmeyer flask to be irradiated from each side. The entire light source could be attached to the platform of an Innova incubator, and 180 rpm could be applied to the liquid cultures, and the contents could be kept at the appropriate temperature for continued growth of the cultures during irradiation experiments. Surprisingly, the probe **65** could be efficiently deprotected by the much weaker, 22W, UVA lamp (**Table 3**, also Section 4.3 and 4.2).

Once the conditions for the release of the probe **66** had been determined, the effect of the presence of biosynthetic enzymes, and also *in vivo* on the rate of photolysis was to be explored.

Chapter 3: Chemoenzymatic preparation of a carrier protein probe for the capture of polyketide intermediates

3. Chemoenzymatic preparation of a carrier protein probe **63** for the capture of polyketide intermediates

3.1. Probe rationale and design

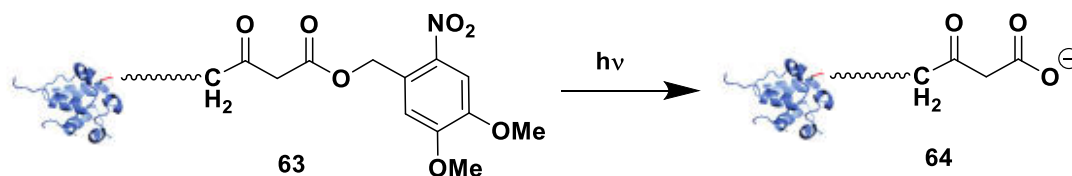
As previously described, mimics of the acyl carrier protein phosphopantetheinyl (PPant) arm, in the form of nonhydrolysable malonyl *N*-acetyl-cysteamine analogues, have proven successful as tools to chemically ‘trap’ biosynthetic intermediates.^{22, 136, 154, 155} It seemed plausible that altering the PPant arm attached to the acyl carrier protein (ACP), making it nonhydrolysable, would have the potential to off-load intermediates directly onto the acyl carrier protein.

The proposed ACP probe **64** would be a very close mimic to the ‘natural’ malonyl-ACP **7**, and is likely to interact more efficiently with the PKSs than the NAC analogues. Additionally, the ACP may stabilise the trapped intermediates more effectively than the small molecule chain terminators, allowing the off-loaded species to be detected in their natural structure, without cyclisation, for instance.

It has been shown that carba(dethia) analogues have been the most effective trapping agents, in comparison to oxa(dethia).^{11, 154} In particular, this comparison was demonstrated in the context of malonyl-CoA analogues,¹¹ as CoA represents the simplest form of malonyl/intermediate carrier that uses a PPant cofactor, it was decided to pursue the preparation of a malonyl carba(dethia) ACP **64** as a more advanced tool for the investigation of systems employing discrete carrier proteins (**Scheme 17**).

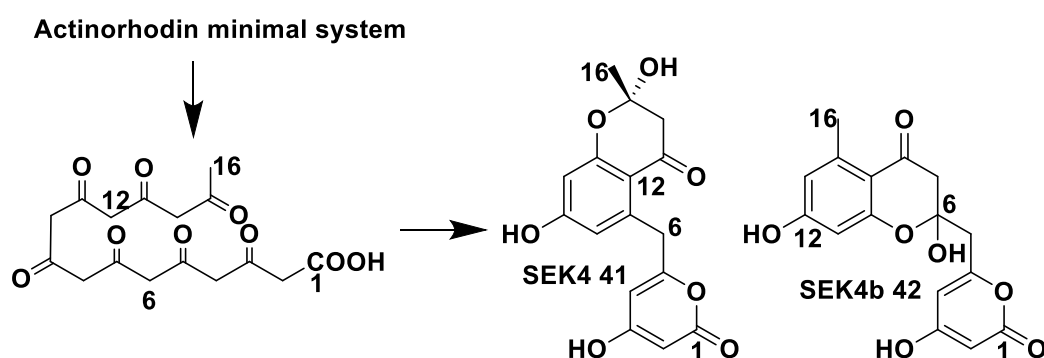
As in the case of the previous malonyl carba(dethia) analogues, the carboxylic acid group must be readily released *in situ*, to react with PKS-bound intermediates ahead of its complete decarboxylation. Previously a methyl ester²² protecting group was

employed for the protection and the use of small molecule probes *in vitro*, however, this requires an additional enzyme, for example pig liver esterase, to release the active probe. This approach has shown limitations in the optimal pH range for esterases (approximately pH 8) as most of the β -keto acid promptly decarboxylates.¹¹



Scheme 17 ‘Protected’ 4,5-dimethoxy-2-nitrobenzyl malonyl carba(dethia) ACP analogue **63** and its product after irradiation to the ‘active’ malonyl carba(dethia) ACP analogue **64**.

To remove the need for another enzyme within PKS assays and also to limit the fast and premature decarboxylation of the probe, a photolabile protecting group, 4,5-dimethoxy-2-nitrobenzyl (DMNB), removable in mild conditions, was chosen (**Scheme 17**). An in depth discussion on this particular protecting group choice will be given in section 2.2.



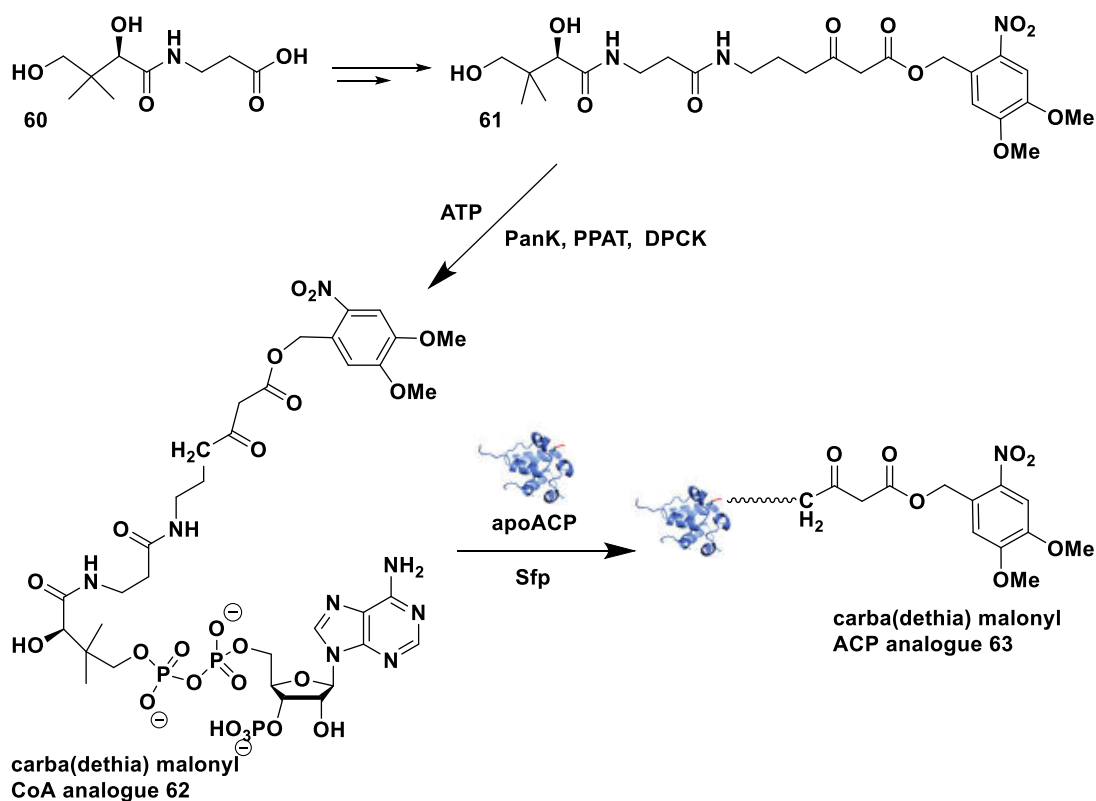
Scheme 18 Products of the actinorhodin minimal system, SEK4 **41** and SEK4b **42**, via the synthesis of an octaketide chain.

In this work, a well-studied^{13, 19, 76, 207, 208} model system for type II PKS biosynthesis, the actinorhodin (*act*) **2** minimal system, has been used to develop and probe this new intermediate capture methodology. The *act* ACP will be modified as **63** to investigate the generation of an octaketide intermediate chain, and its cyclisation to produce SEK4 **41** and SEK4b **42** (**Scheme 18**, Section 1.3.1).^{36, 208}

While working on this project, the Townsend group demonstrated that by loading a nonhydrolysable pantetheine analogue onto the acyl carrier protein, from the aflatoxin PKS (a type I iterative PKS from *Aspergillus parasiticus*), a diketide intermediate could be captured by the ACP.²⁰⁹ They had not protected the malonyl group on the ACP analogue in their assays, and therefore the actual concentration of malonyl carba(dethia) pantetheine present on the ACP was very low. Nonetheless, they had been successful in offloading an early stage polyketide intermediate.²⁰⁹ We then envisaged that photoactivatable acyl carrier proteins such as **63** would hold the promise of being a more effective trapping agent due to the possibility of uncaging *in situ* in mild conditions.

3.2. Preparation of a carrier protein probe

In order to prepare the *act* ACP photolabile probe **63** a pantetheine derivative **61** had to be chemically synthesised, which could then be converted to the corresponding CoA analogue **62** utilising the enzymes pantothenate kinase (PanK), phosphopantetheine adenylyltransferase (PPAT) and dephosphocoenzyme A kinase (DPCK),¹⁰¹ and that, from the CoA analogue **62**, could be transferred to the *apo act* ACP **44** using the phosphopantetheinyl transferase, Sfp (**Scheme 19**).^{99, 100, 210}

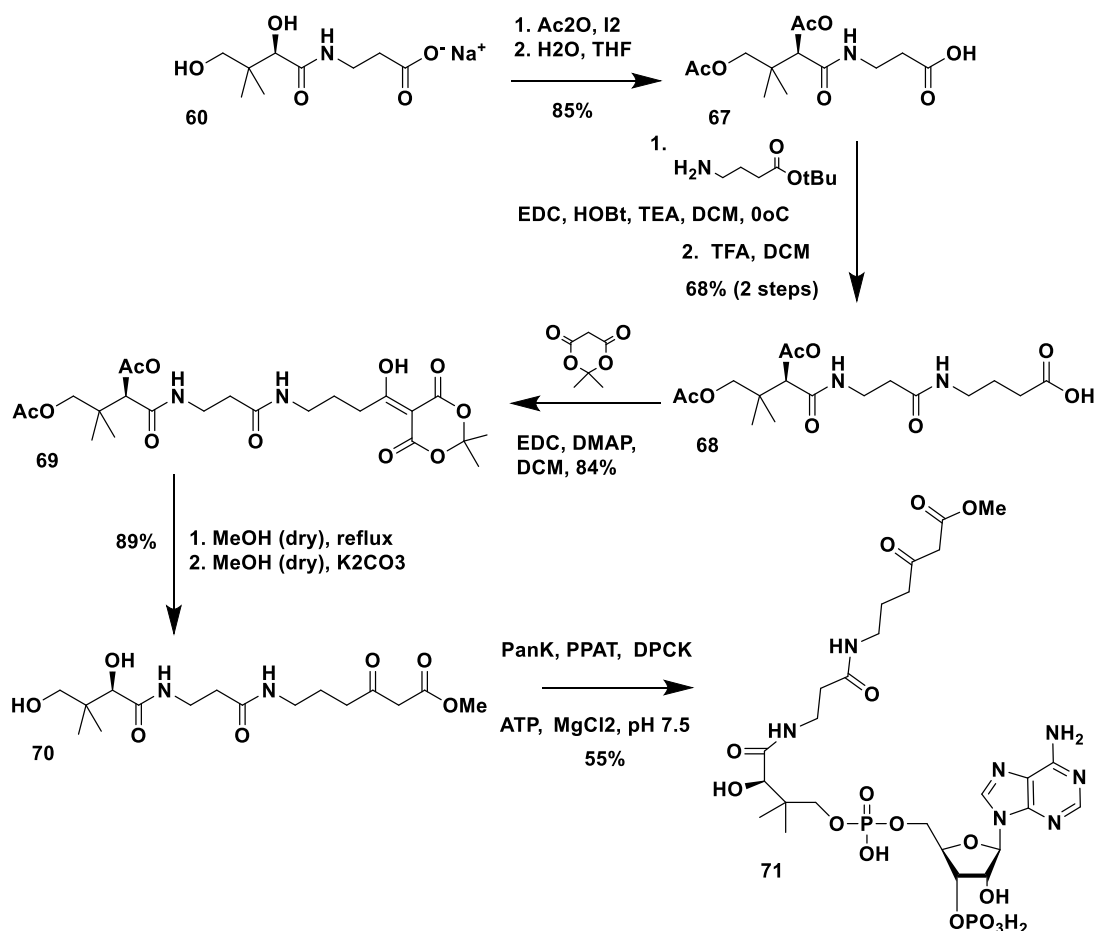


Scheme 19 Overview of the planned chemoenzymatic synthesis of a nonhydrolysable photolabile malonyl acyl carrier protein **63** from pantothenic acid **60**.

3.2.1. Synthesis of the 4,5-dimethoxy-2-nitrobenzyl malonyl carba(dethia) pantetheine **61**

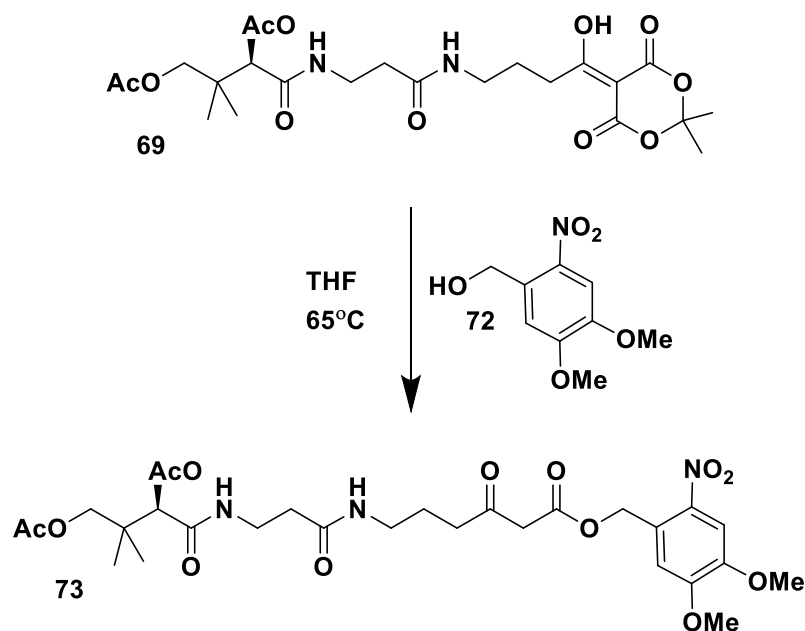
3.2.1.1. Synthesis via acetyl protection of the pantetheine diol moiety

The initial route undertaken for synthesising a nonhydrolysable pantetheine analogue **61** was based on a previously published route to synthesise a methyl ester protected malonyl carba(dethia) coenzyme A **71** (Scheme 20).¹¹ This route was first trialled during research for my Masters project, and further investigated for this PhD project.



Scheme 20 Previous preparation of a nonhydrolysable malonyl carba(dethia) coenzyme A analogue **71** by Tosin and co-workers.¹¹ PanK=Pantothenate kinase, PPAT=phosphopantetheine adenylyltransferase, and DPCK=dephosphocoenzyme A kinase.

Compound **69** was provided by Dr Manuela Tosin. This compound was reacted with 4,5-dimethoxy-2-nitrobenzyl alcohol **72** under reflux, in order to provide **73** (Scheme 21). Difficulties were encountered during the deprotection of the acetyl groups in **73** towards the desired compound **61**. The DMNB ester proved sensitive to both acidic and basic conditions; despite a range of mild methods for acetyl deprotection (chemical and enzymatic) none of them succeeded in generating **61** in good yield. Therefore, a new way of protecting the diol moiety of pantothenic acid **60** had to be envisaged.



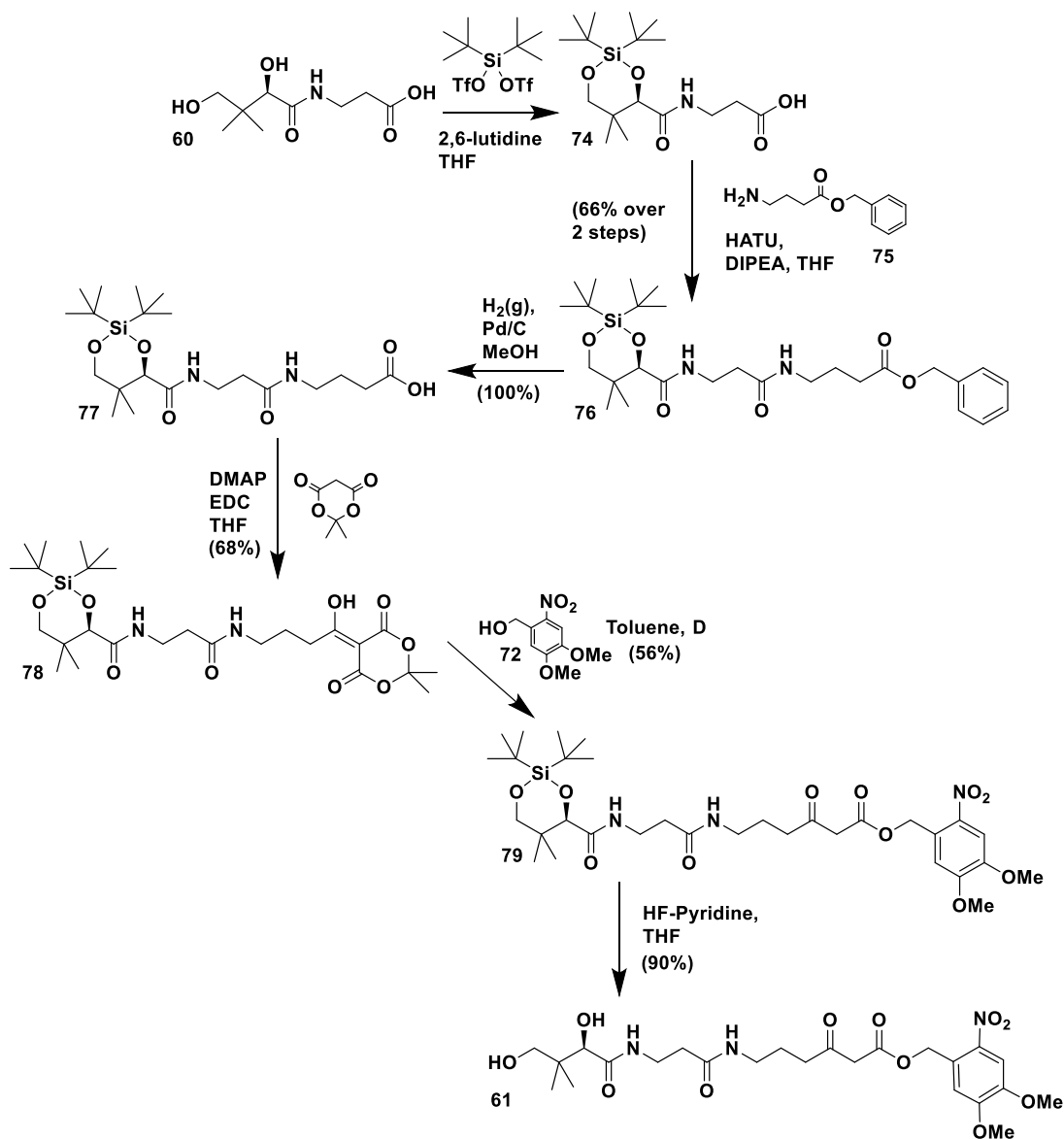
Scheme 21 Synthesis of a nonhydrolysable 4,5-dimethoxy-2-nitrobenzyl malonyl carba(dethia) pantetheine analogue with acetyl protection of the diol **73**.

3.2.1.2. Synthesis via di-tert-butylsilyl protection of the pantetheine 41 diol moiety

By considering the literature available on diol protecting groups, we envisaged that a silyl protecting group could be a good choice for pantetheine substrates; silyl groups are easy to introduce and can be selectively removed in the late stages of complex and multigram scale synthesis *via* mild fluoride ion donors. In particular, a 2,4-*O*-di-tert-butylsilylene (TBS) group,²¹¹⁻²¹³ was chosen for its stability and for its ability to protect both the primary and secondary alcohols of pantothenic acid **60** simultaneously (**Scheme 22**).

D-pantothenic acid **60** was then protected with a 2,4-*O*-di-tert-butylsilylene (TBS) group to afford the crude pantothenic acid **74**, which was directly used in the next step. Amide coupling of **74** to the γ -aminobutyric acid (GABA) benzyl ester **75** was

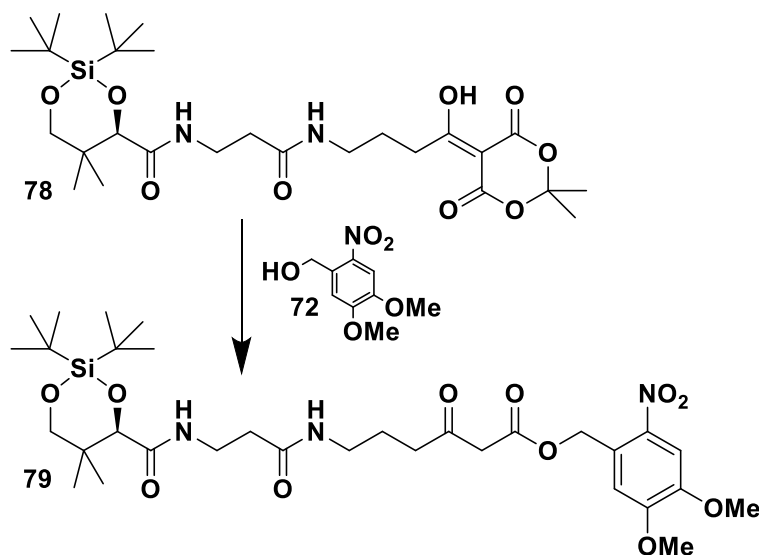
carried out with *N,N,N',N'*-Tetramethyl-O-(7-azabenzotriazol-1-yl)uronium hexafluorophosphate (HATU) to afford **76** (66% yield over the two steps, and after flash chromatography purification).



Scheme 22 Final synthesis of a nonhydrolysable 4,5-dimethoxy-2-nitrobenzyl malonyl carba(dethia) pantetheine analogue **61**.

Hydrogenolysis of **76** with palladium on carbon was carried out next to remove the benzyl ester. It was observed that the yield of this reaction can be significantly affected by substrate concentration and reaction scale.

The resulting carboxylate **77** was coupled to Meldrum's acid with the aid of 1-ethyl-3-(3-dimethylaminopropyl) carbodiimide) (EDC) to yield **78** in 68% after column chromatography.



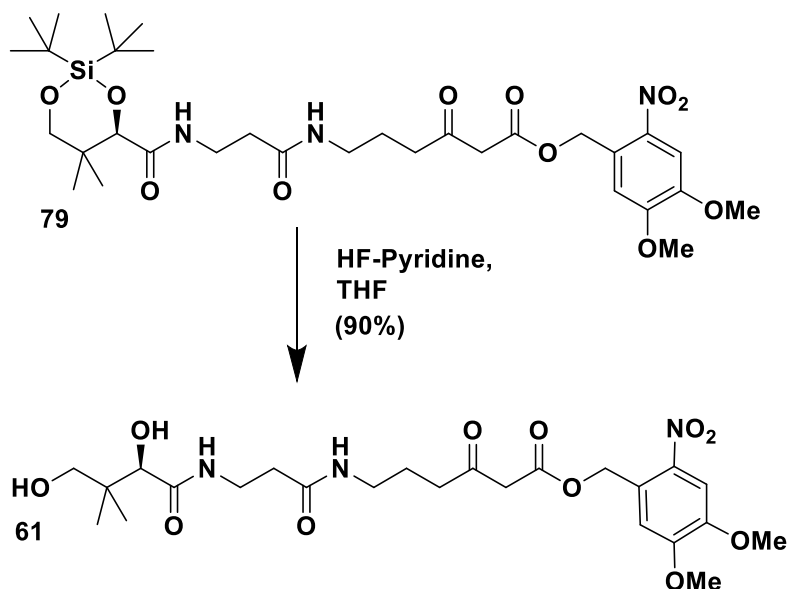
Conditions

Temperature	Solvent	Other	Reaction Time	Yield
65°C	THF	none	24 hrs	29%
65°C	THF	ZnCl ₂ (catalyst)	11.5 hrs	5%
65°C	THF	DMAP	30 hrs	26%
100°C	Toluene	3Å molecular sieves	8 hrs	56%

Table 4 Reaction conditions trialled for the synthesis of **79** from **78**, shown. Yields shown after purification by flash chromatography.

78 was refluxed at 100°C in toluene in the presence of 4,5-dimethoxy-2-nitrobenzyl alcohol **72** for conversion to **61**. This step requires strict anhydrous conditions in order to avoid the nucleophilic attack of water and decarboxylation of the resulting

β -keto acid. Limiting the reaction time to just 8 hours, refluxing at a high temperature in toluene, rather than THF, and the addition of 3Å molecular sieves to the reaction resulted in the best yield of 56% (**Table 4**).



Reagent	Conditions				
	Temperature	Solvent	Equivalents of Reagent	Reaction Time	Yield
TBAF	RT	THF	5 eq	24 hours	traces, unpurified
Fluoride on polymer support	RT	MeOH	2 eq	24 hours	0%
Fluoride on polymer support	RT	MeOH	5 eq	24 hours	0%
Fluoride on polymer support	RT	MeOH	10 eq	24 hours	0%
HF-pyridine	RT	THF	5 eq	2 mins	90%

Table 5 Reaction conditions trialled for the deprotection **79**. Yields given were calculated after HPLC purification.

A range of fluoride ion donors were tested for the diol selective deprotection of **79**. The use of fluoride for desilylation is very common as the Si-F bond is very strong and selective.^{214, 215}

Fluoride on polymer support²¹⁶ and tetrabutylammonium fluoride (TBAF)²¹⁷ were trialled, over long reaction times and different amounts, to no success, only starting material **79** remained (**Table 5**). Eventually, the use of hydrogen fluoride-pyridine (HF·pyr) complex²¹⁸ afforded the desired product in quantitative yield (**Table 5**).

The overall yield of **61**, from D-pantothenic acid **60**, was approximately 23% over six steps on a gram scale. This was overall satisfactory, although weak steps (**74** to **75**, **77** to **78** and **78** to **79**) could be improved.

An efficient chemical preparation of 4,5-dimethoxy-2-nitrobenzyl malonyl carba(dethia) pantetheine **61** has been devised. This pantetheine analogue **61** is an important analogue in its own right, however, for this project the compound was used to prepare **62** and **63**, and also for mass spectrometry studies.

The synthesis of coenzyme A (CoA) **46** from pantetheine **48** is possible *in vitro* utilising three enzymes, a pantothenate kinase (PanK), a phosphopantetheine adenylyltransferase (PPAT) and a dephosphocoenzyme A kinase (DPCK).¹⁰¹ PanK acts first to phosphorylate the primary alcohol of pantetheine **48**, then PPAT adenylates 4'-phosphopantetheine, and lastly DPCK phosphorylates to generate CoA.

PanK, PPAT and DPCK from *E. coli* have been shown to accept a wide variety of pantetheine derivatives, including those bearing bulky chemical groups.^{219, 220} These enzymes can be overexpressed, in *E. coli*, as His-tagged proteins, allowing for simple purification.¹⁰¹

The chemical synthesis of CoA derivatives was considered, however, due to the large number of potential steps towards a final CoA derivative with a likely low yield, it was decided to pursue a chemoenzymatic preparation.

Each of the three enzymes (for which plasmids were available in the Tosin laboratory) were overexpressed in *E. coli*; in hexahistidine-tagged form for bench-top Ni-NTA purification, as previously reported.¹⁰¹ Successful expression and purification were verified by SDS-PAGE (**Figure 22**).

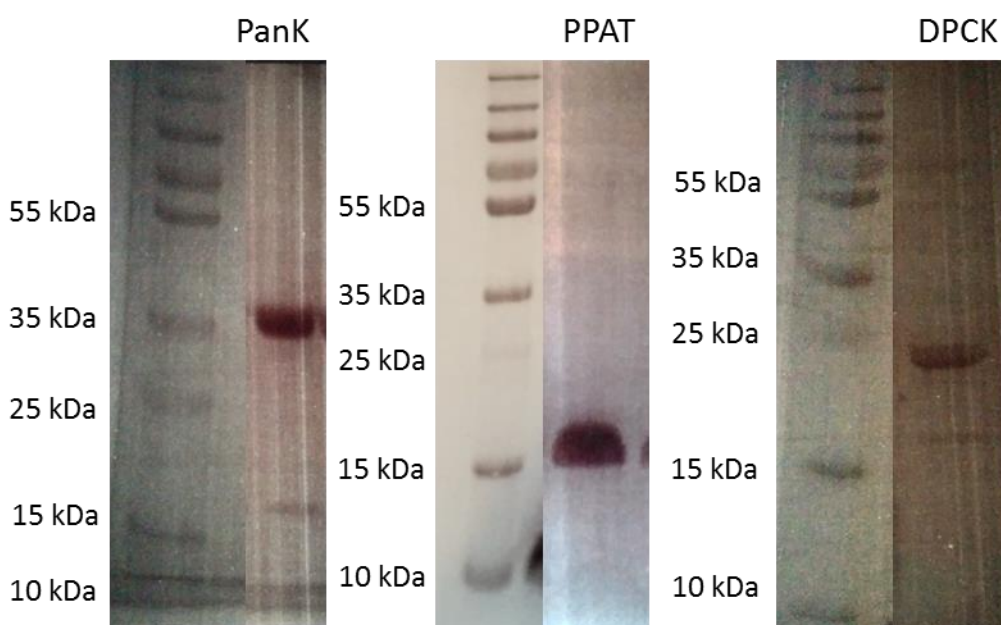
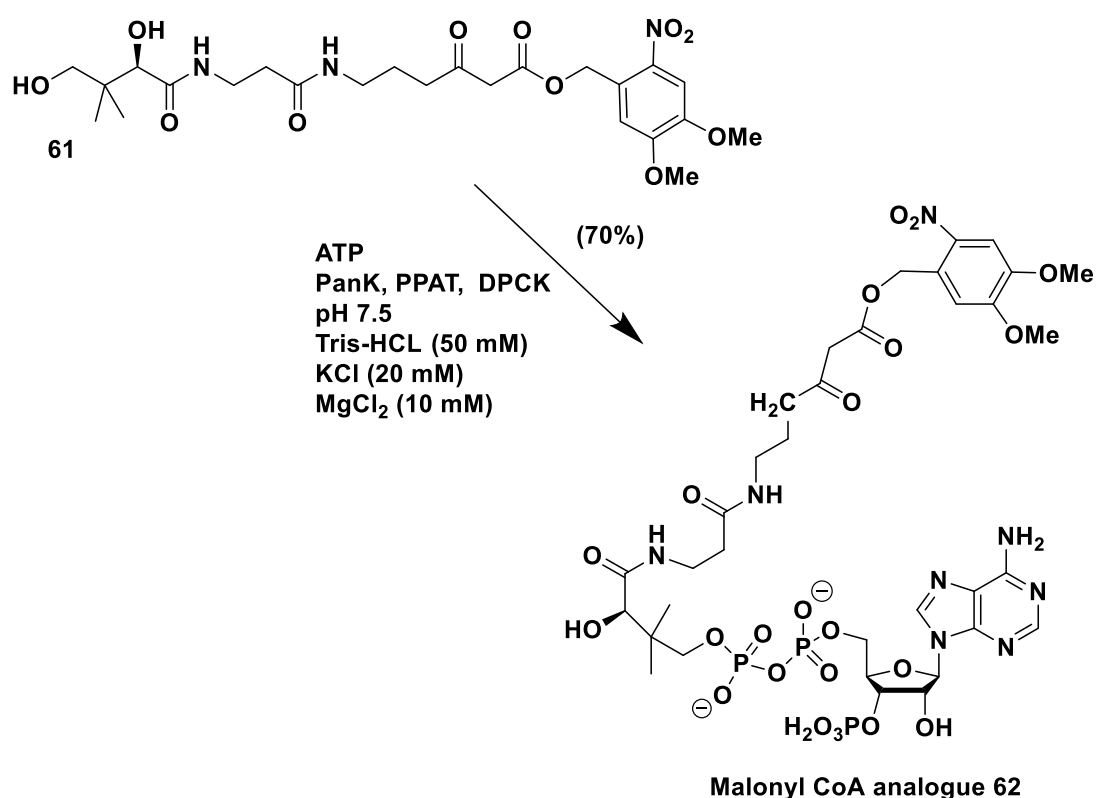


Figure 22 SDS-PAGE results showing expression of the Pantothenate Kinase (*PanK* or *CoaA*)²²¹ (~38 kDa), the phosphopantetheine adenylyltransferase (*PPAT* or *CoaD*)²²² (~19 kDa) and the dephosphocoenzyme A kinase (*DPCK* or *CoaE*)²²³ (~24 kDa) from *E. coli*.

The activity of the enzymes was preliminarily tested with pantetheine **48** as the starting material, as previously reported and carried out in my Master thesis.²²⁴

The 4,5-dimethoxy-2-nitrobenzyl malonyl carba(dethia) pantetheine **61** was incubated with PanK, PPAT and DPCK, in the presence of ATP at room temperature

and overnight (**Scheme 23**). The reaction outcome was analysed by LC-MS, which showed the formation of **62**, but also the presence of unreacted intermediates in the pathway. In particular, it is known that the last enzymatic step catalysed by DPCK is inhibited by the product itself. Therefore, it was necessary to use additional enzyme amounts to achieve full conversion of **61** to **62**. After initial small scale trials, the enzymatic preparation of **62** was scaled up to 15 mg and the crude product purified by HPLC. NMR analyses confirmed the coenzyme A nature of the product, and the presence of the DMNB group as protection of the carboxylate. The overall yield of this enzymatic one-pot preparation was 70% after HPLC purification.



Scheme 23 Enzymatic synthesis of a nonhydrolysable 4,5-dimethoxy-2-nitrobenzyl malonyl carba(dethia) coenzyme A analogue **62** from a corresponding, chemically synthesised, pantetheine analogue **61**. Yield is shown after HPLC purification. PanK = Pantothenate kinase, PPAT = phosphopantotheine adenylyltransferase, and DPCK = dephosphocoenzyme A kinase.

The coenzyme A analogue **62**, is already itself an important compound that can be directly used for the investigation of type III polyketide synthases (out of the scope of this work). **62** was herein used to prepare chemically modified *holo*-acyl carrier proteins for assaying type II PKS biosynthetic pathways.

3.2.2. Enzymatic preparation of a 4,5-dimethoxy-2-nitrobenzyl malonyl carba(dethia) acyl carrier protein

Acyl carrier proteins (ACPs) bear a 4'-phosphopantotheinyl (PPant) chain at the active site serine which facilitates interaction with other domains within a polyketide synthase. Phosphopantetheinyl transferase enzymes catalyse the transfer of PPant cofactors from coenzyme A (CoA) **46** to *apo*-ACPs **44**, *in vitro* and *in vivo*.^{99, 121, 225}

A phosphopantetheinyl transferase from *B. subtilis*, Sfp, presents broad substrate specificity and is widely used for the preparation of modified carrier proteins.⁹⁹ The enzyme was overexpressed in *E. coli* in an hexahistidine-tagged form and purified by Ni-NTA chromatography (**Figure 23**).

The *apo act* ACP **44** (plasmid gift from Dr Hui Hong, University of Cambridge) was also similarly expressed and purified (**Figure 23**).

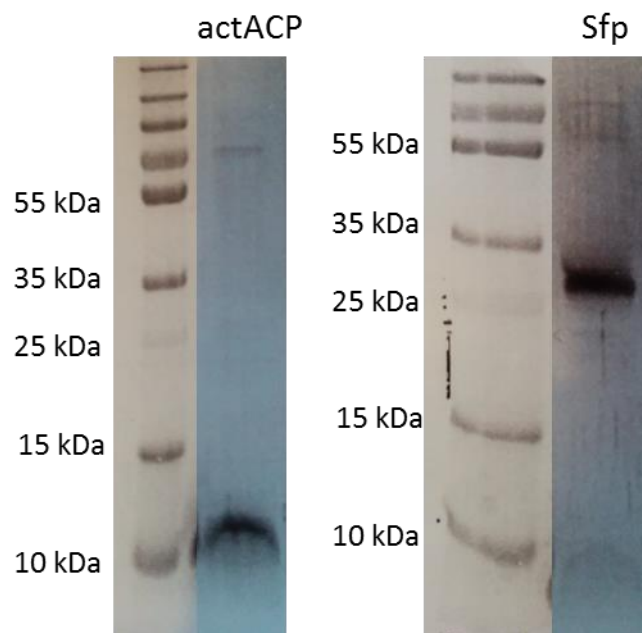
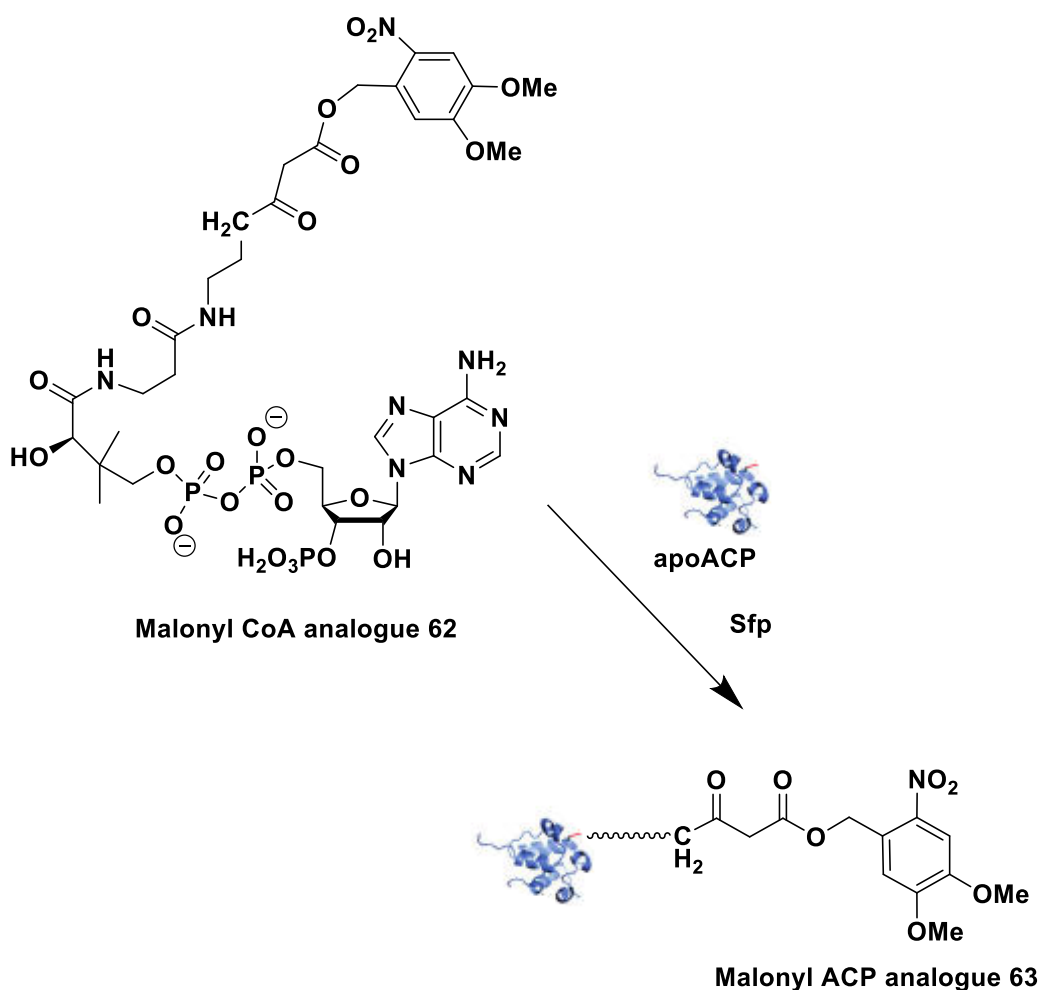


Figure 23 SDS-PAGE analyses showing expression of the apo acyl carrier protein **44** (~11 kDa) from the actinorhodin minimal system, and the phosphopantetheinyl transferase, *Sfp*, (~28 kDa) from *B. subtilis*.

The activity of both *apo act ACP 44* and *Sfp* was tested with commercially available coenzyme A **46**. Complete conversion of *apo 44* to *holo act ACP 43* was shown by LC-MS (**Figure 24**). The same conditions were used for the CoA analogue **62** as substrate: the photolabile malonyl carba(dethia) act ACP **63** was obtained (**Scheme 24, Figure 24**).



Scheme 24 Enzymatic preparation of a nonhydrolysable 4,5-dimethoxy-2-nitrobenzyl malonyl carba(dethia) acyl carrier protein analogue **63** from the corresponding chemoenzymatically synthesised coenzyme A analogue **62**. apo-ACP = apo-acyl carrier protein **44**, Sfp = phosphopantetheinyl transferase from *B. subtilis*, CoA = coenzyme A **46**.

The modified act ACP **63** was characterised by mass spectrometry, including fragmentation by collisionally activated dissociation (CAD) (**Figure 24**). This method of fragmentation is known to preferentially cleave phosphodiester bonds, and it has previously been exploited as a reliable method to characterise PPant modifications of acyl carrier proteins (**Scheme 13**).

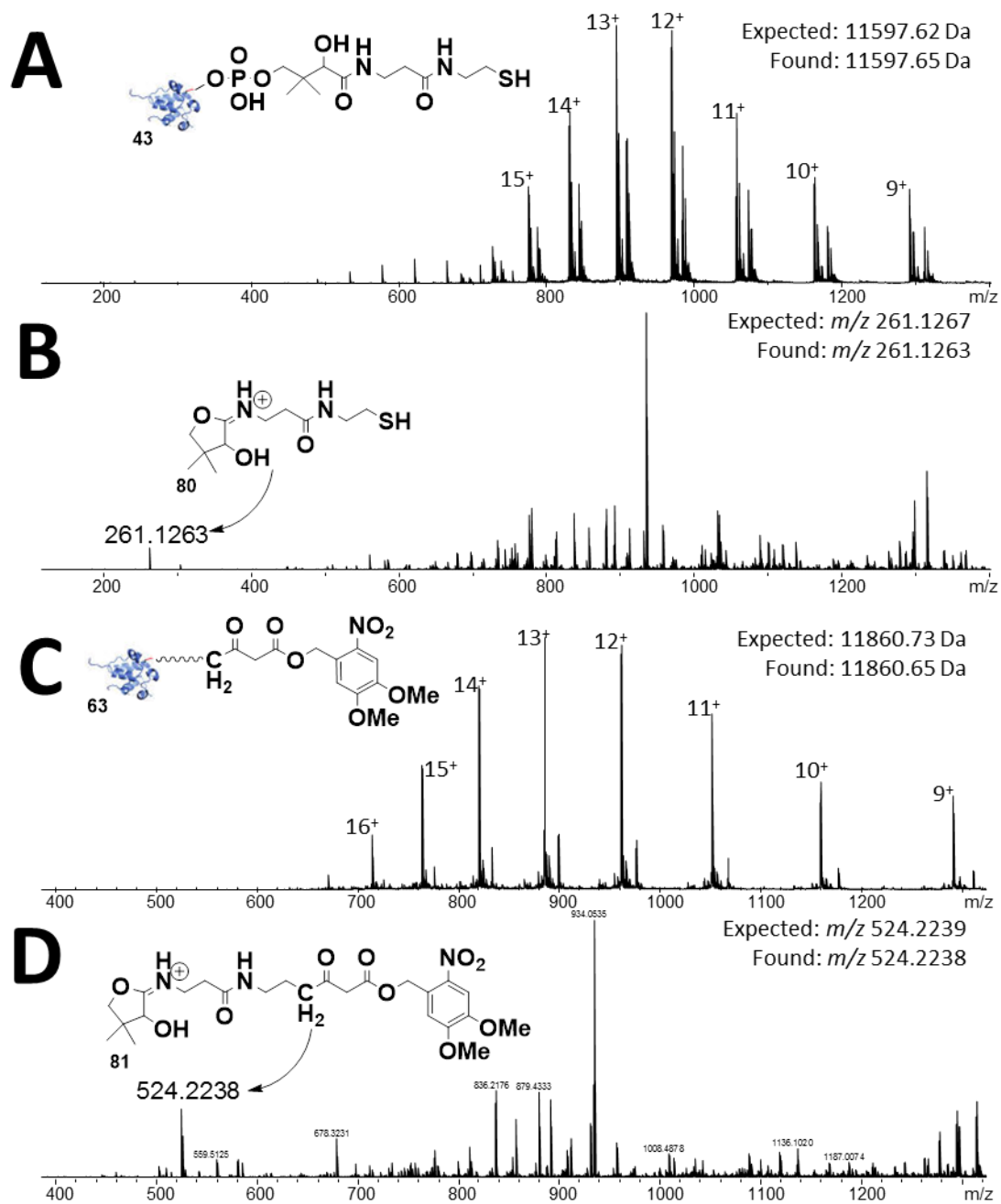


Figure 24 A: (Parent) mass spectrum of (hexahistidine-tagged) holo-acyl carrier protein (ACP) **43** from the actinorhodin minimal system. B: Collisionally activated dissociation (CAD) of the 12^+ parent ion of holo-ACP **43**, generating a singly charged, characteristic, pantetheine ion **80**. C: (Parent) mass spectrum of 4,5-dimethoxy-2-nitrobenzyl (DMNB) malonyl carba(dethia) ACP analogue. ACP is from the actinorhodin minimal system. D: CAD of the 12^+ parent ion of DMNB malonyl carba(dethia) ACP analogue, generating a singly charged, characteristic, pantetheine ion **81**.

Although not demonstrated within this project, we view that it is now possible to load acyl carrier proteins from different biosynthetic pathways with the new photolabile PPant arm. For instance, the Tosin group has already begun to explore the use of this tool in the investigation of saturated and polyunsaturated fatty acid assembly. In Chapter 5.2 of this thesis, the validation of **63** for the investigation of the actinorhodin **2** type II PKS will be presented.

Chapter 4: Trapping of polyketide intermediates *in vivo* and *in vitro* with the aid of a photolabile malonyl *N*-acetyl cysteamine analogue

4. Trapping of polyketide intermediates *in vivo* and *in vitro* with the aid of a photolabile malonyl *N*-acetyl cysteamine analogue **65**

4.1. *In vitro* trapping of intermediates from the actinorhodin minimal system with the nonhydrolysable photolabile NAC probe **65**

4.1.1. Analysis by LC-MS

The established irradiation conditions for the uncaging of the nonhydrolysable photolabile NAC probe **65** were applied in the study of the actinorhodin minimal system generating the polyketides SEK4 **41** and SEK4b **42** *in vitro* (Chapter 1.3). These products have identical molecular formulae hence mass, however SEK4 **41** presents a shorter retention time by RP-LC than SEK4b **42** (Figure 25).³⁶

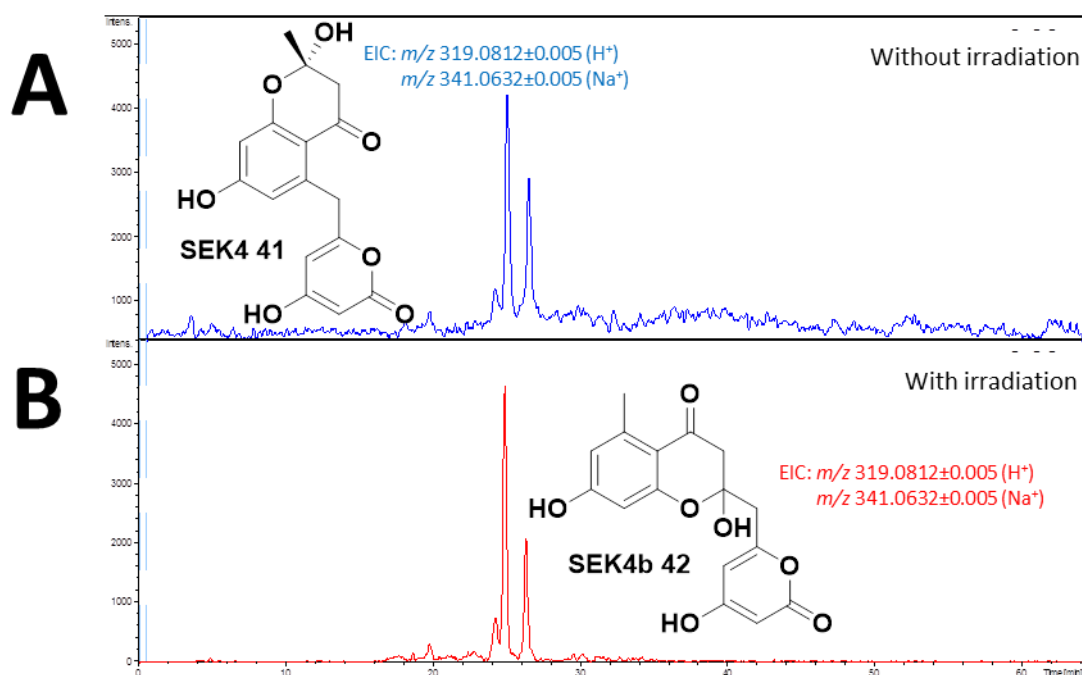


Figure 25 LC-MS chromatogram showing the protonated and sodiated EIC for the isomers SEK4 **41** and SEK4b **42** produced by the actinorhodin minimal system. Peak assignments of SEK4/4b **41/42** based on Fu, et al., 1994.³⁶ A) Production of shunt metabolites, SEK4/4b **41/42**, by the actinorhodin minimal system. B) Production of SEK4/4b **41/42** by the actinorhodin minimal system following photolysis for 2 hours at 365 nm, 1000W.

The ability of the minimal system to produce SEK4/4b **41/42** under the irradiation conditions was established by comparison of the yield of identical assays with and without 2 hours of irradiation. This irradiation time was selected as a significant amount of shunt products can be generated by the type II PKS within this time.^{13, 76, 207, 285} The yields of the two shunt products were shown to be unchanged (**Figure 25**).

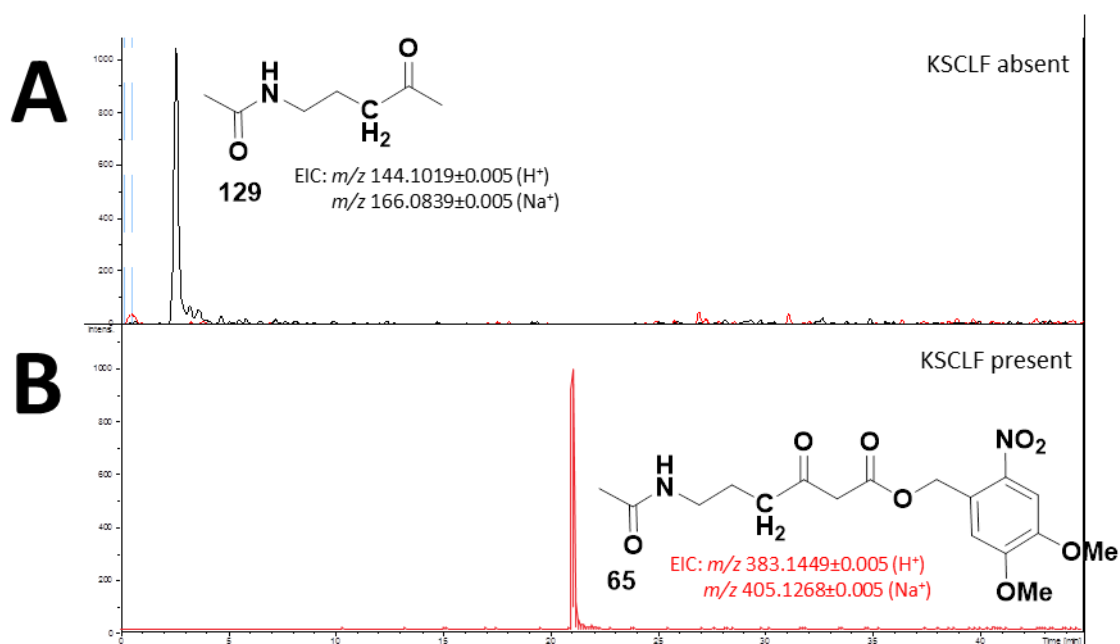


Figure 26 LC-MS chromatograms showing the photolysis of the DMNB NAC analogue **65** to **129** in the absence (A) and in the presence of the ketosynthase and chain length factor from the actinorhodin minimal system (B) with 365 nm, 1000W for 4 hours.

Following these results, the yield of photolysis of the NAC analogue **65** with the ketosynthase and chain length factor (KS-CLF) of the actinorhodin minimal system was compared. Identical assays were set up, and after 4 hours of irradiation, or bench top incubation for the control, the samples were compared by LC-MS following extraction. Unfortunately, the yield of photolysis is substantially affected by the presence of KS-CLF, being almost null (**Figure 26**). This is likely due to the

NAC analogue **65** diffusing within the KS-CLF which protects **65** from photolysis. Based on this evidence, it was decided that the NAC probe **65**, and therefore likely the ACP probe **65** as well, would be irradiated prior to incubation with the minimal system.

Results showed that almost 50% of active probe **66** is released within 10 minutes of irradiation of the protected probe **65**, and that the decarboxylated product **129** is not the major product, even after 5 hours of irradiation (**Figure 27**).

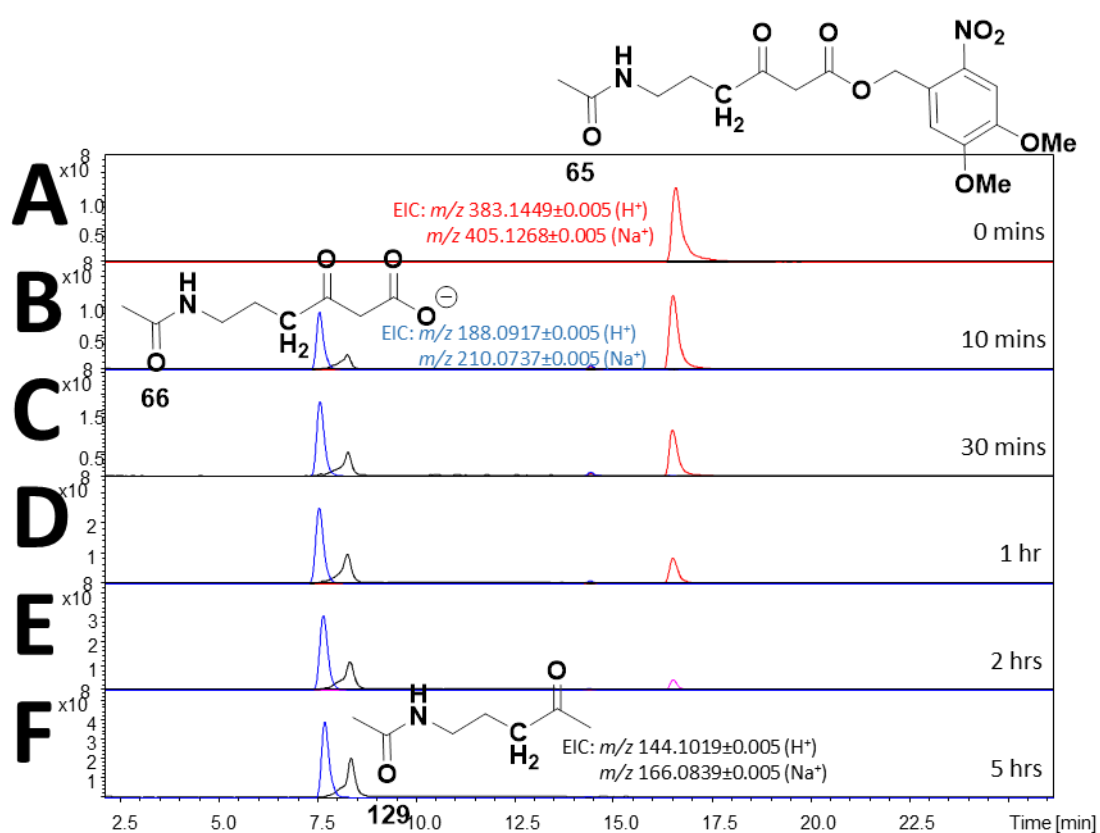


Figure 27 Irradiation of the nonhydrolysable photolabile NAC analogue **65** with 365 nm, 1000 W for 0 mins (A), 10 mins (B), 30 mins (C), 1 hour (D), 2 hours (E) and 5 hours (F), showing the release of the active probe **66** after just 10 mins, and its stability after 5 hours. Also shown is the slow decarboxylation to **129**. Samples were stored in dry ice and defrosted just before analysis by HPLC-MS on the same day.

A light box was designed and specifically built for this project at the University of Warwick by Mr Rod Wesson of our in-house electrical workshop. The light box is fitted with a 22W circular UVA lamp (Actinic BL TL-E 22W/10 1CT), cooling fans, an interchangeable mount for a 50 mL Erlenmeyer flask or a 5 mL petri dish, and the ability to fix the box within an Eppendorf Innova incubator shaker. Photolysis yields were not expected to be much greater than with the handheld UVA lamps already tested, however, after 4 hours of irradiation approximately 75% of decarboxylated product **129** is produced.

Following these preliminary experiments, the protected probe **65** was irradiated for 4 hours and then added to the actinorhodin minimal system.^{13, 76} Each sample was extracted into EtOAc and then analysed by UPLC-MS. pH adjustment to approximately 4 proved critical for the extraction of SEK4 **41** and SEK4b **42** with EtOAc. Predictions for the potential trapped intermediates are based upon the two different cyclisations observed in the octaketide shunt products, SEK4 **41** and SEK4b **42**. The data were analysed for these compounds, but unfortunately no intermediates were detected.

Additionally, varying the ratio of *holo*-ACP **43** to active probe **66** was explored. It has been previously shown that this ratio can be important for trapping intermediates with other nonhydrolysable NAC probes *in vitro*.^{11, 153} For example, when probing the biosynthetic pathway of resveratrol **4** with a nonhydrolysable malonyl carba(dethia) analogue, it was found that a ratio of 3:4, malonyl-CoA analogue:malonyl-CoA **15**, is the most effective.¹¹

The ratios 10:1, 5:1, 1:1, 1:5 and 1:10 of *holo*-ACP **43** to active probe **66** were tested in duplicate copy experiments, however none of these experiments result in any detectable intermediates.

4.1.2. Effect of delayed addition of active NAC probe 66 to the actinorhodin minimal system on SEK4/4b 41/42 production

A series of additional experiments were set up to observe the effect of timing of the addition of the active probe **66** on SEK4/4b **41/42** production. This was carried out by activating the minimal system, and subsequently adding the active probe **66** at set time points. Each assay was left overnight at room temperature, and then extracted with EtOAc, and SEK4/4b **41/42** were detected by LC-MS (Figure 28). Adding *holo*-ACP **43** and active probe **66** at the same time, a time delay of 0, would have introduced a significant error, so this was not attempted.

There was an observation of a decrease in SEK4/4b **41/42** production the longer the time delay between activation of the minimal system and addition of the NAC probe **66**. It was expected that SEK4/4b **41/42** production would be most affected by the addition of the active probe **66** at early time points, however, results showed that SEK4/4b **41/42** production was reduced by longer delays. (**Figure 28**).

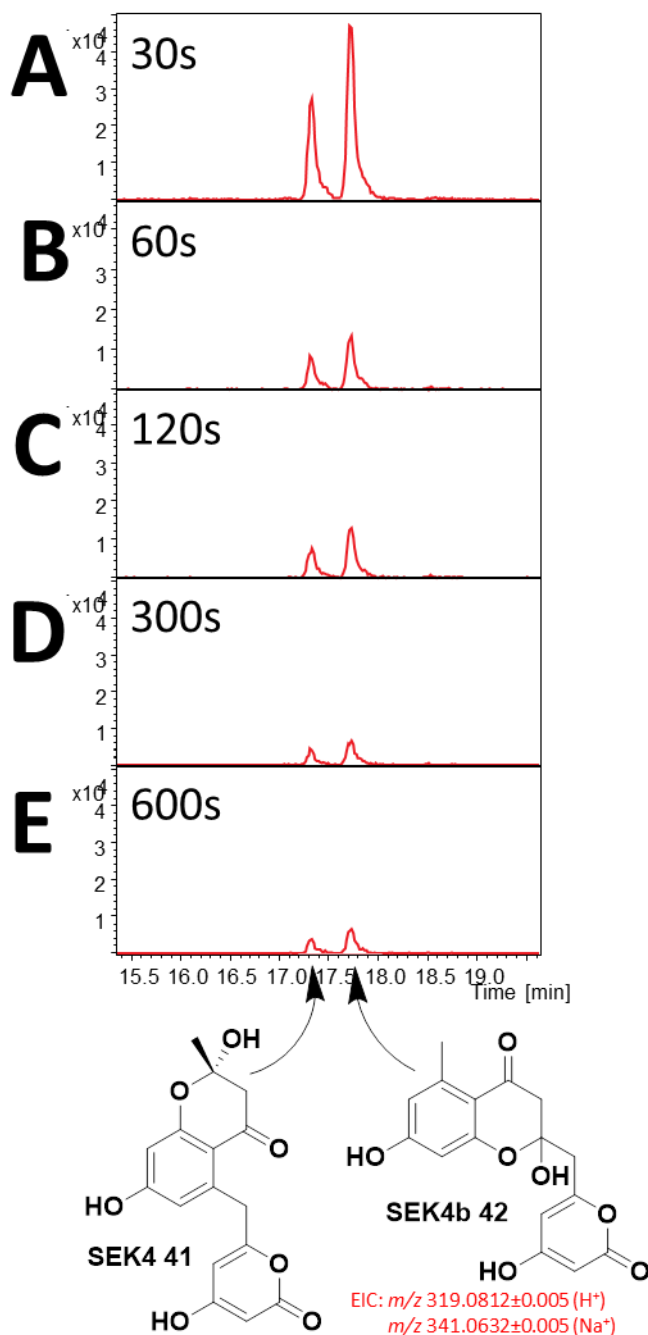


Figure 28 The effect of delayed addition of active probe **66** to the actinorhodin minimal system on the production of SEK4 **41** and SEK4b **42**. The actinorhodin minimal system was activated by the addition of final enzyme, holo-ACP **43**, then 30 (A), 60 (B), 120 (C), 300 (D) and 600 (E) seconds later the active probe **66**, obtained from a 4 hour irradiation of the nonhydrolyzable photolabile NAC analogue **65** in the home built UVA light source, was added. Following incubation overnight at room temperature, EtOAc extracts were analysed by UPLC-MS. The addition of active probe **66** at time point 0 seconds was not feasible by hand. This experiment was repeated with similar results (see **Appendix 1**).

A possible explanation for these results could be that diffusion of the probe **66** into the active site of the enzymes is affected by how long the biosynthesis has been proceeding for. At the early stages of biosynthesis, there is an abundance of malonyl-ACP **7** and the PKS complex may be tightly associated, and therefore the probe **66** may not be able to interfere in this complex at early time points. At later time points, 60 seconds onwards, there would be less malonyl-ACP **7** (see Chapter 5.1.2), which could result in the PKS complex becoming more susceptible to interference from the probe **66**. These experiments require further verifications to draw definitive conclusions.

4.1.3. Analysis by UV-Vis spectroscopy

The ability to demonstrate the effect of the active probe **66** on the production of SEK4/4b **41/42** in real time is desirable. A method published by Beltran-Alvarez *et al.*¹³ used UV spectroscopy to measure the production of SEK4/4b **41/42**. They found that the shunt products have a characteristic wavelength of 293 nm that can be monitored to detect their production in real time. Our goal was to detect an effect of the addition of the active probe **66** on the production of SEK4/4b **41/42**.

The minimal system was activated with the addition of *holo*-ACP **43** and then 293 nm was recorded from 1 to 90 minutes. It was not possible to record absorbance from 0 minutes due to the UV/vis spectrophotometer basic operational settings. Differences between the experiments and control samples (**Figure 29**) indicated that it was possible to detect SEK4/4b **41/42** production by this method.

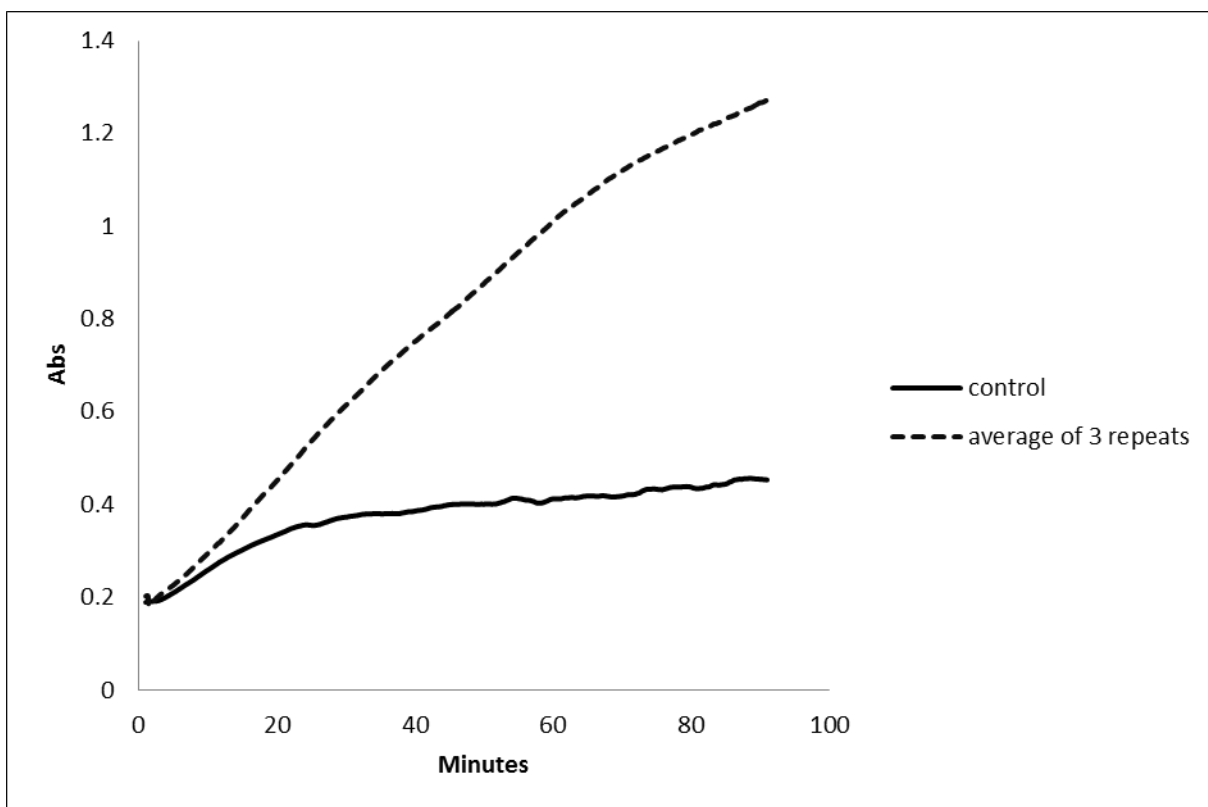


Figure 29 SEK4/4b 41/42 production in the actinorhodin minimal system monitored by absorbance at 293 nm. The dashed line represents the average of three identical repeats. The control does not contain malonyl-CoA 15 and, therefore, no SEK4/4b 41/42 can be produced in that assay.

The active probe **66** was generated as before, after 4 hours of irradiation, and then added 30 seconds after *holo*-ACP **43**. Attempts were made to record absorbance variations from 1 minute to 90 minutes, however the irradiated probe **65** absorbed very strongly at 293 nm, saturating the detector and effectively precluding the use of this method to monitor the biocatalysis.

4.2. *In vivo* trapping of intermediates from the actinorhodin 2 biosynthetic pathway in *Streptomyces coelicolor* with the nonhydrolysable photolabile NAC probe 65

The actinorhodin **2** biosynthetic pathway is a model system for type II polyketide synthases (PKSs). Actinorhodin **2** was first isolated from *Streptomyces coelicolor* in the 1950s^{67, 68} and has been studied extensively ever since.^{77, 207, 208}

S. coelicolor M510²⁸⁷ strain was used for feeding experiments with the protected probe **65**. M510 is a $\Delta redD$ mutant which is an activator gene of Red (undecylprodigiosin) synthesis.^{287, 288} Other than actinorhodin **2**, Red is produced in significant quantities in *S. coelicolor*. Utilising a strain that does not produce Red for *in vivo* feeding experiments allows a cleaner background for off-loading biosynthetic intermediates from actinorhodin **2**. CDA (calcium-dependent antibiotic) is still produced by the *S. coelicolor* M510 strain.²⁸⁹

Solid media was used for the bacterium growth, as liquid culture growth appeared inconsistent. A variety of different solid media, GYM, R5, SFM and R4, were compared for their reproducibility and the amounts of produced actinorhodin **2** determined by the colour of the media. R4 media proved to be superior to the other media types for growing *S. coelicolor* and for the expression of actinorhodin **2** reliably.²⁹⁰⁻²⁹²

R4 media was supplemented with 1 mM protected probe **65** and *S. coelicolor* was grown for five days, followed by plate extraction with EtOAc. SEK4/4b **41/42** proved too hydrophilic to be extracted from the aqueous layer with EtOAc alone, therefore, the media had to be adjusted to approximately pH 4 immediately prior to extraction with EtOAc. Preliminary experiments were carried out with media

supplemented with, 0, 1 mM, 5 mM and 10 mM of protected probe **65** to find the maximum amount of **65** that *S. coelicolor* could tolerate. There was very minimal growth after 5 days with 5 mM and no growth at all in 10 mM of **65**, the plate with just 1 mM of **65** grew well, and the distinctive blue of actinorhodin **2** could be seen (**Figure 30**). Therefore, all further experiments were carried out at a concentration of 1 mM **65**, which was comparable to the cultures grown without **65**.

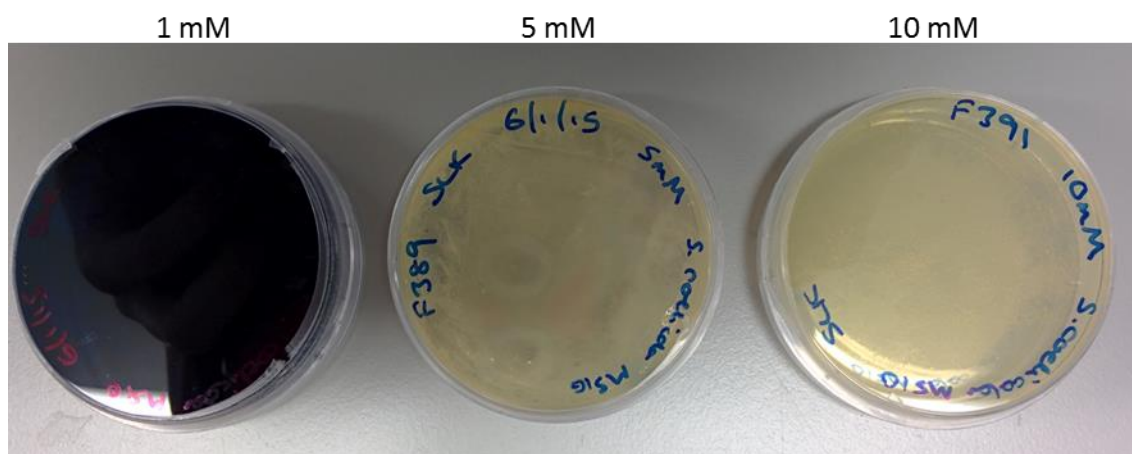


Figure 30 *S. coelicolor* M510 after 5 days growth supplemented with 1 mM, 5 mM and 10 mM nonhydrolysable photolabile NAC probe **65** showing growth inhibition with increasing concentration. Actinorhodin **2** has a strong blue colour, which can be seen in the plate grown with just 1 mM probe **65**.

The extent of deprotection of the DMNB probe **65** by *S. coelicolor* was monitored by extractions on each day of growth. The protected probe **65** proved quite stable during the first two days, possibly due to the low cell density. After three days of growth, however, extensive deprotection was observed and this did not increase much further across days 4 to 5 (**Figure 31**).

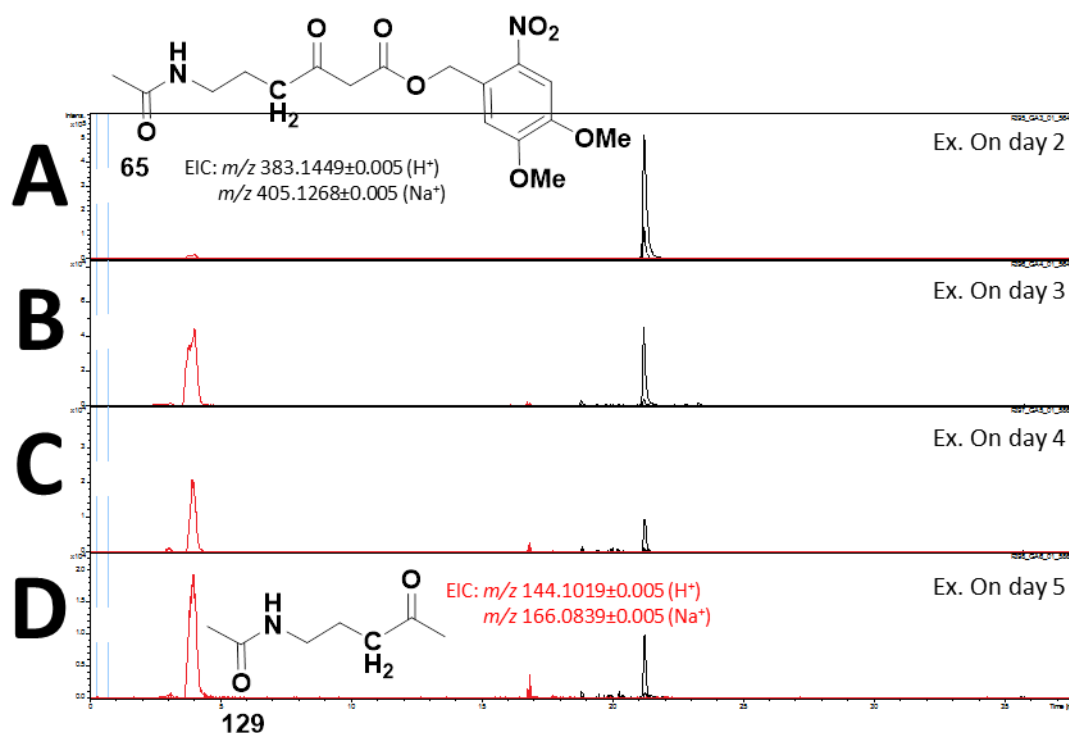


Figure 31 EIC from LC-MS analyses of the DMNB NAC analogue **65** showing its hydrolysis and subsequent decarboxylation to **129** after ethyl acetate extraction at the end of (A) day 2, (B) day 3, (C) day 4 and (D) day 5 of growth on solid media in the presence of *S. coelicolor* M510. Hydrolysis of **65** begins on day 3.

The production of SEK4/4b **41/42** was monitored by MS daily to evaluate the impact of the DMNB probe **65**, whereas the presence of actinorhodin **2** itself was visually followed by the culture's blue-colour increase. In the absence of the protected probe **65** SEK4 **41** and 4b **42** appeared after four days, whereas in the presence of **65** they appeared in substantial amount after 3 days, remaining unaffected afterwards. Overall, more SEK4/4b **41/42** was produced in the absence of the probe **65** (**Figure 32**): this indicates that the probe **65** likely interferes in SEK4/4b **41/42** polyketide assembly.

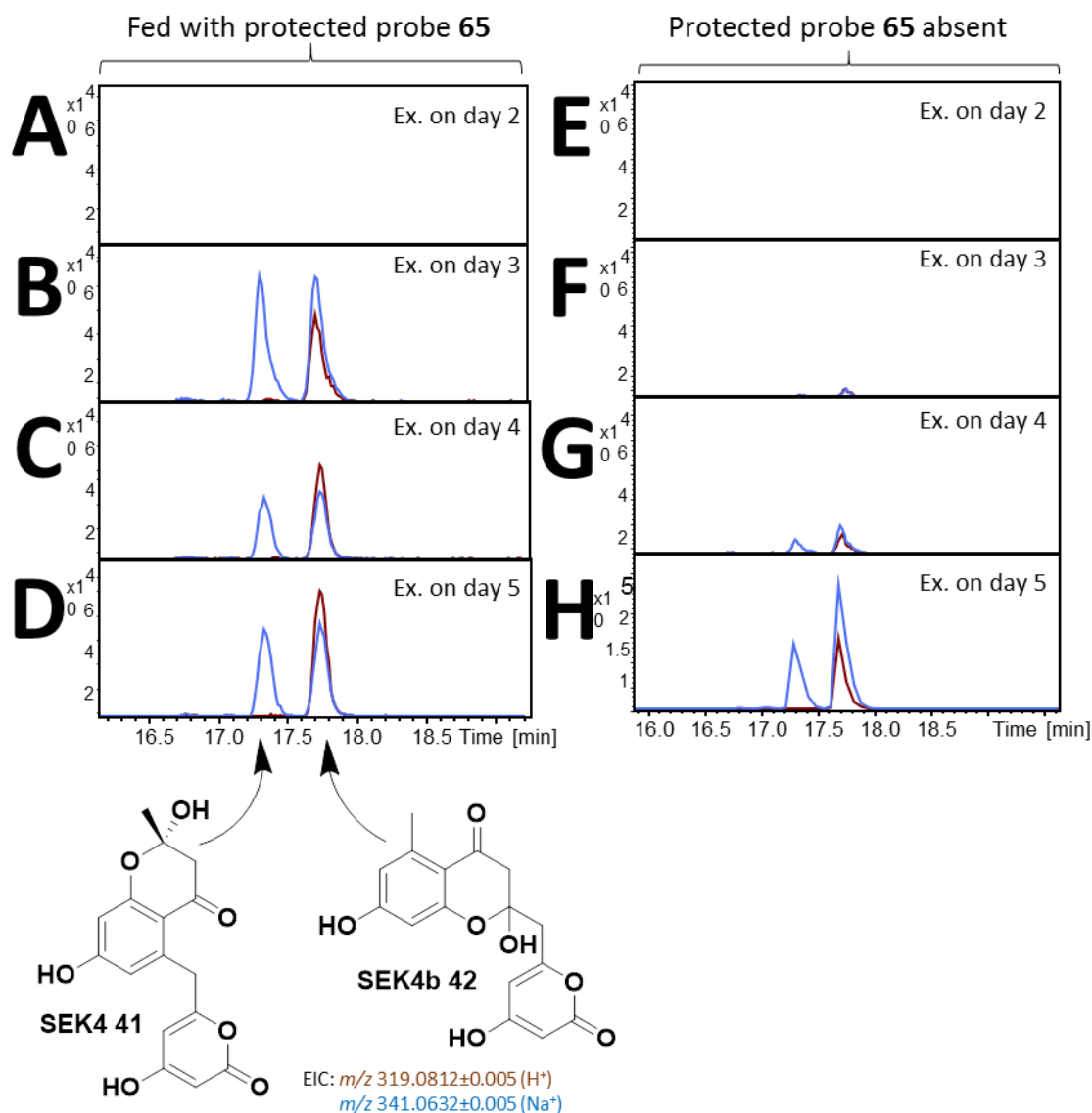


Figure 32 EIC from LC-MS analyses of shunt products of the actinorhodin minimal system, SEK4/4b 41/42, (shown underneath) produced by *S. coelicolor* M510 in the presence of DMNB NAC analogue 65 extracted on (A) day 2, (B) day 3, (C) day 4, (D) day 5 and absence of DMNB NAC analogue 65 extracted on (E) day 2, (F) day 3, (G) day 4 and (H) day 5. Note the increase of the intensity scale in (H).

4.2.1. Photolysis experiments

Based on the previously tested deprotection of the DMNB probe 65 in *S. coelicolor* (Figure 31), irradiation experiments were carried out on days 3 and 4 of growth.

The plates were exposed to irradiation for one, two, and three hours in the home built UVA light box, on either day three or four, and afterwards left to grow until day 5 as usual. In all irradiation experiments, very minimal quantities of protected probe **65** remained in comparison with the amount present in control experiments not subjected to UVA exposure (**Figure 33**).

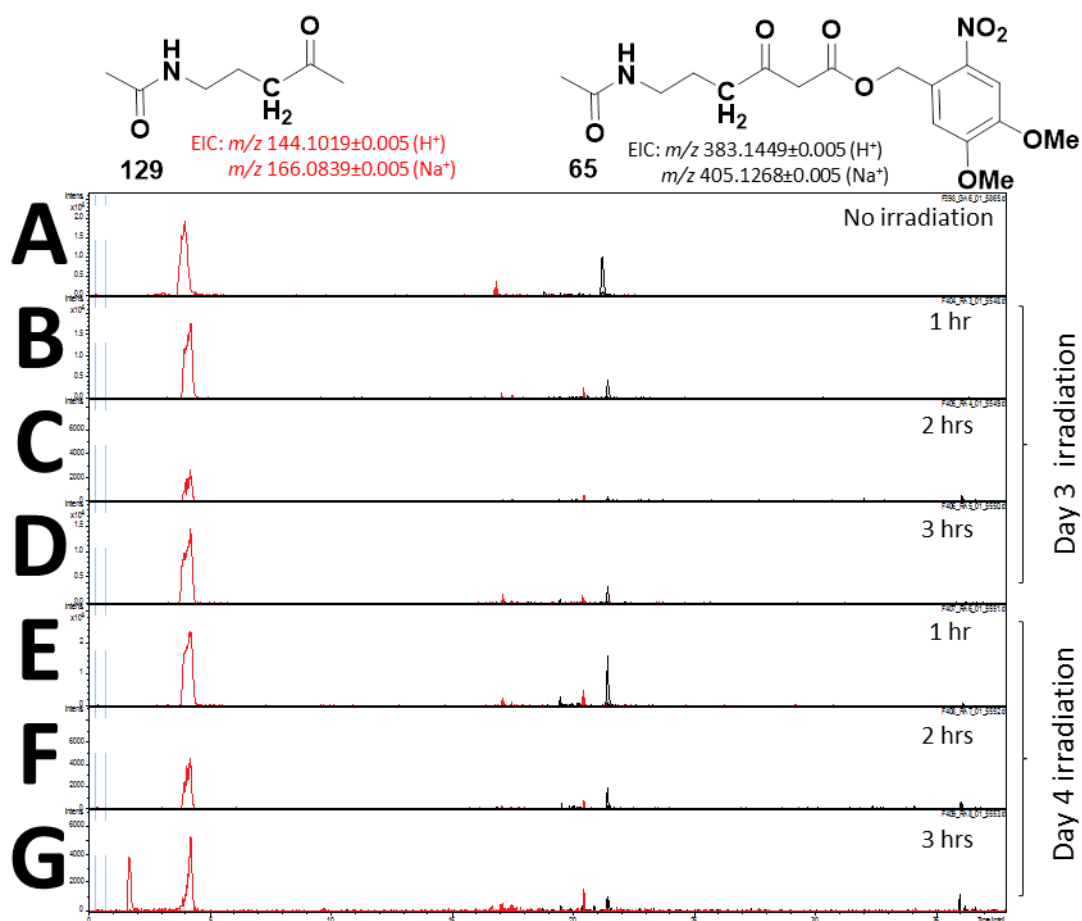


Figure 33 EIC from LC-MS analyses of the DMNB NAC analogue **65** showing its hydrolysis and subsequent decarboxylation to **129** after ethyl acetate extraction on day 5 of growth on solid media in the presence of *S. coelicolor* M510 with (A) no irradiation, (B) 1 hour, (C) 2 hours, (D) 3 hours of irradiation on day 3 and (E) 1 hour, (F) 2 hours, (G) 3 hours of irradiation on day 4.

The biosynthesis of SEK4/4b **41/42** was negatively affected by UVA exposure in the presence and in the absence of the probe **65** (Figure 34).

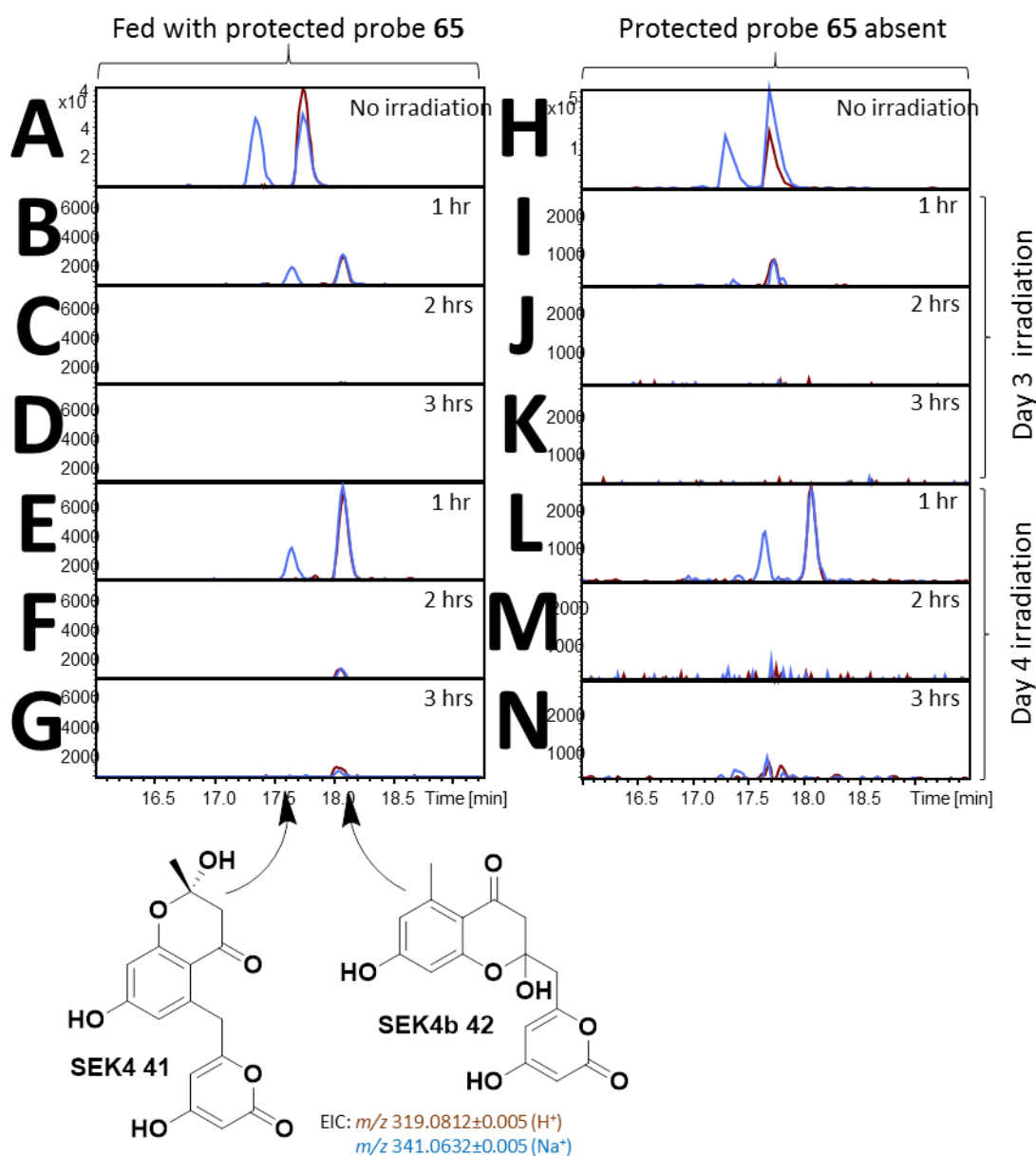


Figure 34 EIC from LC-MS analyses of shunt products of the actinorhodin minimal system, SEK4/4b **41/42**, (shown underneath) produced by *S. coelicolor* M510 in the presence (A-G) and absence (H-N) of DMNB NAC analogue **65**, extracted on day 5, following (A and H) no irradiation, (B and I) 1 hour, (C and J) 2 hours, (D and K) 3 hours of irradiation on day 3, and (E and L) 1 hour, (F and M) 2 hours, and (G and N) 3 hours of irradiation on day 4. Note: Samples A, H and I retention times vary due to analysis performed at an earlier date.

Nonetheless potential trapped intermediates deriving from SEK4 **41** and SEK4b **42** were searched for, such as an off-loaded triketide **141**, tetraketide, etc. (**Figure 35**). Unfortunately, none of them were detected. This could be due to the need for an alternative extraction protocol, or simply indicate that these probes are yet not optimal for intermediate capture in this system.

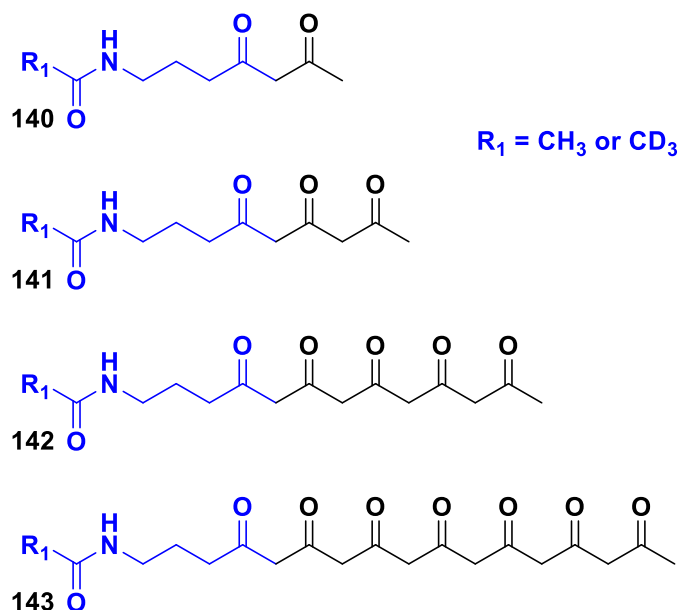


Figure 35 A sample of potential intermediates off-loaded from the actinorhodin **2** biosynthetic pathway by the DMNB NAC analogue **65**. Examples are a potential off-loaded diketide **140**, triketide **141**, pentaketide **142**, and heptaketide **143**.

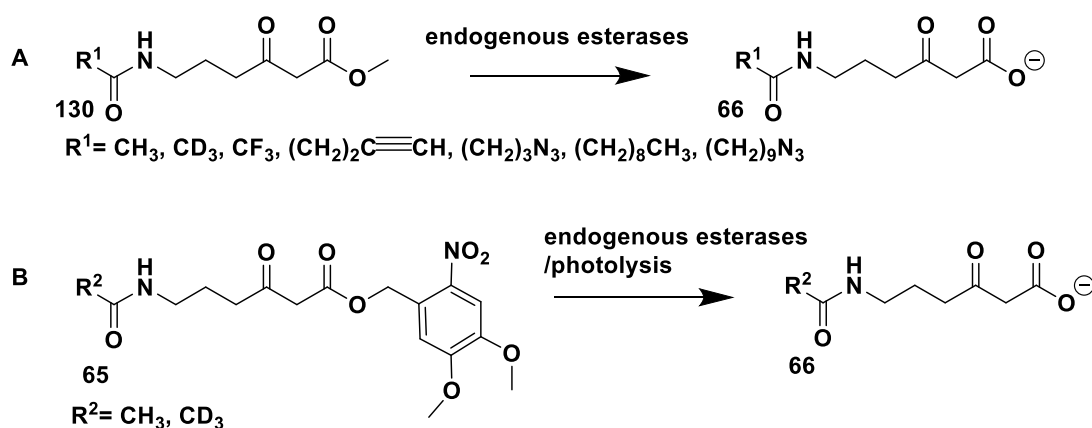
Recently the Tosin group have shown that increasing the bioavailability of chain termination probes (e.g. by increasing the hydrophobicity of the *N*-acyl chain) led to a substantial improvement in both the range and titre of off-loaded intermediates from lasalocid A **1** synthase in *S. lasaliensis*¹⁵⁶ and from 6-methylsalicylic acid **50** synthase *in vitro*²⁹³. It would therefore be useful in the near future to test newly prepared *N*-decanoyl probes bearing the DMNB photolabile group on both *S.*

coelicolor producing actinorhodin **2** *in vivo* and on the type II *act* minimal PKS *in vitro*.

4.3. *In vivo* trapping of intermediates from the lasalocid **1 biosynthetic pathway in *Streptomyces lasaliensis* with the nonhydrolysable photolabile NAC probe **65****

Previously, NAC analogues (**Figure 12**) have been successfully used to probe the lasalocid A **1**^{22, 155} pathway *in vivo*, resulting in a variety of complex off-loaded intermediates. The malonate protecting group has, thus far, only been reported with methyl ester protection. The efficiency of the DMNB photolabile group protection was directly compared with the ability of other NAC analogues to off-load intermediates from the lasalocid **1** biosynthetic pathway.

Streptomyces lasaliensis is a producer of the polyether antibiotic, lasalocid A **1**. This compound is synthesised *via* a type I modular polyketide synthase (PKS). A mutant strain (“ACP12 (S970A)”) of *S. lasaliensis* has been constructed previously,²² this contains a point mutation of the active site serine of the last acyl carrier protein to an alanine residue. The strain does not yield the final product, lasalocid A **1**, but results in intermediates remaining bound to the PKS. Previously in the Tosin group, derivatised chemical probes bearing methyl ester protection of the malonyl group **130**, have been shown to successfully off-load intermediates from the lasalocid A **1** PKS by feeding experiments with this ACP12 mutant strain.¹⁵⁵



Scheme 25 A) *In vivo* generation of the active probe **66** from the methyl ester protected probe **130**.¹⁵⁵ B) *In vivo* generation of the active probe **66**, via endogenous esterases, or photolysis, from the 4,5-Dimethoxy-2-Nitrobenzyl (DMNB) protected probe **65**.

Chemical protection of the malonyl group is essential to allow the probe to enter the cell, the malonyl group is too hydrophilic to pass through the cell membrane, and therefore activation of the probe must occur within the cell. The methyl ester protection of the malonyl group, shown previously¹⁵⁵, relies upon endogenous esterases present within the cell to hydrolyse the compound to provide the ‘active’ probe. It was hypothesised that the ability to ‘trap’ intermediates from biosynthetic pathways could be improved upon if the activation of the probe was controlled (**Scheme 25**). Thus, as described previously, the analogue, **65**, with photolabile protection of the malonyl group was synthesised, with the view to be able to activate the probe at the optimal time in the growth of the culture, as this bulky ester linkage is less likely to be accepted by endogenous esterases.

Initially, the DMNB NAC analogue **65** was fed to the *S. lasaliensis* ACP12 mutant strain without additional UV irradiation. Cultures grown on solid and liquid media were supplemented with probe **65** and the amount of hydrolysis, and ‘trapped’ intermediates, were compared. Additionally, cultures were supplied with probe **65**

either daily, or once at the beginning of the incubation, each up to the same final concentration of 2.5 mM, based upon previous successful results in the Tosin group.¹⁵⁵

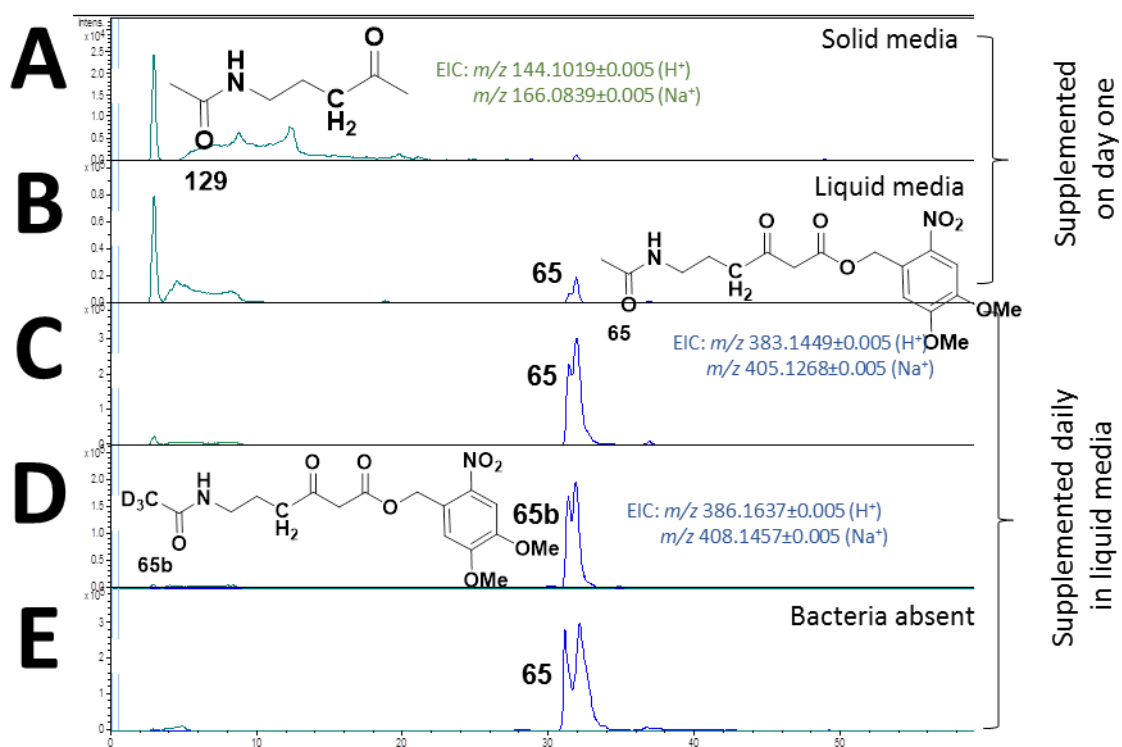
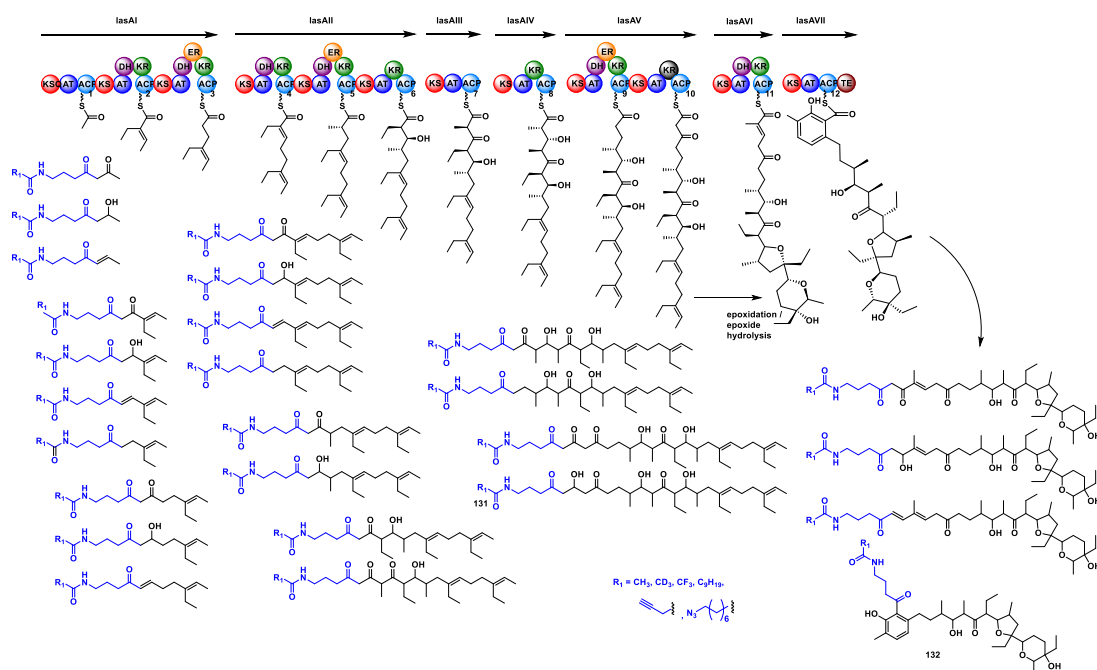


Figure 36 EIC from LC-MS analyses of the DMNB NAC analogue **65** hydrolysing and subsequent decarboxylating to **129** after ethyl acetate extraction of the media in the presence (A to D) and in the absence (E) of *S. lasaliensis* ACP12, with a comparison of the different supplementation strategies. A) Ethyl acetate extraction of *S. lasaliensis* ACP12 grown on solid media (A) or liquid media (B to D) containing 2.5 mM substrate **65** from day one (A and B) or supplemented daily (C to E). D contained deuterated substrate **65b**. NB. Small amounts of hydrolysed and decarboxylated probe **129** were detected in C, D and E.

Figure 36 shows the significant hydrolysis in solid media, and also in liquid media, when all of the substrate **65** is fed on day one of growth. However, the yield of the hydrolysed and decarboxylated product **129** from supplementing daily, up to a

concentration of 2.5 mM, in the presence and in the absence of *S. lasaliensis* ACP12 is comparable, with the majority of probe **65** remaining after five days of incubation.



Scheme 26 Lasalocid A **1** biosynthetic pathway from *S. lasaliensis* showing previously ‘trapped’ intermediates generated by the incubation with NAC analogues. Intermediates **131** and **132** also detected by the photolabile probe **65** are shown.

Extracted ion chromatograms were generated for expected biosynthetic intermediates from the lasalocid A **1** pathway (**Scheme 26**). Two of those polyketide intermediates were detected in the ethyl acetate extracts of the cultures fed with probe **65** to the *S. lasaliensis* ACP12 deletion mutant. The first intermediate **131** was off-loaded from the sixth module, LasAVI, prior to the extension with ACP11 and subsequent epoxidation (**Figure 37**). Both the protonated and sodiated ions were detected, as well as the incorporation of deuterium labelling with the respective probe **65b**, and these peaks were absent in control experiments. This intermediate **131** has undergone further reduction by the KR of the next module, likely once it has been off-loaded.

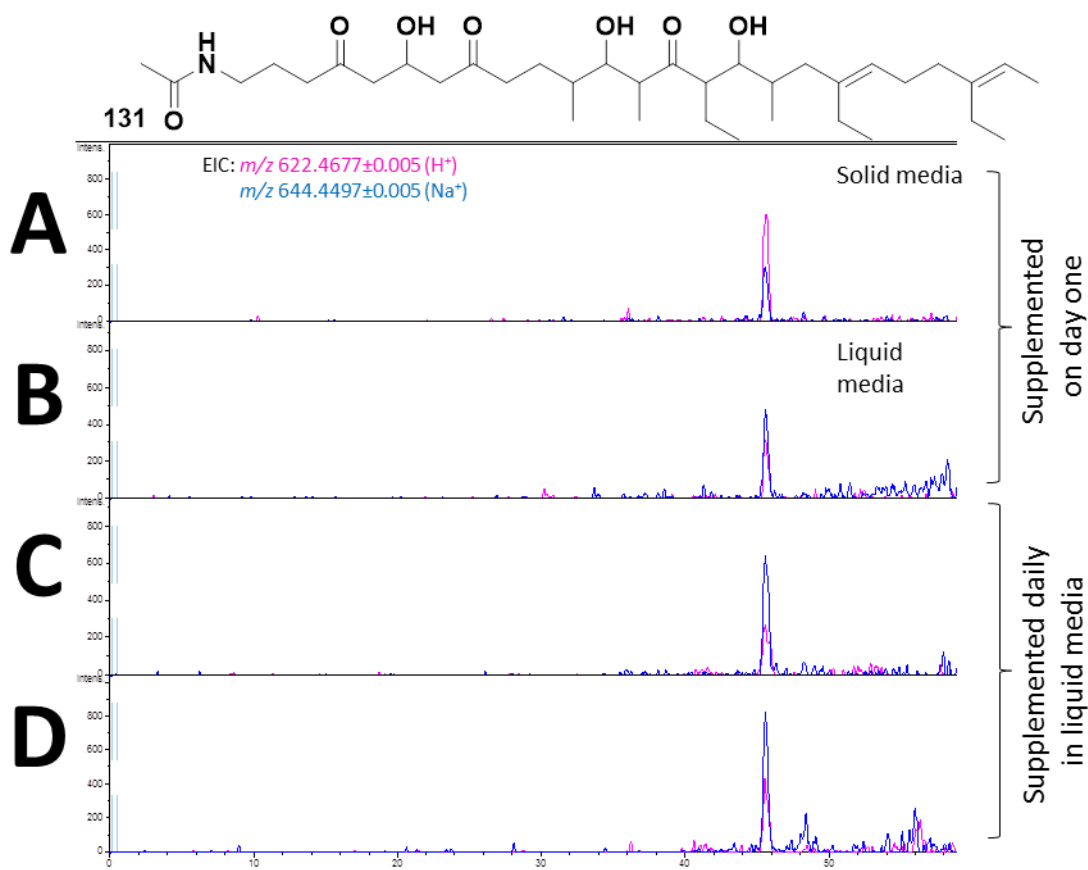


Figure 37 EIC from LC-MS analyses of the extracts from feeding experiments with the DMNB NAC analogue **65** to *S. lasaliensis* ACP12 mutant. Traces shown are the protonated and sodiated ions of compound **131**, a ‘trapped’ intermediate from lasalocid **A 1** biosynthetic pathway, off-loaded from ACP10 and further reduced by KR11. A-B) *S. lasaliensis* ACP12 grown in (A) solid media and (B) liquid media supplemented with substrate **65** to a concentration of 2.5 mM. C-D) *S. lasaliensis* ACP12 grown in liquid media supplemented daily with (C) substrate **65** and (D) deuterated substrate **65b** up to a final concentration of 2.5 mM.

A second, more prominent, intermediate **132** was off-loaded from the seventh module, LasAVII, prior to the final extension with ACP12 and release from the PKS (**Figure 38**). As mentioned previously, this mutant does not bear an active ACP12, thus, it is to be expected that this intermediate **132** would accumulate and increase the chances for off-loading by the NAC analogue. This ‘trapped’ intermediate is detected as two peaks, but both having the same MS fragmentation pattern,¹⁵⁵

therefore it has been hypothesised that this is due to conformational isomerism. NMR spectroscopy will be used to characterise the isomers, however, the low yield of ‘trapped’ intermediates does not facilitate NMR analysis at this stage.

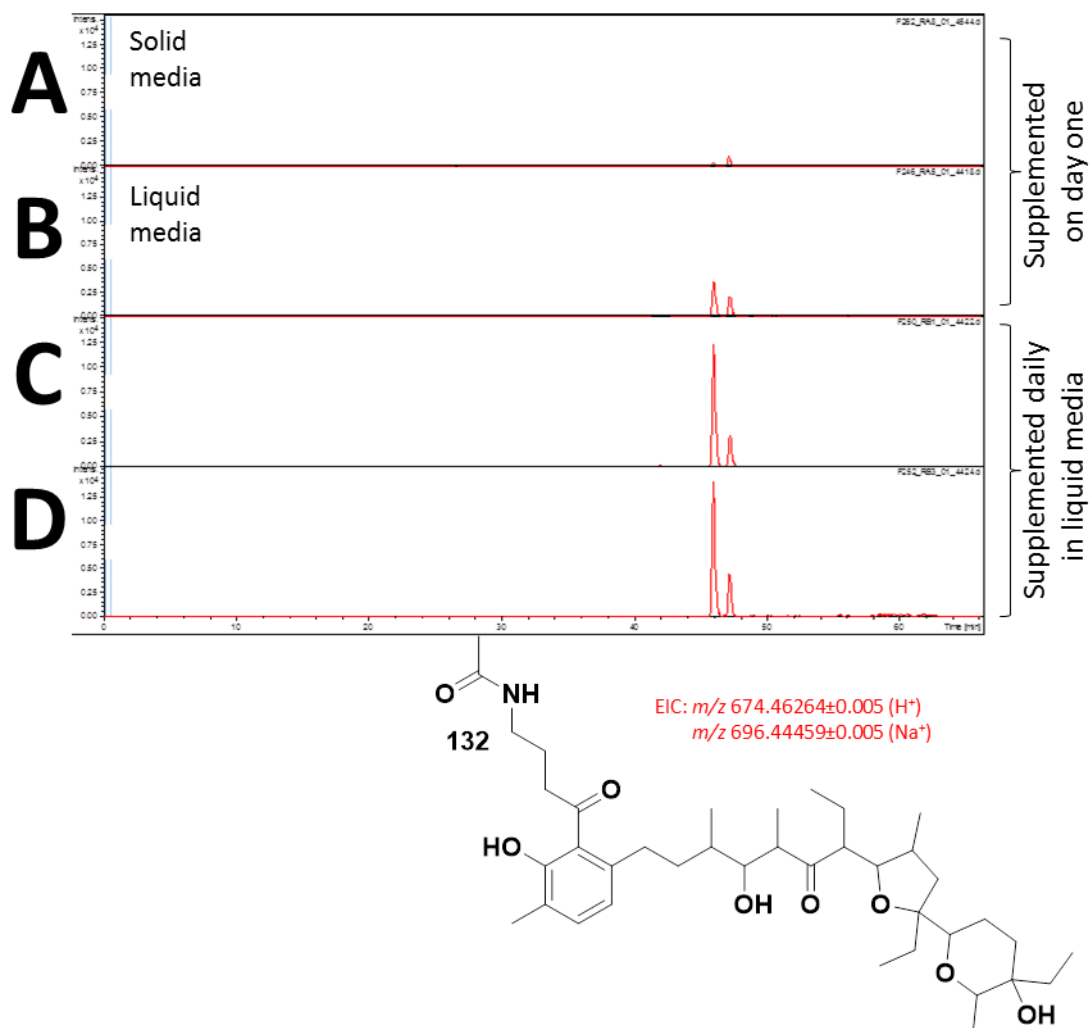


Figure 38 EIC from LC-MS analyses of the extracts from feeding experiments with the DMNB NAC analogue **65** to *S. lasaliensis* ACP12 mutant. Trace shown is compound **132**, a ‘trapped’ intermediate from lasalocid **A 1** biosynthetic pathway, offloaded from ACP11. A-B) *S. lasaliensis* ACP12 grown in (A) solid media and (B) liquid media supplemented with substrate **65** to a concentration of 2.5 mM. C-D) *S. lasaliensis* ACP12 grown in liquid media supplemented daily with (C) substrate **65** and (D) deuterated substrate **65b** up to a final concentration of 2.5 mM.

The yields of **132** were compared from experiments in solid and liquid media, and also from supplementing the media with the probe **65** on day one or stepwise on days two to five (**Figure 37** and **Figure 38**). For compound **131**, the yield was considerably lower than that of intermediate **132** offloaded from ACP11, but the amount was also comparable for all experiments, both in solid and liquid media, and regardless of the method of feeding (**Figure 37**). However, for compound **132**, the yields varied by at least one order of magnitude from solid to liquid cultures, and also more than doubling from supplementing the media with probe **65** on day one, to stepwise feeding. This result agreed with previous research from the Tosin group with different probe analogues.¹⁵⁵

It was initially thought that that the probe **65** might not be a suitable substrate for esterases within the cell due to the unnatural nature of the DMNB group. However, the results showed that there must be a small amount of hydrolysis occurring to release the active probe **66** (**Figure 36**). The stability of the malonyl group of the active probe **66** *in vivo* has not been investigated, although the active probe **66** generated *in vivo* has not been detected in any of the feeding experiments.

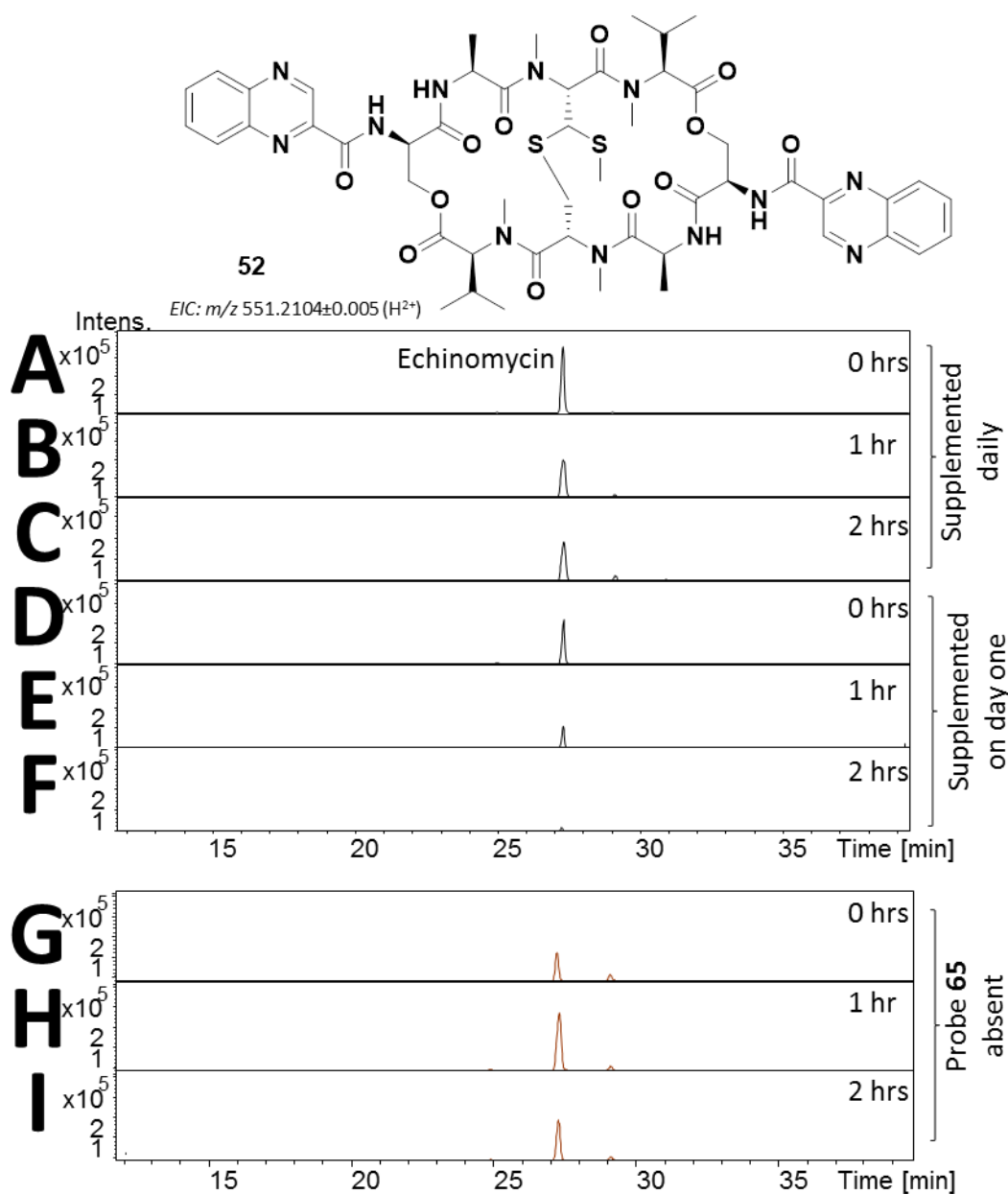


Figure 39 EIC from LC-MS analyses of the extracts from feeding experiments with the DMNB NAC analogue **65** to *S. lasaliensis* ACP12 mutant. Trace shown is the doubly charged ion of echinomycin **52**, a natural product produced by a non-ribosomal peptide synthetase (NRPS) in *S. lasaliensis*. A-C) Supplemented on day one (A-C) or daily (D-F) with substrate **65** to a final concentration of 2.5 mM and G-I) without supplementation. (A, D and G) without irradiation, (B, E and H) with 1 hour or (C, F and I) with 2 hours of irradiation on days 2 to 5.

Following on from the success of the experiments without irradiation of the probe **65**, *in vivo* photolysis experiments were carried out within the home built light box, which is capable of being fixed to the base of an Eppendorf Innova incubator shaker. Preliminary experiments, reported in chapter 2, showed complete photolysis of the protected probe **65** within 4 hours (**Table 3**). To minimise disruption on cell growth, just one and two hours a day of irradiation were applied to the cultures between days two to five. Liquid cultures had provided the greatest amount of trapped intermediates thus far, therefore liquid media was utilised for the photolysis experiments. Control cultures were grown to ensure that irradiation would not alter growth. The production of echinomycin **52**²⁸⁶, also known as quinomycin A, a natural product produced by a non-ribosomal peptide synthetase (NRPS) in *S. lasaliensis*, was monitored by LC-MS (**Figure 39**).

The production of echinomycin **52** is largely unaffected by irradiation, its detection remained within the same order of magnitude for each experiment (**Figure 39**). The combination of feeding the probe **65** on day one and two hours of daily irradiation during days 2-5 led to a decreased production of echinomycin **52** by an order of magnitude, although cell growth did not visually appear to be affected by irradiation alone.

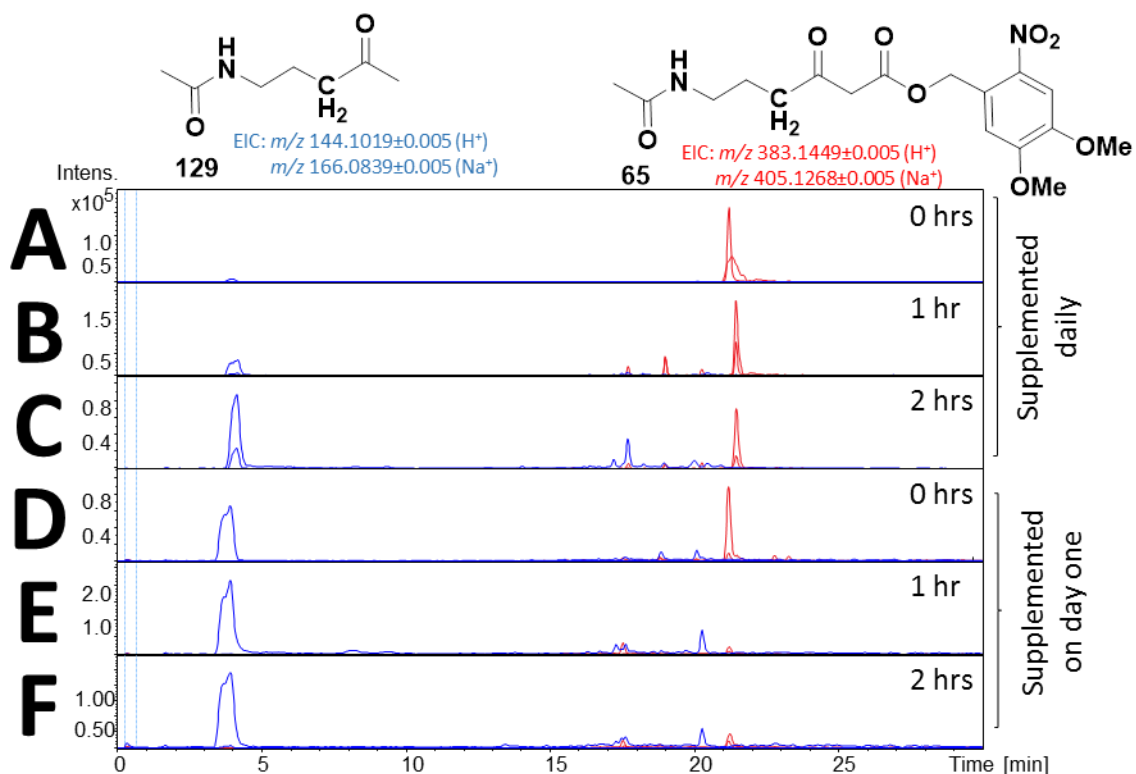


Figure 40 EIC from LC-MS analyses of the DMNB NAC analogue **65** showing its hydrolysis and subsequent decarboxylation to **129** after ethyl acetate extraction of liquid media in the presence of *S. lasaliensis* ACP12. A-C) Supplemented on day one (A-C) or daily (D-F) with substrate **65** to a final concentration of 2.5 mM, (A and D) without irradiation, (B and E) with 1 hour or (C and F) with 2 hours of irradiation on days 2 to 5. Retention times vary slightly due to when LC-MS was performed.

The ratio of protected probe **65** to decarboxylated probe **129** after five days incubation in *S. lasaliensis* does depend upon both the feeding and the irradiation conditions (**Figure 40**). Daily supplementation without any irradiation results in the greatest amount of protected probe **65** remaining intact after five days. Both supplementation conditions were affected similarly by irradiation, with a decrease in amount of protected probe **65** (**Figure 40**). Hence, it was not possible to establish the effective irradiation contribution to the deprotection process.

The same two putative intermediates **131** and **132** off-loaded from feeding experiments without irradiation were also off-loaded upon UV irradiation. However both the yields of intermediates **131** and **132** increased following one hour of daily irradiation when the protected probe **65** was supplied daily (**Figure 41** and **Figure 42**); oppositely, irradiation did not improve the titer of the trapped species when the protected probe **65** supplied exclusively on the first day of growth.

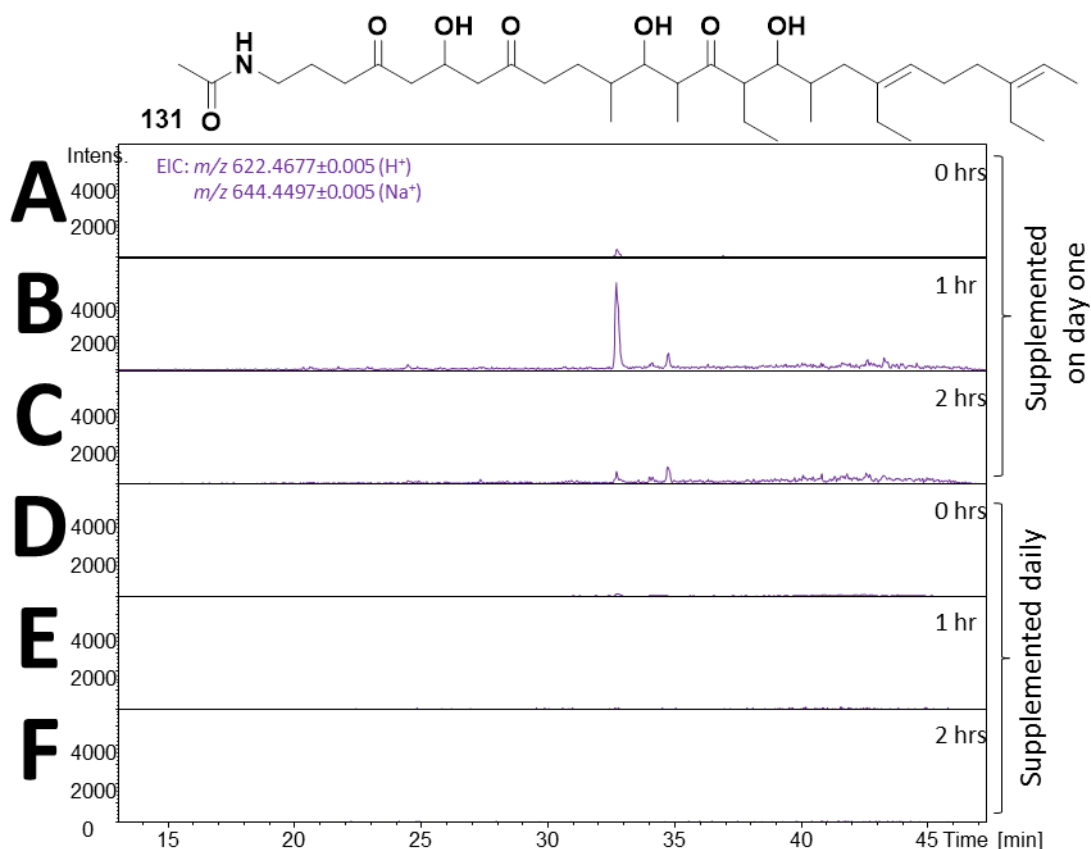


Figure 41 EIC from LC-MS analyses of the extracts from feeding experiments with the DMNB NAC analogue **65** to *S. lasaliensis* ACP12 mutant in liquid media. Trace shown is compound **131**, a ‘trapped’ intermediate from lasalocid **A 1** biosynthetic pathway, off-loaded from ACP10 and further reduced by KR11. A-C) Supplemented on day one (A-C) or daily (D-F) with substrate **65** to a final concentration of 2.5 mM, (A and D) without irradiation, (B and E) with 1 hour or (C and F) with 2 hours of irradiation on days 2 to 5.

The putative undecaketide intermediate **132** from ACP11 (**Figure 42**) titre increased approximately six-fold with one hour of daily irradiation compared to without irradiation. When each irradiation event was increased to two hours a day, however, the yield decreased back to similar levels as without any irradiation. It is possible that exposure to UV light for that length of time was damaging to the cell and resources are drawn away from PKS secondary biosynthesis. The same response was observed with off-loaded intermediate **131** from ACP10.

Two additional putative intermediates from the lasalocid A **1** biosynthetic pathway were observed upon cell feeding with the DMNB probe **65** and its UV activation. One species, allegedly off-loaded from ACP8 as **133**, was detected and, from its MS fragmentation pattern¹⁵⁵, it appears to have undergone epoxidation and cyclisation with dehydration to provide **135** (**Figure 43**). An additional intermediate, **136**, is likely the product of an oxidation of the same off-loaded intermediate **133**, providing a compound that is 2 Da less than **135** (**Figure 44**); the ratio **135** to **136** was approximately 3:4.

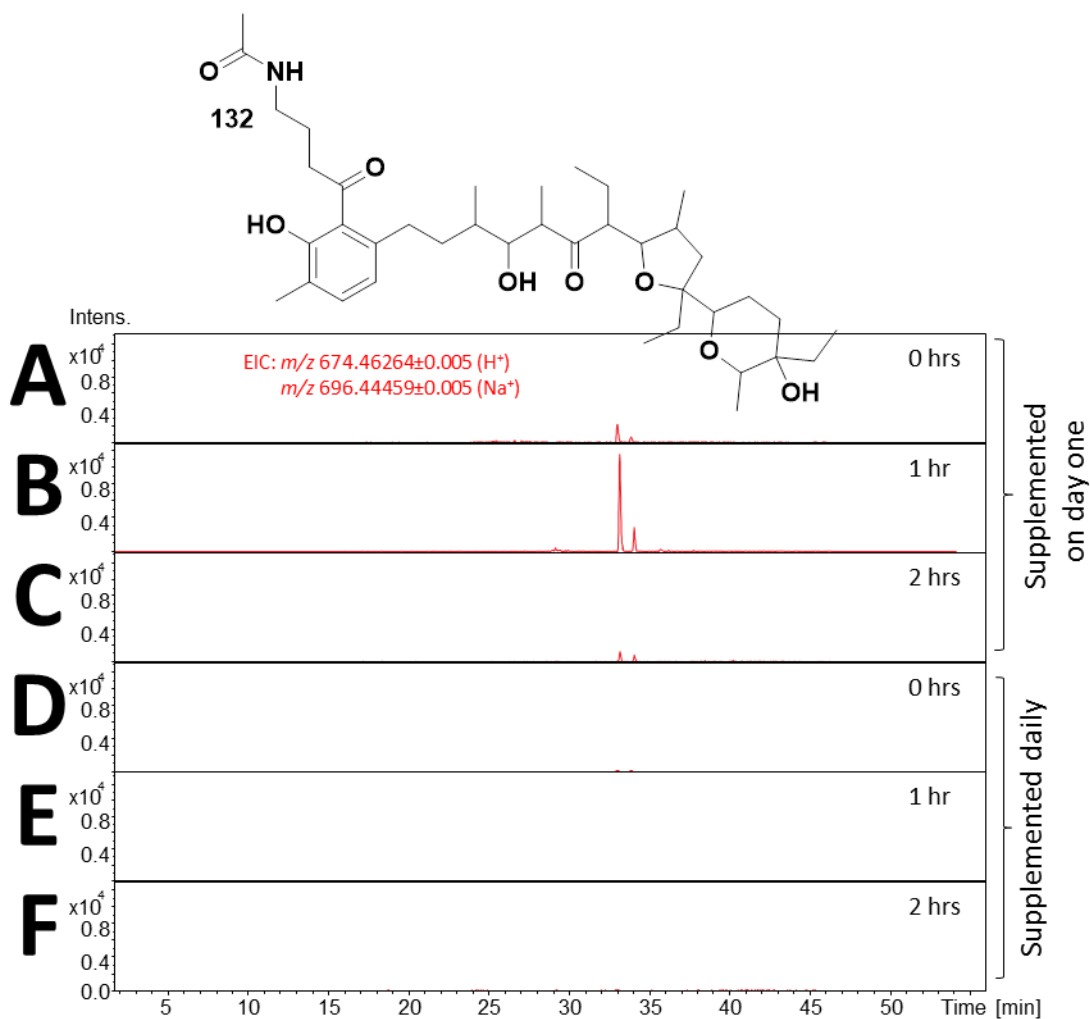


Figure 42 EIC from LC-MS analyses of the extracts from feeding experiments with the DMNB NAC analogue **65** to *S. lasaliensis* ACP12 mutant in liquid media. Trace shown is compound **132**, a 'trapped' intermediate from lasalocid **A 1** biosynthetic pathway, off-loaded from ACP11. A-C) Supplemented on day one (A-C) or daily (D-F) with substrate **65** to a final concentration of 2.5 mM, (A and D) without irradiation, (B and E) with 1 hour or (C and F) with 2 hours of irradiation on days 2 to 5.

The proposed pathway to intermediates **135** and **136** can be seen in **Scheme 27**. The point of oxidation in the structure of **136** is approximated from the lack of MS fragment **138** in the MS/MS of the oxidised species **136** (**Figure 44**).

Both one and two hour long daily irradiation events, when the media is supplemented daily with probe **65**, improves the yield of both the reduced and the

unreduced intermediates **135** and **136** (**Figure 43** and **Figure 44**). As with more advanced off-loaded intermediates **131** and **132**, for both cases, just one hour a day of irradiation is superior for off-loading these intermediates **131** and **132** than two hours a day. In the case of species **135** and **136**, a marginal improvement is seen in the samples that were supplemented on day one with probe **65** from no irradiation to one hour a day of irradiation. Daily supplementation remained overall superior to feeding all of the protected probe **65** on day one for trapping intermediates **135** and **136**.

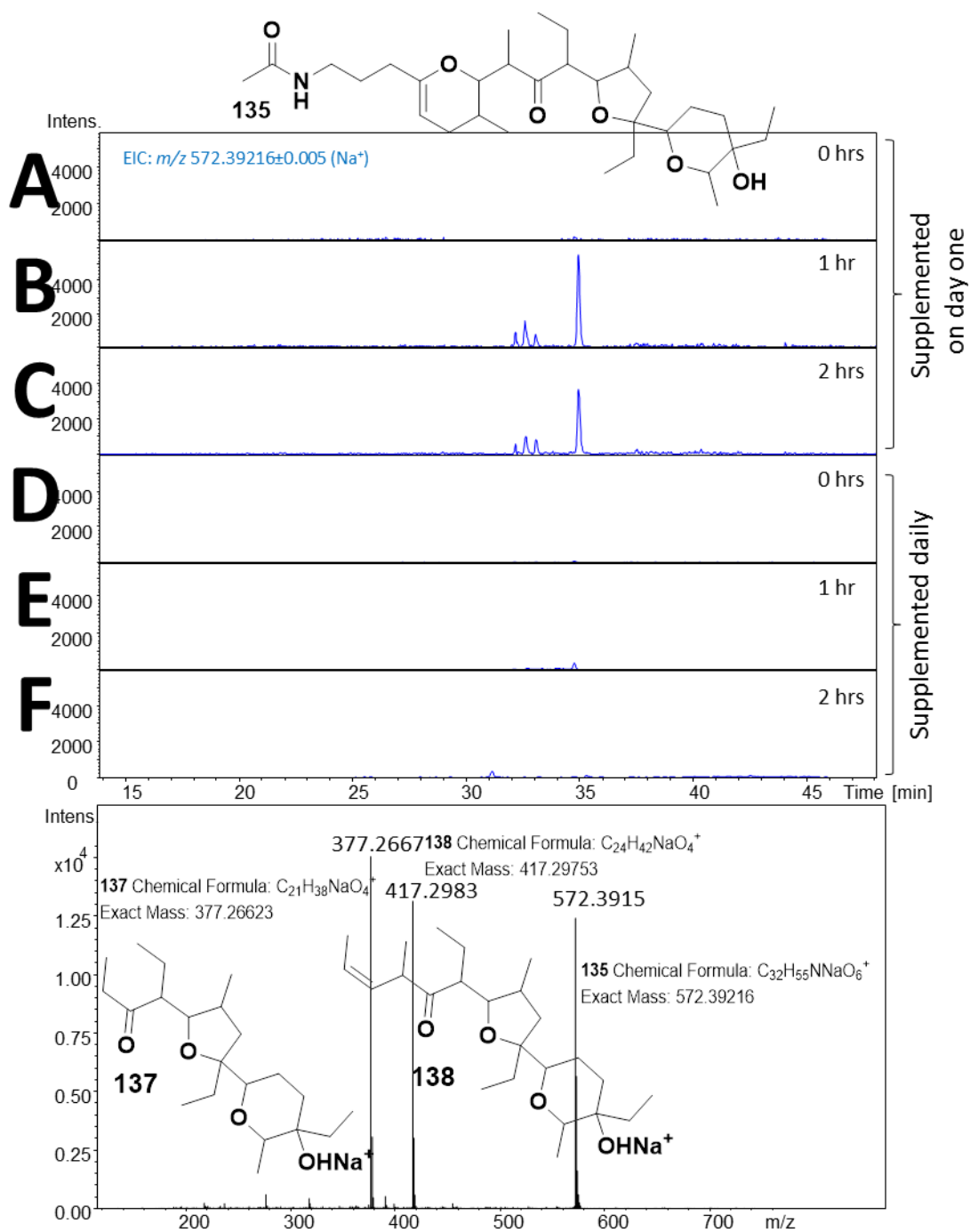


Figure 43 EIC from LC-MS and MS/MS analyses of the extracts from feeding experiments with the DMNB NAC analogue **65** to *S. lasaliensis* ACP12 mutant in liquid media. Trace shown and MS/MS is compound **135**, a 'trapped' intermediate from lasalocid A **1** biosynthetic pathway, off-loaded from ACP8 with subsequent epoxidation and cyclisation. A-C) Supplemented on day one (A-C) or daily (D-F) with substrate **65** to a final concentration of 2.5 mM, (A and D) without irradiation, (B and E) with 1 hour or (C and F) with 2 hours of irradiation on days 2 to 5.

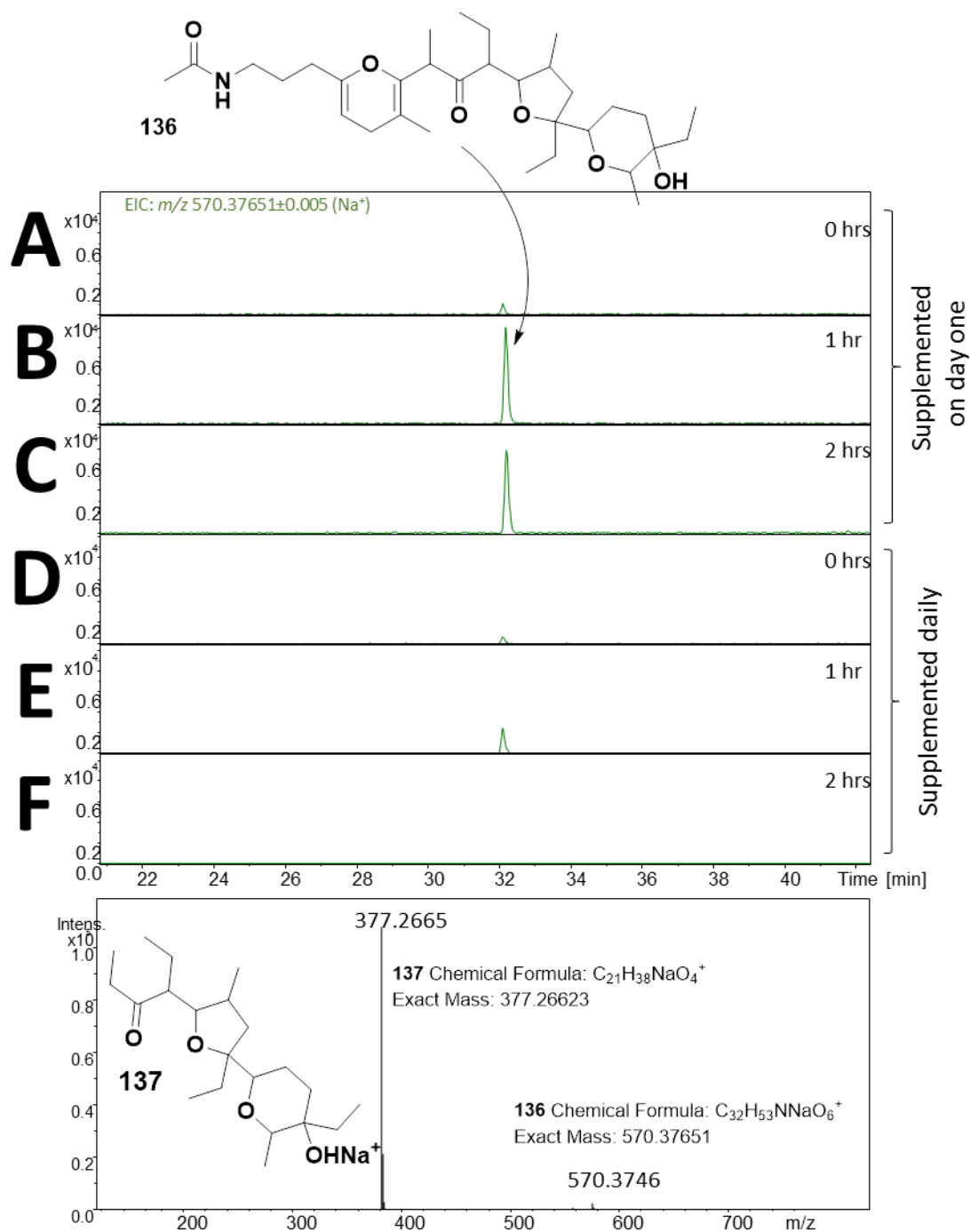
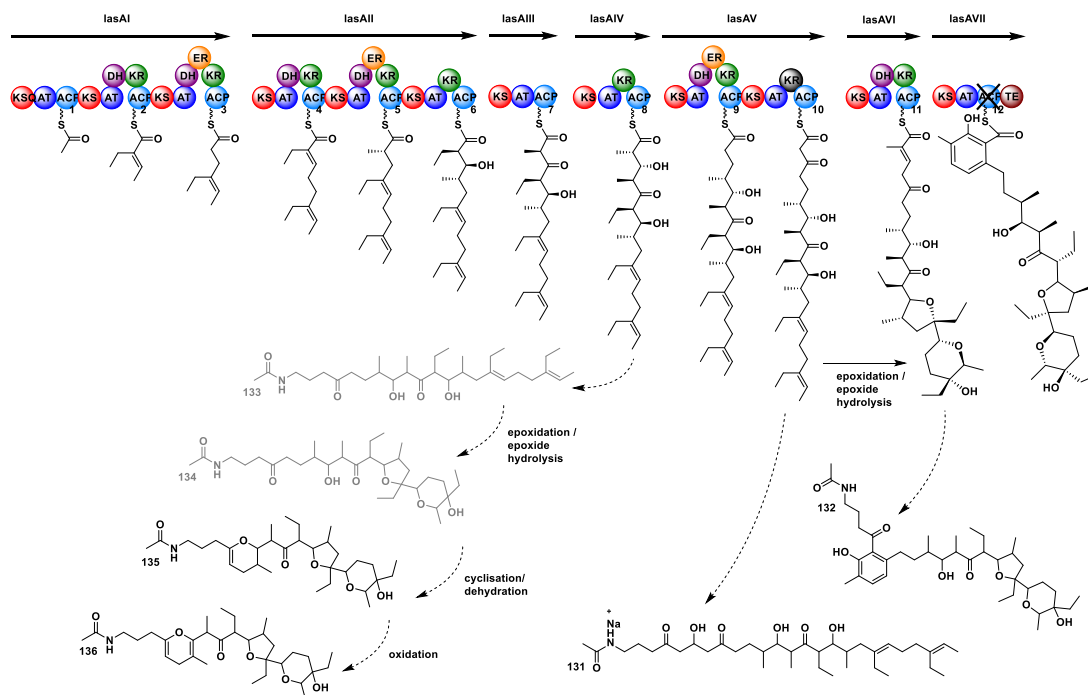


Figure 44 EIC from LC-MS and MS/MS analyses of the extracts from feeding experiments with the DMNB NAC analogue **65** to *S. lasaliensis* ACP12 mutant in liquid media. Trace shown and MS/MS is compound **136**, a ‘trapped’ intermediate from lasalocid A **1** biosynthetic pathway, off-loaded from ACP8, with subsequent epoxidation, cyclisation and oxidation. A-C) Supplemented on day one (A-C) or daily (D-F) with substrate **65** to a final concentration of 2.5 mM, (A and D) without irradiation, (B and E) with 1 hour or (C and F) with 2 hours of irradiation on days 2 to 5.



Scheme 27 Lasalocid A **1** biosynthetic pathway from *S. lasaliensis* showing newly putative ‘trapped’ intermediates **135** and **136** generated by the incubation with DMNB NAC analogue **65** in an ACP12 deletion mutant following UV irradiation. Compounds in grey **133** and **134** were not detected.

Unfortunately, trapped intermediates **135** and **136** were not detected with deuterium labelling in cultures fed with labelled ester probe **65b**. Time did not allow further repeats of these experiments, however MS fragmentation of the sodiated species **135** and **136** showed common fragment ions (**Figure 43** and **Figure 44**) strongly indicative of polyether ring formation.¹⁵⁵ If these results are confirmed, the oxidative steps taking place through lasalocid A **1** polyketide chain assembly to generate the polyether rings would take place earlier than previously hypothesised.

Irradiation with UV light produces significantly more active probe **66** than in its absence, as can be seen by more decarboxylated final product **129** present in the cell

extract (**Figure 40**). Additionally, irradiation events catalysed more trapping of intermediates **131** and **132** from ACP10 and ACP11 than without irradiation, as well as two more newly detected intermediates off-loaded from ACP8 (**Scheme 27**).

**Chapter 5: Capture of polyketide
intermediates with the aid of a
nonhydrolysable malonyl acyl carrier
protein analogue**

5. Capture of polyketide intermediates with the aid of a nonhydrolysable malonyl acyl carrier protein analogue **63**

5.1. Photolysis of the carrier protein **63**

5.1.1. Rate of photolysis of the nonhydrolysable photoactivatable malonyl acyl carrier protein analogue **63**

As described previously, the newly devised acyl carrier protein (ACP) **63** bears a photolabile 4,5-dimethoxy-2-nitrobenzyl (DMNB) group for the protection of the malonyl-like moiety. Section 0 reports the photolysis conditions established for the small molecule NAC probe **65**. These conditions were tested on the carrier protein **63** and proved to be equally suitable for the uncaging of **63** to **64**.

After 4 hours of irradiation at 365 nm in TrisCl (50 mM), KCl (20 mM), MgCl₂ (10 mM) at pH 8 almost all the DMNB group had been removed, and, subsequently, the malonyl group decarboxylates to produce **144** (**Figure 45**). Similar results were obtained by using both a KiloArc Broadband Arc lamp at 365 nm, and also with a home built light box equipped with a circular UVA lamp.

MS protein analyses showed no sign of protein degradation throughout the photolysis. Furthermore, *holo act* ACP **43** was subjected to the same irradiation conditions and its activity proved to be unaffected by it, generating the same amount of SEK4 **41** and SEK4b **42** in reaction with KS-CLF (Section 4.1, **Figure 25**).

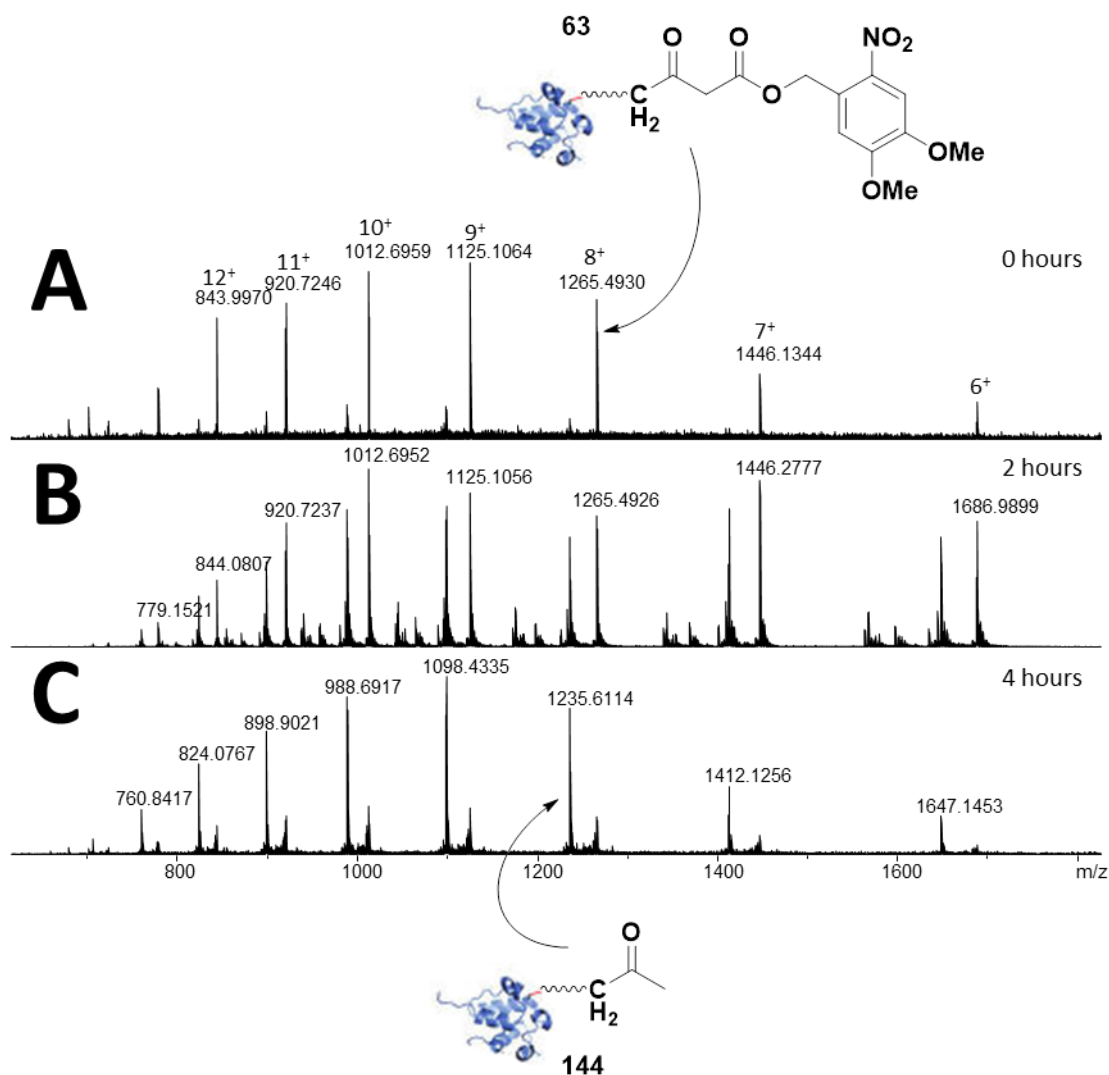


Figure 45 Irradiation of the photolabile acyl carrier protein (ACP) analogue **63** in TrisCl (50 mM), KCl (20 mM), MgCl₂ (10 mM) at pH 8, with 365 nm, 1000 W for 0 (A), 2 (B), and 4 (C) hours, showing the synthesis of the decarboxylated product **144** by TOF-MS. After 4 hours, only a minor amount of ACP analogue **63** could be detected.

5.1.2. Incubation of Ketosynthase-Chain Length Factor (KS-CLF) with malonyl and acetyl acyl carrier proteins (ACPs) and the protein probe **63**

The components of the actinorhodin minimal system, KS-CLF and the discrete *act* ACP, work together and iteratively process acetyl **17** and malonyl-CoA **15**,

generating an octaketide product **31** which spontaneously cyclises to SEK4 **41** and SEK4b **42** (Section 1.3.2 and **Scheme 5**).

More specifically, malonyl-ACP **7** is decarboxylated by the KS-CLF and then the acetate unit, from the newly generated acetyl-ACP **40**, is loaded onto the KS-CLF which initiates polyketide chain extension, as described before. The ability of the KS and the CLF to catalyse the polyketide synthesis has been studied using mutations of the active site cysteine of the KS to alanine, and the glutamine of the CLF to alanine.²⁷

The conversion of malonyl-ACP **7** to acetyl-ACP **40**, and then to *holo*-ACP **43** was monitored with each mutant and it was found that both the KS and the CLF were able to catalyse the decarboxylation, but, not surprisingly, the KS was crucial to the full synthesis of SEK4 **41** and SEK4b **42**.²⁷

5.1.2.1. *Incubation of KS-CLF with malonyl-ACP 7 and acetyl-ACP*

40

Acetyl-ACP **40** and malonyl-ACP **7** were separately incubated with and without KS-CLF, in a 1:1 ratio to prevent chain extension steps, and then analysed by FTICR-MS. Conversion of acetyl-ACP **40** to *holo*-ACP **43** was observed as expected from the loading of the KS with an acetate unit (**Figure 46**).²⁷ When malonyl-ACP **7** was incubated with KS-CLF a substantial difference was seen in comparison to without KS-CLF. Without KS-CLF, malonyl-ACP **7** decarboxylated to acetyl-ACP **40** and a small amount of *holo*-ACP **43** was also detected. However, when malonyl-ACP **7** was incubated with KS-CLF, only a very small amount of **7** was detected: the majority of the ACP was detected as acetyl-ACP **40** and there was also an increase in

the amount of *holo*-ACP **43** present in comparison to incubation without KS-CLF (Figure 47).

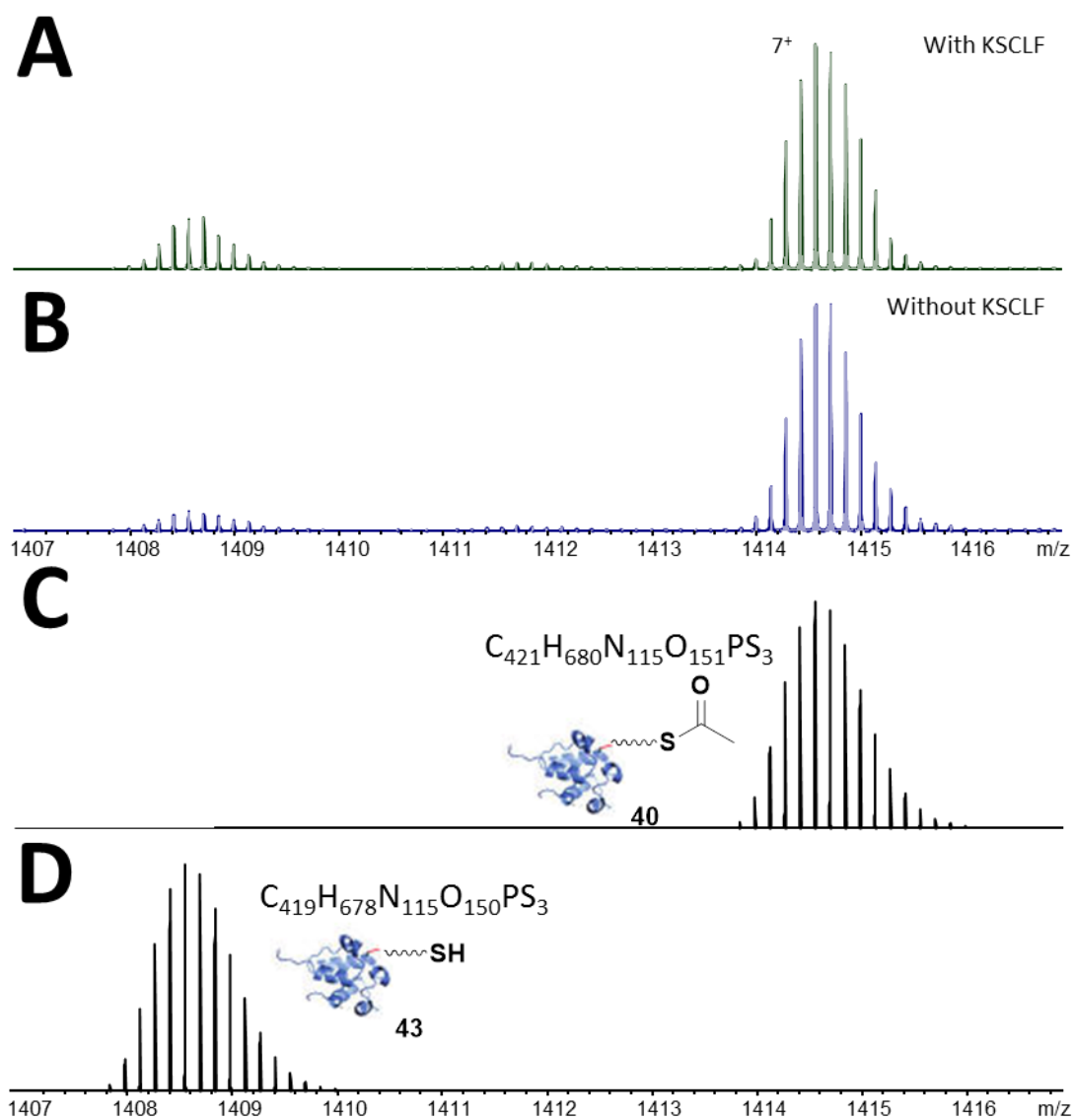


Figure 46 Comparison of the ratio of acetyl **40** to *holo* **43** (not hexahistidine-tagged) acyl carrier protein (ACP) from the actinorhodin minimal system following 2 hours of incubation (A) with and (B) without the actinorhodin ketosynthase-chain length factor (KS-CLF). Simulated isotope distributions for the 7^+ charge state of (C) acetyl-ACP **40** and (D) *holo*-ACP **43**.

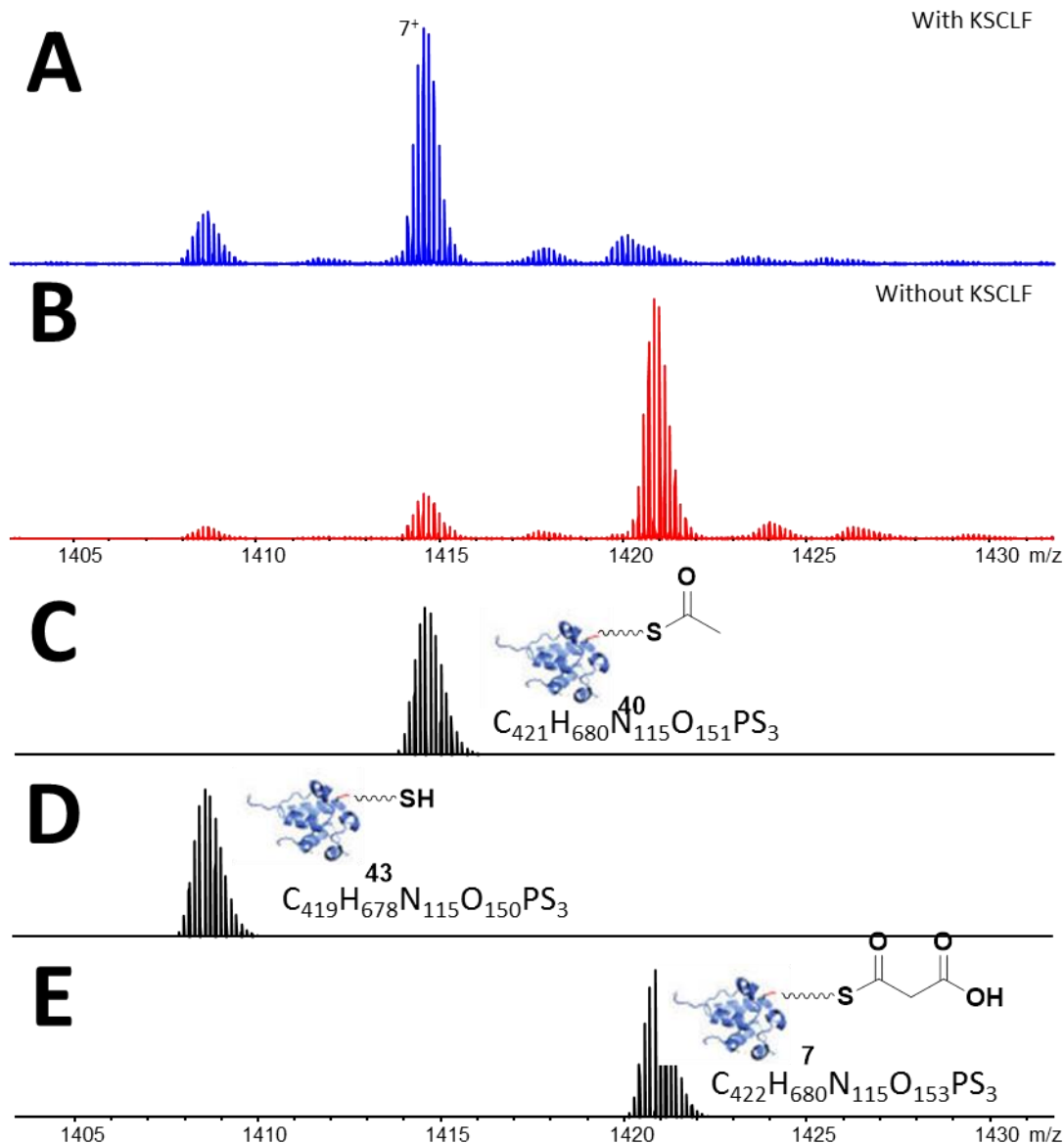


Figure 47 Comparison of the ratios of malonyl **7**, acetyl **40** and holo **43** acyl carrier proteins (ACPs) from the actinorhodin minimal system following 2 hours of incubation (A) with and (B) without the actinorhodin 2 ketosynthase-chain length factor (KS-CLF). Simulated isotope distributions for the 7⁺ charge state of (C) acetyl-ACP **40**, (D) holo-ACP **43** and (E) malonyl-ACP **7**.

The incubated samples were monitored from 2 to 5 hours to determine if the malonyl group would further decarboxylate in the presence or absence of the KS-CLF, or if further holo-ACP **43** would be produced from acetyl-ACP **40**. There was no change

in relative abundances over the 5 hours, suggesting that all action by the KS-CLF is complete within the first two hours. Samples were not analysed within the first two hours. Surprisingly, there is no increase in decarboxylation of malonyl-ACP **7** after the initial two hours, it was expected that even in the absence of KS-CLF that decarboxylation of the malonyl group would occur within five hours at room temperature.

5.1.2.2. The impact of KS-CLF on photolysis of the ACP analogue

63

The photolytic cleavage of the DMNB group of the ACP analogue **63** in the presence and in the absence of the KS-CLF was investigated. In the absence of KS-CLF and after 4 hour irradiation, approximately 50% of carba(dethia) malonyl-ACP analogue **64** was generated, with only a minor amount of decarboxylated carba(dethia) acetyl-ACP **144** present (**Figure 48**). In comparison, when DMNB ACP **63** was irradiated in the presence of the KS-CLF, only a very minimal amount of carba(dethia) acetyl-ACP **144** could be detected (**Figure 49**). By magnifying, it can be seen that no carba(dethia) malonyl-ACP **64** was present and that some decarboxylated product **144** was generated (**Figure 49**). Rapid decarboxylation of the malonyl group of **64** to provide **144** would explain this result, and this agrees with previous observation of the behaviour of malonyl carba(dethia) derivatives (**Figure 47**). Nonetheless these results show how the presence of KS-CLF unequivocally hampers photodeprotection of **63**. This is interesting as it suggests a tight association of the ACP to the KS-CLF, with the modified PPant arm possibly 'buried' within the KS hosting tunnel.

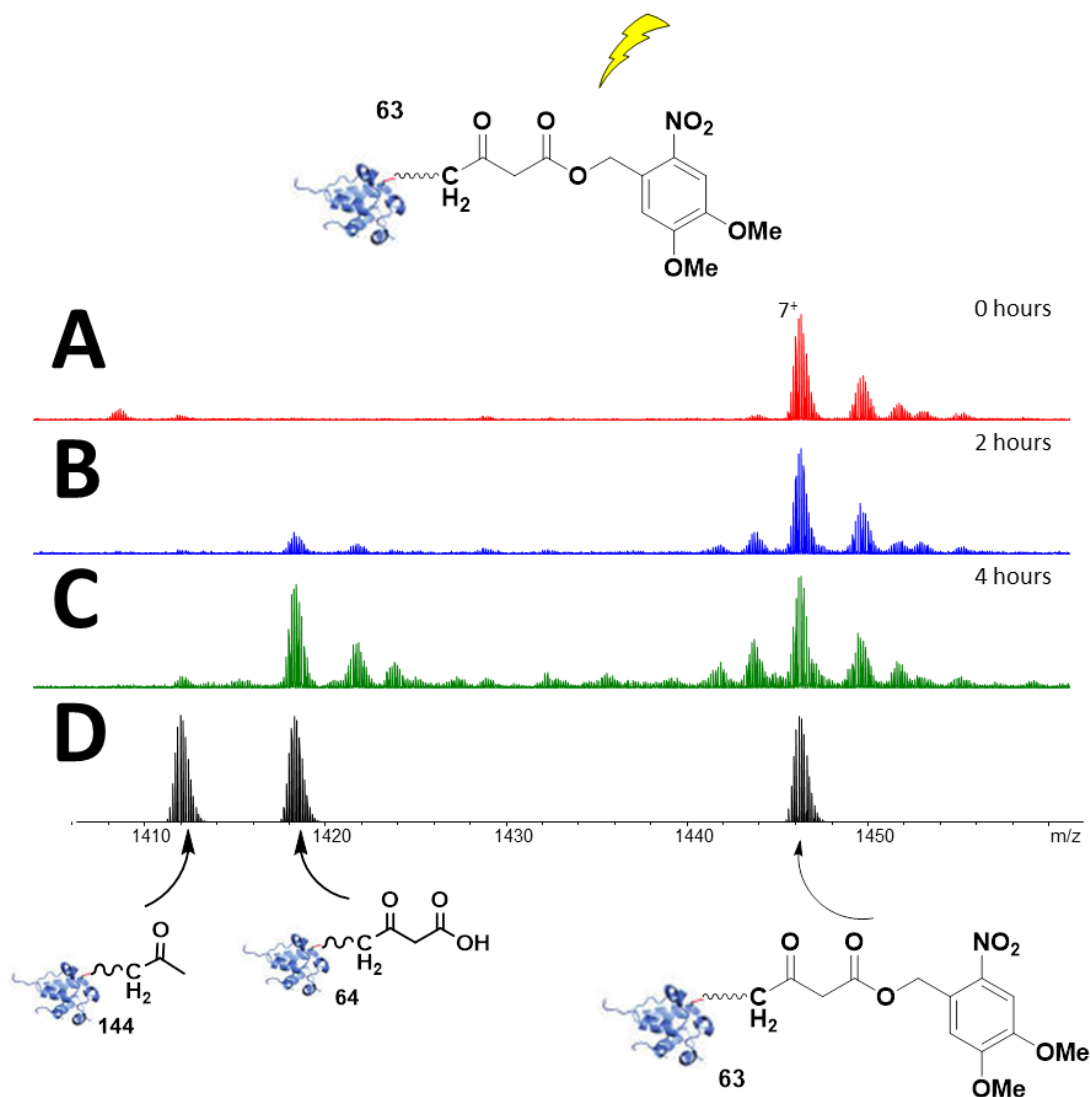


Figure 48 FTICR-MS analyses showing the irradiation of the nonhydrolysable photolabile acyl carrier protein (ACP) analogue **63** with 365 nm, 1000 W, without the ketosynthase chain length factor (KS-CLF), analysed immediately after 0 (**A**), 2 (**B**), and 4 (**C**) hours, showing the synthesis of the deprotected malonyl product **64** and limited decarboxylated product **144**. (**D**) Simulated isotope patterns for the 7^+ ions.

A more direct comparison between the rates of decarboxylation of the carba(dethia) malonyl-ACP analogue **64** and its ‘natural’ malonyl-ACP counterpart **7** in the presence of the KS-CLF was made by performing similar experiments to those shown in **Figure 47** using a readily uncaged sample of deprotected ACP analogue **64**.

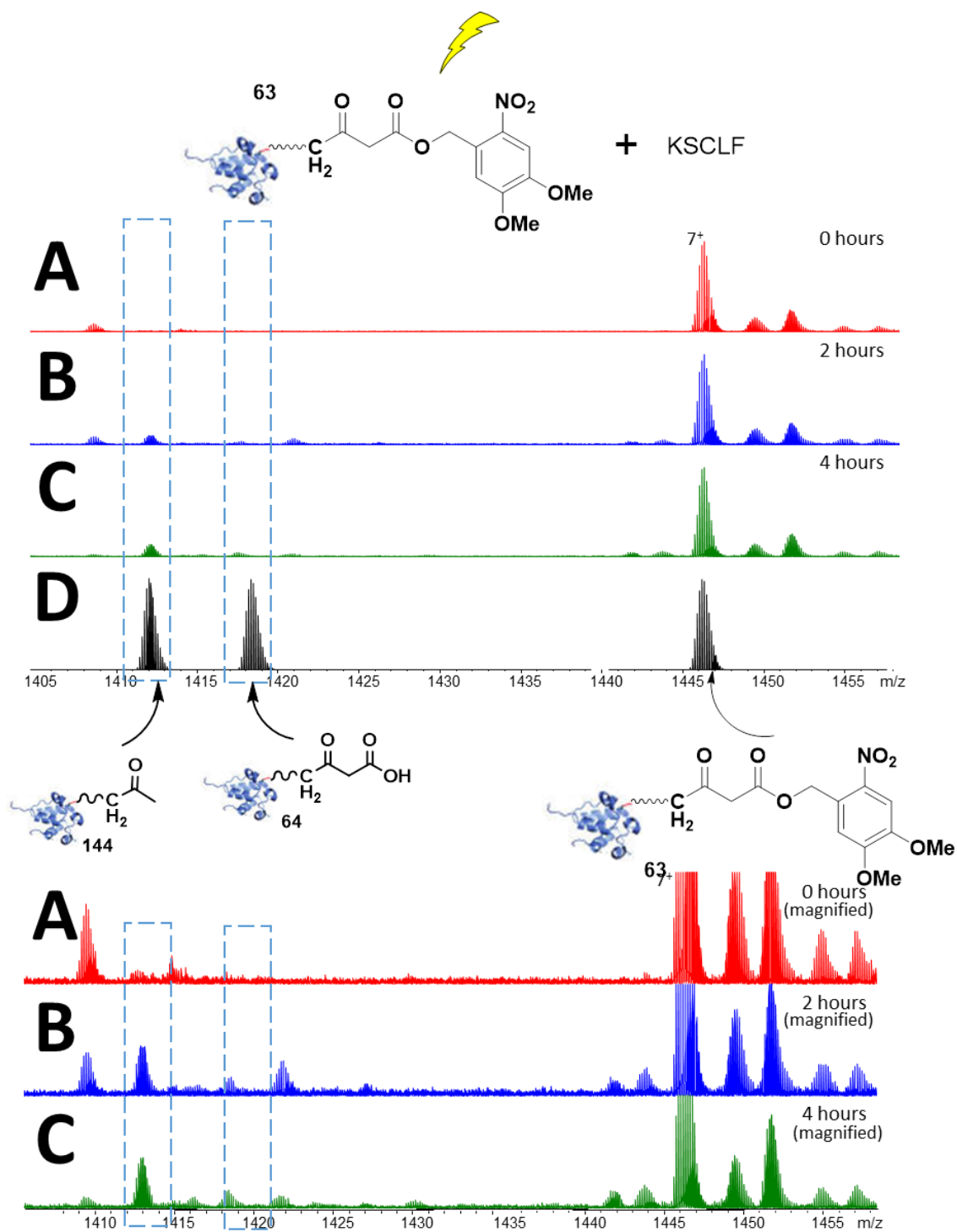


Figure 49 FTICR-MS analyses showing the irradiation of the nonhydrolysable photolabile acyl carrier protein (ACP) analogue **63** with 365 nm, 1000 W, in the presence of the ketosynthase chain length factor (KS-CLF), analysed immediately after 0 (A), 2 (B), and 4 (C) hours: limited deprotected malonyl product **64** and decarboxylated product **144**. (D) Simulated isotope patterns for the 7^+ ions. (A), (B) and (C) underneath are magnified to show the presence of carba(dethia) acetyl-ACP **144** and the absence of carba(dethia) malonyl-ACP **64** in the spectra.

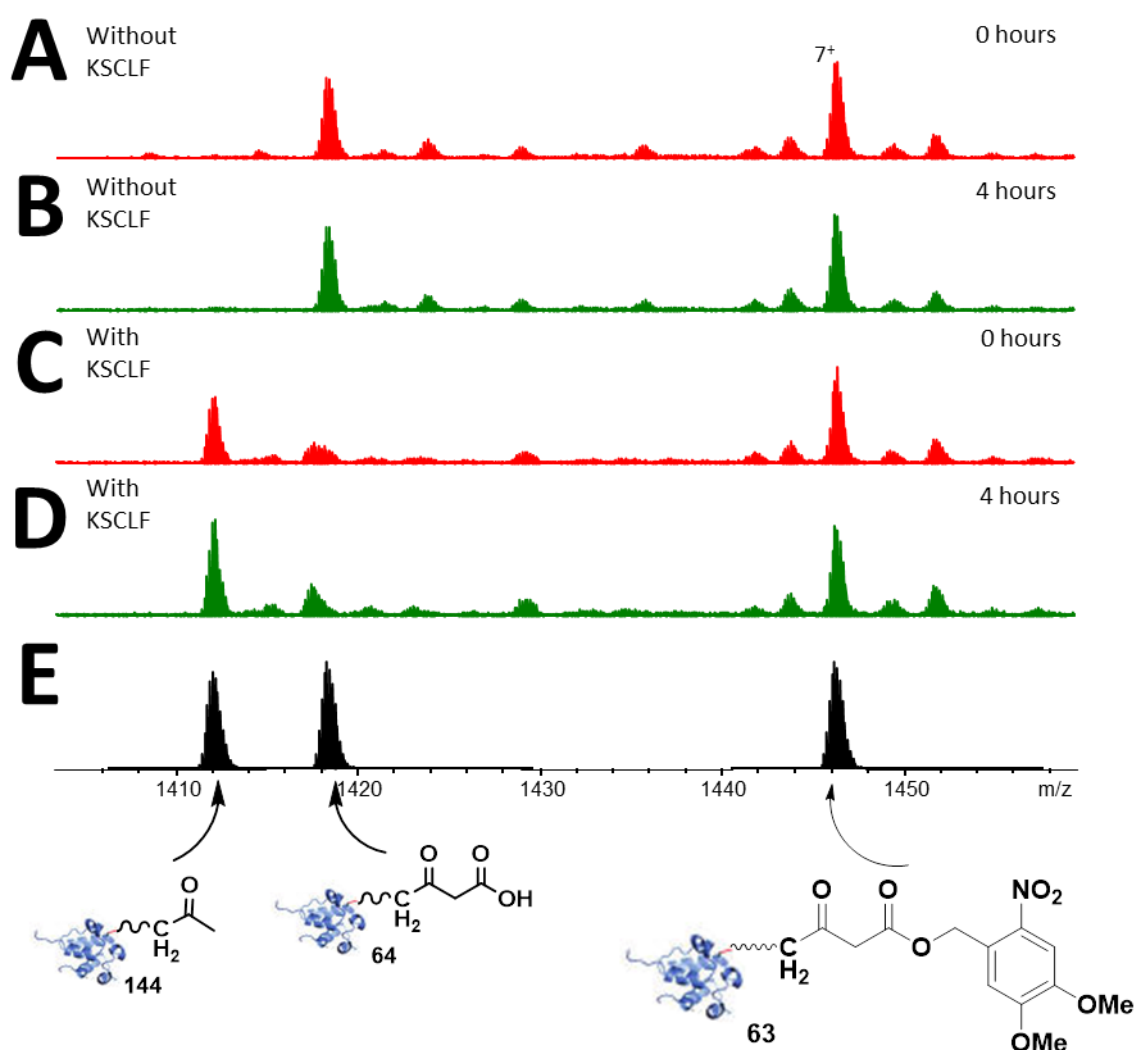


Figure 50 FTICR-MS time-dependant analysis showing a readily uncaged sample of photolabile carrier protein **63**, in the absence, (A and B) and in the presence (C and D), KS-CLF: the uncaged probe **64** decarboxylates instantaneously to **144** in the presence of the KS-CLF. (E) Simulated isotope patterns for the 7⁺ ions. ‘0 hours’ incubation refers to samples analysed immediately after the addition of KS-CLF.

Carba(dethia) DMNB protected malonyl-ACP **63** was irradiated for 4 hours and then incubated either in the presence or in the absence of the KS-CLF for a further 4 hours (**Figure 50**). Samples were analysed hourly from 0 to 4 hours. Samples at ‘0 hours’ were infused into the FTICR mass spectrometer immediately after the addition of the KS-CLF. As previously observed with the ‘natural’ malonyl-ACP **7**,

carba(dethia) malonyl-ACP **64** is remarkably stable alone in buffer at pH 8 and at room temperature for 4 hours, whereas immediately upon the addition of KS-CLF it decarboxylates to produce carba(dethia) acetyl-ACP **144** (**Figure 50**).

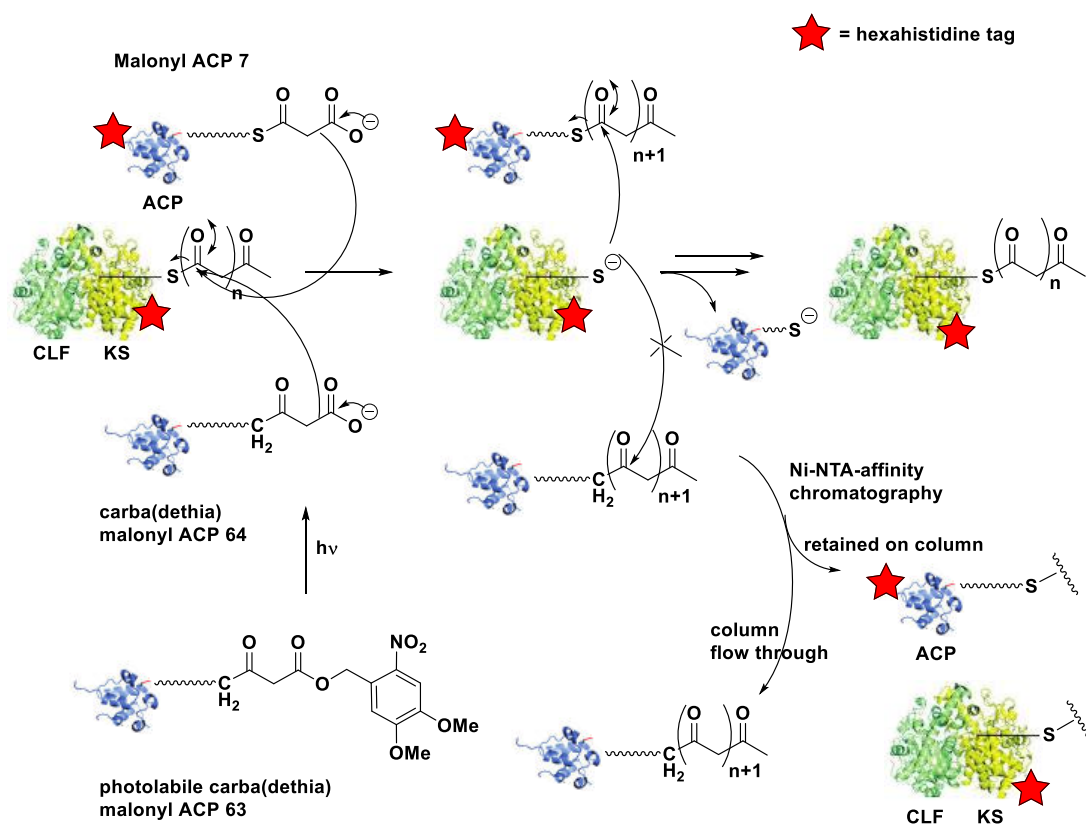
From observing that the photolysis of the DMNB group for **63** was hampered by the presence of KS-CLF, it was envisaged that the ‘active’ probe **64** had to be prepared separately by photolysis prior to its use with the minimal system enzymes. The malonyl groups of both ‘natural’ and carba(dethia) malonyl-ACPs **7** and **64** are stable in the absence of KS-CLF up to approximately 4 hours at room temperature. This facilitates *in vitro* experiments with readily irradiated **63**. The rates of decarboxylation of the ‘natural’ malonyl-ACP **7** and the carba(dethia) malonyl-ACP **64** do not appear to be that different, both in the presence and the absence of the KS-CLF.

5.2. *In vitro* trapping of intermediates from the actinorhodin minimal system with the nonhydrolysable photoactivatable malonyl acyl carrier protein analogue **63**

5.2.1. Experimental set up

Each of the enzymes that reconstitute the act minimal system were expressed and purified with hexahistidine tags (His-tag) for purification by Ni-NTA-affinity chromatography. The act ACP used to prepare the protein probe **63** was the only enzyme for which the His-tag was removed by thrombin, a protease selective for the short amino acid sequence linking the His-tag to the act ACP sequence. This allowed the removal of all the proteins of the act minimal system by affinity chromatography, leaving the probe **63** and any other **63**-derived species readily

isolated for analysis by FTICR-MS (**Scheme 28**). Specific details of this experimental set up are provided in chapter 7.3.



Scheme 28 Investigation of the actinorhodin minimal type II polyketide synthase by means of a protein probe **63**. Purification of enzymatic assays by Ni-NTA affinity chromatography allowed the protein probe **63** and any other derived species to be isolated in the flow through. A hexahistidine tag is indicated by a red star.

5.2.2. Analysis of chain termination assays with protein probe **63** by FTICR-MS

The DMNB protected carba(dethia) ACP analogue **63** was irradiated for 4 hours prior to addition to the actinorhodin minimal system. Malonyl-ACP **7** was either generated from apo-ACP **44** with a phosphopantetheinyl transferase, Sfp⁹⁹, or from self-malonylation¹⁹ of holo-ACP **43** (kind gift of Dr John Crosby, Bristol).

To begin with, a ratio of 1:1 irradiated DMNB protected malonyl-ACP **63** to malonyl-ACP **7** was used for trapping experiments. As discussed in Section 5.2.1, the protein probe **63** was not His-tagged, whereas the malonyl-ACP **7** and KS-CLF retained the His-tag for selective purification of the protein probe **63** and derived species by Ni-NTA affinity chromatography (**Scheme 28**).

It was observed that each repeated experiment did not consistently generate identical results. For example, only a few of the multiple repeats of the 1:1 ratio experiment led to the observation of putative intermediates from the minimal system (**Table 6**). This was not completely unexpected considering the variability of enzymatic activity within sample preparation, the lack of tight control over the timing of enzyme addition, and other experimental variables, coupled with the genuine challenge of analysing a highly heterogeneous sample by direct infusion MS.

It has been previously shown that the ratio of probe to malonyl substrate can be crucial for PKS intermediate trapping *in vitro*.^{11, 153} Different ratios (10:1, 5:1, 1:1, 1:5 and 1:10) of probe **63** to malonyl-ACP **7** were therefore trialled with both ¹³C labelled and unlabelled malonyl-ACP **7b**. The results of these experiments are reported in **Table 6**. ACP probe **63** to malonyl-ACP **7** ratio of 5:1 and 1:10 proved to be the best conditions in which a range of putative intermediates were successfully captured (**Table 6**). In lieu of MS² data, these intermediates are putatively assigned based on accurate mass and isotope distribution.

An additional set of experiments were carried out in a ‘step-wise’ or ‘reversed’ manner, whereby the minimal system enzymes (KS-CLF and malonyl-ACP **7**) were added hourly during irradiation of the DMNB protected ACP probe **63**, resulting in a ratio of 1:4 ACP probe **63** to malonyl-ACP **7**. These experiments led to the ACP

capture of a diketide **145** and a hexaketide **149** species, together with dehydrated and doubly dehydrated hexaketides **156** and **157**, and of a ^{13}C labelled pentaketide **148** in the corresponding labelled assay. The MS analyses of these captured intermediates will be presented in the following sections.

	(with unlabelled malonyl-ACP 7)					(with ^{13}C labelled malonyl-ACP 7b)			
	1:1	1:4 (step-wise)	5:1	1:1 30s delay	1:1 5m delay	1:1	1:10	5:1	1:4 (step-wise)
Diketide 145	Blue	Blue							
Triketide 146									
Tetraketide 147						Red	Red		
Pentaketide 148									Red
Hexaketide 149		Blue							
Heptaketide 150									
Octaketide 151									
Dehydro tetraketide 152									
Didehydro tetraketide 153									
Dehydro pentaketide 154			Blue						
Didehydro pentaketide 155								Red	
Dehydro hexaketide 156		Blue	Blue						
Didehydro hexaketide 157	Blue	Blue		Blue	Blue				
Dehydro heptaketide 158									
Didehydro heptaketide 159									
Dehydro octaketide 160									
Didehydro octaketide 161									
Tridehydro octaketide 162									

Table 6 Intermediates from the actinorhodin minimal system trapped by the carba(dethia) malonyl-ACP probe **64** were detected by FTICR-MS direct injection. Each column shows a separate experiment conducted with the respective ratio of probe **63** to malonyl-ACP **7**. Blue in-fill represents an unlabelled trapped intermediate detected and red in-fill represents a ^{13}C labelled trapped intermediate detected. “Step-wise” indicates the reverse and gradual addition of the actinorhodin minimal system enzymes to an irradiated sample of the DMNB protected protein probe **63**. “30s delay” and “5 m delay” refer to the time delay upon addition of ‘active’ probe **64** to the actinorhodin minimal system. (See **Appendices 1-68**)

The MS samples were very complex and variable, however the major ions observed in each spectrum were typically decarboxylated protein probe **144** and, in much less

intensity, the DMNB protected probe **63**. These species allowed accurate internal calibration of each spectrum, achieving sub ppm error on the majority of assigned peaks.

With the complexity of the samples, control assays proved crucial for peak assignment. These included the DMNB protected probe **63** without the presence of the *act* minimal system enzymes, the irradiated probe **64** without the minimal system enzymes and the DMNB protected probe **63** with the enzymes of the minimal system. Each control assay was compared with the trapping assays for confirmation of the presence of novel isotopic distributions (See **Appendices 51-58**).

5.2.2.1. Detection of a putative captured diketide intermediate 145

A putative trapped diketide intermediate **145** was detected in a 1:1 ACP probe **63** to malonyl-ACP **7** standard experiments as well as 1:4 step-wise addition assays. In both cases the isotopic distribution of **145** very closely overlaps with another unknown distribution (**Figure 51**). Unfortunately, when the peaks merge, this increases the error on those peaks; for example, the A+3 peak shown in **Figure 51** presents a much higher error of 3.22 ppm than the subsequent peaks. Discounting the A+3 peak reduces the average error to -0.60 ppm. Unfortunately, there was no detectable labelled diketide found in any of the labelled assays. Additionally, due to both the low intensity and the overlapping distributions, it is not possible to compare the ion abundance in the simulated isotopic distributions to that of the collected spectra.

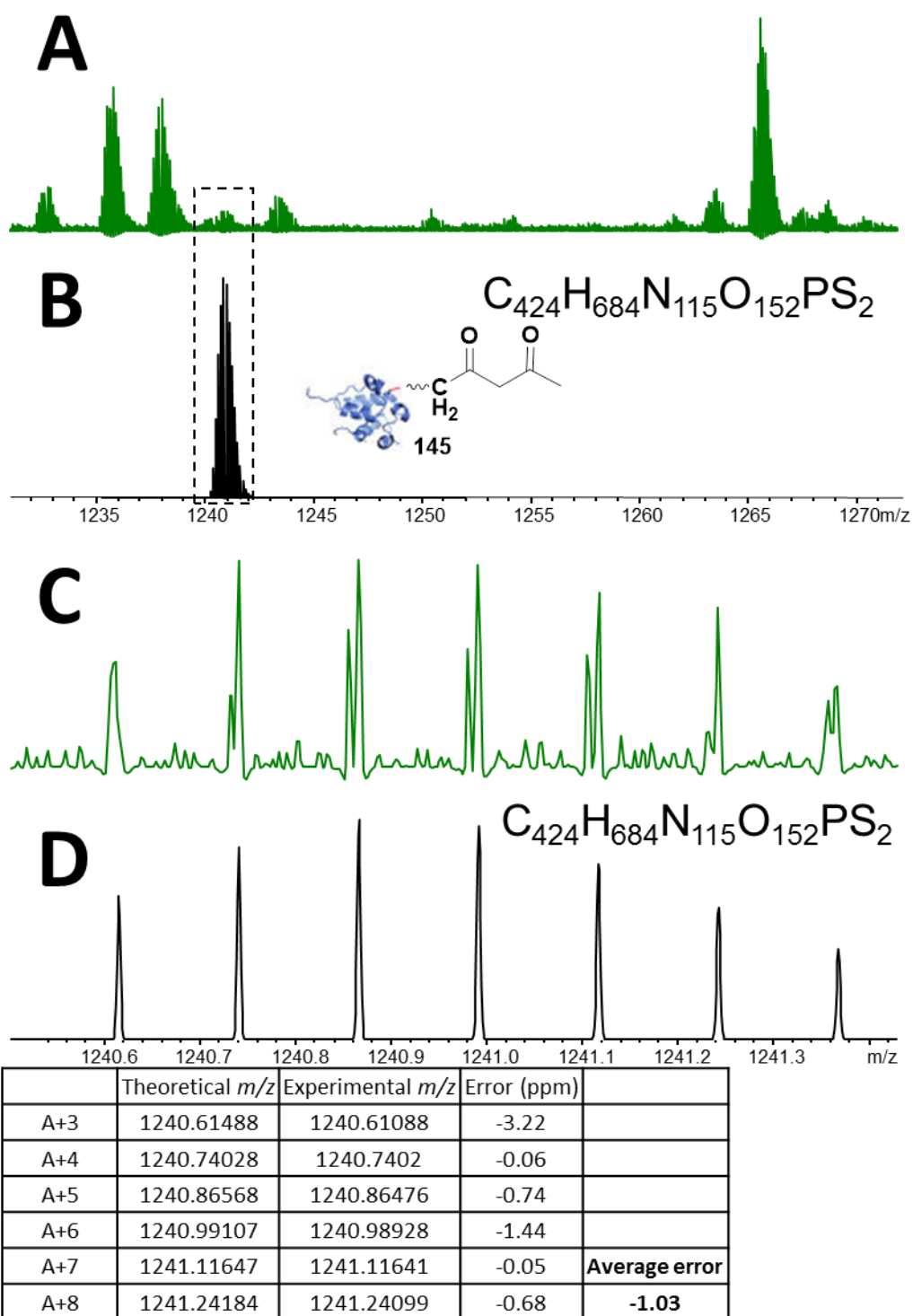


Figure 51 FTICR-MS analysis of active acyl carrier protein (ACP) probe **64** incubated in the actinorhodin minimal system (1:1 ratio, protected ACP probe **63** to malonyl-ACP **7**) showing an off-loaded diketide **145**. (A) Acquired spectrum, (C) acquired spectrum magnified, (B) and (D) are simulated mass spectra (δ^+) of **145**. Underneath displays the peak list and errors for each.

5.2.2.2. *Detection of a putative captured tetraketide intermediate 147*

On two accounts a labelled putative trapped tetraketide **147** was detected. Unfortunately, the respective unlabelled tetraketide intermediate **147** was not detected in any of the assays. The intermediate **147** was detected in experiments at 1:1, ACP probe **63** to malonyl-ACP **7**, and in greater abundance at a ratio of 1:10 (**Figure 52**). Additionally, in the 1:10 assay the adduction of sodium to the tetraketide intermediate **147** can be seen in the spectra.

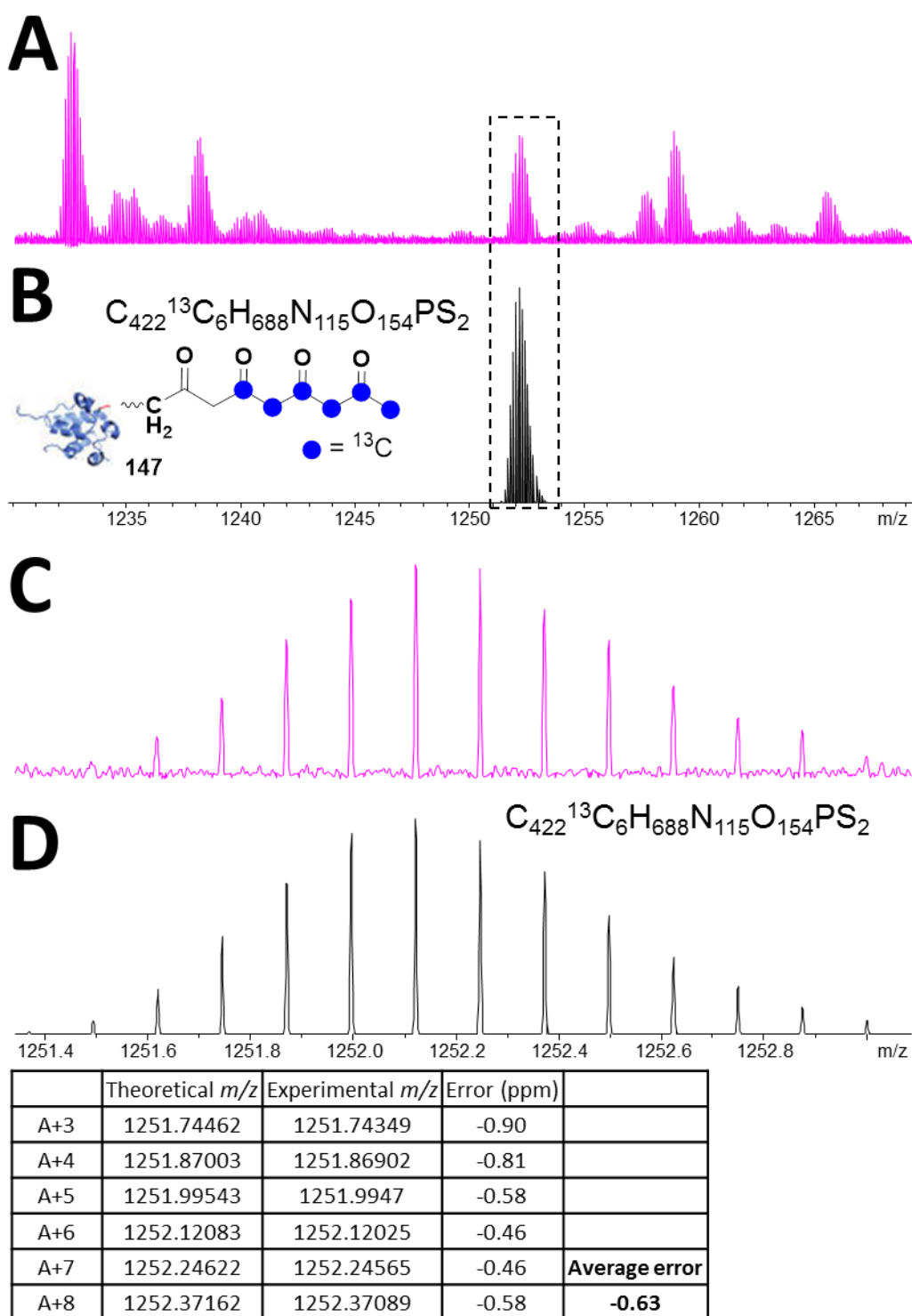


Figure 52 FTICR-MS analysis of active acyl carrier protein (ACP) probe **64** incubated in the actinorhodin minimal system (1:10 ratio, protected ACP probe **63** to labelled malonyl-ACP **7b**) showing an off-loaded labelled tetraketide **147**. (A) Acquired spectrum, (C) acquired spectrum magnified, (B) and (D) are simulated mass spectra (8^+) of **147**. Underneath displays the peak list and errors for each.

form, but spontaneously undergo keto-enol tautomerisation and cyclisation. Nonetheless the fact that it has been detected in an uncyclised form suggests that this polyketone intermediate **148** is sequestered and stabilised within the ACP.²⁹⁴

Beside the putative uncyclised **148**, a putative dehydrated cyclised pentaketide **154** and of a further dehydrated species **155** were identified. Their proposed structures are shown in **Scheme 29** and have been inferred on the basis of the folding of the natural octaketide chain leading to dehydro SEK4 **163** and dehydro SEK4b **164**.²⁹⁵ The presence of these species is reasonable on chemical grounds and consistent with the limited detection of the linear pentaketide **148**.

Pentaketide dehydration/cyclisation could take place either within the PKS, or following its capture by the ACP probe **64** if the pentaketide chain becomes exposed to the solvent. However, without further characterisation of **154** and **155**, the exact location of the cyclisation is unknown. Additionally, the dehydration could take place elsewhere on the protein rather than on the putative intermediate. Due to low intensity signal as well as multiple overlapping isotopic distributions, the “PPant ejection assay” could not be successfully carried out, and the errors on some of the assigned peaks are not consistently as low as they could be (**Figure 55**).

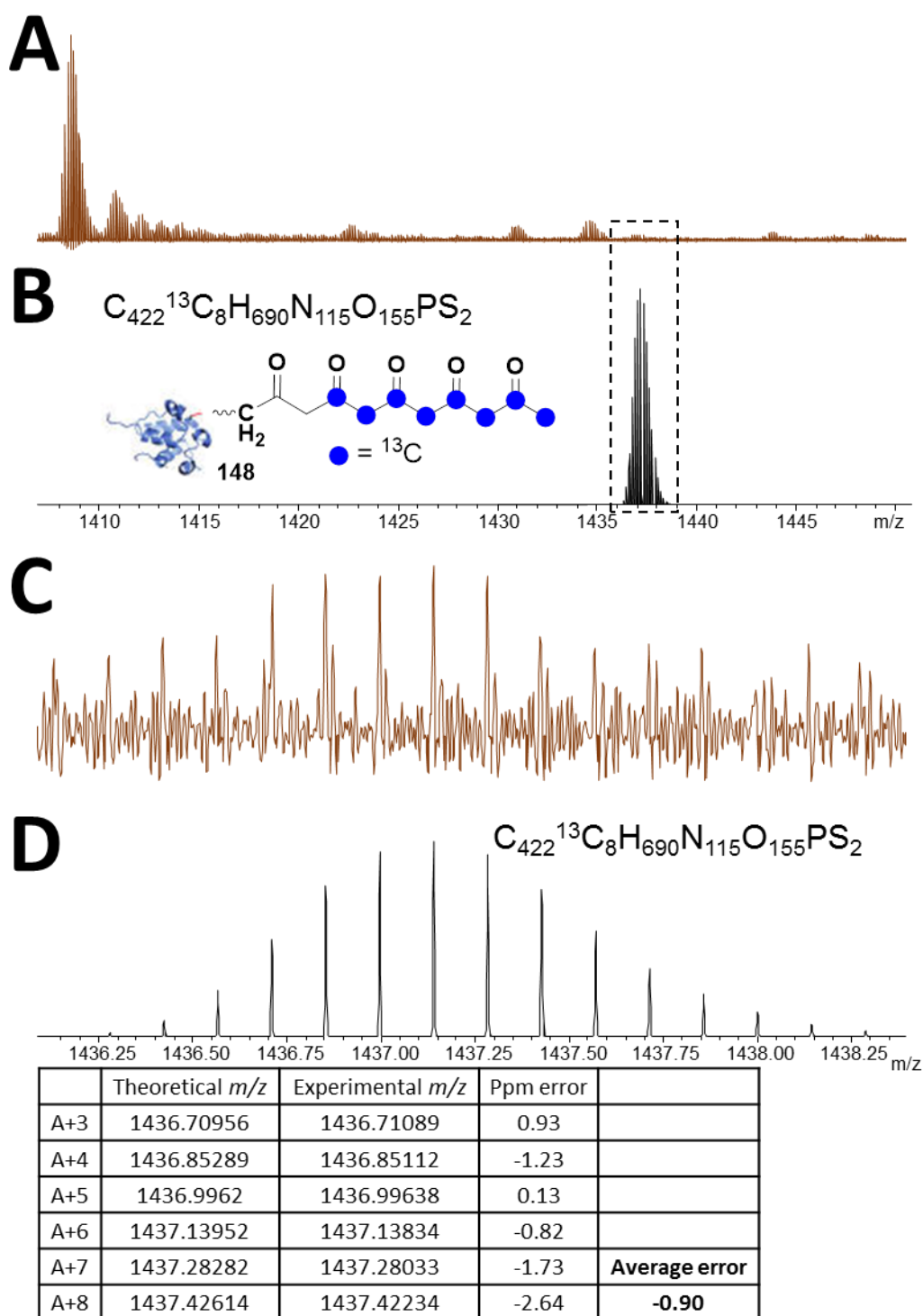


Figure 53 FTICR-MS analysis of ACP probe **64** incubated in the actinorhodin minimal system (1:4 protected ACP probe **63** to labelled malonyl-ACP **7b**), showing a putative captured labelled linear pentaketide **148**. (A) Acquired spectrum, (C) Acquired spectrum magnified, (B) and (D) are simulated mass spectra (7^+) of **148**. Underneath displays the peak list and errors for each.

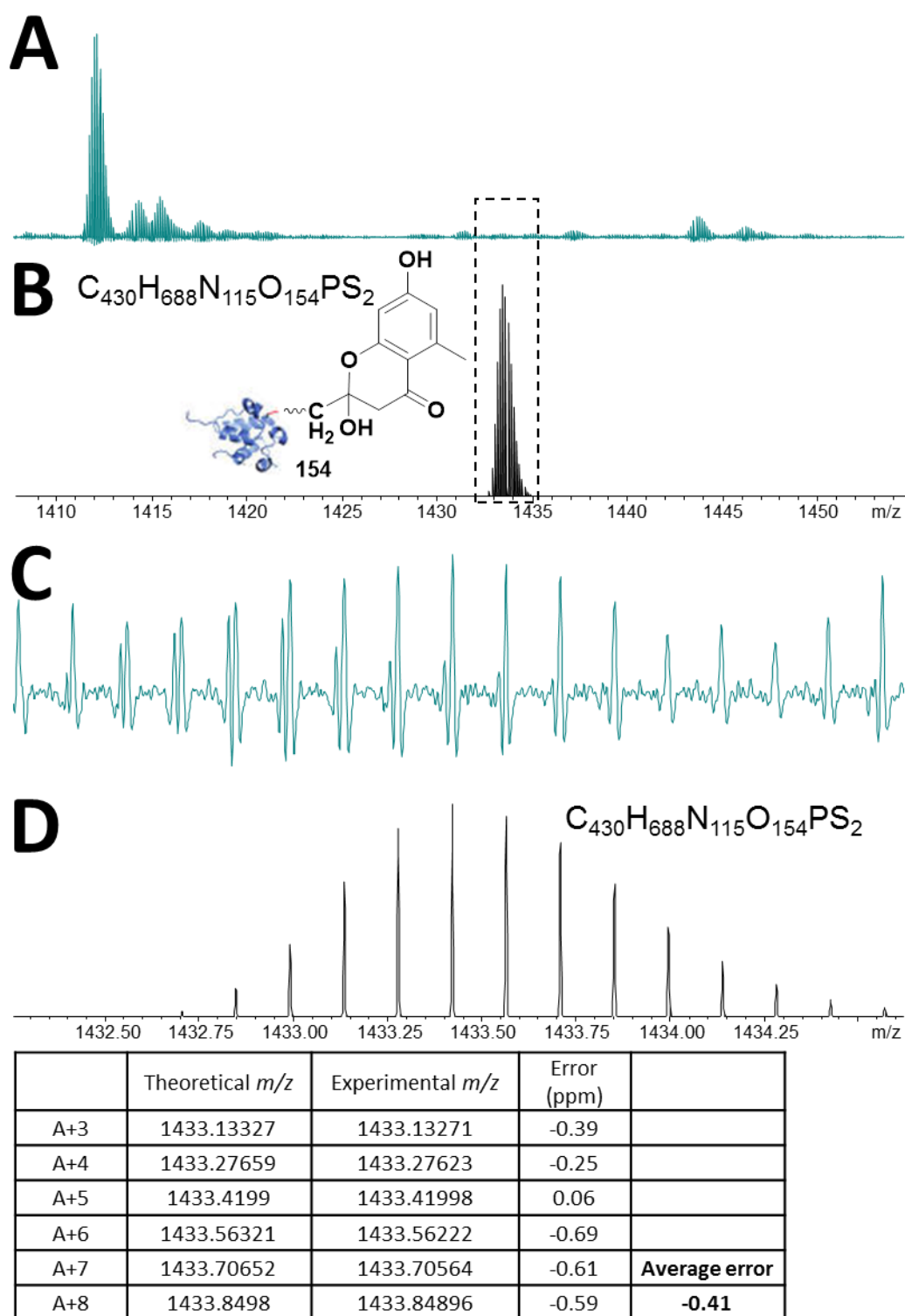


Figure 54 FTICR-MS analysis of the ACP probe **64** incubated in the actinorhodin minimal system (5:1 protected ACP probe **63** to malonyl-ACP **7**) showing a captured putative cyclised pentaketide **154**. (A) Acquired spectrum, (C) acquired spectrum magnified, (B) and (D) are simulated mass spectra (7^+) of **154**. Underneath displays the peak list and errors for each.

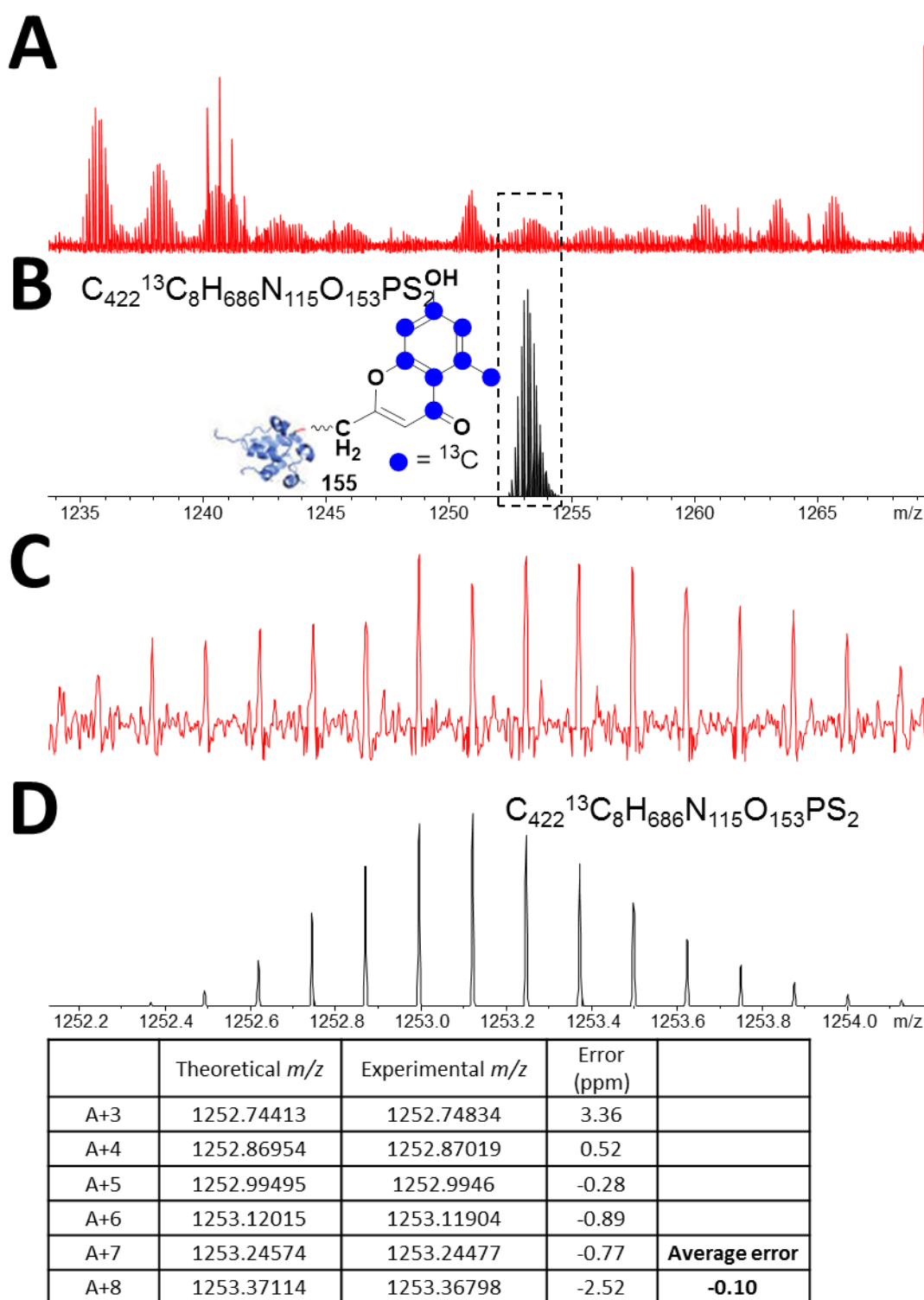
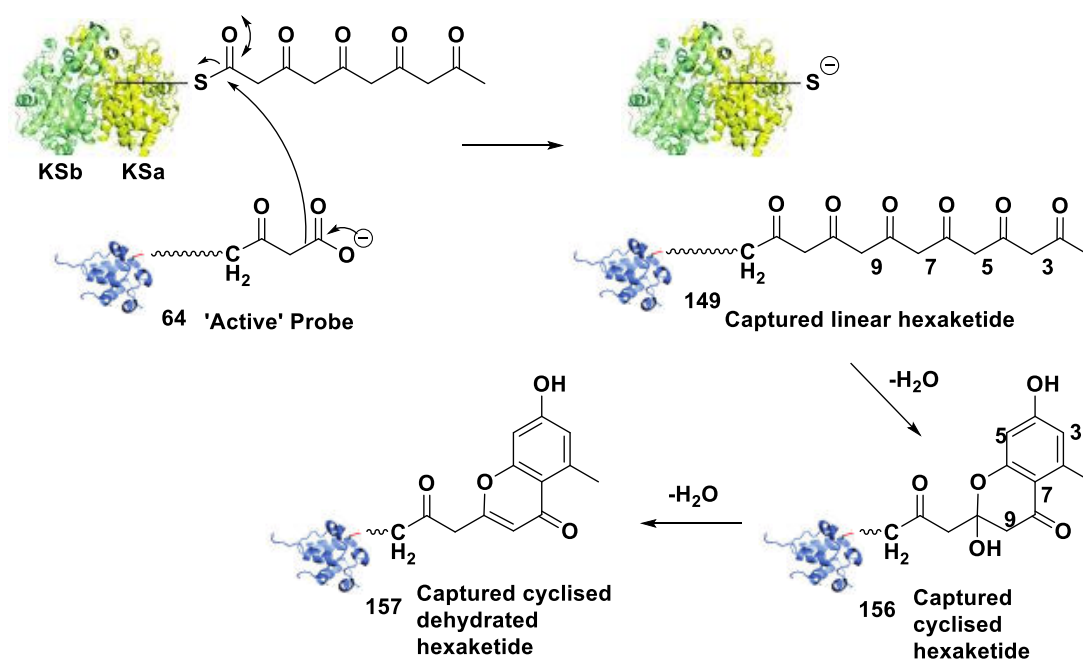


Figure 55 FTICR-MS analysis of the ACP probe **64** incubated in the actinorhodin minimal system (5:1 protected ACP probe **63** to labelled malonyl-ACP **7b**), showing a captured putative cyclised dehydrated pentaketide **155**. (A) Acquired spectrum, (C) acquired spectrum magnified, (B) and (D) are simulated mass spectra (8^+) of **155**. Underneath displays the peak list and errors for each.

5.2.2.4. *Detection of a putative captured hexaketide intermediate 149 and dehydrated species 156 and 157*

A hexaketide **149**, and two likely cyclised **156** and dehydrated **157** captured species were detected on a few occasions (**Scheme 30**). The putative uncyclised hexaketide intermediate **149** was only detected once across all samples and at a very low intensity (**Figure 56**). This is likely due to the unstable nature of a polyketide chain which will spontaneously undergo cyclisation. **149** was only detected in the 1:4 step-wise experiment described previously.



Scheme 30 Capture of putative hexaketide intermediates from the actinorhodin minimal system: predicted linear intermediate **149** can undergo cyclisation and dehydration to produce **156** and **157**.

The intensity of the detected species **156** was low, additionally overlapping isotopic distributions negatively affected the error in some cases. **156** was detected in 1:4 step-wise assays, and also in a 5:1 probe **63** to malonyl-ACP **7** experiment (**Figure 57**).

The last hexaketide derived intermediate **157** is the result of a further dehydration of **156** (**Scheme 30**). Loss of water is quite recurrent within compounds of this nature, and, as mentioned previously, has been observed in the minimal system products.²⁹⁵ The intensity of the detected species **157** is greater than for the other hexaketide and hexaketide derived species **149** and **156**, and there is possibly only one nearby isotopic distribution affecting the error and overall shape of the distribution (**Figure 58**). This intermediate **157** was the most recurrently detected intermediate in 1:1 assays, including those with time delays and in step-wise 1:4 experiments.

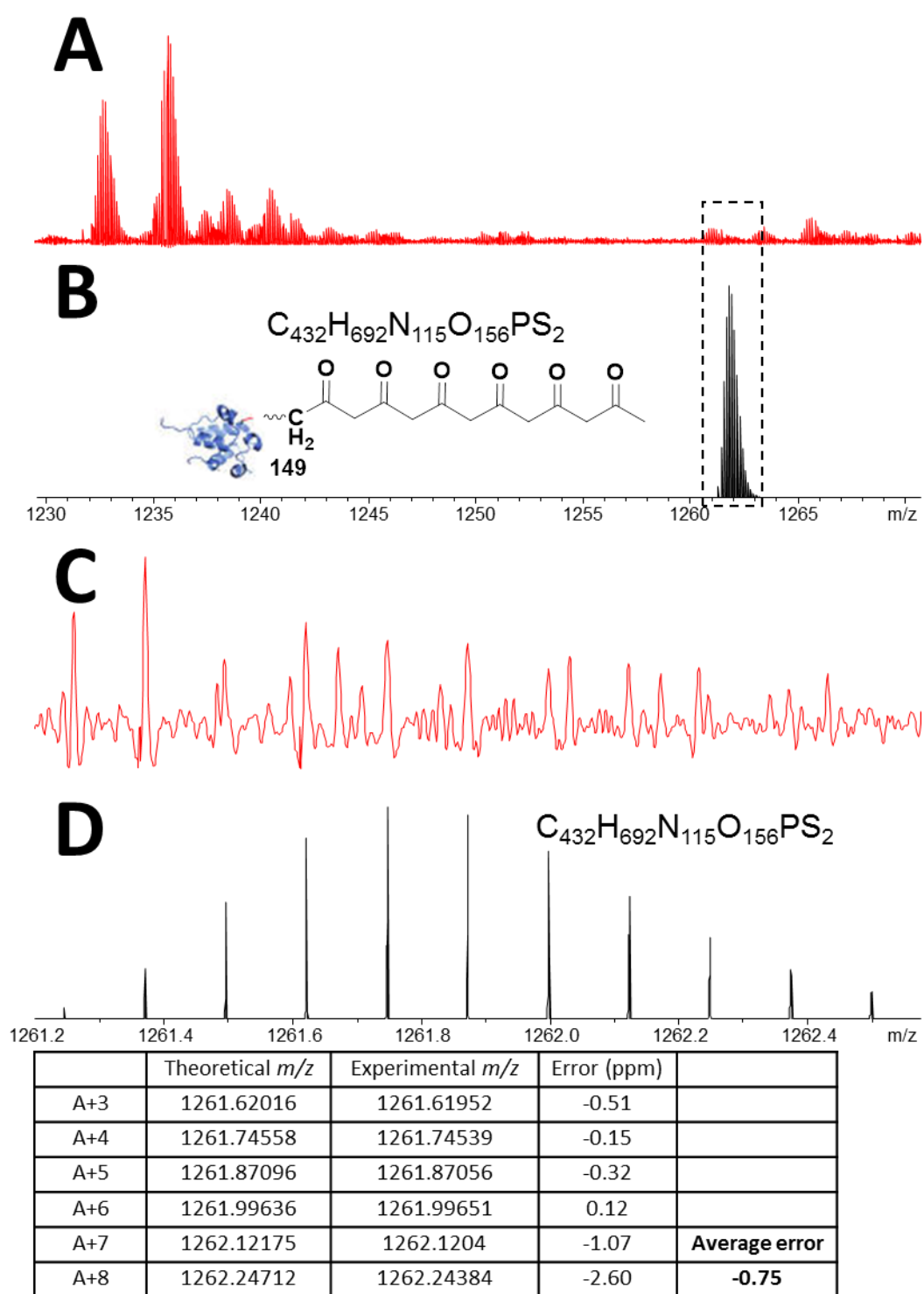


Figure 56 FTICR-MS analysis of ACP probe **64** incubated in the actinorhodin minimal system (1:4 protected ACP probe **63** to malonyl-ACP **7**), showing a putative captured linear hexaketide **149**. (A) Acquired spectrum, (C) acquired spectrum magnified, (B) and (D) are simulated mass spectra (8^+) of **149**. Underneath displays the peak list and errors for each.

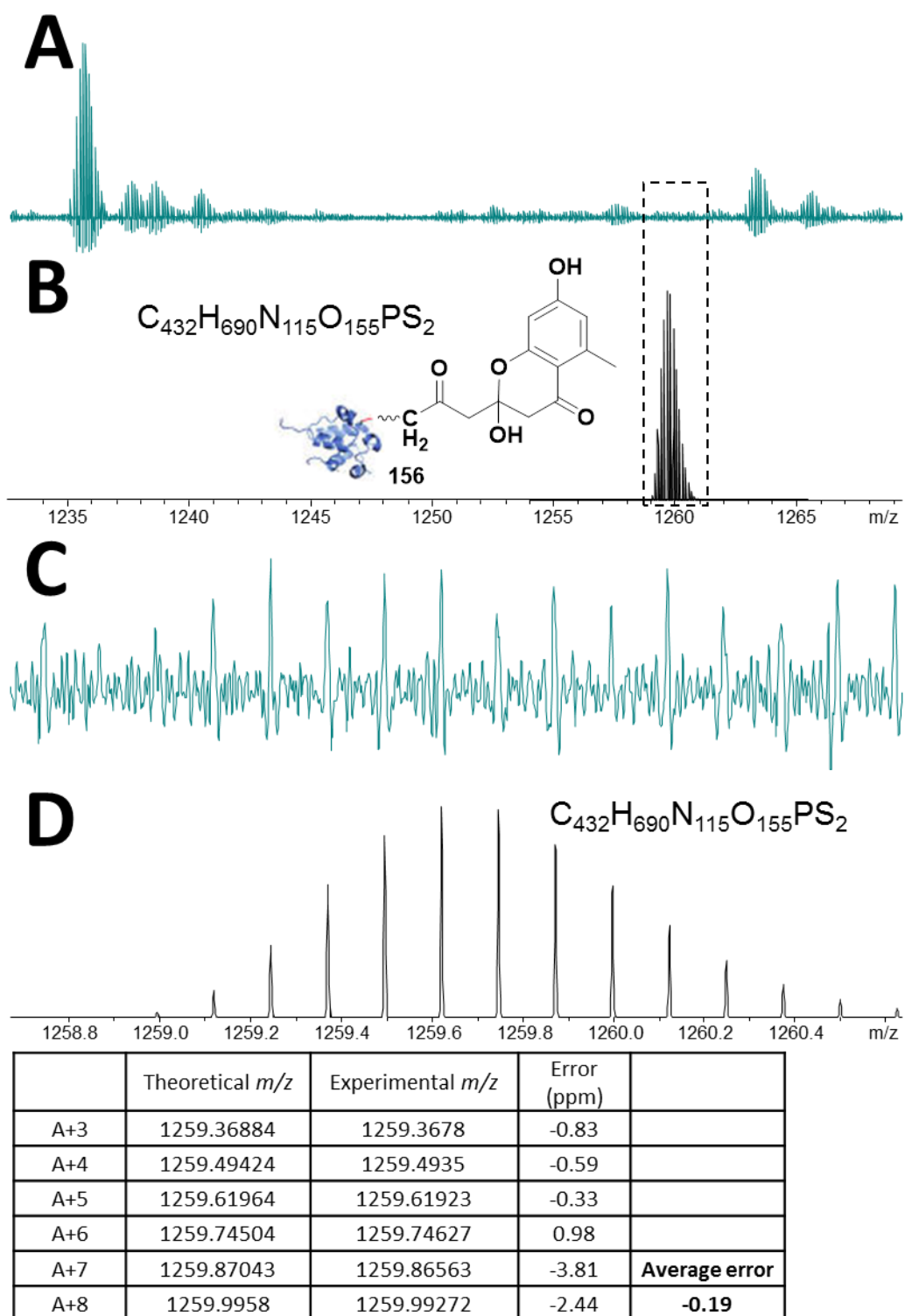


Figure 57 FTICR-MS analysis of ACP probe **64** incubated in the actinorhodin minimal system (5:1 protected ACP probe **63** to malonyl-ACP **7**), showing a putative captured cyclised hexaketide **156**. (A) Acquired spectrum, (C) acquired spectrum magnified, (B) and (D) are simulated mass spectra (8^+) of **156**. Underneath displays the peak list and errors for each.

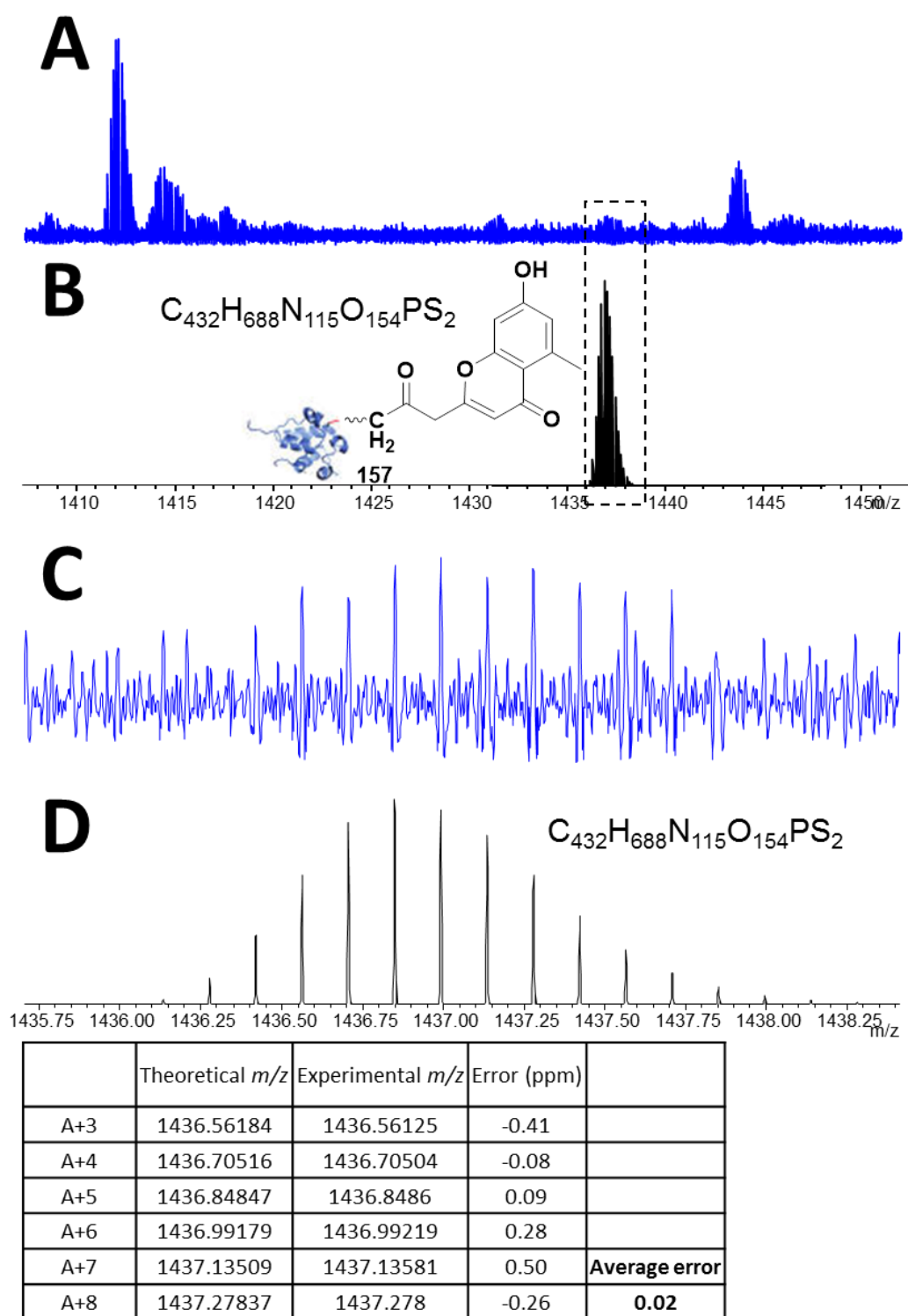


Figure 58 FTICR-MS analysis of ACP probe **64** incubated in the actinorhodin minimal system (1:1 protected ACP probe **63** to malonyl-ACP **7**), showing a putative captured cyclised dehydrated hexaketide **157**. (A) Acquired spectrum, (C) acquired spectrum magnified, (B) and (D) are simulated mass spectra (7^+) of **157**. Underneath displays the peak list and errors for each.

5.2.2.5. *Summary of off-loaded intermediates*

The samples obtained by chain termination experiments with the protein probe **63** and directly infused into the FTICR-MS proved extremely complex to analyse, with multiple isotopic distributions overlapping throughout the spectra. As discussed, major peaks found in the spectra included decarboxylated probe **144**, residual DMNB protected probe **63**, as well as *apo*-ACP **44** and *holo*-ACP **43** deriving from the photolabile probe **63** preparation, whereas the putative intermediates **145**, **147-149**, and **154-157** were of considerably lower abundance. Charge states ranging from 11⁺ to 7⁺ were observed for all these intermediates, with selected spectral regions shown within Section 5.2.2 and the appendices reporting further full peak lists and additional figures for the different charge states.

Unfortunately, due to the low intensity of the species **145**, **147-149**, and **154-157** (only detected after accumulation of spectra over 300 scans) and the complexity of the sample, no MSⁿ fragmentation of these ions could be carried out.

LC retention times would have been useful to gain some insight into the nature of the detected intermediates. LC-FTICR-MS was not possible on this occasion due to the large quantity of samples and file sizes reaching approximately 100 GB per LC-MS run. However, as each direct infusion sample required approximately 20 mins of acquisition, it is possible that, although the LC would purify the sample, the low intensity intermediates would not be detected within the peak elution time.

Analysis of these samples was only performed on an FTICR-MS as lower resolution instruments are not able to resolve the isotopic distributions necessary for confident identification of the species bound to the ~10 kDa protein.

Putative hexaketide derived intermediates **149**, **156** and **157** were detected in the most number of samples, however shorter chain intermediates such as the diketide **145** and the tetraketide **147** were more abundant when detected. Putative longer chain polyketide intermediates, such as heptaketide **150** and octaketide **151** were not detected in any sample, including dehydrated species. It is likely that the observed putative captured species are an indicator of the slow steps of polyketide chain extension. Keatinge-Clay *et al.* suggested that the cyclisation event occurs after the heptaketide stage of chain elongation as the KS-CLF ‘tunnel’ was shown by X-ray crystallography to only accommodate a chain of this length.²⁵ It is possible that as the chain length approaches its maximum the elongation becomes slower or more susceptible to interruption by the ACP probe **64**.

5.2.2.6. Autocorrelation of low intensity isotopic distributions for detecting trapped polyketide intermediates

As the putative detected intermediates trapped by the ACP probe **64** were of very low intensity, additional data analysis of the isotopic distributions was performed to confirm their presence as ‘real’ peaks. A ‘real’ set of peaks would have an isotopic distribution, the detection of such peaks can be accomplished by performing autocorrelation of the region in the spectrum. This method of data analysis has been previously carried out for complex spectra such as polymer mixtures and naphthalene pitch.²⁹⁶⁻³⁰¹ The autocorrelation algorithm, essentially, finds periodic patterns in data, or the cross-correlation of signals with themselves at different points. These patterns infer the charge state, for example, a m/z 0.5 spacing indicates

a 2^+ charge state. If the region of the spectrum does not contain these patterns then that region is ‘noise’, or random data points.^{297, 302}

Figure 59 presents an example of the autocorrelation of a very intense region of the spectrum, the 8^+ isotopic distribution of the signal for the protected ACP probe **63**. A large peak in the autocorrelation spectrum (inset) can be seen at a charge state of 8. For comparison, a region of known ‘noise’ in the spectrum, at high m/z , was chosen and, as expected, no autocorrelation can be seen for that region (**Figure 60**).

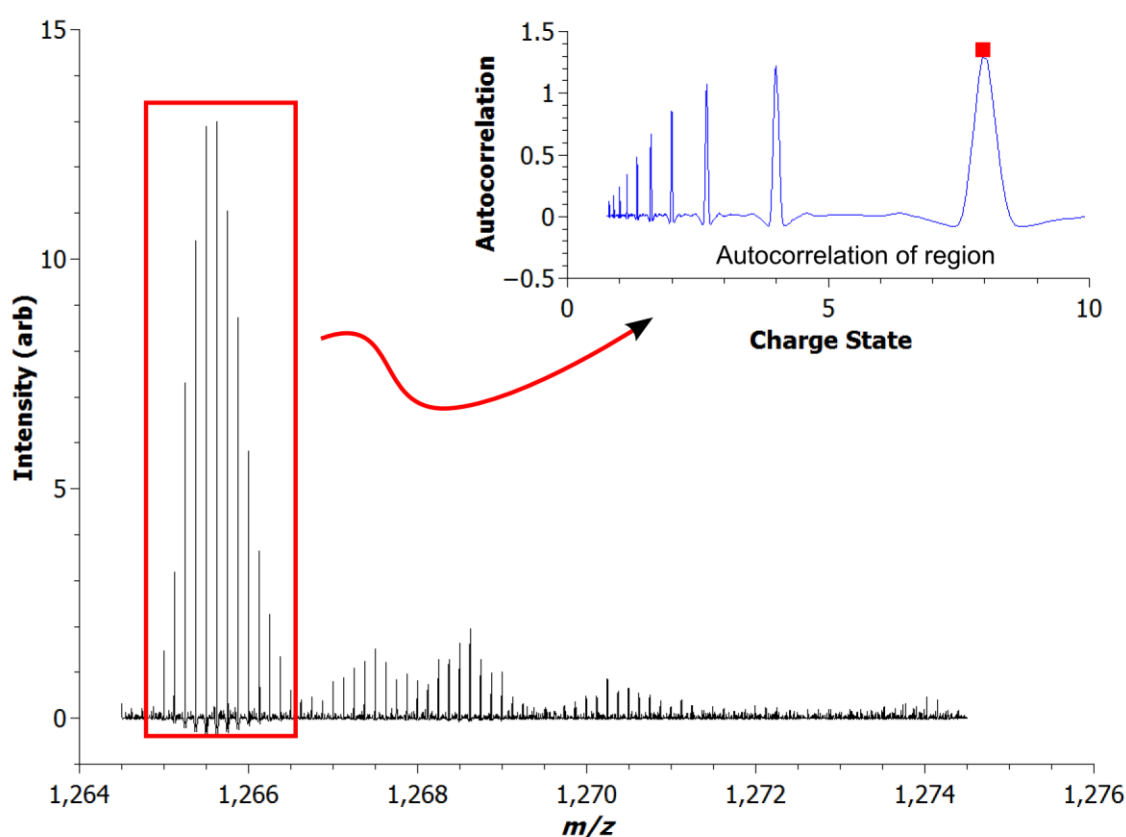


Figure 59 Example of a region of a spectrum with a very intense peak (protected ACP probe **63** at charge state 8^+) with the inset showing the auto-correlation of the region indicated, confirming the 8^+ charge state.

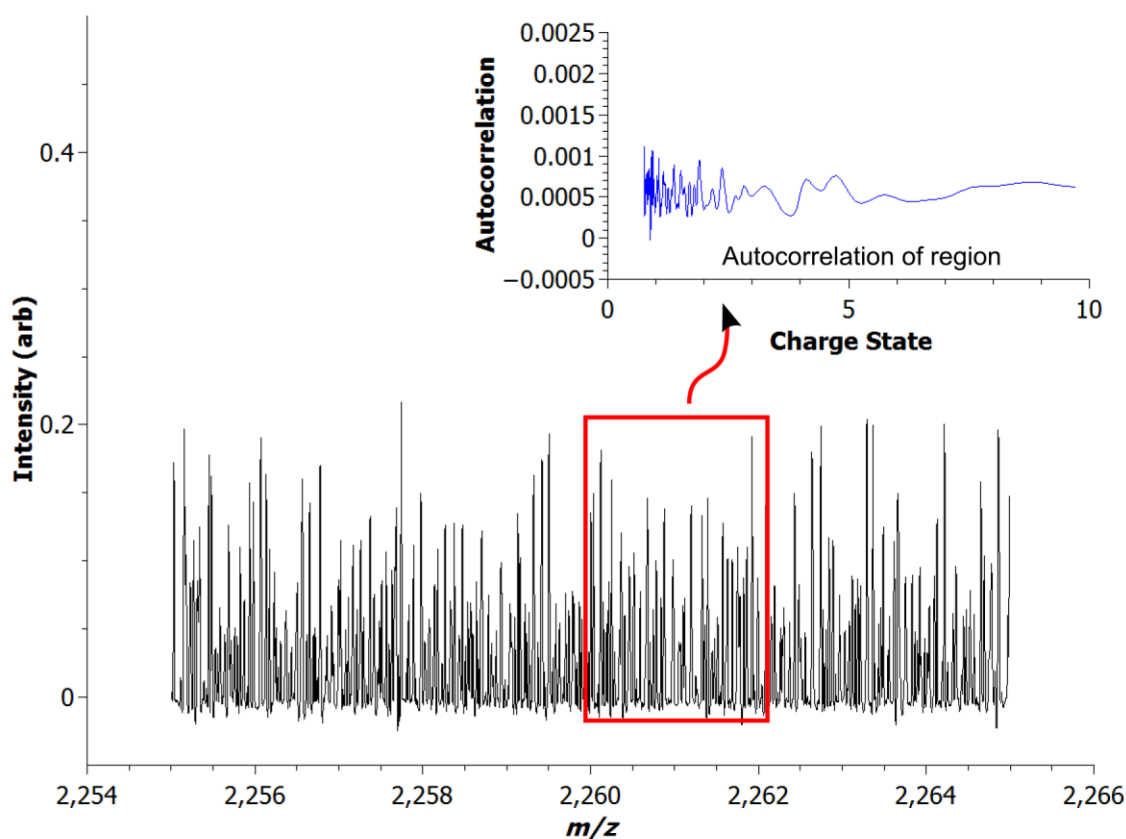


Figure 60 A blank region of a spectrum with the inset showing the auto-correlation of the region indicated, confirming that no isotopic distributions were detected, and this region of the spectrum is, indeed, noise.

The autocorrelation algorithm was applied to those regions of low intensity that had been previously manually identified to contain isotopic distributions for putative captured intermediates by the ACP probe **64** (See appendices).

The region of the spectrum generated from a ‘stepwise’ 1:4 protected ACP probe **63** to malonyl-ACP **7** chain termination assay and suspected to contain a cyclised hexaketide intermediate **156** bound to the ACP, at a charge state of 8^+ , was analysed. These sets of peaks had previously been identified by comparison with the simulated isotopic distribution, and from A+3 to A+7 the average error was calculated to be -0.41 ppm. The autocorrelation of this region detected a strong 8^+ charge state

(**Figure 61**). The detection of this charge state confirms that this is not a region of noise or random data in the spectrum, but is a real set of peaks. That information, combined with the low ppm error, confirms the annotation of that distribution to be a trapped dehydro hexaketide **156**.

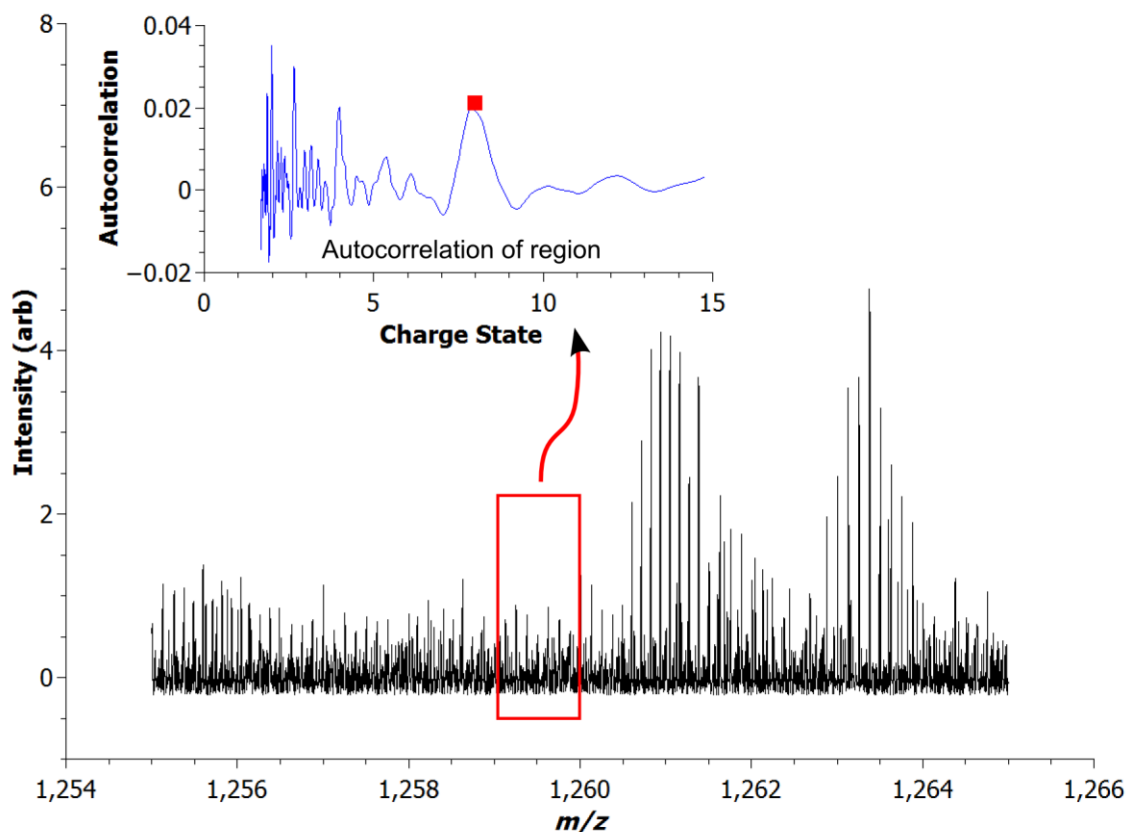


Figure 61 Spectrum of a detected cyclised hexaketide **156** of charge state 8^+ with inset showing autocorrelation of region indicated confirming an 8^+ charge state.

All other isotope distributions of low intensity were analysed with the autocorrelation algorithm. This method allowed additional confirmation of the presence of intermediates manually identified. Since completion of the analysis of this data, a way of using the algorithm to identify isotope distributions in the spectra simultaneously with their assignment has been developed.³⁰³ This greatly helps the

identification and characterisation of the multiple isotopic distributions observed in these complex samples.

5.2.2.7. Tryptic digestion of the acyl carrier protein from the actinorhodin minimal system

Trypsin is a widely used protease for ‘bottom-up’ proteomics, or cleavage of proteins for low resolution MS analysis. The smaller peptides are more easily resolved and identified by LC and MS. The protease cleaves the amide bond on the C-terminal side of arginine or lysine. The *act* ACP contains two arginine residues flanking the active site serine, when cleaved this generates a 17 amino acid long peptide **165/166**.

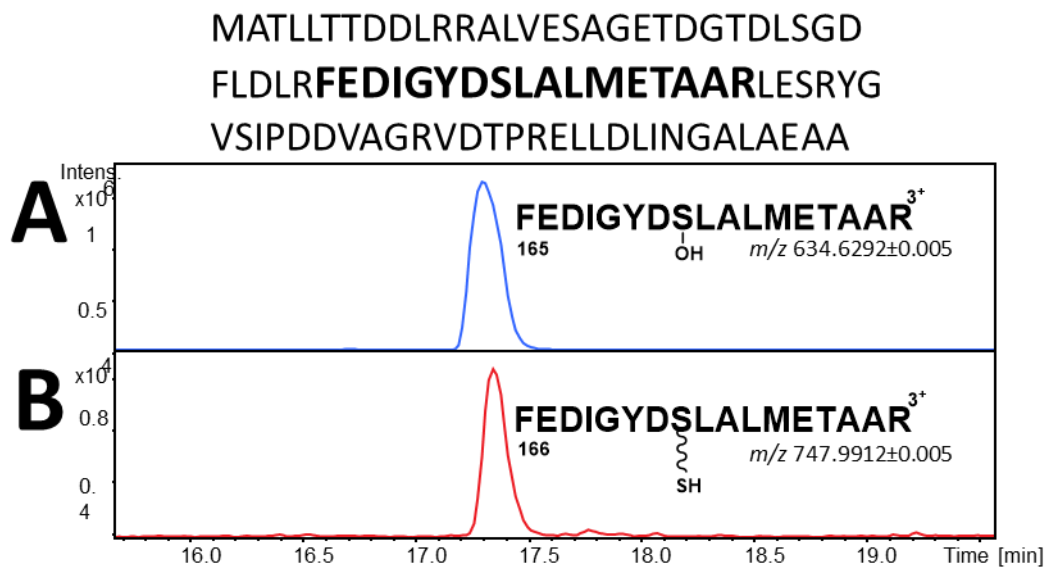


Figure 62 EIC of the peptide containing the active site serine generated by trypsin digestion of the apo and holo acyl carrier proteins **44** and **45** from the actinorhodin minimal system. A) apo acyl carrier protein peptide **165**. B) holo acyl carrier protein peptide **166**.

Apo 44 and *holo 43 act* ACPs were separately digested with trypsin and analysed by LC-MS (**Figure 62**). The peptide of interest containing the active site serine elutes at approximately 17.3 mins, with a very small difference in retention time between the *apo 165* and *holo 166* peptides. However, the LC gradient was not optimised for separation of the two species, although this should be relatively easy to achieve given their chemical differences.

Unfortunately, due to a combination of time constraints and instrument complications, no further samples were analysed with this method. Ultimately, each trapping experiment utilising the ACP probe **63** would have been digested with trypsin, to allow LC-MS analysis on a lower resolution instrument than the FTICR-MS.

5.2.3. UV-Vis spectroscopy analyses of SEK4/SEK4b 41/42 production

As was reported in Section 4.1.3, it is possible to monitor the production of the actinorhodin minimal system shunt products in real time by UV spectroscopy.¹³ SEK4/4b **41/42** have a characteristic wavelength of 293 nm which can be seen to increase steadily upon activation of the minimal system. It was hoped that the effect of the ACP probe **63** on the titer of SEK4/4b **41/42** could be monitored by this method, however, as in the case of the NAC probe **65**, it was soon observed that either the ‘active’ ACP probe **64** or the by-product of its photolysis, **125**, absorbed strongly at 293nm, saturating the detector. Therefore LC-MS was used to fulfil this task.

5.2.4. Effect of delayed addition of active ACP probe **64** on SEK4/4b **41/42** production

Following on from the early time delay experiments with the NAC probe **65**, which revealed an interesting and unexpected time dependent effect on SEK4/4b **41/42** biosynthesis, a small set of experiments were carried out with the ACP probe **63**. As before, the actinorhodin minimal system was activated by addition of the *holo*-ACP **43** and after 30 seconds or 5 minutes ‘active’ ACP probe **64** was added. The assays were incubated overnight at room temperature and assay duplicates using ¹³C labelled malonyl-CoA **15b**, instead of ‘natural’ malonyl-CoA **15**, were also set up. Half of each assay was extracted as usual to analyse SEK4/4b **41/42**, and the remainder was kept for analysis of the ACP probe **64** off-loading ability, as described previously (**Table 6**).

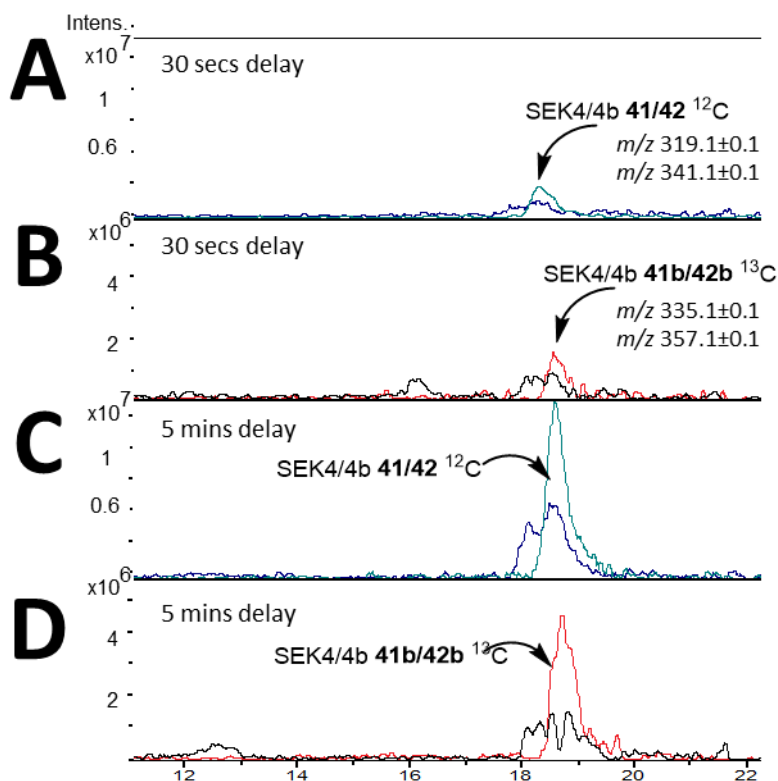


Figure 63 LC-MS chromatogram showing the EIC for the isomers SEK4 **41** and SEK4b **42** produced by the actinorhodin minimal system. The (A and C) unlabelled and (B and D) ^{13}C labelled actinorhodin minimal system was activated by the addition of final enzyme, holo-ACP **43**, then (A and B) 30 seconds and (C and D) 5 minutes later ‘active’ ACP probe **64**, irradiated for 4 hours in the home built UVA light source, was added. Following incubation overnight at room temperature, EtOAc extracts were analysed by low resolution LC-MS. “SEK4/4b ^{13}C ” **41b/42b** are fully ^{13}C labelled compounds.

Analysis of the extracts was carried out by low resolution LC-MS, and thus the two shunt products, SEK4 **41** and SEK4b **42**, did not fully separate by HPLC (**Figure 63**).

In both the labelled and unlabelled minimal systems the addition of the ACP probe **64** after 5 minutes produced approximately three times the quantity of SEK4/4b **41/42** than when the probe **64** was added after just 30 seconds (**Figure 63**). Adding the NAC probe **66** at later time points results in a decrease in SEK4/4b **41/42**

production (section 4.1.2), whereas the ACP probe **64** caused the opposite effect. The NAC probe **66** was unable to offload biosynthetic intermediates under those conditions, however, the ACP probe **64**, in the unlabelled system, can offload a cyclised dehydrated hexaketide **157** (Table 6). The abundance of **157** by the ACP probe **64** seem comparable in the 30 second and 5 minute delays, whereas variations in SEK4/4b **41/42** production are more pronounced (See section 5.2.4). This is likely due to the use of two different LC-MS methods and different analyses complexity; however, it should be further explored in the future.

Unfortunately, due to time constraints and the sample costly nature of the assay, additional time points and more repetitions of these experiments were not carried out.

5.3. *In vivo* labelling of the acyl carrier protein of the actinorhodin minimal system in *E. coli*

Thus far, efforts have been made to reconstitute the actinorhodin minimal system *in vitro* and modifying the acyl carrier protein from the pathway after expression by *E. coli* for trapping experiments. However, the Burkart group^{115-117, 304} have demonstrated that it is possible to utilise the CoA biosynthetic machinery to generate CoA and ACP analogues within cells. Mercer and co-workers have been able to label endogenous carrier proteins in Gram-positive, Gram-negative bacteria and in a human carcinoma cell line with fluorescent reporter tags for imaging purposes.¹¹⁷ When analogues of pantetheine are fed to cell cultures, they can be taken up by the cell and enzymatically transformed into CoA derivatives *via* the endogenous CoA

metabolic pathway. These CoA derivatives can then be transferred to a carrier protein by a promiscuous phosphopantetheinyl transferase from *B. subtilis*.

Co-expression of KS-CLF and ACP from the minimal system would allow for *in vivo* trapping experiments. In our experience *in vivo* chain termination assays are generally more insightful than comparative experiments *in vitro* due to enzyme abundances and optimal working environment.^{22, 154} Additionally, for PKSs or FAS systems where purification of the proteins is challenging or not possible, this method would still allow the biosynthetic pathways to be probed.

E. coli BAP1 cells¹³⁷ harbouring the phosphopantetheinyl transferase Sfp²¹⁰ were transformed with the *actACP* pET-28 plasmid resulting in the overexpression of *holo-ACP 43*. To generate DMNB protected ACPs **63** *in vivo* the pantetheine analogue **61** was added to the LB media at the point of IPTG induction and the cells were incubated overnight at 15°C, as or normal protein expression. Addition of the pantetheine analogue **61** at two different concentrations (1 mM and 10 mM final concentration) and at two different optical densities (0.3 and 0.6 at 600 nm) during IPTG induction were trialled. Enzyme purification was carried out as usual *via* Ni-NTA affinity chromatography, and protein analysis performed by LC-MS (**Figure 64**).

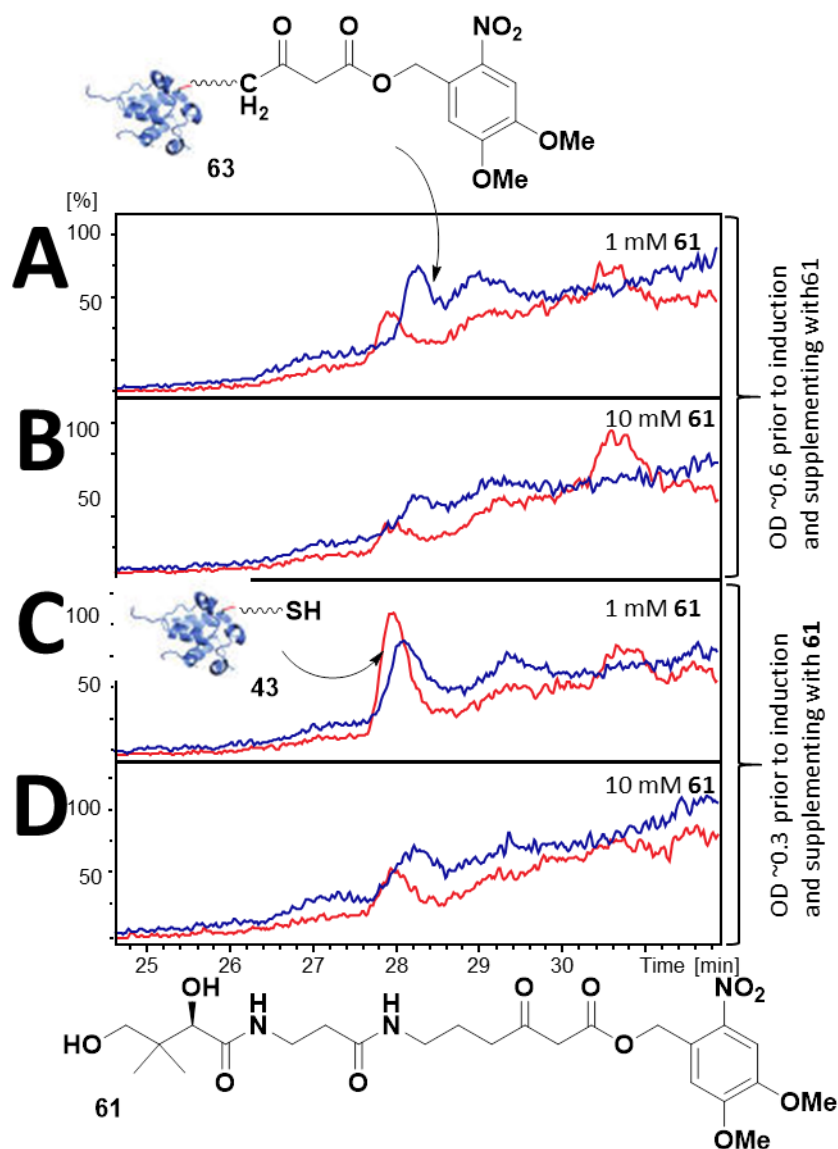


Figure 64 LC-MS chromatograms showing EIC of holo-ACP **43** (red trace) and DMNB protected carba(dethia) malonyl-ACP analogue **63** (blue trace) expressed in *E. coli* BAP1 cells by supplementing with (A and C) 1 mM and (B and D) 10 mM DMNB protected carba(dethia) malonyl pantetheine analogue **61** (shown) at the same time as induction with Isopropyl β -D-1-thiogalactopyranoside (IPTG) at optical densities 600 nm of (A and B) 0.6 and (C and D) 0.3. Ni-NTA affinity chromatography was used to purify the histidine tagged acyl carrier proteins prior to analysis by LC-MS.

In each condition, both holo-ACP **43** and ACP analogue **63** were detected and no apo-ACP **44**. It was not possible to compare the quantities of the holo-ACP **43** and the ACP analogue **63** as the latter contains more potential ionising sites than holo-

ACP **43**, which can affect their MS detection. Additionally, the retention times of the two species, **43** and **63**, are very similar which could lead to signal suppression. However, from these preliminary data, it is possible to say that 10 mM of pantetheine analogue **61** negatively affected the expression of ACPs; less of both *holo*-ACP **43** and ACP analogue **63** were detected at that concentration compared to the 1 mM **61** experiments.

It is likely that at higher concentrations the pantetheine analogue **61** begins to inhibit the enzymes in the biosynthesis of coenzyme A **46**. There is not a substantial difference between induction at the two different optical densities, although there is a small increase in expression of ACP when induced earlier at OD_{600nm} of 0.3. Further repeats of these experiments are required to come to a definitive answer.

Unfortunately, due to time constraints, no further experiments were carried out. Nonetheless, it has been shown that it is possible to generate the ACP probe **63** in *E. coli*. In the future, it would be of interest to show that this is possible within other organisms, such as *S. coelicolor*, the actinorhodin **2** producer, for the capture of biosynthetic intermediates from PKSs and also fatty acid biosynthetic pathways.

5.4. Conclusions and future work

Comparative results from incubation of the malonyl-ACP **7** and the carba(dethia) malonyl-ACP **64** with the KS-CLF strongly indicate that the carba(dethia) malonyl-ACP **64** interacts with the KS-CLF in a similar way to the ‘natural’ malonyl-ACP **7**. With both ACPs, the KS-CLF can efficiently decarboxylate the malonyl groups to produce acetyl within the same time frame. This result itself cannot directly indicate how they compare for chain extension, however.

Adding the ‘active’ ACP probe **64** after just 30 seconds from the activation of the minimal system, led to a decrease in SEK4/4b **41/42** production compared to a 5 minute delayed addition. These time delay experiments behaved in the way that we would have expected: they suggest that the active probe **64** interferes in the biosynthesis of the SEK4/4b **41/42** in its early stages by interacting with the KS-CLF in competition with ‘natural’ malonyl-ACP **7**.

By utilising the nonhydrolysable photoactivatable malonyl-ACP analogue **63** putative enzyme-bound captured intermediates from the actinorhodin minimal system were observed and preliminarily characterised by FTICR-MS. Putative hexaketide species **149**, **156**, and **157** were the most recurrently observed species in samples deriving from a variety of different chain termination assays. Off-loading of KS-bound intermediates at this stage of chain elongation may indicate that this stage is rate limiting, possibly due to a change in protein conformation or cyclisation of the polyketide chain.

Burkart and co-workers modelled the linear and cyclic polyketide intermediates of the actinorhodin minimal system through selective atom replacement. They substituted carbonyl groups that were not essential for cyclisation or reduction with either isoxazole rings or sulphur atoms, creating stable mimics of the intermediates for structural characterisation by NMR. It was shown that heptaketide and octaketide substrates bound strongly to helices II and IV, whereas the tetraketide substrate did not bind within the ACP.²⁹⁴ This conformational change may be the reason why hexaketide intermediates were more easily off-loaded with the ACP probe **64**. It is worth highlighting that putative PKS-bound ‘linear’ pentaketides **148** and hexaketides **149** were detected. If further confirmed in their nature by additional MSⁿ studies, they would represent the first direct evidence of polyketone species

bound to an ACP; due to their intrinsic instability, we hypothesise that they must be residing within the ACP to avoid dehydration and further processing.

Unfortunately, the isotopic distributions for the intermediates detected were all of relatively low intensity, and no further analyses of these ions, such as fragmentation, was possible. Nonetheless we can be confident that the observed species are 'real' as autocorrelation of the regions can confirm the presence of isotopic distributions, alongside sub ppm mass errors on the peaks.

Scaling up the experiments, by at least 10 fold, and isolating the intermediates by preparative LC or by other separation techniques, would likely lead to a more intense signal for characterisation. Alternatively, further optimisation of the method in regards to the ratio of malonyl-ACP **7** to carba(dethia) malonyl-ACP **64** could improve the ability to capture intermediates in terms of amount and range.

An additional way of looking at ACP-bound intermediates, not explored in this project, has been recently reported. It involves the use of an acyl carrier protein hydrolase (AcpH) which can regenerate *apo*-ACPs by selectively hydrolysing the phosphopantetheinyl (PPant) cofactor. *S. coelicolor* does not contain a protein of this type, however an AcpH from *Pseudomonas fluorescens* has been proven to cleave the PPant arm from the actinorhodin **2** *holo*-ACP **43**.³⁰⁵ In theory, PPant arms could be hydrolysed from the carba(dethia) ACP providing the small molecule intermediates bound to the PPant for detection by LC-MS. The small molecular ion is preferable for mass spectrometry, as the lower the molecular weight the lower the mass error will be. Additionally, LC separation of these species could be carried out on a RP C18 column, aiding their identification and characterisation. Conversely, significant information on substrate-protein interaction might be lost by using AcpH

or trypsin digestion, therefore the intact protein analysis, ‘top-down’ approach, for the dissection of type II PKS catalysis should be pursued in the future.

Throughout this project, we have shown that the capture of intermediates from iterative polyketide biocatalysis is not trivial. This confirms that type II PKS biosynthetic machineries are as challenging as previously assumed because of fast and tightly controlled chain extension. Little is known about the interactions between the ACP and the KS-CLF during chain extension. These results could indicate that chain extension is too fast, and tightly controlled, for efficient chain termination, however, the preliminary observation of putative captured intermediates with the ACP probe **64** *in vitro* is promising. With the preliminary evidence that ACP probes such as **63** can be generated *in vivo*, the new chain termination approach herein developed holds the promise of gaining further in depth insights into natural product assembly. In the future, alternative type II PKS systems, as well as other types of iterative enzymes, such as type I iterative and type I-II fatty acid synthases, should be probed with their respective ACP probes. This will ultimately contribute to generate a detailed and comprehensive picture of how iterative systems operate, from which new synthetic biology can be developed.

**Chapter 6: Improving molecular structural
determination by combining the results of
alkali metal adductin tandem mass
spectrometry**

6. Improving molecular structural determination by combining the results of alkali metal adduction assisted tandem mass spectrometry

In chapters 4 and 5, the use of photolabile small molecule and protein probes for the investigation of type II iterative catalysis were reported. This chapter will focus on the investigation of mass spectrometry methods to assist the characterisation of both pantetheines and acyl carrier proteins, in view of improving our ability to characterise ACP-bound intermediates. The effect of alkali metals for the structural characterisation of pantetheines in their free and ACP-bound form will be described.

6.1. The use of alkali metal assisted tandem mass spectrometry for structural determination

The structural characterization of compounds by mass spectrometry is an essential analytical technique for the study of organic molecules. Multiple fragmentation methods are frequently used to generate complementary sets of cleavages, which can produce extensive structural information.^{182, 186, 191, 306-310} The development of a robust method to obtain a wide range of structurally significant fragments for a molecule (or more specifically, an ion) of interest within one tandem mass spectrometry experiment would provide a useful tool for the mass spectrometry community.

Protonated and sodiated ions are common in the mass spectra of most samples analysed by electrospray ionization mass spectrometry (MS) and they are the most commonly used parent ions for tandem MS. Unfortunately, these ions can often produce limited fragmentation of the compound of interest; this is especially the case

with Collisionally Activated Dissociation (CAD), the most frequently used fragmentation technique. This can lead to incorrect or non-specific identification of the compound of interest, or the need for an alternative, often costlier and more time consuming, method of analysis, such as NMR or X-ray crystallography. Both of these alternate techniques require pure and substantial amounts of the compound, which is frequently not possible.

Metal adduction has been shown to alter the fragmentation pathways in Electron Capture Dissociation (ECD),^{311, 312} Electron induced dissociation (EID),³¹³⁻³¹⁶ CAD,^{313, 316, 317} and Infra-Red Multiphoton Dissociation (IRMPD).³¹⁸ Preparation of these metal adducted ions is facile, and applicable to a wide range of samples. The addition of 1 mM LiCl to a sample will provide a lithiated ion that is suitable for analysis.

EID is a tandem MS technique for fragmentation of singly charged, positive or negative, ions with electrons of moderate kinetic energies in the range of 10 – 25 eV.¹⁸²⁻¹⁸⁴ The technique has been shown to produce many of the same fragments that are produced by the more common CAD and IRMPD, but also to generate additional unique fragments.¹⁸⁵⁻¹⁸⁸

Mosely and co-workers¹⁸⁶ analysed singly charged cations (proton, sodium, ammonium and potassium) of pharmaceutical molecules by EID and CAD. They found that the fragmentation techniques, EID and CAD, produced complementary data, but EID produced far more product ions compared to CAD. They also demonstrated that the charge carrying species had a very significant effect on the fragmentation as well as on the type of product ion after EID. Wills *et al.*¹⁹¹ reported similar results when analysing the isomeric natural polyketide products lasalocid A **1**

and *iso*-lasalocid A by EID and CAD; the collection of fragment ions obtained by competition with Li⁺ allowed, for the first time, the structural differentiation between the two isomers (**Figure 65**).

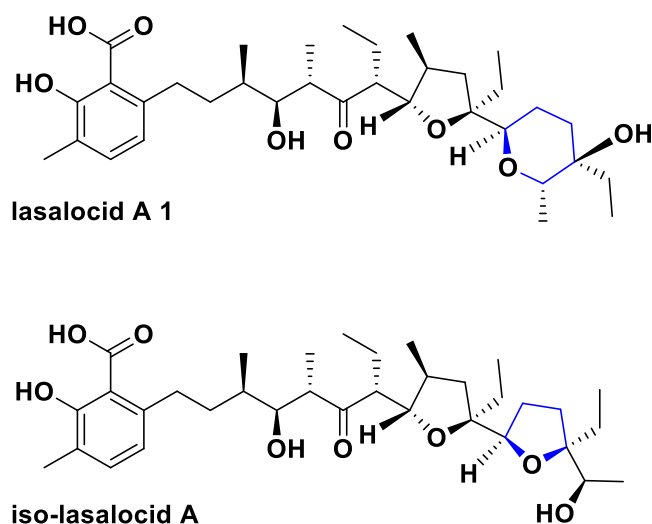


Figure 65 Structures of *lasalocid A 1* and *iso-lasalocid A*.

Alkali adduction to enhance fragmentation of oligosaccharides is commonly employed. Zhou and co-workers³¹⁹ found that monolithiated disaccharides showed abundant reducing end cleavages, and with dilithiated disaccharides linkage isomers could be easily differentiated.³²⁰ Cancilla *et al.*³²¹ demonstrated that fragmentation yields were inversely related to the size of the cation, following the order H⁺>Li⁺>Na⁺>K⁺>Rb⁺>Cs⁺. There are three proposed fragmentation pathways for metal cationised oligosaccharides: either the loss of the metal ion (resulting in a neutral product ion), cross ring cleavage, or glycosidic bond cleavage. It has been demonstrated that the loss of the metal ion increases with its size and dissociation was greatest for caesium and weakest for lithium and sodium.^{320, 322}

Triacylglycerols have been analysed as lithium, sodium and potassium cations by CAD; the sodiated species was the only species of the three, in this case, to provide

useful structural diagnostic fragmentation.³²³ Denekamp and co-workers³²⁴ fragmented sodiated and lithiated product ions of dirhamnosyl lipids and discovered that, with high energy CAD, unique cross ring cleavages occurred, which was not detected with the protonated species.

Beyond the cases mentioned above, there have been a few specific uses of EID reported in the literature. For instance, electron-ion interactions can be used to differentiate between aspartic acid and isoaspartic acid, something that has not been proven possible with CAD.³²⁵ The location of double bonds in fatty acids has also been shown to be traceable by EID of manganese adducted ions.¹⁹⁰

Pantetheine **48** is a small molecule precursor to Coenzyme A **46**, which functions as an acyl carrier in many biological processes such as transcription, cell-cell mediated recognition, the tricarboxylic acid cycle, and the biosynthesis of secondary metabolites.³²⁶⁻³²⁸ The 4-phosphopantetheinyl group of Coenzyme A **46** is transferred to *apo*-acyl carrier proteins (ACPs) and peptidyl carrier proteins (PCPs) by phosphopantetheinyl transferases. These ‘active’ *holo*-ACPs and PCPs are further responsible for the biosynthesis of a variety of natural products, including polyketides, fatty acids and non-ribosomal peptides.³²⁸ Pantetheine **48** is, therefore, a fundamental molecule in both prokaryotes and eukaryotes.³²⁸

The groups of Dorrestein and Kelleher have reported an important method for analysing the phosphopantetheinyl (PPant) group of carrier proteins. The “PPant ejection assay” involves fragmentation by CAD which selectively cleaves the PPant moiety **58/59** from a conserved and specific serine residue of the carrier protein. This provides a characteristic fragment ion for detection and the low m/z allows accurate mass identification.

The PPant group covalently binds and causes a plethora of biosynthetic intermediates: detecting these and fully characterising them would provide key insights into the understanding of mechanisms and kinetics of natural product biosynthesis and other biological processes.^{157, 192, 193, 329, 330}

Dorrestein *et al.* reported the “PPant ejection assay” performed on *holo*-ACPC, a putative acyl carrier protein from *Streptococcus agalactiae*. The ejection assay was followed by further fragmentation of the ejected ion by CAD and produced 12 fragment ions.³³⁰ Nine of these fragments contained the thiol group of the pantetheine **48** group, which carries the substrate during the biosynthesis of natural products, whereas they reported just three ions that would provide a diagnostic pattern for the PPant arm itself. These masses would remain unchanged even with biosynthetic intermediates bound to the thiol group.

In this work, the tandem MS characterisation of a synthetic analogue of pantetheine **61** is reported. This analogue **61** contains a variety of functional groups, including a non-hydrolysable malonyl moiety and a photolabile group (**Figure 66**). Sodium and lithium adducted ions were fragmented with CAD and EID to compare the fragmentation pathways in each case. In addition, a caesiated precursor ion was prepared and analysed by EID.

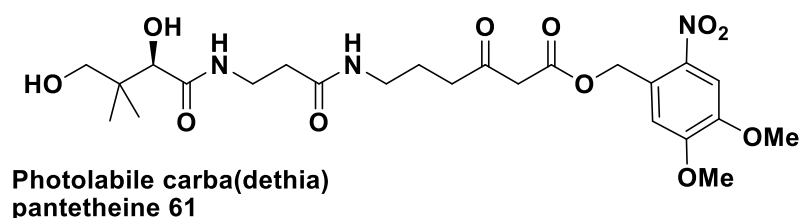


Figure 66 Structure of the nonhydrolysable photolabile carba(dethia) pantetheine **61**.

Lithium and caesium adducted ACP analogues were prepared, and the impact of the alkali metal ions on the “PPant ejection assay” was explored.

6.2. Alkali metal adduction assisted CAD and EID of the nonhydrolysable photolabile malonyl carba(dethia) pantetheine analogue 61

The pantetheine analogue **61** was chemically synthesised, as previously discussed in chapter 3 and its structure was elucidated by NMR prior to MS analysis. The samples for MS analysis were prepared in 50% MeCN with 1 mM NaCl, LiCl or CsCO₃ in H₂O. Samples were analysed on a 12T Bruker Solarix Fourier Transform Ion Cyclotron Resonance (FT-ICR) mass spectrometer (Bruker Daltonics, Billerica) with nanospray ionization; 1-5 µL of approximately 10 µM solutions were electrosprayed using custom-pulled glass capillary tips, grounded with a stainless steel wire. The precursor ions were isolated in the quadrupole, then accumulated in the collision cell for 4 seconds, before being transferred to the ICR Infinity cell.³³¹ For EID, the ions were subsequently irradiated with electrons from a 1.7 A, heated, hollow cathode dispenser, biased with an offset potential of 14 V. Fragmentation for CAD occurred in the collision cell (30 V), prior to the ICR cell. The voltages applied were the same for every spectrum for an unbiased comparison of each condition.

The FT-ICR mass spectra have been assigned in absorption mode, providing improved resolution, and signal to noise ratio over the normal magnitude mode spectra (**Figure 67**). A software programme, Autophaser, was used to produce the absorption mode spectra.³³²

The molecule of interest, a malonyl pantetheine analogue **61** (**Figure 66**), has been fragmented by CAD (**Figure 68**) and EID (**Figure 69**) with both sodium and lithium adduction separately. The CAD spectra present noticeably fewer assigned fragments and peaks than the EID spectra. Most peaks in the CAD spectra could be assigned potential fragment structures based on the known structure of the parent ion. However, several of the peaks in the EID spectra are still undetermined. It is hypothesised that this may be due to an unknown rearrangement and secondary fragmentation occurring during fragmentation. To confirm this, further MS fragmentation of these peaks would have to be carried out, however, this was not possible due to the low intensity of the fragments generated in EID. Furthermore, this was not deemed essential for a comparison of the MS fragmentation techniques.

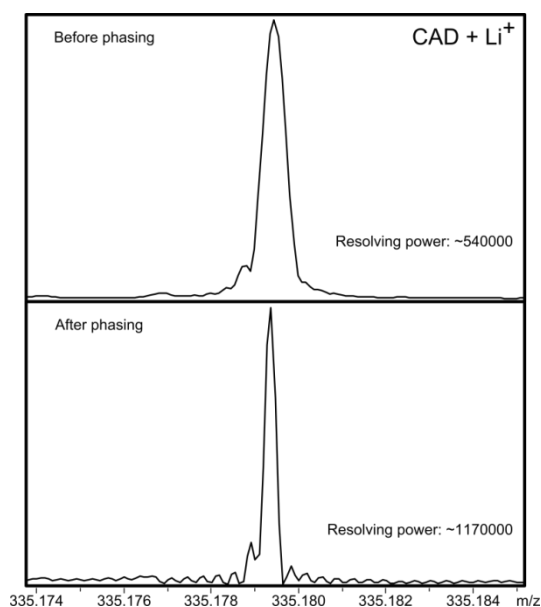


Figure 67 Example peak displaying the increased resolving power before (top) and after (bottom) phasing. Top is the magnitude mode spectrum, bottom is the absorption mode spectrum produced by Autophaser³³².

CAD tandem MS is commonly carried out on sodiated molecular ions. This method produces few fragments when applied to the pantetheine analogue **61** herein

described, and none of these fragments are unique. In this context, unique would mean that a fragment was not detected in the other MS/MS spectra resulting from the fragmentation of different alkali adducts, by either CAD or EID. However, a sodiated molecular ion of the pantetheine analogue fragmented with EID or CAD does generate two unique fragments, as shown in **Figure 69A**. Both of these (“x” and “gg”) have a mass which would be consistent with the loss of the nitro group, a loss of one or two methoxy groups, and cleavage around the hydroxyl and carbonyl groups. Fragments are labelled in ascending order by mass (Da); ‘a’ is the smallest fragment and ‘vv’ is the fragment with the largest mass. A fragment ion may be produced from fragmentation of multiple bonds as can be seen in **Figure 68**. For example, fragment ion ‘x’ is the result of the cleavage of three bonds: one cleavage between the two amide groups, and two cleavages on the DMNB ring. Fragment ions are listed from ‘a’ to ‘z’, and then ‘aa’, ‘bb’, ‘cc’, onwards.

Two fragments exclusive for CAD are found in the fragmentation of both sodium and lithium adducted ions. Both occur from simple fragmentation; “pp” has a mass which would be consistent with a loss of both methoxy groups and the nitro group, and fragment “tt” from a loss of one of the methoxy groups and loss of H₂O (**Figure 68**).

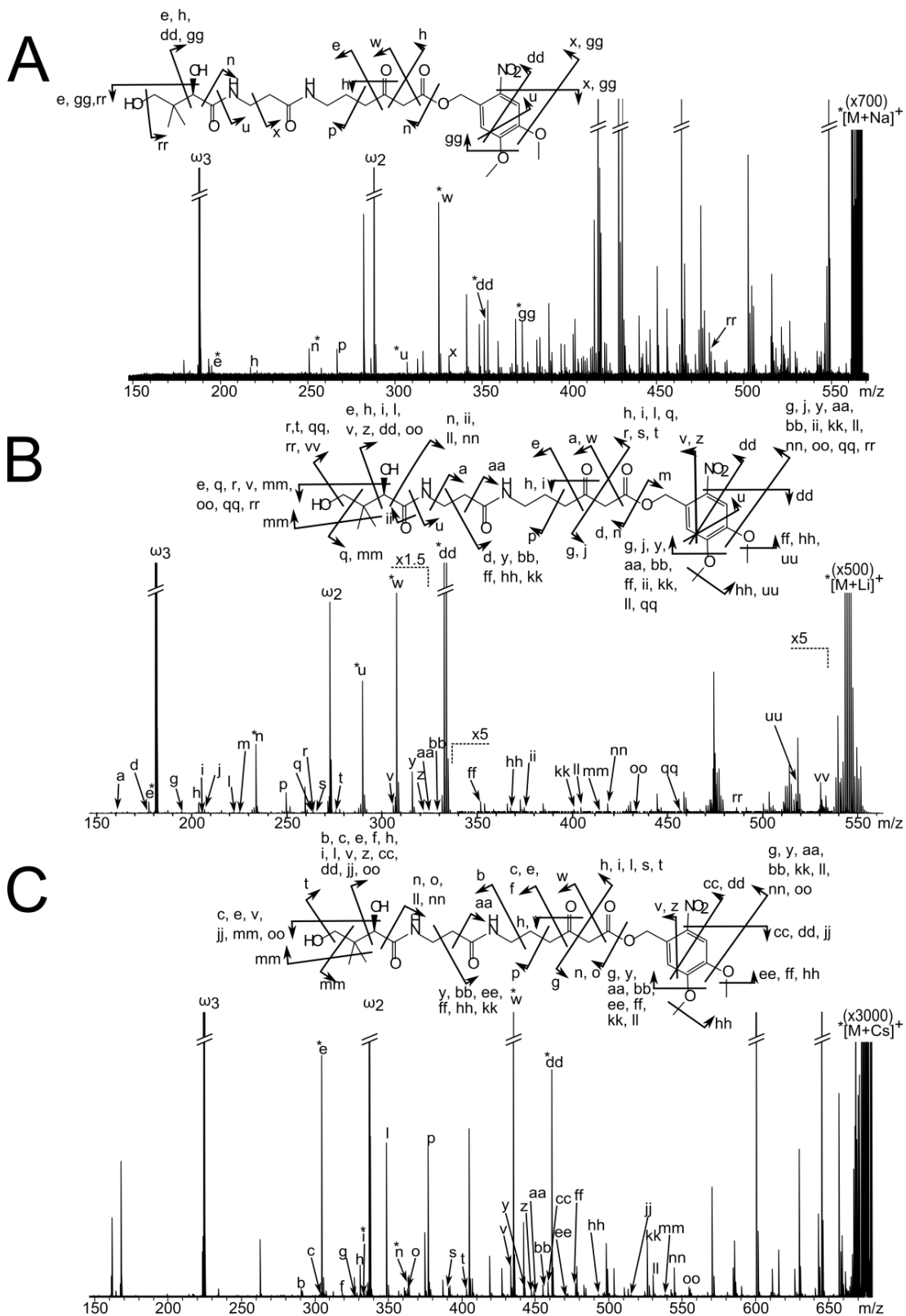


Figure 69 Mass spectra of: A) electron induced dissociation (EID) of $[M+Na]^+$ parent ion **61**; B) EID of $[M+Li]^+$ parent ion **61**; C) EID of $[M+Cs]^+$ parent ion **61**. Inset: assigned fragmentation diagram. An asterisk indicates a peak used for internal calibration.

The adduction of a lithium ion to the molecule yields seven unique fragments with both CAD (**Figure 68B**) and EID (**Figure 69B**): “a”, “d”, “j”, “m”, “q”, “r” and “qq”. Aside from fragment “a”, the majority of the fragments may come from carbon-oxygen bond cleavage. EID with a lithium adducted produces two additional unique peaks corresponding to fragments “uu” and “vv”. These new fragments would result from the loss of two methyl groups and, in the latter fragment, a loss of H₂O. CAD with the lithium adduct also provides two further unique fragments, absent in all other spectra. Fragment “k” has an accurate mass which would be consistent with two fragmentations near to carbonyl groups, both in oxygen rich environments, and fragment “ss” has a mass which correlates with the loss of the nitro group and a methyl group from the parent ion.

The pantetheine analogue **61** was also investigated in complex with caesium. The caesiated molecular ion was fragmented with EID (**Figure 69C**). Once again, the fragmentation pathways were different from the other alkali adducts. In addition, complementary ions were also generated and these provide further insights into the molecular structure. Fragment “u” is found in every spectrum, but is not detected with caesium adduction and EID. This fragment has a mass which would be consistent with a cross ring cleavage and an amide bond cleavage, each cleavage at opposite ends of the compound.

Amide bond fragmentation is abundant in peptide and protein fragmentation; therefore, it was expected that that amide bond cleavage would be one of the most prevalent bond cleavages. However, this was not the case, this could be due to a lack of a mobile proton to induce fragmentation of this type.^{179, 333-335}

Six fragments are detected exclusively in the EID spectrum with Cs adducted to the compound (**Figure 69C**). All of the fragments, “b”, “c”, “f”, “o”, “cc”, and “ee”, have masses that correlate with containing two nitrogen atoms; only fragment “ee” has a mass indicating a fragment containing the nitrogen atom in the nitro group. Lastly, fragment “b” is the only fragment predicted to include a bond cleaved within the most aliphatic portion of the molecule.

Lithium and caesium adductions cause quite similar behaviour under EID: there are many common fragments, “l”, “v”, “z”, “aa”, “bb”, “ff”, “hh”, “kk”, “mm” and “nn”. All of these fragments have masses consistent with bonds cleaved around the first carbonyl group, and, aside from “l”, cleavages in or around the benzene ring.

There are also three fragments, “g”, “s”, and “t”, that are common to both lithium and caesium adduction with both CAD and EID and have masses which would be consistent with cleavage within the malonyl moiety. The fragments “g” and “s” happen to be almost complementary fragments with additional side chain losses.

There is a high degree of overlap of detected fragments across all of the spectra (i.e. the same proposed fragments arising from multiple different fragmentation experiments). Certain fragments are common with both lithium and caesium adduction under EID and CAD, but are not found with sodium adduction. “p” is not present with sodium adduction and CAD, and “y” is not present with sodium adduction and EID, but these ions are found in every other spectrum. “g”, “s”, “t” and “oo” are not found with sodium adduction with either fragmentation technique, but are found in all of the other spectra.

A caesiated ion under EID produces fragment “jj”, having a mass which would be consistent with coming from a cleavage between the hydroxyl and carbonyl group,

loss of the nitro group and two methyl groups. This fragment is not found in any of the other spectra.

There are only a few peaks that are present in both CAD and EID spectra with each of the alkali metal adducts corresponding to the same fragments: “e”, “h”, “n”, “dd” and “w”. Each of these fragments has a mass consistent with the ion containing the middle portion of the compound with two nitrogen atoms. A hypothesis is that the presence of multiple nitrogen atoms could contribute to increased chance of protonation and, therefore, detection. The most common fragmentation sites appear to fall within the malonyl moiety and near to the first amide bond where there is a neighbouring hydroxyl group.

Simply in terms of the total number of identified fragments with each alkali ion, with EID, the lithiated compound generates the most fragments and sodiated, the least. Caesium adduction provides seven new assigned fragments, but a further 23 complementary species.

When switching from sodium to lithium adduction with CAD, only 8 of the fragments are found in both spectra, but, for this molecule, there was an increase from 11 assigned fragments to 25. EID with a lithiated parent ion, however, generates 10 more identifiable fragmentation peaks than the 25 with CAD; 21 of the fragments are detected in both spectra.

In conclusion, five spectra were collected of the malonyl pantetheine analogue **61** in the presence of different alkali ions. The sodiated and lithiated ions were fragmented with CAD and EID, and, additionally, a caesiated ion was fragmented with EID.

Each spectrum was unique; only four fragments are detected in all five conditions.

There was a strong increase in the number of fragmentation sites by CAD when the

molecule was lithium adducted, compared to sodiated (**Figure 70B**). Lithium adduction produced fragments from throughout the molecule, whereas sodium adduction tended towards more localised fragmentation patterns.

Figure 70A shows the number of new fragments provided by EID compared to CAD. It appears that cross ring cleavages are more prevalent with EID, and are also more common with lithium or caesium adduction. These types of cleavages can assist with the important identification of the position of functional groups around an aromatic ring. The compound is hypothesised to have undergone a cyclisation during fragmentation, leading to some, as yet, undefined rearrangements.

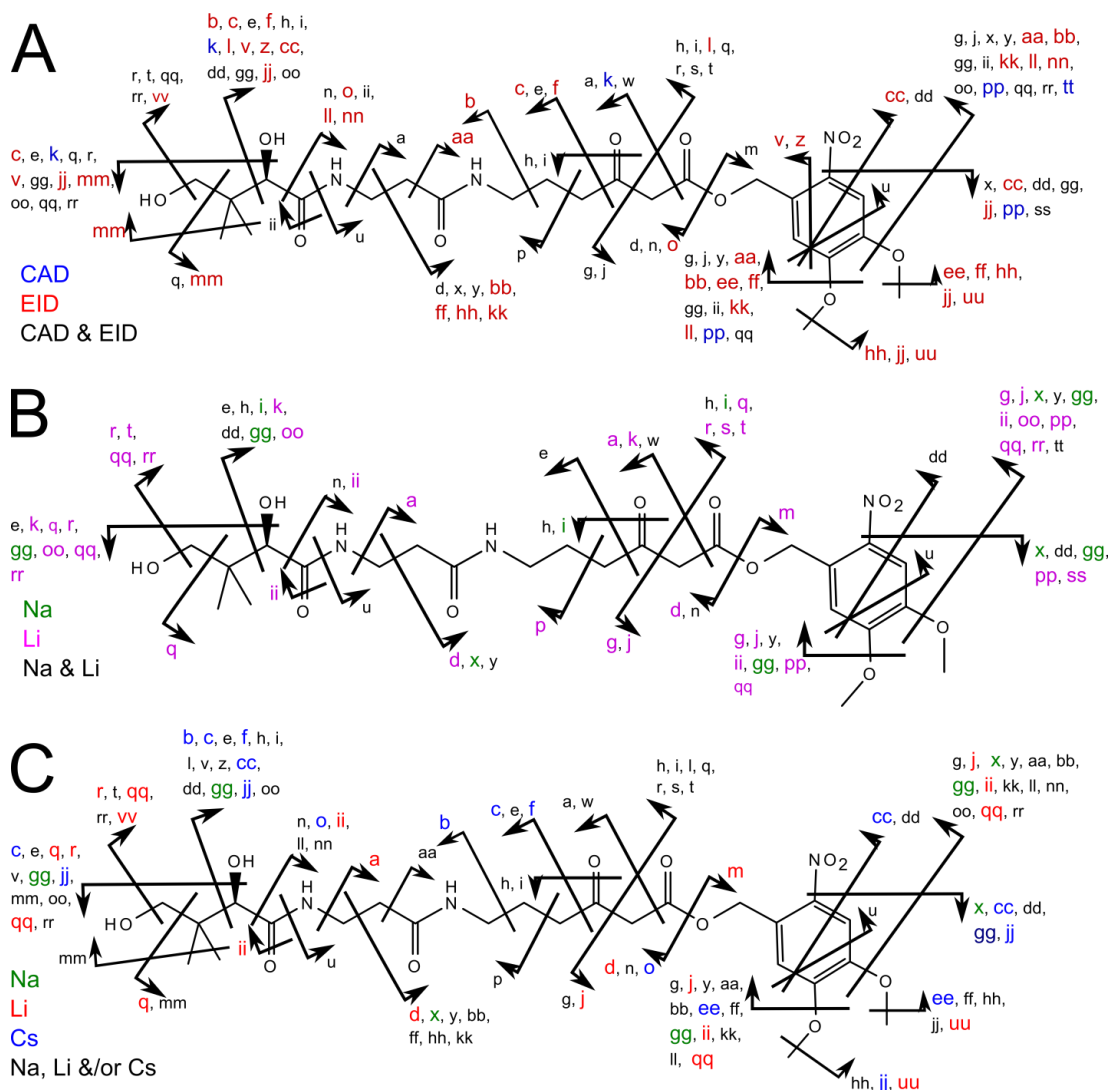


Figure 70 Fragmentation diagrams showing all the assigned fragments for: A) CAD and EID. In blue are those fragments only seen with CAD, in red are the fragments only seen with EID, and in black are the fragments seen with both CAD and EID; B) CAD with sodium and lithium ion adduction. In purple are fragments only seen with lithium adducted, in green are fragments only seen with sodium adducted and in black are the fragments that are seen in both spectra; C) EID with sodium, lithium and caesium ion adduction. In blue are fragments only seen with sodium adduction, in red are fragments only seen with lithium adduction, in green are fragments only seen with caesium adduction and in black are the fragments that are seen in more than one of the EID spectra.

As shown in **Figure 70C**, the combinations of fragmentations with each of the different metal ions present varied, but only lithium and caesium gave new bond

cleavages that were not shown in any of the other spectra, including by CAD. Fragmentation between the two carbonyl groups in the malonyl moiety is a very abundant fragmentation pathway; fragment “w”, which has a mass which would be consistent with this cleavage, was present in all of the spectra and was always one of the most intense peaks in the spectrum. This is likely due to the position of the alkali metal on the compound **61**.

The pantetheine **48** molecule holds strong biological importance, particularly for the natural products field. Detailed insight into the fragmentation patterns for these types of compounds has been demonstrated by mass spectrometry. Combining the “PPant ejection assay”^{158, 192, 193} with alkali metal adduction and EID at the MS³ stage is promising for characterisation of biosynthetic intermediates bound to acyl carrier proteins. The ejection assay provides a small, singly charged molecule which would be susceptible to fragmentation by EID for improved structural characterisation. This work has demonstrated that fragmentation of the target compound is facilitated by the addition of the alkali metal as well as with EID as a fragmentation method. Whether the metal ion remains bound to the ejected pantetheinyl is investigated in section 6.3.

For this compound **61**, carrying out EID with a lithiated ion produced the most assigned fragments compared to the other alkali metals tested in this study and provided sufficient information for a thorough analysis of the structure of the compound. In the future, researchers may wish to consider investigating which is the best adduct, or adducts, for their particular molecule of interest. For the characterisation of a new compound by mass spectrometry, preparing ions for fragmentation with each of the different alkali metals adducted is a worthwhile practice. Also, due to the complementary nature of EID and CAD, combining the

data from both fragmentation techniques could reveal more detailed structural information.

The method of alkali adduction to compounds is a facile sample preparation technique, applicable to a wide range of molecules with benefits including a greater amount of fragmentation throughout the molecule, as well as unique fragmentations. Alongside EID capabilities, robust structural characterisation by mass spectrometry is possible.

6.3. The effect of alkali metal adduction assisted CAD of modified acyl carrier proteins on the generation of phosphopantetheinyl (PPant) ejection ions 58/59

6.3.1. Background and aim

CAD has been used for the identification of ACPs and in generating characteristic phosphopantetheinyl (PPant) ejection ions **58/59**. This technique has been used in proteomics for identifying PKSs, but also in off-loading intermediates from ACPs (**Scheme 13**).^{141, 142, 157-159, 192-195}

Unfortunately, the “PPant ejection assay” often generates a fragment ion that is of low intensity, and the energy of CAD is key to producing the PPant ejection ions **58/59**. Method development of that type can be time consuming, use up sample and can lead to missed ACPs when the technique is used in proteomics.¹⁵⁷ Because of these drawbacks, the technique is only available to expert users on advanced instruments with the ability to trap ions, such as FT-ICRs. Improvements to the method would be beneficial to the scientific community, and provide a robust tool for the investigation of biosynthetic pathways in more laboratories.

Following on from the work carried out on the small molecule pantetheine analogue **61** explored in section 6.2, the effect of alkali metal ions bound to ACPs on their fragmentation, specifically in regards to the PPant ejection was explored.

6.3.2. Generation of lithium and caesium adducted ACP species

At just 7 Da the adduction of lithium to a ~10 kDa acyl carrier protein (ACP) makes a minimal difference to the isotope distribution, and this is complicated further by a mixture of multiply lithiated and protonated ions causing a ‘tailed’ isotope distribution (**Figure 71**). Unfortunately, this meant that it was not possible to isolate a solely lithiated species for fragmentation. However, the fragmentation patterns of the partially lithiated ions were still compared to solely protonated ions.

Sodium adduction was also present in all spectra, due to the preparation of the ACP and its analogues. Its close m/z to the protonated and lithiated species meant that the sodium adducted ACPs were not able to be separated in the isolations for fragmentation experiments.

The affinity of the ACP analogues to caesium was surprisingly successful. At a higher mass than lithium, a single adduction of caesium was sufficient to be isolated separately to the protonated species. Up to five caesium adducted species were detected on the nonhydrolysable photolabile malonyl carba(dethia) ACP **63** (**Figure 72**).

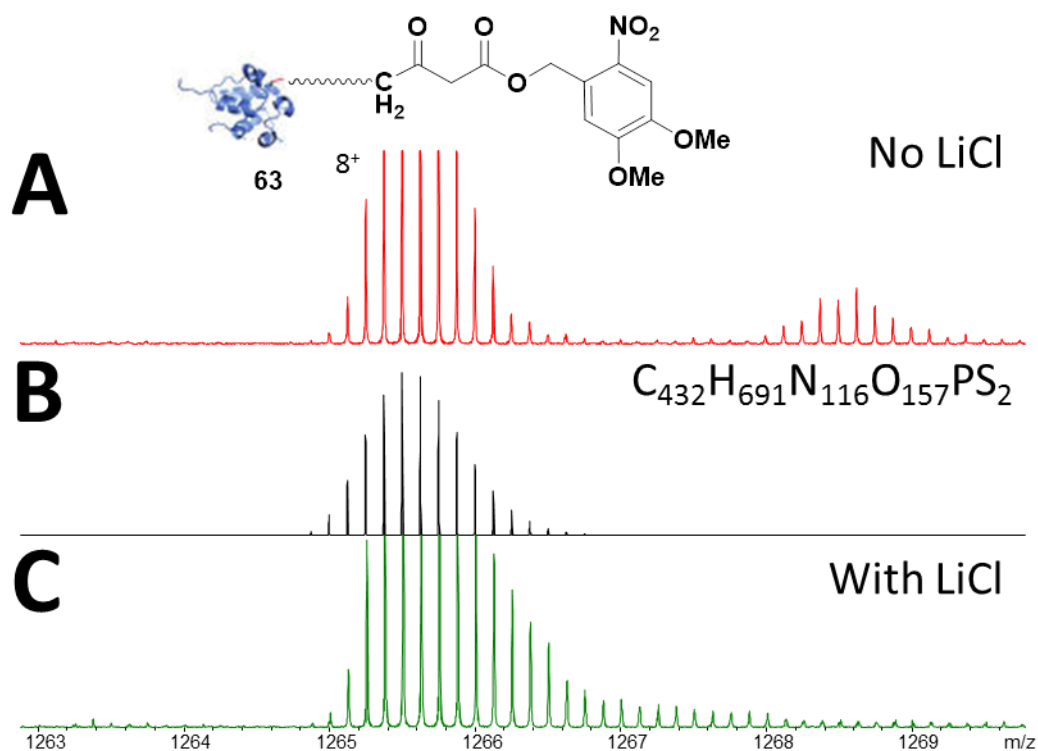


Figure 71 Adduction of lithium to the nonhydrolysable photolabile malonyl carba(dethia) acyl carrier protein (ACP) analogue **63** demonstrated on the 8⁺ ion. A) ACP **63** without the addition of LiCl to the sample. B) Simulated isotopic pattern for ACP **63** 8⁺ ion. C) ACP **63** with the addition of 1 mM LiCl. Multiple lithium adductions can be seen by the 'tailing' of the isotope distribution to higher m/z values.

Five different ACP analogues, nonhydrolysable photolabile malonyl carba(dethia) ACP **63**, acetyl-ACP **40**, malonyl-ACP **7**, acetoacetyl-ACP **167** and myristoyl-ACP **168**, were prepared from apo-ACP **44** using the corresponding CoA analogues and a phosphopantetheinyl transferase, Sfp. The MS samples were prepared with 1 mM lithium chloride or caesium carbonate for fragmentation experiments.

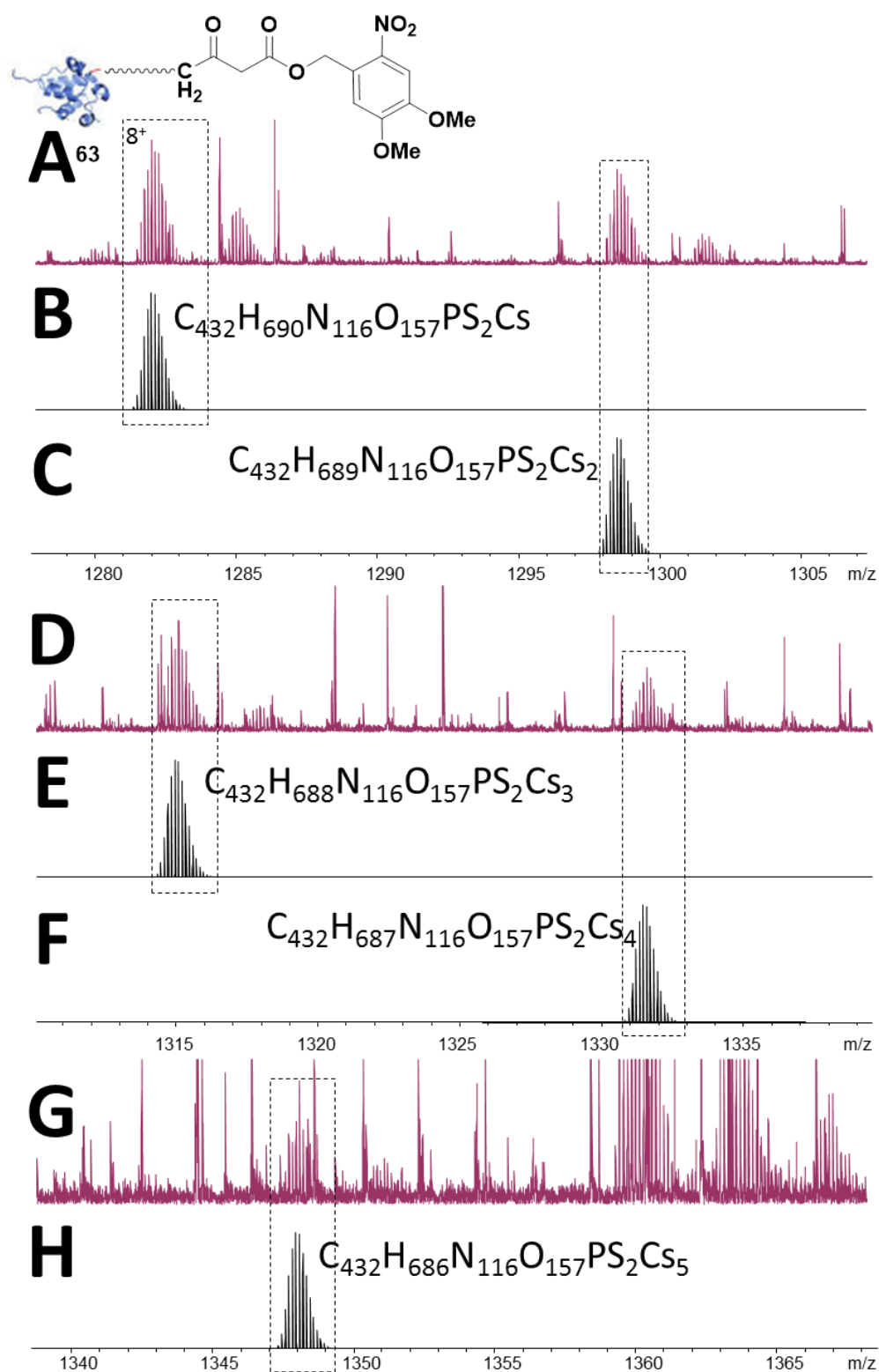


Figure 72 (A, D, G) Mass spectra showing caesium adduction to the nonhydrolysable photolabile malonyl carba(dethia) acyl carrier protein (ACP) **63** by sample preparation with 1 mM Cs_2CO_3 . Simulated isotopic distributions for the 8^+ ions for (B) one, (C) two, (E) three, (F) four and (G) five caesiums adducted and loss of a hydrogen for each caesium adduction.

Acetyl-ACP **40** and malonyl-ACP **7** both are necessary for the biosynthesis of polyketide and fatty acid biosynthesis. Acetoacetyl-ACP **167** would be the product resulting from one round of the polyketide or fatty acid chain extension of acetyl-ACP **40**, whereas myristoyl-ACP **168** is a lipid modification produced by fatty acid synthases (FAS), and, therefore, would naturally be attached to those ACPs.

A range of CAD voltages were applied to each sample, the upper voltage used in each case was the maximum possible before the signal of the precursor ion was lost. Each spectrum was acquired with the same parameters for comparative purposes.

6.3.3. The effect of alkali metal adduction on generation of a pantetheinyl ion by CAD of the nonhydrolysable photolabile malonyl carba(dethia) ACP **63**

The nonhydrolysable photolabile malonyl carba(dethia) ACP **63** without lithium or caesium adduction can produce a Pant ion **81**, as well as a phospho-Pant ion **169**, with CAD of 25V. Increasing the voltage to 28V improves the yield of phospho-ACP **170**, however, there is a decrease in the relative abundance of the Pant ion **81**, and the phospho-Pant ion **169** was not able to be detected under those conditions. The adduction of caesium does not provide either ejection ion **81** or **169** upon CAD, however, lithium adduction does generate Pant ion **81**.

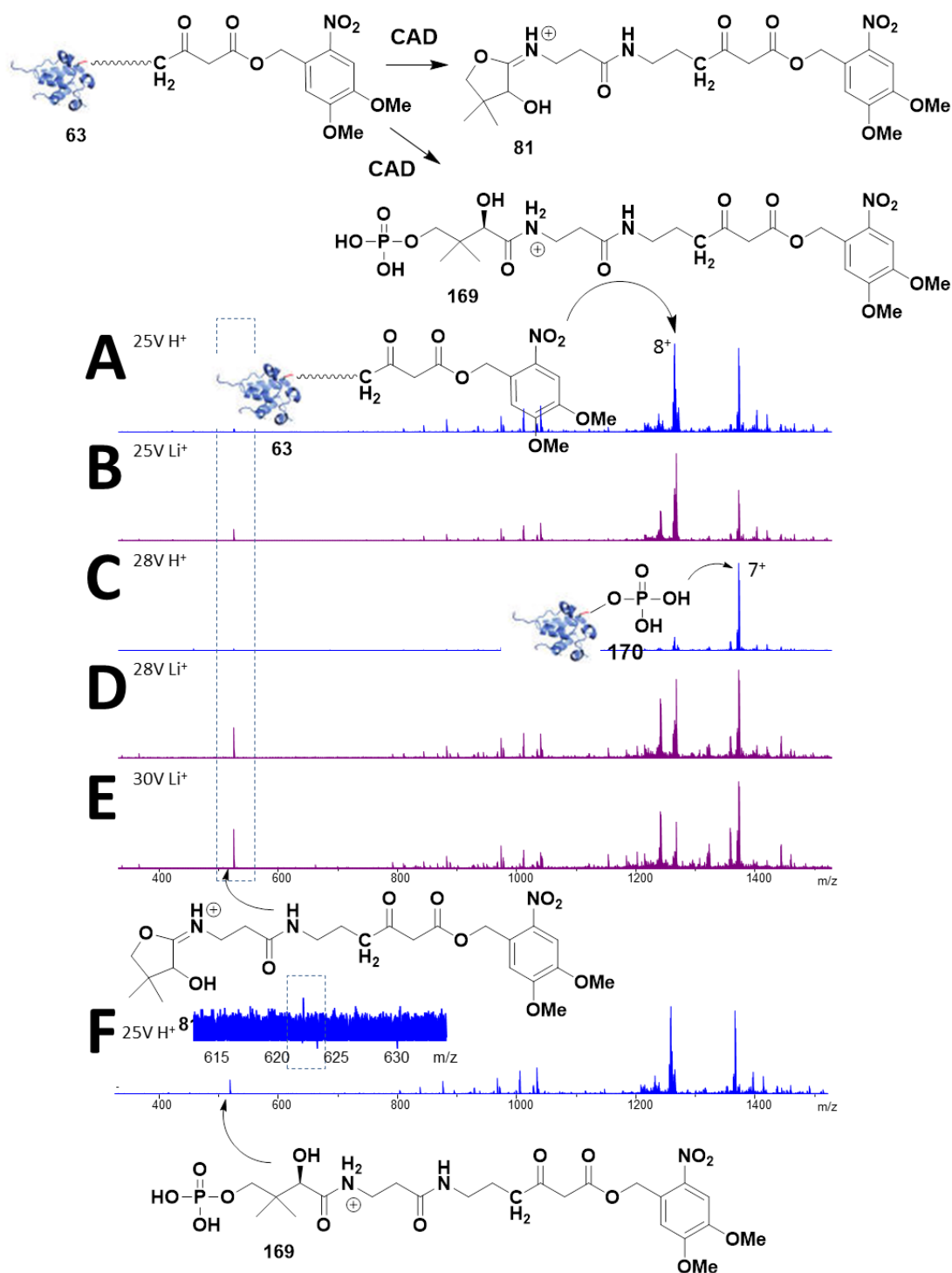


Figure 73 The effect of adduction of lithium to the nonhydrolysable photolabile malonyl carba(dethia) acyl carrier protein (ACP) **63** on the yield of cleaved pantetheine analogue **81** (m/z 524.2239) and the phosphopantetheine analogue **169** (m/z 622.2008) via bond cleavage under collisionally activated dissociation (CAD). (A, C and F) CAD of 8^+ ACP **63**. B, D and E) CAD of lithium adducted 8^+ ACP **63**. CAD voltages of 25V (A, B and F), 28V (C and D), 30V (E) were used. Scheme above shows the expected fragmentation pathway. Phospho-ACP **170** is a by-product of the cleavage.

The relative abundance of the Pant ion **81** produced at 25V is comparable to without lithium adduction. However, at 28V, the intensity of the Pant ion **81** continues to increase when fragmenting the lithium adducted species. Additionally, the CAD voltage could be increased up to 30V with lithium adduction, and the Pant ion **81** intensity increases further (**Figure 73**). Higher voltages were not able to be applied due to loss of signal strength over 30V.

6.3.4. The effect of alkali metal adduction on generation of a pantetheinyl ion by CAD of acetyl-ACP 40

Acetyl-ACP **40** without lithium adduction could be fragmented up to a CAD voltage of 25V before loss of signal. At this voltage the corresponding acetyl Pant ion **171** is produced, but the acetyl phospho-Pant **172** is not. A caesium adducted acetyl-ACP **40** was generated, however the Pant **171** or phospho-Pant **172** were not produced by CAD fragmentation. As with the nonhydrolysable photolabile malonyl carba(dethia) ACP **63**, with lithium adduction, the CAD voltage could be increased up to 35V. From 25V to 30V, the signal strength of the Pant ion **171** increased, but past 30V the abundance of the Pant ion **171** did not increase any further (**Figure 74**).

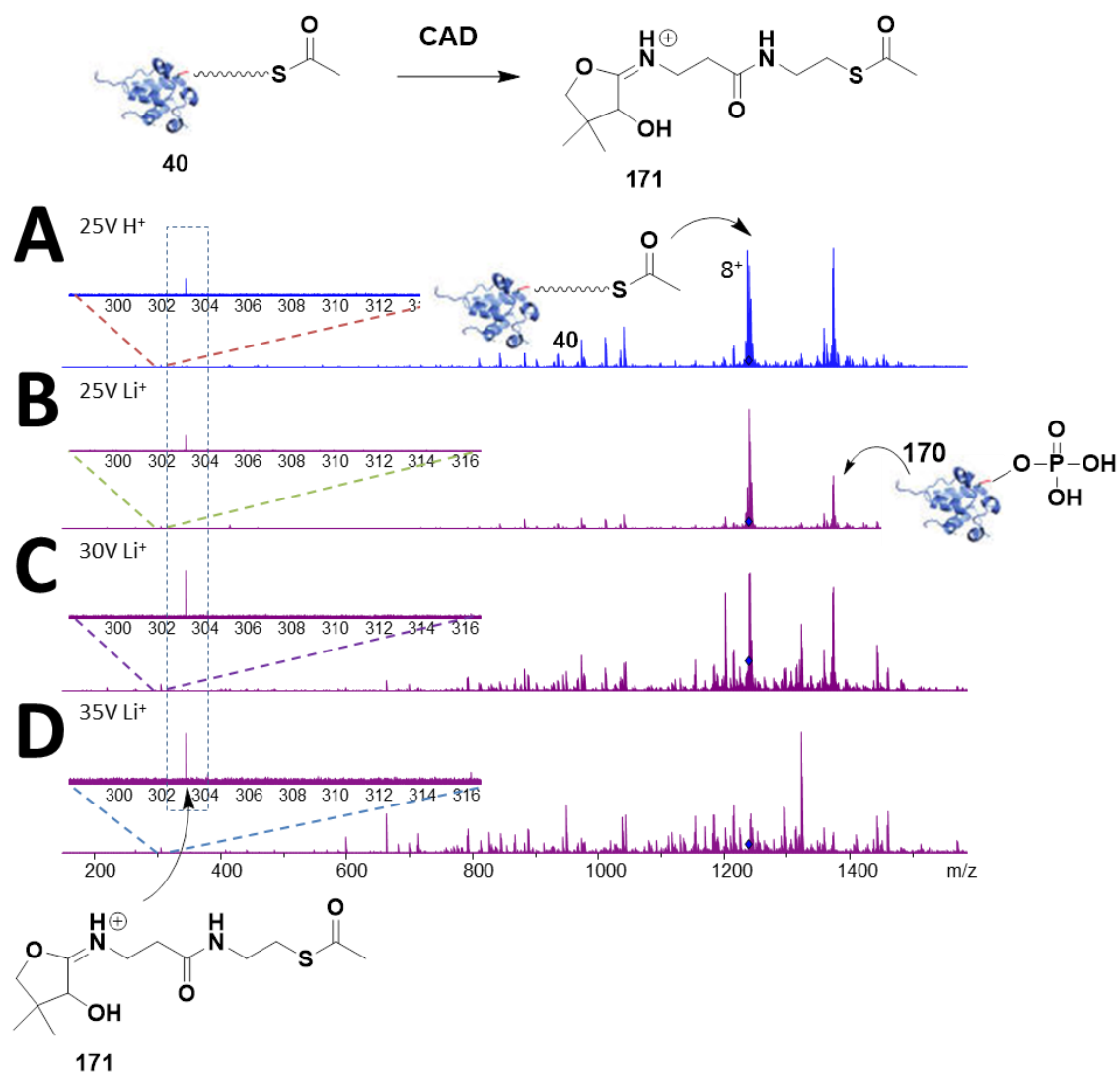


Figure 74 Adduction of Lithium to acetyl acyl carrier protein (ACP) **40** shows improved yield of cleaved acetylated pantetheine **171** (m/z 303.1373) via phosphodiester bond cleavage under collisionally activated dissociation (CAD). A) CAD of 8^+ acetyl-ACP **40**. B, C and D) CAD of lithium adducted 8^+ acetyl-ACP **40**. CAD voltages of 25V (A and B), 30V (C) and 35V (D) were used. Scheme above shows the expected fragmentation pathway. Phospho-ACP **170** is a by-product of the cleavage.

6.3.5. The effect of alkali metal adduction on generation of a pantetheinyl ion by CAD of malonyl-ACP 7

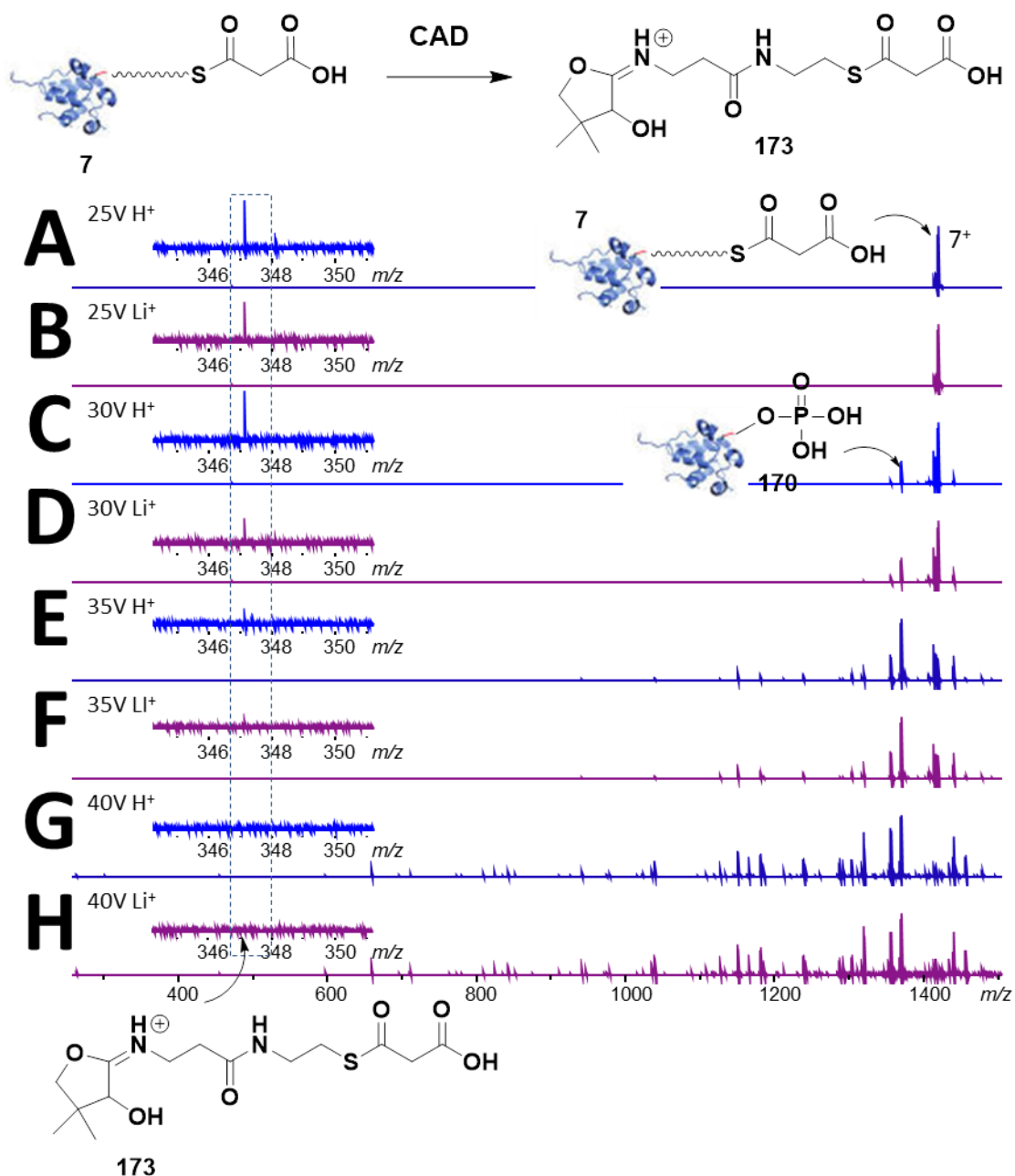


Figure 75 The effect of adduction of lithium to malonyl acyl carrier protein (ACP) 7, on the yield of cleaved malonyl pantetheine 173 (m/z 347.1271) via phosphodiester bond cleavage under collisionally activated dissociation (CAD). A, C, E, and G) CAD of 7⁺ malonyl-ACP 7. B, D, F and H) CAD of lithium adducted 7⁺ malonyl-ACP 7. CAD voltages of 25V (A and B), 30V (C and D), 35V (E and F), and 40V (G and H) were used. Scheme above shows the expected fragmentation pathway. Phospho-ACP 170 is a by-product of the cleavage.

CAD voltages up to 40V could be applied for malonyl-ACP **7** with and without lithium adduction. As with the other ACPs, caesium adduction does not result in the corresponding Pant ion **173**. On this occasion, lithium adduction does not improve the ejection of the Pant ion **173**. No malonyl phospho-Pant ion **174** was detected in any of the spectra (**Figure 75**).

6.3.6. The effect of alkali metal adduction on CAD of acetoacetyl-ACP 167

The acetoacetyl Pant ion **175** was detected with and without lithium or caesium adduction to the acetoacetyl-ACP **167**. At 25V and 30V, the precursor ion without alkali adduction produced the most intense Pant fragment ion **175**, with lithium adduction the second most and with caesium adduction to the acetoacetyl-ACP **167**, the fragment ion **175** generated is very low intensity. A higher voltage could not be applied to the caesiated acetoacetyl-ACP **167** than 30V, but the protonated and lithiated ions could be fragmented with voltages of 35V and 40V. At these higher voltages the signal of the Pant ion **175** is weaker than at lower voltages, but the intensities are comparable, whether lithiated or not (**Figure 76**). No phospho-Pant ion **176** was detected in any of the spectra.

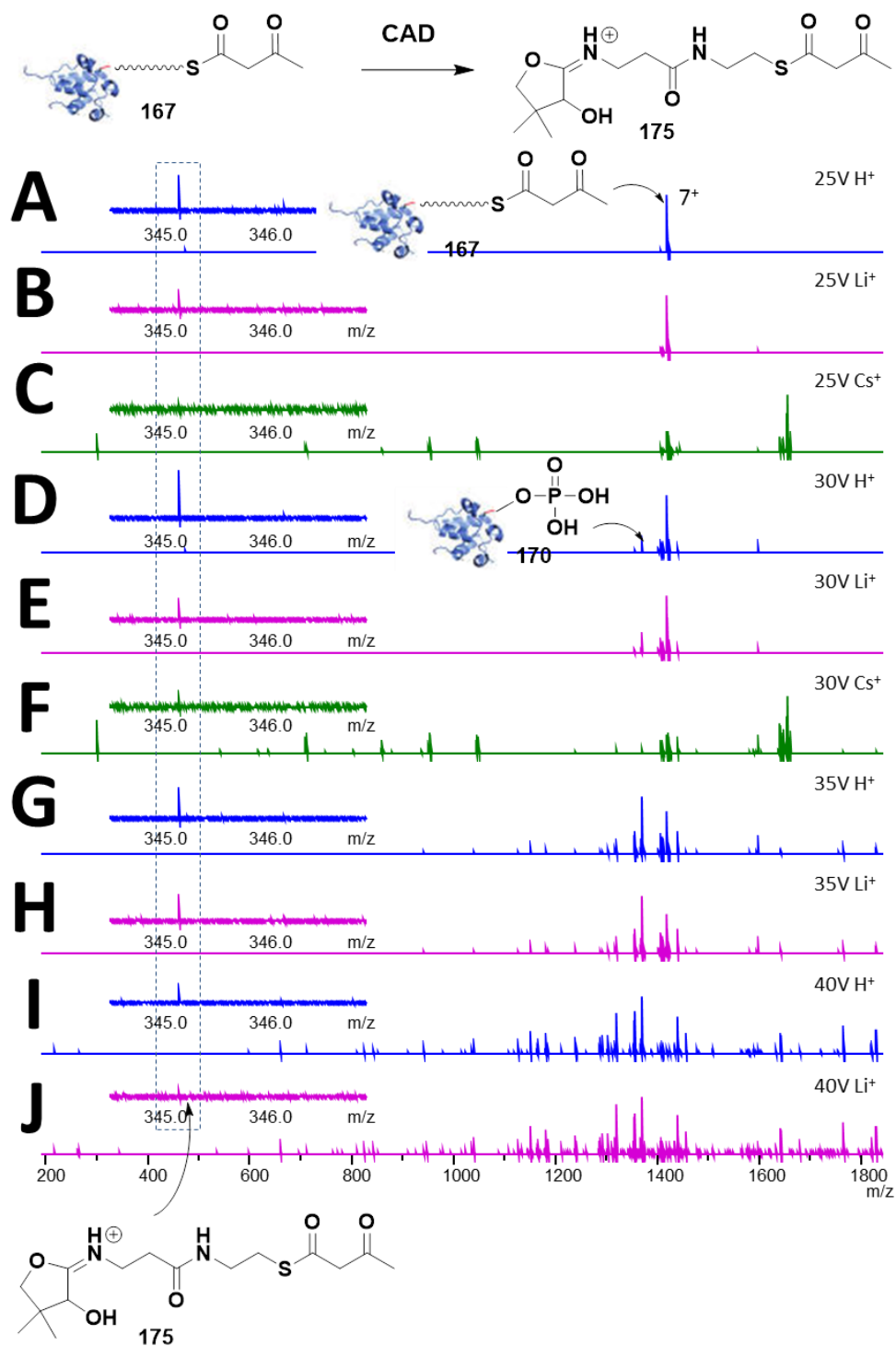


Figure 76 The effect of adduction of lithium or caesium to acetoacetyl-ACP **167**, on the yield of cleaved acetoacetyl pantetheine **175** (m/z 345.1479) via phosphodiester bond cleavage under collisionally activated dissociation (CAD). A, D, G, I) CAD of 7^+ acetoacetyl-ACP **167**. CAD of lithium (B, E, H, and J) and caesium (C and F) adducted 7^+ acetoacetyl-ACP **167**. CAD voltages of 25V (A, B and C), 30V (D, E and F), 35V (G and H) and 40V (I and J) were applied. Scheme above shows the expected fragmentation pathway. Phospho-ACP **170** is a by-product of the cleavage.

6.3.7. The effect of alkali metal adduction on generation of a pantetheinyl ion by CAD of myristoyl-ACP 168

Both the Pant ion **177** and the phospho-Pant ion **178** from myristoyl-ACP **168** were generated by CAD with and without lithium adduction. Unfortunately, due to the low intensity of the caesium adducted ACP **168**, CAD was not possible with that alkali metal. The most abundant Pant ion **177** is generated with 30V CAD without lithium adduction to the parent ion **168**, voltages above 30V were not achievable due to loss of signal of the parent ion **168**. 35V CAD of the lithium adducted species **168** is possible, however, it produces the most intense Pant ion **177** among those lithiated experiments, but the intensity was not as great as without this alkali metal (**Figure 77**). Low abundant phospho-Pant ions **178** were detected in all spectra fragmented with 25V and 30V CAD, both with and without lithium adduction (**Figure 78**).

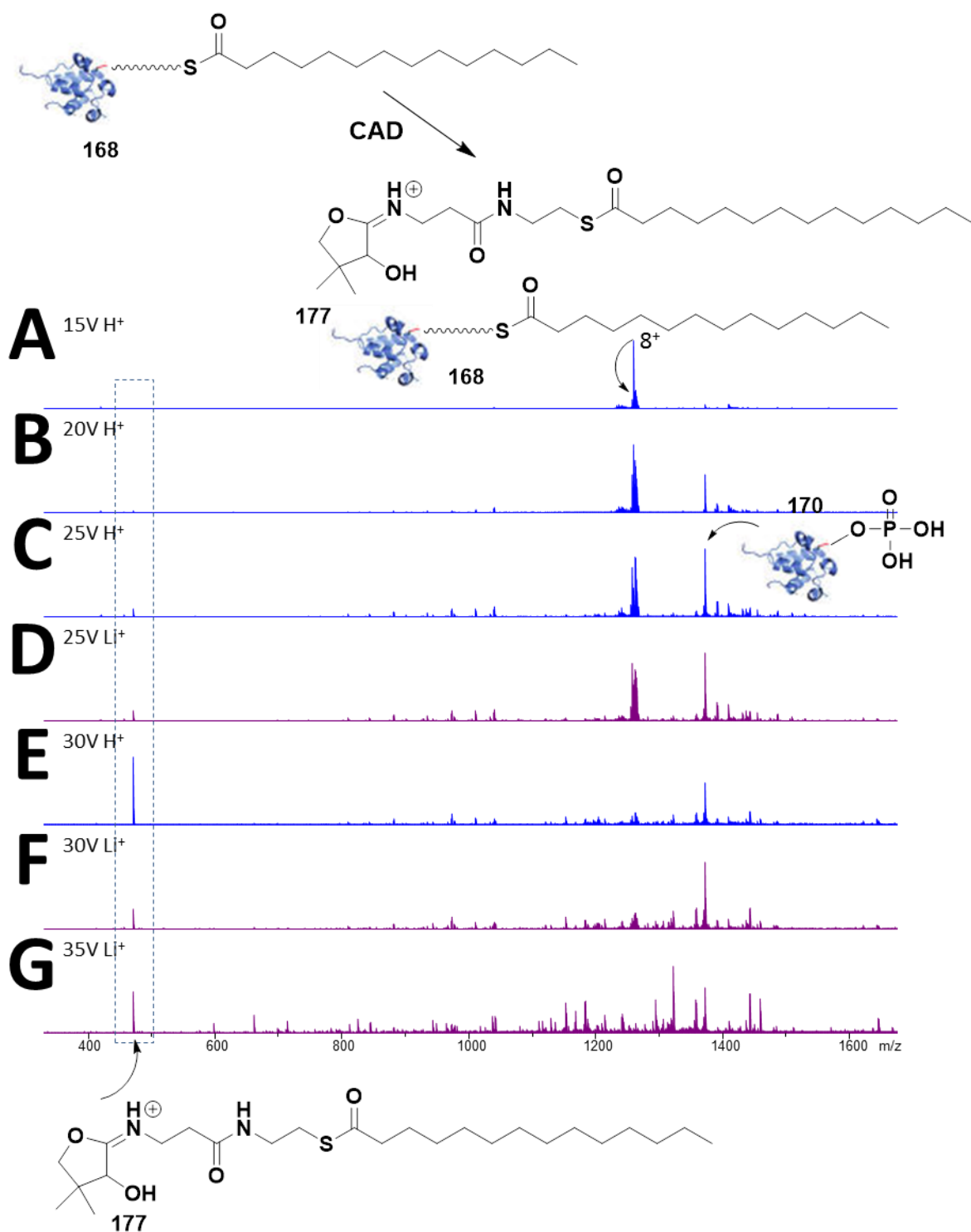


Figure 77 The effect of lithium adduction to myristoyl-ACP **168** on the yield of cleaved myristoyl pantetheine **177** (m/z 471.32511) via phosphodiester bond cleavage under collisionally activated dissociation (CAD). **A**, **B**, **C** and **E**) CAD of 8^+ myristoyl-ACP **168**. **D**, **F** and **G**) CAD of lithium adducted 8^+ myristoyl-ACP **168**. CAD voltages of 15V (**A**), 20V (**B**), 25V (**C** and **D**), 30V (**E** and **F**) and 35V (**G**) were applied. Above shows the expected fragmentation pathway. Phospho-ACP **170** is a by-product of this cleavage.

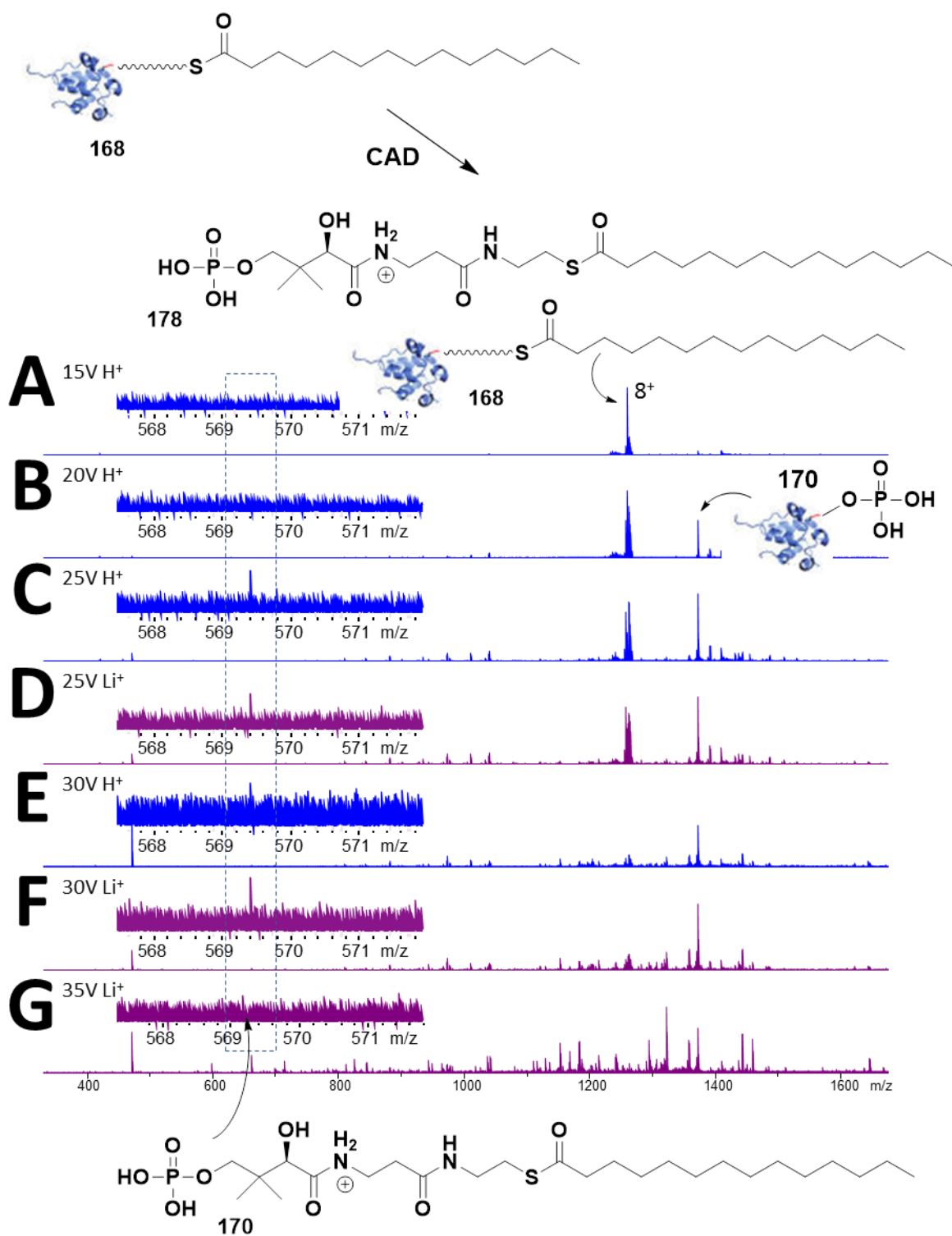


Figure 78 The effect of lithium adduction to myristoyl-ACP **168** on the yield of cleaved myristoyl phosphopantetheine **178** (m/z 569.3020) via phosphodiester bond cleavage under collisionally activated dissociation (CAD). A, B, C and E) CAD of 8^+ myristoyl-ACP **168**. D, F and G) CAD of lithium adducted 8^+ myristoyl-ACP **168**. CAD voltages of 15V (A), 20V (B), 25V (C and D), 30V (E and F) and 35V (G) were applied. Above shows the expected fragmentation pathway. Phospho-ACP **170** is a by-product of this cleavage.

6.3.8. CAD of caesium adducted ACP species

The most common fragmentation pathway for caesiated ACP ions (**63**, **40**, **167** and **7**) is the loss of the caesium ion and charge reduction. For caesiated malonyl-ACP **7** a decarboxylation was also produced by CAD (**Figure 79**). This pathway is likely the cause of the low abundant, or absent, PPant ejection ions for all caesiated ACP species.

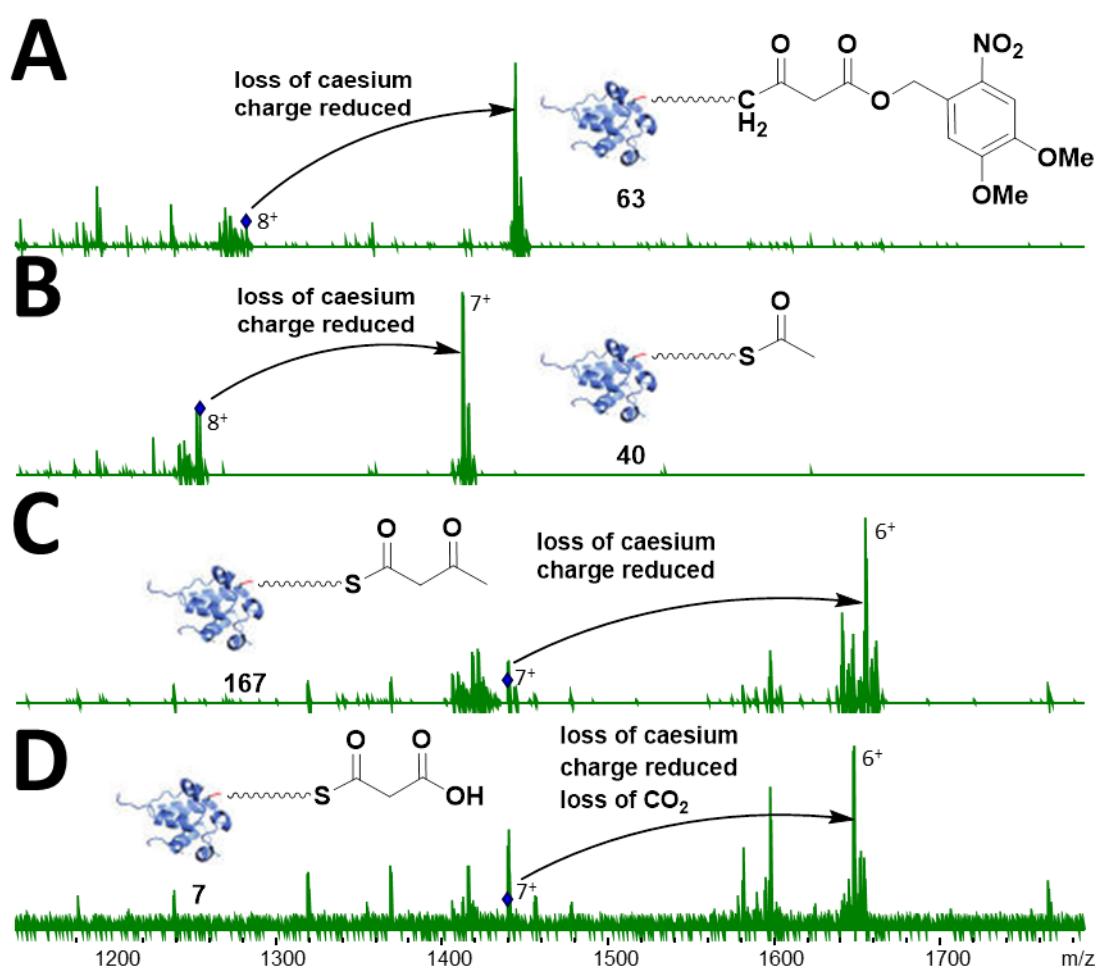


Figure 79 The effect of caesium adduction to four different ACPs **63**, **40**, **167**, and **7** on fragmentation pathways with collisionally activated dissociation (CAD). A) 18V CAD of caesium adducted 8⁺ nonhydrolysable photolabile malonyl carba(dethia) ACP analogue **63**. B) 16V CAD of caesium adducted 8⁺ acetylated ACP **40**. C) 30V CAD of caesium adducted 7⁺ acetoacetyl-ACP **167**. D) 35V CAD of caesium adducted 7⁺ malonyl-ACP **7**.

6.3.9. Summary and conclusions

Alkali metals were at no time found bound to the Pant or phospho-Pant ejection ions, in all cases the ions were detected as protonated species. This could indicate that the alkali metal is adducting to somewhere within the protein, rather than along the PPant modification, however, it is equally likely that the alkali metal falls off upon fragmentation.

It is still unclear whether the adduction of lithium is beneficial to the generation of a Pant ion. The lithiated nonhydrolysable photolabile malonyl carba(dethia) ACP analogue **63** and the lithiated acetyl-ACP **40** provided more intense Pant ions **81** and **171** than the respective non-lithiated species. However, CAD of malonyl and acetoacetyl-ACP ions **7** and **167** generated similar intensities of their Pant ions **173** and **175** with and without lithium. Lithium adduction to myristoyl-ACP **168** was the only ACP species to show a decrease in abundance of the fragment ion **177** compared to unlithiated. It may be worthwhile to test ACP species of interest with and without lithium adduction, as the variation in the effect of the alkali metal is unpredictable with these preliminary results. What can be deduced is that caesium adduction is not a favourable alkali metal ion for promoting the generation of a Pant ion or a phospho-Pant ion, as the primary fragmentation pathway is simply the loss of caesium.

6.4. The effect of alkali metal adduction to acyl carrier proteins (ACPs) on the production of peptides by CAD, and the application to post-translational modification mapping

Collisionally activated dissociation (CAD) is the most common fragmentation technique for sequencing peptides and proteins. The amide bonds of the proteins are highly susceptible to fragmentation by CAD, generating, so called, ‘b’ and ‘y’ ions.^{179, 334, 335} A ‘b’ ion is a fragment containing the N-terminus, whereas a ‘y’ ion is containing the C-terminus. Typically, protonated and sodiated peptides and proteins are used for the sequencing. The effect of metal binding to proteins has been explored in limited detail, in regards to the fragments generated by CAD.³³⁶⁻³³⁸ The effect of alkali metals on CAD, in particular, has not been widely documented in the literature.³³⁸

The same samples and spectra analysed for the ability to produce PPant ions by CAD were also analysed for the production of peptide fragment ions. The effect of the alkali metal on the fragments produced was compared to without that metal ion.

Five ACPs were prepared from *apo act* ACP **44** as previously described in Section 6.3.2; acetyl **40**, malonyl **7**, acetoacetyl **167**, myristoyl **168** ACPs and the ACP analogue **63** explored in detail in this thesis. Each ACP was prepared with and without 1 mM LiCl or CsCO₃, as before, and these ions were isolated and fragmented in the collision cell. A range of CAD voltages were applied to the isolated parent ions, up to the point where signal was lost.

The FT-ICR mass spectra have been assigned in absorption mode, providing improved resolution, and signal to noise ratio over the normal magnitude mode

spectra (**Figure 67**). A software programme, Autophaser, was used to produce the absorption mode spectra.³³²

For this section, the same voltages are compared between each ACP, however, the effect of increasing voltages, where applicable, will be discussed.

Locating the position of a post-translational modification (PTM) on a protein is important for biochemical characterisation. As discussed, the acyl carrier protein from the actinorhodin minimal system used in this study bears a phosphopantetheinyl (PPant) arm at serine 45 of the protein. CAD will often cleave the PTM from the protein, producing a Pant ion **58**, or a phospho-Pant ion **59**, this will leave a phosphorylated protein or peptide fragment ion. The PTM can, however, remain bound, and the peptide fragment ions will contain the PTM. This information can be used to locate which amino acid the PTM is bound to. The influence of the metal ion on whether the PPant arm, or phosphorylation, remains bound to the peptide fragment ions is explored, as this is essential for PTM mapping.

6.4.1. The effect of alkali metal adduction to modified ACPs from the actinorhodin minimal system from *S. coelicolor* on the production of peptide ions by CAD

To identify proteins by mass spectrometry, ‘b’ and ‘y’ ions are compared against a library, the more of these types of ions produced will result in more confidence in the protein’s assignment. This section explores whether the simple sample preparation with an alkali metal salt can improve the sequence coverage for a selection of ACPs from the model actinorhodin minimal system. Identifying ACPs from organisms is a relatively new technique for detecting expressed polyketide synthases (PKSs).^{158, 159}

This information can lead to discovering new compounds of pharmaceutical and agricultural significance.

6.4.1.1. Acetyl-ACP 40

Acetyl-ACP **40** is a ‘natural’ ACP analogue, it is used by the PKS and FAS for loading the ketosynthase domain, prior to chain extension and elongation, a key process for the biosynthesis of polyketides. It would be likely that this ACP could be detected in a proteomics sample.

25V is the highest voltage that is able to generate an adequate signal for the non-lithiated acetyl-ACP **40**, and this voltage was also applied to the lithium adducted acetyl-ACP **40**. The caesiated acetyl-ACP **40** does not produce any peptide fragments, therefore it was rapidly ruled out as an adduct that can improve sequence coverage for this sample.

The cleavage coverage maps for each sample at 25V CAD are shown in **Figure 80**, and the corresponding spectrum is shown in **Figure 81**. The difference between the sequence coverages for the two samples clearly shows improvements with lithium adduction. In particular, there are six new ‘b’ and ‘y’ ions within the first ten amino acids at the N-terminus of the protein. The other differences are distributed evenly throughout the protein.

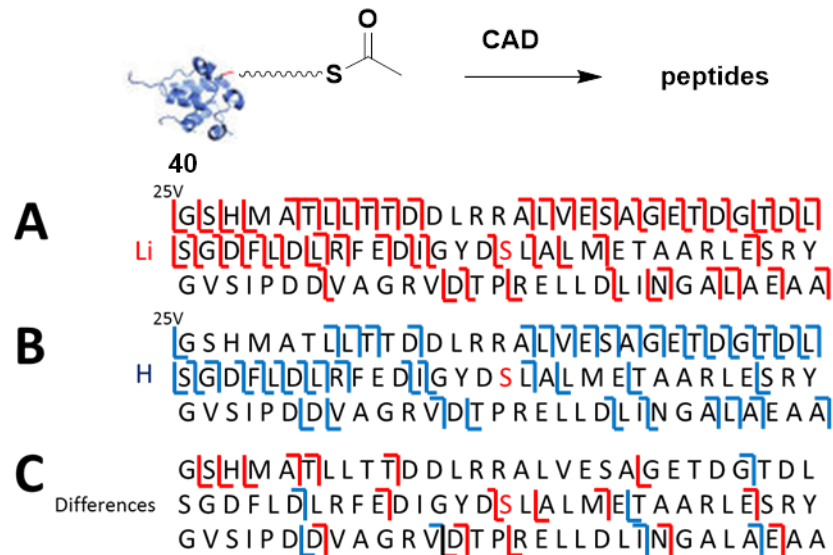


Figure 80 Cleavage coverage maps showing *b* and *y* ions resulting from collisionally activated dissociation (25V) of acetyl-ACP 40 with (A, red) and without (B, blue) lithium adduction. The differences between the maps is shown (C).

The adduction of lithium to the protein also allows for higher CAD voltages, up to 35V. The increased voltage produces a few different ‘b’ and ‘y’ ions, but the improvement in sequence coverage, compared to without lithium adduction, is not significant. (**Appendix 71**)

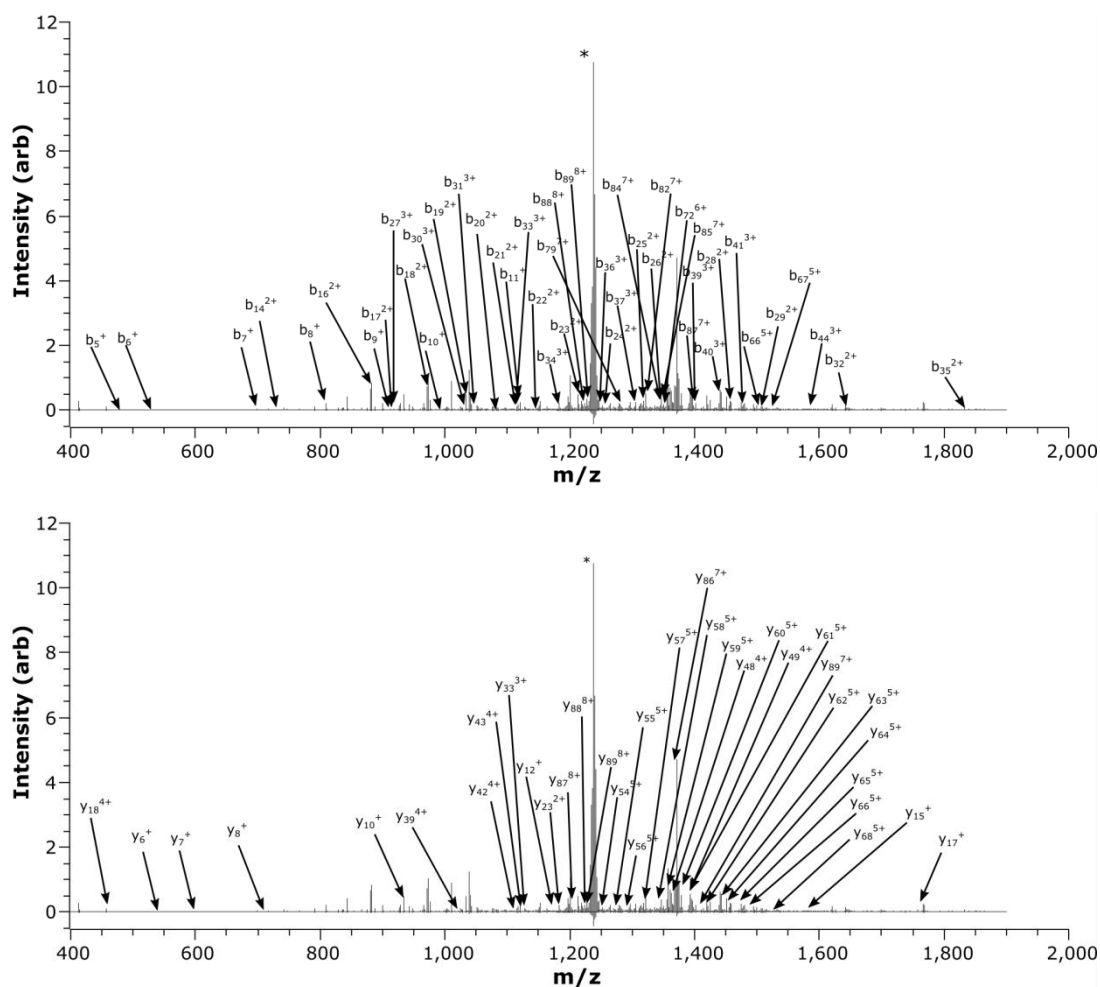


Figure 81 Example spectrum showing *b* (top) and *y* (bottom) ions resulting from collisionally activated dissociation (25V) of acetyl-ACP **40** with lithium adduction. The parent ion (8^+) is indicated with an asterisk. The corresponding cleavage coverage map is shown in **Figure 80**.

6.4.1.2. Malonyl-ACP **7**

Chain elongation is initiated by malonyl-ACP **7** in PKSs and FASs, a key process for the production of polyketides and fatty acids. 35V can be applied to all samples; non-alkali adducted, lithiated and caesiated, without loss of signal (**Figure 82**). The caesiated ACP **7** does not produce any unique fragments. The lithium adducted sample produces a similar number of fragments to the sample without alkali adduction. There are differences between with and without lithium adduction,

however, they are spread throughout the protein. There is no clear difference between the sequence coverage of the two samples.

The voltage applied to the samples with and without lithium adduction could be increased to 40V, but there is still no clear improvements to the sequence coverage with either sample. (**Appendix 72**)

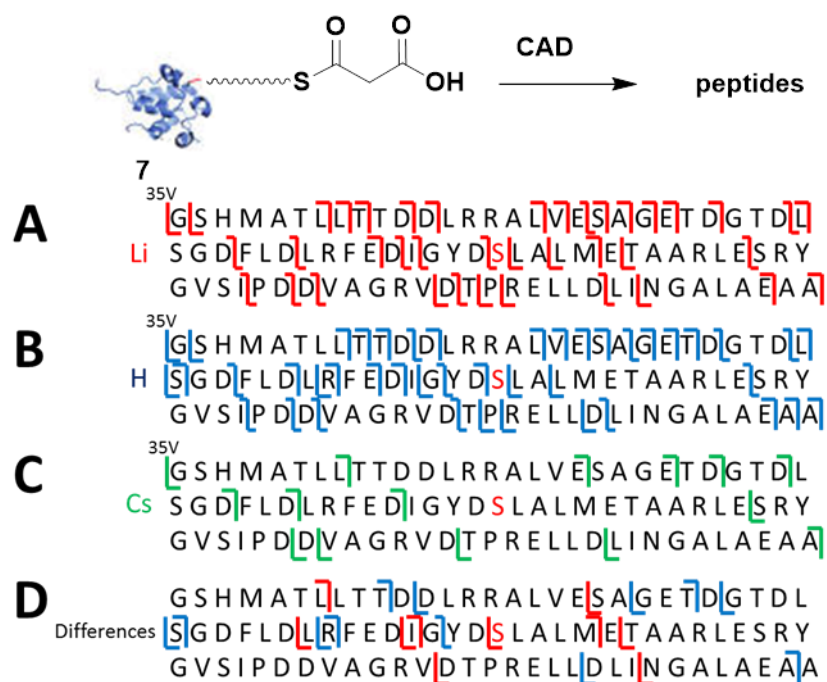


Figure 82 Cleavage coverage maps showing *b* and *y* ions resulting from collisionally activated dissociation (35V) of malonyl-ACP 7 with lithium (A, red), with caesium (C, green) and without alkali (B, blue) adduction. The differences between the maps is shown (D).

6.4.1.3. Acetoacetyl-ACP 167

Acetoacetyl-ACP 167 is the product of a single extension of the polyketide chain, a common intermediate to both PKS and FAS biosynthetic pathways. CAD of 30V could be applied to all three samples. The caesiated sample, again, provides the lowest sequence coverage, but does generate three unique ‘b’ and ‘y’ ions not

detected in the other spectra. On this occasion, the sample without additional alkali metal adduction produces greater sequence coverage than with lithium adduction, most notably due to increased fragmentation between residues 17 and 27 (**Figure 83**).

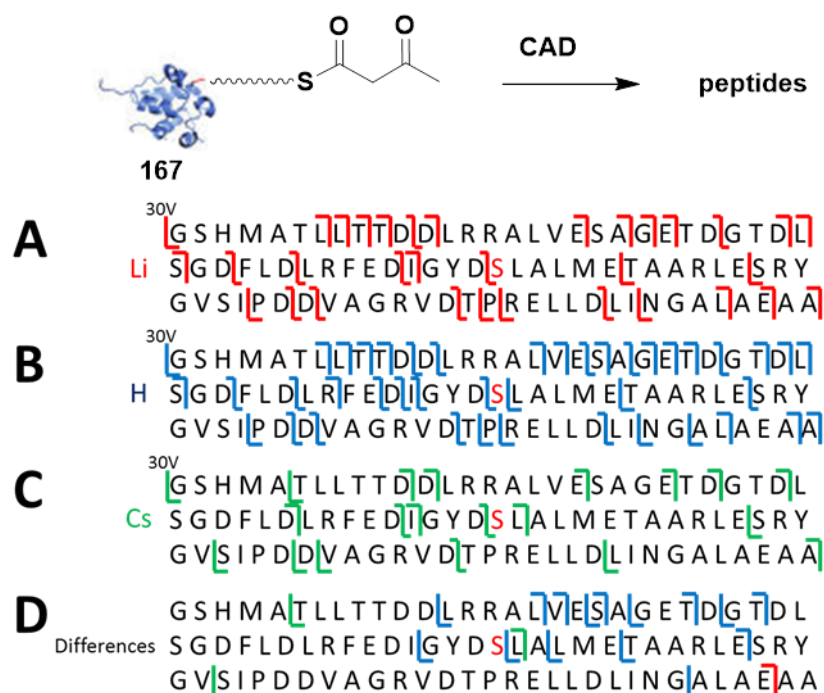


Figure 83 Cleavage coverage maps showing *b* and *y* ions resulting from collisionally activated dissociation (30V) of acetoacetyl-ACP **167** with lithium (A, red), with caesium (C, green) and without alkali (B, blue) adduction. The differences between the maps is shown (D).

The voltage for the samples with and without lithium adduction could be increased to 40V. At this voltage the sequence coverage shows more similarities between the samples, however, the sample without lithium adduction still provides the greatest sequence coverage. (**Appendix 73**)

6.4.1.4. Myristoyl-ACP 168

The myristoyl group is a lipid modification to proteins, biosynthesised by FASs, for promoting protein-membrane and protein-protein interactions, it is involved in a range of signal transduction cascades.³³⁹ Myristoyl-ACP **168** is a late stage biosynthetic intermediate following a number of chain extensions and reductions.

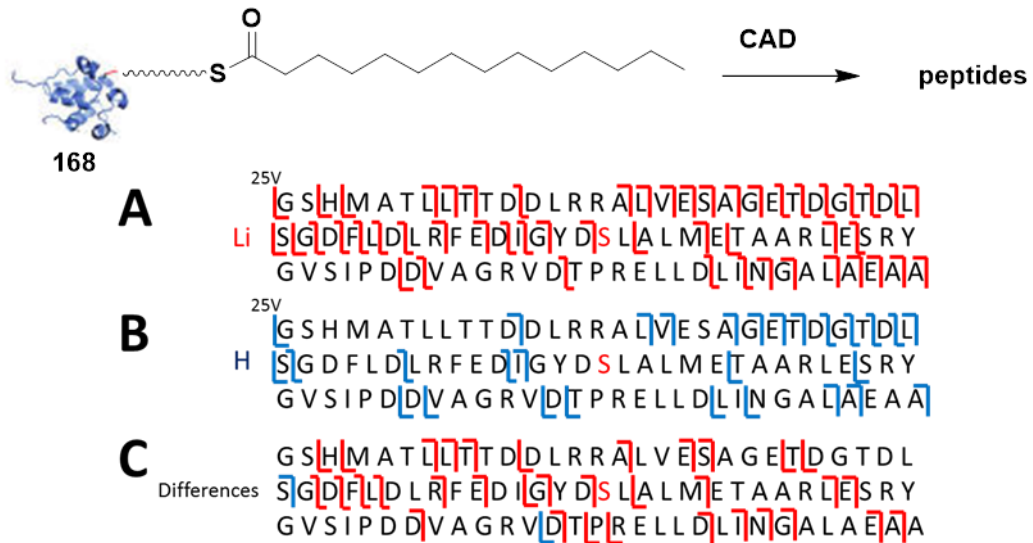


Figure 84 Cleavage coverage maps showing *b* and *y* ions resulting from collisionally activated dissociation (25V) of myristoyl-ACP **168** with (A, red) and without (B, blue) lithium adduction. The differences between the maps is shown (C).

Unfortunately, the signal for the caesiated myristoyl-ACP **168** was too weak for isolation and subsequent fragmentation. The maximum voltage that could be applied to the non-lithiated sample was 25V. At this voltage, the lithiated sample, by far, provides the greater sequence coverage (**Figure 84**). Increasing the voltage to 35V for the lithiated myristoyl-ACP **168** reduces the sequence coverage, but there was still more sequence coverage than without lithium adduction at 25V. (**Appendix 74**)

6.4.1.5. Nonhydrolysable photolabile malonyl carba(dethia) ACP analogue

63

The nonhydrolysable photolabile malonyl carba(dethia) ACP analogue **63** was designed to be activated by light to act as a probe for polyketide chain extension. It is not a ‘natural’ ACP, however, many polyketide intermediates contain bulky aromatic constituents, and its response to alkali adduction can still be worthwhile to investigate.

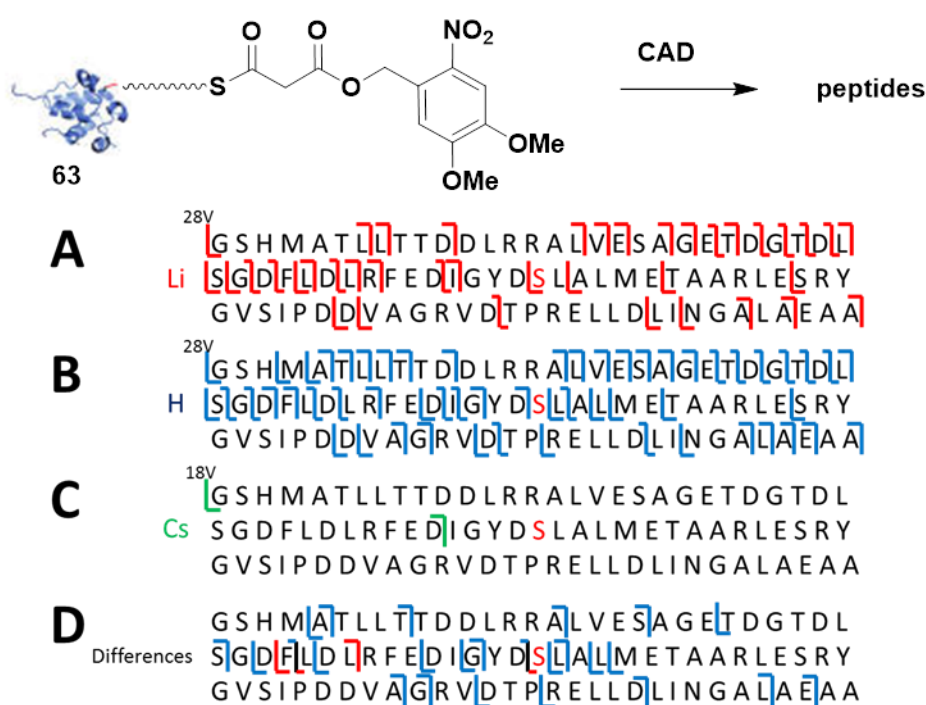


Figure 85 Cleavage coverage maps showing *b* and *y* ions resulting from collisionally activated dissociation (28V and 18V) of nonhydrolysable photolabile malonyl carba(dethia) ACP analogue **63** with lithium (A, red), with caesium (C, green) and without alkali (B, blue) adduction. The differences between the maps is shown (D).

The maximum voltage that could be used for the caesiated ACP analogue **63** was just 18V, and only generates two fragment ions. The sample without alkali adduction could be fragmented with voltages up to 28V, which provides substantial sequence

coverage, more so than the lithium adducted sample at the same voltage. The lithiated ACP **63** could be fragmented at 30V, providing a few different fragment ions, however, the non-lithiated sample is still superior for optimum sequence coverage. (**Appendix 75**)

6.4.2. The effect of alkali metal adduction to ACPs on the production of phospho-peptide ions for post-translational modification mapping

The cleavage of the phosphodiester bond of the phosphopantetheinyl (PPant) arm of the ACP under CAD is a common fragmentation pathway, in doing so, a phospho group remains bound to the ACP. Subsequent fragmentation of the protein can lead to locating the amino acid on which the PPant arm, the PTM, was originally bound. This technique is often called ‘PTM mapping’, a key technique in mass spectrometry for characterising known proteins, and identifying or classifying unknown proteins. The use of alkali metals in improving the technique of PTM mapping is explored in this section.

6.4.2.1. Acetyl-ACP 40

Phospho-peptide ions, only, are shown in **Figure 86** produced from fragmentation of acetyl-ACP **40** with 25V. The lithiated sample provides ten ‘b’ ions and just two ‘y’ ions bearing the phospho group, whereas the sample without additional alkali adduction provides eight ‘b’ ions and three ‘y’ ions. There are eleven differences in the ions generated by the two samples, combining the data from the two samples’ spectra narrows down the location of the active site amino acid by just a single

amino acid. However, the lithiated sample's spectra has more phosphorylated fragment ions than the non-lithiated.

Increasing the voltage to 35V for the lithiated ACP parent ion **40** reduces the number of 'b' ions to eight, but increases the number of 'y' ions to six. It also restricts the location of the active site amino acid by two more amino acids. Some of the new fragment ions were originally detected without the lithium adduction. (**Appendix 76**)

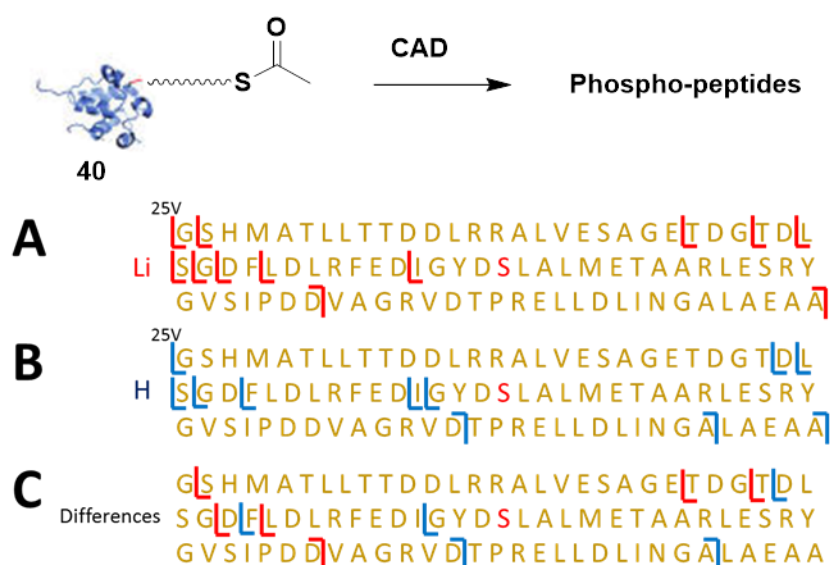


Figure 86 Cleavage coverage maps only showing phosphorylated b and y ions resulting from collisionally activated dissociation (25V) of acetyl-ACP **40** with (A, red) and without (B, blue) lithium adduction. The differences between the maps is shown (C).

6.4.2.2. Malonyl-ACP 7

There is good coverage of phosphorylated peptide ions for both malonyl-ACP **7** samples with and without lithium adduction. No phospho-peptides were detected in the caesiated sample **7**. At 35V, the sample without lithium adduction provides more phospho-peptides for PTM mapping, but both preparations allow mapping to within

twelve amino acids (**Figure 87**). Increasing the CAD voltage to 40V reduces the number of phosphorylated fragment ions detected. (**Appendix 77**)

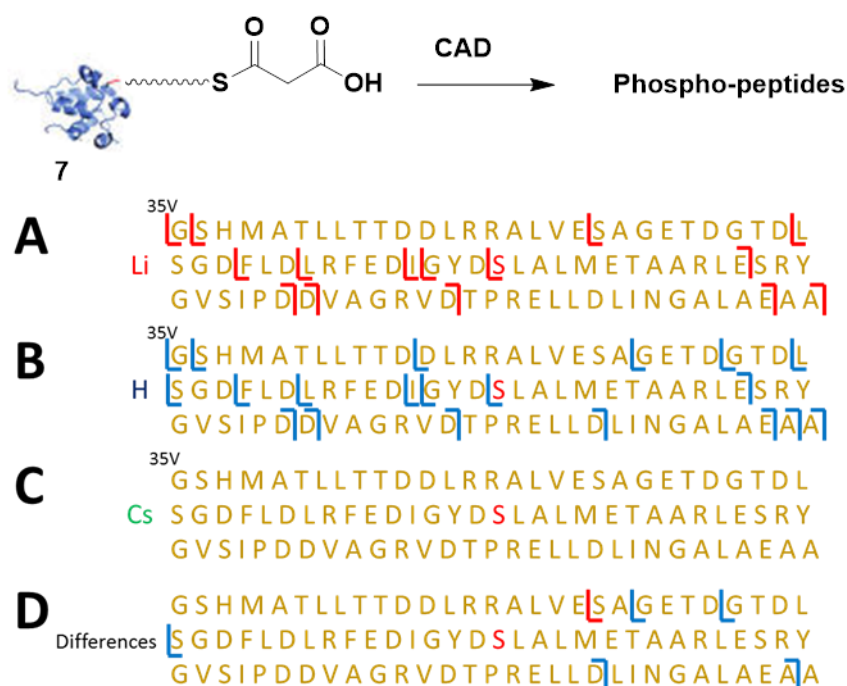


Figure 87 Cleavage coverage maps only showing phosphorylated b and y ions resulting from collisionally activated dissociation (35V) of malonyl-ACP 7 with lithium (A, red), with caesium (C, green) (Note: none detected) and without alkali (B, blue) adduction. The differences between the maps is shown (D).

6.4.2.3. Acetoacetyl-ACP 167

The sample without additional alkali metal adduction maps the active site amino acid of acetoacetyl-ACP 167 to within twelve amino acids, substantially less than in the lithiated and caesiated samples. Additionally, that sample without alkali adduction provides one extra ‘b’ ion, and three extra ‘y’ ions than the other two samples (**Figure 88**). Increasing the CAD voltage did not increase the sequence coverage of the phospho-peptide ions, and did not improve the ability to map the PTM. (**Appendix 78**)

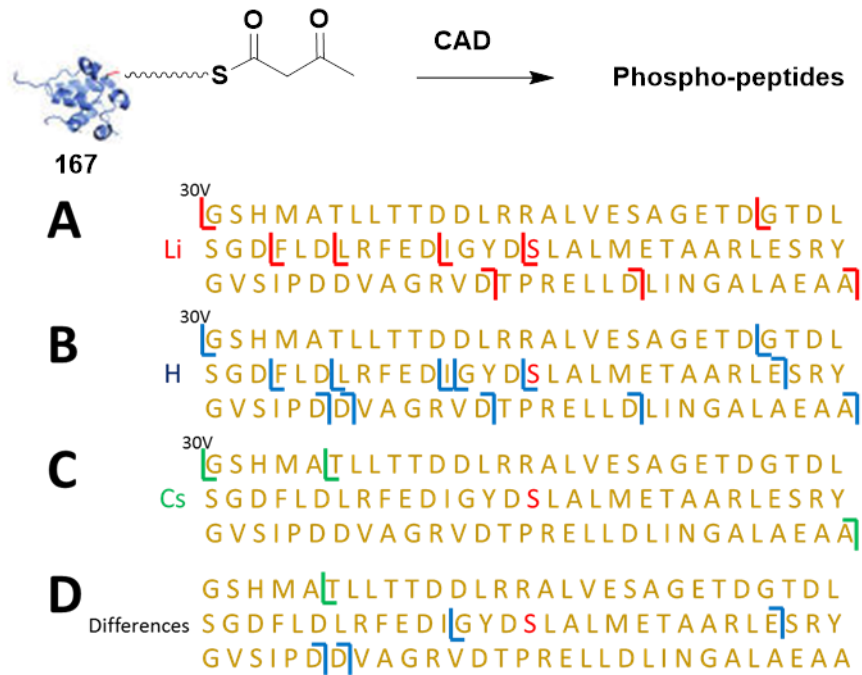


Figure 88 Cleavage coverage maps only showing phosphorylated b and y ions resulting from collisionally activated dissociation (30V) of acetoacetyl-ACP 167 with lithium (A, red), with caesium (C, green) and without alkali (B, blue) adduction. The differences between the maps is shown (D).

6.4.2.4. Myristoyl-ACP 168

Lithium adduction to myristoyl-ACP 168 significantly improves the sequence coverage of phosphorylated fragment ions compared to without lithium adduction. However, fragments near to the active site serine are lacking (**Figure 89**). Increasing the CAD voltage, on the lithiated parent ion, does not improve the sequence coverage, but it is still superior to the non-lithiated sample. (**Appendix 79**)

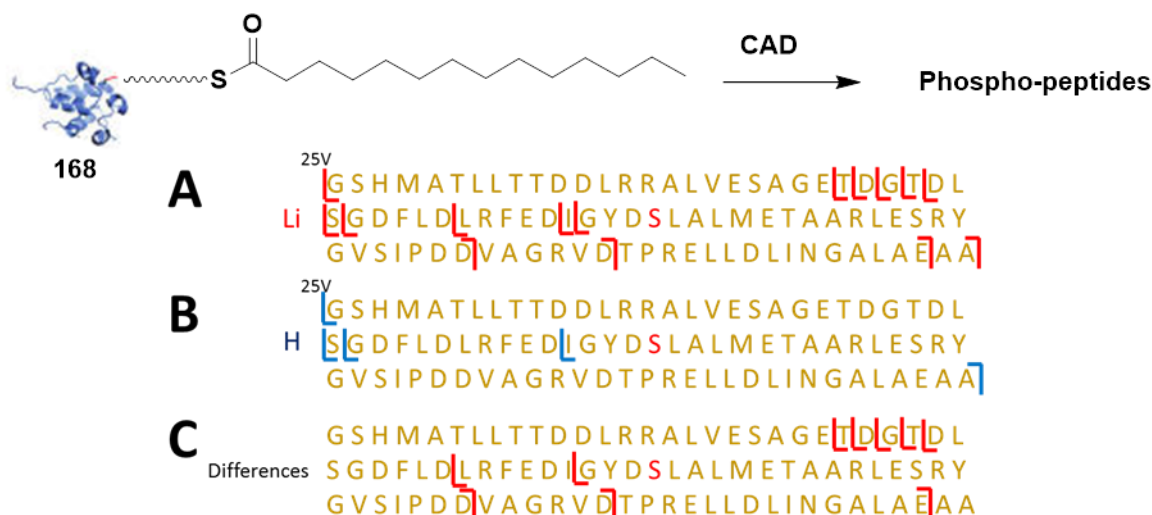


Figure 89 Cleavage coverage maps only showing phosphorylated *b* and *y* ions resulting from collisionally activated dissociation (25V) of myristoyl-ACP **168** with (A, red) and without (B, blue) lithium adduction. The differences between the maps is shown (C).

6.4.2.5. Nonhydrolysable photolabile malonyl carba(dethia) ACP analogue

63

The sequence coverage of phospho-peptide ions is superior for the ACP analogue **63** sample without alkali adduction, compared to both the lithiated and caesiated. However, sequence coverage specifically in the region of the active site serine is better in the lithiated sample, but would only narrow down the amino acid to within 28 amino acids. The caesiated sample fails to generate any phosphorylated fragment ions (**Figure 90**). Increasing the voltage of CAD on the lithium adducted ACP **63** to 30V reduces the sequence coverage, and decreases the number of phospho-peptide ions around the active site serine. (**Appendix 80**)

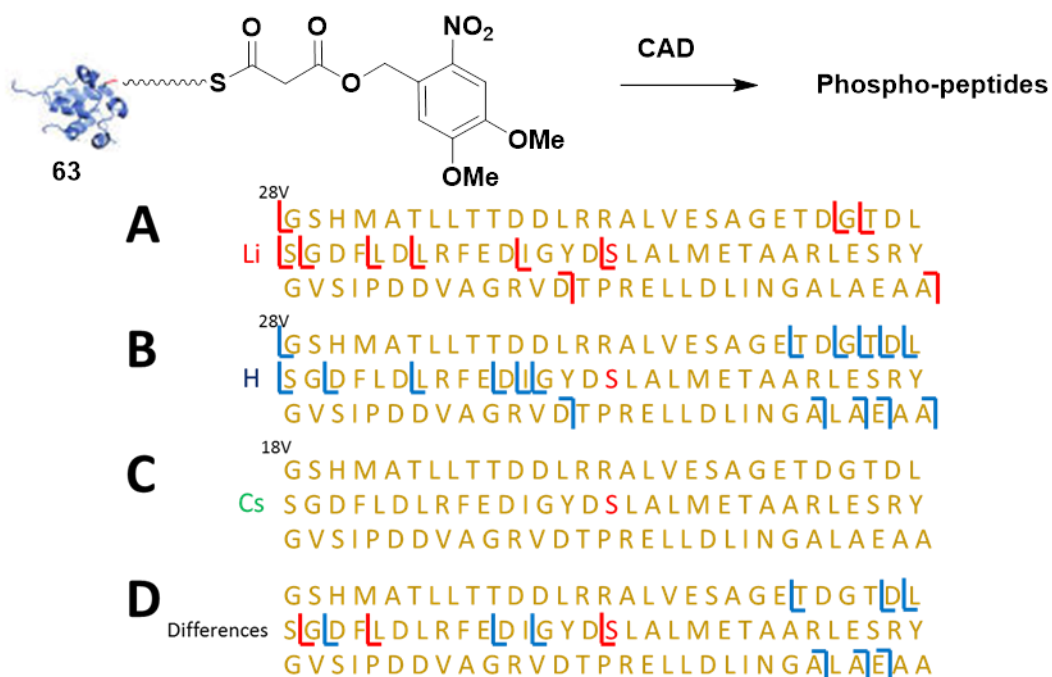


Figure 90 Cleavage coverage maps only showing phosphorylated b and y ions resulting from collisionally activated dissociation (28V and 18V) of nonhydrolysable photolabile malonyl carba(dethia) ACP analogue **63** with lithium (A, red), with caesium (C, green) (Note: none detected) and without alkali (B, blue) adduction. The differences between the maps is shown (D).

6.4.3. The effect of alkali metal adduction to ACPs on the production of peptide ions bearing the phosphopantetheinyl arm for post-translational modification mapping

CAD will typically cleave a phosphodiester bond, or a phospho group from a peptide or protein, however, this is not favourable for PTM mapping. This section explores whether the addition of an alkali metal salt to protein samples prior to CAD analysis can improve the technique of PTM mapping for modifications linked by a phosphodiester bond, by analysing a range of modified ACPs.

6.4.3.1. Acetyl-ACP 40

The acetyl-phosphopantetheinyl (PPant) group remains bound to many of the ‘b’ and ‘y’ ions upon 25V CAD fragmentation, both with and without lithium adduction, however, with lithium bound there is a greater number of both types of ions. Fragments near to the active site serine in the middle of the protein are lacking, however (**Figure 91**).

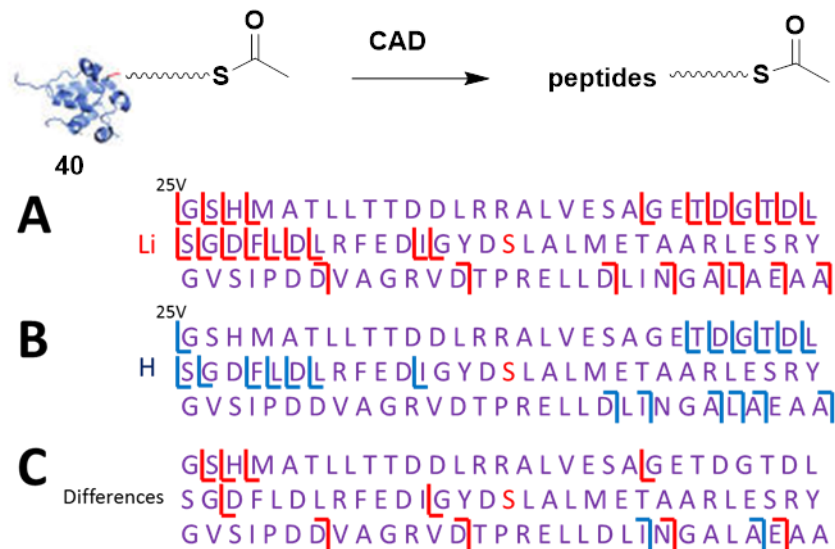


Figure 91 Cleavage coverage maps only showing ‘b’ and ‘y’ ions with the acetyl-phosphopantetheinyl arm bound, resulting from collisionally activated dissociation (25V) of acetyl-ACP 40 with (A, red) and without (B, blue) lithium adduction. The differences between the maps is shown (C).

The voltage, with lithium bound to the parent ion, could be increased to 35V, but this significantly reduces the number of ions with the PPant group remaining bound.

(**Appendix 81**)

6.4.3.2. Malonyl-ACP 7

The malonyl-PPant group remains bound to a small amount of the ‘b’ and ‘y’ ions, distributed evenly throughout the protein, with and without lithium adduction, but these ions are not detected from caesium adducted to the parent malonyl-ACP ion **7**. Only two more ‘b’ ions are found in the spectra from CAD without lithium adduction (**Figure 92**). When the voltage is increased to 40V, both with and without lithium adduction, no malonyl-PPant ‘b’ or ‘y’ ions are detected in the spectra.

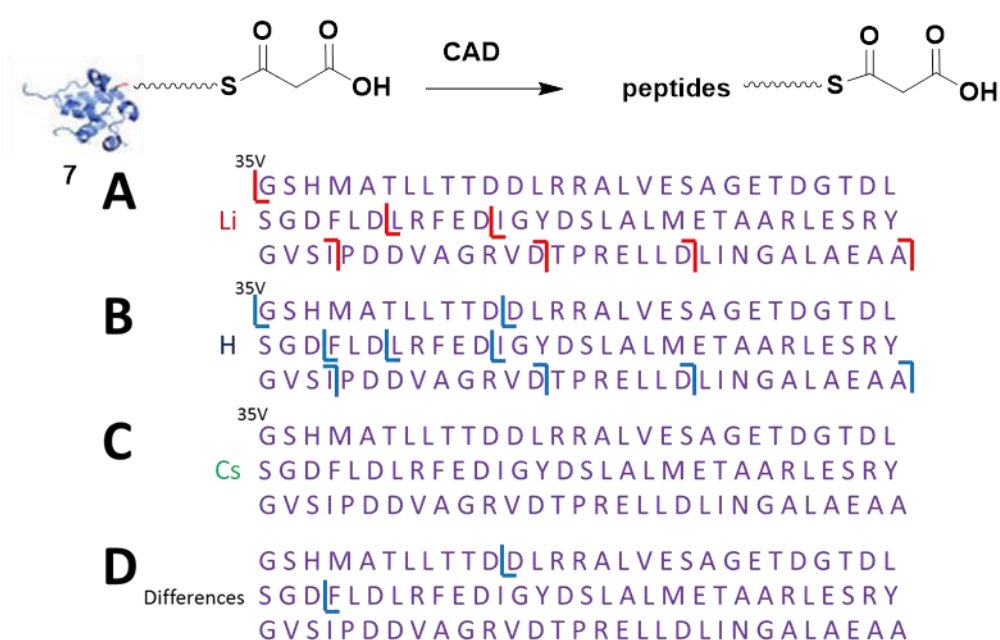


Figure 92 Cleavage coverage maps only showing ‘b’ and ‘y’ ions with the malonyl-phosphopantetheinyl arm bound, resulting from collisionally activated dissociation (35V) of malonyl-ACP **7** with lithium (A, red), with caesium (C, green) (Note: none detected) and without alkali (B, blue) adduction. The differences between the maps is shown (D).

6.4.3.3. Acetoacetyl-ACP 167

The addition of an alkali metal salt to the acetoacetyl-ACP **167** samples does not increase the number of ‘b’ or ‘y’ ions with the acetoacetyl-PPant group bound. Six

more PPant ions are detected without the additional sample preparation (**Figure 93**). Increasing the CAD voltage from 30V to 40V to the parent ions with and without lithium adduction results in no acetoacetyl-PPant bound peptides.

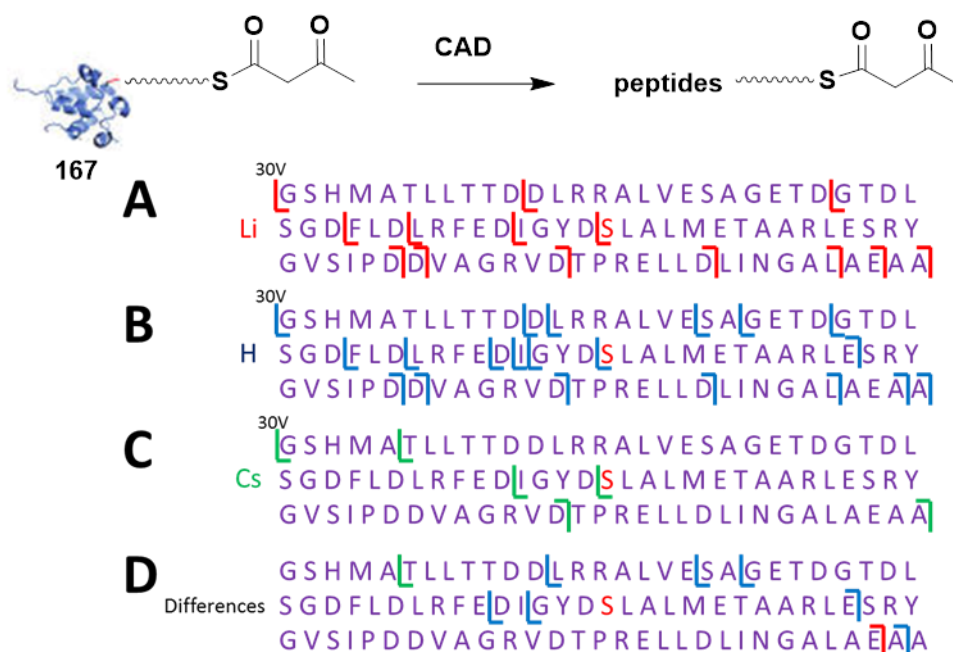


Figure 93 Cleavage coverage maps only showing ‘b’ and ‘y’ ions with the acetoacetyl-phosphopantetheinyl arm bound, resulting from collisionally activated dissociation (30V) of acetoacetyl-ACP **167** with lithium (A, red), with caesium (C, green) and without alkali (B, blue) adduction. The differences between the maps is shown (D).

6.4.3.4. Myristoyl-ACP **168**

At 25V CAD, the lithiated myristoyl-ACP **168** produces many more myristoyl-PPant peptide ions than in the non-lithiated sample. The ions are mainly from the termini of the protein, and not as many near to the active site serine, at amino acid 45 (**Figure 94**). Increasing the CAD voltage to 35V, only capable with the lithiated parent ion **168**, abolishes all production of PPant bound peptide ions.

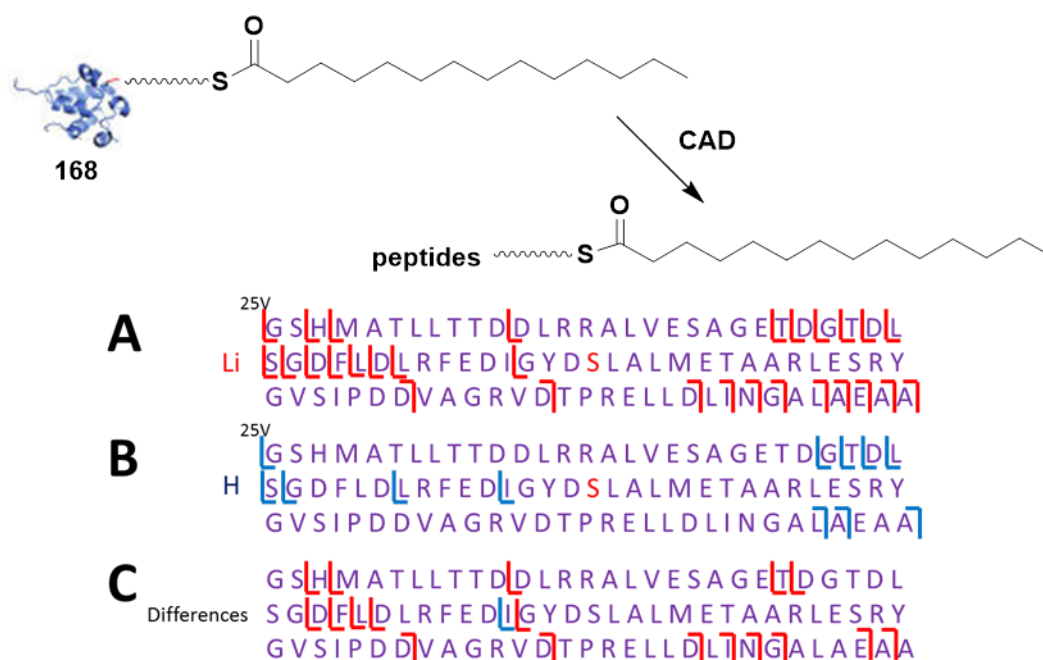


Figure 94 Cleavage coverage maps only showing ‘b’ and ‘y’ ions with the myristoyl-phosphopantetheinyl arm bound, resulting from collisionally activated dissociation (25V) of myristoyl-ACP **168** with (A, red) and without (B, blue) lithium adduction. The differences between the maps is shown (C).

6.4.3.5. Nonhydrolysable photolabile malonyl carba(dethia) ACP analogue **63**

The CAD spectra resulting from fragmentation of both lithiated and non-lithiated ACP analogue **63** parent ions were quite similar in number of PPant peptide ions, but the peptide ions generated are slightly different. Combining the data from the two spectra results in a much higher sequence cover. The caesiated parent ion **63** does not provide PPant bound ‘b’ or ‘y’ ions (**Figure 95**). Increasing the voltage to 30V for fragmentation of the lithiated parent ion **63** reduces the sequence coverage of PPant bound ions. (**Appendix 82**)

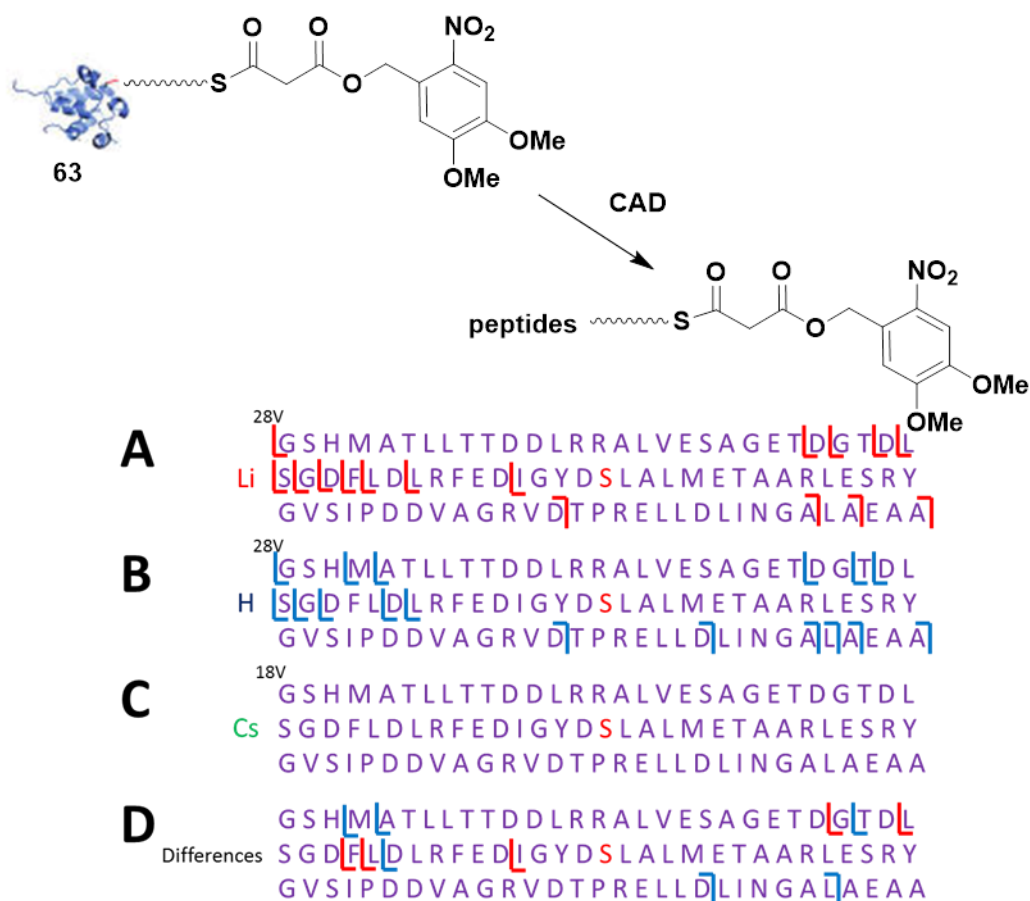


Figure 95 Cleavage coverage maps only showing ‘b’ and ‘y’ ions with the nonhydrolysable photolabile malonyl carba(dethia)-phosphopantetheinyl arm bound, resulting from collisionally activated dissociation (28V and 18V) of nonhydrolysable photolabile malonyl carba(dethia) ACP analogue **63** with lithium (A, red), with caesium (C, green) (Note: none detected) and without alkali (B, blue) adduction. The differences between the maps is shown (D).

6.4.4. Summary and conclusions: The application of alkali metal adduction to acyl carrier proteins (ACPs) on the production of peptides by CAD, and the application to post-translational modification mapping

Five different ACPs, acetyl **40**, malonyl **7**, acetoacetyl **167**, myristoyl **168** and, an unnatural analogue, nonhydrolysable photolabile malonyl carba(dethia) **63**, were

prepared for analysis by CAD on an FTICR-MS. Each sample was prepared with 1 mM of either lithium chloride or caesium carbonate, to provide the respective alkali adducted parent ions for isolation and subsequent fragmentation. Lithium parent ions were produced for each ACP, however a caesiated precursor ion for myristoyl-ACP **168** was not generated with sufficient intensity to be isolated for CAD analysis.

Each lithium adducted parent ion could be fragmented with a higher CAD voltage than its respective non-lithiated ion; increasing the voltage did not increase the sequence coverage, however, it did alter the type of fragments.

Caesiated parent ions never generated a substantial number of peptide fragments, in most cases they did not produce any. This is likely due to the primary fragmentation pathway of the loss of the caesium ion and charge reduction.

At the same voltages, the lithiated parent ion was not always the sample to provide the highest sequence coverage. Acetyl **40** and myristoyl **168** ACPs were the only two samples to clearly show an increase in sequence cover with lithium adduction compared to without. Malonyl-ACP **7** had similar sequence coverage with and without lithium adduction, but without the alkali adduction was marginally better. Acetoacetyl-ACP **167** and the unnatural ACP analogue **63** demonstrated clear improvements to the sequence cover without lithium adduction. It would be hard to predict this outcome; however, the simple sample preparation and possible improvements could prove beneficial for identifying and characterising proteins. An extended study on a wider variety of ACPs with varying chain lengths and chemical moieties may discover a link between the PPant group and the sequence cover.

PTM mapping is an important characterisation technique for peptides and proteins. The PPant group of ACPs can either remain bound to the fragment peptide ions, be

partially cleaved, often leaving a phosphorylated ion, or be cleaved entirely resulting in an *apo*-peptide ion. The latter is not useful for PTM mapping, however both the partially fragmented and intact PPant group can be used to locate the active site serine.

Increasing the voltage for fragmentation of the lithiated precursor ions resulted in losses of phosphorylated or PPant peptide ions with all ACPs except for acetyl-ACP **40**, however that only resulted in two more phospho-peptide ions being detected. Increasing the voltage resulted in a more substantial loss of PPant bound 'b' and 'y' ions, it is likely that the group is being cleaved off at higher voltages.

Caesium adduction resulted in very few peptides ions with either the phospho or PPant group bound.

The adduction of lithium improved the sequence coverage of phosphorylated 'b' and 'y' ions in the spectra of acetyl **40** and myristoyl **168** ACPs. In all other spectra, the samples without additional alkali adduction generated more phosphorylated peptide ions.

The number of PPant-peptide ions generated was improved by lithium adduction in the fragmentation of, again, acetyl **40** and myristoyl **168** ACPs. In the spectra of the malonyl-ACP **7** and the ACP analogue **63** the difference between lithiated and non-lithiated was marginal. Acetoacetyl-PPant fragment ions, from fragmentation of acetoacetyl-ACP **167**, were more abundant in the spectra produced without additional alkali adduction.

The benefits of alkali adduction for mapping PTMs of proteins appears to depend upon the specific ACP as the results varied from ACP to ACP. A wider study with a range of ACPs, as well as with a variety of modifications, such as polyketide

intermediates, would reveal when alkali metal adduction can be effective for locating PTMs.

6.5. Summary and conclusions: Alkali metal adduction assisted tandem mass spectrometry for molecular structural determination

The influence of alkali metal adduction to a small molecule **61** and five ACPs has been explored through CAD, and with EID to the small molecule.

The impact of the simple sample preparation technique on the fragmentation pathways of the small molecule **61** in both CAD and EID was determined by direct comparison with the same MS methods applied to each sample. Although EID is the more advanced and time consuming technique, several new fragments were generated with this fragmentation method compared to CAD. The adduction of lithium, by far, provided the most fragment ions by CAD, and lithium and caesium adduction generated new fragments by EID that were not seen with sodium adduction. Although this study was carried out with just one compound, the improvements indicate that adding lithium chloride to a small molecule sample prior to fragmentation could be beneficial for structural characterisation. Analysis of a database of small molecules could determine whether this increase in fragments is common to a variety of compounds when lithiated, as well as reveal why this enhancement occurs.

The production of a small Pant ion upon CAD fragmentation of *holo*-ACPs was explored with lithium and caesium adduction. The addition of caesium carbonate to the samples did not benefit the ‘ejection’ of a Pant ion, mostly due to the primary

fragmentation pathway being the loss of the caesium adduct and the reduction of charge.

	PPant bound to ACP	Most successful sample preparation	
		Non-lithiated	Lithiated
Production of PPant ion – most intense PPant ion	Acetyl 40		✓
	Malonyl 7	✓	
	Acetoacetyl 167	✓	
	Myristoyl 168	✓	
	Unnatural analogue 63		✓
Sequence cover – greatest abundance of ‘b’ and ‘y’ ions	Acetyl 40		✓
	Malonyl 7	✓	
	Acetoacetyl 167	✓	
	Myristoyl 168		✓
	Unnatural analogue 63	✓	
Production of phospho-peptides – greatest abundance of phosphorylated ‘b’ and ‘y’ ions	Acetyl 40		✓
	Malonyl 7	✓	
	Acetoacetyl 167	✓	
	Myristoyl 168		✓
	Unnatural analogue 63	✓	
Production of PPant-peptides – greatest abundance of PPant bound ‘b’ and ‘y’ ions	Acetyl 40		✓
	Malonyl 7	✓	
	Acetoacetyl 167	✓	
	Myristoyl 168		✓
	Unnatural analogue 63	✓	

Table 7 Comparison of lithiated and non-lithiated ACP samples. A tick indicates whether samples with or without lithium adduction resulted in a more insightful spectrum from CAD fragmentation, either to produce a phosphopantetheinyl (PPant) ion, sequence cover, and for post-translational modification mapping (the detection of phosphorylated or Pant ions).

Lithium adduction had varying influence on providing the Pant ion, depending upon the specific ACP being analysed. This response was also seen with the sequence coverage, and PTM mapping potential. The acetyl **40** and myristoyl **168** ACPs responded most favourably towards lithium adduction of the five ACPs (**Table 7**).

There was always a variance between samples prepared with lithium chloride and those without, although not necessarily to the benefit of the original goal, this aspect needs to be investigated further for its potential. Both the types of modifications to the ACP, as well as the ACP protein itself, need to be broadened to discover a relationship between the alkali metal adducted and the influence on CAD fragmentation pathways.

Chapter 7: Conclusions and future work

7. Conclusions and future work

The core aim of this project was to develop a new method to trap biosynthetic intermediates from an iterative type II PKS, a task that had yet to be accomplished before. The method herein devised utilised a photoactivatable nonhydrolysable malonyl acyl carrier protein probe **63** to off-load and capture enzyme-bound biosynthetic intermediates from the minimal system of the actinorhodin **2** PKS.

The secondary research aim was to compare the efficiency of intermediates caught by a small molecule photolabile probe **65** with the ACP probe **63**. Unfortunately, the small molecule probe **65** was unsuccessful in capturing any intermediates from the actinorhodin minimal system PKS. There was insufficient time to explore this in more detail, however, the small molecule photolabile probe **65** proved capable of capturing intermediates from the lasalocid A **1** biosynthetic pathway *in vivo*.

The final aim was to investigate the future potential for mass spectrometry in the analysis of polyketides, and proteins associated with natural product biosynthesis. Alkali metal adduction to samples showed promise for structural characterisation of small molecules, as well as boosting the signal of fragment ions from *holo*-ACPs. In addition, a less known technique, electron impact dissociation (EID), was compared with the widely used collisionally activated dissociation (CAD) for its possible advantages for structural characterisation of small molecules.

7.1. Probing the biosynthesis of an iterative polyketide PKS with a photoactivatable nonhydrolysable malonyl acyl carrier protein probe **63** and future work

A photoactivatable ACP probe **63**, the first of its kind, was chemoenzymatically synthesised *via* six chemical steps to pantetheine analogue **61**, then over three enzymatic steps in a one pot reaction to CoA analogue **62**, and finally enzymatically loaded onto *apo act*ACP **44** to generate the protected ACP probe **63**. This synthesis was repeated numerous times throughout the project, and optimised to produce a robust protocol.

The *act* ACP probe **64** proved promising in capturing selected putative intermediates from the actinorhodin minimal system, spanning from diketide **145** to hexaketide **149** (Scheme 31). If further confirmed by MSⁿ experiments, these would be the very first intermediates ever captured from type II PKS assembly.

The intermediate capture *via* probe **64** did prove inconsistent though, with different intermediates captured in experiment repeats. If this was somehow expected, reproducibility could perhaps be improved upon with the use of stopped flow equipment whereby each enzyme component is handled by a robot.

An autocorrelation algorithm allowed confirmation of the presence of the putative species manually identified. This is the first time that such a technique has been used within the natural products field and, in the future, it will be possible to use the algorithm to identify isotope distributions in the spectra simultaneously with their assignment.³⁰³

'trap'. This instrument generates very high resolution data and can accumulate ions in the ICR cell resulting in high sensitivity. Unfortunately, LC on the FTICR-MS was not feasible as the file size exceeded the capabilities at the time. Retention time of the intermediates on a RP column would have provided additional characterisation by way of an insight into the polarity of the trapped intermediates, in particular for cyclised/dehydrated species.

A trypsin digest of *actACP* was shown to provide two different peptides containing the active site serine, and these peptide ions were detected on a QTOF at sufficient resolution to be able to accurately identify species bound to the PPant arm. Optimising this method of analysis would allow those without access to FTMS to carry out the intermediate trapping; unfortunately, this was not pursued within the time constraints.

Fragmentation by CAD of the ACP-bound intermediate ion to generate a PPant fragment ion was not possible because of their low intensity, but this challenge could be overcome by scaling up the reactions to provide enough material for further MSⁿ characterisation. Further fragmentation of the ejected Pant ion would generate a plethora of information towards structural characterisation.

NMR or crystallography, however, would be the ideal techniques for characterisation of cleaved PPant moieties in detail, and this could be achieved by utilising an ACP hydrolase (AcpH) to cleave the PPant arm^{305, 340}. Additionally, the mixture of cleaved PPant arms produced from such a reaction could be analysed by LC-MS/MS.

Ion mobility MS is a mass spectrometric technique by which gas phase ions are separated by their movement through a drift tube containing a carrier gas and an

electric charge. More compact ions travel through the drift tube faster than less compact ions resulting in separation of ions. This method of separation could be used for characterisation of the biosynthetic intermediates bound to the ACP, and it could provide an insight into the structure of the ACP during biosynthesis.

The use of UV analysis for real time detection of SEK4/4b¹³ **41/42** was explored within this project, however the DMNB group absorbed too strongly at the wavelength of interest. Either investigation into alternative wavelengths for detection of SEK4/4b **41/42** or the use of a different photolabile group may allow this highly valuable avenue of analysis to be explored further in the future.

Labelling of the *act* ACP *in vivo* in *E. coli* was achieved showing the potential for *in vivo* off-loading of intermediates with the ACP probe **64**.^{115-117, 304} Time constraints did not allow further experiments, however complete reconstruction of the minimal system within a suitable host, likely *S. coelicolor*, and similar labelling of the *act* ACP will be possible in the future for off-loading *in vivo*.

Lastly, synthesising ACP probes from other PKSs is the next obvious step. Type II PKSs were the aim in this project, but type I PKSs, both iterative and modular, as well as FASs, could also be investigated. Not explored within this project is the potential for the CoA analogue **62** to be used as a probe for type III PKSs, but also in other processes that require malonyl-CoA **15** as a cofactor such as in the regulation of carnitine acyltransferase.³⁴¹ Using AcpH to cleave the PPant arms with bound intermediates would generate a library of unnatural polyketide derivatives which could be more efficient than the natural compound, or even have a new bioactivity.^{155, 156}

7.2. Capture of intermediates by the small molecule NAC probe **65** and future work

A photoactivatable NAC probe **65**, the first of its kind, was chemically synthesised via three chemical steps. This probe was utilised both *in vivo* and *in vitro*. **66** was unable to off-load intermediates from the actinorhodin minimal system both *in vivo* and *in vitro*, whereas the ACP probe **64** was successful in capturing intermediates *in vitro*. It may be possible to further optimise the *in vitro* conditions, such as the timing and length of photoirradiation, to enable the DMNB NAC probe **65** to capture intermediates, but, without further improvements, the ACP probe **64** is currently the most promising *in vitro* trapping agent for the actinorhodin minimal system.

Delayed addition of the active DMNB probes **63** and **65** was explored *in vitro* with the actinorhodin minimal system (Sections 4.1.2 and 5.2.4). The addition of active NAC probe **66** reduced the production of SEK4/4b **41/42** when it was added after 60 seconds and later (Figure 28). Further repeats (for example, with the use of stopped flow equipment to gather more time points and increase accuracy) would be able to confirm and rationalise this result, especially in comparison with the opposite effect obtained *via* the use of the ACP probe **64** in the same settings. This could indeed indicate a difference in the interactions of the two probes **64** and **66** with the actinorhodin minimal system, but for which no definitive conclusion can be inferred at this stage.

Within the Tosin group, success had been achieved in the investigation of the lasalocid A **1** biosynthetic pathway from *S. lasaliensis* utilising NAC probes.^{22, 155, 156} Herein *S. lasaliensis* was fed with the DMNB probe **65** and this led to the capture of two lasalocid A advanced intermediates **131** and **132** previously observed. Besides

two new putative intermediate species, the **135** and **136**, resulting from off-loading from ACP8, and further modification was detected and characterised.

Optimisation of these experiments with the DMNB NAC probe **65** in *S. lasaliensis* was not pursued within the project timeframe. Further exploration of time and duration of irradiation events could play a crucial role in improving the ability to capture intermediates, as well as if other factors such as photolysis quantum yield and bioavailability.

As discussed in Section 2.2, there are a variety of photolabile protecting groups that can be used for the masking of carboxylic acid groups. The DMNB group was chosen as it is widely studied and easily introduced *via* established synthetic routes, however the use of alternative groups should be explored in the future. The DMNPP group **112** has a higher quantum yield than the DMNB group²⁶⁵, however the synthetic route for its incorporation into chain termination probes would become more complex. Cell permeability may be a factor affecting the efficiency of the NAC probe **65**, and this could be altered by hydrophilic or hydrophobic substitutions to the benzene ring as in **108**, **109** or **110**.²⁵⁵ Coumarin based protecting groups can offer alternative non-protein damaging cleavage wavelengths, such as MCM **92** (cleaving at 340 nm)²³² or tBhc **91** (at 397 nm)²³⁴. SEK4/4b **41/42** production was demonstrated to be affected by the irradiation with 365nm (**Figure 34**), therefore a different investigatory wavelength may prove useful. Possible next generation photolabile probes are illustrated in **Figure 96**.

Alternative photolabile protecting groups may open up opportunities for real time UV detection of SEK4/4b **41/42**, which was prohibited by the strong absorption of the DMNB group at the wavelength required for detection of SEK4/4b **41/42**.

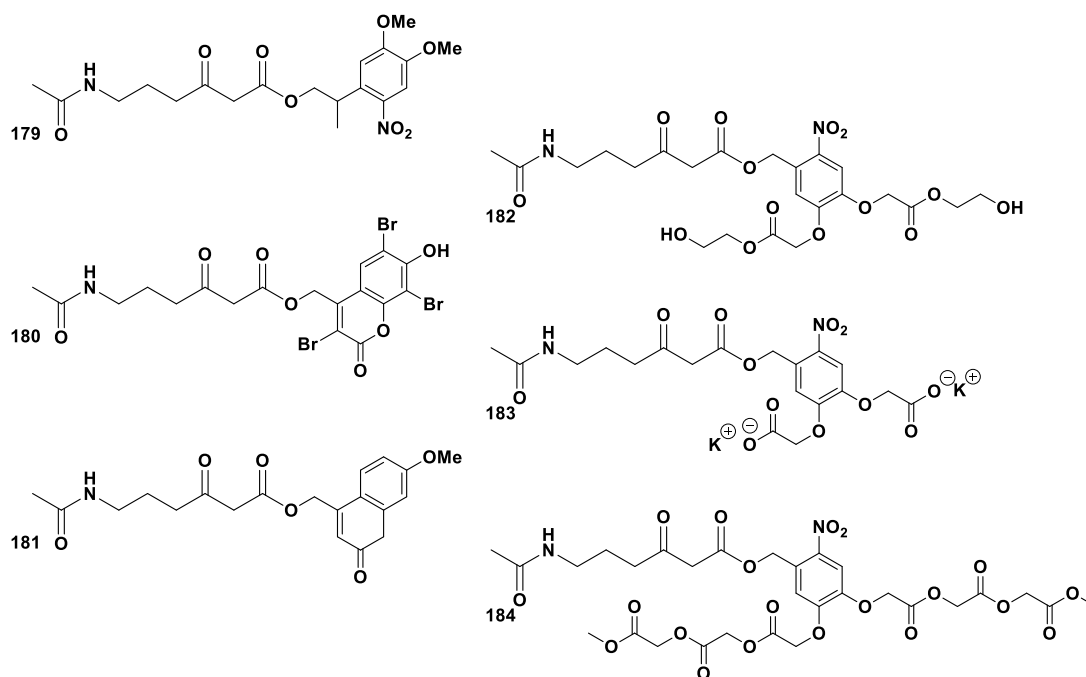


Figure 96 Potential next generation photolabile NAC analogues for off-loading of biosynthetic intermediates. **179** presents the DMNPP group that is reported to have a higher quantum yield than the DMNB group²⁶⁵. **180** presents the tBhc group that cleaves at 397 nm²³⁴. **181** presents the MCM group that cleaves at 340 nm²³². **182-184** have hydrophobic or hydrophilic substitutions to the benzene ring affecting their membrane permeability²⁵⁵.

Lasalocid A **1** present stereogenic centres that are likely crucial in determining its bioactivity, although this has not been explored extensively due to the complexity of its chemical synthesis. At this point, the chirality of the putative off-loaded intermediates from the lasalocid A **1** PKS is unknown. The putative undecaketide **131** and the two putative nonaketides **135** and **136** present a single peak in the LC chromatograms (**Figure 37**, **Figure 43**, and **Figure 44**), however the off-loaded dodecaketide **132** is detected in two distinct peaks (**Figure 42**). These are likely due to stereochemical differences. The characterisation of these two stereoisomers would require large scale feeding experiments to produce enough material for a detailed NMR analysis. A MS fragmentation technique, EID, has been proven to be

able to differentiate iso-lasalocid A from lasalocid A **1**¹⁹¹. EID of the two isolated peaks of dodecaketide **132** would aid the characterisation of the compounds, furthermore, EID analysis requires less material than NMR.

Lastly, as discussed in greater detail in chapter 6, the addition of alkali metals, in particular lithium, to the LC solvent has the potential to boost the MS signal of off-loaded biosynthetic intermediates from *in vivo* and *in vitro* feeding experiment extracts or aid MSMS analysis.

7.3. Alkali metal assisted tandem MS and future work

A synthetic analogue of pantetheine **61** was extensively analysed by CAD and EID with sodium, lithium or caesium ions. The impact of the alkali metal ions on the “PPant ejection assay” was also explored. The preliminary conclusion was that the addition of the alkali metal salts to samples was beneficial towards the goal of characterisation. It is not possible, at this point, to determine which alkali metal provided the most useful information, but analysing compounds with each alkali metal in turn and combining the results would allow full structural characterisation.

To gather a full picture of the benefits of this sample preparation requires a broader study using additional fragmentation techniques and mass spectrometers, more adducted ions, and many more compounds. In particular, whether the type of ACP (type I iterative, type I modular, type II, etc.), the PPant arm of the ACP (acetyl-ACP **40**, malonyl-ACP **7**, etc.) or the alkali metal ion have the greatest influence on the efficiency of the PPant ejection.

A full library of fragmentation spectra could then be statistically analysed and predictions could be made as to the most useful adduct for the desired purpose.

Chapter 8: Experimental

8. Experimental

8.1. General methods for synthetic chemistry

NMR spectra were recorded on Bruker DPX 300, 400, 500 or 700 spectrometers. For ^1H - and ^{13}C -NMR the chemical shifts are reported relative to the solvent signal (CDCl_3 δ_{H} 7.26, D_2O δ_{H} 4.80, CDCl_3 δ_{C} 77.0). TLC was performed on aluminium sheets precoated with silica gel 60 (F₂₅₄, Merck) and spots were visualized by UV and charring with permanganate dip. Flash column chromatography was carried out with silica gel 60 (0.040-0.630 mm, Merck) using a stepwise solvent polarity gradient. Anhydrous solvents were purchased from Sigma-Aldrich. Preparative HPLC was carried out on Agilent Technologies 1200 series HPLC with a C18 column (Zorbax® XDB-C18 21.2x15mm, 5 μm), at a flow rate of 20 mL/min and UV detection set at 280, 254, and 210 nm.

Semi-preparative HPLC was carried out on Agilent Technologies 1200 series HPLC with a C18 column (Phenomenex Synergi™ 4 μm Polar-RP 80 Å, 250 x 10 mm), at a flow rate of 2.5 mL/min and UV detection set at 280, 254, and 210 nm.

High resolution mass spectrometry data was recorded on a Bruker MaXis mass spectrometer. Ultra high resolution mass spectrometry data was recorded on a solariX 12T FT-ICR mass spectrometer (Bruker Daltonik GmbH, Bremen, Germany), equipped with an Infinity cell.³³¹

8.2. Irradiation procedures

8.2.1. *In vitro*

Samples were placed in a quartz cuvette for irradiation with an OBB Tunable KiloArc™ Illuminator. Unless otherwise stated, a wavelength of 365 nm was used for all irradiation events, at 1000W.

8.2.2. *In vivo*

Cultures in liquid or solid media were placed within a home built light box, equipped with a circular 22W UVA lamp, able to be fixed to an Innova™ 4300 Incubator Shaker, New Brunswick Scientific platform for temperature and shaking. The light box was purposely built by Rod Wesson (Electronics workshop, University of Warwick, UK). Cultures were irradiated for varying lengths of time, as stated.

8.3. Expression and purification of Histidine-tagged proteins in *E. coli* – *act* *apoACP 44, Sfp, PanK, PPAT, and DPCK*

His-tagged proteins were expressed and purified from cultures of *E. coli* BL21*, DE3 and Rosetta 2* strains grown in autoclaved (Astell autoclave) LB broth media (Miller, BP1426-2, 25g/L). The *actACP* and *Sfp* plasmids were gifts from Dr Hui Hong, University of Cambridge. The *actACP* gene was inserted as NdeI-BamHI fragment in pET28a, *PanK* and *DPCK* genes were inserted as NdeI-HindIII fragments into pET28a, and the *PPAT* gene were inserted as NheI-HindIII fragments into pET28a, all with N-terminal hexa-histadine tags. Precultures of approximately 10 mL of LB media, containing the appropriate antibiotic (10 µL of 25 mg/mL kanamycin for *actACP*, *Sfp*, *PanK* and *PPAT*, 10 µL of 100 mg/mL Carbenicillin for *DPCK*, and 10 µL of 100 mg/mL ampicillin for *ACPP* and *FabH*) were incubated overnight at 30°C, at 180 rpm (Innova™ 4300 Incubator Shaker, New Brunswick Scientific). The preculture was transferred to 1L flasks of LB media with 1 mL of the appropriate antibiotic (as previous), and incubated at 37°C, 180 rpm (Innova^(R) 44 Incubator shaker series) until an optical density of between 0.5 and 0.8 at 600 nm was reached. At this point 1 mL of Isopropyl β-D-1-thiogalactopyranoside (IPTG)

0.5M was added to each 1 L flask to induce protein expression. The flasks were incubated at 15°C and 180 rpm overnight (Innova^(R) 44 Incubator shaker series).

The cultures were centrifuged at 5000 rpm at 4°C, for 15 minutes (Sorvall^(R) RC6 Plus, SLA 3000 Super-lite rotor). The pellets, containing the whole cells, were resuspended in binding buffer (100 mM potassium phosphate, 20 mM imidazole, 10% glycerol, pH 7.3). The cells were lysed with a cell disruptor (Constant systems, Ltd), at 20 kPSI, one shot. The lysed cells were then centrifuged at 20000 rpm for 30 minutes (Beckman Coulter AvantiTM J-30I centrifuge). The supernatant was added to 1 mL of charged Ni-sepharoseTM 6 Fast Flow resin (equilibrated into the binding buffer), and mixed at 4°C.

After 1 hour, the resin was washed with 20 mL of wash/binding buffer (100 mM potassium phosphate, 20 mM imidazole, 10% glycerol, pH 7.3) was used to wash off loosely bound proteins, and finally 6 mL of elution buffer (100 mM potassium phosphate, 500 mM imidazole, 10% glycerol, pH 7.3) was added to the column to elute the His-tagged proteins. This final fraction was buffer exchanged with a PD10 desalting column (GE Healthcare) into tris (50 mM), potassium chloride (20 mM), magnesium chloride (10 mM), pH 8 buffer and stored in 50% glycerol at -80°C.

Bradford assay was used to determine protein concentration using bovine serum albumin (0.1 mg/mL to 0.7 mg/mL) as calibrant.

8.4. SDS-PAGE analysis

At each step of the expression and the purification a sample was kept for Sodium Dodecyl Sulphate-Protein Agarose Gel Electrophoresis (SDS-PAGE) analysis (**Table 8**). A PageRulerTM Plus Prestained Protein Ladder from Fermentas was run

alongside all samples. SDS-PAGE loading dye (4.8 mL H₂O, 1.2 mL 1 M Tris-HCl pH 6.8, 1 mL 100% glycerol, 2 mL 10% w/v SDS, 0.5 mL 0.1% w/v bromophenol blue) was added to each sample. A 10X SDS PAGE running buffer (10X) 288 g glycine, 60.4 g tris, 20g SDS in 2L distilled H₂O, diluted by a factor of 10 for each SDS-PAGE analysis. The gels were pre-run for 30 mins, then loaded with the samples and run at 200V. The gels were stained with InstantBlue™ Dye and viewed with white light.

	10% (5 mL)	12% (5 mL)	15% (5 mL)	18% (5 mL)	Stacking Gel (1 mL)
Water	1.9 mL	1.6 mL	1.1 mL	0.6 mL	0.68 mL
30% Acrylamide mix	1.7 mL	2 mL	2.5 mL	3 mL	0.17 mL
1.5 M Tris (pH 8.8)	1.3 mL	1.3 mL	1.3 mL	1.3 mL	-
1.0 M Tris (pH 6.8)	-	-	-	-	0.13 mL
10% SDS	50 µL	50 µL	50 µL	50 µL	10 µL
10% APS	50 µL	50 µL	50 µL	50 µL	10 µL
Tetramethylethylene diamine (TEMED)	2 µL	2 µL	2 µL	2 µL	1 µL

Table 8 SDS-PAGE recipes

8.5. Expression and purification of *act* KS-CLF in *S. coelicolor*

KS-CLF was expressed and purified from frozen *S. coelicolor* CH999/pRJC006, previously transformed with the required KS-CLF expression vector, pCB84, (gift of Dr Cosby, University of Bristol¹⁴) grown in autoclaved (Astell autoclave) Super YEME media (1.5 g yeast extract, 2.5 g bacto peptone, 1.5 g malt extract, 5 g glucose, 170 g sucrose in 500 mL dH₂O and autoclaved, then 37.5 mg L-proline, 37.5 mg L-arginine, 37.5 mg L-cysteine, 50 mg L-histidine, 7.5 mg uracil, 6.25 mL glycine (20%) and 500 µL MgCl₂.6H₂O (2.5 M)). A preculture of 10 mL was

incubated at 30°C, 180 rpm for 5 days, and then 250 mL super YEME was inoculated with 5 mL preculture, 500 µL kanamycin (50 mg/mL) and 250 µL nalidixic acid (25 mg/mL) for a further 2 days at 30°C, 180 rpm. The cultures were induced with 250 µL fresh thiostrepton in DMSO (10 mg/mL), and incubated at 30°C, 180 rpm for 5 days.

The cells were pelleted at 9000 rpm for 25 mins, and the supernatant was discarded. The cells were resuspended in binding buffer (0.1 M potassium phosphate buffer, 10% glycerol, pH 7.3) and disrupted with 30 kPsi, one shot. The lysed cell suspension was centrifuged at 20000 rpm, for 30 mins. Streptomycin sulphate was added (0.5 g per 25 mL) to the supernatant to precipitate the DNA, and mixed for 20 mins before centrifugation at 20000 rpm, 30 mins. The supernatant was purified by Ni-sepharoseTM resin as before (see section 8.3). (Wash buffer: 0.1 M potassium phosphate, 40 mM imidazole, 10% glycerol, pH 7.3. Elution buffer: 0.1 M potassium phosphate, 500 mM imidazole, 10% glycerol, pH 7.3. A PD10 column was used to buffer exchange into a storage buffer (0.1 M potassium phosphate, 2 mM DTT, 10% glycerol, pH 7.3), before storage in 50% glycerol at -80°C.

SDS-PAGE analysis of the purified protein showed two discrete bands at approximately 50 kDa and 43 kDa, as previously reported.¹⁹

Bradford assay was used to determine protein concentration using bovine serum albumin (0.1 mg/mL to 0.7 mg/mL) as calibrant.

8.6. Trypsin digestion of acyl carrier proteins

0.38 µL trypsin (1 mg/mL) was added to 2 µmol acyl carrier protein in ammonium bicarbonate (100 mM) pH 8.5 to a final volume of 50 µL, and incubated for 4 hours at 37°C.

8.7. Thrombin cleavage of the Histidine-tag from *act* ACP

The overexpressed ACP from the actinorhodin minimal system contains a His-tag linked with a thrombin cleavage site (Leu-Val-Pro-Arg-Gly-Ser). Thrombin can be used to cleave the His-tag between the arginine and glycine, providing a cleaved protein, minus a His-tag.

A Thrombin CleanCleave Kit™, Sigma, containing 50% slurry of immobilised bovine thrombin on agarose. The resin was buffer exchanged into cleavage buffer (10X: 500 mM Tris-HCl, pH 8.0, 100 mM CaCl₂) prior to use. 100 µL of thrombin-agarose slurry will cleave 1 mg of target protein, at a concentration of 1 mg/mL (target protein) after six hours at room temperature with mixing by a see-saw rocker.

The cleaved protein was purified from His-tagged protein by bench top purification with Ni-sepharose™ 6 Fast Flow resin, as described previously (Section 8.3).

Cleavage of the His-tag was confirmed by SDS-PAGE and mass spectrometry.

8.8. Phosphopantetheinylation of *act apo*-ACPs **44 *in vitro***

Unless otherwise stated, in reaction buffer TrisCl (50 mM), KCl (20 mM), MgCl₂ (10 mM), pH 8, final concentrations of 0.3 mM of *apo*- acyl carrier protein **44**, 0.03 mM Sfp and 0.7 mM CoA analogue (3.2 mM malonyl-CoA **15**, excess due to rapid decarboxylation), were incubated at room temperature for 2 hours. Samples were monitored for full phosphopantetheinylation by UPLC-MS analysis (Section 8.16.3).

8.9. Loading of *act* KS-CLF

Unless otherwise stated, KS-CLF was primed with acetyl groups by incubation of 0.12 mM KS-CLF with 1.2 mM acetyl-CoA **17**, 0.12 mM *apo*- acyl carrier protein **44**, 0.012 mM Sfp, final concentrations, in TrisCl (50 mM), KCl (20 mM), MgCl₂ (10 mM), pH 8, at room temperature for 2 hours.

8.10. Reconstitution of enzymatic activity for the *act* PKS minimal system

Unless otherwise stated, the actinorhodin minimal system was reconstituted *in vitro* as follows. *Holo*- ACPs and the acetyl loading of KS-CLF were generated immediately prior to this reaction.

Final concentrations of 0.16 mM malonyl-ACP **7**, 3 μM loaded acetyl-KSCLF and excess 1 mM malonyl-CoA **15** were incubated in TrisCl (50 mM) pH 8 buffer at room temperature, overnight. Enzymes were tested for activity by the production of SEK4/4b **41/42** (Sections 8.15 and 8.16.4).

8.11. Trapping of intermediates from the *act* minimal system with the protein probe **63**

The nonhydrolysable photolabile ACP analogue was not His-tagged for these experiments to enable selective isolation of these species and others related to it from the other enzymatic components. The cleavage of the His-tag is described in section 8.7.

Unless otherwise stated, cleaved *apo*-ACP **44** was phosphopantetheinylated with DMNB protected carba(dethia) CoA **63** as described in section 8.8. His-tagged *apo*-ACP **44** was phosphopantetheinylated with malonyl-CoA **15**, also as described in section 8.8.

DMNB protected ACP probe **63** was irradiated for 4 hours, either at 365 nm, 1000W, with a KiloArc mercury lamp, or with a home built, 22W, UVA light source. Following irradiation, malonyl-ACP **7** (0.16 mM), KS-CLF (3 μ M) and excess malonyl-CoA **15** (1 mM) were added to the irradiated DMNB protected ACP probe **63**, in TrisCl (50 mM) pH 8 buffer, and allowed to react over night at room temperature.

The cleaved ACP analogue **63** and species deriving from it were separated from the other protein assay components by use of a Ni-NTA spin column (Thermo Scientific, HisPur Ni-NTA spin column, 0.2 mL resin bed). Samples were mixed with the Ni-NTA resin for 1 hour, at 4°C, and then washed three times with distilled H₂O to elute the cleaved ACP of interest. All other His-tagged proteins remained bound to the Ni resin.

8.12. Trapping of intermediates from the *act* minimal system with the small molecule probe 65

Unless otherwise stated, His-tagged *apo*-ACP **44** was phosphopantetheinylated with malonyl-CoA **15**, as described in section 8.8. The nonhydrolysable photolabile NAC analogue **65** was irradiated for 4 hours, either at 365 nm, 1000W, with a KiloArc mercury lamp, or with a home built, 22W, UVA light source. Following irradiation, malonyl-ACP **7** (0.16 mM), KS-CLF (3 μ M) and excess malonyl-CoA **15** (1 mM)

were added to the irradiated NAC analogue **65** and allowed to react over night at room temperature.

HCl was added to each completed reaction, to acidify to pH 4, followed by EtOAc extraction three times, evaporation and reconstitution in 50 μ L MeCN/H₂O (1:1) for a 100 μ L reaction volume.

8.13. Feeding of DMNB NAC probe 65 to *S. lasaliensis* and preparation for LC-MS analysis

All media and glassware were sterilized prior to use by autoclave (Astell). Liquid cultures were incubated at 30°C, at 180 rpm (Innova 44 incubator/shaker (New Brunswick scientific)).

M79 medium: 2.5 g glucose, 2.5 g peptone, 0.5 g yeast extract, 1.5 g NaCl, 2.5 g casein hydrolysate in 250 mL of tap water adjusted to pH 7.1.

MYM medium: 1.0 g maltose, 1.0 g yeast extract, 2.5 g malt extract in 250 mL of tap water adjusted to pH 7.1. For solid medium, 2.2 g of agar was added to 100 mL of this media.

Precultures of *S. lasaliensis* ACP12 (S970A) were grown in 10 mL M79 medium for 3 days, then 100 μ L of this preculture was used to inoculate 10 mL of MYM liquid cultures and grown for 5 days. On days 2-5 6.25 μ mol of probe **65** (previously dissolved in the minimum amount of DMSO), was added daily to the cultures to reach a final concentration of 2.5 mM. Control cultures (without *S. lasaliensis*, without probe **65**, without *S. lasaliensis* or probe **65**, and with and without photolysis) were also grown in parallel. After 5 days, the fermentation cultures were

extracted with EtOAc, evaporated and reconstituted in 1 mL MeCN/H₂O (1:1) for LC-MS analysis.

Solid MYM plates (5 mL) were prepared with 2.5 mM probe **65**, and inoculated with 5 µL *S. lasaliensis* ACP12 (S970A) spore stock, and grown at 30°C for 5 days. Plates were extracted with EtOAc, evaporated and reconstituted in 0.5 mL MeCN/H₂O (1:1) for LC-MS analysis.

8.14. Feeding to *S. coelicolor* and preparation for LC-MS analysis

All media and glassware were sterilized prior to use by autoclave (Astell).

Liquid cultures were incubated at 30°C, at 180 rpm (Innova 44 incubator/shaker (New Brunswick scientific)). Solid cultures were incubated at 30°C.

R4 medium: 2.5 g glucose, 750 mg proline, 2.5 g MgCl₂·6H₂O, 50 mg K₂SO₄, 25 mg Bacto casamino acids, 625 µL trace elements solution, 250 mg yeast extract and 1.4 g TES in 250 mL of distilled water adjusted to pH 7.2. (Trace elements solution: 40 mg ZnCl₂, 200 mg FeCl₃·6H₂O, 10 mg CuCl₂·2H₂O, 10 mg MnCl₂·4H₂O, 10 mg Na₂B₄O₇·10H₂O, (NH₄)₆Mo₇O₂₄·4H₂O in 1 L distilled water). For solid medium, 2.2 g agar was added to 100 mL of this media.

Precultures were grown in 10 mL R4 medium for 3 days, then 100 µL of the preculture was used to inoculate 10 mL R4 liquid media and grown for 5 days. On days 2-5 (of 5) 6.25 µmol of probe, in DMSO, was added each day to the cultures, to a final concentration of 2.5 mM. Control cultures were also grown in parallel: without *S. coelicolor*, without probe **65**, without either *S. coelicolor* or probe **65**, and with and without photolysis.

After 5 days, the liquid cultures were pH adjusted to pH 4 with HCl (conc.), extracted with EtOAc, evaporated and then reconstituted in 1 mL MeCN/H₂O (1:1) for LC-MS analysis.

Solid R4 plates (5 mL) were prepared with 2.5 mM probe **65**, and inoculated with 5 μ L *S. coelicolor* M510 spore stock, and grown at 30°C for 5 days. Cultures were extracted with EtOAc and 20 μ L conc. HCl, evaporated, and reconstituted in 0.5 mL MeCN/H₂O (1:1) for LC-MS analysis.

8.15. Enzyme assay extraction

Unless otherwise stated, all extractions from the actinorhodin minimal system *in vitro* assays were pH adjusted with conc. HCl to approximately pH 4, and extracted into EtOAc three times. EtOAc was removed *in vacuo* and reconstituted in MeCN/H₂O.

8.16. LC-MS analysis

8.16.1. HPLC analysis of NAC probe 65 photolysis experiments

The samples were analysed on an Agilent 1200 HPLC system coupled to a Bruker HCT Ultra mass spectrometer.

HPLC Column: Waters Atlantis T3, 5 μ m, 2.1 x 150 mm C18 column.

Flow rate: 0.3 mL/min

Solvents: H₂O/MeCN containing 0.1% formic acid

Oven temperature: 25°C

Time (mins)	% MeCN
0	5
5	5
35	95
40	95
45	5

Table 9 LC-MS gradient for the analysis of the nonhydrolysable photolabile SNAC analogue 65 photolysis experiments

8.16.2. UPLC-MS analysis of proteins (not including *act* ACPs)

The samples were analysed on a Dionex UPLC system coupled to a Bruker MaXis mass spectrometer.

Column: ACE C4-300 (UPLC)

Flow rate: 0.2 mL/min

Solvents: H₂O/MeCN containing 0.05% trifluoroacetic acid

Oven temperature: 30°C

Time (mins)	% MeCN
0	5
5	5
45	100
50	100
55	5
60	5

Table 10 UPLC-MS gradient for the analysis of proteins

8.16.3. UPLC-MS analysis of *act* ACPs

The samples were analysed on a Dionex UPLC system coupled to a Bruker MaXis mass spectrometer.

Column: ACE C4-300 (UPLC)

Flow rate: 0.2 mL/min

Solvents: H₂O/MeCN containing 0.05% trifluoroacetic acid

Oven temperature: 30°C

Time (mins)	% MeCN
0	5
5	5
10	40
40	45
50	100
55	100
60	5

Table 11 UPLC-MS gradient for the analysis of acyl carrier proteins

8.16.4. UPLC-MS analysis of cell and enzyme reaction extracts

Samples were prepared as discussed in section 8.14 and 8.15.

The samples were analysed on a Dionex UPLC system coupled to a Bruker MaXis mass spectrometer.

Column: Eclipse plus C18, 1.8 µm, 2.1 x 100 mm (UPLC)

Flow rate: 0.2 mL/min

Solvents: H₂O/MeCN containing 0.1% formic acid

Oven temperature: 30°C

Time (mins)	% MeCN
0	5
5	5
35	100
40	100
45	5
50	5

Table 12 UPLC-MS gradient for the analysis of cell and enzyme reaction extracts

8.16.5. UPLC-MS analysis of trypsin digested *act* ACPs

Trypsin digested acyl carrier protein samples were prepared for LC-MS analysis by filtering and diluting through a 10 kDa cut off filter.

Samples were analysed on a Dionex UPLC system coupled to a Bruker MaXis mass spectrometer.

Column: Eclipse plus C18, 1.8 μ m, 2.1 x 100 mm (UPLC)

Flow rate: 0.2 mL/min

Solvents: H₂O/MeCN containing 0.1% formic acid

Oven temperature: 30°C

Time (mins)	% MeCN
0	5
5	5
35	100
40	100
45	5
50	5

Table 13 UPLC-MS gradient for the analysis of trypsin digested acyl carrier proteins

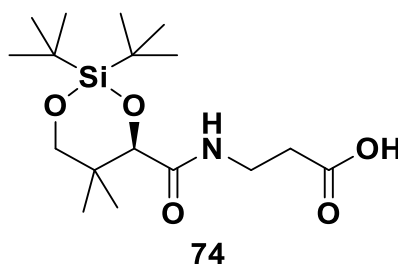
8.17. FTICR-MS analyses

A calibration mix (Agilent HP tune mix) was used to externally calibrate the instrument prior to analysis of samples. Internal calibration was used to calibrate the data once it has been acquired from the instrument using Data Analysis software. A series of peaks in the spectra were chosen, in as wide a range as possible. The software was instructed to fit a calibration curve to the peaks chosen, and this was then applied to the spectrum. Each spectrum was internally calibrated separately, with its own calibration curve, and a range spanning the whole m/z range required.

Nanospray Ionisation (nESI) or Electrospray Ionisation (ESI) was used for sample injection.

For CAD analyses the precursor ion was isolated in the quadrupole, and then fragmented in the collision cell (the collision gas was argon).

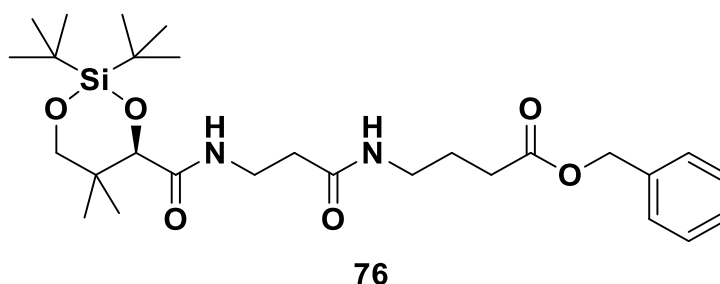
8.18. Synthetic procedures



3-[[[(4R)-2,2-ditert-butyl-5,5-dimethyl-1,3,2-dioxasilinane-4-

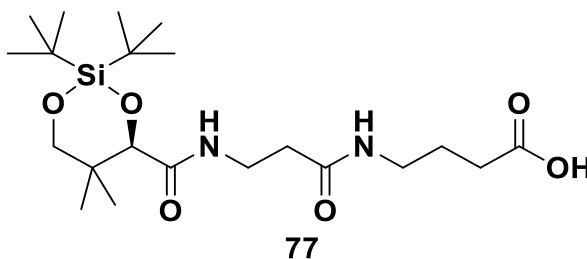
carbonyl]amino]propanoic acid (74): To a solution of D-pantothenic acid **60** (1 g, 4.2 mmol) in dry THF (10 mL) was added 2,6-lutidine (1.46 mL, 12.6 mmol). This was cooled to 0°C and then Di-*tert*-butylsilyl bis(trifluoromethanesulfonate) (1.75 mL, 5.4 mmol) was added, drop wise and the reaction mixture stirred for 18h at

room temperature. The solvent was removed *in vacuo* to give **74** as a crude yellow oil; a portion of it was purified by prep-HPLC for characterisation whereas most of the crude material was utilised directly in the next reaction; $^1\text{H-NMR}$ (400 MHz, CDCl_3): δ 7.41 (t, 1H, $J = 5.5$ Hz, NH), 6.54 (br, 1H, OH), 4.44 (s, 1H, CH), 4.04 (d, 1H, $J = 11.5$ Hz, CH), 3.67 (m, 1H, $J = 5.5$ Hz, 6.0 Hz, 6.5 Hz, CH), 3.51 (d, 1H, $J = 11.5$ Hz, CH), 3.48 (m, 1H, $J = 6.5$ Hz, 7.0 Hz, CH), 2.61 (t, 2H, $J = 5.5$ Hz, 6.0 Hz, CH_2), 1.09 (s, 9H, CCH_3), 1.08 (s, 9H, CCH_3), 1.05 (s, 3H, CCH_3), 1.04 (s, 3H, CCH_3); $^{13}\text{C-NMR}$ (100 MHz, CDCl_3): δ 17.2, 171.4, 81.3, 75.4, 33.9, 28.7, 27.6, 23.4, 23.3, 18.7; HRMS: m/z $[\text{M} + \text{Na}]^+$, found: 382.2033, calculated: 382.2026.



benzyl 4-[3-[[[(4R)-2,2-ditert-butyl-5,5-dimethyl-1,3,2-dioxasilinane-4-carbonyl]amino]propanoylamino]butanoate (76): To a solution of crude **74** (4.2 mmol) and γ -aminobutyric acid benzyl ester p-tosylate **75** (0.97 g, 5.04 mmol) in dry THF (16 mL) was added *N,N*-Diisopropylethylamine (1.5 mL, 8.40 mmol). This was cooled to 0°C for 10 minutes and O-(7-Azabenzotriazol-1-yl)-*N,N,N',N'*-tetramethyluronium hexafluorophosphate (HATU) (2.08 g, 5.46 mmol) was added. This was stirred at 0°C for 30 minutes, allowed to warm to room temperature, and then stirred at room temperature for a further 18h. The solvent was removed *in vacuo*, and the product was extracted with EtOAc, washing the organic layer with

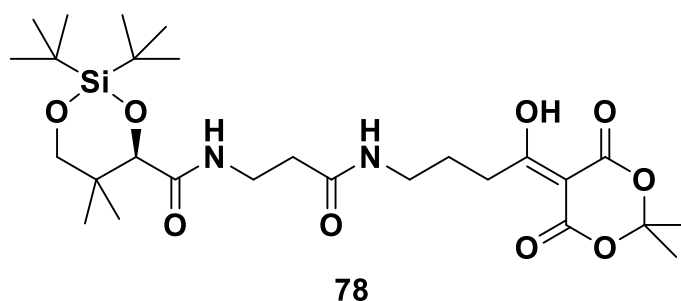
deionised water. The organic layer was dried and concentrated, and the crude residue purified *via* flash chromatography with gradient elution ($R_f = 0.4$ in EtOAc:DCM 3:2 containing 1% Et₃N) (1.48 g, 2.8 mmol, 66% over two steps) to afford **76**; ¹H-NMR (500 MHz, CDCl₃): δ 7.37 (m, 6H, NH and ArH), 5.94 (t, $J = 5.0$ Hz, 1H, NH), 5.14 (s, 2H, CH₂), 4.43 (s, 2H, CH), 4.05 (d, 1H, $J = 11.5$ Hz, CH), 3.66 (m, 1H, $J = 6.0$ Hz, 6.5 Hz, CH), 3.52 (d, 1H, $J = 11.5$ Hz, CH), 3.52 (m, 1H, $J = 6.0$ Hz, CH), 3.30 (m, 2H, $J = 6.5$ Hz, 7.0 Hz, CH₂), 2.41 (m, 2H, $J = 6.0$ Hz, CH₂), 2.41 (m, 2H, $J = 7.0$ Hz, 7.5 Hz, CH₂), 1.87 (dt, 2H, $J = 7.0$ Hz, CH₂), 1.11 (s, 9H, CCH₃), 1.10 (s, 9H, CCH₃), 1.05 (s, 3H, CCH₃), 1.05 (s, 3H, CCH₃); ¹³C-NMR (126 MHz, CDCl₃): δ 173.1, 171.4, 171.0, 135.8, 128.6, 128.3, 128.2, 81.3, 75.4, 66.4, 38.8, 37.3, 35.8, 34.7, 31.7, 28.6, 27.6, 23.3, 20.3, 18.9; HRMS: m/z [M + H]⁺, found: 535.3201, calculated: 535.3198.



4-[3-[[[(4R)-2,2-ditert-butyl-5,5-dimethyl-1,3,2-dioxasilinane-4-

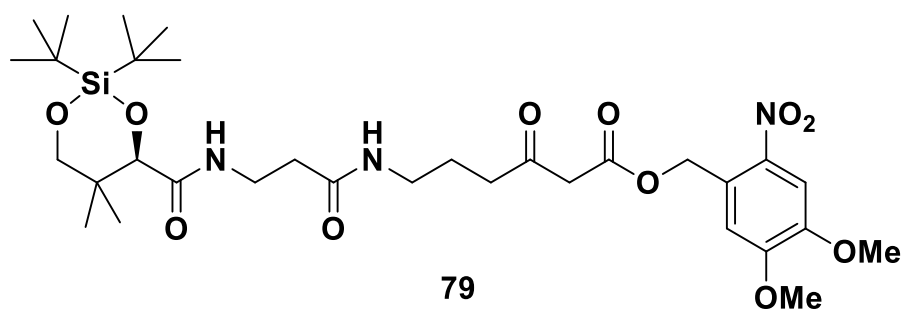
carbonyl]amino]propanoylamino]butanoic acid (77): A solution of **76** (1.48 g, 2.8 mmol) and Palladium on carbon, 10 wt. % (1.47 g, 1.39 mmol) in dry EtOAc (296 mL) was stirred for 2 hours flushing H₂ throughout. The reaction mixture was filtered through Celite and the solvent removed *in vacuo* affording **77** as a white solid (1.24 g, 100%); ¹H-NMR (500 MHz, CDCl₃): δ 7.37 (t, 1H, $J = 6.0$ Hz, NH), 6.71 (t, 1H, $J = 5.5$ Hz, NH), 4.35 (s, 1H, CH), 3.96 (d, 1H, $J = 11.5$ Hz, CH), 3.55 (m, 1H, $J = 6.0$ Hz, 6.5 Hz, 7.0 Hz, CH), 3.46 (m, 1H, $J = 6.0$ Hz, 6.5 Hz, CH), 3.43

(d, 1H, $J = 11.5$ Hz, CH), 3.21 (m, 2H, $J = 6.5$ Hz, 7.0 Hz, CH₂), 2.40 (m, 2H, $J = 6.0$ Hz, 6.5 Hz, 7.0 Hz, CH₂), 2.30 (t, 2H, $J = 7.0$ Hz, CH₂), 1.76 (quin, 2H, $J = 7.0$ Hz, CH₂), 1.02 (s, 9H, CCH₃), 1.01 (s, 9H, CCH₃), 0.97 (m, 3H, $J = 5.0$ Hz, 5.5 Hz, CCH₃), 0.94 (s, 3H, CCH₃); ¹³C-NMR (126 MHz, CDCl₃): δ 175.5, 171.1, 170.5, 80.3, 74.3, 38.0, 36.4, 34.9, 30.4, 27.6, 26.6, 23.5, 22.4, 22.3, 19.3, 17.8; HRMS: m/z [M - H]⁻, found: 443.2653, calculated: 443.2583.



(4R)-2,2-ditert-butyl-N-[3-[[4-(2,2-dimethyl-4,6-dioxo-1,3-dioxan-5-ylidene)-4-hydroxy-butyl]amino]-3-oxo-propyl]-5,5-dimethyl-1,3,2-dioxasilinane-4-carboxamide (78): To a solution of **77** (317.3 mg, 0.71 mmol) and Meldrum's acid (113.3 mg, 0.79 mmol) in dry THF (4 mL) was added 4-dimethylaminopyridine (109.2 mg, 0.89 mmol). After 10 minutes, 1-ethyl-3-(3-dimethylaminopropyl) carbodiimide (154 mg, 1.0 mmol) (was added and the reaction mixture was stirred for 18 hours at room temperature. The solvent was removed *in vacuo*, and the crude residue purified using flash chromatography with gradient elution ($R_f = 0.4$ in EtOAc:MeOH (4:1) containing 1% Et₃N) to afford **78** as a yellow oil (274.2 mg, 68%); ¹H-NMR (400 MHz, CDCl₃): δ 7.36 (t, 1H, $J = 6.0$ Hz, NH), 7.01 (t, 1H, $J = 5.0$ Hz, NH), 4.40 (s, 2H, CH₂), 4.02 (d, 1H, $J = 11.5$ Hz, CH), 3.64 (m, 1H, $J = 6.5$ Hz, 7.0 Hz, CH), 3.49 (d, 1H, $J = 11.5$ Hz, CH), 3.49 (m, 1H, CH), 3.21 (m, 2H, $J =$

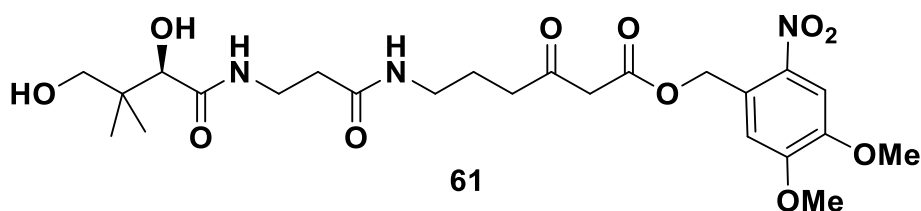
7.0 Hz, 7.5 Hz, CH₂), 2.85 (m, 2H, *J* = 7.0 Hz, CH₂), 2.44 (m, 2H, *J* = 6.5 Hz, 7.0 Hz, CH₂), 1.77 (dt, 2H, *J* = 6.0 Hz, 6.5 Hz, CH₂), 1.64 (s, 6H, CCH₃), 1.09 (s, 9H, CCH₃), 1.08 (s, 9H, CCH₃), 1.03 (s, 3H, CCH₃), 1.01 (s, 3H, CCH₃); ¹³C-NMR (100 MHz, CDCl₃): δ 198.3, 171.3, 171.0, 166.6, 101.2, 89.3, 81.2, 75.5, 39.1, 39.0, 37.3, 36.0, 35.0, 28.6, 27.6, 26.2, 25.4, 23.3, 20.3, 18.9; HRMS: *m/z* [M + Na]⁺, found: 593.2870, calculated: 593.2865.



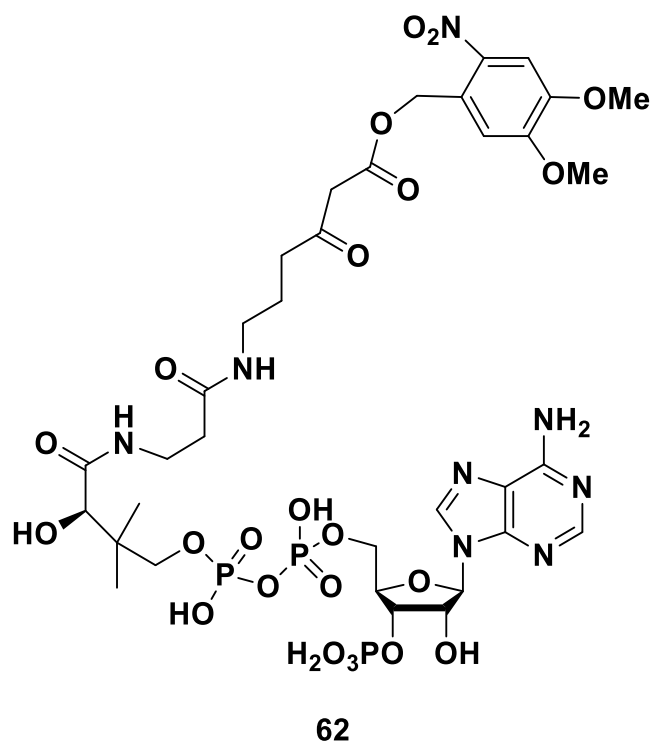
(4,5-dimethoxy-2-nitro-phenyl)methyl 6-[3-[[[(4R)-2,2-ditert-butyl-5,5-dimethyl-1,3,2-dioxasilinane-4-carbonyl]amino]propanoylamino]-3-oxo-hexanoate (79):

To a solution of **78** (190 mg, 0.33 mmol) and 4,5-dimethoxy-2-nitrobenzyl alcohol **72** (213 mg, 0.99 mmol) in dry toluene (10 mL), refluxed for 8 hours. The solvent was removed *in vacuo* and purified by semi-preparative HPLC (H₂O/MeCN containing 0.1% FA, 70 to 95% MeCN over 40 mins, R_f = 20.3 mins) to give **79** as a yellow solid (127 mg, 56%). ¹H-NMR (700 MHz, CDCl₃): δ 7.64 (s, 1H, ArH), 7.30 (t, 1H, *J* = 6.0 Hz, 6.5 Hz, NH), 7.08 (s, 1H, ArH), 6.44 (t, 1H, *J* = 5.5 Hz, NH), 5.51 (s, 2H, CH₂), 4.33 (s, 1H, CH), 3.97 (s, 3H, OCH₃), 3.95 (d, 1H, *J* = 11.5 Hz, CH), 3.88 (s, 3H, OCH₃), 3.56 (m, 1H, *J* = 6.0 Hz, 6.5 Hz, CH), 3.52 (s, 2H, CH₂), 3.42 (m, 1H, *J* = 6.0 Hz, CH), 3.42 (d, 1H, *J* = 11.5 Hz, CH), 3.17 (m, 2H, *J* = 6.5 Hz, 7.0 Hz, CH₂), 2.54 (t, 2H, *J* = 7.0 Hz, CH₂), 2.35 (m, 2H, *J* = 5.5 Hz, 6.5 Hz, CH₂), 1.73 (m, 2H, *J* = 7.0 Hz, CH₂), 1.01 (s, 9H, CCH₃), 1.00 (s, 9H, CCH₃), 0.96 (s, 3H,

CCH₃), 0.95 (s, 3H, CCH₃); ¹³C-NMR (126 MHz, CDCl₃): δ 207.5, 201.3, 170.4, 170.2, 165.6, 153.4, 152.9, 147.3, 138.6, 125.8, 109.5, 107.2, 80.3, 74.4, 63.1, 55.8, 55.4, 48.1, 39.4, 37.5, 35.0, 33.7, 27.6, 26.6, 22.4, 22.3, 17.9; HRMS: *m/z* [M + Na]⁺, found: 704.3188, calculated: 704.3185.



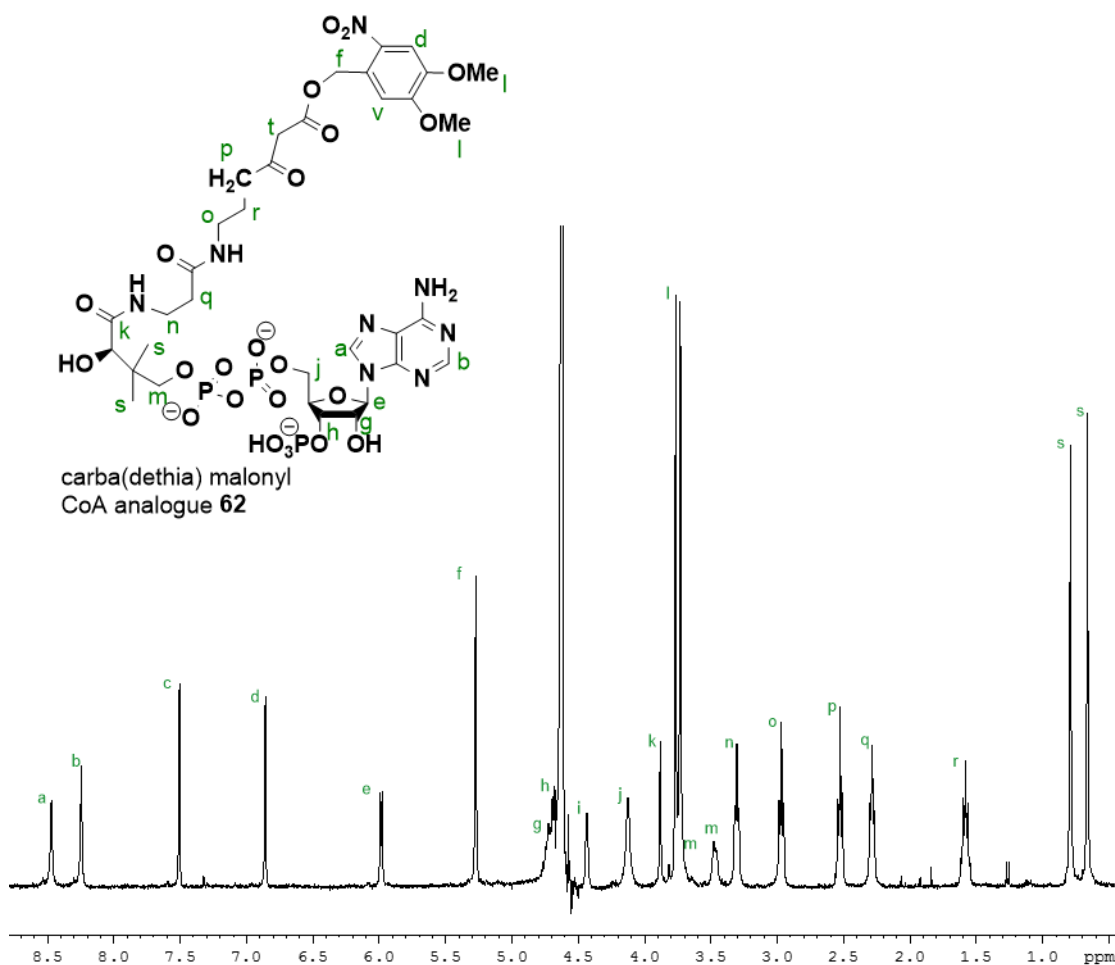
(4,5-dimethoxy-2-nitro-phenyl)methyl 6-[3-[[[(2R)-2,4-dihydroxy-3,3-dimethylbutanoyl]amino]propanoylamino]-3-oxo-hexanoate (61): A solution of **79** (79.1 mg, 0.12 mmol) and hydrogen fluoride pyridine (70% HF) (11.6 mg, 0.58 mmol) in dry THF (0.5 mL) was stirred at room temperature for 2 mins to yield **61**. The solvent and hydrogen fluoride pyridine were removed *in vacuo* and product purified by semi-preparative HPLC (H₂O/MeOH, 5 to 95% MeOH over 30 mins, R_f = 18 mins) to give **61** as a yellow solid (58 mg, 90%); ¹H-NMR (500 MHz, CDCl₃): δ 7.74 (s, 1H, ArH), 7.41 (t, 1H, *J* = 6.0 Hz, NH), 7.14 (s, 1H, ArH), 6.43 (t, 1H, *J* = 5.5 Hz, 6.0 Hz, NH), 5.59 (s, 2H, CH₂), 4.06 (s, 3H, OCH₃), 4.01 (s, 1H, CH), 3.98 (s, 3H, OCH₃), 3.63 (s, 2H, CH₂), 3.57 (m, 2H, *J* = 6.0 Hz, 6.5 Hz, 7.0 Hz, CH₂), 3.49 (s, 2H, HOCH₂), 3.27 (m, 2H, 6.0 Hz, 6.5 Hz, 7.0 Hz, CH₂), 2.65 (t, 2H, *J* = 7.0 Hz, CH₂), 2.45 (t, 2H, *J* = 6.0 Hz, CH₂), 1.82 (q, 2H, *J* = 7.0 Hz, CH₂); ¹³C-NMR (126 MHz, CDCl₃): δ 202.6, 173.7, 171.7, 166.9, 153.8, 148.4, 139.8, 126.5, 110.9, 108.3, 77.6, 70.9, 64.3, 56.8, 56.4, 49.1, 40.5, 39.3, 38.6, 35.9, 35.2, 23.3, 21.5, 20.4; HRMS: *m/z* [M + Na]⁺, found: 564.2156, calculated: 564.2164.

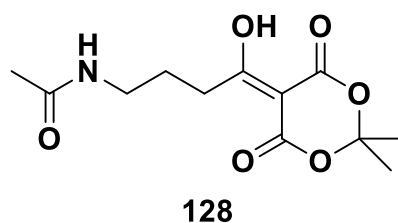


(4,5-dimethoxy-2-nitro-phenyl)methyl 6-[3-[[4-[[[5-(4-amino-7H-pyrrolo[3,2-d]pyrimidin-7-yl)-4-hydroxy-3-phosphonooxy-tetrahydrofuran-2-yl]methoxy-hydroxy-phosphoryl]oxy-hydroxy-phosphoryl]oxy-2-hydroxy-3,3-dimethylbutanoyl]amino]propanoylamino]-3-oxo-hexanoate (62):

A solution of adenosine-5'-triphosphate disodium salt (90 mg, 0.18 mmol) in Tris-HCl (50 mM), KCl (20 mM), MgCl₂ (10 mM) buffer and adjusted to pH 7.5. **61** (15 mg, 0.28 mmol) was dissolved in this buffer and PanK, PPAT and DPCK (to a final concentration of 500 µg/mL, 500 µg/mL and 700 µg/mL) were added to a final volume of 7.5 mL. After overnight incubation the enzymes were precipitated by addition of CHCl₃ (7.5 mL) and purified immediately by semi-preparative HPLC (H₂O/MeCN containing 0.05% TFA, 5 to 95% MeCN over 30 mins, t_R = 16.1 mins) to yield **62** as a white powder (20 mg, 70%); ¹H-NMR (500 MHz, D₂O): δ 8.57 (s, 1H, ArH), 8.33 (s, 1H, ArH), 7.64 (t, 1H, J = 6.0 Hz, ArH), 6.99 (t, 1H, J = 5.0 Hz, ArH), 6.08 (d, 1H, J = 6.0 Hz, ArH), 5.39 (s, 2H, CH₂), 4.78 (m, 1H, J = 6.0 Hz,

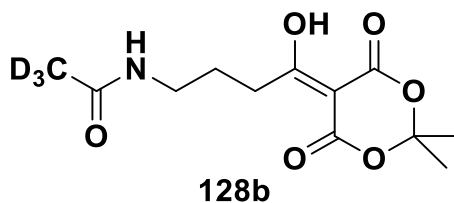
ArH), 4.78 (m, 1H, ArH), 4.51 (s, 1H, ArH), 4.19 (s, 2H, CH₂), 3.96 (s, 1H, CH), 3.87 (s, 3H, OCH₃), 3.83 (s, 3H, OCH₃), 3.80 (m, 1H, *J* = 9.5 Hz, CH₂), 3.53 (m, 1H, *J* = 9.5 Hz, CH₂), 3.38 (t, 2H, *J* = 6.5 Hz, CH₂), 3.04 (t, 2H, *J* = 7.0 Hz, CH₂), 2.60 (t, 2H, *J* = 7.0 Hz, 7.5 Hz, CH₂), 2.36 (t, 2H, *J* = 6.5 Hz, 7.0 Hz, CH₂), 1.66 (q, 2H, *J* = 7.0 Hz, CH₂), 0.87 (s, 3H, CH₃), 0.73 (s, 3H, CH₃); ¹³C-NMR (151 MHz, D₂O): δ 207.1, 174.7, 173.8, 168.9, 153.1, 149.8, 148.3, 147.6, 144.4, 142.3, 139.6, 126.2, 118.4, 111.1, 108.4, 87.5, 83.5, 74.1, 74.1, 74.1, 71.9, 71.9, 65.0, 64.3, 56.4, 56.1, 40.1, 38.4, 38.4, 35.4, 35.3, 22.3, 20.8, 18.2; ³¹P-NMR (151 MHz, D₂O): δ 0.25 (1P, OPO₃H₂), -11.01 (2P, O(PO₃H)₂). HRMS: *m/z* [M-2H]²⁻, found: 514.0974, calculated: 514.0978.



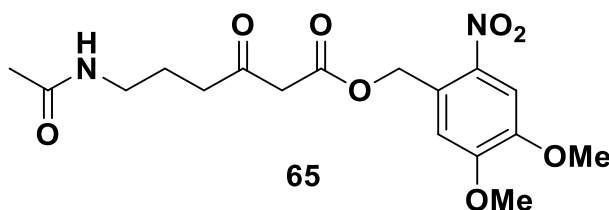


***N*-(4-(2,2-dimethyl-4,6-dioxo-1,3-dioxan-5-ylidene)-4-hydroxybutyl)acetamide**

(128): γ -aminobutyric acid **126** (2.00 g, 19.5 mmol) was suspended in dry methanol (120 mL) in the presence of triethylamine (11.60 mL, 83.2 mmol). The mixture was cooled to 0°C and acetyl chloride (1.57 mL, 20.0 mmol) was added dropwise. The reaction was stirred at 0°C for 1 h and at room temperature for 16 h. The solvent was evaporated to afford crude *N*-acetyl- γ -butyric acid **127** (triethylammonium salt, 5.69 g). This material was directly treated with 2,2-dimethyl-1,3-dioxane-4,6-dione (Meldrum's acid; 2.81 g, 19.5 mmol), 4-(dimethylamino)pyridine (2.95 g, 24.2 mmol) and *N*-(3-dimethylaminopropyl)-*N*'-ethylcarbodiimide hydrochloride (4.11 g, 21.5 mmol) in dry THF (300 mL) for 18 h. The solvent was removed *in vacuo* and the crude residue was redissolved in dichloromethane (200 mL), washed with 1M HCl (200 mL) and water (200 mL). After being dried (on MgSO₄) and concentrated, the crude yellow residue was purified by silica gel chromatography by using a stepwise gradient of DCM and EtOAc to yield **128** (2.98 g, 57%); ¹H-NMR (400 MHz, CDCl₃) δ 15.31 (br s, 1H, OH), 6.03 (br s, 1H, NH), 3.32 (apt q, *J* = 6.0 Hz, 2H, CH₂), 3.08 (apt t, *J* = 7.5 Hz, 2H, CH₂), 1.98 (s, 3H, COCH₃), 1.96–1.89 (m, 2H, CH₂), 1.74 (s, 6H, C(CH₃)₂); ¹³C-NMR (100 MHz, CDCl₃) δ 196.8, 170.3, 162.8, 104.9, 91.5, 38.4, 32.7, 26.6, 25.8, 23.0; HRMS: *m/z* [M + H]⁺, found: 272.1130, calculated: 272.1134.

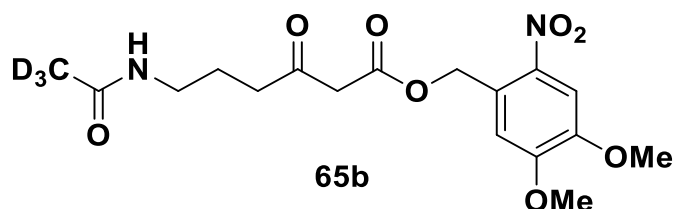


***N*-(4-(2,2-dimethyl-4,6-dioxo-1,3-dioxan-5-ylidene)-4-hydroxybutyl)acetamide- d_3 (128b):** This compound was obtained in a similar manner as **128** but by using acetyl chloride- d_3 to acetylate GABA; $^1\text{H-NMR}$ (300 MHz, CDCl_3) δ 15.29 (br s, 1H, OH), 5.94 (br s, 1H, NH), 3.31 (apt q, $J = 6.0$ Hz, 2H, CH_2), 3.06 (apt t, $J = 7.5$ Hz, 2H, CH_2), 1.92 (m, 2H, CH_2), 1.74 (s, 6H, $\text{C}(\text{CH}_3)_2$); $^{13}\text{C-NMR}$ (100 MHz, CDCl_3) δ 196.0, 169.5, 159.6, 104.1, 90.7, 37.5, 31.8, 25.8, 25.1, 23.3; HRMS: m/z $[\text{M} + \text{Na}]^+$, found: 297.1129, calculated: 297.1136.



(4,5-dimethoxy-2-nitro-phenyl)methyl 6-acetamido-3-oxo-hexanoate (65): To a solution of **128** (20 mg, 0.07 mmol), 4,5-dimethoxy-2-nitrobenzyl alcohol **72** (15.7 mg, 0.07 mmol) and zinc chloride (4.8 mg, 0.04 mmol, cat.) in dry THF (0.2 mL). This reaction mixture was refluxed at 65°C for 2.5 h. The solvent was removed *in vacuo* and **65** was purified by semi-preparative HPLC (with MeCN/ H_2O) (50 to 100% MeCN over 15 mins, $R_f = 14.3$ mins) (18.7 mg, 70%); $^1\text{H-NMR}$ (400 MHz, CDCl_3) δ 7.66 (s, 1H, CH), 7.08 (s, 1H, CH), 5.57 (br s, 1H, NH), 5.53 (s, 2H, CH_2), 3.99 (s, 3H, OCH_3), 3.90 (s, 3H, OCH_3), 3.54 (s, 2H, CH_2), 3.20 (dt, 2H, $J = 6.5$ Hz, CH_2), 2.56 (t, 2H, $J = 7.0$ Hz, CH_2), 1.90 (s, 3H, CCH_3), 1.75 (tt, 2H, $J = 7.0$ Hz, CH_2); $^{13}\text{C-NMR}$ (100 MHz, CDCl_3) δ 201.4, 169.7, 16.7, 12.9, 146.9, 138.7, 131.5,

109.9, 107.1, 63.1, 55.5, 55.4, 39.4, 37.7, 22.5, 22.5, 22.3; HRMS: m/z $[M + Na]^+$,
found: 405.1270, calculated: 405.1268.



(4,5-dimethoxy-2-nitro-phenyl)methyl 6-acetamido-3-oxo-hexanoate (65b): This compound was obtained in a similar manner as **65** but with **128b** as starting material; $^1\text{H-NMR}$ (400 MHz, CDCl_3) δ 7.66 (s, 1H, CH), 7.08 (s, 1H, CH), 5.57 (br s, 1H, NH), 5.53 (s, 2H, CH_2), 3.99 (s, 3H, OCH_3), 3.90 (s, 3H, OCH_3), 3.54 (s, 2H, CH_2), 3.20 (dt, 2H, $J = 6.5$ Hz, CH_2), 2.56 (t, 2H, $J = 7.0$ Hz, CH_2), 1.75 (tt, 2H, $J = 7.0$ Hz, CH_2); $^{13}\text{C-NMR}$ (100 MHz, CDCl_3) δ 201.4, 169.7, 16.7, 12.9, 146.9, 138.7, 131.5, 109.9, 107.1, 63.1, 55.5, 55.4, 39.4, 37.7, 22.5, 22.3; HRMS: m/z $[M + Na]^+$, found: 408.1456, calculated: 408.1457.

References

- 1 O'Hagan, D. *The Polyketide Metabolites*. Ellis Horwood: Chichester, **1991**.
- 2 O'Hagan, D. *Nat. Prod. Rep.* **1995**, *12*, 1-32.
- 3 Das, A.; Khosla, C. *Acc. Chem. Res.* **2009**, *42*, 631-639.
- 4 Staunton, J.; Weissman, K. J. *Nat. Prod. Rep.* **2001**, *18*, 380-416.
- 5 Khosla, C. *J. Org. Chem.* **2009**, *74*, 6416-6420.
- 6 Foreyt, W. J.; Rice, D. H.; Wescott, R. B. *Am. J. Vet. Res.* **1986**, *47*, 2031-5.
- 7 Wright, L. F.; Hopwood, D. A. *J. Gen. Microbiol.* **1976**, *96*, 289-97.
- 8 Pal Singh, I.; Bharate, S. B. *Nat. Prod. Rep.* **2006**, *23*, 558-591.
- 9 Jang, M. S.; Cai, E. N.; Udeani, G. O.; Slowing, K. V.; Thomas, C. F.; Beecher, C. W. W.; Fong, H. H. S.; Farnsworth, N. R.; Kinghorn, A. D.; Mehta, R. G.; Moon, R. C.; Pezzuto, J. M. *Sci* **1997**, *275*, 218-220.
- 10 Campbell, C. D.; Vederas, J. C. *Biopolymers* **2010**, *93*, 755-63.
- 11 Tosin, M.; Spitteller, D.; Spencer, J. B. *ChemBioChem* **2009**, *10*, 1714-1723.
- 12 Hertweck, C.; Luzhetskyy, A.; Rebets, Y.; Bechthold, A. *Nat. Prod. Rep.* **2007**, *24*, 162-190.
- 13 Beltran-Alvarez, P.; Cox, R. J.; Crosby, J.; Simpson, T. J. *Biochemistry* **2007**, *46*, 14672-14681.
- 14 Wang, C. C. C. *Front. Microbiol.* **2014**, *5*, 717.
- 15 Dunn, B. J.; Watts, K. R.; Robbins, T.; Cane, D. E.; Khosla, C. *Biochemistry* **2014**, *53*, 3796-806.
- 16 Cheng, Y. Q.; Tang, G. L.; Shen, B. *Proc. Natl. Acad. Sci. U. S. A.* **2003**, *100*, 3149-3154.
- 17 Lopanik, N. B.; Shields, J. A.; Buchholz, T. J.; Rath, C. M.; Hothersall, J.; Haygood, M. G.; Hakansson, K.; Thomas, C. M.; Sherman, D. H. *Chem. Biol.* **2008**, *15*, 1175-1186.
- 18 Carvalho, R.; Reid, R.; Viswanathan, N.; Gramajo, H.; Julien, B. *Gene* **2005**, *359*, 91-98.
- 19 Matharu, A. L.; Cox, R. J.; Crosby, J.; Byrom, K. J.; Simpson, T. J. *Chem. Biol.* **1998**, *5*, 699-711.
- 20 Keatinge-Clay, A. T.; Stroud, R. M. *Structure* **2006**, *14*, 737-748.
- 21 Boldi, A. M. *Combinatorial Synthesis of Natural Product-Based Libraries*. CRC Press: **2006**.
- 22 Tosin, M.; Smith, L.; Leadlay, P. F. *Angew. Chem. Int. Ed.* **2011**, *50*, 11930-11933.
- 23 Nakata, T.; Schmid, G.; Vranesic, B.; Okigawa, M.; Smithpalmer, T.; Kishi, Y. *J. Am. Chem. Soc.* **1978**, *100*, 2933-2935.
- 24 Weissman, K. J. *Methods Enzymol.* **2009**, *459*, 3-16.
- 25 Keatinge-Clay, A.; Maltby, D. A.; Medzihradzky, K. F.; Khosla, C.; Stroud, R. M. *Nat. Struct. Mol. Biol.* **2004**, *11*, 888-893.
- 26 Byers, D. M.; Gong, H. *Biochem. Cell Biol.* **2007**, *85*, 649-62.
- 27 Bisang, C.; Long, P. F.; Cortes, J.; Westcott, J.; Crosby, J.; Matharu, A. L.; Cox, R. J.; Simpson, T. J.; Staunton, J.; Leadlay, P. F. *Nature* **1999**, *401*, 502-505.
- 28 Okamoto, S.; Taguchi, T.; Ochi, K.; Ichinose, K. *Chem. Biol.* **2009**, *16*, 226-236.
- 29 Malla, S.; Prasad Niraula, N.; Singh, B.; Liou, K.; Kyung Sohng, J. *Microbiol. Res.* **2010**, *165*, 427-435.
- 30 Waldman, A. J.; Balskus, E. P. *Org. Lett.* **2014**, *16*, 640-3.
- 31 Piel, J.; Hertweck, C.; Shipley, P. R.; Hunt, D. M.; Newman, M. S.; Moore, B. S. *Chem. Biol.* **2000**, *7*, 943-55.
- 32 Bibb, M. J.; Sherman, D. H.; Ōmura, S.; Hopwood, D. A. *Gene* **1994**, *142*, 31-39.
- 33 Bililign, T.; Hyun, C.-G.; Williams, J. S.; Czisny, A. M.; Thorson, J. S. *Chem. Biol.* **2004**, *11*, 959-969.
- 34 Moore, B. S.; Hertweck, C. *Nat. Prod. Rep.* **2002**, *19*, 70-99.
- 35 Revill, W. P.; Bibb, M. J.; Hopwood, D. A. *J. Bacteriol.* **1995**, *177*, 3946-52.
- 36 Fu, H.; Ebertkhosla, S.; Hopwood, D. A.; Khosla, C. *J. Am. Chem. Soc.* **1994**, *116*, 4166-4170.
- 37 Fu, H.; Hopwood, D. A.; Khosla, C. *Chem. Biol.* **1994**, *1*, 205-10.
- 38 Pan, H.; Tsai, S.-c.; Meadows, E. S.; Miercke, L. J. W.; Keatinge-Clay, A. T.; O'Connell, J.; Khosla, C.; Stroud, R. M. *Structure* **2002**, *10*, 1559-1568.
- 39 Pan, H.; Tsai, S.; Meadows, E. S.; Miercke, L. J.; Keatinge-Clay, A. T.; O'Connell, J.; Khosla, C.; Stroud, R. M. *Structure* **2002**, *10*, 1559-68.
- 40 Tang, Y.; Tsai, S. C.; Khosla, C. *J. Am. Chem. Soc.* **2003**, *125*, 12708-12709.
- 41 Shen, Y.; Yoon, P.; Yu, T.-W.; Floss, H. G.; Hopwood, D.; Moore, B. S. *Proc. Natl. Acad. Sci. U. S. A.* **1999**, *96*, 3622-3627.
- 42 Petkovič, H.; Thamchaipenet, A.; Zhou, L.-H.; Hranueli, D.; Raspor, P.; Waterman, P. G.; Hunter, I. S. *J. Biol. Chem.* **1999**, *274*, 32829-32834.

- 43 Crump, M. P.; Crosby, J.; Dempsey, C. E.; Parkinson, J. A.; Murray, M.; Hopwood, D. A.; Simpson, T. J. *Biochemistry* **1997**, *36*, 6000-6008.
- 44 Li, Q.; Khosla, C.; Puglisi, J. D.; Liu, C. W. *Biochemistry* **2003**, *42*, 4648-4657.
- 45 Findlow, S. C.; Winsor, C.; Simpson, T. J.; Crosby, J.; Crump, M. P. *Biochemistry* **2003**, *42*, 8423-8433.
- 46 Evans, S. E.; Williams, C.; Arthur, C. J.; Burston, S. G.; Simpson, T. J.; Crosby, J.; Crump, M. P. *ChemBioChem* **2008**, *9*, 2424-2432.
- 47 Qiu, X.; Janson, C. A. *Acta Crystallogr. D Biol. Crystallogr.* **2004**, *60*, 1545-54.
- 48 Hertweck, C.; Xiang, L. K.; Kalaitzis, J. A.; Cheng, Q.; Palzer, M.; Moore, B. S. *Chem. Biol.* **2004**, *11*, 461-468.
- 49 Wohler, S.-E.; Wendt-Pienkowski, E.; Bao, W.; Hutchinson, C. R. *J. Nat. Prod.* **2001**, *64*, 1077-1080.
- 50 Chen, Y.-H.; Wang, C.-C.; Greenwell, L.; Rix, U.; Hoffmeister, D.; Vining, L. C.; Rohr, J.; Yang, K.-Q. *J. Biol. Chem.* **2005**, *280*, 22508-22514.
- 51 Mayer, A.; Taguchi, T.; Linnenbrink, A.; Hofmann, C.; Luzhetskyy, A.; Bechthold, A. *ChemBioChem* **2005**, *6*, 2312-2315.
- 52 Jansson, A.; Koskiniemi, H.; Mäntsälä, P.; Niemi, J.; Schneider, G. *J. Biol. Chem.* **2004**, *279*, 41149-41156.
- 53 Jansson, A.; Niemi, J.; Lindqvist, Y.; Mäntsälä, P.; Schneider, G. *J. Mol. Biol.* **2003**, *334*, 269-280.
- 54 Fetzner, S. *Appl. Microbiol. Biotechnol.* **2002**, *60*, 243-257.
- 55 Sciarra, G.; Kendrew, S. G.; Miele, A. E.; Marsh, N. G.; Federici, L.; Malatesta, F.; Schimperna, G.; Savino, C.; Vallone, B. *EMBO J.* **2003**, *22*, 205-215.
- 56 Caballero, J. L.; Martinez, E.; Malpartida, F.; Hopwood, D. A. *Mol. Gen. Genet.* **1991**, *230*, 401-412.
- 57 Gibson, M.; Nur-e-alam, M.; Lipata, F.; Oliveira, M. A.; Rohr, J. *J. Am. Chem. Soc.* **2005**, *127*, 17594-17595.
- 58 Xu, Z.; Jakobi, K.; Welzel, K.; Hertweck, C. *Chem. Biol.* **2005**, *12*, 579-588.
- 59 Walczak, R. J.; Dickens, M. L.; Priestley, N. D.; Strohl, W. R. *J. Bacteriol.* **1999**, *181*, 298-304.
- 60 Walczak, R. J.; Hines, J. V.; Strohl, W. R.; Priestley, N. D. *Org. Lett.* **2001**, *3*, 2277-2279.
- 61 Rix, U.; Fischer, C.; Remsing, L. L.; Rohr, J. *Nat. Prod. Rep.* **2002**, *19*, 542-580.
- 62 Kamerbeek, N. M.; Janssen, D. B.; van Berkel, W. J. H.; Fraaije, M. W. *Adv. Synth. Catal.* **2003**, *345*, 667-678.
- 63 Baeyer, A.; Villiger, V. *Ber. Dtsch. Chem. Ges.* **1899**, *32*, 3625-3633.
- 64 Doull, J. L.; Singh, A. K.; Hoare, M.; Ayer, S. W. *J. Ind. Microbiol.* **1994**, *13*, 120-5.
- 65 Claesson, M.; Siitonen, V.; Dobritzsch, D.; Metsä-Ketelä, M.; Schneider, G. *FEBS J.* **2012**, *279*, 3251-3263.
- 66 Nicholson, T. P.; Winfield, C.; Westcott, J.; Crosby, J.; Simpson, T. J.; Cox, R. J. *Chem. Commun.* **2003**, 686-687.
- 67 Brockmann, H.; Hieronymus, E. *Chem. Ber.* **1955**, *88*, 1379-1390.
- 68 Brockmann, H.; Pini, H.; v. Plotho, O. *Chem. Ber.* **1950**, *83*, 161-167.
- 69 Brockmann, H.; Zeeck, A.; Merwe, K. V. D.; Müller, W. *Justus Liebigs Ann. Chem.* **1966**, *698*, 209-229.
- 70 Craney, A.; Ahmed, S.; Nodwell, J. *J. Antibiot.* **2013**, *66*, 387-400.
- 71 Floriano, B.; Bibb, M. *Mol. Microbiol.* **1996**, *21*, 385-396.
- 72 McDaniel, R.; Ebertkhosla, S.; Hopwood, D. A.; Khosla, C. *J. Am. Chem. Soc.* **1993**, *115*, 11671-11675.
- 73 McDaniel, R.; Ebertkhosla, S.; Hopwood, D. A.; Khosla, C. *Sci* **1993**, *262*, 1546-1550.
- 74 Burson, K. K.; Khosla, C. *Tetrahedron* **2000**, *56*, 9401-9408.
- 75 Zhang, Y. M.; Rao, M. S.; Heath, R. J.; Price, A. C.; Olson, A. J.; Rock, C. O.; White, S. W. *J. Biol. Chem.* **2001**, *276*, 8231-8238.
- 76 Beltran-Alvarez, P.; Arthur, C. J.; Cox, R. J.; Crosby, J.; Crump, M. P.; Simpson, T. J. *Mol. Biosyst.* **2009**, *5*, 511-518.
- 77 Javidpour, P.; Bruegger, J.; Srithahan, S.; Crump, M. P.; Crosby, J.; Burkart, M. D.; Tsai, S.-C. *Chem. Biol.* **2013**, *20*, 1225-1234.
- 78 Khosla, C.; McDaniel, R.; Ebertkhosla, S.; Torres, R.; Sherman, D. H.; Bibb, M. J.; Hopwood, D. A. *J. Bacteriol.* **1993**, *175*, 2197-2204.
- 79 McDaniel, R.; Ebertkhosla, S.; Fu, H.; Hopwood, D. A.; Khosla, C. *Proc. Natl. Acad. Sci. U. S. A.* **1994**, *91*, 11542-11546.

- 80 Zawada, R. J. X.; Khosla, C. *Chem. Biol.* **1999**, *6*, 607-615.
- 81 McDaniel, R.; Ebertkhosla, S.; Hopwood, D. A.; Khosla, C. *J. Am. Chem. Soc.* **1994**, *116*, 10855-10859.
- 82 Taguchi, T.; Itou, K.; Ebizuka, Y.; Malpartida, F.; Hopwood, D. A.; Surti, C. M.; Booker-Milburn, K. I.; Stephenson, G. R.; Ichinose, K. *J. Antibiot. (Tokyo)* **2000**, *53*, 144-52.
- 83 Ichinose, K.; Surti, C.; Taguchi, T.; Malpartida, F.; Booker-Milburn, K. I.; Stephenson, G. R.; Ebizuka, Y.; Hopwood, D. A. *Bioorg. Med. Chem. Lett.* **1999**, *9*, 395-400.
- 84 Booker-Milburn, K. I.; Gillan, R.; Kimberley, M.; Taguchi, T.; Ichinose, K.; Stephenson, G. R.; Ebizuka, Y.; Hopwood, D. A. *Angew. Chem. Int. Ed. Engl.* **2005**, *44*, 1121-5.
- 85 Fernandez-Moreno, M. A.; Martinez, E.; Caballero, J. L.; Ichinose, K.; Hopwood, D. A.; Malpartida, F. *J. Biol. Chem.* **1994**, *269*, 24854-63.
- 86 Kendrew, S. G.; Hopwood, D. A.; Marsh, E. N. *J. Bacteriol.* **1997**, *179*, 4305-10.
- 87 Kendrew, S. G.; Federici, L.; Savino, C.; Miele, A.; Marsh, E. N.; Vallone, B. *Acta Crystallogr. D Biol. Crystallogr.* **2000**, *56*, 481-3.
- 88 Valton, J.; Filisetti, L.; Fontecave, M.; Niviere, V. *J. Biol. Chem.* **2004**, *279*, 44362-44369.
- 89 Valton, J.; Fontecave, M.; Douki, T.; Kendrew, S. G.; Niviere, V. *J. Biol. Chem.* **2006**, *281*, 27-35.
- 90 Valton, J.; Fontecave, M.; Douki, T.; Kendrew, S. G.; Niviere, V. *J. Biol. Chem.* **2006**, *281*, 27-35.
- 91 Valton, J.; Mathevon, C.; Fontecave, M.; Niviere, V.; Ballou, D. P. *J. Biol. Chem.* **2008**, *283*, 10287-10296.
- 92 Taguchi, T.; Okamoto, S.; Itoh, T.; Ebizuka, Y.; Ochi, K.; Ichinose, K. *Tetrahedron Lett.* **2008**, *49*, 1208-1211.
- 93 Taguchi, T.; Ebihara, T.; Furukawa, A.; Hidaka, Y.; Ariga, R.; Okamoto, S.; Ichinose, K. *Bioorg. Med. Chem. Lett.* **2012**, *22*, 5041-5045.
- 94 Evans, S. E.; Williams, C.; Arthur, C. J.; Ploskon, E.; Wattana-Amorn, P.; Cox, R. J.; Crosby, J.; Willis, C. L.; Simpson, T. J.; Crump, M. P. *J. Mol. Biol.* **2009**, *389*, 511-528.
- 95 Ploskon, E.; Arthur, C. J.; Evans, S. E.; Williams, C.; Crosby, J.; Simpson, T. J.; Crump, M. P. *J. Biol. Chem.* **2008**, *283*, 518-528.
- 96 Mootz, H. D.; Finking, R.; Marahiel, M. A. *J. Biol. Chem.* **2001**, *276*, 37289-37298.
- 97 Majerus, P. W.; Alberts, A. W.; Vagelos, P. R. *Proc Nat Acad Sci USA* **1964**, *51*, 1231-1238.
- 98 Crosby, J.; Byrom, K. J.; Hitchman, T. S.; Cox, R. J.; Crump, M. P.; Findlow, I. S. C.; Bibb, M. J.; Simpson, T. J. *FEBS Lett.* **1998**, *433*, 132-138.
- 99 Quadri, L. E. N.; Weinreb, P. H.; Lei, M.; Nakano, M. M.; Zuber, P.; Walsh, C. T. *Biochemistry* **1998**, *37*, 1585-1595.
- 100 Yin, J.; Lin, A. J.; Golan, D. E.; Walsh, C. T. *Nat. Protoc.* **2006**, *1*, 280-285.
- 101 Nazi, I.; Koteva, K. P.; Wright, G. D. *Anal. Biochem.* **2004**, *324*, 100-105.
- 102 Padmakumar, R.; Padmakumar, R.; Banerjee, R. *Methods Enzymol.* **1997**, *279*, 220-4.
- 103 Yin, J.; Straight, P. D.; McLoughlin, S. M.; Zhou, Z.; Lin, A. J.; Golan, D. E.; Kelleher, N. L.; Kolter, R.; Walsh, C. T. *Proc. Natl. Acad. Sci. U. S. A.* **2005**, *102*, 15815-15820.
- 104 Zhou, Z.; Cironi, P.; Lin, A. J.; Xu, Y.; Hrvatin, S.; Golan, D. E.; Silver, P. A.; Walsh, C. T.; Yin, J. *ACS Chem. Biol.* **2007**, *2*, 337-346.
- 105 La Clair, J. J.; Foley, T. L.; Schegg, T. R.; Regan, C. M.; Burkart, M. D. *Chem. Biol.* **2004**, *11*, 195-201.
- 106 Shute, T. S.; Matsushita, M.; Dickerson, T. J.; La Clair, J. J.; Janda, K. D.; Burkart, M. D. *Bioconjugate Chem.* **2005**, *16*, 1352-1355.
- 107 Kosa, N. M.; Foley, T. L.; Burkart, M. D. *J. Antibiot.* **2014**, *67*, 113-120.
- 108 Meier, J. L.; Mercer, A. C.; Burkart, M. D. *J. Am. Chem. Soc.* **2008**, *130*, 5443-+.
- 109 Sieber, S. A.; Walsh, C. T.; Marahiel, M. A. *J. Am. Chem. Soc.* **2003**, *125*, 10862-10866.
- 110 Belshaw, P. J.; Walsh, C. T.; Stachelhaus, T. *Sci* **1999**, *284*, 486-489.
- 111 Finzel, K.; Lee, D. J.; Burkart, M. D. *ChemBioChem* **2015**, *16*, 528-547.
- 112 Worthington, A. S.; Rivera, H.; Torpey, J. W.; Alexander, M. D.; Burkart, M. D. *ACS Chem. Biol.* **2006**, *1*, 687-691.
- 113 Blatti, J. L.; Beld, J.; Behnke, C. A.; Mendez, M.; Mayfield, S. P.; Burkart, M. D. *PLoS One* **2012**, *7*.
- 114 Chi, N.; Haushalter, R. W.; Lee, D. J.; Markwick, P. R. L.; Bruegger, J.; Caldara-Festin, G.; Finzel, K.; Jackson, D. R.; Ishikawa, F.; O'Dowd, B.; McCammon, J. A.; Opella, S. J.; Tsai, S.-C.; Burkart, M. D. *Nature* **2014**, *505*, 427-431.
- 115 Clarke, K. M.; Mercer, A. C.; La Clair, J. J.; Burkart, M. D. *J. Am. Chem. Soc.* **2005**, *127*, 11234-11235.

- 116 Meier, J. L.; Mercer, A. C.; Rivera, H.; Burkart, M. D. *J. Am. Chem. Soc.* **2006**, *128*, 12174-12184.
- 117 Mercer, A. C.; Meier, J. L.; Torpey, J. W.; Burkart, M. D. *ChemBioChem* **2009**, *10*, 1091-1100.
- 118 George, N.; Pick, H.; Vogel, H.; Johnsson, N.; Johnsson, K. *J. Am. Chem. Soc.* **2004**, *126*, 8896-8897.
- 119 Vivero-Pol, L.; George, N.; Krumm, H.; Johnsson, K.; Johnsson, N. *J. Am. Chem. Soc.* **2005**, *127*, 12770-12771.
- 120 Meyer, B. H.; Martinez, K. L.; Segura, J. M.; Pascoal, P.; Hovius, R.; George, N.; Johnsson, K.; Vogel, H. *FEBS Lett.* **2006**, *580*, 1654-1658.
- 121 Yin, J.; Lin, A. J.; Buckett, P. D.; Wessling-Resnick, M.; Golan, D. E.; Walsh, C. T. *Chem. Biol.* **2005**, *12*, 999-1006.
- 122 Meyer, B. H.; Segura, J. M.; Martinez, K. L.; Hovius, R.; George, N.; Johnsson, K.; Vogel, H. *Proc. Natl. Acad. Sci. U. S. A.* **2006**, *103*, 2138-2143.
- 123 Yin, J.; Liu, F.; Li, X. H.; Walsh, C. T. *J. Am. Chem. Soc.* **2004**, *126*, 7754-7755.
- 124 Yin, J.; Liu, F.; Schinke, M.; Daly, C.; Walsh, C. T. *J. Am. Chem. Soc.* **2004**, *126*, 13570-13571.
- 125 Clifton, G.; Bryant, S. R.; Skinner, C. G. *Arch. Biochem. Biophys.* **1970**, *137*, 523-528.
- 126 Zhang, Y. M.; Frank, M. W.; Virga, K. G.; Lee, R. E.; Rock, C. O.; Jackowski, S. *J. Biol. Chem.* **2004**, *279*, 50969-50975.
- 127 Strauss, E.; Begley, T. P. *J. Biol. Chem.* **2002**, *277*, 48205-48209.
- 128 Mercer, A. C.; Burkart, M. D. *Nat. Prod. Rep.* **2007**, *24*, 750-773.
- 129 Collie, N.; Myers, W. S. *J. Chem. Soc., Trans.* **1893**, *63*, 122-128.
- 130 Birch, A.; Massy-Westropp, R.; Moye, C. *Aust. J. Chem.* **1955**, *8*, 539-544.
- 131 Minto, R. E.; Townsend, C. A. *Chem. Rev.* **1997**, *97*, 2537-2555.
- 132 Hill, R. A.; Carter, R. H.; Staunton, J. *J. Chem. Soc., Perkin Trans. 1* **1981**, 2570-2576.
- 133 Cane, D. E.; Prabhakaran, P. C.; Tan, W. T.; Ott, W. R. *Tetrahedron Lett.* **1991**, *32*, 5457-5460.
- 134 Barry, S. M.; Kers, J. A.; Johnson, E. G.; Song, L.; Aston, P. R.; Patel, B.; Krasnoff, S. B.; Crane, B. R.; Gibson, D. M.; Loria, R.; Challis, G. L. *Nat. Chem. Biol.* **2012**, *8*, 814-816.
- 135 Siegel, B. Z.; Galston, A. W. *Proc Nat Acad Sci Us Amer* **1966**, *56*, 1040-1042.
- 136 Tosin, M.; Demydchuk, Y.; Parascandolo, J. S.; Per, C. B.; Leeper, F. J.; Leadlay, P. F. *Chem. Commun.* **2011**, *47*, 3460-3462.
- 137 Pfeifer, B. A.; Admiraal, S. J.; Gramajo, H.; Cane, D. E.; Khosla, C. *Sci* **2001**, *291*, 1790-1792.
- 138 Watanabe, K.; Hotta, K.; Praseuth, A. P.; Koketsu, K.; Migita, A.; Boddy, C. N.; Wang, C. C. C.; Oguri, H.; Oikawa, H. *Nat. Chem. Biol.* **2006**, *2*, 423-428.
- 139 Schmidt, E. W.; Nelson, J. T.; Rasko, D. A.; Sudek, S.; Eisen, J. A.; Haygood, M. G.; Ravel, J. *Proc. Natl. Acad. Sci. U. S. A.* **2005**, *102*, 7315-7320.
- 140 Jenner, M.; Afonso, J. P.; Bailey, H. R.; Frank, S.; Kampa, A.; Piel, J.; Oldham, N. J. *Angew. Chem. Int. Ed.* **2015**, *54*, 1817-1821.
- 141 Dutta, S.; Whicher, J. R.; Hansen, D. A.; Hale, W. A.; Chemler, J. A.; Congdon, G. R.; Narayan, A. R. H.; Hakansson, K.; Sherman, D. H.; Smith, J. L.; Skiniotis, G. *Nature* **2014**, *510*, 512-+.
- 142 Whicher, J. R.; Dutta, S.; Hansen, D. A.; Hale, W. A.; Chemler, J. A.; Dosey, A. M.; Narayan, A. R. H.; Hakansson, K.; Sherman, D. H.; Smith, J. L.; Skiniotis, G. *Nature* **2014**, *510*, 560-+.
- 143 Wilkinson, B.; Micklefield, J. *Nat. Chem. Biol.* **2007**, *3*, 379-386.
- 144 Miller, W. W.; Richards, J. H. *Biochem. Biophys. Res. Commun.* **1968**, *33*, 569-573.
- 145 Pohl, N. L.; Gokhale, R. S.; Cane, D. E.; Khosla, C. *J. Am. Chem. Soc.* **1998**, *120*, 11206-11207.
- 146 Richardson, M. T.; Pohl, N. L.; Kealey, J. T.; Khosla, C. *Metab. Eng.* **1999**, *1*, 180-187.
- 147 Klopries, S.; Sundermann, U.; Schulz, F. *Beilstein J. Org. Chem.* **2013**, *9*, 664-674.
- 148 Crawford, J. M.; Dancy, B. C. R.; Hill, E. A.; Udworthy, D. W.; Townsend, C. A. *Proc. Natl. Acad. Sci. U. S. A.* **2006**, *103*, 16728-16733.
- 149 Bravo-Rodriguez, K.; Ismail-Ali, A. F.; Klopries, S.; Kushnir, S.; Ismail, S.; Fansa, E. K.; Wittinghofer, A.; Schulz, F.; Sanchez-Garcia, E. *ChemBioChem* **2014**, *15*, 1991-1997.
- 150 Xie, X.; Watanabe, K.; Wojcicki, W. A.; Wang, C. C. C.; Tang, Y. *Chem. Biol.* **2006**, *13*, 1161-1169.
- 151 Deska, J.; Hähn, S.; Kazmaier, U. *Org. Lett.* **2011**, *13*, 3210-3213.

- 152 Kohlhaas, C.; Jenner, M.; Kampa, A.; Briggs, G. S.; Afonso, J. P.; Piel, J.; Oldham, N. J. *Chem. Sci.* **2013**, *4*, 3212-3217.
- 153 Spiteller, D.; Waterman, C. L.; Spencer, J. B. *Angew. Chem. Int. Ed.* **2005**, *44*, 7079-7082.
- 154 Tosin, M.; Betancor, L.; Stephens, E.; Li, W. M. A.; Spencer, J. B.; Leadlay, P. F. *ChemBioChem* **2010**, *11*, 539-546.
- 155 Riva, E.; Wilkening, I.; Gazzola, S.; Li, W. M. A.; Smith, L.; Leadlay, P. F.; Tosin, M. *Angew. Chem. Int. Ed.* **2014**, *53*, 11944-11949.
- 156 Wilkening, I.; Gazzola, S.; Riva, E.; Parascandolo, J. S.; Song, L.; Tosin, M. *Chem. Commun.* **2016**, *52*, 10392-10395.
- 157 Meier, J. L.; Patel, A. D.; Niessen, S.; Meehan, M.; Kersten, R.; Yang, J. Y.; Rothmann, M.; Cravatt, B. F.; Dorrestein, P. C.; Burkart, M. D.; Bafna, V. *J. Proteome Res.* **2011**, *10*, 320-329.
- 158 Bumpus, S. B.; Kelleher, N. L. *Curr. Opin. Chem. Biol.* **2008**, *12*, 475-482.
- 159 Bumpus, S. B.; Evans, B. S.; Thomas, P. M.; Ntai, I.; Kelleher, N. L. *Nat. Biotechnol.* **2009**, *27*, 951-U120.
- 160 Meier, J. L.; Niessen, S.; Hoover, H. S.; Foley, T. L.; Cravatt, B. F.; Burkart, M. D. *ACS Chem. Biol.* **2009**, *4*, 948-957.
- 161 Kebarle, P.; Verkerk, U. H. in *Electrospray and Maldi Mass Spectrometry*. John Wiley & Sons, Inc., **2010**, pp 1-48.
- 162 Gross, J. in *Mass Spectrometry*. Springer Berlin Heidelberg, **2011**, pp 561-620.
- 163 Knochenmuss, R. in *Electrospray and Maldi Mass Spectrometry*. John Wiley & Sons, Inc., **2010**, pp 147-183.
- 164 Gross, J. in *Mass Spectrometry*. Springer Berlin Heidelberg, **2011**, pp 507-559.
- 165 Gross, J. in *Mass Spectrometry*. Springer Berlin Heidelberg, **2011**, pp 67-116.
- 166 Gross, J. in *Mass Spectrometry*. Springer Berlin Heidelberg, **2011**, pp 117-221.
- 167 He, F.; Hendrickson, C. L.; Marshall, A. G. *Anal. Chem.* **2001**, *73*, 647-650.
- 168 Bossio, R. E.; Marshall, A. G. *Anal. Chem.* **2002**, *74*, 1674-1679.
- 169 Hughey, C. A.; Rodgers, R. P.; Marshall, A. G. *Anal. Chem.* **2002**, *74*, 4145-4149.
- 170 Comisarow, M. B.; Marshall, A. G. *J. Mass Spectrom.* **1996**, *31*, 581-585.
- 171 Comisarow, M. B.; Marshall, A. G. *Chem. Phys. Lett.* **1974**, *25*, 282-283.
- 172 Comisarow, M. B.; Marshall, A. G. *The Journal of Chemical Physics* **1976**, *64*, 110-119.
- 173 Comisarow, M. B. *J. Chem. Phys.* **1978**, *69*, 4097-4104.
- 174 Marshall, A. G.; Grosshans, P. B. *Anal. Chem.* **1991**, *63*, A215-A229.
- 175 Hu, Q.; Noll, R. J.; Li, H.; Makarov, A.; Hardman, M.; Graham Cooks, R. *J. Mass Spectrom.* **2005**, *40*, 430-43.
- 176 Lanucara, F.; Holman, S. W.; Gray, C. J.; Eyers, C. E. *Nat. Chem.* **2014**, *6*, 281-294.
- 177 Sleno, L.; Volmer, D. A. *J. Mass Spectrom.* **2004**, *39*, 1091-112.
- 178 Syka, J. E. P.; Coon, J. J.; Schroeder, M. J.; Shabanowitz, J.; Hunt, D. F. *Proc. Natl. Acad. Sci. U. S. A.* **2004**, *101*, 9528-9533.
- 179 Roepstorff, P.; Fohlman, J. *Biomed. Mass Spectrom.* **1984**, *11*, 601-601.
- 180 Gross, J. in *Mass Spectrometry*. Springer Berlin Heidelberg, **2011**, pp 21-66.
- 181 Mikhailov, V. A.; Cooper, H. J. *J. Am. Soc. Mass. Spectrom.* **2009**, *20*, 763-771.
- 182 Yoo, H. J.; Liu, H. C.; Hakansson, K. *Anal. Chem.* **2007**, *79*, 7858-7866.
- 183 Cody, R. B.; Freiser, B. S. *Anal. Chem.* **1979**, *51*, 547-551.
- 184 Budnik, B. A.; Haselmann, K. F.; Elkin, Y. N.; Gorbach, V. I.; Zubarev, R. A. *Anal. Chem.* **2003**, *75*, 5994-6001.
- 185 Lioe, H.; O'Hair, R. A. J. *Anal. Bioanal. Chem.* **2007**, *389*, 1429-1437.
- 186 Mosely, J. A.; Smith, M. J. P.; Prakash, A. S.; Sims, M.; Bristow, A. W. T. *Anal. Chem.* **2011**, *83*, 4068-4075.
- 187 Wolff, J. J.; Laremore, T. N.; Aslam, H.; Linhardt, R. J.; Amster, I. J. *J. Am. Soc. Mass. Spectrom.* **2008**, *19*, 1449-1458.
- 188 Nguyen, V. H.; Afonso, C.; Tabet, J. C. *Int. J. Mass spectrom.* **2012**, *316*, 140-146.
- 189 Doerr, A. *Nat Meth* **2008**, *5*, 24-24.
- 190 Yoo, H. J.; Hakansson, K. *Anal. Chem.* **2010**, *82*, 6940-6946.
- 191 Wills, R. H.; Tosin, M.; O'Connor, P. B. *Anal. Chem.* **2012**, *84*.
- 192 Meehan, M. J.; Xie, X. K.; Zhao, X. L.; Xu, W.; Tang, Y.; Dorrestein, P. C. *Biochemistry* **2011**, *50*, 287-299.
- 193 Dorrestein, P. C.; Bumpus, S. B.; Calderone, C. T.; Garneau-Tsodikova, S.; Aron, Z. D.; Straight, P. D.; Kolter, R.; Walsh, C. T.; Kelleher, N. L. *Biochemistry* **2006**, *45*, 12756-12766.

- 194 Poust, S.; Phelan, R. M.; Deng, K.; Katz, L.; Petzold, C. J.; Keasling, J. D. *Angew. Chem. Int. Ed.* **2015**, *54*, 2370-2373.
- 195 Van Lanen, S. G.; Dorrestein, P. C.; Christenson, S. D.; Liu, W.; Ju, J. H.; Kelleher, N. L.; Shen, B. *J. Am. Chem. Soc.* **2005**, *127*, 11594-11595.
- 196 Kislinger, T.; Gramolini, A. O.; MacLennan, D. H.; Emili, A. *J. Am. Soc. Mass. Spectrom.* **2005**, *16*, 1207-20.
- 197 Washburn, M. P.; Wolters, D.; Yates, J. R. *Nat Biotech* **2001**, *19*, 242-247.
- 198 Evans, B. S.; Ntai, I.; Chen, Y.; Robinson, S. J.; Kelleher, N. L. *J. Am. Chem. Soc.* **2011**, *133*, 7316-7319.
- 199 Chen, Y.; McClure, R. A.; Zheng, Y.; Thomson, R. J.; Kelleher, N. L. *J. Am. Chem. Soc.* **2013**, *135*, 10449-10456.
- 200 Chen, Y.; Unger, M.; Ntai, I.; McClure, R. A.; Albright, J. C.; Thomson, R. J.; Kelleher, N. L. *Medchemcomm* **2013**, *4*, 233-238.
- 201 Bochet, C. G. *J. Chem. Soc. Perk. Trans. 1* **2002**, 125-142.
- 202 Atkins, P.; de Paula, J. *Atkins' Physical Chemistry*. OUP Oxford: **2010**.
- 203 Maxwell, K.; Johnson, G. N. *J. Exp. Bot.* **2000**, *51*, 659-668.
- 204 Vile, G. F.; Tyrrell, R. M. *J. Biol. Chem.* **1993**, *268*, 14678-81.
- 205 Scattino, C.; Castagna, A.; Neugart, S.; Chan, H. M.; Schreiner, M.; Crisosto, C. H.; Tonutti, P.; Ranieri, A. *Food Chem.* **2014**, *163*, 51-60.
- 206 Huang, L. X.; McCluskey, M. P.; Ni, H.; LaRossa, R. A. *J. Bacteriol.* **2002**, *184*, 6845-6858.
- 207 Dreier, J.; Shah, A. N.; Khosla, C. *J. Biol. Chem.* **1999**, *274*, 25108-25112.
- 208 Carreras, C. W.; Pieper, R.; Khosla, C. *J. Am. Chem. Soc.* **1996**, *118*, 5158-5159.
- 209 Vagstad, A. L.; Bumpus, S. B.; Belecki, K.; Kelleher, N. L.; Townsend, C. A. *J. Am. Chem. Soc.* **2012**, *134*, 6865-6877.
- 210 Lambalot, R. H.; Gehring, A. M.; Flugel, R. S.; Zuber, P.; LaCelle, M.; Marahiel, M. A.; Reid, R.; Khosla, C.; Walsh, C. T. *Chem. Biol.* **1996**, *3*, 923-936.
- 211 Corey, E. J.; Hopkins, P. B. *Tetrahedron Lett.* **1982**, *23*, 4871-4874.
- 212 Barrett, A. G. M.; Pena, M.; Willardsen, J. A. *J. Org. Chem.* **1996**, *61*, 1082-1100.
- 213 Evans, D. A.; Kaldor, S. W.; Jones, T. K.; Clardy, J.; Stout, T. J. *J. Am. Chem. Soc.* **1990**, *112*, 7001-7031.
- 214 Krouse, I. H.; Wenthold, P. G. *J. Am. Soc. Mass. Spectrom.* **2005**, *16*, 697-707.
- 215 Larson, G. L. in *Organic Silicon Compounds (1989)*. John Wiley & Sons, Ltd, **2004**, pp 763-808.
- 216 Cardillo, G.; Orena, M.; Sandri, S.; Tomasini, C. *Chem. Ind.* **1983**, 643-644.
- 217 DiLauro, A. M.; Seo, W.; Phillips, S. T. *J. Org. Chem.* **2011**, *76*, 7352-7358.
- 218 Boschelli, D.; Takemasa, T.; Nishitani, Y.; Masamune, S. *Tetrahedron Lett.* **1985**, *26*, 5239-5242.
- 219 Akinnusi, T. O.; Vong, K.; Auclair, K. *Biorg. Med. Chem.* **2011**, *19*, 2696-2706.
- 220 Awuah, E.; Ma, E.; Hoegl, A.; Vong, K.; Habib, E.; Auclair, K. *Biorg. Med. Chem.* **2014**, *22*, 3083-3090.
- 221 Song, W. J.; Jackowski, S. *J. Bacteriol.* **1992**, *174*, 6411-6417.
- 222 Geerlof, A.; Lewendon, A.; Shaw, W. V. *J. Biol. Chem.* **1999**, *274*, 27105-27111.
- 223 Mishra, P. K.; Park, P. K.; Drueckhammer, D. G. *J. Bacteriol.* **2001**, *183*, 2774-2778.
- 224 Kilgour, S. L., O'Connor, P. B., Tosin, Manuela **2011**.
- 225 Walsh, C. T.; Gehring, A. M.; Weinreb, P. H.; Quadri, L. E. N.; Flugel, R. S. *Curr. Opin. Chem. Biol.* **1997**, *1*, 309-315.
- 226 Corrie, J. E. T.; Furuta, T.; Givens, R.; Yousef, A. L.; Goeldner, M. in *Dynamic Studies in Biology*. Wiley-VCH Verlag GmbH & Co. KGaA, **2005**, pp 1-94.
- 227 Pirrung, M. C.; Fallon, L.; Zhu, J.; Lee, Y. R. *J. Am. Chem. Soc.* **2001**, *123*, 3638-3643.
- 228 Pirrung, M. C.; Lee, Y. R. *J. Org. Chem.* **1993**, *58*, 6961-6963.
- 229 Kitani, S.; Sugawara, K.; Tsutsumi, K.; Morimoto, T.; Kakiuchi, K. *Chem. Commun.* **2008**, 2103-2105.
- 230 Furuta, T.; Hirayama, Y.; Iwamura, M. *Org. Lett.* **2001**, *3*, 1809-1812.
- 231 Givens, R. S.; Matuszewski, B. *J. Am. Chem. Soc.* **1984**, *106*, 6860-6861.
- 232 Furuta, T.; Torigai, H.; Osawa, T.; Iwamura, M. *Chem. Lett.* **1993**, *22*, 1179-1182.
- 233 Eckardt, T.; Hagen, V.; Schade, B.; Schmidt, R.; Schweitzer, C.; Bendig, J. *J. Org. Chem.* **2002**, *67*, 703-710.
- 234 Furuta, T.; Wang, S. S. H.; Dantzker, J. L.; Dore, T. M.; Bybee, W. J.; Callaway, E. M.; Denk, W.; Tsien, R. Y. *Proc. Natl. Acad. Sci. U. S. A.* **1999**, *96*, 1193-1200.

- 235 Takaoka, K.; Tatsu, Y.; Yumoto, N.; Nakajima, T.; Shimamoto, K. *Bioorg. Med. Chem. Lett.* **2003**, *13*, 965-970.
- 236 Barltrop, J. A.; Schofield, P. *Tetrahedron Lett.* **1962**, *3*, 697-699.
- 237 Chamberlin, J. W. *J. Org. Chem.* **1966**, *31*, 1658-1660.
- 238 Zimmerman, H. E.; Somasekhara, S. *J. Am. Chem. Soc.* **1963**, *85*, 922-927.
- 239 Zimmerman, H. E. *J. Phys. Chem. A* **1998**, *102*, 5616-5621.
- 240 Wang, P. *Asian J. Org. Chem.* **2013**, *2*, 452-464.
- 241 Birr, C.; Lochinger, W.; Stahnke, G.; Lang, P. *Justus Liebigs Ann. Chem.* **1972**, *763*, 162-172.
- 242 Conrad, P. G.; Givens, R. S.; Weber, J. F. W.; Kandler, K. *Org. Lett.* **2000**, *2*, 1545-1547.
- 243 Barton, D. H. R.; Chow, Y. L.; Cox, A.; Kirby, G. W. *Tetrahedron Lett.* **1962**, *3*, 1055-1057.
- 244 Il'ichev, Y. V.; Schworer, M. A.; Wirz, J. *J. Am. Chem. Soc.* **2004**, *126*, 4581-4595.
- 245 Singh, A. K.; Khade, P. K. *Tetrahedron* **2005**, *61*, 10007-10012.
- 246 Reichmanis, E.; Gooden, R.; Wilkins, C. W.; Schonhorn, H. *J. Polym. Sci. Polym. Chem. Ed.* **1983**, *21*, 1075-1083.
- 247 Reichmanis, E.; Smith, B. C.; Gooden, R. *J. Polym. Sci. Polym. Chem. Ed.* **1985**, *23*, 1-8.
- 248 Houlihan, F. M.; Shugard, A.; Gooden, R.; Reichmanis, E. *Macromolecules* **1988**, *21*, 2001-2006.
- 249 Wan, P.; Yates, K. *Can. J. Chem.* **1986**, *64*, 2076-2086.
- 250 Cameron, J. F.; Frechet, J. M. J. *J. Am. Chem. Soc.* **1991**, *113*, 4303-4313.
- 251 Wieboldt, R.; Gee, K. R.; Niu, L.; Ramesh, D.; Carpenter, B. K.; Hess, G. P. *Proc. Natl. Acad. Sci. U. S. A.* **1994**, *91*, 8752-8756.
- 252 Gee, K. R.; Wieboldt, R.; Hess, G. P. *J. Am. Chem. Soc.* **1994**, *116*, 8366-8367.
- 253 Schaper, K.; Mobarekeh, S. A. M.; Grewer, C. *Eur. J. Org. Chem.* **2002**, 1037-1046.
- 254 Xia, J.; Huang, X. P.; Sreekumar, R.; Walker, J. W. *Bioorg. Med. Chem. Lett.* **1997**, *7*, 1243-1248.
- 255 Makings, L. R.; Tsien, R. Y. *J. Biol. Chem.* **1994**, *269*, 6282-6285.
- 256 Hasan, A.; Stengele, K. P.; Giegrich, H.; Cornwell, P.; Isham, K. R.; Sachleben, R. A.; Pfeleiderer, W.; Foote, R. S. *Tetrahedron* **1997**, *53*, 4247-4264.
- 257 Gorner, H. *Photochem. Photobiol. Sci.* **2005**, *4*, 822-828.
- 258 Patchornik, A.; Amit, B.; Woodward, R. B. *J. Am. Chem. Soc.* **1970**, *92*, 6333-6335.
- 259 Bochet, C. G. *Tetrahedron Lett.* **2000**, *41*, 6341-6346.
- 260 Shamma, M.; Whitesell, J. K.; Warner Jr, P. L. *Tetrahedron Lett.* **1965**, *6*, 3869-3871.
- 261 Wilcox, M.; Viola, R. W.; Johnson, K. W.; Billington, A. P.; Carpenter, B. K.; McCray, J. A.; Guzikowski, A. P.; Hess, G. P. *J. Org. Chem.* **1990**, *55*, 1585-1589.
- 262 Corrie, J. E.; DeSantis, A.; Katayama, Y.; Khodakhah, K.; Messenger, J. B.; Ogden, D. C.; Trentham, D. R. *The Journal of Physiology* **1993**, *465*, 1-8.
- 263 Solomek, T.; Mercier, S.; Bally, T.; Bochet, C. G. *Photochem. Photobiol. Sci.* **2012**, *11*, 548-555.
- 264 Specht, A.; Thomann, J. S.; Alarcon, K.; Wittayanan, W.; Ogden, D.; Furuta, T.; Kurakawa, Y.; Goeldner, M. *ChemBioChem* **2006**, *7*, 1690-1695.
- 265 Schelkle, K. M.; Griesbaum, T.; Ollech, D.; Becht, S.; Buckup, T.; Hamburger, M.; Wombacher, R. *Angew. Chem. Int. Ed.* **2015**, *54*, 2825-2829.
- 266 Yamaguchi, K.; Tsuda, Y.; Shimakage, T.-a.; Kusumi, A. *Bull. Chem. Soc. Jpn.* **1998**, *71*, 1923-1929.
- 267 Zhang, Z.-Y.; Smith, B. D. *Bioconjugate Chem.* **1999**, *10*, 1150-1152.
- 268 Luchian, T.; Shin, S.-H.; Bayley, H. *Angew. Chem. Int. Ed.* **2003**, *42*, 1926-1929.
- 269 Zehavi, U.; Amit, B.; Patchornik, A. *J. Org. Chem.* **1972**, *37*, 2281-2285.
- 270 Lu, J.; Koo, S. C.; Li, N.-S.; Piccirilli, J. A. *Nucleosides Nucleotides Nucl. Acids* **2015**, *34*, 114-129.
- 271 Fodor, S.; Read, J.; Pirrung, M.; Stryer, L.; Lu, A.; Solas, D. *Sci* **1991**, *251*, 767-773.
- 272 Lemke, E. A.; Summerer, D.; Geierstanger, B. H.; Brittain, S. M.; Schultz, P. G. *Nat. Chem. Biol.* **2007**, *3*, 769-772.
- 273 Li, W.-h.; Llopis, J.; Whitney, M.; Zlokarnik, G.; Tsien, R. Y. *Nature* **1998**, *392*, 936-941.
- 274 Binschik, J.; Zettler, J.; Mootz, H. D. *Angew. Chem. Int. Ed.* **2011**, *50*, 3249-3252.
- 275 Van Ryssen, M. P.; Avlonitis, N.; Giniatullin, R.; McDougall, C.; Carr, J. L.; Stanton-Humphreys, M. N.; Borgstrom, E. L. A.; Brown, C. T. A.; Fayuk, D.; Surin, A.; Niittykoski, M.; Khiroug, L.; Conway, S. J. *Org. Biomol. Chem.* **2009**, *7*, 4695-4707.
- 276 Bochet, C. G. *Pure Appl. Chem.* **2006**, *78*, 241-247.
- 277 Kessler, M.; Glatthar, R.; Giese, B.; Bochet, C. G. *Org. Lett.* **2003**, *5*, 1179-1181.

- 278 Avlonitis, N.; Chalmers, S.; McDougall, C.; Stanton-Humphreys, M. N.; Brown, C. T. A.; McCarron, J. G.; Conway, S. J. *Mol. Biosyst.* **2009**, *5*, 450-457.
- 279 Deiters, A. *ChemBioChem* **2010**, *11*, 47-53.
- 280 Brieke, C.; Rohrbach, F.; Gottschalk, A.; Mayer, G.; Heckel, A. *Angew. Chem. Int. Ed.* **2012**, *51*, 8446-8476.
- 281 Zhang, R.; Sioma, C. S.; Thompson, R. A.; Xiong, L.; Regnier, F. E. *Anal. Chem.* **2002**, *74*, 3662-3669.
- 282 Rigo, B.; Fasseur, D.; Cauliez, P.; Couturier, D. *Tetrahedron Lett.* **1989**, *30*, 3073-3076.
- 283 Miller, J. S.; Olejnik, D. *Water Res.* **2001**, *35*, 233-243.
- 284 Beltran, F. J.; Ovejero, G.; Garcia-Araya, J. F.; Rivas, J. *Ind. Eng. Chem. Res.* **1995**, *34*, 1607-1615.
- 285 Dreier, J.; Khosla, C. *Biochemistry* **2000**, *39*, 2088-95.
- 286 Steinerová, N.; Lipavská, H.; Stajner, K.; Čáslavská, J.; Blumauerová, M.; Cudlín, J.; Vank, Z. *Folia Microbiol* **1987**, *32*, 1-5.
- 287 Kieser, T.; Bibb, M.; Buttner, M.; Chater, K.; Hopwood, D., **2000**.
- 288 Takano, E.; Gramajo, H. C.; Strauch, E.; Andres, N.; White, J.; Bibb, M. J. *Mol Microbiol* **1992**, *6*, 2797-804.
- 289 Hopwood, D. A. *Proc. R. Soc. Lond. B. Biol. Sci.* **1988**, *235*, 121-+.
- 290 Shima, J.; Hesketh, A.; Okamoto, S.; Kawamoto, S.; Ochi, K. *J. Bacteriol.* **1996**, *178*, 7276-7284.
- 291 Ochi, K.; Hu, H.; Hino, M.; Fujie, A.; Muramatsu, H. Google Patents, **2002**.
- 292 Hu, H.; Ochi, K. *Appl. Environ. Microbiol.* **2001**, *67*, 1885-92.
- 293 Parascandolo, J. S.; Havemann, J.; Potter, H. K.; Huang, F.; Riva, E.; Connolly, J.; Wilkening, I.; Song, L.; Leadlay, P. F.; Tosin, M. *Angew. Chem. Int. Ed.* **2016**, *55*, 3463-3467.
- 294 Shakya, G.; Rivera, H., Jr.; Lee, D. J.; Jaremko, M. J.; La Clair, J. J.; Fox, D. T.; Haushalter, R. W.; Schaub, A. J.; Bruegger, J.; Barajas, J. F.; White, A. R.; Kaur, P.; Gwozdzowski, E. R.; Wong, F.; Tsai, S.-C.; Burkart, M. D. *J. Am. Chem. Soc.* **2014**, *136*, 16792-16799.
- 295 Xiang, L.; Kalaitzis, J. A.; Moore, B. S. *Proc. Natl. Acad. Sci. U. S. A.* **2004**, *101*, 15609-15614.
- 296 Apicella, B.; Bruno, A.; Wang, X.; Spinelli, N. *Int. J. Mass spectrom.* **2013**, *338*, 30-38.
- 297 Wallace, W. E.; Guttman, C. M. *J. Res. Natl. Inst. Stand. Technol.* **2002**, *107*, 1-17.
- 298 Sarker, M.; Graham Glen, W.; Yin, L.-B.; Dunn Iii, W. J.; Scott, D. R.; Swanson, S. *Anal. Chim. Acta* **1992**, *257*, 229-238.
- 299 Georgakopoulos, C. G.; Statheropoulos, M. C.; Montaudo, G. *Anal. Chim. Acta* **1998**, *359*, 213-225.
- 300 Stein, S. E. *J. Am. Soc. Mass. Spectrom.* **1999**, *10*, 770-781.
- 301 Nicola, A. J.; Gusev, A. I.; Proctor, A.; Hercules, D. M. *Anal. Chem.* **1998**, *70*, 3213-3219.
- 302 Owens, K. G. *ApSRv* **1992**, *27*, 1-49.
- 303 Kilgour, D. P. A.; Hughes, S.; Kilgour, S. L.; Mackay, C. L.; Palmblad, M.; Tran, B. Q.; Goo, Y. A.; Ernst, R. K.; Clarke, D. J.; Goodlett, D. R. *J. Am. Soc. Mass. Spectrom.* **2017**, *28*, 253-262.
- 304 Worthington, A. S.; Hur, G. H.; Burkart, M. D. *Mol. Biosyst.* **2011**, *7*, 365-370.
- 305 Kosa, N. M.; Pham, K. M.; Burkart, M. D. *Chem. Sci.* **2014**, *5*, 1179-1186.
- 306 Zubarev, R. A.; Zubarev, A. R.; Savitski, M. M. *J. Am. Soc. Mass. Spectrom.* **2008**, *19*, 753-761.
- 307 Zhao, C.; Xie, B.; Chan, S. Y.; Costello, C. E.; O'Connor, P. B. *J. Am. Soc. Mass. Spectrom.* **2008**, *19*, 138-150.
- 308 Chowdhury, S. M.; Munske, G. R.; Tang, X. T.; Bruce, J. E. *Anal. Chem.* **2006**, *78*, 8183-8193.
- 309 Koster, S.; Duursma, M. C.; Boon, J. J.; Heeren, R. M. A.; Ingemann, S.; van Benthem, R.; de Koster, C. G. *J. Am. Soc. Mass. Spectrom.* **2003**, *14*, 332-341.
- 310 Olsen, J. V.; Haselmann, K. F.; Nielsen, M. L.; Budnik, B. A.; Nielsen, P. E.; Zubarev, R. A. *Rapid Commun. Mass Spectrom.* **2001**, *15*, 969-974.
- 311 Kleinnijenhuis, A. J.; Mihalca, R.; Heeren, R. M. A.; Heck, A. J. R. *Int. J. Mass spectrom.* **2006**, *253*, 217-224.
- 312 Liu, H.; Yoo, H. J.; Hakansson, K. *J. Am. Soc. Mass. Spectrom.* **2008**, *19*, 799-808.
- 313 Wills, R. H.; Tosin, M.; O'Connor, P. B. *Anal. Chem.* **2012**, *84*, 8863-8870.
- 314 Kaczorowska, M. A.; Cooper, H. J. *J. Am. Soc. Mass. Spectrom.* **2010**, *21*, 1398-1403.
- 315 Kaczorowska, M. A.; Cooper, H. J. *Chem. Commun.* **2011**, *47*, 418-420.

- 316 Feketeova, L.; Wong, M. W.; O'Hair, R. A. J. *EPJD* **2010**, *60*, 11-20.
- 317 Wei, J.; Bristow, A. W.; McBride, E.; Kilgour, D. P.; O'Connor, P. B. *Anal. Chem.* **2014**.
- 318 Yang, B.; Wu, R. R.; Polfer, N. C.; Berden, G.; Oomens, J.; Rodgers, M. T. *J. Am. Soc. Mass. Spectrom.* **2013**, *24*, 1523-1533.
- 319 Zhou, Z. R.; Ogden, S.; Leary, J. A. *J. Org. Chem.* **1990**, *55*, 5444-5446.
- 320 Zaia, J. *Mass Spectrom. Rev.* **2004**, *23*, 161-227.
- 321 Cancilla, M. T.; Penn, S. G.; Carroll, J. A.; Lebrilla, C. B. *J. Am. Chem. Soc.* **1996**, *118*, 6736-6745.
- 322 Cancilla, M. T.; Wang, A. W.; Voss, L. R.; Lebrilla, C. B. *Anal. Chem.* **1999**, *71*, 3206-3218.
- 323 Pittenauer, E.; Allmaier, G. *J. Am. Soc. Mass. Spectrom.* **2009**, *20*, 1037-1047.
- 324 Denekamp, C.; Claeys, M.; Pocsfalvi, G. *Rapid Commun. Mass Spectrom.* **2000**, *14*, 794-799.
- 325 Sargaeva, N. P.; Lin, C.; O'Connor, P. B. *Anal. Chem.* **2009**, *81*, 9778-9786.
- 326 Mishra, P. K.; Drucekhammer, D. G. *Chem. Rev.* **2000**, *100*, 3283-3309.
- 327 Yu, D.; Xu, F.; Zeng, J.; Zhan, J. *IUBMB Life* **2012**, *64*, 285-295.
- 328 Leonardi, R.; Zhang, Y.-M.; Rock, C. O.; Jackowski, S. *Prog. Lipid Res.* **2005**, *44*, 125-153.
- 329 Hicks, L. M.; Mazur, M.; Miller, L. M.; Dorrestein, P. C.; Schnarr, N. A.; Khosla, C.; Kelleher, N. L. *ChemBioChem* **2006**, *7*, 904-907.
- 330 Meluzzi, D.; Zheng, W. H.; Hensler, M.; Nizet, V.; Dorrestein, P. C. *Bioorg. Med. Chem. Lett.* **2008**, *18*, 3107-3111.
- 331 Caravatti, P.; Allemann, M. *Org. Mass Spectrom.* **1991**, *26*, 514-518.
- 332 Kilgour, D. P. A.; Wills, R.; Qi, Y. L.; O'Connor, P. B. *Anal. Chem.* **2013**, *85*, 3903-3911.
- 333 Wysocki, V. H.; Tsaprailis, G.; Smith, L. L.; Brechi, L. A. *J. Mass Spectrom.* **2000**, *35*, 1399-1406.
- 334 Paizs, B.; Suhai, S. *Mass Spectrom. Rev.* **2005**, *24*, 508-548.
- 335 Senko, M. W.; Speir, J. P.; McLafferty, F. W. *Anal. Chem.* **1994**, *66*, 2801-2808.
- 336 Kaczorowska, M. A.; Cooper, H. J. *J. Am. Soc. Mass. Spectrom.* **2009**, *20*, 674-681.
- 337 Watson, H. M.; Vincent, J. B.; Cassidy, C. J. *J. Mass Spectrom.* **2011**, *46*, 1099-1107.
- 338 Tomlinson, M. J.; Scott, J. R.; Wilkins, C. L.; Wright, J. B.; White, W. E. *J. Mass Spectrom.* **1999**, *34*, 958-68.
- 339 Farazi, T. A.; Waksman, G.; Gordon, J. I. *J. Biol. Chem.* **2001**, *276*, 39501-39504.
- 340 WO2014043561-A1.
- 341 Brindle, N. P.; Zammit, V. A.; Pogson, C. I. *Biochem. J* **1985**, *232*, 177-182.

10. Appendices

Please see attached CD for full appendix.

Appendices

Appendix 1 The effect of delayed addition of active NAC probe 66 to the actinorhodin minimal system on the production of SEK4 41 and SEK4b 42	1
Appendix 2 FTICR-MS analysis of active acyl carrier protein (ACP) probe 64 incubated in the actinorhodin minimal system (1:1 ratio, protected ACP probe 63 to malonyl-ACP 7) showing an off-loaded putative diketide 145	2
Appendix 3 FTICR-MS analysis of active ACP probe 64 incubated in the actinorhodin minimal system (1:1 ratio, protected ACP probe 63 to malonyl-ACP 7) showing an off-loaded putative diketide 145	3
Appendix 4 FTICR-MS analysis of active ACP probe 64 incubated in the actinorhodin minimal system (1:1 ratio, protected ACP probe 63 to malonyl-ACP 7) showing an off-loaded putative diketide 145	4
Appendix 5 FTICR-MS analysis of active ACP probe 64 incubated in the actinorhodin minimal system (1:1 ratio, protected ACP probe 63 to malonyl-ACP 7) showing an off-loaded putative diketide 145	5
Appendix 6 FTICR-MS analysis of active ACP probe 64 incubated in the actinorhodin minimal system (1:1 ratio, protected ACP probe 63 to malonyl-ACP 7) showing an off-loaded putative diketide 145	6
Appendix 7 FTICR-MS analysis of active ACP probe 64 incubated in the actinorhodin minimal system (1:4 ratio, protected ACP probe 63 to malonyl-ACP 7) showing an off-loaded putative diketide 145	7
Appendix 8 FTICR-MS analysis of active ACP probe 64 incubated in the actinorhodin minimal system (1:4 ratio, protected ACP probe 63 to malonyl-ACP 7) showing an off-loaded putative diketide 145	8
Appendix 9 FTICR-MS analysis of active ACP probe 64 incubated in the actinorhodin minimal system (1:4 ratio, protected ACP probe 63 to malonyl-ACP 7) showing an off-loaded putative diketide 145	9
Appendix 10 FTICR-MS analysis of active ACP probe 64 incubated in the actinorhodin minimal system (1:4 ratio, protected ACP probe 63 to malonyl-ACP 7) showing an off-loaded putative diketide 145	10
Appendix 11 FTICR-MS analysis of active ACP probe 64 incubated in the actinorhodin minimal system (1:1 ratio, protected ACP probe 63 to labelled malonyl-ACP 7b) showing an off-loaded putative labelled tetraketide 147	11

Appendix 12	FTICR-MS analysis of active ACP probe 64 incubated in the actinorhodin minimal system (1:1 ratio, protected ACP probe 63 to labelled malonyl-ACP 7b) showing an off-loaded putative labelled tetraketide 147	12
Appendix 13	FTICR-MS analysis of active ACP probe 64 incubated in the actinorhodin minimal system (1:1 ratio, protected ACP probe 63 to labelled malonyl-ACP 7b) showing an off-loaded putative labelled tetraketide 147 at a charge state of 7 ⁺	13
Appendix 14	FTICR-MS analysis of active ACP probe 64 incubated in the actinorhodin minimal system (1:10 ratio, protected ACP probe 63 to labelled malonyl-ACP 7b) showing an off-loaded putative labelled tetraketide 147	14
Appendix 15	FTICR-MS analysis of active ACP probe 64 incubated in the actinorhodin minimal system (1:10 ratio, protected ACP probe 63 to labelled malonyl-ACP 7b) showing an off-loaded putative labelled tetraketide 147	15
Appendix 16	FTICR-MS analysis of active ACP probe 64 incubated in the actinorhodin minimal system (1:10 ratio, protected ACP probe 63 to labelled malonyl-ACP 7b) showing an off-loaded putative labelled tetraketide 147	16
Appendix 17	FTICR-MS analysis of active ACP probe 64 incubated in the actinorhodin minimal system (1:10 ratio, protected ACP probe 63 to labelled malonyl-ACP 7b) showing an off-loaded putative labelled tetraketide 147	17
Appendix 18	FTICR-MS analysis of active ACP probe 64 incubated in the actinorhodin minimal system (1:10 ratio, protected ACP probe 63 to labelled malonyl-ACP 7b) showing an off-loaded putative labelled tetraketide 147	18
Appendix 19	FTICR-MS analysis of active ACP probe 64 incubated in the actinorhodin minimal system (1:4 ratio, protected ACP probe 63 to labelled malonyl-ACP 7b) showing an off-loaded putative labelled linear pentaketide 148	19
Appendix 20	FTICR-MS analysis of active ACP probe 64 incubated in the actinorhodin minimal system (5:1 ratio, protected ACP probe 63 to malonyl-ACP 7) showing an off-loaded putative cyclised pentaketide 154	20
Appendix 21	FTICR-MS analysis of active ACP probe 64 incubated in the actinorhodin minimal system (5:1 ratio, protected ACP probe 63 to malonyl-ACP 7) showing an off-loaded putative cyclised pentaketide 154	21
Appendix 22	FTICR-MS analysis of active ACP probe 64 incubated in the actinorhodin minimal system (5:1 ratio, protected ACP probe 63 to malonyl-ACP 7) showing an off-loaded putative cyclised pentaketide 154	22

Appendix 23	FTICR-MS analysis of active ACP probe 64 incubated in the actinorhodin minimal system (5:1 ratio, protected ACP probe 63 to labelled malonyl-ACP 7b) showing an off-loaded putative cyclised dehydrated pentaketide 155	23
Appendix 24	FTICR-MS analysis of active ACP probe 64 incubated in the actinorhodin minimal system (5:1 ratio, protected ACP probe 63 to labelled malonyl-ACP 7b) showing an off-loaded putative cyclised dehydrated pentaketide 155	24
Appendix 25	FTICR-MS analysis of active ACP probe 64 incubated in the actinorhodin minimal system (5:1 ratio, protected ACP probe 63 to labelled malonyl-ACP 7b) showing an off-loaded putative cyclised dehydrated pentaketide 155	25
Appendix 26	FTICR-MS analysis of active ACP probe 64 incubated in the actinorhodin minimal system (5:1 ratio, protected ACP probe 63 to labelled malonyl-ACP 7b) showing an off-loaded putative cyclised dehydrated pentaketide 155	26
Appendix 27	FTICR-MS analysis of active ACP probe 64 incubated in the actinorhodin minimal system (1:4 ratio, protected ACP probe 63 to malonyl-ACP 7b) showing an off-loaded putative linear hexaketide 149	27
Appendix 28	FTICR-MS analysis of active ACP probe 64 incubated in the actinorhodin minimal system (1:4 ratio, protected ACP probe 63 to malonyl-ACP 7b) showing an off-loaded putative labelled tetraketide 147 at a charge state of 6 ⁺	28
Appendix 29	FTICR-MS analysis of active ACP probe 64 incubated in the actinorhodin minimal system (1:4 ratio, protected ACP probe 63 to malonyl-ACP 7) showing an off-loaded putative linear hexaketide 149	29
Appendix 30	FTICR-MS analysis of active ACP probe 64 incubated in the actinorhodin minimal system (1:4 ratio, protected ACP probe 63 to malonyl-ACP 7) showing an off-loaded putative linear hexaketide 149	30
Appendix 31	FTICR-MS analysis of active ACP probe 64 incubated in the actinorhodin minimal system (1:4 ratio, protected ACP probe 63 to malonyl-ACP 7) showing an off-loaded putative linear hexaketide 149 at a charge state of 8 ⁺	31
Appendix 32	FTICR-MS analysis of active ACP probe 64 incubated in the actinorhodin minimal system (1:4 ratio, protected ACP probe 63 to malonyl-ACP 7) showing an off-loaded putative cyclised hexaketide 156	32
Appendix 33	FTICR-MS analysis of active ACP probe 64 incubated in the actinorhodin minimal system (1:4 ratio, protected ACP probe 63 to malonyl-ACP 7) showing an off-loaded putative cyclised hexaketide 156 at a charge state of 8 ⁺	33

Appendix 34	FTICR-MS analysis of active ACP probe 64 incubated in the actinorhodin minimal system (1:4 ratio, protected ACP probe 63 to malonyl-ACP 7 , repeat) showing an off-loaded putative cyclised hexaketide 156	34
Appendix 35	FTICR-MS analysis of active ACP probe 64 incubated in the actinorhodin minimal system (1:4 ratio, protected ACP probe 63 to malonyl-ACP 7 , repeat) showing an off-loaded putative cyclised hexaketide 156	35
Appendix 36	FTICR-MS analysis of active ACP probe 64 incubated in the actinorhodin minimal system (1:4 ratio, protected ACP probe 63 to malonyl-ACP 7 , repeat) showing an off-loaded putative cyclised hexaketide 156 at a charge state of 8 ⁺	36
Appendix 37	FTICR-MS analysis of active ACP probe 64 incubated in the actinorhodin minimal system (5:1 ratio, protected ACP probe 63 to malonyl-ACP 7) showing an off-loaded putative cyclised hexaketide 156	37
Appendix 38	FTICR-MS analysis of active ACP probe 64 incubated in the actinorhodin minimal system (5:1 ratio, protected ACP probe 63 to malonyl-ACP 7) showing an off-loaded putative cyclised hexaketide 156	38
Appendix 39	FTICR-MS analysis of active ACP probe 64 incubated in the actinorhodin minimal system (1:1 ratio, protected ACP probe 63 to malonyl-ACP 7) showing an off-loaded putative cyclised dehydrated hexaketide 157	39
Appendix 40	FTICR-MS analysis of active ACP probe 64 incubated in the actinorhodin minimal system (1:1 ratio, protected ACP probe 63 to malonyl-ACP 7) showing an off-loaded putative cyclised dehydrated hexaketide 157	40
Appendix 41	FTICR-MS analysis of active ACP probe 64 incubated in the actinorhodin minimal system (1:1 ratio, protected ACP probe 63 to malonyl-ACP 7 , repeat) showing an off-loaded putative cyclised dehydrated hexaketide 157	41
Appendix 42	FTICR-MS analysis of active ACP probe 64 incubated in the actinorhodin minimal system (1:1 ratio, protected ACP probe 63 to malonyl-ACP 7 , repeat) showing an off-loaded putative cyclised dehydrated hexaketide 157 at a charge state of 6 ⁺	42
Appendix 43	FTICR-MS analysis of active ACP probe 64 incubated in the actinorhodin minimal system (1:1 ratio, protected ACP probe 63 to malonyl-ACP 7 , repeat) showing an off-loaded putative cyclised dehydrated hexaketide 157	43

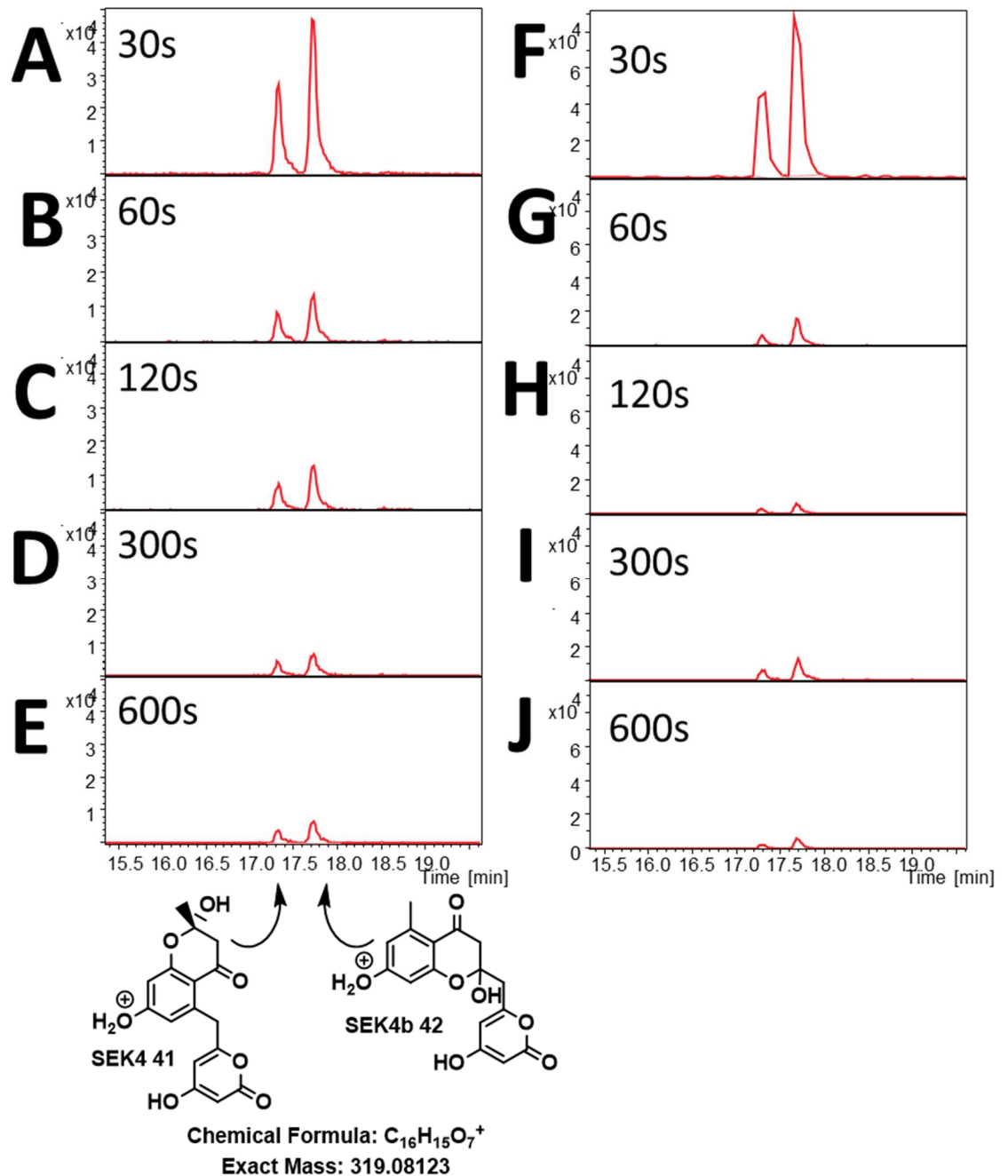
Appendix 44	FTICR-MS analysis of active ACP probe 64 incubated in the actinorhodin minimal system (1:1 ratio, protected ACP probe 63 to malonyl-ACP 7 , repeat) showing an off-loaded putative cyclised dehydrated hexaketide 157	44
Appendix 45	FTICR-MS analysis of active ACP probe 64 incubated in the actinorhodin minimal system (1:4 ratio, protected ACP probe 63 to malonyl-ACP 7) showing an off-loaded putative cyclised dehydrated hexaketide 157	45
Appendix 46	FTICR-MS analysis of active ACP probe 64 incubated in the actinorhodin minimal system (1:4 ratio, protected ACP probe 63 to malonyl-ACP 7) showing an off-loaded putative cyclised dehydrated hexaketide 157	46
Appendix 47	FTICR-MS analysis of active acyl carrier protein (ACP) probe 64 incubated in the actinorhodin minimal system (1:1 ratio, protected ACP probe 63 to malonyl-ACP 7 , probe added after 30 seconds) showing an off-loaded putative cyclised dehydrated hexaketide 157	47
Appendix 48	FTICR-MS analysis of active ACP probe 64 incubated in the actinorhodin minimal system (1:1 ratio, protected ACP probe 63 to malonyl-ACP 7 , probe added after 30 seconds) showing an off-loaded putative cyclised dehydrated hexaketide 157	48
Appendix 49	FTICR-MS analysis of active ACP probe 64 incubated in the actinorhodin minimal system (1:1 ratio, protected ACP probe 63 to malonyl-ACP 7 , probe added after five minutes) showing an off-loaded putative cyclised dehydrated hexaketide 157	49
Appendix 50	FTICR-MS analysis of active ACP probe 64 incubated in the actinorhodin minimal system (1:1 ratio, protected ACP probe 63 to malonyl-ACP 7 , probe added after five minutes) showing an off-loaded putative cyclised dehydrated hexaketide 157	50
Appendix 51	FTICR-MS analysis of the ACP probe 63 (A) with irradiation but without the actinorhodin minimal system, (B) without irradiation and incubated in the actinorhodin minimal system (1:1 ratio, protected ACP probe 63 to malonyl-ACP 7), (C) without irradiation and without the actinorhodin minimal system. (D) Simulated mass spectrum (7^+) of an off-loaded putative diketide 145	51
Appendix 52	FTICR-MS analysis of the ACP probe 63 (A) with irradiation but without the actinorhodin minimal system, (B) without irradiation and incubated in the actinorhodin minimal system (1:1 ratio, protected ACP probe 63 to malonyl-ACP 7),	

(C) without irradiation and without the actinorhodin minimal system. (D) Simulated mass spectrum (7^+) of an off-loaded putative labelled linear tetraketide 147	52
Appendix 53 FTICR-MS analysis of the ACP probe 63 (A) with irradiation but without the actinorhodin minimal system, (B) without irradiation and incubated in the actinorhodin minimal system (1:1 ratio, protected ACP probe 63 to malonyl-ACP 7), (C) without irradiation and without the actinorhodin minimal system. (D) Simulated mass spectrum (7^+) of an off-loaded putative labelled linear pentaketide 148	53
Appendix 54 FTICR-MS analysis of the ACP probe 63 (A) with irradiation but without the actinorhodin minimal system, (B) without irradiation and incubated in the actinorhodin minimal system (1:1 ratio, protected ACP probe 63 to malonyl-ACP 7), (C) without irradiation and without the actinorhodin minimal system. (D) Simulated mass spectrum (7^+) of an off-loaded putative cyclised pentaketide 154	54
Appendix 55 FTICR-MS analysis of the ACP probe 63 (A) with irradiation but without the actinorhodin minimal system, (B) without irradiation and incubated in the actinorhodin minimal system (1:1 ratio, protected ACP probe 63 to malonyl-ACP 7), (C) without irradiation and without the actinorhodin minimal system. (D) Simulated mass spectrum (7^+) of an off-loaded putative labelled cyclised dehydrated pentaketide 155	55
Appendix 56 FTICR-MS analysis of the ACP probe 63 (A) with irradiation but without the actinorhodin minimal system, (B) without irradiation and incubated in the actinorhodin minimal system (1:1 ratio, protected ACP probe 63 to malonyl-ACP 7), (C) without irradiation and without the actinorhodin minimal system. (D) Simulated mass spectrum (7^+) of an off-loaded putative linear hexaketide 149	56
Appendix 57 FTICR-MS analysis of the ACP probe 63 (A) with irradiation but without the actinorhodin minimal system, (B) without irradiation and incubated in the actinorhodin minimal system (1:1 ratio, protected ACP probe 63 to malonyl-ACP 7), (C) without irradiation and without the actinorhodin minimal system. (D) Simulated mass spectrum (7^+) of an off-loaded putative cyclised hexaketide 156	57
Appendix 58 FTICR-MS analysis of the ACP probe 63 (A) with irradiation but without the actinorhodin minimal system, (B) without irradiation and incubated in the actinorhodin minimal system (1:1 ratio, protected ACP probe 63 to malonyl-ACP 7), (C) without irradiation and without the actinorhodin minimal system. (D) Simulated mass spectrum (7^+) of an off-loaded putative cyclised dehydrated hexaketide 157 ..	58

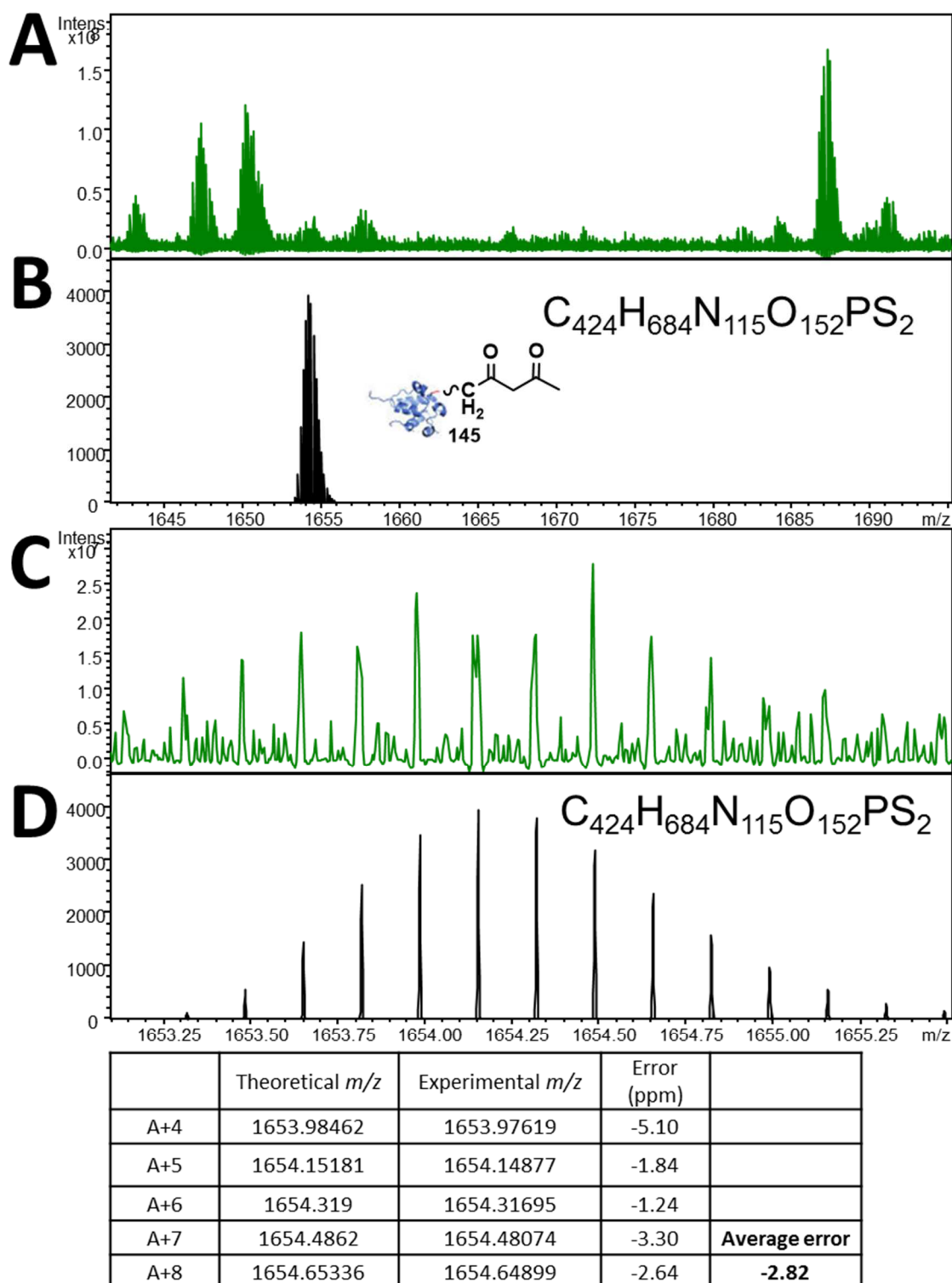
Appendix 59 Peak list - FTICR-MS analysis of active ACP probe 64 incubated in the actinorhodin minimal system (1:1 ratio, protected ACP probe 63 to malonyl-ACP 7) showing an off-loaded putative cyclised dehydrated hexaketide 157.....	59
Appendix 60 Peak list – Repeated FTICR-MS analysis of active ACP probe 64 incubated in the actinorhodin minimal system (1:1 ratio, protected ACP probe 63 to malonyl-ACP 7) showing off-loaded putative diketide 145 and cyclised dehydrated hexaketide 157.	62
Appendix 61 Peak list – FTICR-MS analysis of active ACP probe 64 incubated in the actinorhodin minimal system (1:4 ratio, protected ACP probe 63 to malonyl-ACP 7) showing off-loaded putative linear hexaketide 149 and cyclised hexaketide 156. 64	
Appendix 62 Peak list – Repeated FTICR-MS analysis of active ACP probe 64 incubated in the actinorhodin minimal system (1:4 ratio, protected ACP probe 63 to malonyl-ACP 7) showing off-loaded putative diketide 145, cyclised hexaketide 156 and cyclised dehydrated hexaketide 157.....	66
Appendix 63 Peak list – FTICR-MS analysis of active ACP probe 64 incubated in the actinorhodin minimal system (5:1 ratio, protected ACP probe 63 to malonyl-ACP 7) showing off-loaded putative cyclised pentaketide 154 and cyclised hexaketide 156	68
Appendix 64 Peak list – FTICR-MS analysis of active ACP probe 64 incubated in the actinorhodin minimal system (1:1 ratio, protected ACP probe 63 to malonyl-ACP 7 with 30 seconds delay upon addition of the ACP probe 64) showing an off-loaded putative cyclised dehydrated hexaketide 157.....	69
Appendix 65 Peak list – FTICR-MS analysis of active ACP probe 64 incubated in the actinorhodin minimal system (1:1 ratio, protected ACP probe 63 to malonyl-ACP 7 with 30 seconds delay upon addition of the ACP probe 64) showing an off-loaded putative cyclised dehydrated hexaketide 157.....	70
Appendix 66 Peak list – FTICR-MS analysis of active ACP probe 64 incubated in the actinorhodin minimal system (1:1 ratio, protected ACP probe 63 to ¹³ C-malonyl-ACP 7b) showing an off-loaded putative ¹³ C-labelled tetraketide 147	71
Appendix 67 Peak list – FTICR-MS analysis of active ACP probe 64 incubated in the actinorhodin minimal system (1:10 ratio, protected ACP probe 63 to ¹³ C-malonyl-ACP 7b) showing an off-loaded putative ¹³ C-labelled tetraketide 147	73
Appendix 68 Peak list – FTICR-MS analysis of active ACP probe 64 incubated in the actinorhodin minimal system (1:5 ratio, protected ACP probe 63 to ¹³ C-malonyl-	

ACP 7b) showing an off-loaded putative ¹³ C-labelled cyclised dehydrated pentaketide 155	75
Appendix 69 Peak list – FTICR-MS analysis of active ACP probe 64 incubated in the actinorhodin minimal system (1:4 ratio, protected ACP probe 63 to ¹³ C-malonyl-ACP 7b , step-wise addition) showing an off-loaded putative ¹³ C-labelled linear pentaketide 148	76
Appendix 70 Peak list – FTICR-MS electron induced dissociation (EID) or collisionally activated dissociation (CAD) of the nonhydrolysable photolabile carba(dethia) pantetheine 81 with sodium, lithium or caesium adduction.....	86
Appendix 71 Cleavage coverage maps showing b and y ions resulting from collisionally activated dissociation (35V and 25V) of acetyl-ACP 40 with (A, red) and without (B, blue) lithium adduction.	87
Appendix 72 Cleavage coverage maps showing b and y ions resulting from collisionally activated dissociation (40V and 35V) of malonyl-ACP 7 with lithium (A, red), with caesium (C, green) and without alkali (B, blue) adduction.	87
Appendix 73 Cleavage coverage maps showing b and y ions resulting from collisionally activated dissociation (40V and 30V) of acetoacetyl-ACP 167 with lithium (A, red), with caesium (C, green) and without alkali (B, blue) adduction. .	88
Appendix 74 Cleavage coverage maps showing b and y ions resulting from collisionally activated dissociation (35V and 25V) of myristoyl-ACP 168 with (A, red) and without (B, blue) lithium adduction.	88
Appendix 75 Cleavage coverage maps showing b and y ions resulting from collisionally activated dissociation (30V, 28V and 18V) of nonhydrolysable photolabile malonyl carba(dethia) ACP analogue 63 with lithium (A, red), with caesium (C, green) and without alkali (B, blue) adduction.....	89
Appendix 76 Cleavage coverage maps only showing phosphorylated b and y ions resulting from collisionally activated dissociation (35V and 25V) of acetyl-ACP 40 with (A, red) and without (B, blue) lithium adduction..	89
Appendix 77 Cleavage coverage maps only showing phosphorylated b and y ions resulting from collisionally activated dissociation (40V and 35V) of malonyl-ACP 7 with lithium (A, red), with caesium (C, green) (Note: none detected) and without alkali (B, blue) adduction.	90
Appendix 78 Cleavage coverage maps only showing phosphorylated b and y ions resulting from collisionally activated dissociation (40V and 30V) of acetoacetyl-ACP	

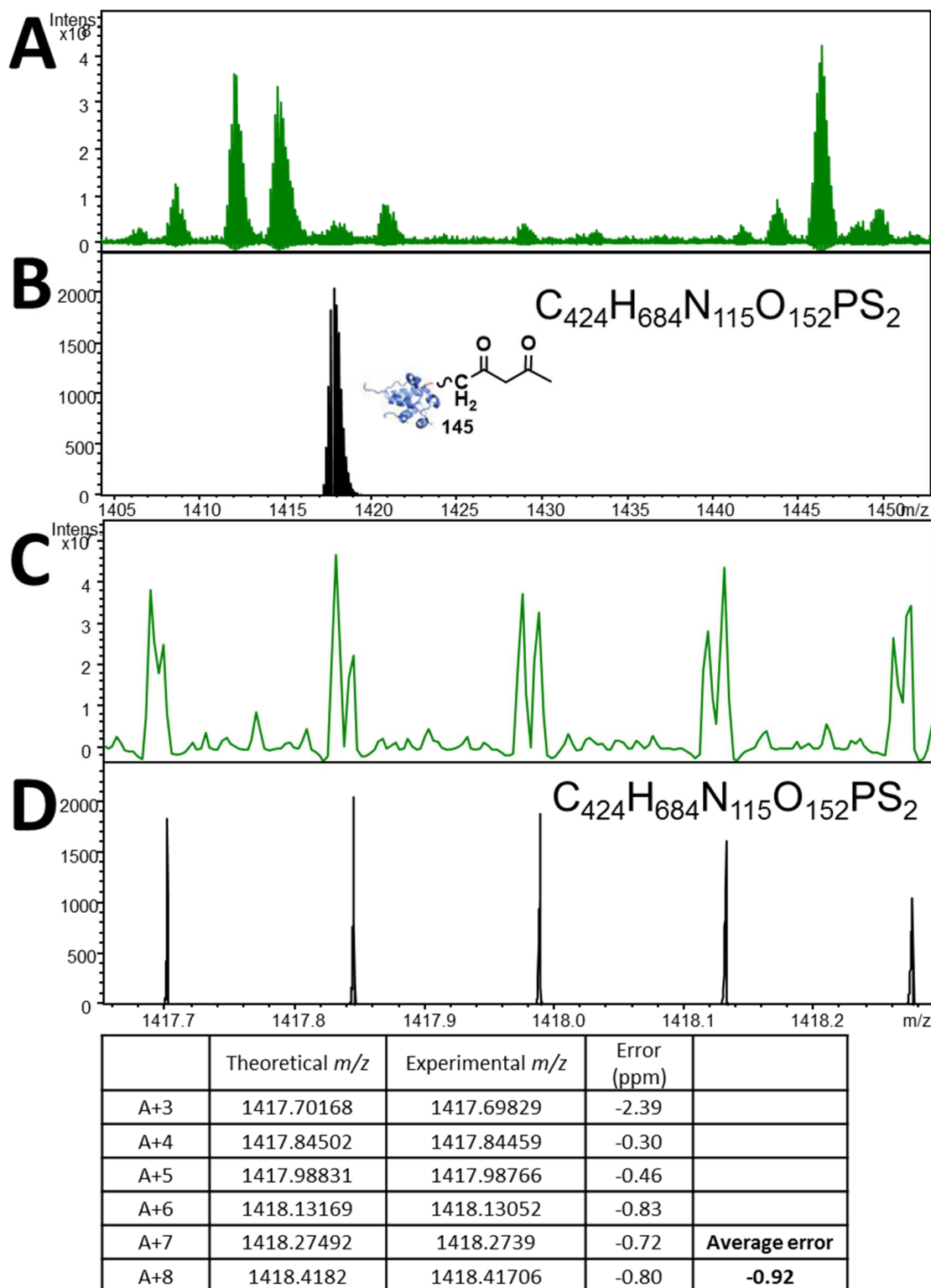
167 with lithium (A, red), with caesium (C, green) and without alkali (B, blue) adduction.	90
Appendix 79 Cleavage coverage maps only showing phosphorylated b and y ions resulting from collisionally activated dissociation (35V and 25V) of myristoyl-ACP 168 with (A, red) and without (B, blue) lithium adduction.	91
Appendix 80 Cleavage coverage maps only showing phosphorylated b and y ions resulting from collisionally activated dissociation (30V, 28V and 18V) of nonhydrolysable photolabile malonyl carba(dethia) ACP analogue 63 with lithium (A, red), with caesium (C, green) (Note: none detected) and without alkali (B, blue) adduction.	91
Appendix 81 Cleavage coverage maps only showing ‘b’ and ‘y’ ions with the acetyl-phosphopantetheinyl arm bound, resulting from collisionally activated dissociation (35V and 25V) of acetyl-ACP 40 with (A, red) and without (B, blue) lithium adduction.	92
Appendix 82 Cleavage coverage maps only showing ‘b’ and ‘y’ ions with the nonhydrolysable photolabile malonyl carba(dethia)-phosphopantetheinyl arm bound, resulting from collisionally activated dissociation (30V, 28V and 18V) of nonhydrolysable photolabile malonyl carba(dethia) ACP analogue 63 with lithium (A, red), with caesium (C, green) (Note: none detected) and without alkali (B, blue) adduction.	92



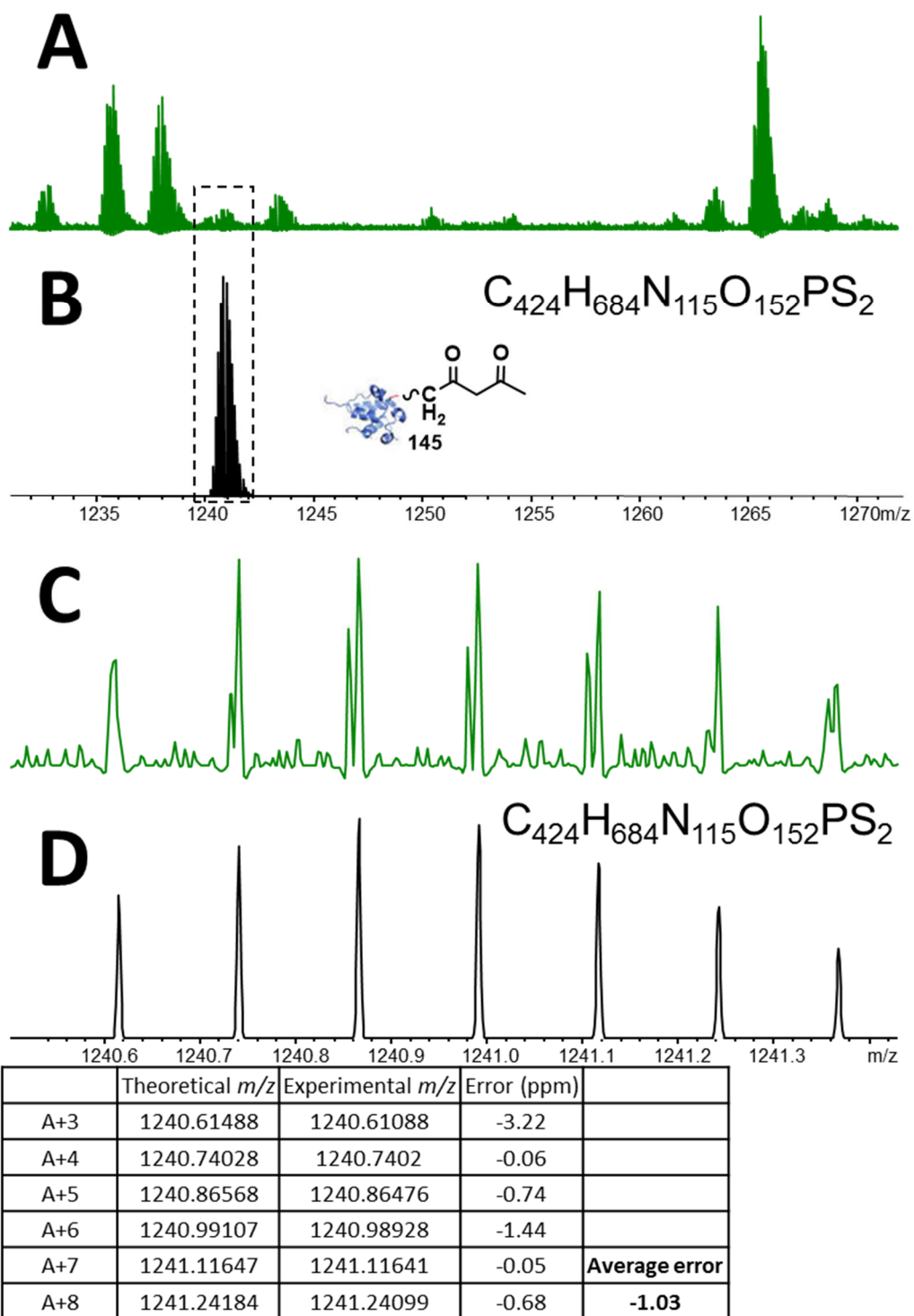
Appendix 1 The effect of delayed addition of active NAC probe **66** to the actinorhodin minimal system on the production of SEK4 **41** and SEK4b **42**. The actinorhodin minimal system was activated by the addition of final enzyme, holo-ACP **43**, then 30 (A and F), 60 (B and G), 120 (C and H), 300 (D and I) and 600 (E and J) seconds later active probe **66**, irradiated for 4 hours in the home built UVA light source, was added. Following incubation overnight at room temperature, EtOAc extracts were analysed by UPLC-MS. The addition of active NAC probe **66** at time point 0 seconds was not feasible by hand. F to J are repeats of A to E.



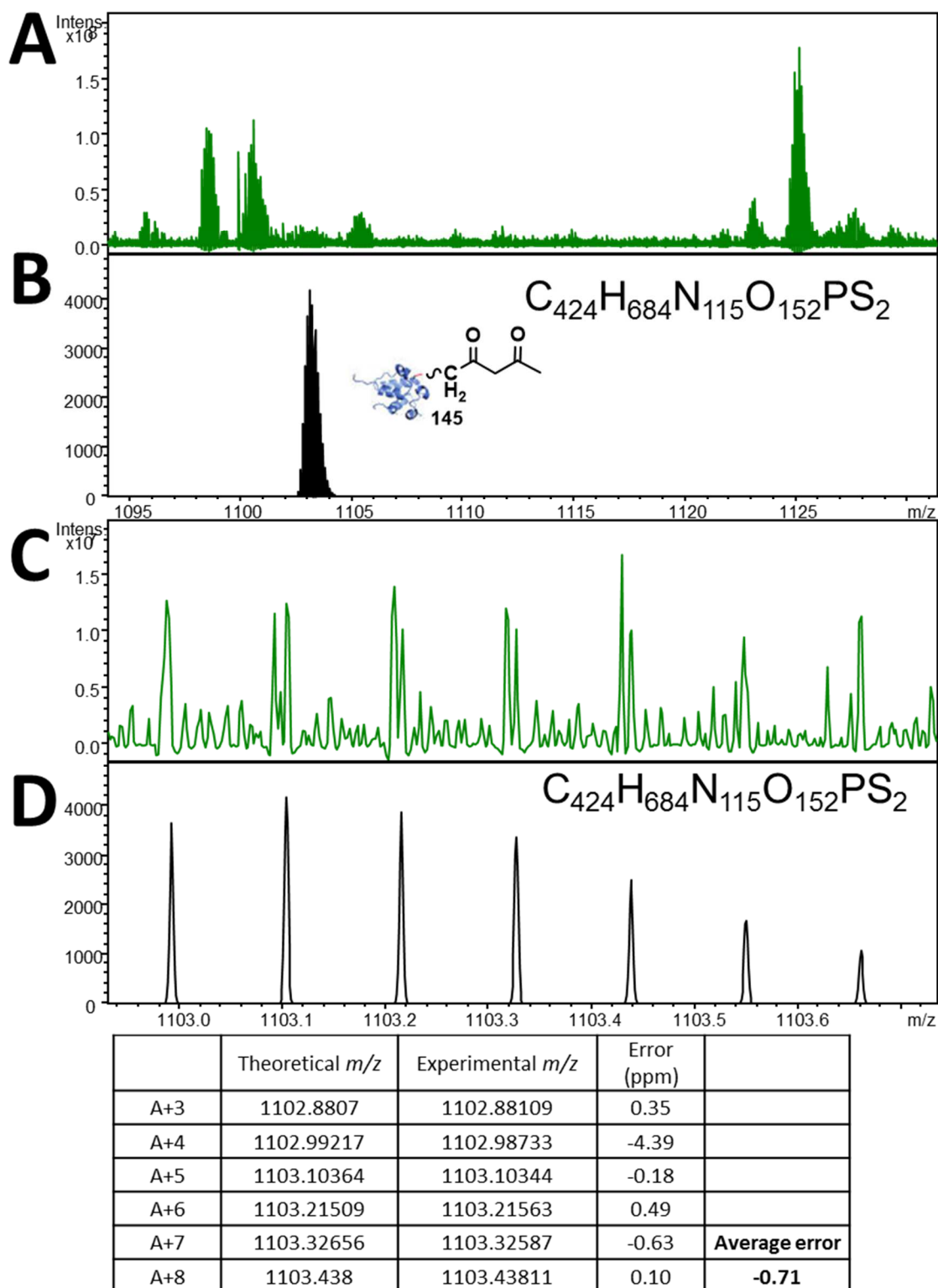
Appendix 2 FTICR-MS analysis of active acyl carrier protein (ACP) probe 64 incubated in the actinorhodin minimal system (1:1 ratio, protected ACP probe 63 to malonyl-ACP 7) showing an off-loaded putative diketide 145. (A) Acquired spectrum, (C) acquired spectrum magnified, (B) and (D) are simulated mass spectra (6^+) of 145. Underneath displays the peak list and errors for each.



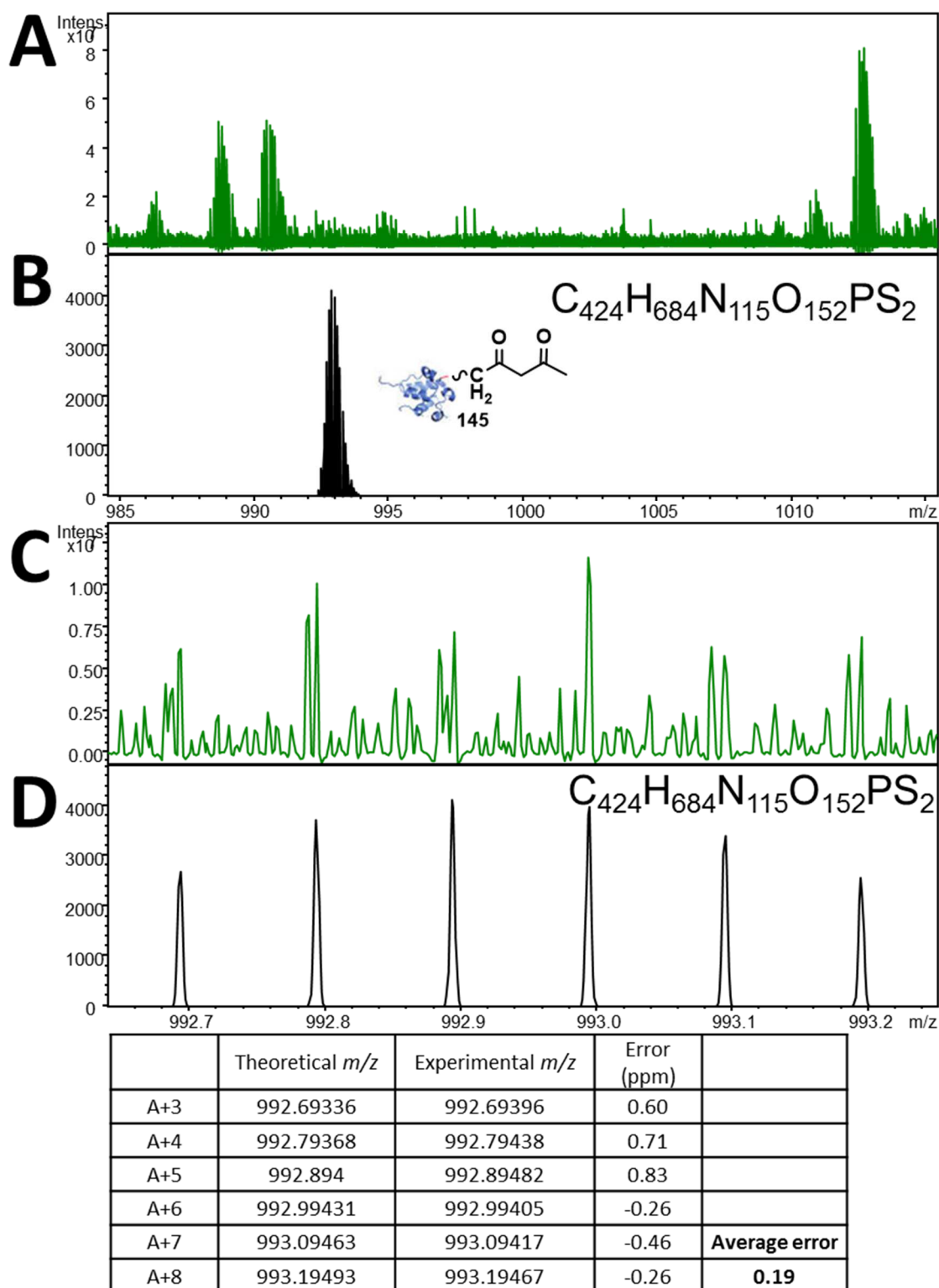
Appendix 3 FTICR-MS analysis of active ACP probe **64** incubated in the actinorhodin minimal system (1:1 ratio, protected ACP probe **63** to malonyl-ACP **7**) showing an off-loaded putative diketide **145**. (A) Acquired spectrum, (C) acquired spectrum magnified, (B) and (D) are simulated mass spectra (7^+). Underneath displays the peak list and errors for each.



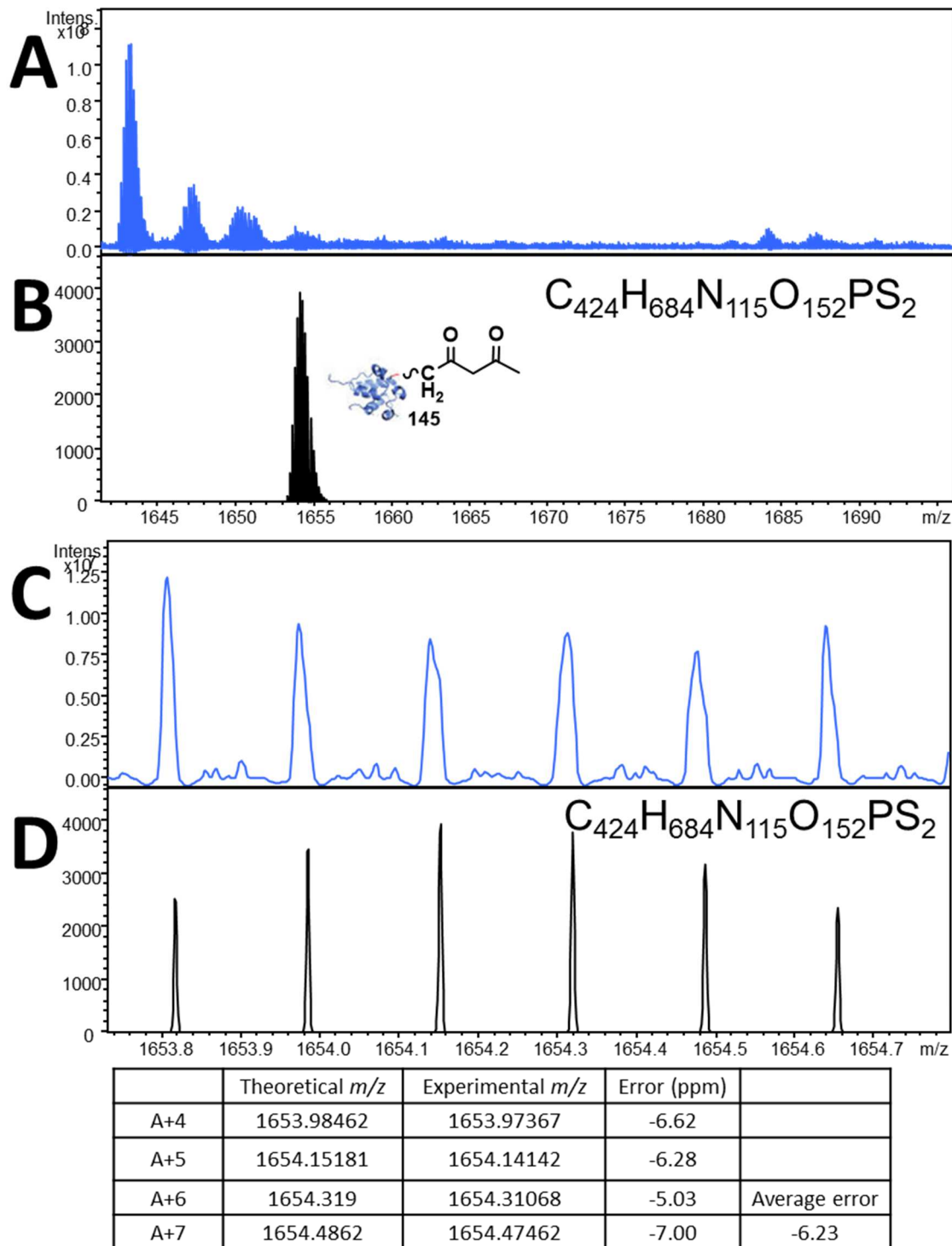
Appendix 4 FTICR-MS analysis of active ACP probe **64** incubated in the actinorhodin minimal system (1:1 ratio, protected ACP probe **63** to malonyl-ACP **7**) showing an off-loaded putative diketide **145**. (A) Acquired spectrum, (C) acquired spectrum magnified, (B) and (D) are simulated mass spectra (8^+). Underneath displays the peak list and errors for each.



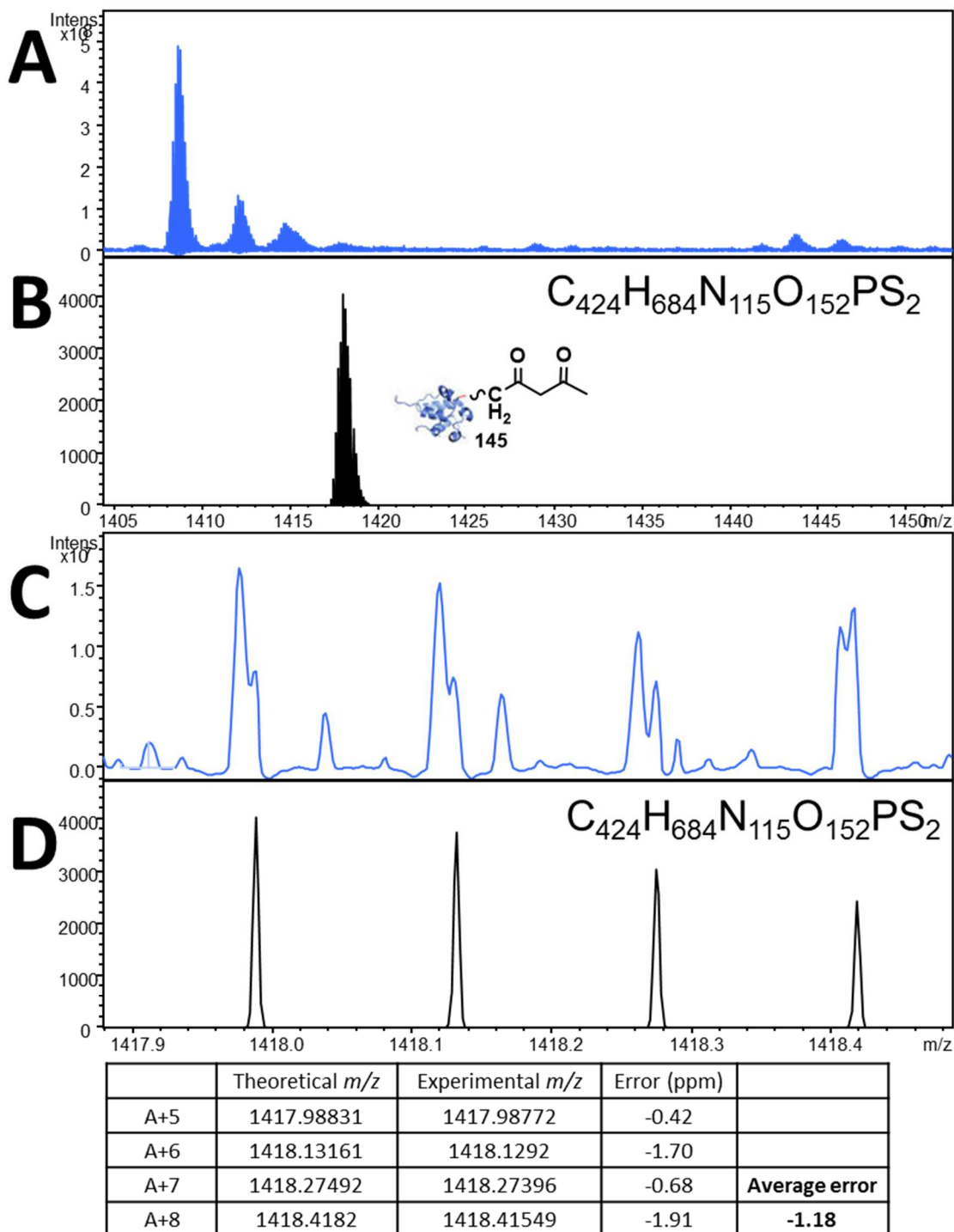
Appendix 5 FTICR-MS analysis of active ACP probe **64** incubated in the actinorhodin minimal system (1:1 ratio, protected ACP probe **63** to malonyl-ACP **7**) showing an off-loaded putative diketide **145**. (A) Acquired spectrum, (C) acquired spectrum magnified, (B) and (D) are simulated mass spectra (9^+). Underneath displays the peak list and errors for each.



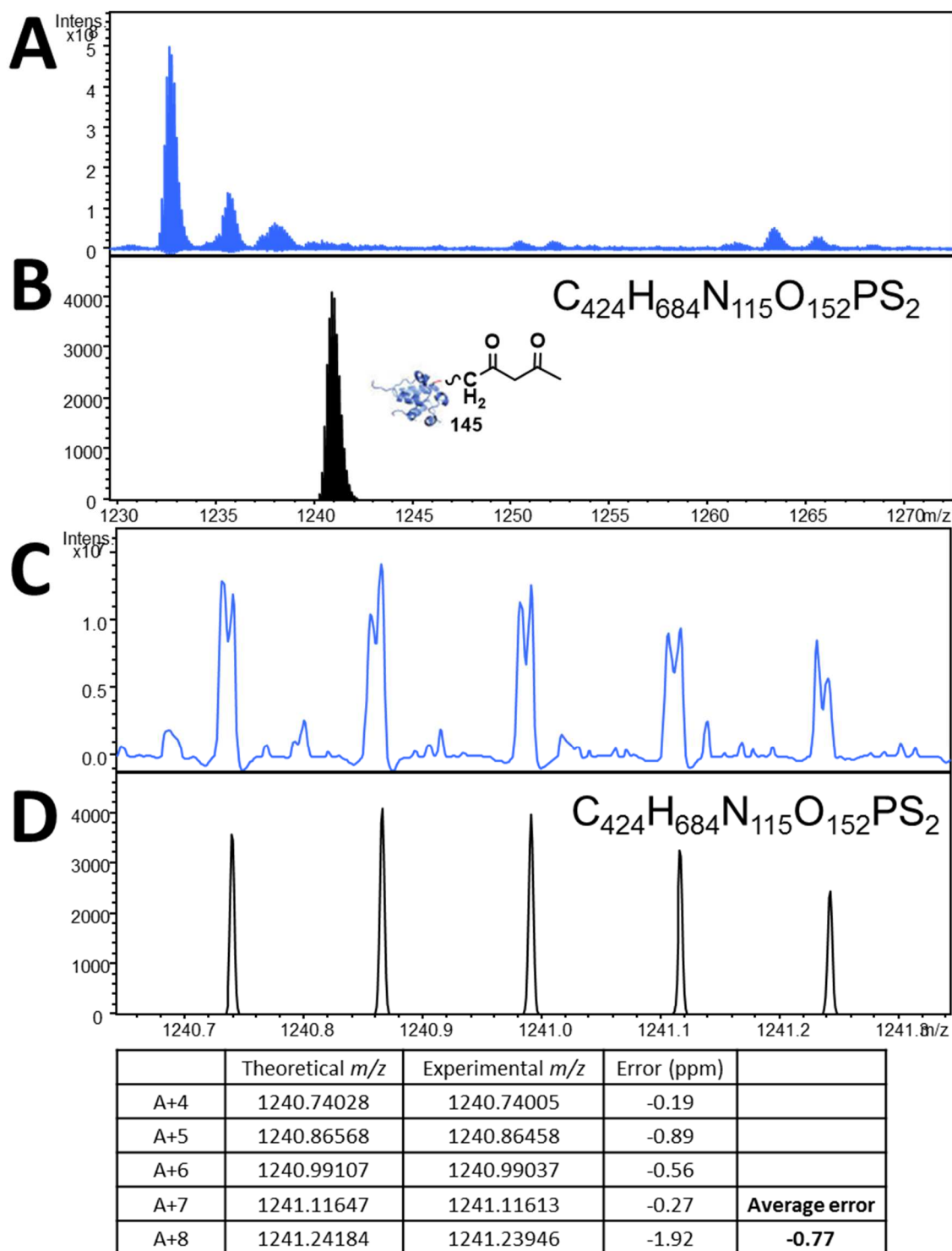
Appendix 6 FTICR-MS analysis of active ACP probe **64** incubated in the actinorhodin minimal system (1:1 ratio, protected ACP probe **63** to malonyl-ACP **7**) showing an off-loaded putative diketide **145**. (A) Acquired spectrum, (C) acquired spectrum magnified, (B) and (D) are simulated mass spectra (10^+). Underneath displays the peak list and errors for each.



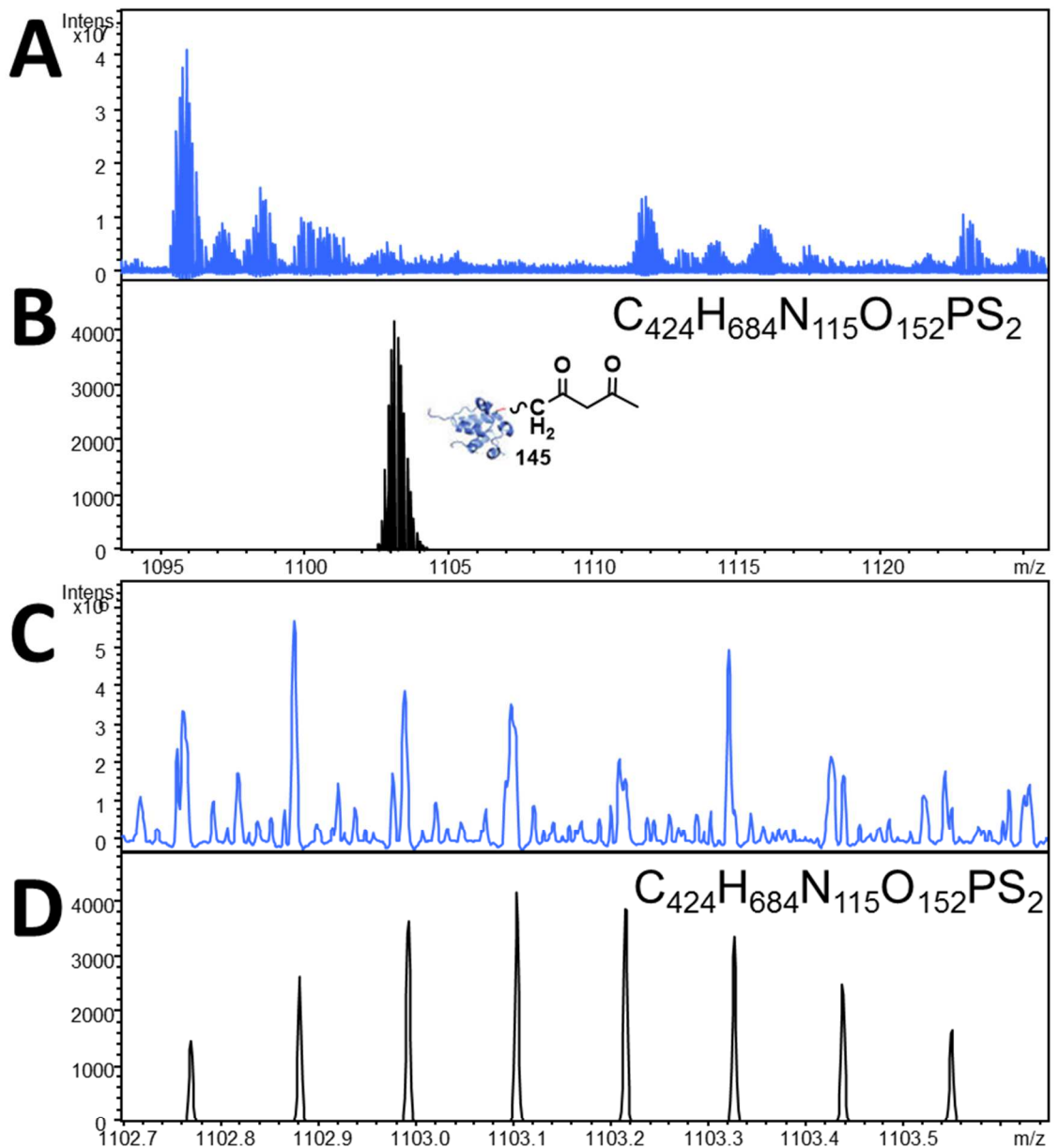
Appendix 7 FTICR-MS analysis of active ACP probe 64 incubated in the actinorhodin minimal system (1:4 ratio, protected ACP probe 63 to malonyl-ACP 7) showing an off-loaded putative diketide 145. (A) Acquired spectrum, (C) acquired spectrum magnified, (B) and (D) are simulated mass spectra (6^+). Underneath displays the peak list and errors for each.



Appendix 8 FTICR-MS analysis of active ACP probe **64** incubated in the actinorhodin minimal system (1:4 ratio, protected ACP probe **63** to malonyl-ACP **7**) showing an off-loaded putative diketide **145**. (A) Acquired spectrum, (C) acquired spectrum magnified, (B) and (D) are simulated mass spectra (7^+). Underneath displays the peak list and errors for each.

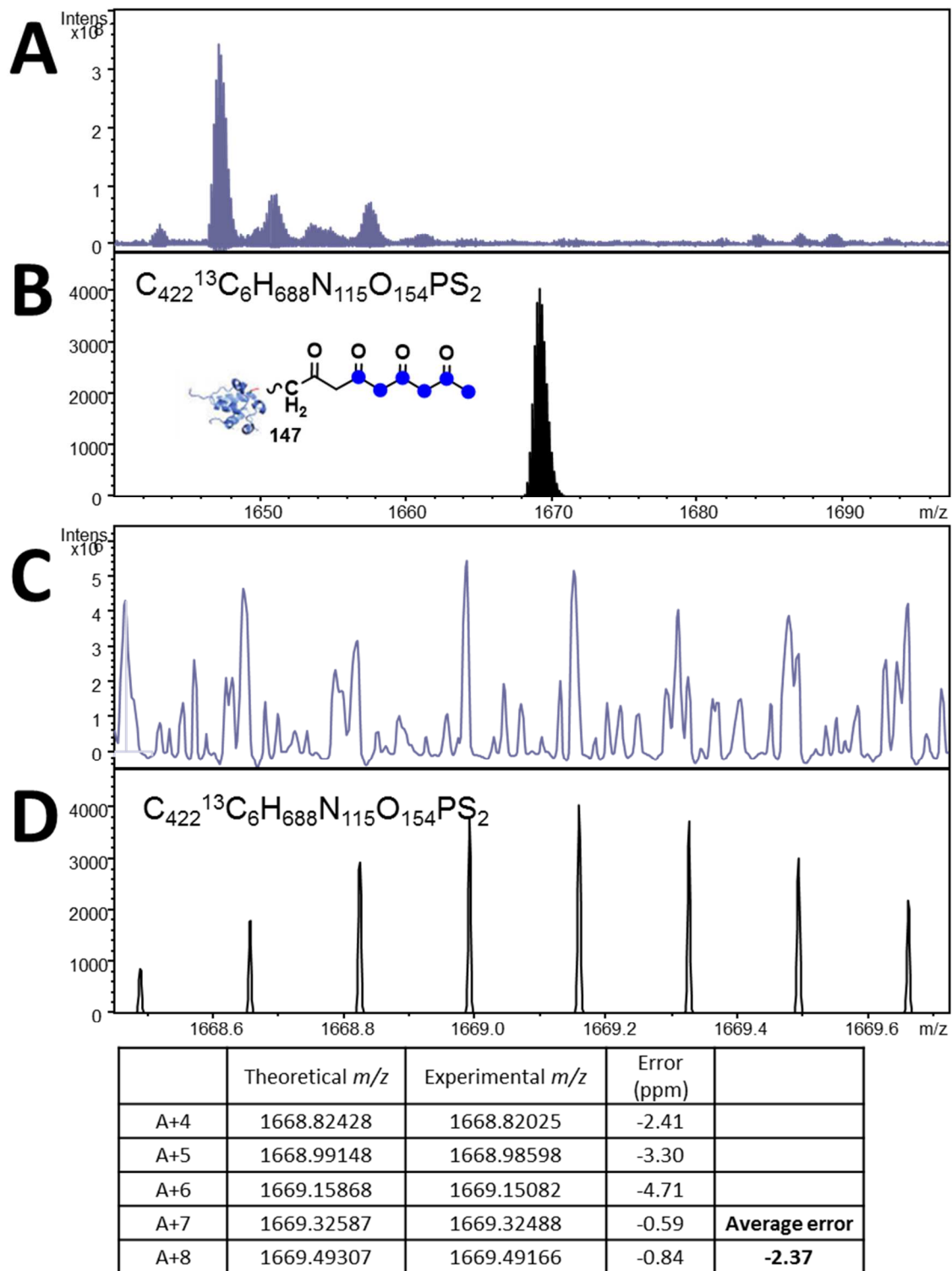


Appendix 9 FTICR-MS analysis of active ACP probe **64** incubated in the actinorhodin minimal system (1:4 ratio, protected ACP probe **63** to malonyl-ACP **7**) showing an off-loaded putative diketide **145**. (A) Acquired spectrum, (C) acquired spectrum magnified, (B) and (D) are simulated mass spectra (8^+). Underneath displays the peak list and errors for each.

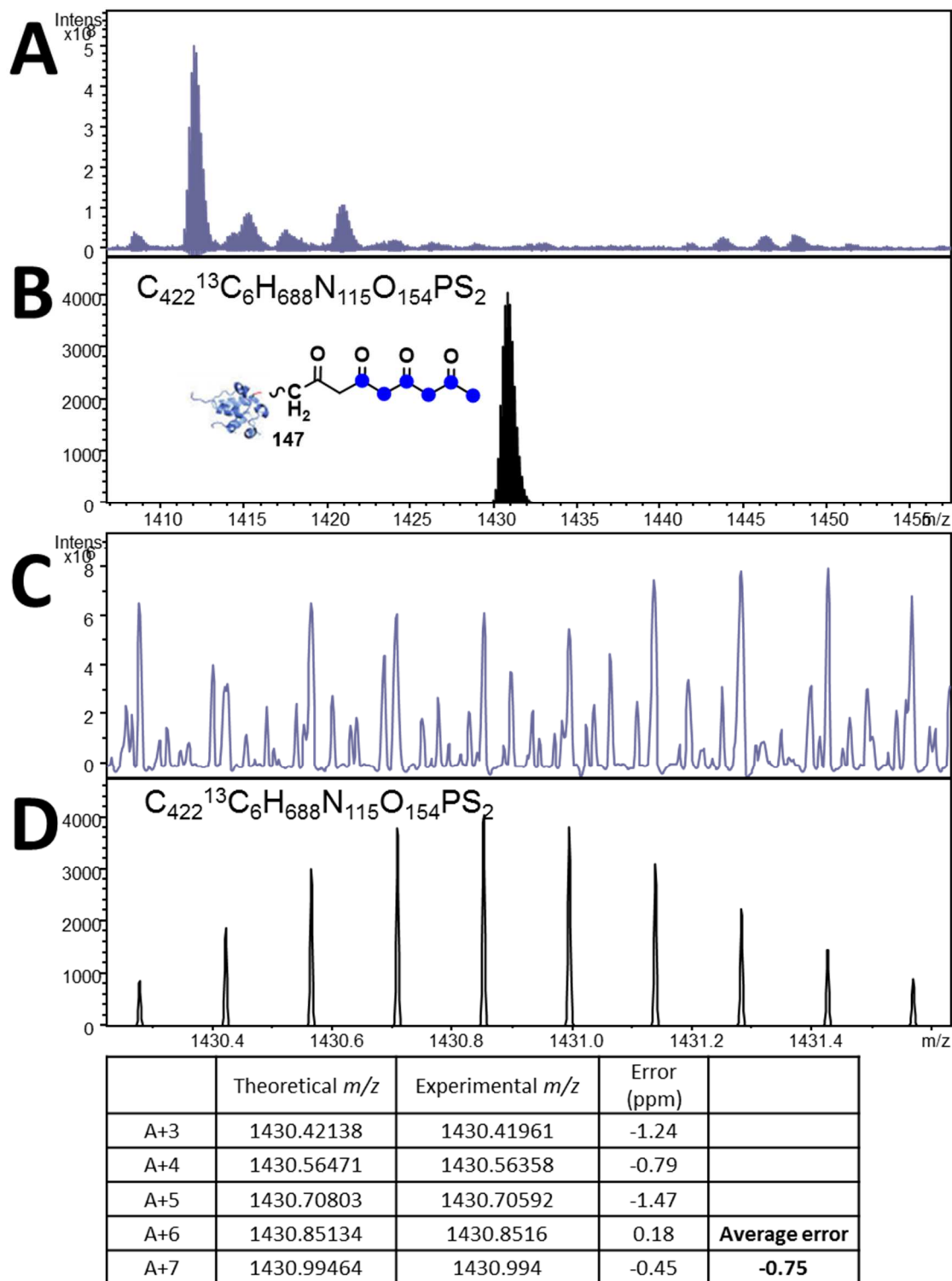


	Theoretical m/z	Experimental m/z	Error (ppm)	
A+4	1102.99217	1102.98835	-3.46	
A+5	1103.10364	1103.09795	-5.16	
A+6	1103.21509	1103.21444	-0.59	
A+7	1103.32656	1103.3207	-5.31	Average error
A+8	1103.438	1103.4379	-0.09	-2.92

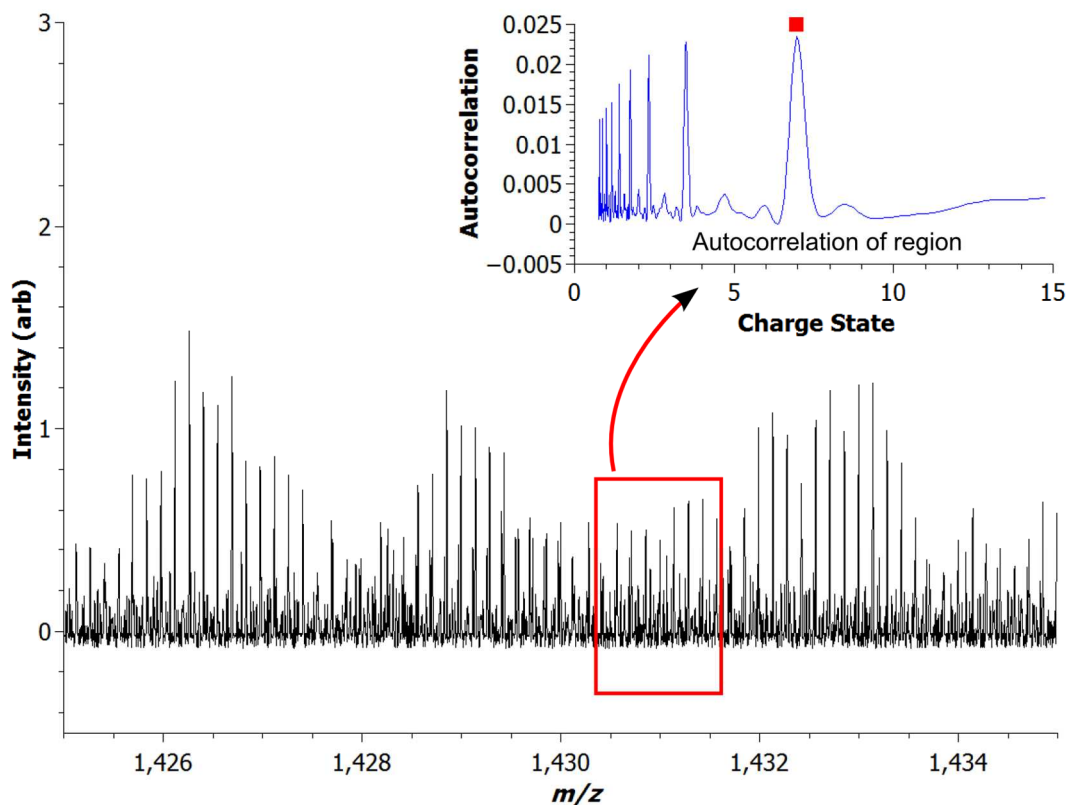
Appendix 10 FTICR-MS analysis of active ACP probe **64** incubated in the actinorhodin minimal system (1:4 ratio, protected ACP probe **63** to malonyl-ACP **7**) showing off-loaded putative diketide **145**. (A) Acquired spectrum, (C) acquired spectrum magnified, (B) and (D) are simulated mass spectra (9^+). Underneath displays the peak list and errors for each.



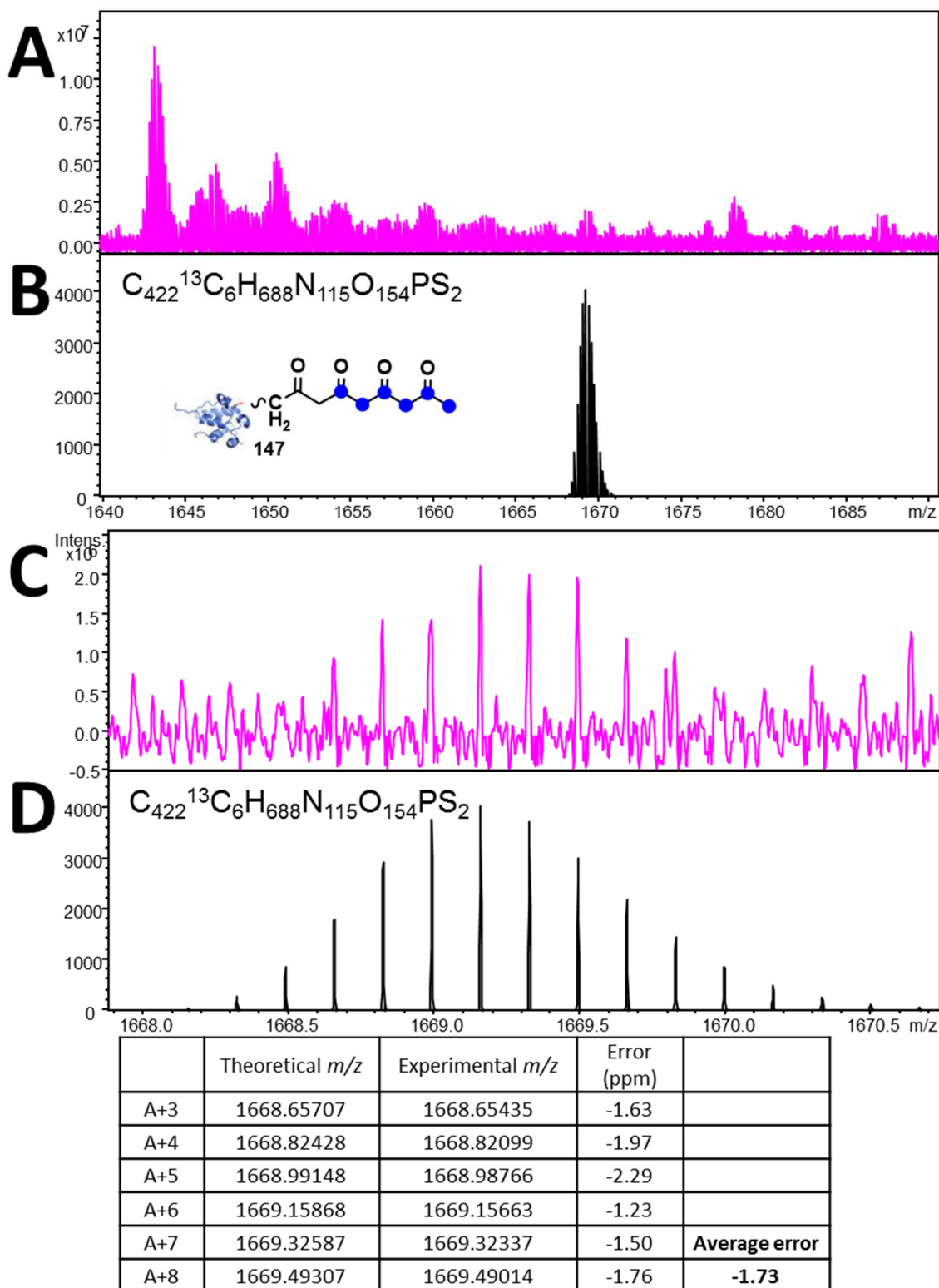
Appendix 11 FTICR-MS analysis of active ACP probe **64** incubated in the actinorhodin minimal system (1:1 ratio, protected ACP probe **63** to labelled malonyl-ACP **7b**) showing an off-loaded putative labelled tetraketide **147**. (A) Acquired spectrum, (C) acquired spectrum magnified, (B) and (D) are simulated mass spectra (6^+). Underneath displays the peak list and errors for each.



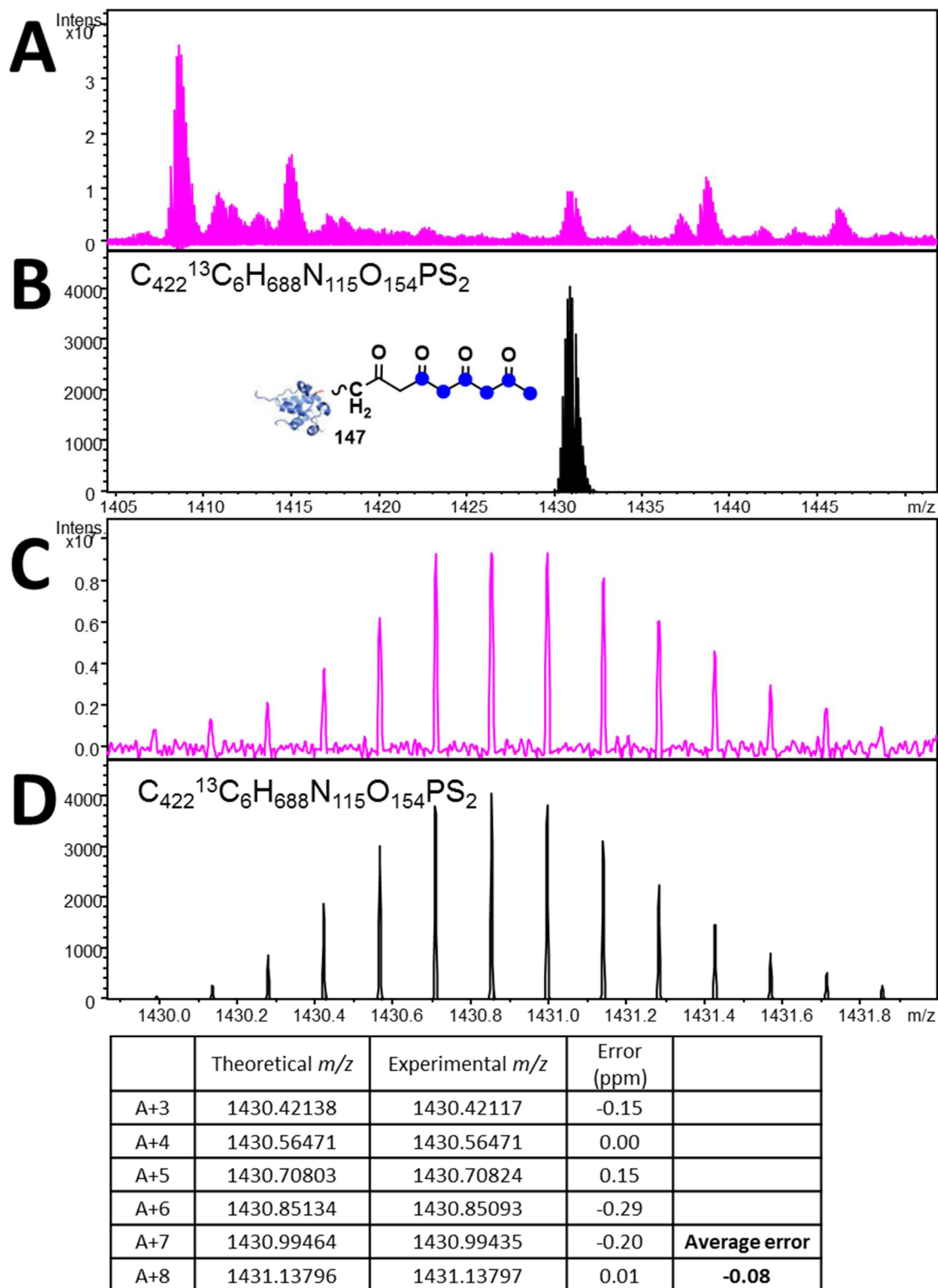
Appendix 12 FTICR-MS analysis of active ACP probe **64** incubated in the actinorhodin minimal system (1:1 ratio, protected ACP probe **63** to labelled malonyl-ACP **7b**) showing an off-loaded putative labelled tetraketide **147**. (A) Acquired spectrum, (C) acquired spectrum magnified, (B) and (D) are simulated mass spectra (7^+). Underneath displays the peak list and errors for each.



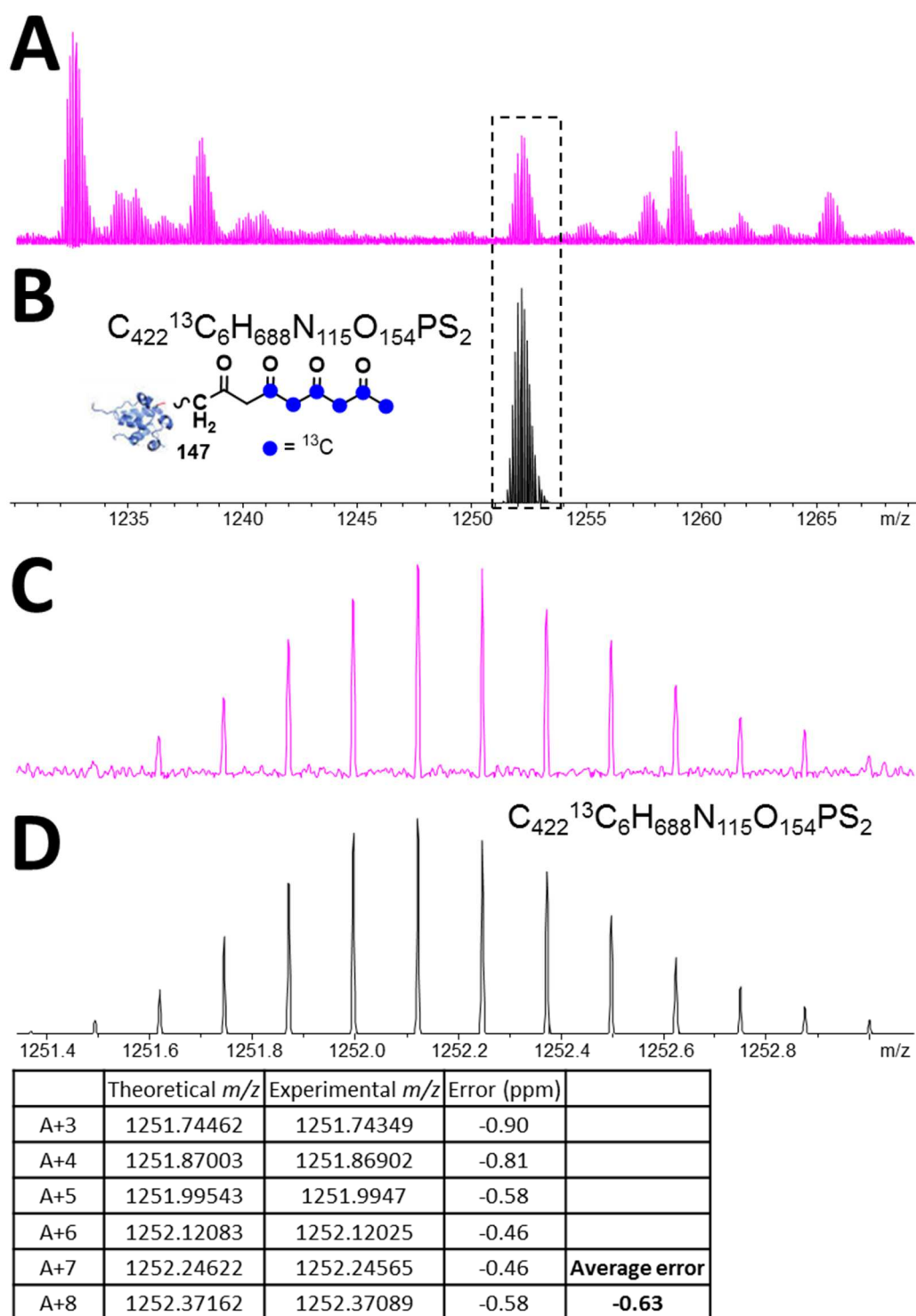
*Appendix 13 FTICR-MS analysis of active ACP probe **64** incubated in the actinorhodin minimal system (1:1 ratio, protected ACP probe **63** to labelled malonyl-ACP **7b**) showing an off-loaded putative labelled tetraketide **147** at a charge state of 7^+ . Inset shows autocorrelation of region indicated confirming a 7^+ charge state.*



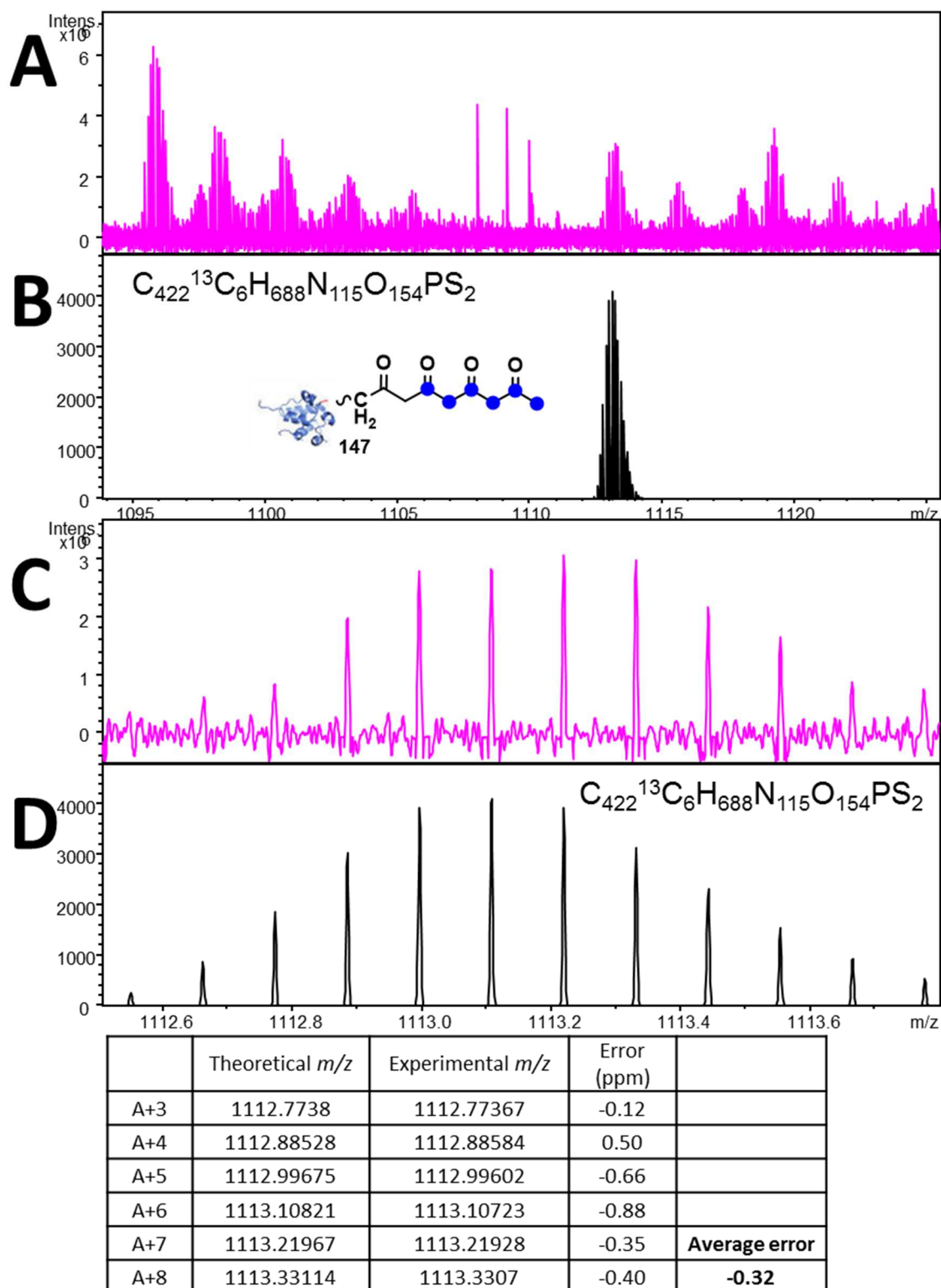
Appendix 14 FTICR-MS analysis of active ACP probe **64** incubated in the actinorhodin minimal system (1:10 ratio, protected ACP probe **63** to labelled malonyl-ACP **7b**) showing an off-loaded putative labelled tetraketide **147**. (A) Acquired spectrum, (C) acquired spectrum magnified, (B) and (D) are simulated mass spectra (6^+). Underneath displays the peak list and errors for each.



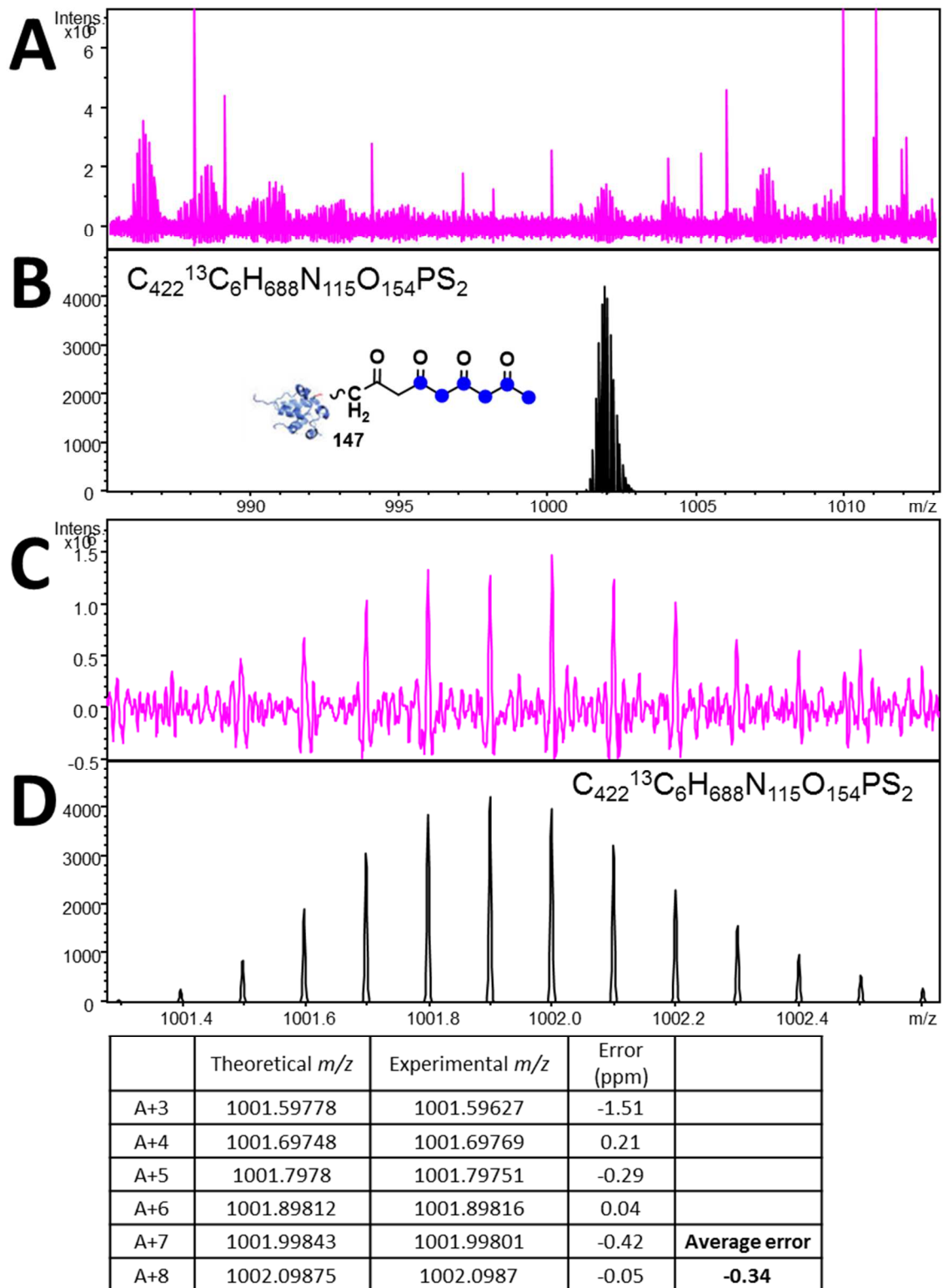
Appendix 15 FTICR-MS analysis of active ACP probe 64 incubated in the actinorhodin minimal system (1:10 ratio, protected ACP probe 63 to labelled malonyl-ACP 7b) showing an off-loaded putative labelled tetraketide 147. (A) Acquired spectrum, (C) acquired spectrum magnified, (B) and (D) are simulated mass spectra (7^+). Underneath displays the peak list and errors for each.



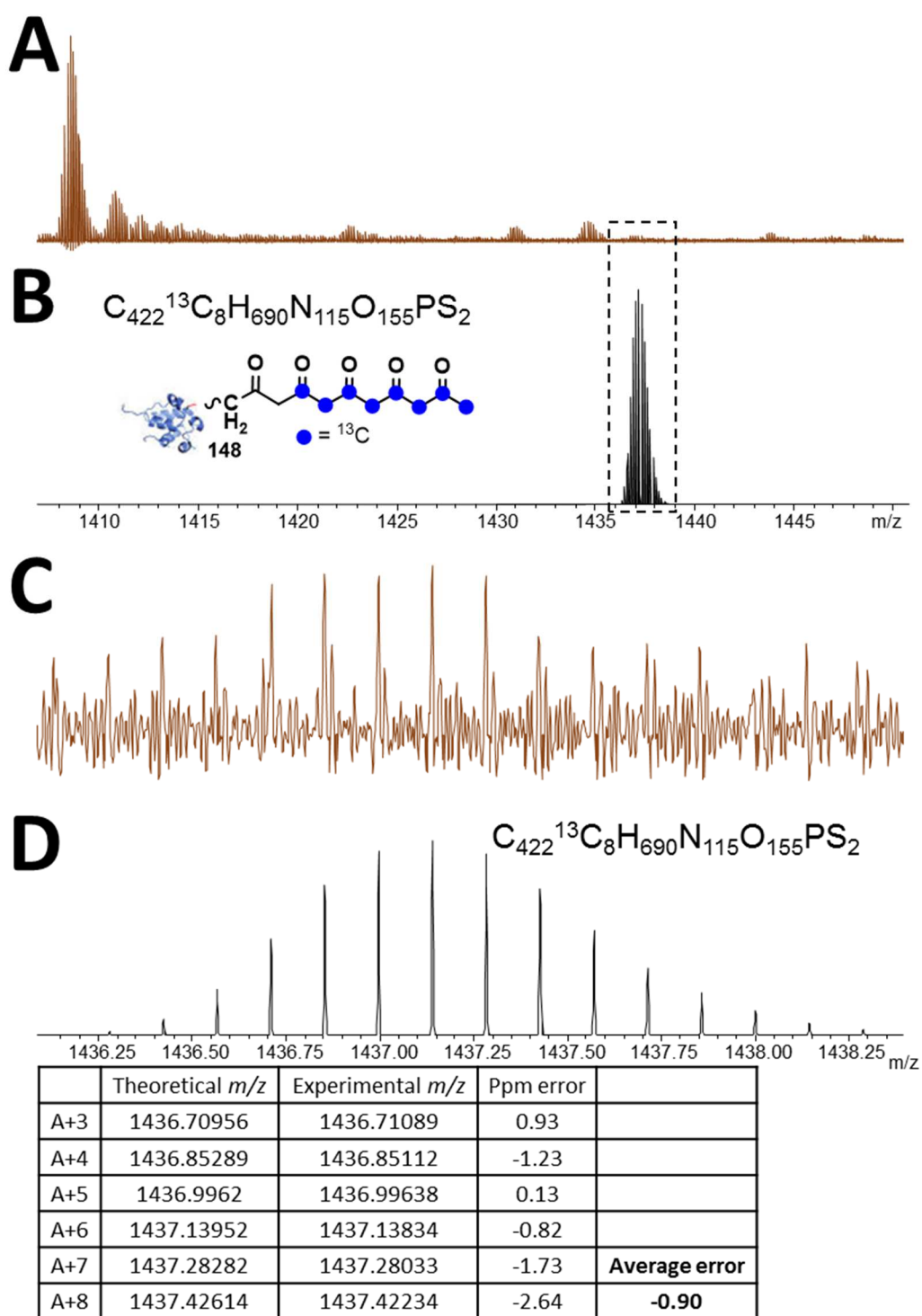
Appendix 16 FTICR-MS analysis of active ACP probe **64** incubated in the actinorhodin minimal system (1:10 ratio, protected ACP probe **63** to labelled malonyl-ACP **7b**) showing an off-loaded putative labelled tetraketide **147**. (A) Acquired spectrum, (C) acquired spectrum magnified, (B) and (D) are simulated mass spectra (8^+). Underneath displays the peak list and errors for each.



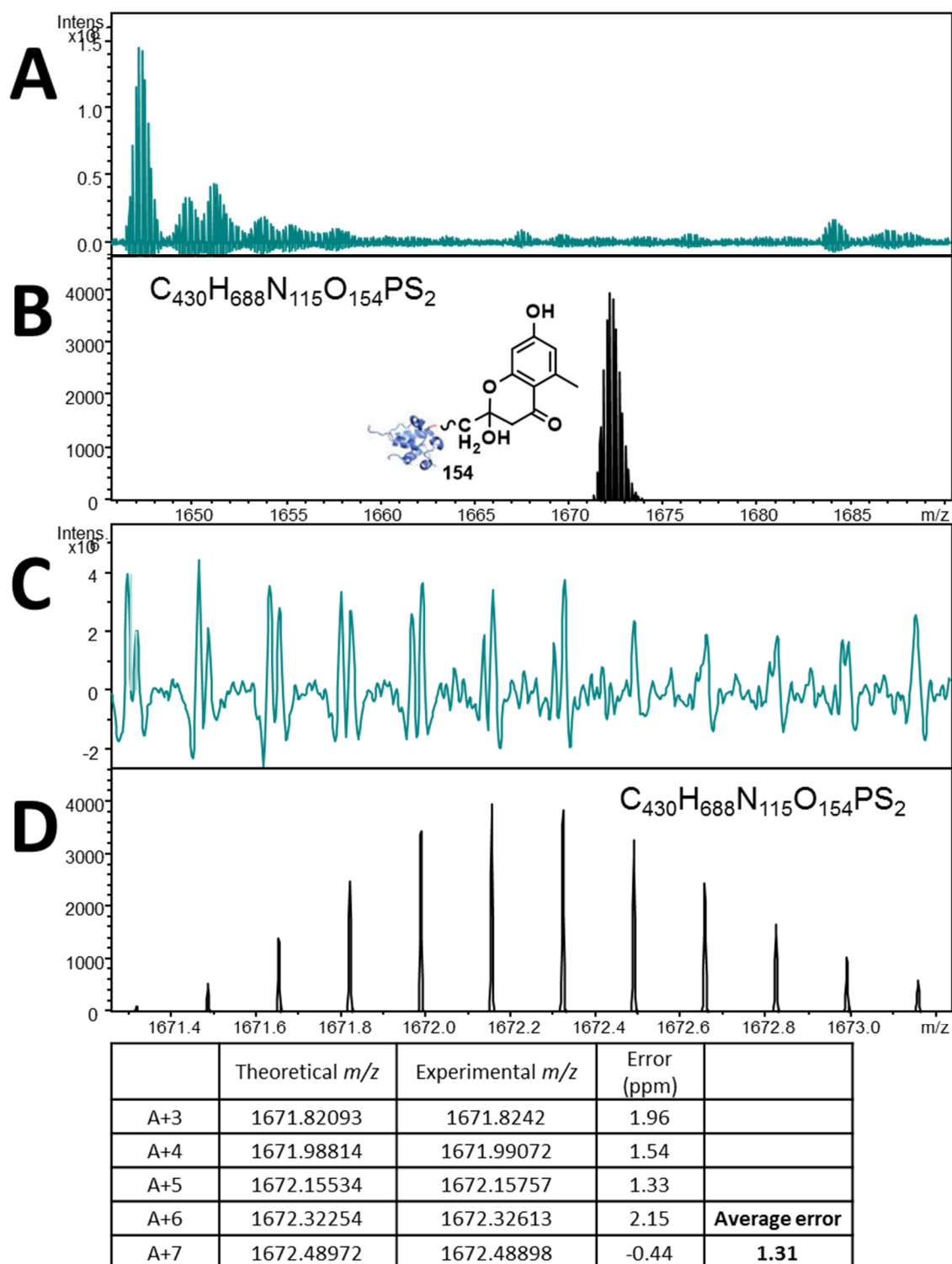
Appendix 17 FTICR-MS analysis of active ACP probe 64 incubated in the actinorhodin minimal system (1:10 ratio, protected ACP probe 63 to labelled malonyl-ACP 7b) showing an off-loaded putative labelled tetraketide 147. (A) Acquired spectrum, (C) acquired spectrum magnified, (B) and (D) are simulated mass spectra (9^+). Underneath displays the peak list and errors for each.



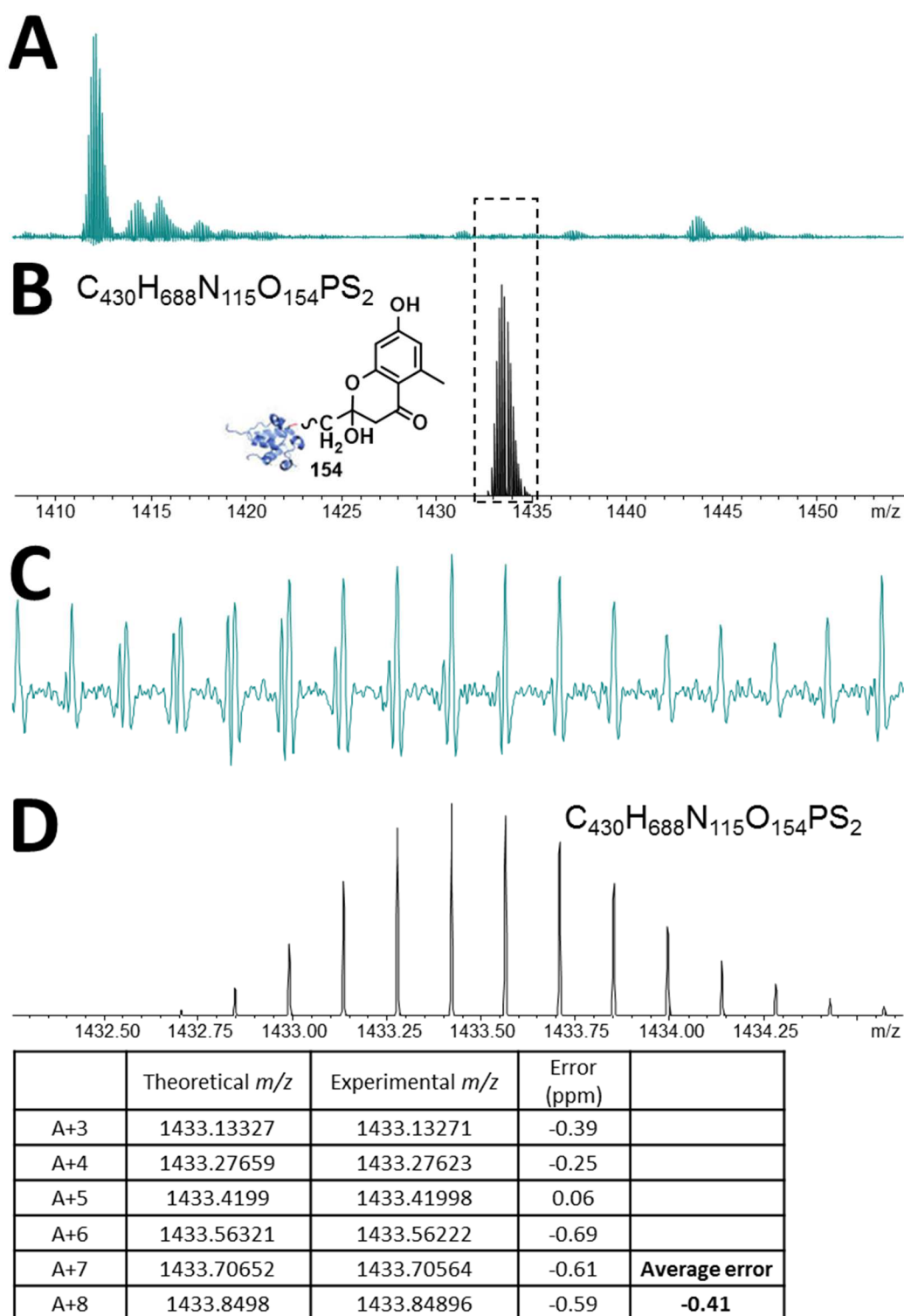
Appendix 18 FTICR-MS analysis of active ACP probe **64** incubated in the actinorhodin minimal system (1:10 ratio, protected ACP probe **63** to labelled malonyl-ACP **7b**) showing an off-loaded putative labelled tetraketide **147**. (A) Acquired spectrum, (C) acquired spectrum magnified, (B) and (D) are simulated mass spectra (10^+). Underneath displays the peak list and errors for each.



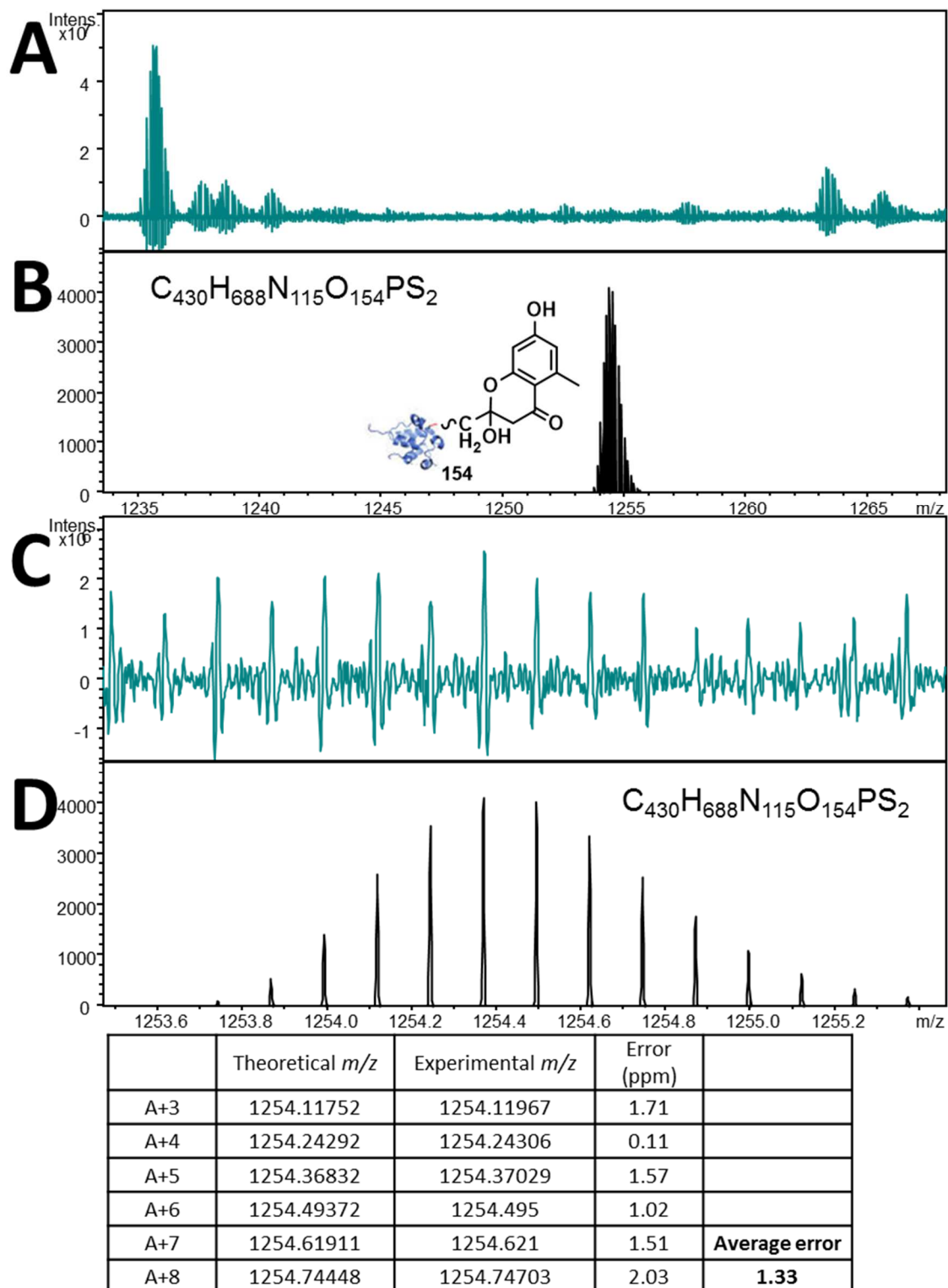
Appendix 19 FTICR-MS analysis of active ACP probe **64** incubated in the actinorhodin minimal system (1:4 ratio, protected ACP probe **63** to labelled malonyl-ACP **7b**) showing an off-loaded putative labelled linear pentaketide **148**. (A) Acquired spectrum, (C) acquired spectrum magnified, (B) and (D) are simulated mass spectra (7^+). Underneath displays the peak list and errors for each.



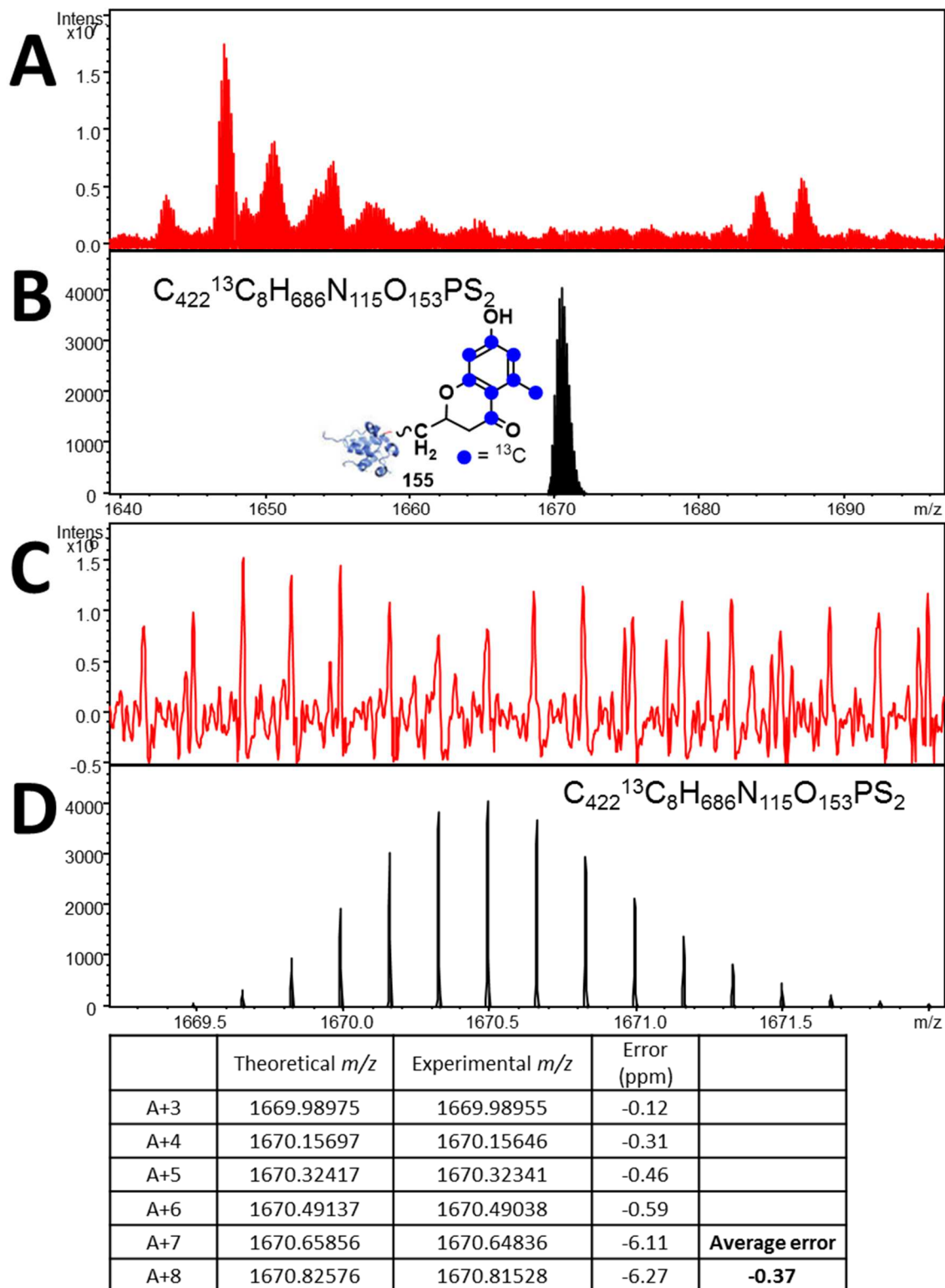
Appendix 20 FTICR-MS analysis of active ACP probe **64** incubated in the actinorhodin minimal system (5:1 ratio, protected ACP probe **63** to malonyl-ACP **7**) showing an off-loaded putative cyclised pentaketide **154**. (A) Acquired spectrum, (C) acquired spectrum magnified, (B) and (D) are simulated mass spectra (6^+). Underneath displays the peak list and errors for each.



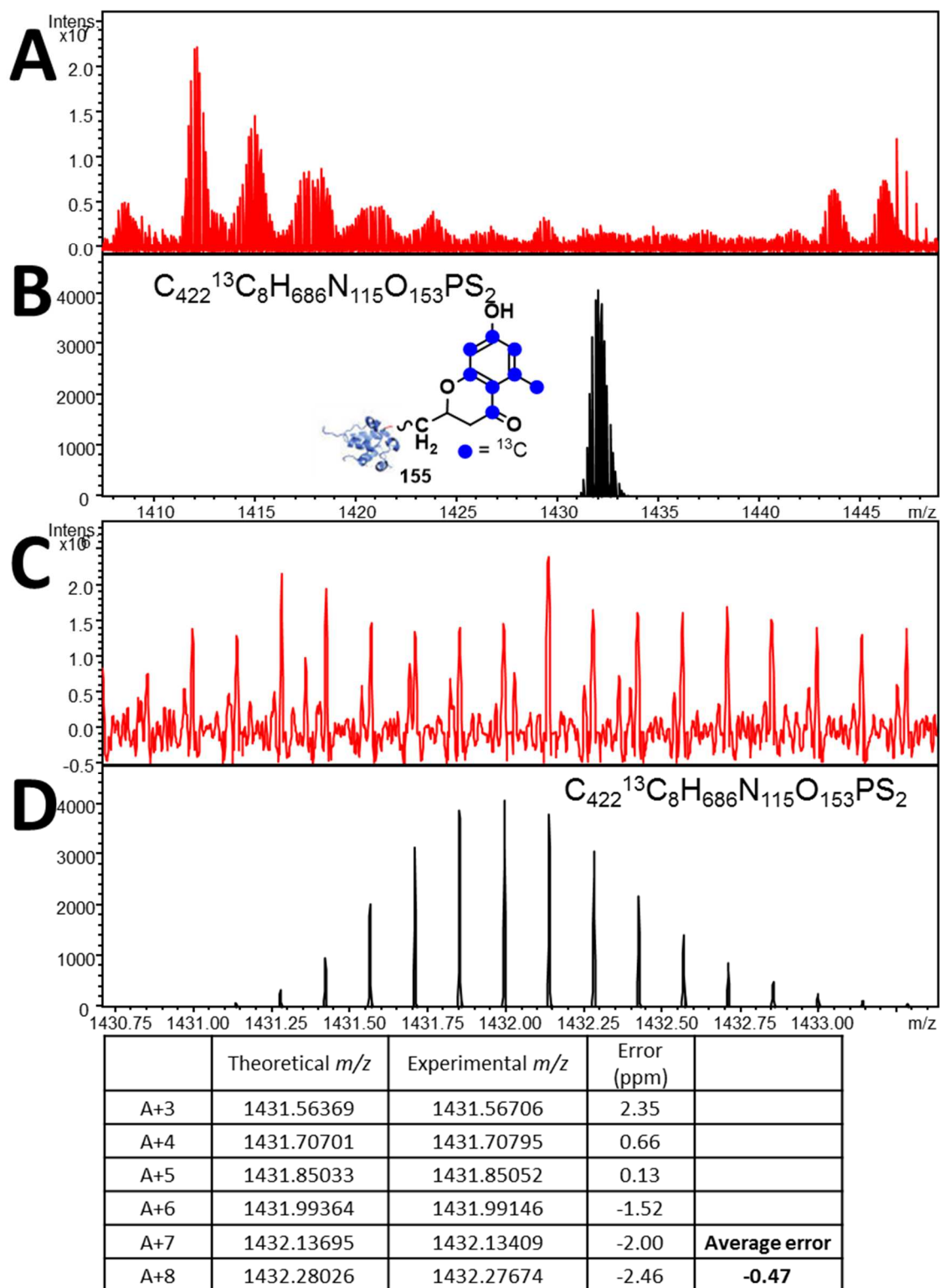
Appendix 21 FTICR-MS analysis of active ACP probe **64** incubated in the actinorhodin minimal system (5:1 ratio, protected ACP probe **63** to malonyl-ACP **7**) showing an off-loaded putative cyclised pentaketide **154**. (A) Acquired spectrum, (C) acquired spectrum magnified, (B) and (D) are simulated mass spectra (7^+). Underneath displays the peak list and errors for each.



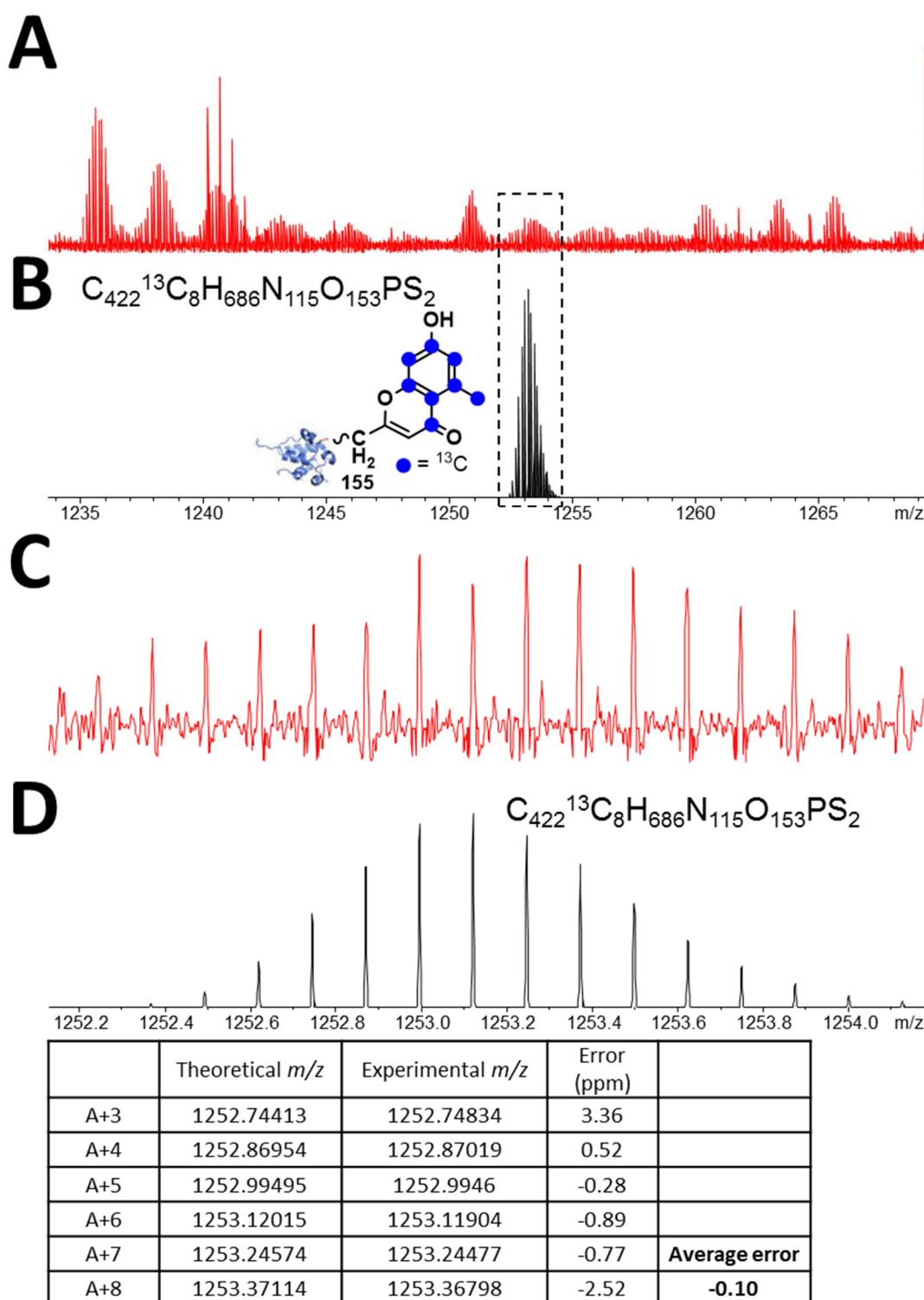
Appendix 22 FTICR-MS analysis of active ACP probe **64** incubated in the actinorhodin minimal system (5:1 ratio, protected ACP probe **63** to malonyl-ACP **7**) showing an off-loaded putative cyclised pentaketide **154**. (A) Acquired spectrum, (C) acquired spectrum magnified, (B) and (D) are simulated mass spectra (8^+). Underneath displays the peak list and errors for each.



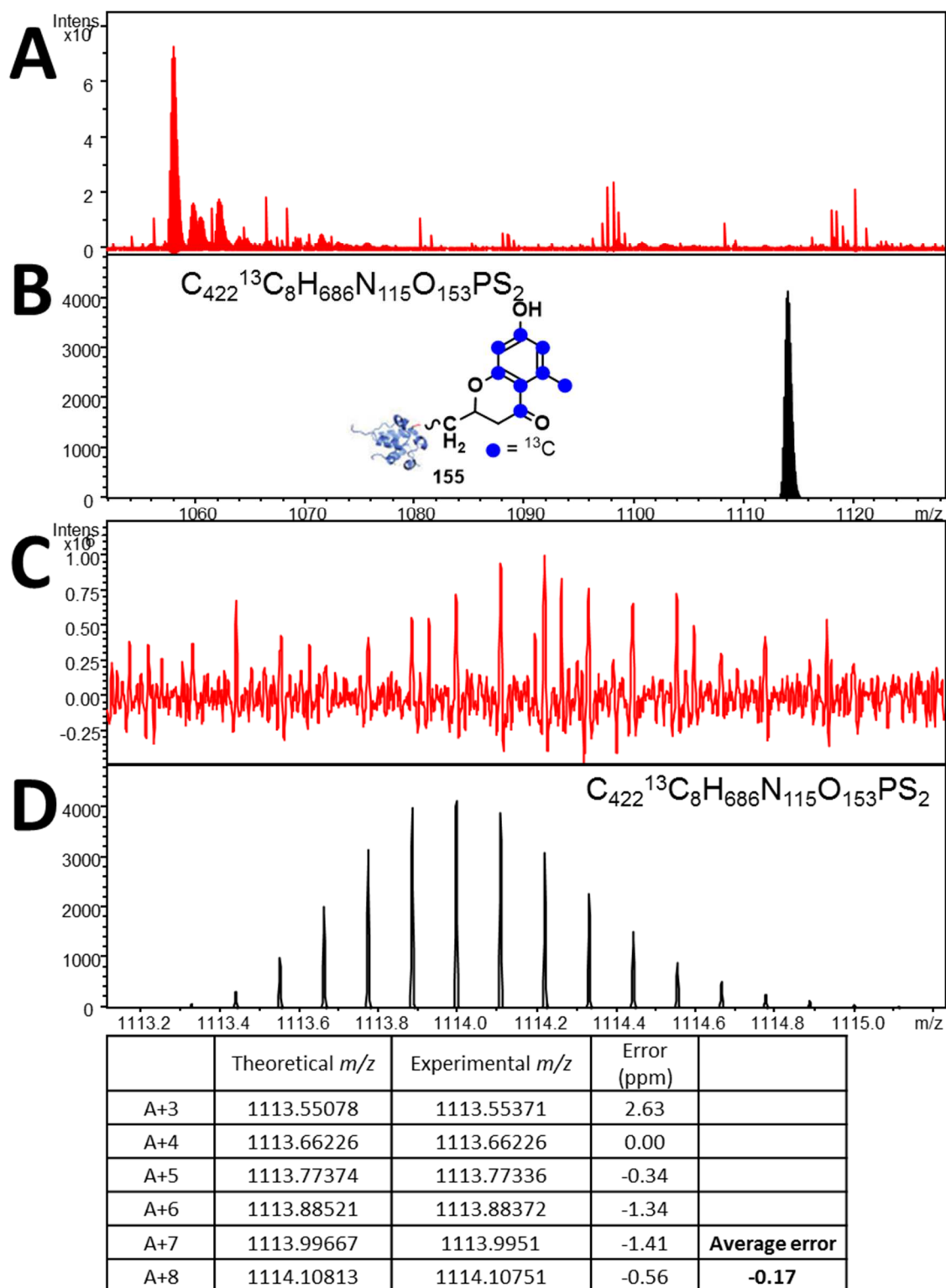
Appendix 23 FTICR-MS analysis of active ACP probe **64** incubated in the actinorhodin minimal system (5:1 ratio, protected ACP probe **63** to labelled malonyl-ACP **7b**) showing an off-loaded putative cyclised dehydrated pentaketide **155**. (A) Acquired spectrum, (C) acquired spectrum magnified, (B) and (D) are simulated mass spectra (6^+). Underneath displays the peak list and errors for each.



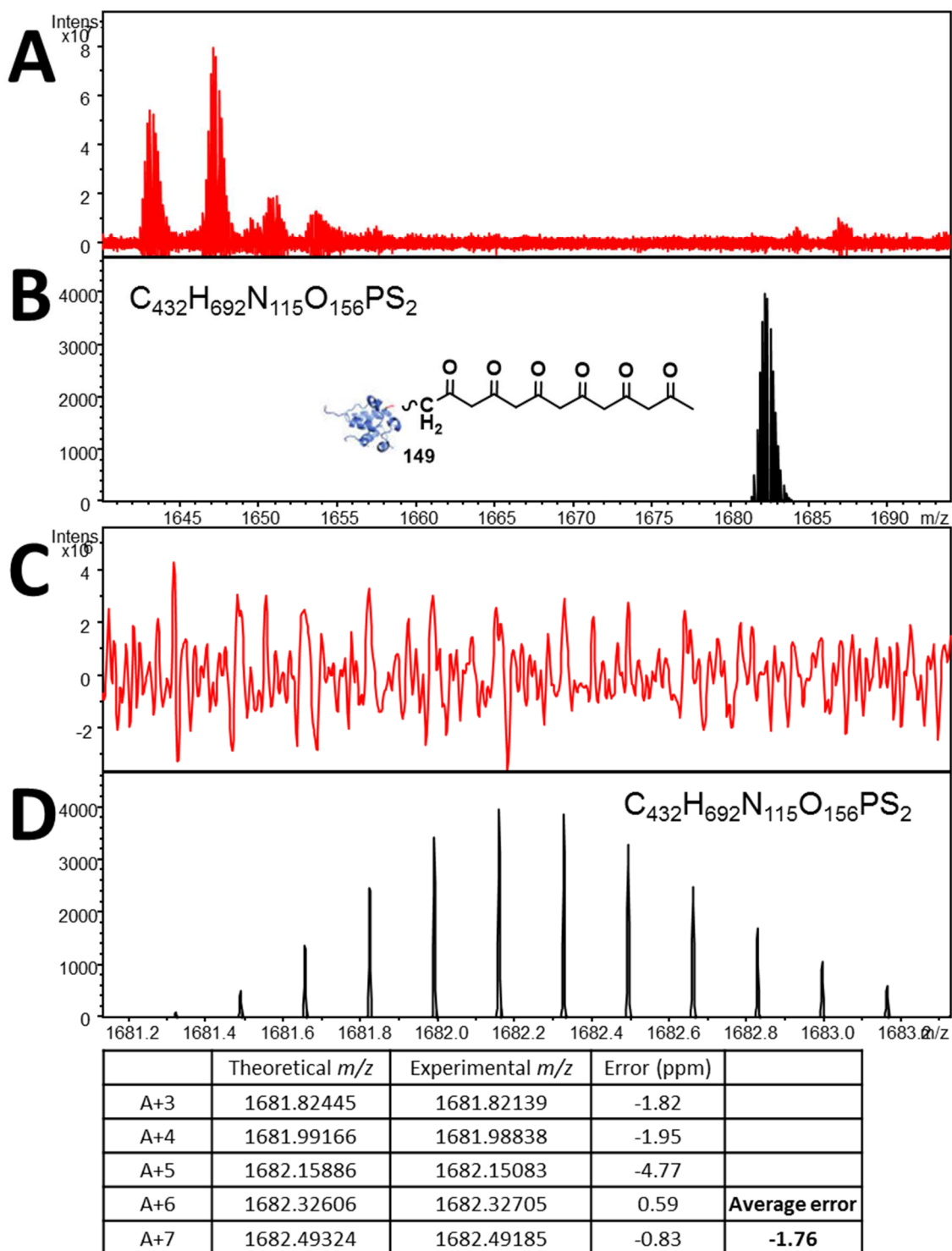
Appendix 24 FTICR-MS analysis of active ACP probe **64** incubated in the actinorhodin minimal system (5:1 ratio, protected ACP probe **63** to labelled malonyl-ACP **7b**) showing an off-loaded putative cyclised dehydrated pentaketide **155**. (A) Acquired spectrum, (C) acquired spectrum magnified, (B) and (D) are simulated mass spectra (7^+). Underneath displays the peak list and errors for each.



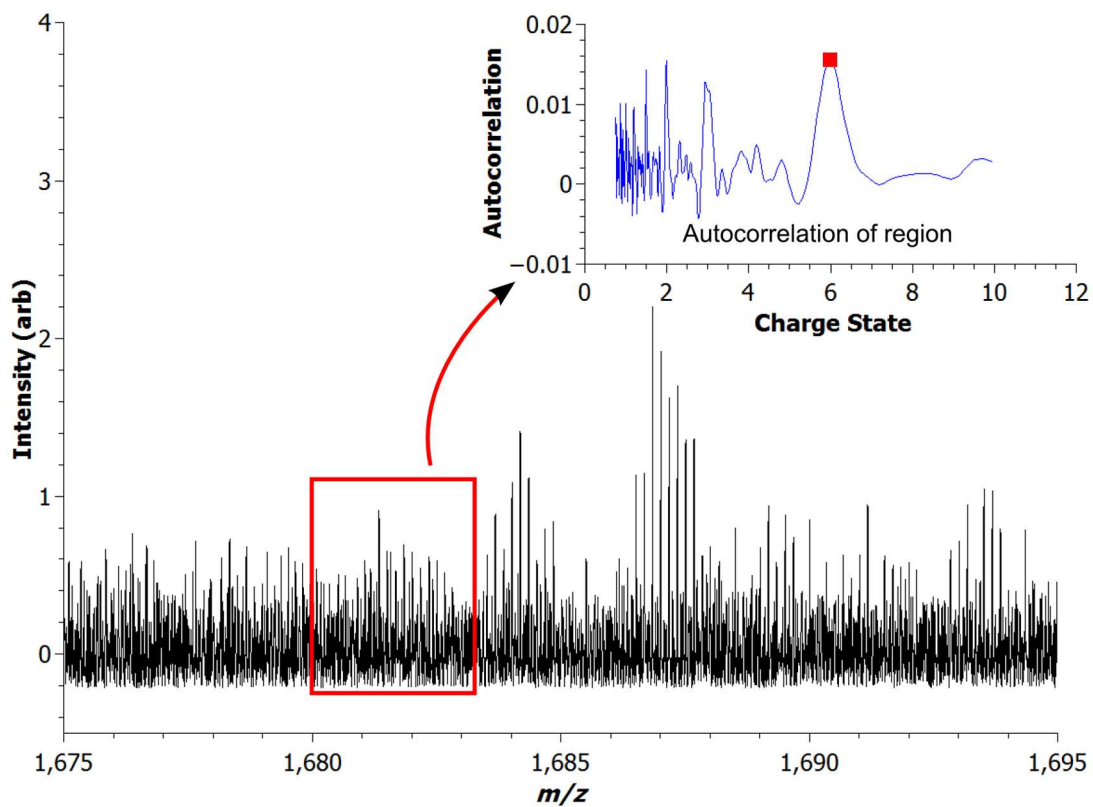
Appendix 25 FTICR-MS analysis of active ACP probe **64** incubated in the actinorhodin minimal system (5:1 ratio, protected ACP probe **63** to labelled malonyl-ACP **7b**) showing an off-loaded putative cyclised dehydrated pentaketide **155**. (A) Acquired spectrum, (C) acquired spectrum magnified, (B) and (D) are simulated mass spectra (8^+). Underneath displays the peak list and errors for each.



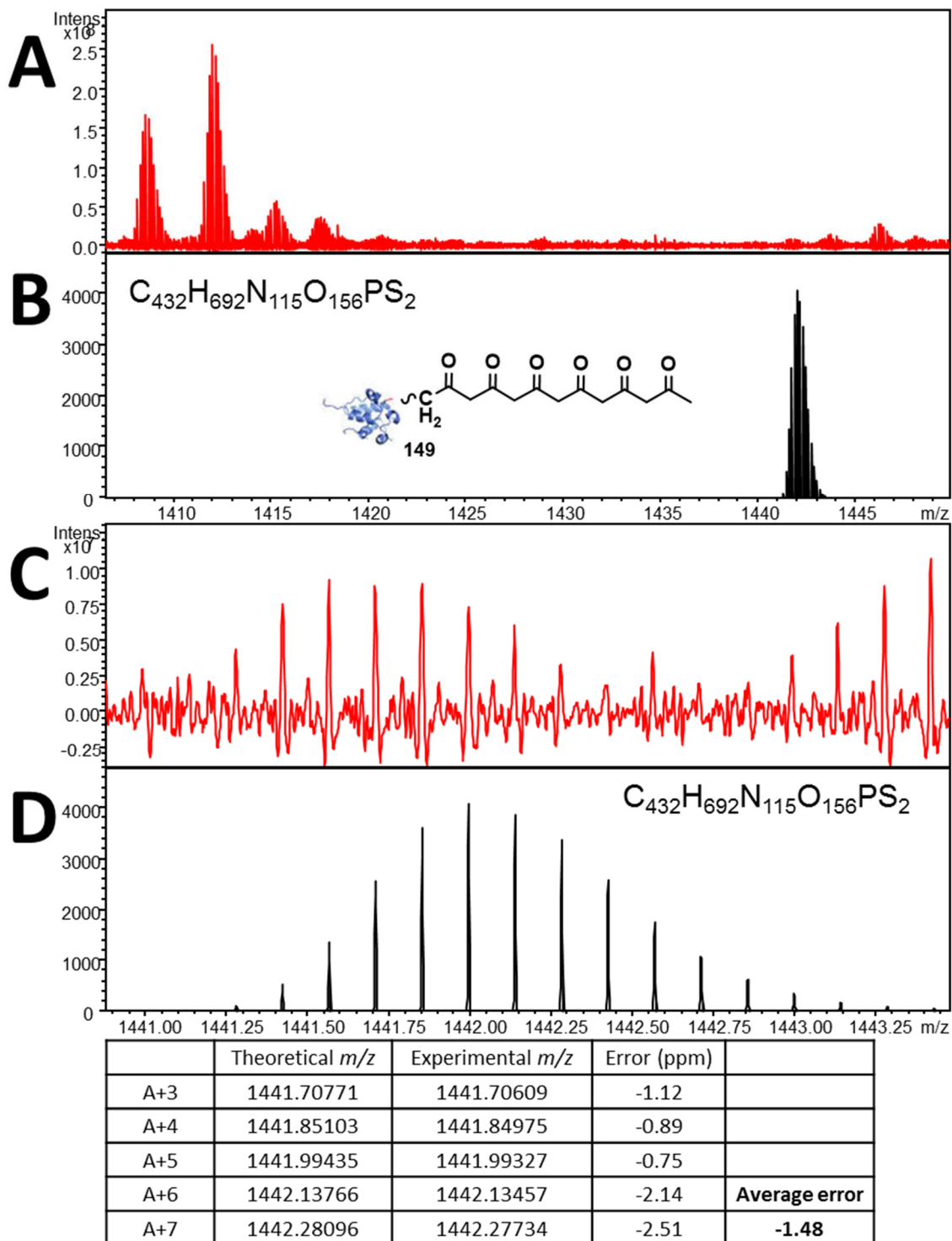
Appendix 26 FTICR-MS analysis of active ACP probe **64** incubated in the actinorhodin minimal system (5:1 ratio, protected ACP probe **63** to labelled malonyl-ACP **7b**) showing an off-loaded putative cyclised dehydrated pentaketide **155**. (A) Acquired spectrum, (C) acquired spectrum magnified, (B) and (D) are simulated mass spectra (9^+). Underneath displays the peak list and errors for each.



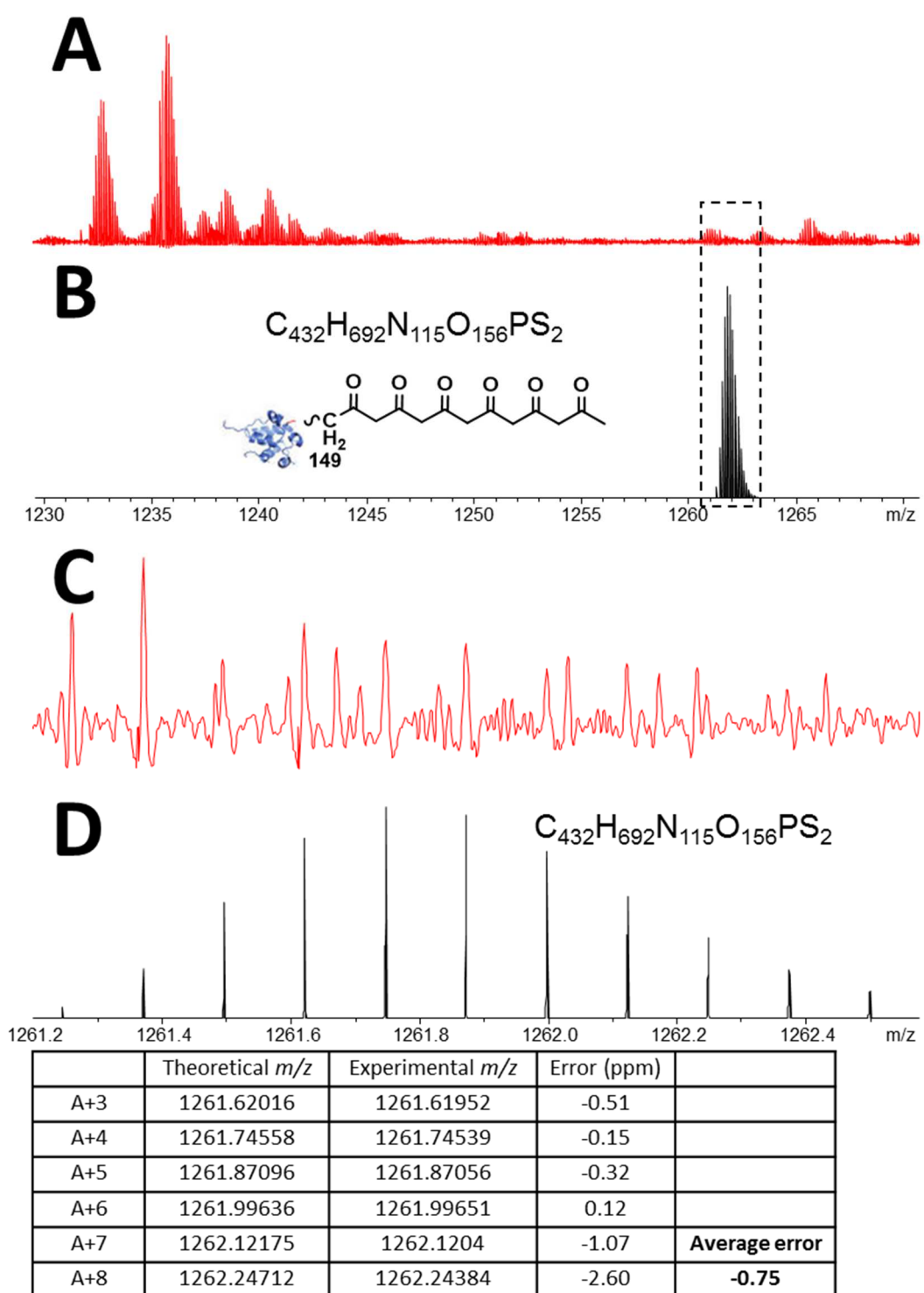
Appendix 27 FTICR-MS analysis of active ACP probe **64** incubated in the actinorhodin minimal system (1:4 ratio, protected ACP probe **63** to malonyl-ACP **7b**) showing an off-loaded putative linear hexaketide **149**. (A) Acquired spectrum, (C) acquired spectrum magnified, (B) and (D) are simulated mass spectra (6^+). Underneath displays the peak list and errors for each.



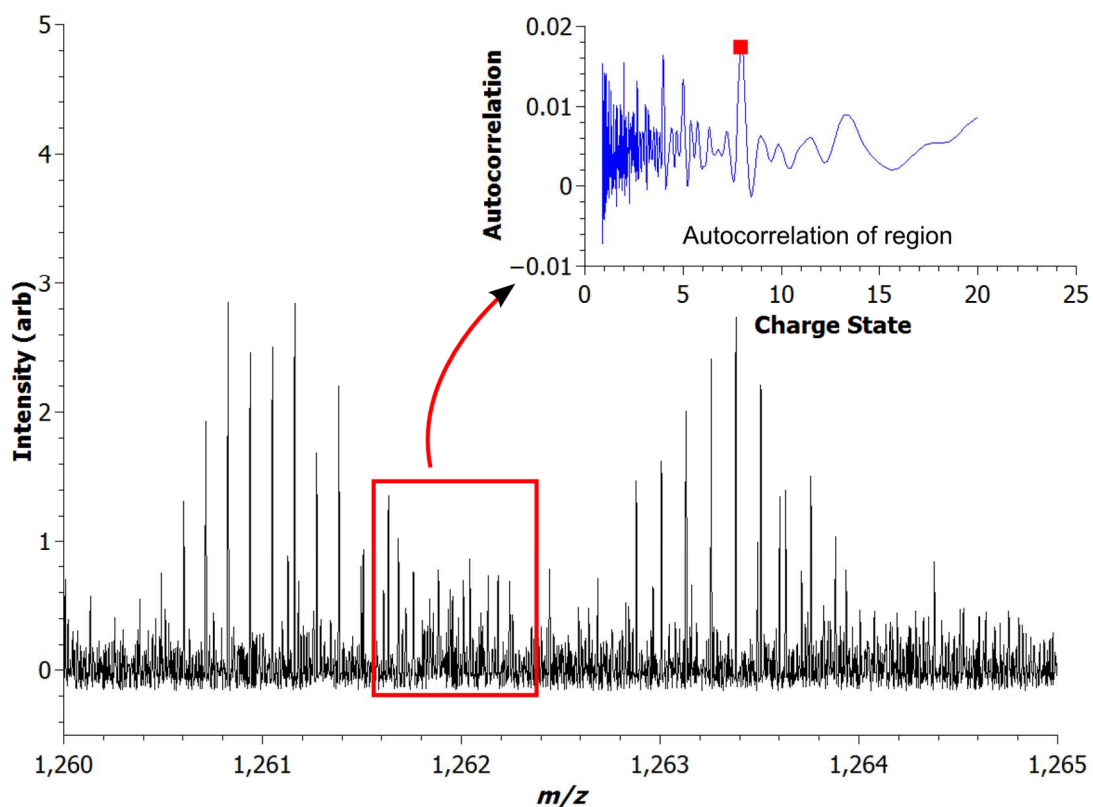
Appendix 28 FTICR-MS analysis of active ACP probe **64** incubated in the actinorhodin minimal system (1:4 ratio, protected ACP probe **63** to malonyl-ACP **7b**) showing an off-loaded putative labelled tetraketide **147** at a charge state of 6^+ . Inset shows autocorrelation of region indicated confirming a 6^+ charge state.



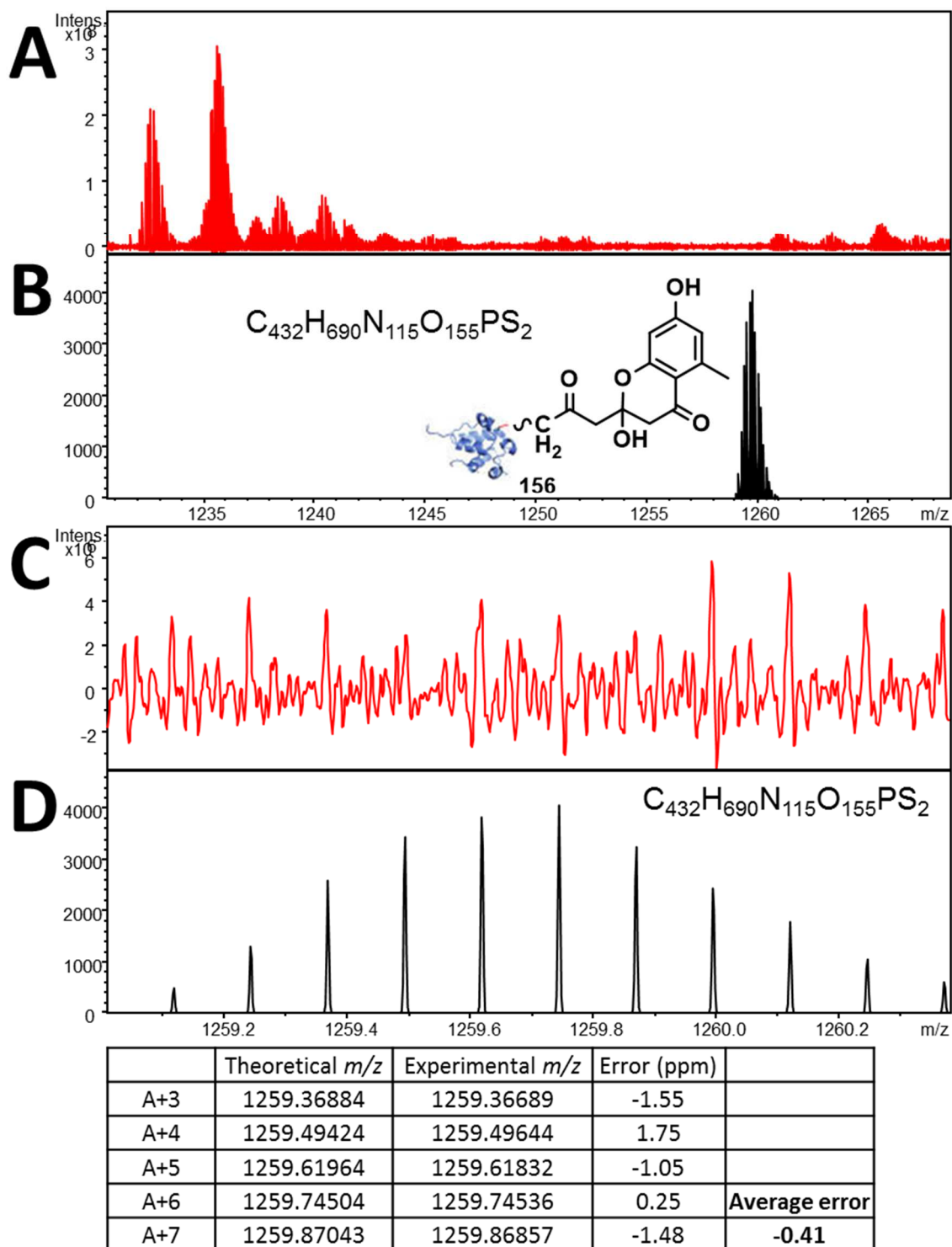
Appendix 29 FTICR-MS analysis of active ACP probe **64** incubated in the actinorhodin minimal system (1:4 ratio, protected ACP probe **63** to malonyl-ACP **7**) showing an off-loaded putative linear hexaketide **149**. (A) Acquired spectrum, (C) acquired spectrum magnified, (B) and (D) are simulated mass spectra (7^+). Underneath displays the peak list and errors for each.



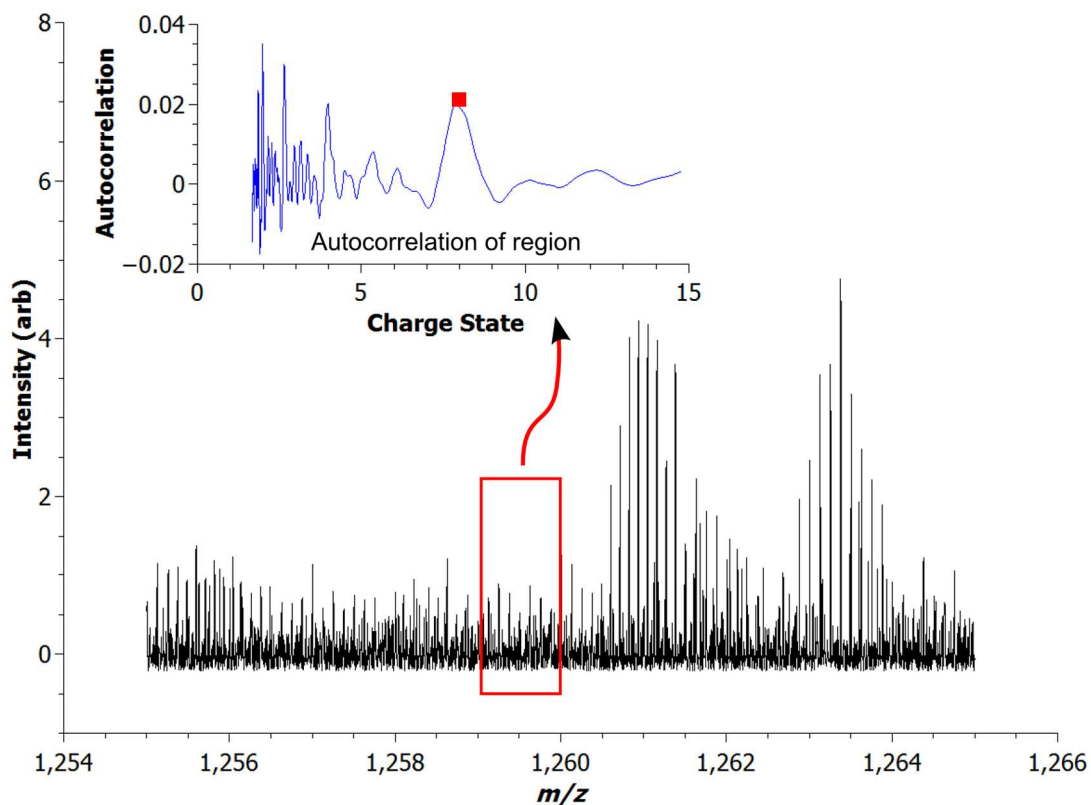
Appendix 30 FTICR-MS analysis of active ACP probe **64** incubated in the actinorhodin minimal system (1:4 ratio, protected ACP probe **63** to malonyl-ACP **7**) showing an off-loaded putative linear hexaketide **149**. (A) Acquired spectrum, (C) acquired spectrum magnified, (B) and (D) are simulated mass spectra (8^+). Underneath displays the peak list and errors for each.



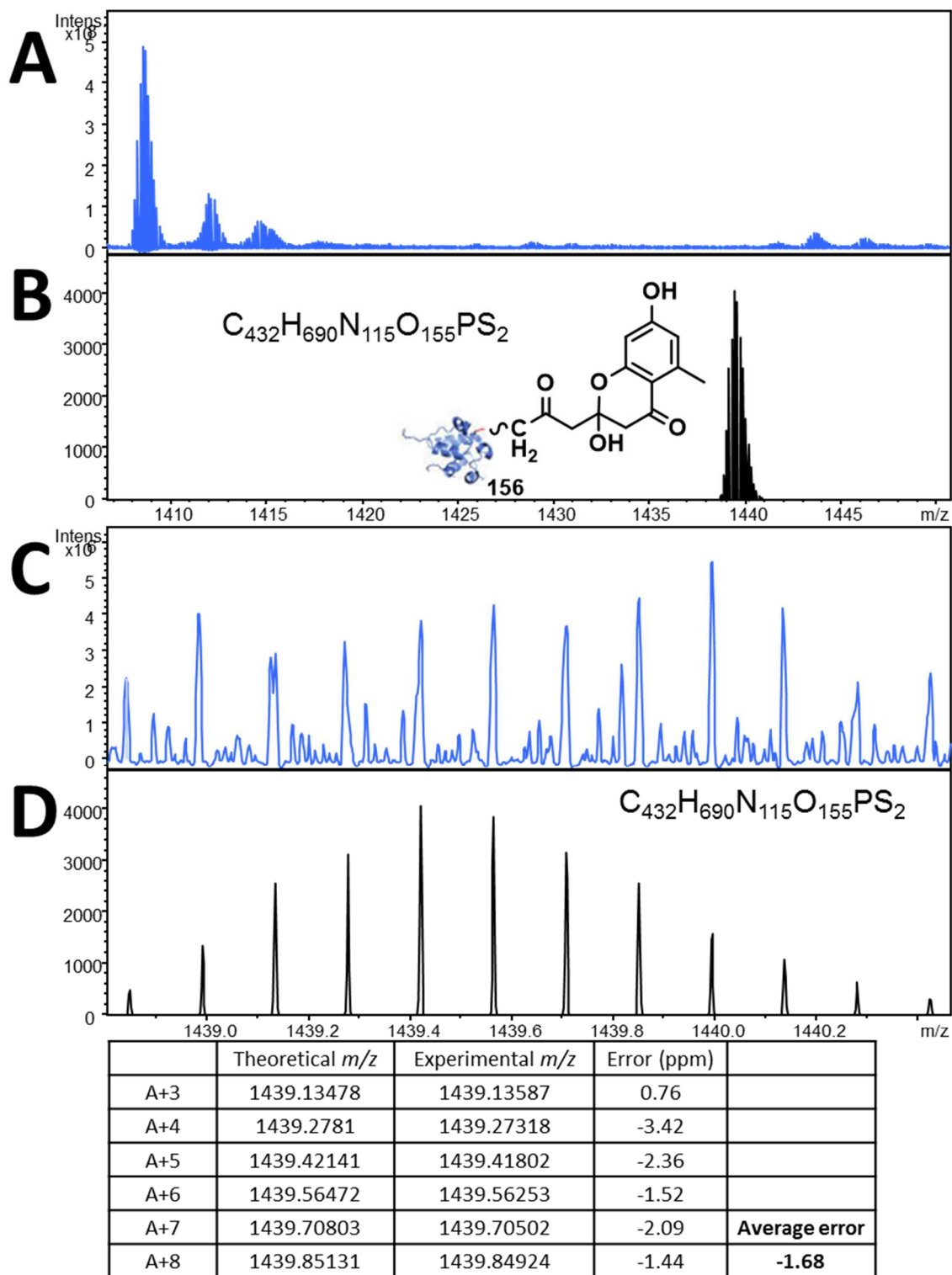
Appendix 31 FTICR-MS analysis of active ACP probe 64 incubated in the actinorhodin minimal system (1:4 ratio, protected ACP probe 63 to malonyl-ACP 7) showing an off-loaded putative linear hexaketide 149 at a charge state of 8⁺. Inset shows autocorrelation of region indicated confirming an 8⁺ charge state.



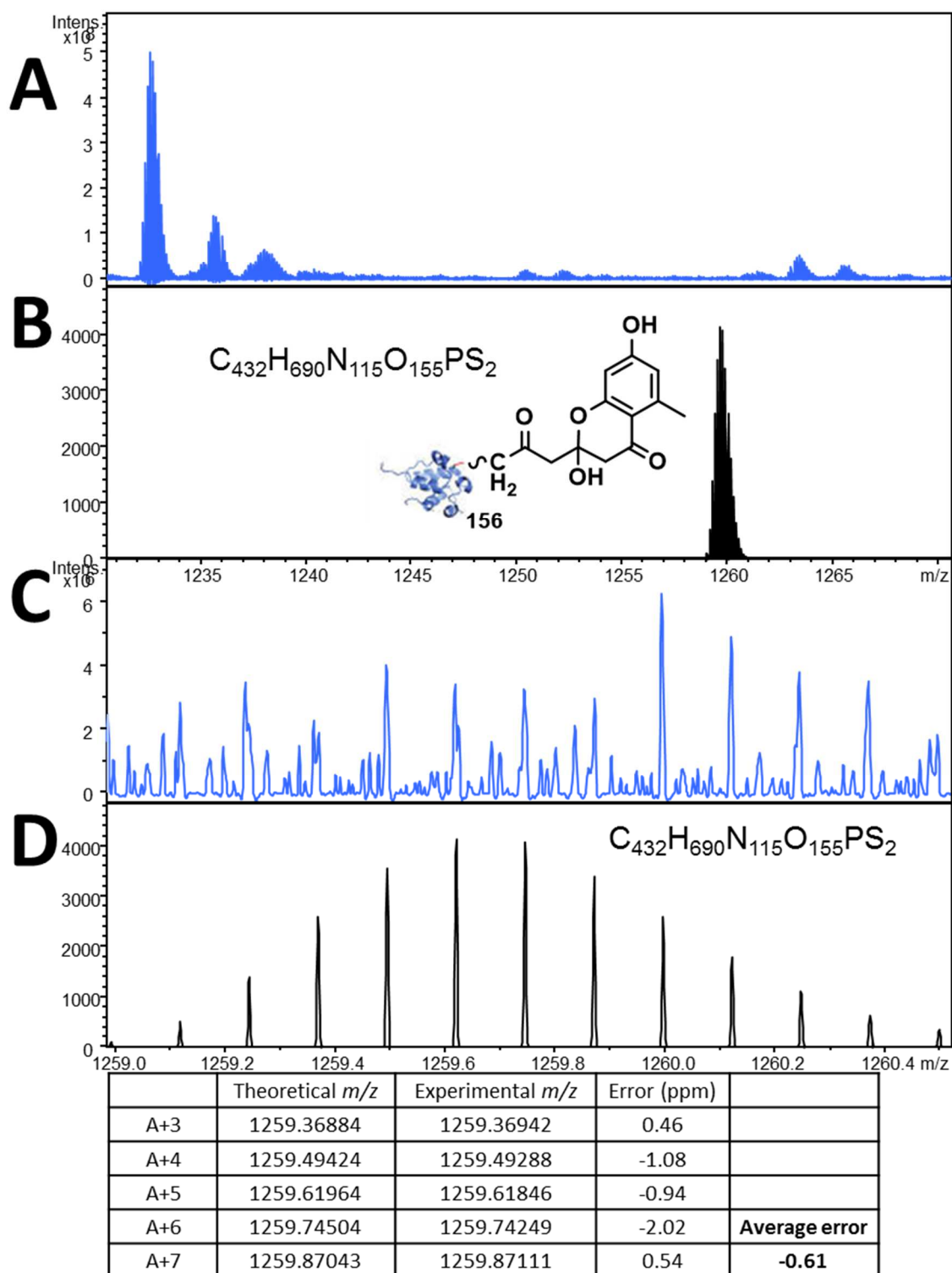
Appendix 32 FTICR-MS analysis of active ACP probe **64** incubated in the actinorhodin minimal system (1:4 ratio, protected ACP probe **63** to malonyl-ACP **7**) showing an off-loaded putative cyclised hexaketide **156**. (A) Acquired spectrum, (C) acquired spectrum magnified, (B) and (D) are simulated mass spectra (8^+). Underneath displays the peak list and errors for each.



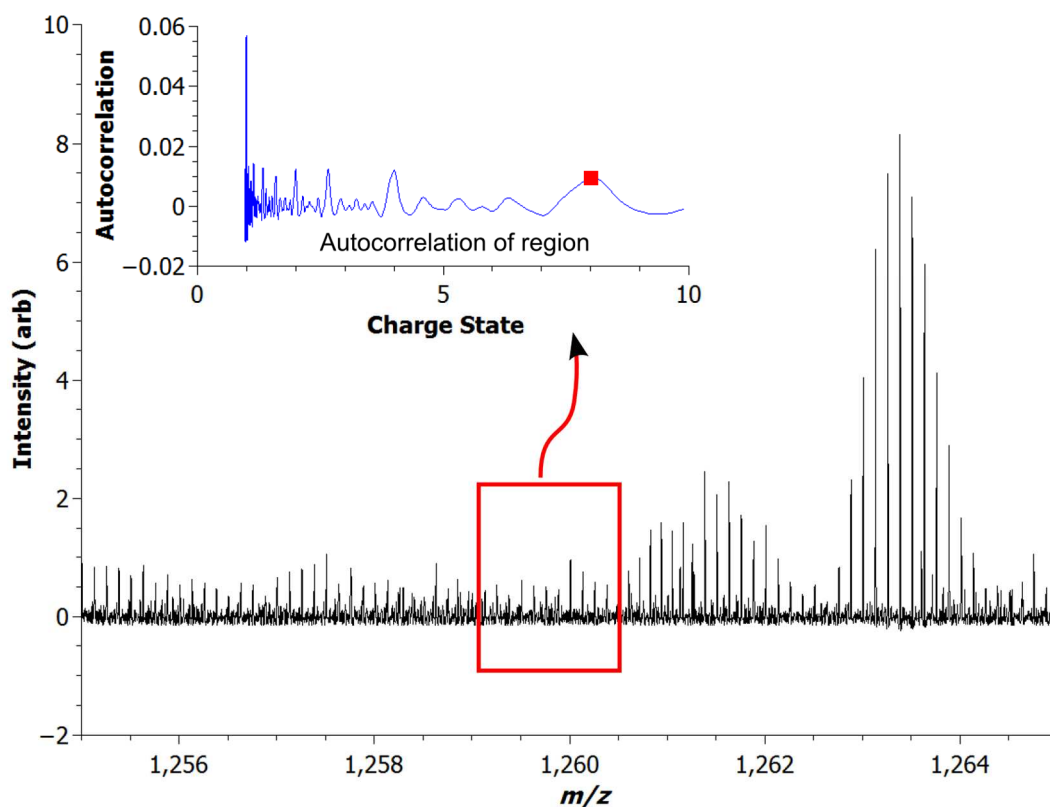
Appendix 33 FTICR-MS analysis of active ACP probe 64 incubated in the actinorhodin minimal system (1:4 ratio, protected ACP probe 63 to malonyl-ACP 7) showing an off-loaded putative cyclised hexaketide 156 at a charge state of 8^+ . Inset shows autocorrelation of region indicated confirming an 8^+ charge state.



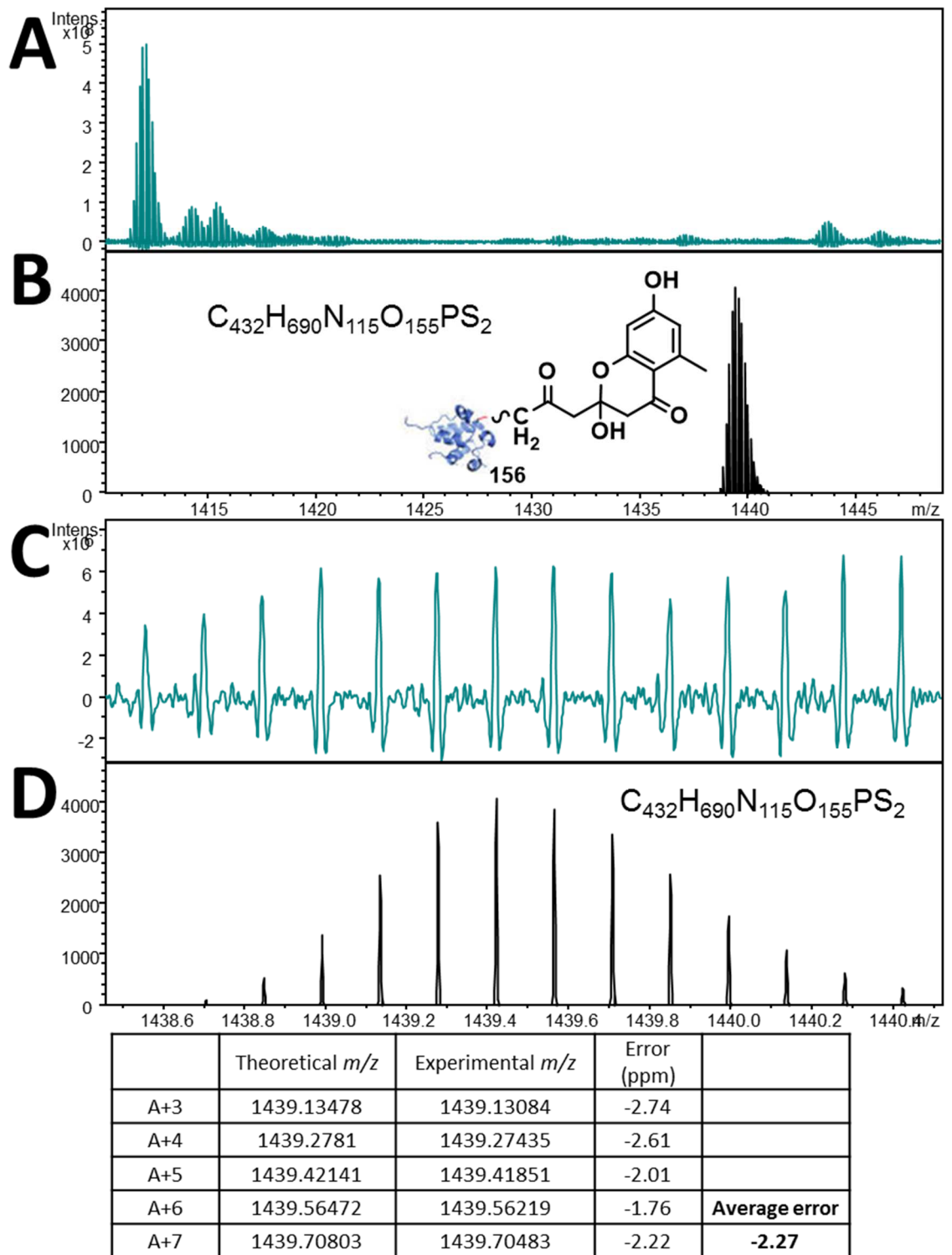
Appendix 34 FTICR-MS analysis of active ACP probe **64** incubated in the actinorhodin minimal system (1:4 ratio, protected ACP probe **63** to malonyl-ACP **7**, repeat) showing an off-loaded putative cyclised hexaketide **156**. (A) Acquired spectrum, (C) acquired spectrum magnified, (B) and (D) are simulated mass spectra (7^+). Underneath displays the peak list and errors for each.



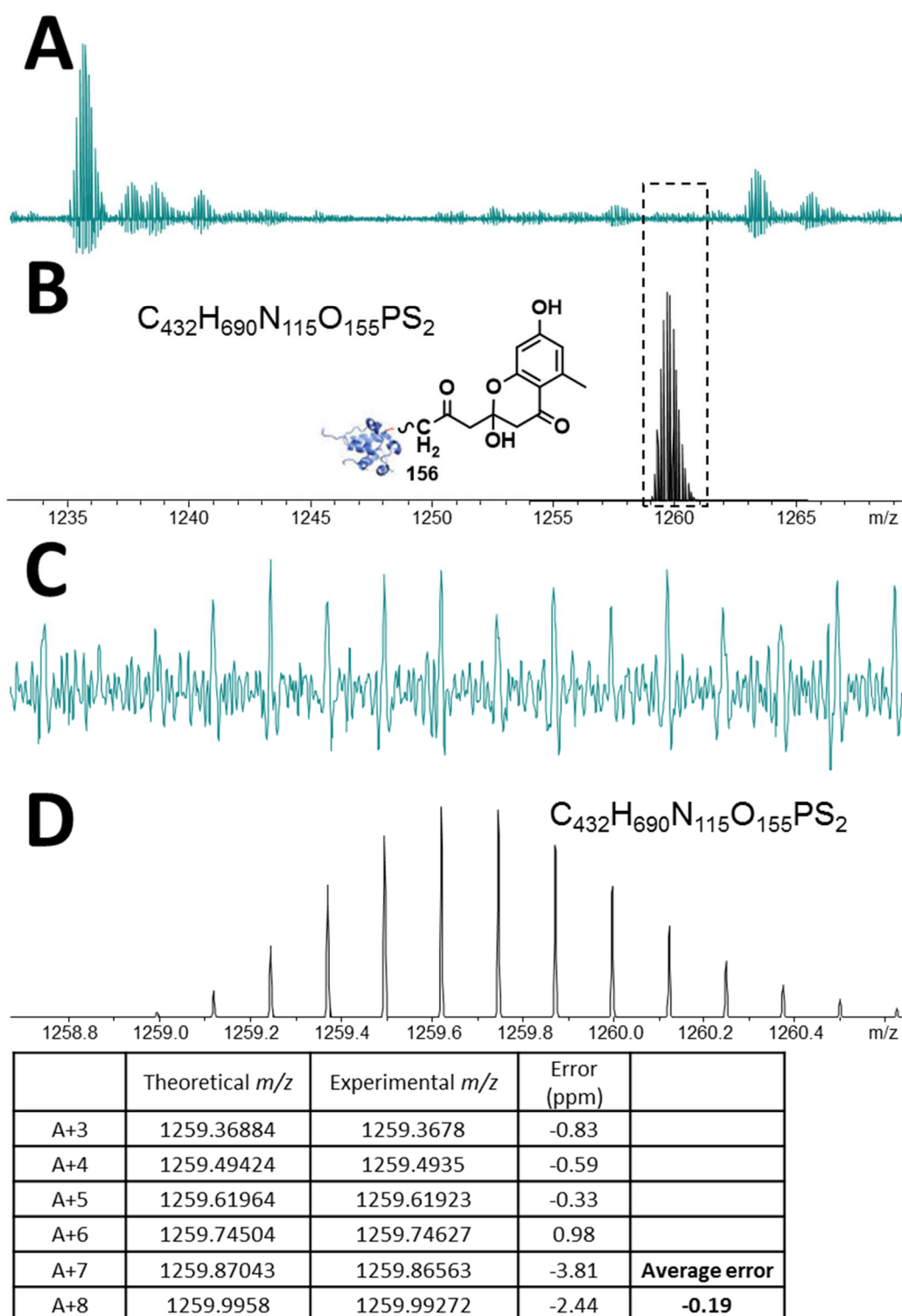
Appendix 35 FTICR-MS analysis of active ACP probe **64** incubated in the actinorhodin minimal system (1:4 ratio, protected ACP probe **63** to malonyl-ACP **7**, repeat) showing an off-loaded putative cyclised hexaketide **156**. (A) Acquired spectrum, (C) acquired spectrum magnified, (B) and (D) are simulated mass spectra (8^+). Underneath displays the peak list and errors for each.



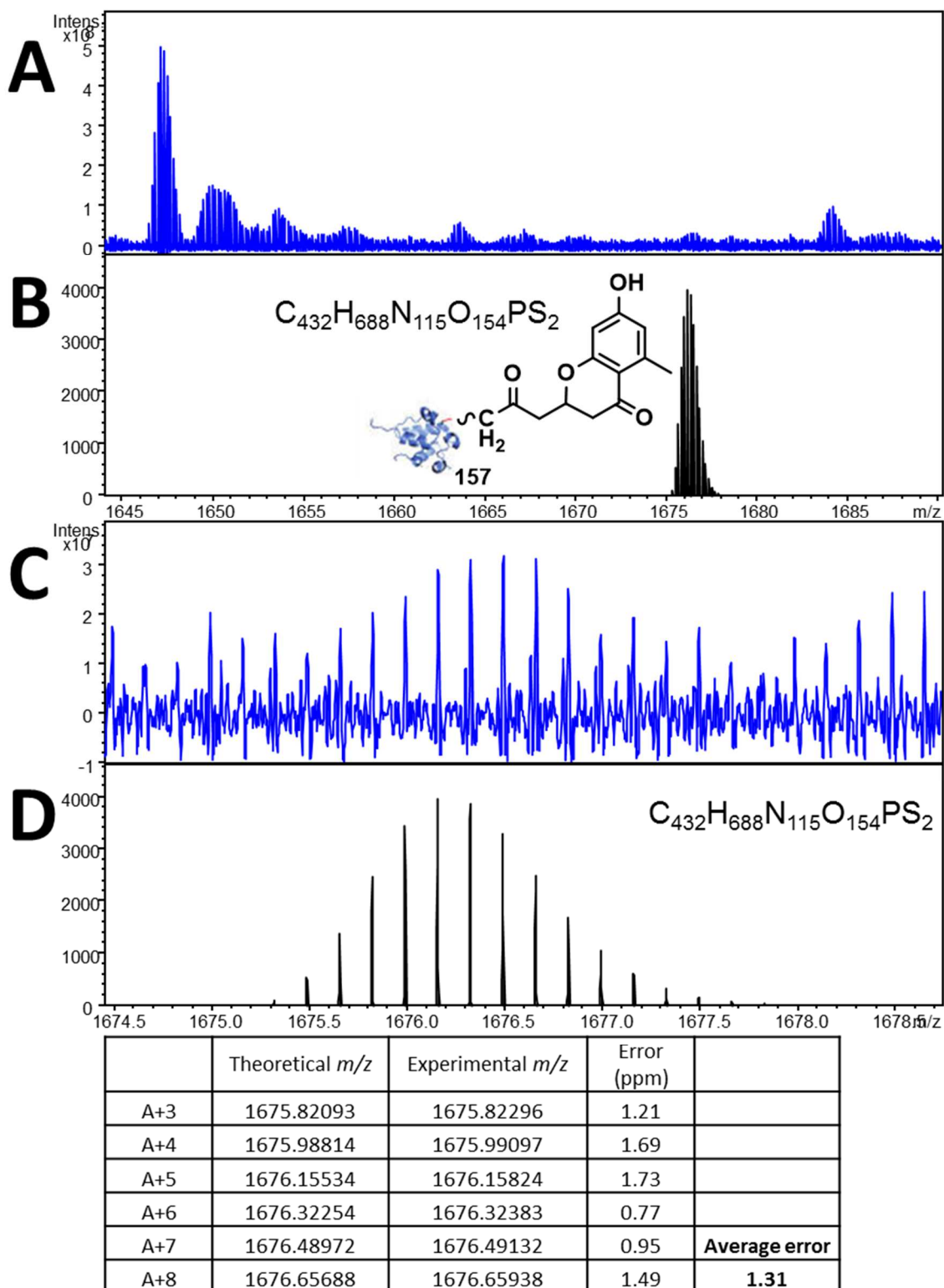
Appendix 36 FTICR-MS analysis of active ACP probe 64 incubated in the actinorhodin minimal system (1:4 ratio, protected ACP probe 63 to malonyl-ACP 7, repeat) showing an off-loaded putative cyclised hexaketide 156 at a charge state of 8^+ . Inset shows autocorrelation of region indicated confirming an 8^+ charge state.



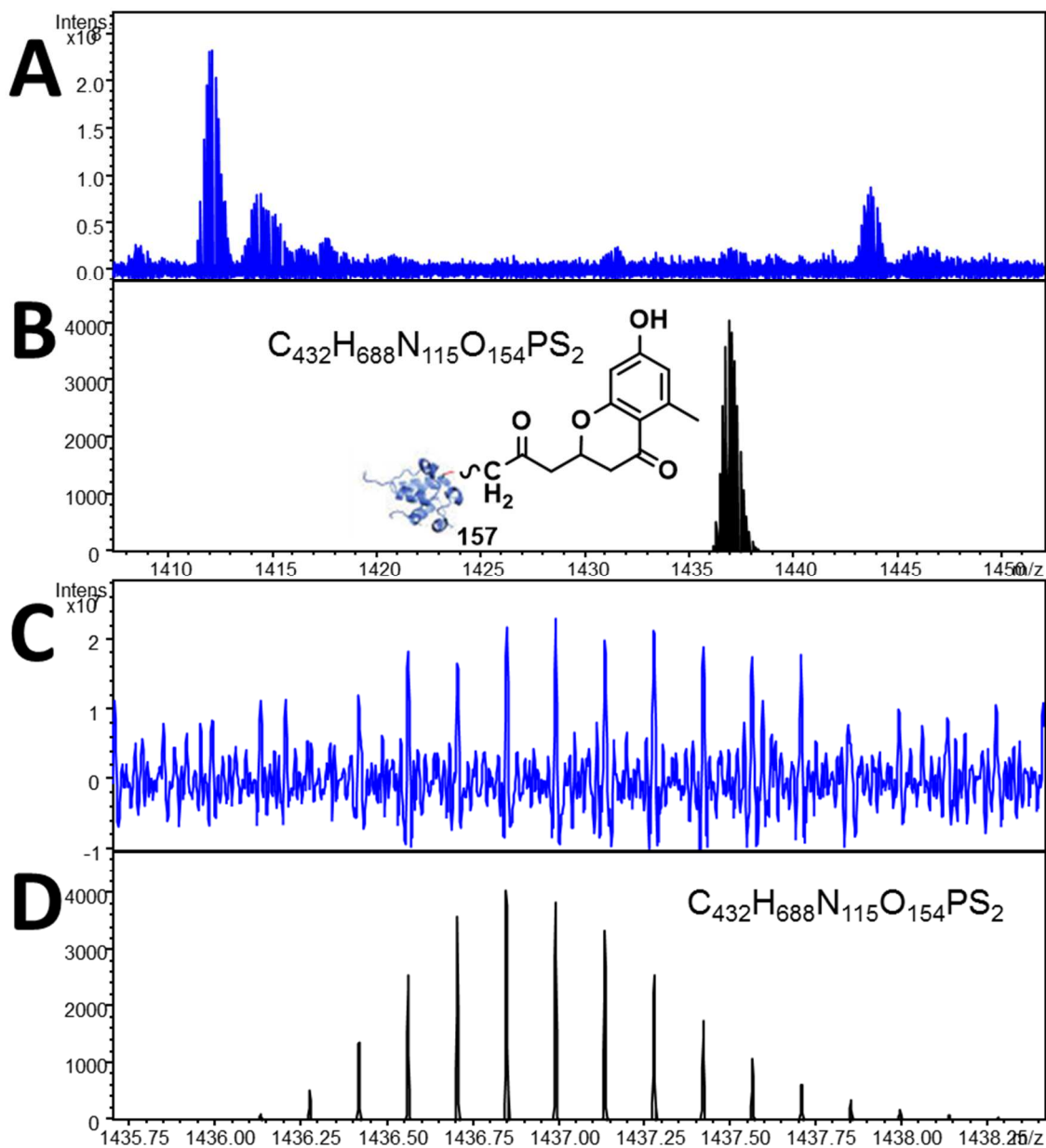
Appendix 37 FTICR-MS analysis of active ACP probe 64 incubated in the actinorhodin minimal system (5:1 ratio, protected ACP probe 63 to malonyl-ACP 7) showing an off-loaded putative cyclised hexaketide 156. (A) Acquired spectrum, (C) acquired spectrum magnified, (B) and (D) are simulated mass spectra (7^+). Underneath displays the peak list and errors for each.



Appendix 38 FTICR-MS analysis of active ACP probe **64** incubated in the actinorhodin minimal system (5:1 ratio, protected ACP probe **63** to malonyl-ACP **7**) showing an off-loaded putative cyclised hexaketide **156**. (A) Acquired spectrum, (C) acquired spectrum magnified, (B) and (D) are simulated mass spectra (8^+). Underneath displays the peak list and errors for each.

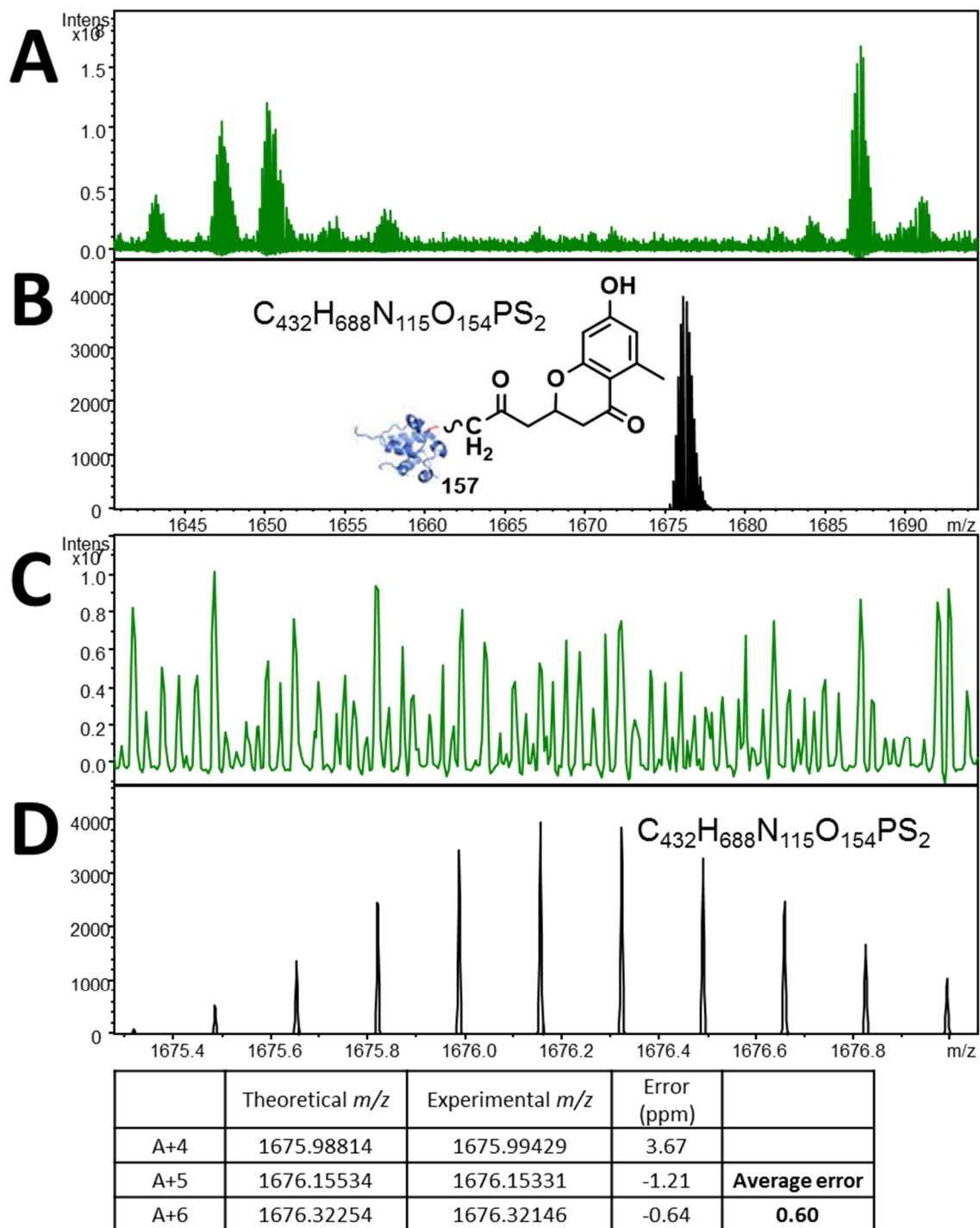


Appendix 39 FTICR-MS analysis of active ACP probe **64** incubated in the actinorhodin minimal system (1:1 ratio, protected ACP probe **63** to malonyl-ACP **7**) showing an off-loaded putative cyclised dehydrated hexaketide **157**. (A) Acquired spectrum, (C) acquired spectrum magnified, (B) and (D) are simulated mass spectra (6^+). Underneath displays the peak list and errors for each.

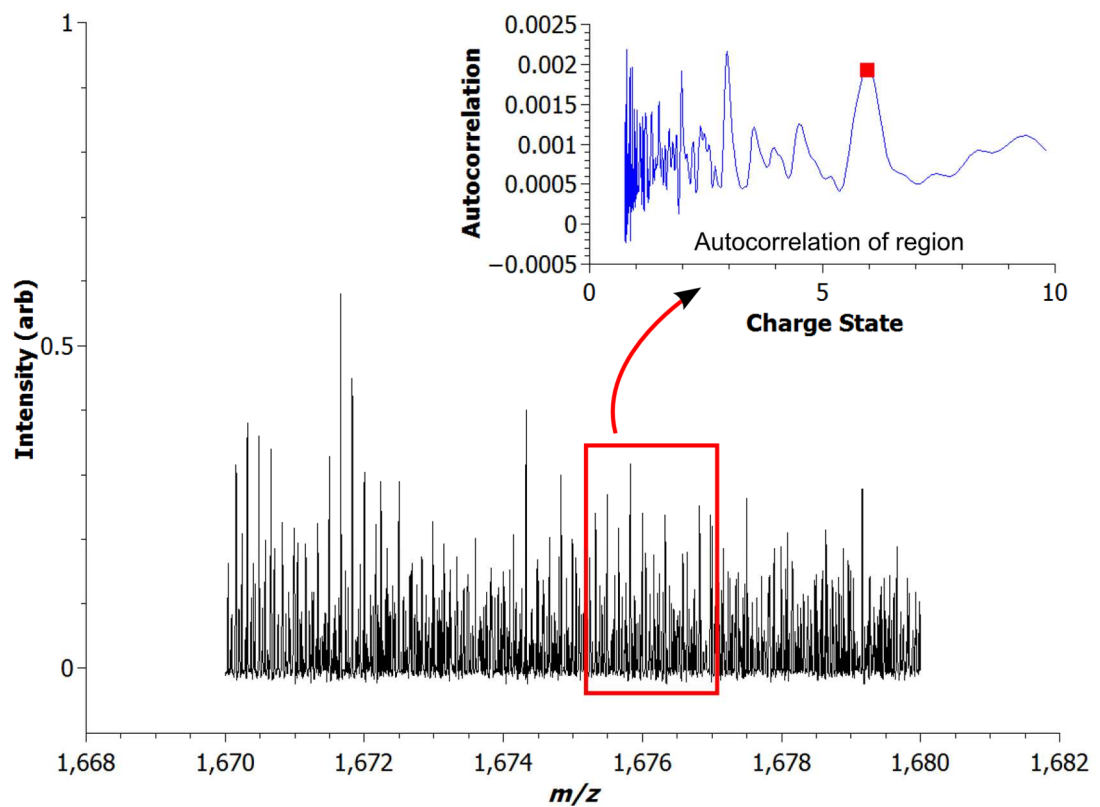


	Theoretical m/z	Experimental m/z	Error (ppm)	
A+3	1436.56184	1436.56125	-0.41	
A+4	1436.70516	1436.70504	-0.08	
A+5	1436.84847	1436.8486	0.09	
A+6	1436.99179	1436.99219	0.28	
A+7	1437.13509	1437.13581	0.50	Average error
A+8	1437.27837	1437.278	-0.26	0.02

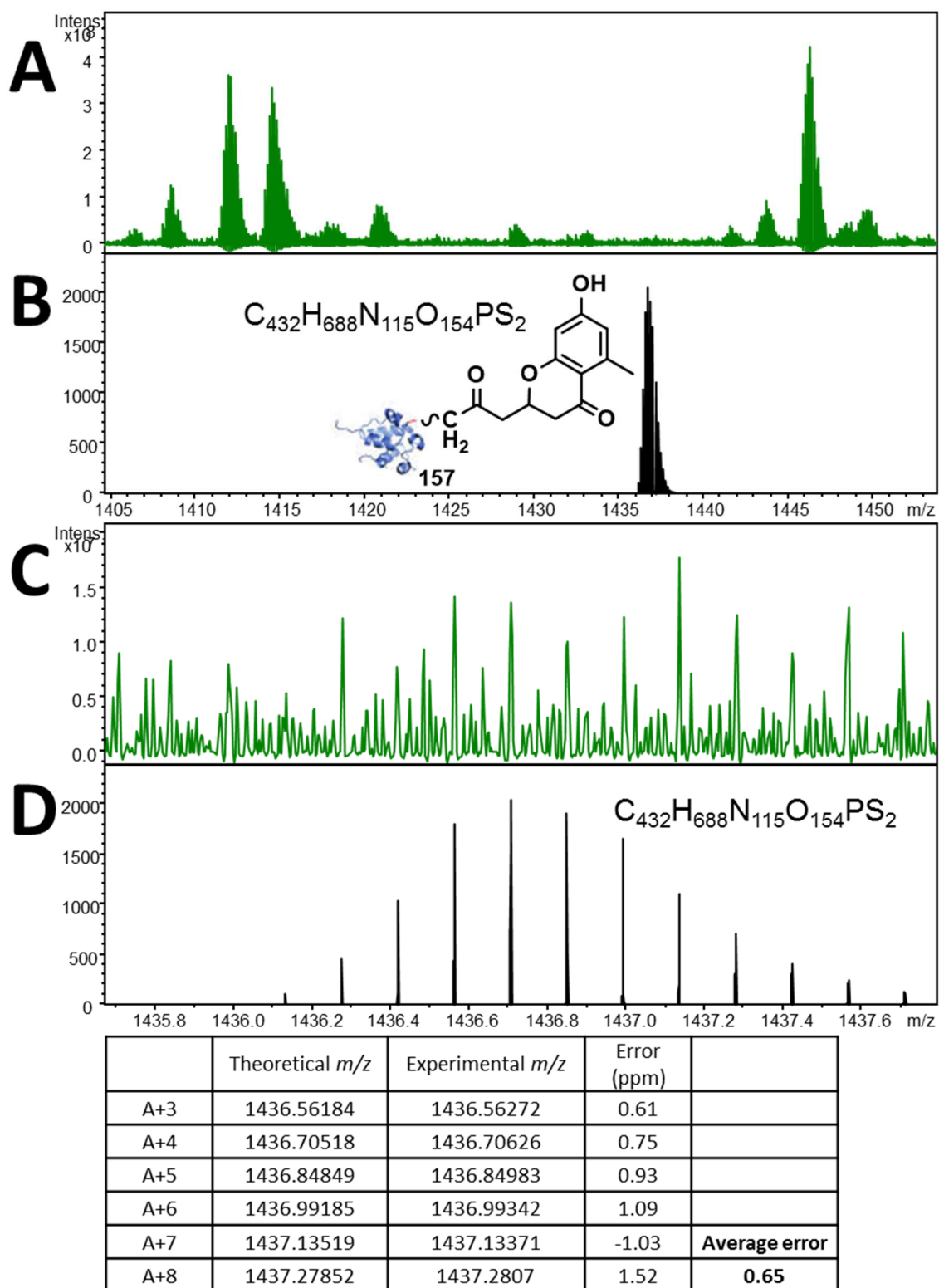
Appendix 40 FTICR-MS analysis of active ACP probe **64** incubated in the actinorhodin minimal system (1:1 ratio, protected ACP probe **63** to malonyl-ACP **7**) showing an off-loaded putative cyclised dehydrated hexaketide **157**. (A) Acquired spectrum, (C) acquired spectrum magnified, (B) and (D) are simulated mass spectra (7^+). Underneath displays the peak list and errors for each.



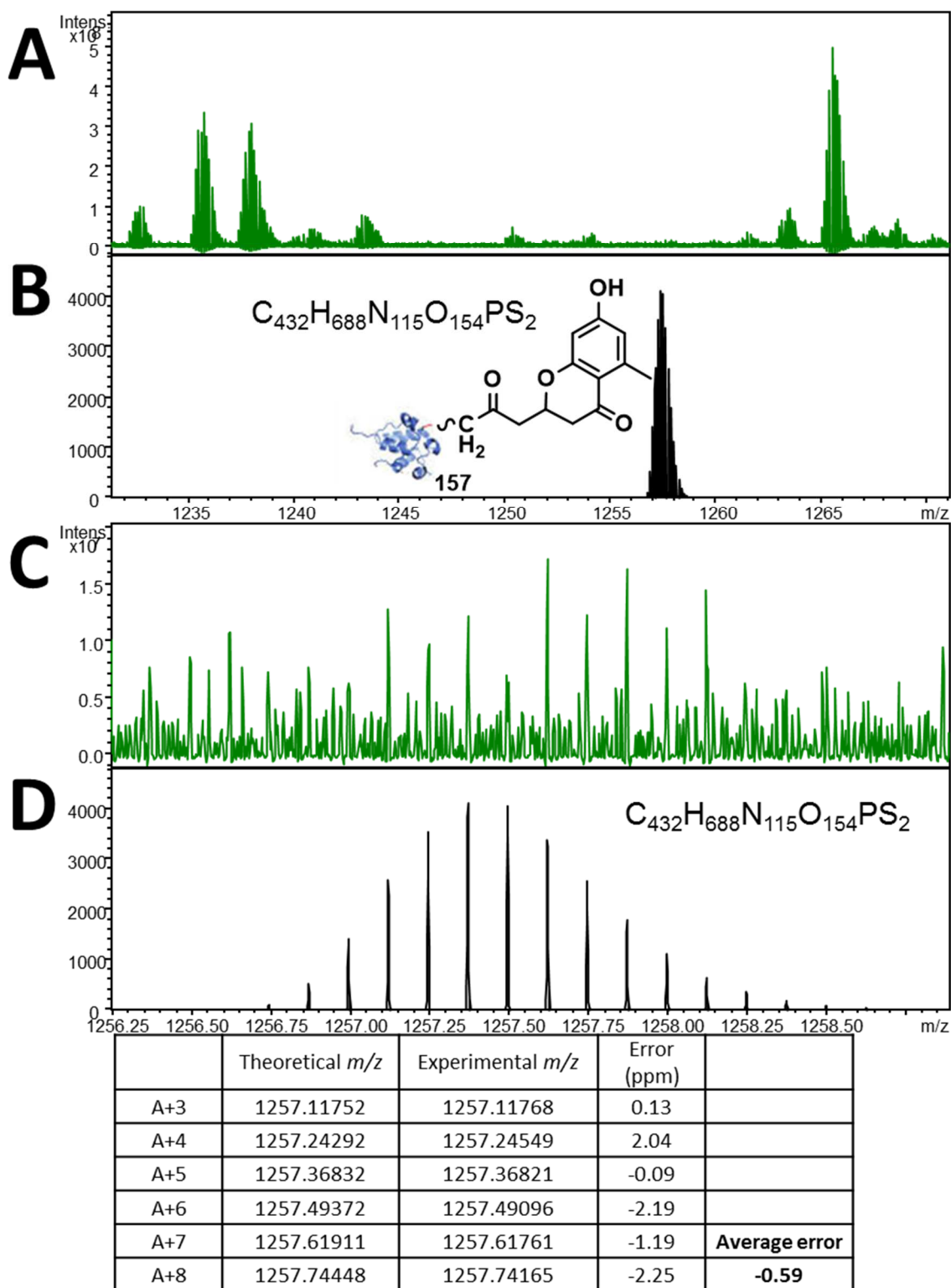
Appendix 41 FTICR-MS analysis of active ACP probe **64** incubated in the actinorhodin minimal system (1:1 ratio, protected ACP probe **63** to malonyl-ACP **7**, repeat) showing an off-loaded putative cyclised dehydrated hexaketide **157**. (A) Acquired spectrum, (C) acquired spectrum magnified, (B) and (D) are simulated mass spectra (6^+). Underneath displays the peak list and errors for each.



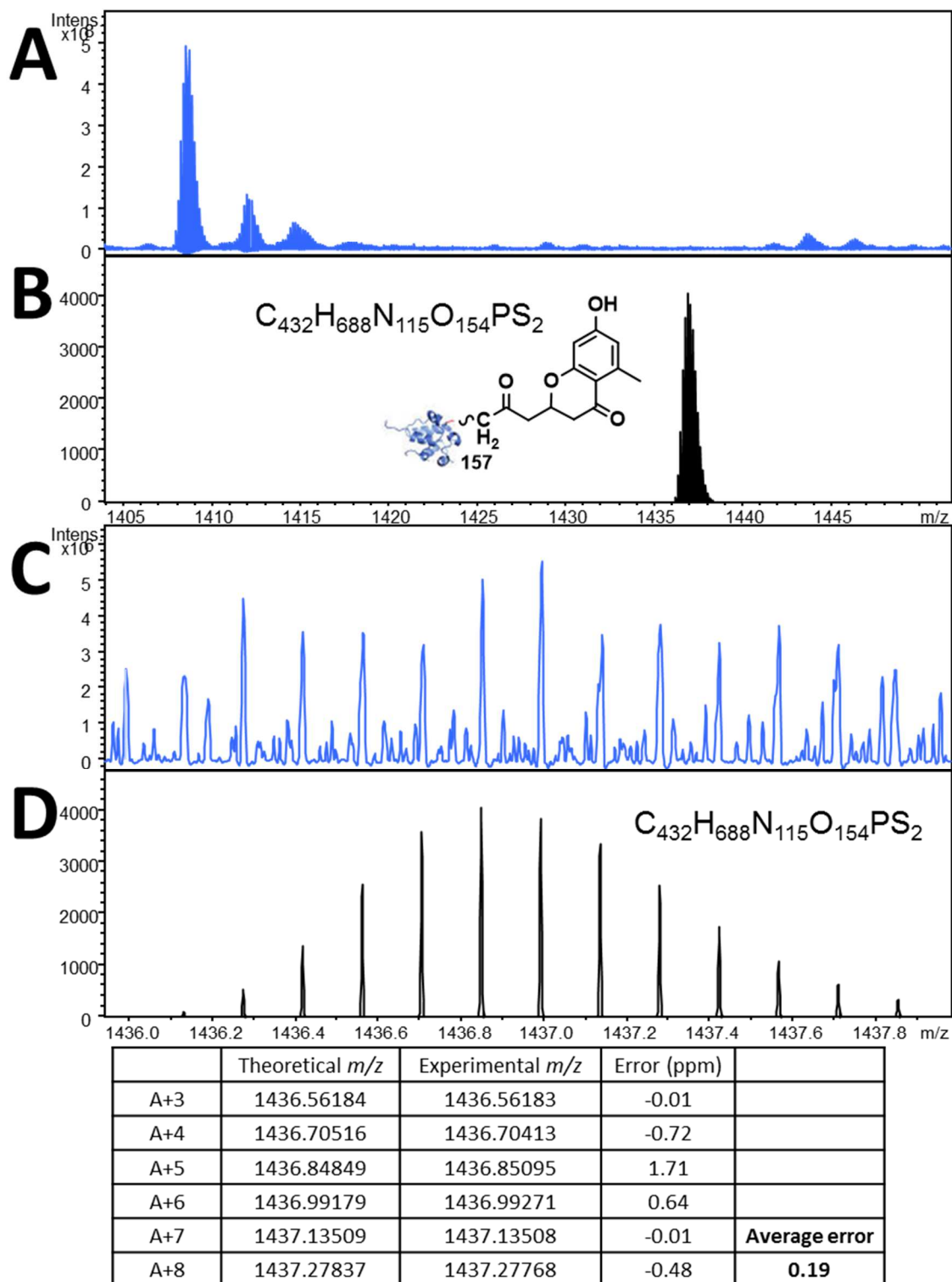
Appendix 42 FTICR-MS analysis of active ACP probe **64** incubated in the actinorhodin minimal system (1:1 ratio, protected ACP probe **63** to malonyl-ACP **7**, repeat) showing an off-loaded putative cyclised dehydrated hexaketide **157** at a charge state of 6^+ . Inset shows autocorrelation of region indicated confirming a 6^+ charge state.



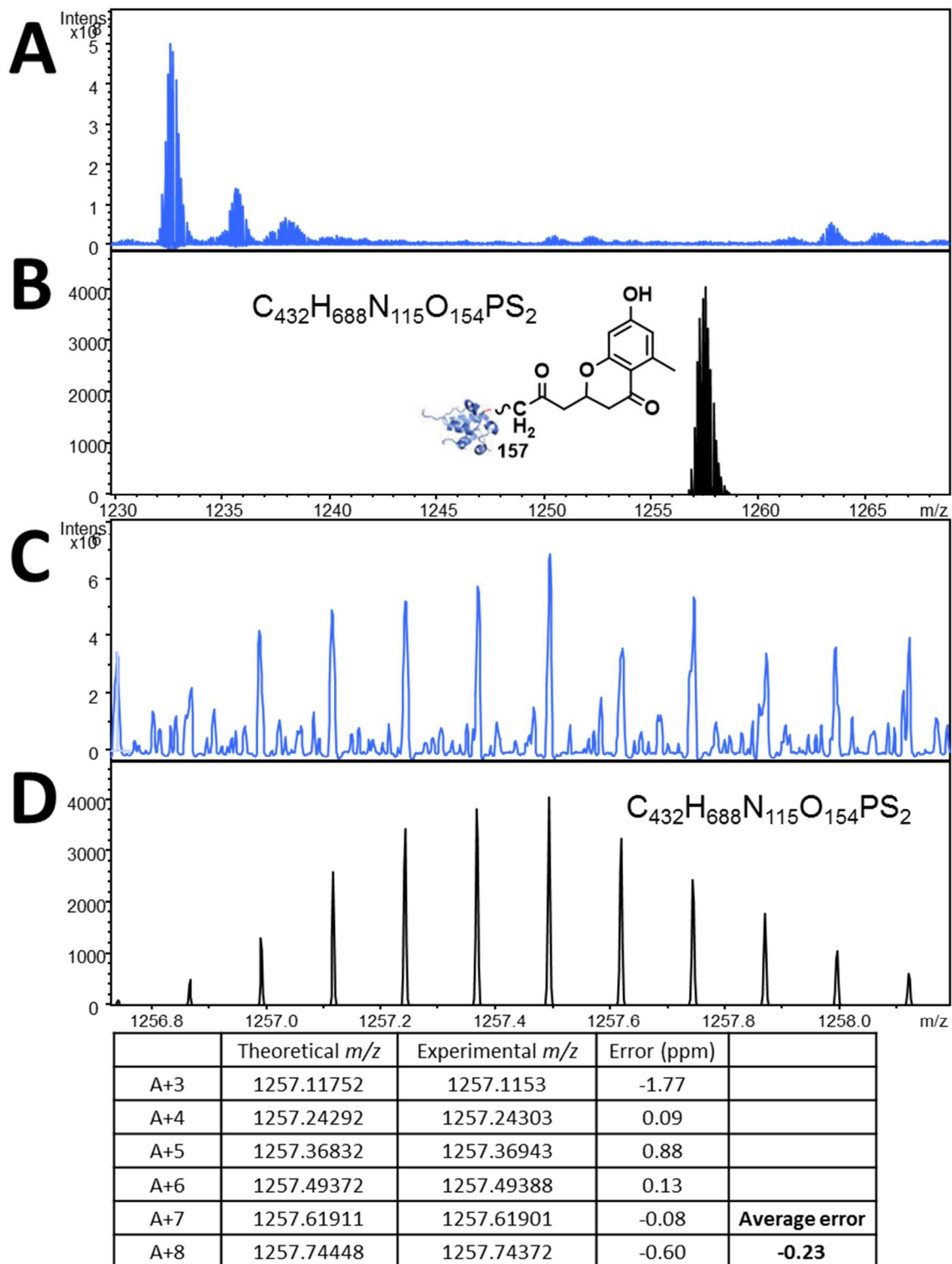
Appendix 43 FTICR-MS analysis of active ACP probe **64** incubated in the actinorhodin minimal system (1:1 ratio, protected ACP probe **63** to malonyl-ACP **7**, repeat) showing an off-loaded putative cyclised dehydrated hexaketide **157**. (A) Acquired spectrum, (C) acquired spectrum magnified, (B) and (D) are simulated mass spectra (7^+). Underneath displays the peak list and errors for each.



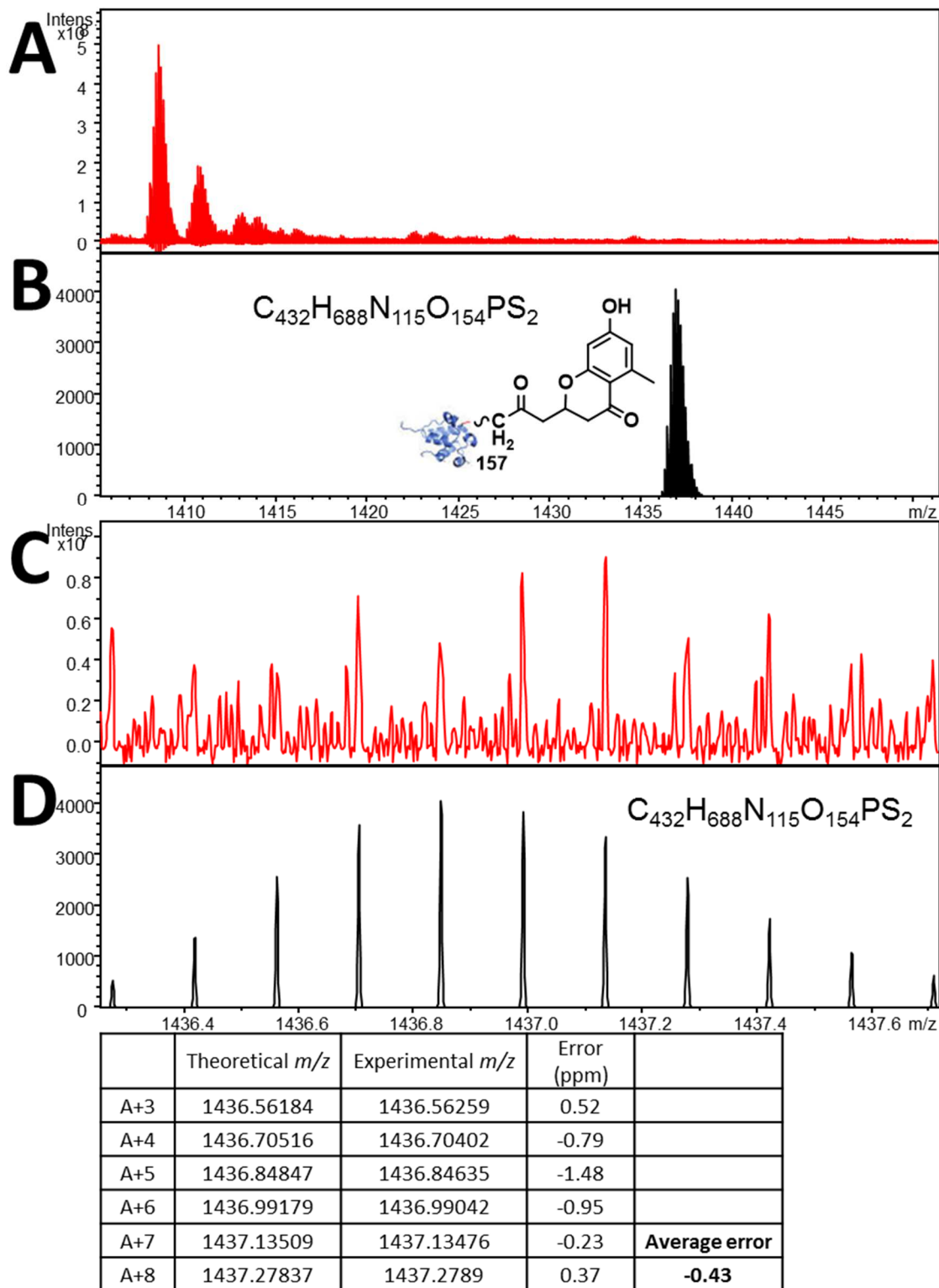
Appendix 44 FTICR-MS analysis of active ACP probe **64** incubated in the actinorhodin minimal system (1:1 ratio, protected ACP probe **63** to malonyl-ACP **7**, repeat) showing an off-loaded putative cyclised dehydrated hexaketide **157**. (A) Acquired spectrum, (C) acquired spectrum magnified, (B) and (D) are simulated mass spectra (8^+). Underneath displays the peak list and errors for each.



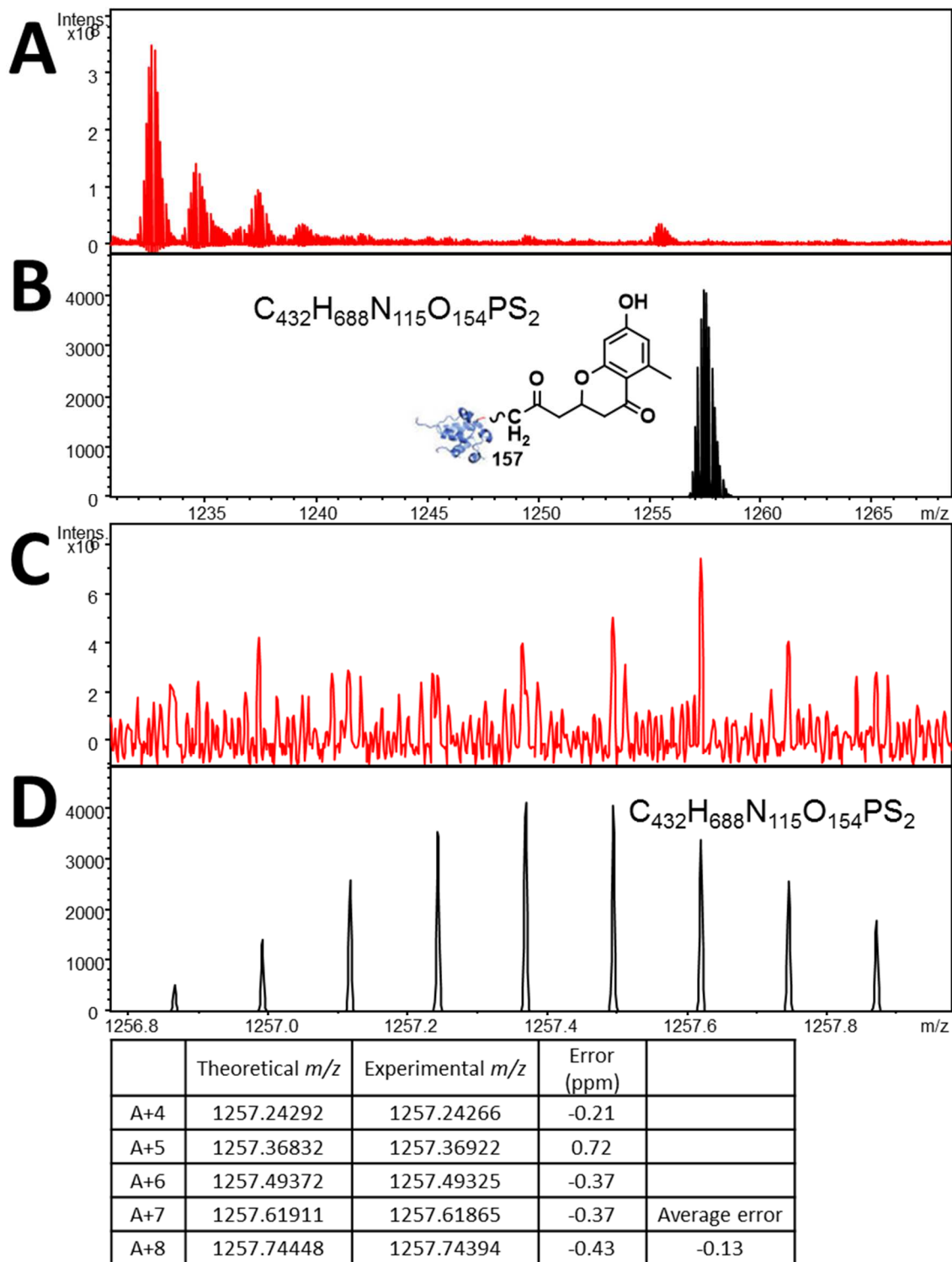
Appendix 45 FTICR-MS analysis of active ACP probe **64** incubated in the actinorhodin minimal system (1:4 ratio, protected ACP probe **63** to malonyl-ACP **7**) showing an off-loaded putative cyclised dehydrated hexaketide **157**. (A) Acquired spectrum, (C) acquired spectrum magnified, (B) and (D) are simulated mass spectra (7⁺). Underneath displays the peak list and errors for each.



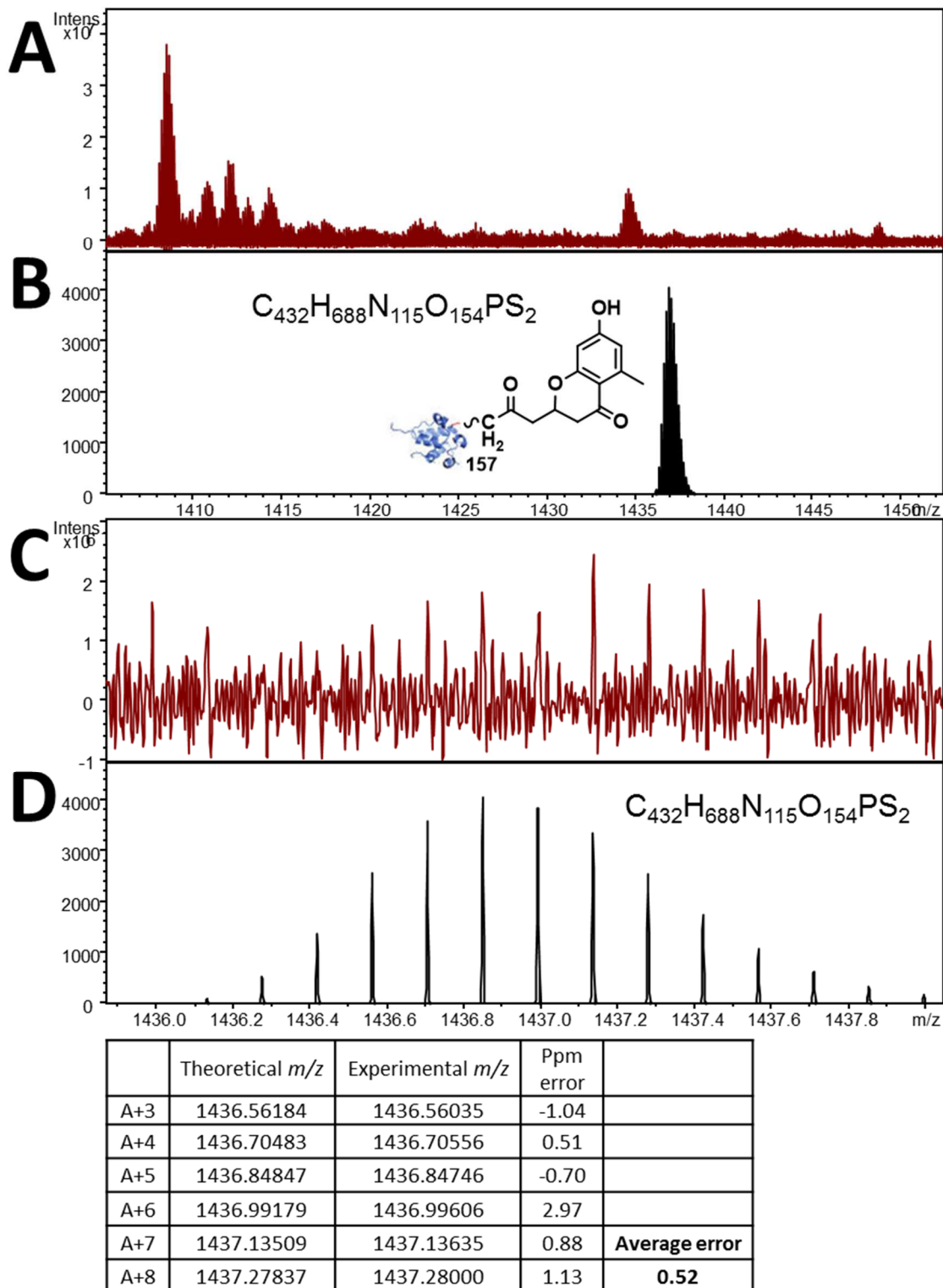
Appendix 46 FTICR-MS analysis of active ACP probe **64** incubated in the actinorhodin minimal system (1:4 ratio, protected ACP probe **63** to malonyl-ACP **7**) showing an off-loaded putative cyclised dehydrated hexaketide **157**. (A) Acquired spectrum, (C) acquired spectrum magnified, (B) and (D) are simulated mass spectra (8^+). Underneath displays the peak list and errors for each.



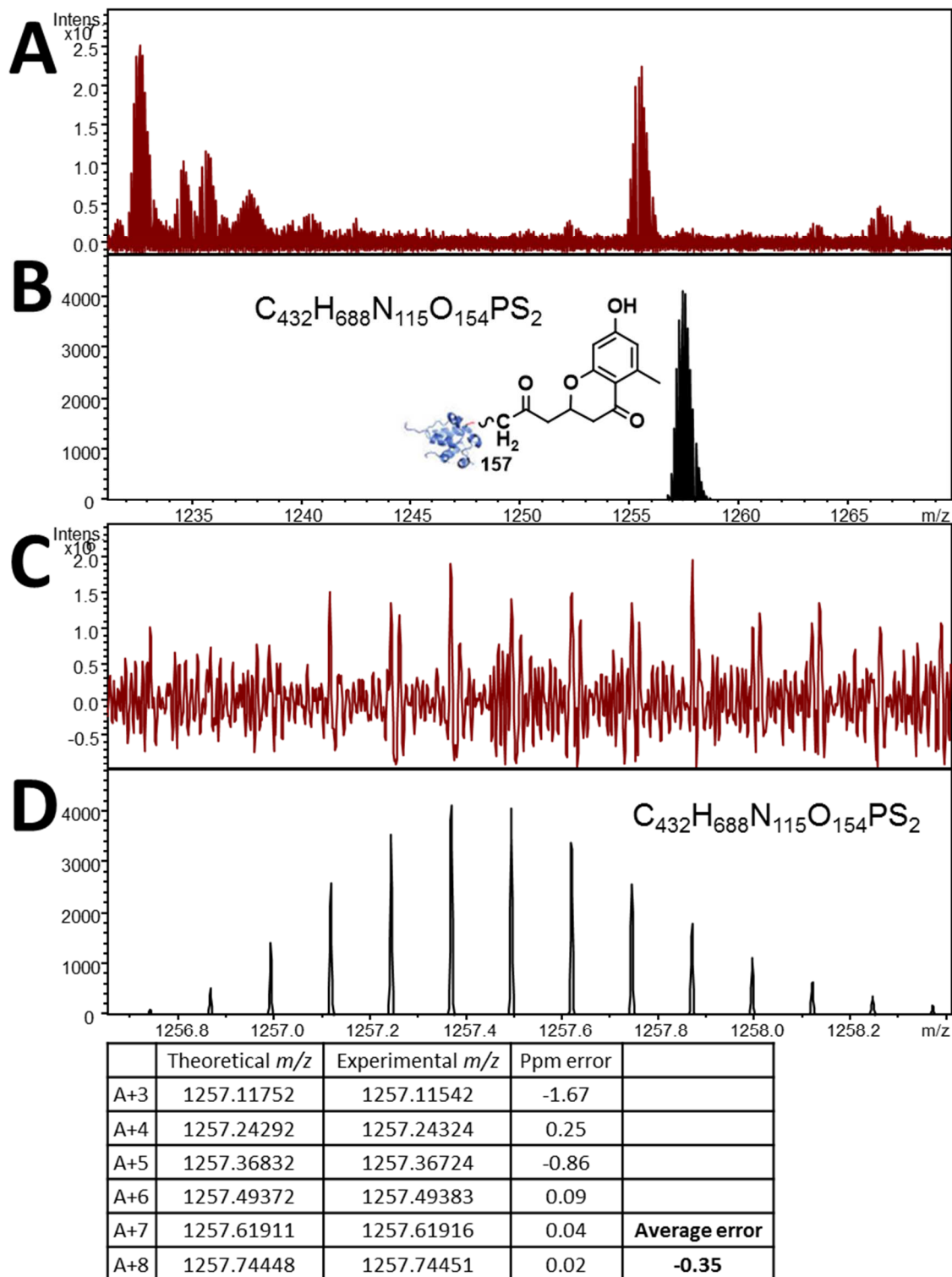
Appendix 47 FTICR-MS analysis of active acyl carrier protein (ACP) probe **64** incubated in the actinorhodin minimal system (1:1 ratio, protected ACP probe **63** to malonyl-ACP **7**, probe added after 30 seconds) showing an off-loaded putative cyclised dehydrated hexaketide **157**. (A) Acquired spectrum, (C) acquired spectrum magnified, (B) and (D) are simulated mass spectra (7^+). Underneath displays the peak list and errors for each.



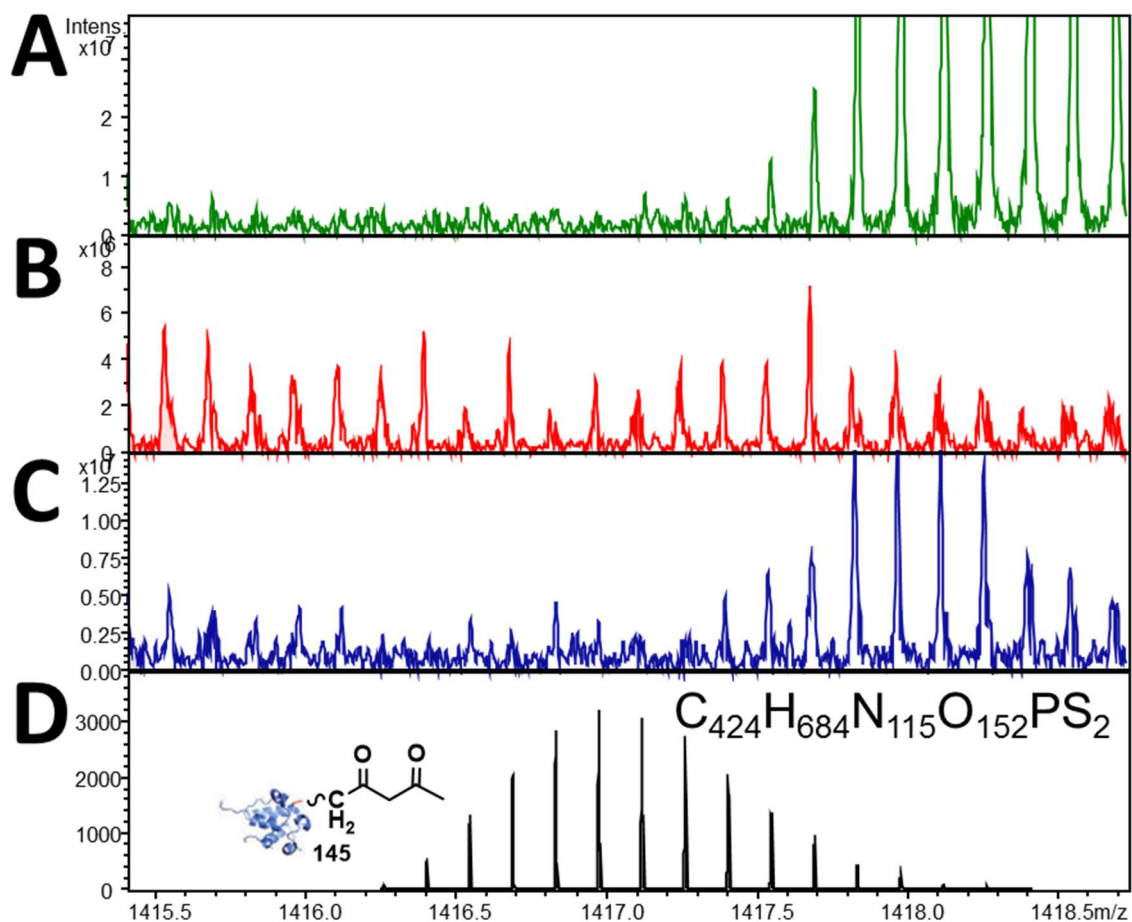
Appendix 48 FTICR-MS analysis of active ACP probe **64** incubated in the actinorhodin minimal system (1:1 ratio, protected ACP probe **63** to malonyl-ACP **7**, probe added after 30 seconds) showing an off-loaded putative cyclised dehydrated hexaketide **157**. (A) Acquired spectrum, (C) acquired spectrum magnified, (B) and (D) are simulated mass spectra (8^+). Underneath displays the peak list and errors for each.



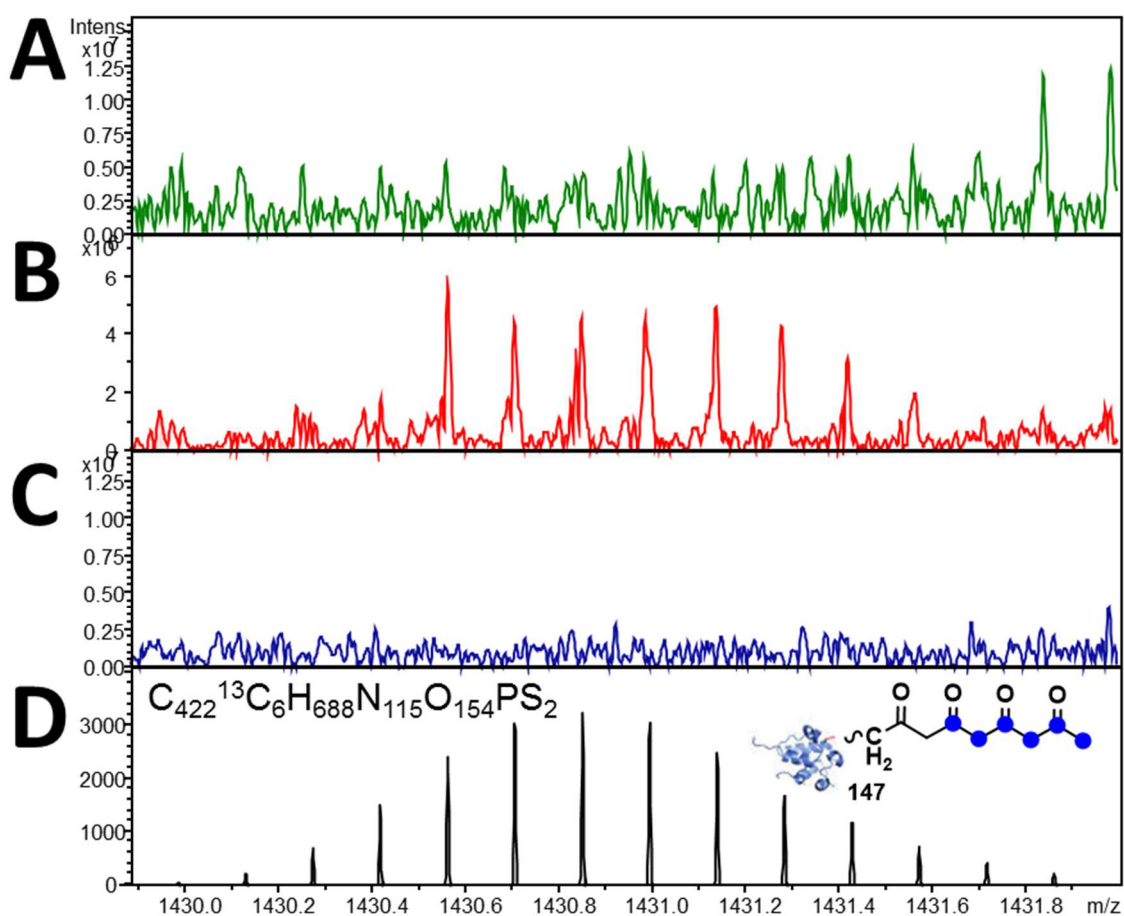
Appendix 49 FTICR-MS analysis of active ACP probe **64** incubated in the actinorhodin minimal system (1:1 ratio, protected ACP probe **63** to malonyl-ACP **7**, probe added after five minutes) showing an off-loaded putative cyclised dehydrated hexaketide **157**. (A) Acquired spectrum, (C) acquired spectrum magnified, (B) and (D) are simulated mass spectra (7^+). Underneath displays the peak list and errors for each.



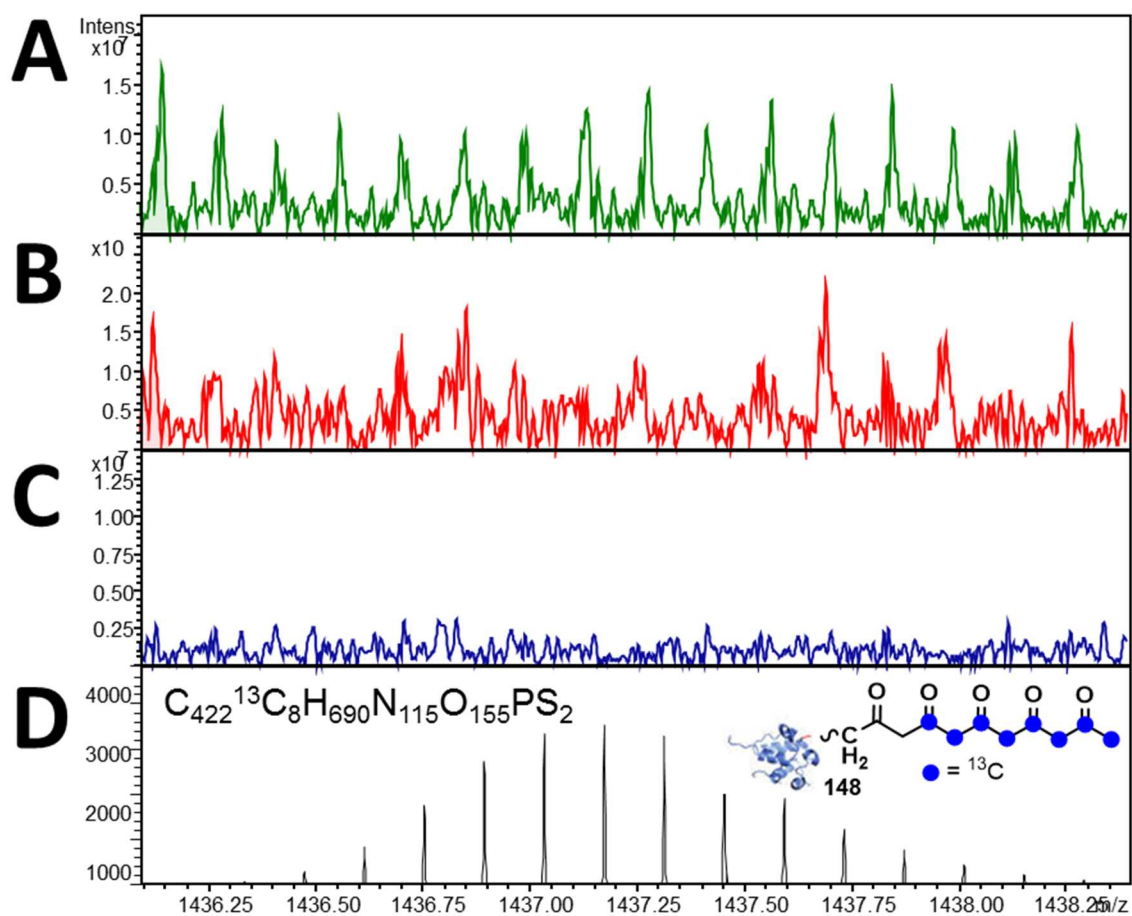
Appendix 50 FTICR-MS analysis of active ACP probe **64** incubated in the actinorhodin minimal system (1:1 ratio, protected ACP probe **63** to malonyl-ACP **7**, probe added after five minutes) showing an off-loaded putative cyclised dehydrated hexaketide **157**. (A) Acquired spectrum, (C) acquired spectrum magnified, (B) and (D) are simulated mass spectra (8^+). Underneath displays the peak list and errors for each.



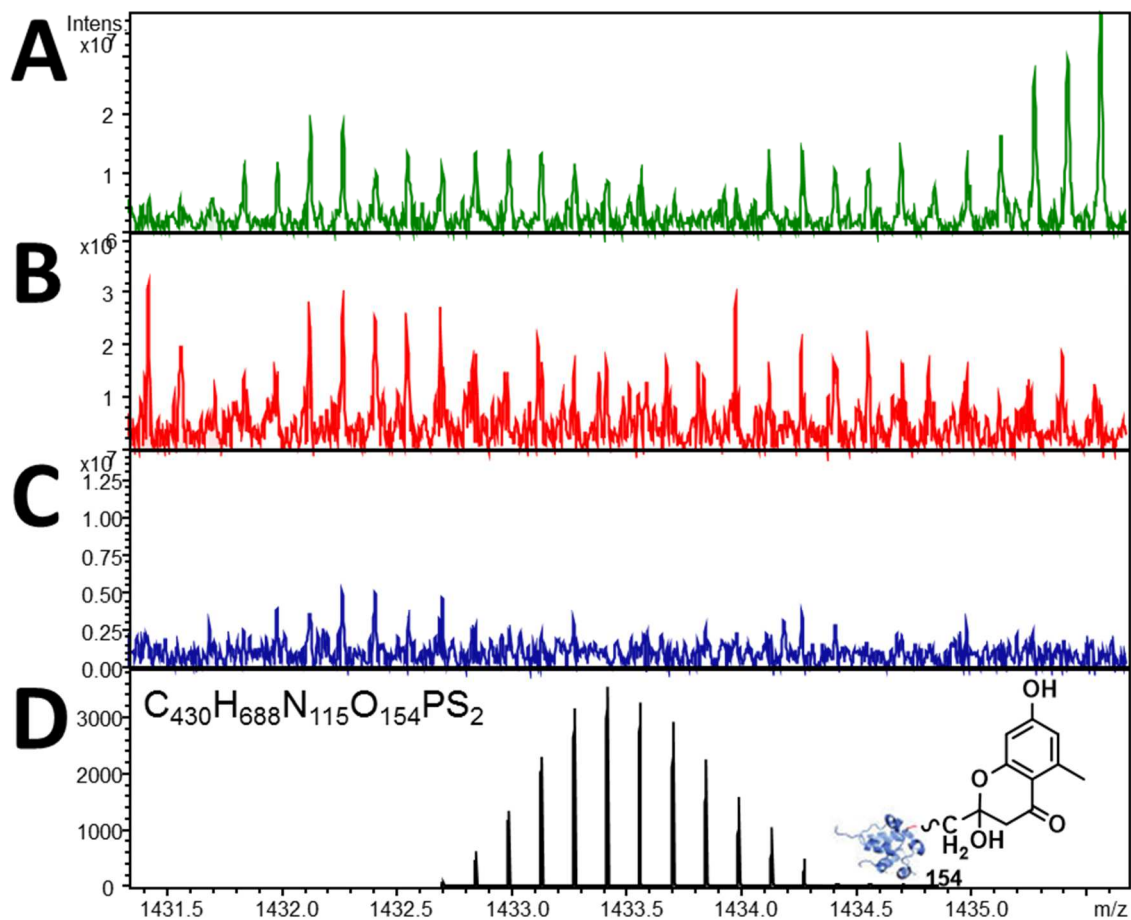
Appendix 51 FTICR-MS analysis of the ACP probe 63 (A) with irradiation but without the actinorhodin minimal system, (B) without irradiation and incubated in the actinorhodin minimal system (1:1 ratio, protected ACP probe 63 to malonyl-ACP 7), (C) without irradiation and without the actinorhodin minimal system. (D) Simulated mass spectrum (7^+) of an off-loaded putative diketide 145.



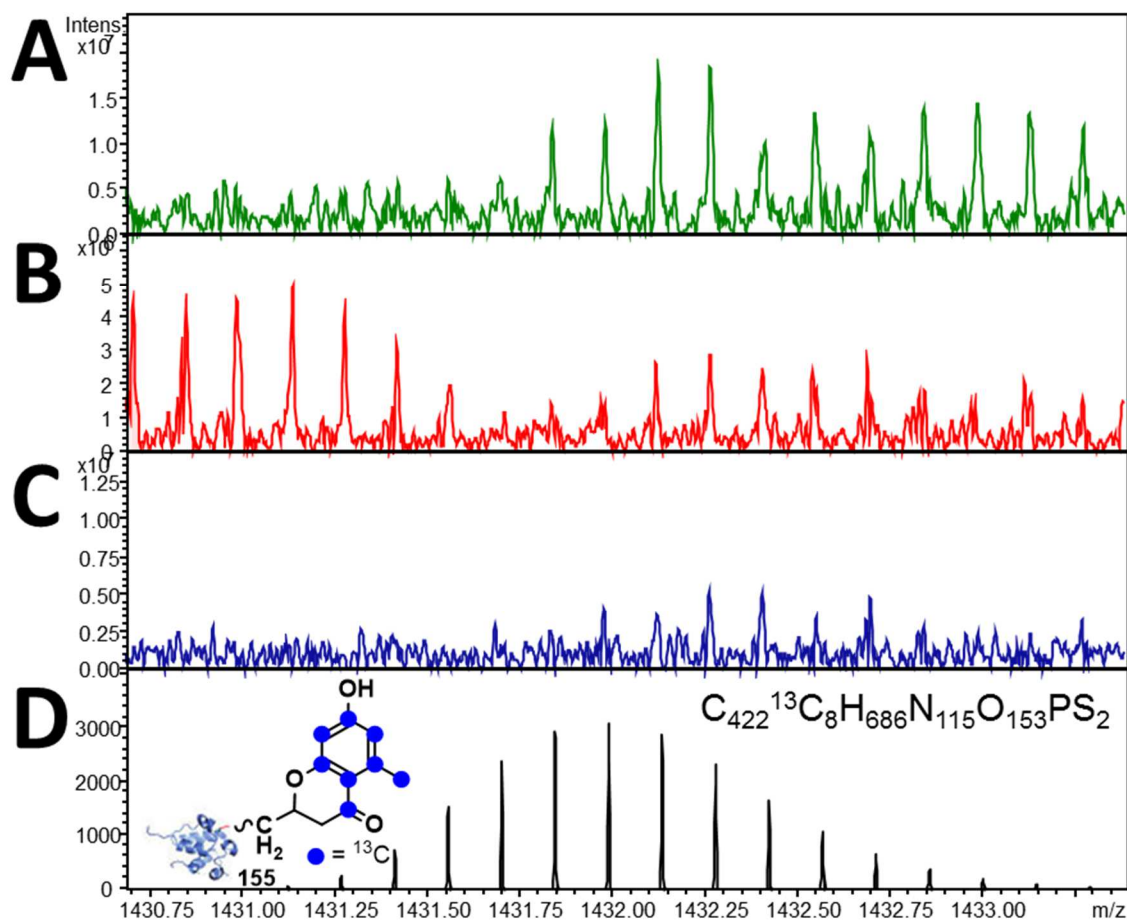
Appendix 52 FTICR-MS analysis of the ACP probe **63** (A) with irradiation but without the actinorhodin minimal system, (B) without irradiation and incubated in the actinorhodin minimal system (1:1 ratio, protected ACP probe **63** to malonyl-ACP **7**), (C) without irradiation and without the actinorhodin minimal system. (D) Simulated mass spectrum (7^+) of an off-loaded putative labelled linear tetraketide **147**.



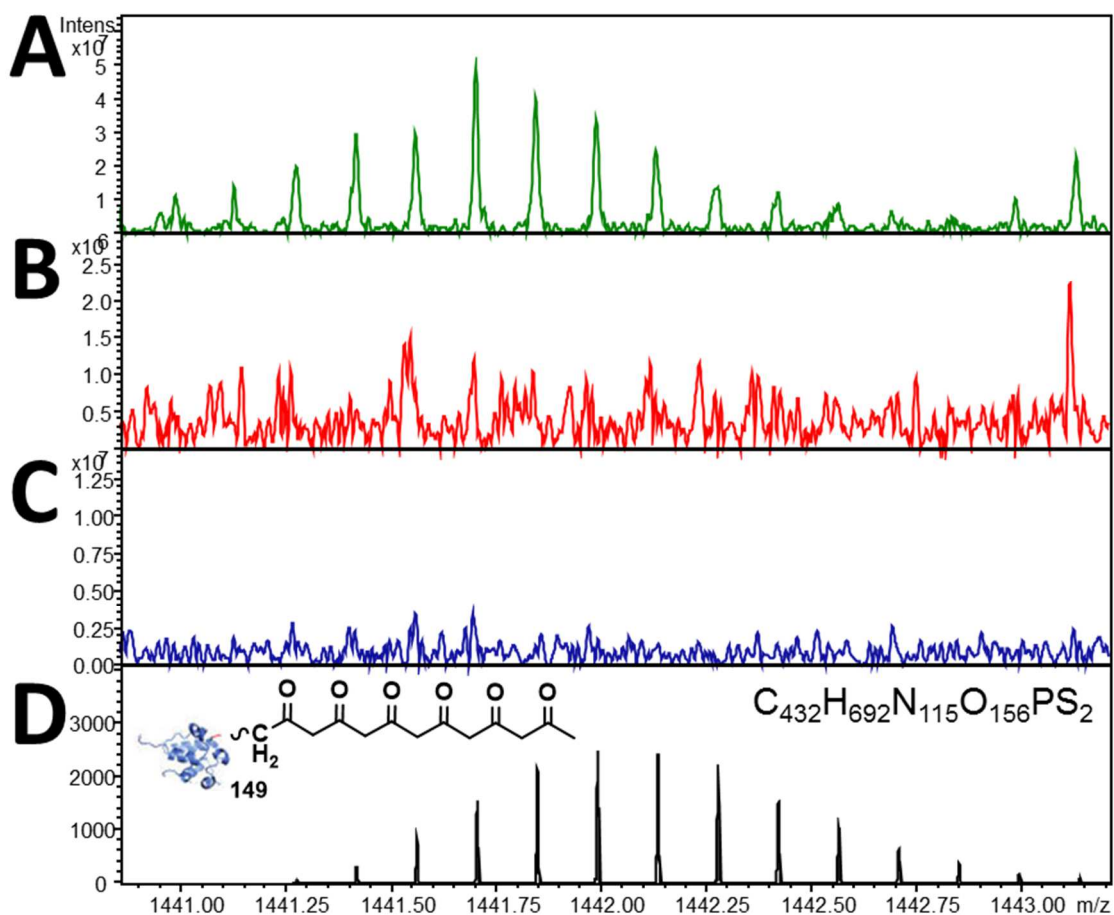
Appendix 53 FTICR-MS analysis of the ACP probe **63** (A) with irradiation but without the actinorhodin minimal system, (B) without irradiation and incubated in the actinorhodin minimal system (1:1 ratio, protected ACP probe **63** to malonyl-ACP **7**), (C) without irradiation and without the actinorhodin minimal system. (D) Simulated mass spectrum (7^+) of an off-loaded putative labelled linear pentaketide **148**.



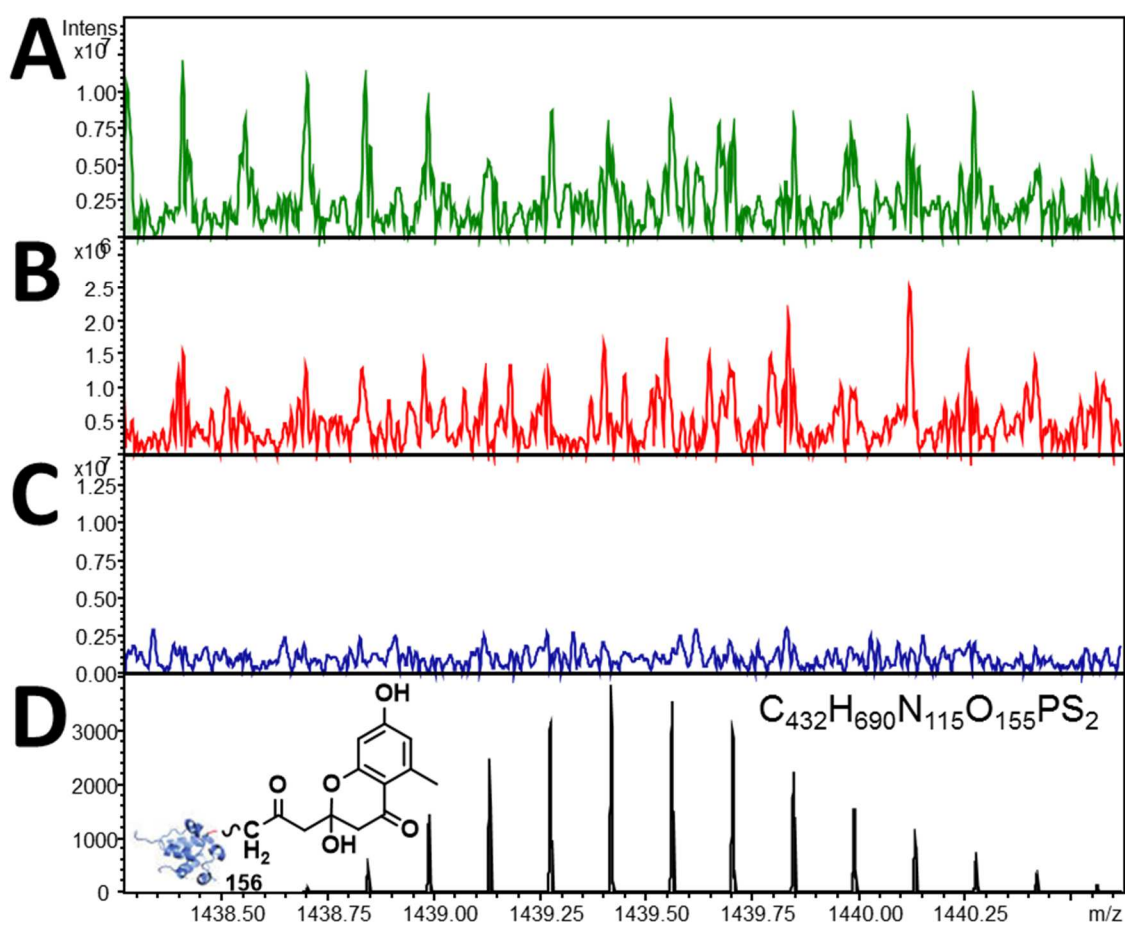
Appendix 54 FTICR-MS analysis of the ACP probe **63** (A) with irradiation but without the actinorhodin minimal system, (B) without irradiation and incubated in the actinorhodin minimal system (1:1 ratio, protected ACP probe **63** to malonyl-ACP **7**), (C) without irradiation and without the actinorhodin minimal system. (D) Simulated mass spectrum (7^+) of an off-loaded putative cyclised pentaketide **154**.



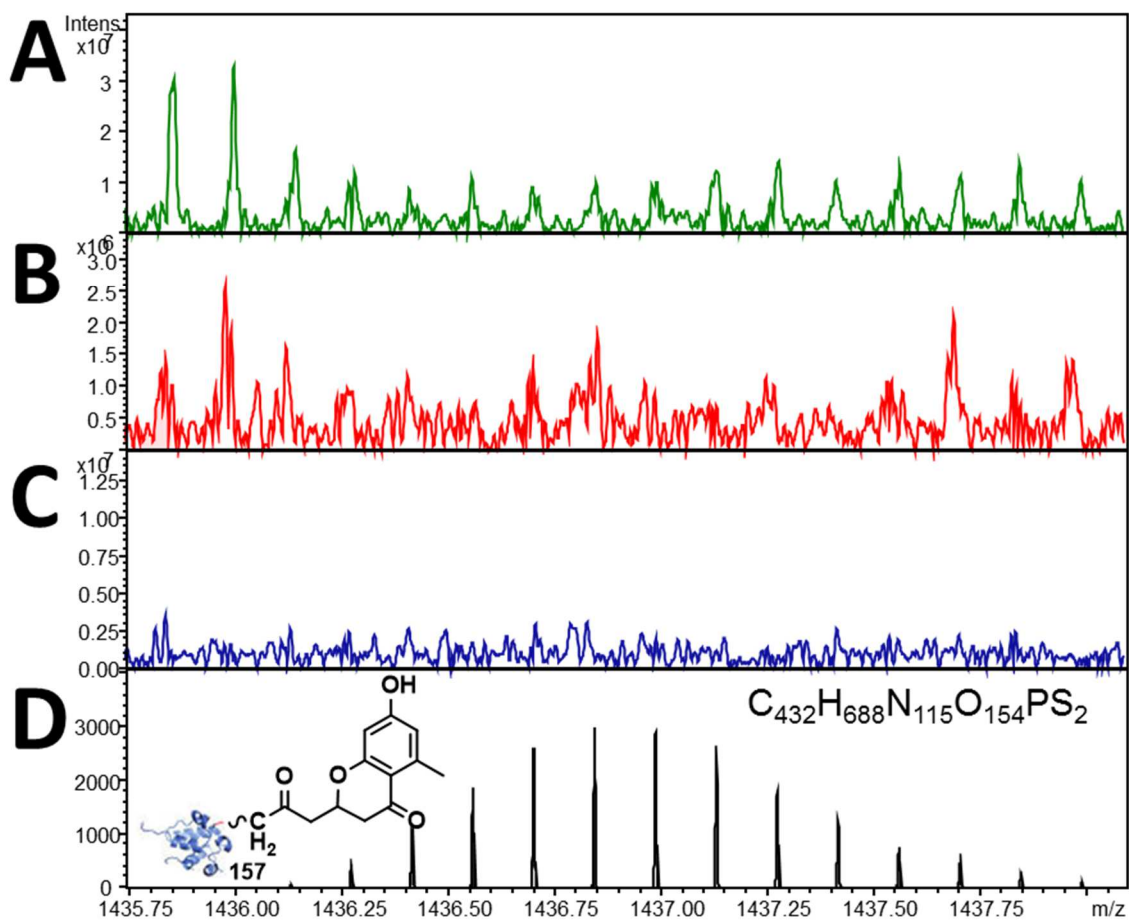
Appendix 55 FTICR-MS analysis of the ACP probe **63** (A) with irradiation but without the actinorhodin minimal system, (B) without irradiation and incubated in the actinorhodin minimal system (1:1 ratio, protected ACP probe **63** to malonyl-ACP **7**), (C) without irradiation and without the actinorhodin minimal system. (D) Simulated mass spectrum (7^+) of an off-loaded putative labelled cyclised dehydrated pentaketide **155**.



Appendix 56 FTICR-MS analysis of the ACP probe **63** (A) with irradiation but without the actinorhodin minimal system, (B) without irradiation and incubated in the actinorhodin minimal system (1:1 ratio, protected ACP probe **63** to malonyl-ACP **7**), (C) without irradiation and without the actinorhodin minimal system. (D) Simulated mass spectrum (7^+) of an off-loaded putative linear hexaketide **149**.



Appendix 57 FTICR-MS analysis of the ACP probe 63 (A) with irradiation but without the actinorhodin minimal system, (B) without irradiation and incubated in the actinorhodin minimal system (1:1 ratio, protected ACP probe 63 to malonyl-ACP 7), (C) without irradiation and without the actinorhodin minimal system. (D) Simulated mass spectrum (7^+) of an off-loaded putative cyclised hexaketide 156.



Appendix 58 FTICR-MS analysis of the ACP probe **63** (A) with irradiation but without the actinorhodin minimal system, (B) without irradiation and incubated in the actinorhodin minimal system (1:1 ratio, protected ACP probe **63** to malonyl-ACP **7**), (C) without irradiation and without the actinorhodin minimal system. (D) Simulated mass spectrum (7^+) of an off-loaded putative cyclised and dehydrated hexaketide **157**.

Peak and error tables – Results of trapping experiments with the ACP probe 63

1:1 ACP probe: malonyl-ACP 7						
Internal calibrant	Charge State	Average error of peaks A+3 to A+8 (ppm)				
Holo-ACP 43 Calibrated with A+4, A+5 and A+6	6	-0.55				
	7	0.18				
Decarboxylated ACP probe 144 Calibrated with A+4, A+5 and A+6	6	1.13				
	7	-0.05				
Protected ACP probe 63 Calibrated with A+4, A+5 and A+6	6	-1.09				
	7	-0.76				
Off-loaded intermediate	Charge State	Peak	Theoretical <i>m/z</i>	Experimental <i>m/z</i>	Error (ppm)	Average error of A+3 to A+8 (where applicable) (ppm)
Cyclised dehydrated hexaketide 157 $C_{432}H_{688}N_{115}O_{154}PS_2$	6	A+3	1675.82093	1675.82296	1.21	
	6	A+4	1675.98814	1675.99097	1.69	
	6	A+5	1676.15534	1676.15824	1.73	
	6	A+6	1676.32254	1676.32383	0.77	
	6	A+7	1676.48972	1676.49132	0.95	
	6	A+8	1676.65688	1676.65938	1.49	1.31
	6	A+9	1676.82407	1676.82372	-0.21	
	6	A+10	1676.99118	1676.99002	-0.69	
	7	A+2	1436.41851	1436.41800	-0.36	
	7	A+3	1436.56184	1436.56125	-0.41	
	7	A+4	1436.70516	1436.70504	-0.08	
	7	A+5	1436.84847	1436.84860	0.09	
	7	A+6	1436.99179	1436.99219	0.28	
	7	A+7	1437.13509	1437.13581	0.50	
	7	A+8	1437.27837	1437.27800	-0.26	0.02
	7	A+9	1437.42167	1437.42191	0.17	
7	A+10	1437.56491	1437.56350	-0.98		

Appendix 59 Peak list - FTICR-MS analysis of active ACP probe 64 incubated in the actinorhodin minimal system (1:1 ratio, protected ACP probe 63 to malonyl-ACP 7) showing an off-loaded putative cyclised dehydrated hexaketide 157 and internal calibration performed with holo-ACP, decarboxylated ACP probe 144 and protected ACP probe 63.

1:1 ACP probe 63:malonyl-ACP 7							
Internal calibrant	Charge State	Average error of peaks A+3 to A+8 (ppm)					
Apo-ACP 44 Calibrated with A+4, A+5 and A+6	7	0.39					
	8	-0.02					
	9	-0.25					
	10	0.23					
Holo-ACP 43 Calibrated with A+4, A+5 and A+6	6	-0.73					
	7	-0.94					
	8	-0.21					
	9	-0.48					
Decarboxylated ACP probe 144 Calibrated with A+4, A+5 and A+6.	6	0.83					
	7	-0.34					
	8	-0.52					
	9	-0.51					
Protected ACP probe 63 Calibrated with A+4, A+5 and A+6	6	-0.27					
	7	0.83					
	8	0.79					
	9	-0.03					
	10	-0.04					
	Off-loaded intermediate	Charge State	Peak	Theoretical m/z	Experimental m/z	Error (ppm)	Average error of A+3 to A+8 (where applicable) (ppm)
	Diketide 145 C ₄₂₄ H ₆₈₄ N ₁₁₅ O ₁₅₂ PS ₂	6	A+4	1653.98462	1653.97619	-5.10	
6		A+5	1654.15181	1654.14877	-1.84		
6		A+6	1654.31900	1654.31695	-1.24		
6		A+7	1654.48620	1654.48074	-3.30	-2.82	
6		A+8	1654.65336	1654.64899	-2.64		
7		A+2	1417.55835	1417.55528	-2.17		
7		A+3	1417.70168	1417.69829	-2.39		
7		A+4	1417.84502	1417.84459	-0.30		
7		A+5	1417.98831	1417.98766	-0.46		
7		A+6	1418.13169	1418.13052	-0.83		
7		A+7	1418.27492	1418.27390	-0.72	-0.92	
7		A+8	1418.41820	1418.41706	-0.80		
7		A+9	1418.56151	1418.56025	-0.89		
7		A+10	1418.70474	1418.70002	-3.33		
8		A+2	1240.48947	1240.48227	-5.80		
8		A+3	1240.61488	1240.61088	-3.22		
8	A+4	1240.74028	1240.74020	-0.06			
8	A+5	1240.86568	1240.86476	-0.74			
8	A+6	1240.99107	1240.98928	-1.44			

Off-loaded intermediate	Charge State	Peak	Theoretical <i>m/z</i>	Experimental <i>m/z</i>	Error (ppm)	Average error of A+3 to A+8 (where applicable) (ppm)
	8	A+7	1241.11647	1241.11641	-0.05	-1.03
	8	A+8	1241.24184	1241.24099	-0.68	
	8	A+9	1241.36723	1241.36560	-1.31	
	8	A+10	1241.49256	1241.49023	-1.88	
	9	A+3	1102.88070	1102.88109	0.35	
	9	A+4	1102.99217	1102.98733	-4.39	
	9	A+5	1103.10364	1103.10344	-0.18	
	9	A+6	1103.21509	1103.21563	0.49	
	9	A+7	1103.32656	1103.32587	-0.63	-0.71
	9	A+8	1103.43800	1103.43811	0.10	
	9	A+9	1103.54946	1103.54643	-2.75	
	9	A+10	1103.66086	1103.66068	-0.16	
	10	A+1	992.49269	992.48840	-4.32	
	10	A+2	992.59303	992.58718	-5.89	
	10	A+3	992.69336	992.69396	0.60	
	10	A+4	992.79368	992.79438	0.71	
	10	A+5	992.89400	992.89482	0.83	
	10	A+6	992.99431	992.99405	-0.26	
	10	A+7	993.09463	993.09417	-0.46	0.19
	10	A+8	993.19493	993.19467	-0.26	
	10	A+9	993.29524	993.29200	-3.26	
	10	A+10	993.39550	993.39254	-2.98	
Cyclised dehydrated hexaketide 157 C ₄₃₂ H ₆₈₈ N ₁₁₅ O ₁₅₄ PS ₂	6	A+4	1675.98814	1675.99429	3.67	
	6	A+5	1676.15534	1676.15331	-1.21	0.60
	6	A+6	1676.32254	1676.32146	-0.64	
	7	A+2	1436.41850	1436.41587	-1.83	
	7	A+3	1436.56184	1436.56272	0.61	
	7	A+4	1436.70518	1436.70626	0.75	
	7	A+5	1436.84849	1436.84983	0.93	
	7	A+6	1436.99185	1436.99342	1.09	
	7	A+7	1437.13519	1437.13371	-1.03	0.65
	7	A+8	1437.27852	1437.28070	1.52	
	7	A+9	1437.42167	1437.42104	-0.44	
	8	A+2	1256.99211	1256.99244	0.26	
	8	A+3	1257.11752	1257.11768	0.13	
	8	A+4	1257.24292	1257.24549	2.04	
	8	A+5	1257.36832	1257.36821	-0.09	
	8	A+6	1257.49372	1257.49096	-2.19	
	8	A+7	1257.61911	1257.61761	-1.19	-0.59
	8	A+8	1257.74448	1257.74165	-2.25	
	8	A+9	1257.86987	1257.86959	-0.22	
	8	A+10	1257.99520	1257.99499	-0.17	
	8	A+11	1258.12058	1258.11786	-2.16	
	9	A+3	1117.54971	1117.55286	2.82	
	9	A+4	1117.66118	1117.66599	4.30	
	9	A+5	1117.77265	1117.77308	0.38	
	9	A+6	1117.88412	1117.88019	-3.52	
	9	A+7	1117.99557	1117.99339	-1.95	0.58
	9	A+8	1118.10701	1118.10863	1.45	

Off-loaded intermediate	Charge State	Peak	Theoretical <i>m/z</i>	Experimental <i>m/z</i>	Error (ppm)	Average error of A+3 to A+8 (where applicable) (ppm)
	9	A+9	1118.21847	1118.21782	-0.58	

Appendix 60 Peak list – Repeated FTICR-MS analysis of active ACP probe 64 incubated in the actinorhodin minimal system (1:1 ratio, protected ACP probe 63 to malonyl-ACP 7) showing off-loaded putative diketide 145 and cyclised dehydrated hexaketide 157 and internal calibration performed with apo-ACP 44, holo-ACP 43, decarboxylated ACP probe 144 and protected ACP probe 63.

1:4 ACP probe 63:malonyl-ACP 7						
Internal calibrant	Charge State	Average error of peaks A+3 to A+8 (ppm)				
Holo ACP Calibrated with A+4, A+5 and A+6	6	-1.38				
	7	-1.08				
	8	-0.50				
	9	0.70				
	10	-0.18				
Decarboxylated ACP probe 144 Calibrated with A+4, A+5 and A+6	6	1.74				
	7	-0.62				
	8	-1.02				
	9	-0.52				
	10	0.06				
Protected ACP probe 63 Calibrated with A+4, A+5 and A+6	6	-1.29				
	7	1.76				
	8	0.96				
	9	-0.26				
	10	-0.21				
Off-loaded intermediate	Charge State	Peak	Theoretical <i>m/z</i>	Experimental <i>m/z</i>	Error (ppm)	Average error of A+3 to A+8 (where applicable) (ppm)
Linear hexaketide C ₄₃₂ H ₆₉₂ N ₁₁₅ O ₁₅₆ PS ₂	6	A+3	1681.82445	1681.82139	-1.82	
	6	A+4	1681.99166	1681.98838	-1.95	
	6	A+5	1682.15886	1682.15083	-4.77	
	6	A+6	1682.32606	1682.32705	0.59	
	6	A+7	1682.49324	1682.49185	-0.83	-1.76
	7	A+2	1441.56439	1441.56330	-0.76	
	7	A+3	1441.70771	1441.70609	-1.12	
	7	A+4	1441.85103	1441.84975	-0.89	
	7	A+5	1441.99435	1441.99327	-0.75	
	7	A+6	1442.13766	1442.13457	-2.14	
	7	A+7	1442.28096	1442.27734	-2.51	-1.48
	8	A+1	1261.36933	1261.36995	0.49	
	8	A+2	1261.49475	1261.49307	-1.33	
	8	A+3	1261.62016	1261.61952	-0.51	
	8	A+4	1261.74558	1261.74539	-0.15	
	8	A+5	1261.87096	1261.87056	-0.32	
	8	A+6	1261.99636	1261.99651	0.12	
	8	A+7	1262.12175	1262.12040	-1.07	
	8	A+8	1262.24712	1262.24384	-2.60	-0.75
	9	A+2	1121.44058	1121.43947	-0.99	
9	A+3	1121.55206	1121.55135	-0.63		
9	A+4	1121.66353	1121.66326	-0.24		

Off-loaded intermediate	Charge State	Peak	Theoretical m/z	Experimental m/z	Error (ppm)	Average error of A+3 to A+8 (where applicable) (ppm)
	9	A+5	1121.77500	1121.77315	-1.65	
	9	A+6	1121.88646	1121.88510	-1.21	
	9	A+7	1121.99792	1121.99707	-0.76	-0.90
Cyclised hexaketide 156 $C_{432}H_{690}N_{115}O_{155}PS_2$	8	A+2	1259.24343	1259.23993	-2.78	
	8	A+3	1259.36884	1259.36689	-1.55	
	8	A+4	1259.49424	1259.49644	1.75	
	8	A+5	1259.61964	1259.61832	-1.05	
	8	A+6	1259.74504	1259.74536	0.25	
	8	A+7	1259.87043	1259.86857	-1.48	-0.41

Appendix 61 Peak list – FTICR-MS analysis of active ACP probe 64 incubated in the actinorhodin minimal system (1:4 ratio, protected ACP probe 63 to malonyl-ACP 7) showing off-loaded putative linear hexaketide 149 and cyclised hexaketide 156 and internal calibration performed with holo-ACP, decarboxylated ACP probe 144 and protected ACP probe 63.

1:4 ACP probe 63:malonyl-ACP 7						
Internal calibrant	Charge State	Average error of peaks A+3 to A+8 (ppm)				
Holo ACP Calibrated with A+4, A+5 and A+6	6	0.00				
	7	-0.69				
	8	-0.40				
	9	0.33				
	10	-0.08				
Decarboxylated ACP probe 144 Calibrated with A+4, A+5 and A+6	6	-1.17				
	7	-0.16				
	8	-0.98				
	9	-0.14				
	10	0.20				
Protected ACP probe 63 Calibrated with A+4, A+5 and A+6	6	0.14				
	7	1.43				
	8	0.68				
	9	-0.52				
Off-loaded intermediate	Charge State	Peak	Theoretical <i>m/z</i>	Experimental <i>m/z</i>	Error (ppm)	Average error of A+3 to A+8 (where applicable) (ppm)
Diketide 145 C ₄₂₄ H ₆₈₄ N ₁₁₅ O ₁₅₂ PS ₂	6	A+4	1653.98462	1653.97367	-6.62	
	6	A+5	1654.15181	1654.14142	-6.28	
	6	A+6	1654.31900	1654.31068	-5.03	
	6	A+7	1654.48620	1654.47462	-7.00	-6.23
	7	A+5	1417.98831	1417.98772	-0.42	
	7	A+6	1418.13161	1418.12920	-1.70	
	7	A+7	1418.27492	1418.27396	-0.68	
	7	A+8	1418.41820	1418.41549	-1.91	-1.18
	7	A+9	1418.56151	1418.56031	-0.85	
	8	A+4	1240.74028	1240.74005	-0.19	
	8	A+5	1240.86568	1240.86458	-0.89	
	8	A+6	1240.99107	1240.99037	-0.56	
	8	A+7	1241.11647	1241.11613	-0.27	
	8	A+8	1241.24184	1241.23946	-1.92	-0.77
	9	A+4	1102.99217	1102.98835	-3.46	
	9	A+5	1103.10364	1103.09795	-5.16	
	9	A+6	1103.21509	1103.21444	-0.59	
9	A+7	1103.32656	1103.32070	-5.31		
9	A+8	1103.43800	1103.43790	-0.09	-2.92	
Cyclised hexaketide 156 C ₄₃₂ H ₆₉₀ N ₁₁₅ O ₁₅₅ PS ₂	7	A+3	1439.13478	1439.13587	0.76	
	7	A+4	1439.27810	1439.27318	-3.42	
	7	A+5	1439.42141	1439.41802	-2.36	
	7	A+6	1439.56472	1439.56253	-1.52	
	7	A+7	1439.70803	1439.70502	-2.09	

Off-loaded intermediate	Charge State	Peak	Theoretical m/z	Experimental m/z	Error (ppm)	Average error of A+3 to A+8 (where applicable) (ppm)
	7	A+8	1439.85131	1439.84924	-1.44	-1.68
	8	A+2	1259.24343	1259.24246	-0.77	
	8	A+3	1259.36884	1259.36942	0.46	
	8	A+4	1259.49424	1259.49288	-1.08	
	8	A+5	1259.61964	1259.61846	-0.94	
	8	A+6	1259.74504	1259.74249	-2.02	
	8	A+7	1259.87043	1259.87111	0.54	-0.61
Cyclised dehydrated hexaketide 157 $C_{432}H_{688}N_{115}O_{154}PS_2$	7	A+1	1436.27518	1436.27556	0.26	
	7	A+2	1436.41851	1436.41785	-0.46	
	7	A+3	1436.56184	1436.56183	-0.01	
	7	A+4	1436.70516	1436.70413	-0.72	
	7	A+5	1436.84849	1436.85095	1.71	
	7	A+6	1436.99179	1436.99271	0.64	
	7	A+7	1437.13509	1437.13508	-0.01	
	7	A+8	1437.27837	1437.27768	-0.48	0.19
	7	A+9	1437.42167	1437.41941	-1.57	
	7	A+10	1437.56491	1437.56488	-0.02	
	7	A+11	1437.70820	1437.70694	-0.88	
	7	A+12	1437.85151	1437.85151	0.00	
	8	A+1	1256.86669	1256.86952	2.25	
	8	A+2	1256.99211	1256.98951	-2.07	
	8	A+3	1257.11752	1257.11530	-1.77	
	8	A+4	1257.24292	1257.24303	0.09	
	8	A+5	1257.36832	1257.36943	0.88	
	8	A+6	1257.49372	1257.49388	0.13	
	8	A+7	1257.61911	1257.61901	-0.08	
	8	A+8	1257.74448	1257.74372	-0.60	-0.23
	8	A+9	1257.86987	1257.87187	1.59	
	8	A+10	1257.99520	1257.99230	-2.31	
	9	A+3	1117.54971	1117.55364	3.52	
	9	A+4	1117.66118	1117.65869	-2.23	
	9	A+5	1117.77265	1117.77083	-1.63	
	9	A+6	1117.88412	1117.88502	0.81	
	9	A+7	1117.99557	1117.99518	-0.35	0.02

Appendix 62 Peak list – Repeated FTICR-MS analysis of active ACP probe **64** incubated in the actinorhodin minimal system (1:4 ratio, protected ACP probe **63** to malonyl-ACP **7**) showing off-loaded putative diketide **145**, cyclised hexaketide **156** and cyclised dehydrated hexaketide **157** and internal calibration performed with holo-ACP, decarboxylated ACP probe **144** and protected ACP probe **63**.

5:1 ACP probe 63:malonyl-ACP 7						
Internal calibrant	Charge State	Average error of peaks A+3 to A+8 (ppm)				
<i>Apo</i>-ACP 44 Calibrated with A+4, A+5 and A+6	6	1.30				
	7	0.63				
	8	-0.01				
	9	0.06				
<i>Holo</i>-ACP 43 Calibrated with A+4, A+5 and A+6	6	-1.28				
	7	-1.07				
	8	-0.19				
Decarboxylated ACP probe 144 Calibrated with A+4, A+5 and A+6	6	1.39				
	7	-0.75				
	8	-0.57				
	9	-0.45				
Protected ACP probe 63 Calibrated with A+4, A+5 and A+6	6	-2.05				
	7	1.08				
	8	0.63				
Off-loaded intermediate	Charge State	Peak	Theoretical <i>m/z</i>	Experimental <i>m/z</i>	Error (ppm)	Average error of A+3 to A+8 (where applicable) (ppm)
Cyclised pentaketide 154 $C_{430}H_{688}N_{115}O_{154}PS_2$	6	A+2	1671.65372	1671.65470	0.59	
	6	A+3	1671.82093	1671.82420	1.96	
	6	A+4	1671.98814	1671.99072	1.54	
	6	A+5	1672.15534	1672.15757	1.33	
	6	A+6	1672.32254	1672.32613	2.15	
	6	A+7	1672.48972	1672.48898	-0.44	1.31
	7	A+1	1432.84661	1432.84570	-0.64	
	7	A+2	1432.98994	1432.99025	0.22	
	7	A+3	1433.13327	1433.13271	-0.39	
	7	A+4	1433.27659	1433.27623	-0.25	
	7	A+5	1433.41990	1433.41998	0.06	
	7	A+6	1433.56321	1433.56222	-0.69	
	7	A+7	1433.70652	1433.70564	-0.61	
	7	A+8	1433.84980	1433.84896	-0.59	-0.41
	7	A+9	1433.99310	1433.98883	-2.98	
	8	A+2	1253.99211	1253.99377	1.32	
	8	A+3	1254.11752	1254.11967	1.71	
	8	A+4	1254.24292	1254.24306	0.11	
	8	A+5	1254.36832	1254.37029	1.57	
	8	A+6	1254.49372	1254.49500	1.02	
8	A+7	1254.61911	1254.62100	1.51		

Off-loaded intermediate	Charge State	Peak	Theoretical m/z	Experimental m/z	Error (ppm)	Average error of A+3 to A+8 (where applicable) (ppm)
	8	A+8	1254.74448	1254.74703	2.03	1.33
Cyclised hexaketide 156 C ₄₃₂ H ₆₉₀ N ₁₁₅ O ₁₅₅ PS ₂	7	A+3	1439.13478	1439.13084	-2.74	
	7	A+4	1439.27810	1439.27435	-2.61	
	7	A+5	1439.42141	1439.41851	-2.01	
	7	A+6	1439.56472	1439.56219	-1.76	
	7	A+7	1439.70803	1439.70483	-2.22	-2.27
	8	A+1	1259.11801	1259.11646	-1.23	
	8	A+2	1259.24343	1259.24340	-0.02	
	8	A+3	1259.36884	1259.36780	-0.83	
	8	A+4	1259.49424	1259.49350	-0.59	
	8	A+5	1259.61964	1259.61923	-0.33	
	8	A+6	1259.74504	1259.74627	0.98	
	8	A+7	1259.87043	1259.86563	-3.81	
	8	A+8	1259.99580	1259.99272	-2.44	-0.19

Appendix 63 Peak list – FTICR-MS analysis of active ACP probe 64 incubated in the actinorhodin minimal system (5:1 ratio, protected ACP probe 63 to malonyl-ACP 7) showing off-loaded putative cyclised pentaketide 154 and cyclised hexaketide 156 and internal calibration performed with apo-ACP 44, holo-ACP 43, decarboxylated ACP probe 144 and protected ACP probe 63.

1:1 ACP probe 63:Malonyl-ACP 7 (30 seconds delay)						
Internal calibrant	Charge State	Average error of peaks A+3 to A+8 (ppm)				
Apo-ACP 44 Calibrated with A+4, A+5 and A+6.	7	0.58				
	8	-0.43				
	9	-0.06				
	10	-0.11				
Holo-ACP 43 Calibrated with A+4, A+5 and A+6.	6	-0.75				
	7	-1.34				
	8	-0.42				
	9	0.46				
Decarboxylated ACP probe 144 Calibrated with A+4, A+5 and A+6	7	-0.59				
	8	-0.35				
	9	0.29				
	10	0.56				
Off-loaded intermediate	Charge State	Peak	Theoretical m/z	Experimental m/z	Error (ppm)	Average error of A+3 to A+8 (where applicable) (ppm)
Cyclised dehydrated hexaketide 157 $C_{432}H_{688}N_{115}O_{154}PS_2$	7	A+1	1436.27518	1436.27393	-0.87	
	7	A+2	1436.41851	1436.41741	-0.77	
	7	A+3	1436.56184	1436.56259	0.52	
	7	A+4	1436.70516	1436.70402	-0.79	
	7	A+5	1436.84847	1436.84635	-1.48	
	7	A+6	1436.99179	1436.99042	-0.95	
	7	A+7	1437.13509	1437.13476	-0.23	
	7	A+8	1437.27837	1437.27890	0.37	-0.43
	7	A+9	1437.42167	1437.41924	-1.69	
	7	A+10	1437.56491	1437.56295	-1.36	
	7	A+11	1437.70820	1437.70669	-1.05	
	8	A+4	1257.24292	1257.24266	-0.21	
	8	A+5	1257.36832	1257.36922	0.72	
	8	A+6	1257.49372	1257.49325	-0.37	
	8	A+7	1257.61911	1257.61865	-0.37	
	8	A+8	1257.74448	1257.74394	-0.43	-0.13
	8	A+9	1257.86987	1257.86932	-0.44	
	8	A+10	1257.99520	1257.99600	0.64	

Appendix 64 Peak list – FTICR-MS analysis of active ACP probe **64** incubated in the actinorhodin minimal system (1:1 ratio, protected ACP probe **63** to malonyl-ACP **7** with 30 seconds delay upon addition of the ACP probe **64**) showing an off-loaded putative cyclised dehydrated hexaketide **157** and internal calibration performed with apo-ACP **44**, holo-ACP **43**, and decarboxylated ACP probe **144**.

1:1 ACP probe 63:malonyl-ACP 7 (5 mins delay)		
Internal calibrant	Charge State	Average error of peaks A+3 to A+8 (ppm)
Apo-ACP 44 Calibrated with A+4, A+5 and A+6.	7	0.73
	8	0.32
	9	-0.04
	10	-0.25
Holo-ACP 43 Calibrated with A+4, A+5 and A+6.	7	-1.04
	8	-0.24
	9	0.73
Decarboxylated ACP probe 144 Calibrated with A+4, A+5 and A+6.	7	-0.61
	8	-0.66
	9	-0.22
	10	0.07

Off-loaded intermediate	Charge State	Peak	Theoretical m/z	Experimental m/z	Error (ppm)	Average error of A+3 to A+8 (where applicable) (ppm)
Cyclised dehydrated hexaketide 157 $C_{432}H_{688}N_{115}O_{154}PS_2$	7	A+3	1436.56184	1436.56035	-1.04	
	7	A+4	1436.70483	1436.70556	0.51	
	7	A+5	1436.84847	1436.84746	-0.70	
	7	A+6	1436.99179	1436.99606	2.97	
	7	A+7	1437.13509	1437.13635	0.88	
	7	A+8	1437.27837	1437.28000	1.13	0.52
	7	A+9	1437.42167	1437.42201	0.24	
	7	A+10	1437.56383	1437.56572	1.31	
	7	A+11	1437.70783	1437.70445	-2.35	
	8	A+3	1257.11752	1257.11542	-1.67	
	8	A+4	1257.24292	1257.24324	0.25	
	8	A+5	1257.36832	1257.36724	-0.86	
	8	A+6	1257.49372	1257.49383	0.09	
	8	A+7	1257.61911	1257.61916	0.04	
	8	A+8	1257.74448	1257.74451	0.02	-0.35
	8	A+9	1257.86987	1257.86990	0.02	
	8	A+10	1257.99520	1257.99530	0.08	
	8	A+11	1258.12058	1258.11945	-0.90	

Appendix 65 Peak list – FTICR-MS analysis of active ACP probe **64** incubated in the actinorhodin minimal system (1:1 ratio, protected ACP probe **63** to malonyl-ACP **7** with 30 seconds delay upon addition of the ACP probe **64**) showing an off-loaded putative cyclised dehydrated hexaketide **157** and internal calibration performed with apo-ACP **44**, holo-ACP **43**, and decarboxylated ACP probe **144**.

1:1 ACP probe 63: ¹³ C-malonyl-ACP 7		
Internal calibrant	Charge State	Average error of peaks A+3 to A+8 (ppm)
Holo ACP Calibrated with A+4, A+5 and A+6	6	-0.67
	7	-0.70
	8	1.20
Decarboxylated ACP probe 144 Calibrated with A+4, A+5 and A+6	6	0.75
	7	-0.16
	8	-0.10
Protected ACP probe 63 Calibrated with A+4, A+5 and A+6	6	-0.23
	7	0.46
	8	0.71

Off-loaded intermediate	Charge State	Peak	Theoretical <i>m/z</i>	Experimental <i>m/z</i>	Error (ppm)	Average error of A+3 to A+8 (where applicable) (ppm)
Labelled tetraketide 147 C ₄₂₂ ¹³ C ₆ H ₆₈₈ N ₁₁₅ O ₁₅₄ PS ₂	6	A+4	1668.82428	1668.82025	-2.41	
	6	A+5	1668.99148	1668.98598	-3.30	
	6	A+6	1669.15868	1669.15082	-4.71	
	6	A+7	1669.32587	1669.32488	-0.59	
	6	A+8	1669.49307	1669.49166	-0.84	-2.37
	6	A+9	1669.66023	1669.65847	-1.05	
	6	A+10	1669.82742	1669.82305	-2.62	
	7	A+3	1430.42138	1430.41961	-1.24	
	7	A+4	1430.56471	1430.56358	-0.79	
	7	A+5	1430.70803	1430.70592	-1.47	
	7	A+6	1430.85134	1430.85160	0.18	
	7	A+7	1430.99464	1430.99400	-0.45	-0.75
	7	A+8	1431.13796	1431.13462	-2.33	
	7	A+9	1431.28124	1431.27960	-1.15	
	7	A+10	1431.42454	1431.42412	-0.29	
	7	A+11	1431.56777	1431.56554	-1.56	

Appendix 66 Peak list – FTICR-MS analysis of active ACP probe **64** incubated in the actinorhodin minimal system (1:1 ratio, protected ACP probe **63** to ¹³C-malonyl-ACP **7b**) showing an off-loaded putative ¹³C-labelled tetraketide **147** and internal calibration performed with holo-ACP, decarboxylated ACP probe **144** and protected probe **63**.

1:10 ACP probe 63:¹³C-malonyl-ACP 7b		
Internal calibrant	Charge State	Average error of peaks A+3 to A+8 (ppm)
<i>Apo</i>-ACP 44 Calibrated with A+4, A+5 and A+6	6	0.99
	7	0.06
	8	-0.08
	9	-0.53
	10	-0.12
<i>Holo</i>-ACP 43 Calibrated with A+4, A+5 and A+6	6	-1.00
	7	-0.98
	8	-0.54
	9	0.20
	10	-0.25
Protected ACP probe 63 Calibrated with A+4, A+5 and A+6	6	-0.31
	7	0.61
	8	0.65
	9	-0.41
	10	-0.55

Off-loaded intermediate	Charge State	Peak	Theoretical <i>m/z</i>	Experimental <i>m/z</i>	Error (ppm)	Average error of A+3 to A+8 (where applicable) (ppm)
Labelled tetraketide 147 C ₄₂₂ ¹³ C ₆ H ₆₈₈ N ₁₁₅ O ₁₅₄ PS ₂	6	A+3	1668.65707	1668.65435	-1.63	
	6	A+4	1668.82428	1668.82099	-1.97	
	6	A+5	1668.99148	1668.98766	-2.29	
	6	A+6	1669.15868	1669.15663	-1.23	
	6	A+7	1669.32587	1669.32337	-1.50	
	6	A+8	1669.49307	1669.49014	-1.76	-1.73
	6	A+9	1669.66023	1669.65695	-1.96	
	7	A+1	1430.13471	1430.13074	-2.78	
	7	A+2	1430.27805	1430.27631	-1.22	
	7	A+3	1430.42138	1430.42117	-0.15	
	7	A+4	1430.56471	1430.56471	0.00	
	7	A+5	1430.70803	1430.70824	0.15	
	7	A+6	1430.85134	1430.85093	-0.29	
	7	A+7	1430.99464	1430.99435	-0.20	
	7	A+8	1431.13796	1431.13797	0.01	-0.08
	7	A+9	1431.28124	1431.28033	-0.64	
	7	A+10	1431.42454	1431.42381	-0.51	
	7	A+11	1431.56777	1431.56275	-3.51	
	7	A+12	1431.71106	1431.70872	-1.63	
	8	A+2	1251.61920	1251.61793	-1.01	
	8	A+3	1251.74462	1251.74349	-0.90	
	8	A+4	1251.87003	1251.86902	-0.81	
	8	A+5	1251.99543	1251.99470	-0.58	
8	A+6	1252.12083	1252.12025	-0.46		
8	A+7	1252.24622	1252.24565	-0.46		
8	A+8	1252.37162	1252.37089	-0.58	-0.63	
8	A+9	1252.49699	1252.49628	-0.57		
8	A+10	1252.62238	1252.62158	-0.64		
8	A+11	1252.74771	1252.74693	-0.62		

Off-loaded intermediate	Charge State	Peak	Theoretical m/z	Experimental m/z	Error (ppm)	Average error of A+3 to A+8 (where applicable) (ppm)
	8	A+12	1252.87309	1252.87177	-1.05	
	8	A+13	1252.99771	1252.99650	-0.97	
	8	A+14	1253.12392	1253.11966	-3.40	
	9	A+2	1112.66232	1112.66353	1.09	
	9	A+3	1112.77380	1112.77367	-0.12	
	9	A+4	1112.88528	1112.88584	0.50	
	9	A+5	1112.99675	1112.99602	-0.66	
	9	A+6	1113.10821	1113.10723	-0.88	
	9	A+7	1113.21967	1113.21928	-0.35	
	9	A+8	1113.33114	1113.33070	-0.40	-0.32
	9	A+9	1113.44258	1113.44198	-0.54	
	9	A+10	1113.55404	1113.55328	-0.68	
	9	A+11	1113.66544	1113.66359	-1.66	
	9	A+12	1113.77689	1113.77493	-1.76	
	9	A+13	1113.88766	1113.88630	-1.22	
	10	A+2	1001.49682	1001.49407	-2.75	
	10	A+3	1001.59778	1001.59627	-1.51	
	10	A+4	1001.69748	1001.69769	0.21	
	10	A+5	1001.79780	1001.79751	-0.29	
	10	A+6	1001.89812	1001.89816	0.04	
	10	A+7	1001.99843	1001.99801	-0.42	
	10	A+8	1002.09875	1002.09870	-0.05	-0.34
	10	A+9	1002.19905	1002.19860	-0.45	
	10	A+10	1002.29936	1002.29770	-1.66	
	10	A+11	1002.39962	1002.39845	-1.17	

Appendix 67 Peak list – FTICR-MS analysis of active ACP probe 64 incubated in the actinorhodin minimal system (1:10 ratio, protected ACP probe 63 to ¹³C-malonyl-ACP 7b) showing an off-loaded putative ¹³C-labelled tetraketide 147 and internal calibration performed with apo-ACP 44, holo-ACP 43, and protected probe 63.

1:5 ACP probe 63:¹³C-malonyl-ACP 7b						
Internal calibrant	Charge State	Average error of peaks A+3 to A+8 (ppm)				
<i>Apo</i>-ACP 44 Calibrated with A+4, A+5 and A+6	6	0.51				
	7	0.12				
	8	0.05				
	9	-0.02				
	10	-0.09				
<i>Holo</i>-ACP 43 Calibrated with A+4, A+5 and A+6	6	-0.64				
	7	-0.64				
	8	-1.95				
Decarboxylated ACP probe 144 Calibrated with A+4, A+5 and A+6	6	0.61				
	7	-0.30				
	8	-0.42				
	9	-0.18				
	10	-0.16				
Protected ACP probe 63 Calibrated with A+4, A+5 and A+6	6	-0.53				
	7	0.54				
	8	0.11				
	9	0.29				
	Charge State	Peak	Theoretical <i>m/z</i>	Experimental <i>m/z</i>	Error ppm	Average error of A+3 to A+8 (where applicable) ppm
Labelled cyclised dehydrated pentaketide 155 $C_{422}^{13}C_8H_{686}N_{115}O_{153}PS_2$	6	A+2	1669.82253	1669.82268	0.09	
	6	A+3	1669.98975	1669.98955	-0.12	
	6	A+4	1670.15697	1670.15646	-0.31	
	6	A+5	1670.32417	1670.32341	-0.46	
	6	A+6	1670.49137	1670.49038	-0.59	
	6	A+7	1670.65856	1670.64836	-6.11	
	6	A+8	1670.82576	1670.81528	-6.27	-0.37
	7	A+3	1431.56369	1431.56706	2.35	
	7	A+4	1431.70701	1431.70795	0.66	
	7	A+5	1431.85033	1431.85052	0.13	
	7	A+6	1431.99364	1431.99146	-1.52	
	7	A+7	1432.13695	1432.13409	-2.00	
	7	A+8	1432.28026	1432.27674	-2.46	-0.47
	7	A+9	1432.42354	1432.41942	-2.88	
	8	A+3	1252.74413	1252.74834	3.36	
	8	A+4	1252.86954	1252.87019	0.52	
8	A+5	1252.99495	1252.99460	-0.28		

Off-loaded intermediate	Charge State	Peak	Theoretical m/z	Experimental m/z	Error (ppm)	Average error of A+3 to A+8 (where applicable) (ppm)
	8	A+6	1253.12015	1253.11904	-0.89	
	8	A+7	1253.24574	1253.24477	-0.77	
	8	A+8	1253.37114	1253.36798	-2.52	-0.10
	8	A+9	1253.49651	1253.49377	-2.19	
	8	A+10	1253.62190	1253.61957	-1.86	
	9	A+1	1113.32781	1113.33014	2.09	
	9	A+2	1113.43930	1113.44041	1.00	
	9	A+3	1113.55078	1113.55371	2.63	
	9	A+4	1113.66226	1113.66226	0.00	
	9	A+5	1113.77374	1113.77336	-0.34	
	9	A+6	1113.88521	1113.88372	-1.34	
	9	A+7	1113.99667	1113.99510	-1.41	
	9	A+8	1114.10813	1114.10751	-0.56	-0.17
	9	A+9	1114.21960	1114.21794	-1.49	
	9	A+10	1114.33104	1114.32939	-1.48	
	9	A+11	1114.44250	1114.44086	-1.47	
	9	A+12	1114.55389	1114.55236	-1.37	
	9	A+13	1114.66535	1114.66388	-1.32	
	9	A+14	1114.77681	1114.77441	-2.15	
	9	A+15	1114.88760	1114.88698	-0.56	
	9	A+16	1114.99930	1114.99756	-1.56	

Appendix 68 Peak list – FTICR-MS analysis of active ACP probe 64 incubated in the actinorhodin minimal system (1:5 ratio, protected ACP probe 63 to ¹³C-malonyl-ACP 7b) showing an off-loaded putative ¹³C-labelled cyclised dehydrated pentaketide 155 and internal calibration performed with apo-ACP 44, holo-ACP, decarboxylated ACP probe 144 and protected probe 63.

1:4 ACP probe 63:¹³C-malonyl-ACP 7b (step-wise addition)						
Internal calibrant		Charge State	Average error of peaks A+3 to A+8 (ppm)			
Apo-ACP 44 Calibrated with A+4, A+5 and A+6		7	0.76			
		8	-0.03			
		9	-0.26			
		10	0.15			
Holo-ACP 43 Calibrated with A+4, A+5 and A+6		6	0.74			
		7	-0.64			
		8	-0.58			
		9	0.40			
Decarboxylated ACP probe 144 Calibrated with A+4, A+5 and A+6		7	0.20			
		8	-0.54			
		9	-0.30			
		10	0.52			
Off-loaded intermediate	Charge State	Peak	Theoretical m/z	Experimental m/z	Error ppm	Average error of A+3 to A+8 (where applicable) (ppm)
Labelled linear pentaketide 148 C ₄₂₂ ¹³ C ₈ H ₆₉₀ N ₁₁₅ O ₁₅₅ PS ₂	7	A+1	1436.42290	1436.41883	-2.83	
	7	A+2	1436.56623	1436.56234	-2.71	
	7	A+3	1436.70956	1436.71089	0.93	
	7	A+4	1436.85289	1436.85112	-1.23	
	7	A+5	1436.99620	1436.99638	0.13	
	7	A+6	1437.13952	1437.13834	-0.82	
	7	A+7	1437.28282	1437.28033	-1.73	
	7	A+8	1437.42614	1437.42234	-2.64	-0.90
	7	A+9	1437.56942	1437.56605	-2.34	

Appendix 69 Peak list – FTICR-MS analysis of active ACP probe 64 incubated in the actinorhodin minimal system (1:4 ratio, protected ACP probe 63 to ¹³C-malonyl-ACP 7b, step-wise addition) showing an off-loaded putative ¹³C-labelled linear pentaketide 148 and internal calibration performed with apo-ACP 44, holo-ACP 43, and decarboxylated ACP probe 144 and protected probe 63.

			EID						CAD			
			<i>m/z</i> detected (<i>m/z</i> before phasing)			Absolute Error (Error before phasing) (ppm)			<i>m/z</i> detected (<i>m/z</i> before phasing)		Absolute Error (Error before phasing) (ppm)	
	Predicted Formula	Theoretical Mass (Da)	Na	Li	Cs	Na	Li	Cs	Na	Li	Na	Li
	C₈H₁₂N₂O	152.09496			285.00057 (285.00047)			0.59 (0.24)				
	C₈H₁₄N₂O	154.11061		161.12672 (161.12664)			0.66 (0.16)					
a	C₈H₁₃NO₂	155.09463		162.11070 (162.11061)			0.41 (0.15)			162.11060 (162.11020)		0.21 (2.68)
b	C₆H₁₀N₂O₃	158.06914			290.97469 (290.97464)			0.37 (0.20)				
c	C₈H₁₄N₂O₂	170.10553			303.01098 (303.01092)			0.03 (0.17)				
d	C₈H₁₃NO₃	171.08954		178.10555 (178.10550)			0.03 (0.25)			178.10554 (178.10558)		0.02 (0.20)
e	C₈H₁₆N₂O₂	172.12118	195.11095 (195.11095)	179.13719 (179.13718)	305.02665 (305.02659)	0.01 (0.01)	0.03 (0.02)	0.10 (0.10)	195.11095 (195.11093)	179.13718 (179.13718)	0.01 (0.11)	0.02 (0.02)
	C₉H₁₂N₂O₂	180.08988		187.10586 (187.10577)			0.13 (0.61)			187.10590 (187.10594)		0.09 (0.30)
	C₉H₁₄N₂O₂	182.10553		189.12154 (189.12150)			0.03 (0.18)			189.12155 (189.12141)		0.08 (0.66)
f	C₈H₁₄N₂O₃	186.10044			319.00586 (319.00579)			0.07 (0.29)				
	C₁₀H₁₁NO₃	193.07389		200.08988 (200.09002)			0.07 (0.63)					
g	C₉H₉NO₄	195.05316		196.06100 (196.06079)	327.95859 (327.95860)		2.87 (1.80)	0.03 (0.00)		196.06101 (196.06102)		2.93 (2.98)
	C₉H₁₂N₂O₃	196.08479			328.99026 (328.99019)			0.09 (0.12)				
h	C₉H₁₄N₂O₃	198.10044	221.09028 (221.09026)	205.11642 (205.11643)	331.00585 (331.00586)	0.31 (0.22)	0.12 (0.07)	0.09 (0.06)	221.09021 (221.09032)	205.11642 (205.11645)	0.00 (0.49)	0.12 (0.03)

			EID						CAD			
			<i>m/z</i> detected (<i>m/z</i> before phasing)			Absolute Error (Error before phasing) (ppm)			<i>m/z</i> detected (<i>m/z</i> before phasing)		Absolute Error (Error before phasing) (ppm)	
	Predicted Formula	Theoretical Mass (Da)	Na	Li	Cs	Na	Li	Cs	Na	Li	Na	Li
i	C ₉ H ₁₆ N ₂ O ₃	200.11609		207.13207 (207.13202)	333.02144 (333.02154)		0.12 (0.36)	0.27 (0.03)	223.10586 (223.10585)		0.00 (0.05)	
j	C ₉ H ₁₅ NO ₄	201.10011		208.11606 (208.11609)			0.25 (0.11)			208.11611 (208.11610)		0.01 (0.06)
	C ₁₀ H ₁₂ N ₂ O ₃	208.08479		215.10067 (215.10059)			0.58 (0.95)			215.10080 (215.10078)		0.03 (0.07)
k	C ₁₀ H ₁₆ N ₂ O ₃	212.11609								219.13207 (219.13207)		0.11 (0.11)
l	C ₉ H ₁₆ N ₂ O ₄	216.11101		223.12695 (223.12696)	349.01634 (349.01642)		0.29 (0.24)	0.32 (0.09)				
m	C ₉ H ₁₇ NO ₅	219.11067		226.12661 (226.12663)			0.28 (0.19)			226.12665 (226.12666)		0.11 (0.06)
	C ₁₂ H ₁₅ NO ₃	221.10519		228.12117 (228.12119)			0.11 (0.02)			228.12117 (228.12114)		0.11 (0.24)
	C ₁₀ H ₁₂ N ₂ O ₄	224.07971		231.09567 (231.09573)	356.98500 (356.98511)		0.19 (0.07)	0.42 (0.11)		231.09567 (231.09577)		0.19 (0.24)
	C ₁₀ H ₁₄ N ₂ O ₄	226.09536		233.11130 (233.11132)	359.00067 (359.00077)		0.27 (0.19)	0.36 (0.09)		233.11132 (233.11140)		0.19 (0.15)
n	C ₁₀ H ₁₆ N ₂ O ₄	228.11101	251.10078 (251.10081)	235.12695 (235.12701)	361.01635 (361.01646)	0.00 (0.12)	0.27 (0.02)	0.28 (0.02)	251.10077 (251.10089)	235.12701 (235.12702)	0.04 (0.43)	0.02 (0.03)
o	C ₁₀ H ₁₈ N ₂ O ₄	230.12666			363.03199 (363.03177)			0.31 (0.91)				
	C ₁₃ H ₁₅ NO ₃	233.10519								240.12119 (240.12119)		0.02 (0.02)
	C ₁₃ H ₂₀ N ₂ O ₂	236.15248		243.16838 (243.16842)			0.43 (0.26)			243.16844 (243.16835)		0.18 (0.55)
	C ₁₃ H ₂₂ N ₂ O ₂	238.16813								245.18408 (245.18413)		0.22 (0.02)

			EID						CAD			
			<i>m/z</i> detected (<i>m/z</i> before phasing)			Absolute Error (Error before phasing) (ppm)			<i>m/z</i> detected (<i>m/z</i> before phasing)		Absolute Error (Error before phasing) (ppm)	
	Predicted Formula	Theoretical Mass (Da)	Na	Li	Cs	Na	Li	Cs	Na	Li	Na	Li
	C₁₂H₁₇NO₄	239.11576			372.02116 (372.02093)			0.11 (0.73)				
	C₁₀H₁₄N₂O₅	242.09027		249.10620 (249.10634)	374.99554 (374.99554)		0.30 (0.26)	0.46 (0.46)				
p	C₁₁H₂₀N₂O₄	244.14231	267.13209 (267.13208)	251.15825 (251.15832)	377.04761 (377.04760)	0.03 (0.00)	0.25 (0.02)	0.37 (0.40)		251.15827 (251.15765)		0.18 (2.64)
	C₁₀H₁₈N₂O₅	246.12157		253.13750 (253.13755)	379.02684 (379.02684)		0.29 (0.09)	0.45 (0.45)				
	C₁₄H₂₀N₂O₂	248.15248		255.16844 (255.16843)			0.17 (0.21)			255.16843 (255.16833)		0.21 (0.60)
	C₁₁H₁₄N₂O₅	254.09027		261.10623 (261.10628)	386.99562 (386.99550)		0.17 (0.02)	0.24 (0.55)	277.08008 (277.08011)	277.08008 (277.08011)	0.14 (0.25)	0.05 (0.02)
	C₁₃H₂₂N₂O₃	254.16304		261.17900 (261.17908)	387.06831 (387.06830)		0.17 (0.14)	0.44 (0.47)	277.15281 (277.15289)	261.17905 (261.17905)	0.00 (0.29)	0.02 (0.02)
q	C₁₂H₂₀N₂O₄	256.14231		263.15828 (263.15823)			0.13 (0.32)			263.15825 (263.15828)		0.24 (0.13)
r	C₁₃H₂₄N₂O₃	256.17870		263.19463 (263.19475)			0.28 (0.17)			263.19464 (263.19463)		0.24 (0.28)
s	C₁₂H₂₂N₂O₄	258.15796		265.17391 (265.17397)	391.06322 (391.06322)		0.20 (0.02)	0.46 (0.46)		265.17391 (265.17396)		0.20 (0.02)
	C₁₄H₁₆N₂O₃	260.11609		267.13199 (267.13205)			0.39 (0.16)			267.13204 (267.13209)		0.20 (0.01)
	C₁₄H₁₈N₂O₃	262.13174								269.14766 (269.14765)		0.31 (0.35)
	C₁₄H₁₆O₅	264.09977			397.00516 (397.00529)			0.13 (0.20)				
	C₁₄H₂₂N₂O₃	266.16304		273.17901 (273.17914)			0.12 (0.35)			273.17903 (273.17902)		0.05 (0.09)

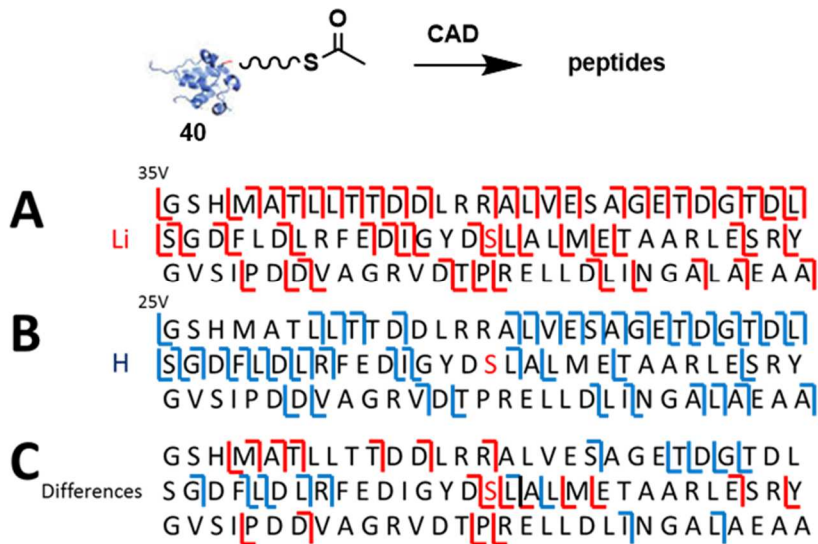
			EID						CAD			
			<i>m/z</i> detected (<i>m/z</i> before phasing)			Absolute Error (Error before phasing) (ppm)			<i>m/z</i> detected (<i>m/z</i> before phasing)		Absolute Error (Error before phasing) (ppm)	
	Predicted Formula	Theoretical Mass (Da)	Na	Li	Cs	Na	Li	Cs	Na	Li	Na	Li
t	C ₁₃ H ₂₂ N ₂ O ₄	270.15796		277.17393 (277.17395)	403.06332 (403.06344)		0.12 (0.05)	0.20 (0.10)		277.17389 (277.17391)		0.27 (0.19)
	C ₁₁ H ₁₆ N ₂ O ₆	272.10084		279.11681 (279.11695)	405.00614 (405.00612)		0.12 (0.38)	0.35 (0.40)				
	C ₁₂ H ₂₂ N ₂ O ₅	274.15287		281.16880 (281.16875)	407.05819 (407.05818)		0.26 (0.44)	0.30 (0.32)				
	C ₁₄ H ₂₀ N ₂ O ₄	280.14231		287.15829 (287.15824)	413.04780 (413.04780)		0.08 (0.26)	0.12 (0.12)		287.15829 (287.15825)		0.08 (0.22)
	C ₁₄ H ₂₂ N ₂ O ₄	282.15796		289.17391 (289.17393)			0.19 (0.12)			289.17398 (289.17403)		0.06 (0.23)
u	C ₁₄ H ₂₄ N ₂ O ₄	284.17361	307.16337 (307.16331)	291.18959 (291.18973)		0.04 (0.23)	0.08 (0.40)		307.16339 (307.16328)	291.18960 (291.18960)	0.03 (0.33)	0.05 (0.05)
	C ₁₃ H ₂₂ N ₂ O ₅	286.15287		293.16887 (293.16890)	419.05820 (419.05820)		0.01 (0.09)	0.26 (0.26)				
	C ₁₅ H ₂₀ N ₂ O ₄	292.14231		299.15835 (299.15860)			0.12 (0.96)			299.15850 (299.15850)		0.62 (0.62)
	C ₉ H ₁₇ N ₃ O ₈	295.10157			428.00659 (428.00674)			0.98 (0.63)				
	C ₁₄ H ₁₉ NO ₆	297.12124		304.13729 (304.13733)			0.15 (0.28)			304.13713 (304.13714)		0.37 (0.34)
	C ₁₄ H ₂₂ N ₂ O ₅	298.15287		305.16886 (305.16890)	431.05829 (431.05814)		0.05 (0.09)	0.05 (0.40)				
v	C ₁₄ H ₂₄ N ₂ O ₅	300.16852		307.18452 (307.18456)	433.07397 (433.07382)		0.01 (0.12)	0.02 (0.33)				
w	C ₁₄ H ₂₆ N ₂ O ₅	302.18417	325.17394 (325.17397)	309.20022 (309.20005)	435.08962 (435.08976)	0.00 (0.09)	0.15 (0.40)	0.02 (0.34)	325.17393 (325.17401)	309.20017 (309.20016)	0.03 (0.21)	0.01 (0.05)
x	C ₁₆ H ₂₁ NO ₅	307.14197	330.13176 (330.13186)			0.06 (0.36)			330.13172 (330.13178)		0.06 (0.12)	

			EID						CAD			
			<i>m/z</i> detected (<i>m/z</i> before phasing)			Absolute Error (Error before phasing) (ppm)			<i>m/z</i> detected (<i>m/z</i> before phasing)		Absolute Error (Error before phasing) (ppm)	
	Predicted Formula	Theoretical Mass (Da)	Na	Li	Cs	Na	Li	Cs	Na	Li	Na	Li
y	C ₁₅ H ₂₂ N ₂ O ₅	310.15287		317.16890 (317.16895)	443.05836 (443.05852)		0.08 (0.24)	0.11 (0.47)	333.14264 (333.14271)	317.16886 (317.16885)	0.00 (0.21)	0.04 (0.08)
z	C ₁₄ H ₂₂ N ₂ O ₆	314.14779		321.16383 (321.16405)	447.05332 (447.05332)		0.11 (0.80)	0.20 (0.20)				
aa	C ₁₄ H ₂₄ N ₂ O ₆	316.16344		323.17955 (323.17985)	449.06888 (449.06888)		0.33 (1.26)	0.00 (0.00)				
bb	C ₁₅ H ₁₈ N ₂ O ₆	322.11649		329.13253 (329.13267)	455.02192 (455.02176)		0.11 (0.53)	0.02 (0.38)				
cc	C ₁₅ H ₂₂ N ₂ O ₆	326.14779			459.05329 (459.05312)			0.13 (0.24)				
dd	C ₁₅ H ₂₄ N ₂ O ₆	328.16344	351.15321 (351.15320)	335.17956 (335.17941)	461.06902 (461.06924)	0.00 (0.03)	0.35 (0.10)	0.30 (0.78)	351.15322 (351.15334)	335.17947 (335.17944)	0.03 (0.37)	0.08 (0.01)
ee	C ₁₅ H ₁₈ N ₂ O ₇	338.11140			471.01685 (471.01685)			0.02 (0.02)				
	C ₁₇ H ₂₆ N ₂ O ₅	338.18417			471.08970 (471.08953)			0.19 (0.17)				
ff	C ₁₅ H ₂₄ N ₂ O ₇	344.15835		351.17452 (351.17448)	477.06396 (477.06397)		0.47 (0.36)	0.35 (0.38)				
gg	C ₁₈ H ₂₆ N ₂ O ₅	350.18417	373.17395 (373.17397)			0.02 (0.08)			373.17396 (373.17406)		0.05 (0.32)	
hh	C ₁₅ H ₂₄ N ₂ O ₈	360.15327		367.16947 (367.16998)	493.05889 (493.05910)		0.53 (1.92)	0.36 (0.79)				
	C ₁₇ H ₂₁ N ₃ O ₆	363.14304			496.04886 (496.04908)			0.76 (1.21)				
	C ₁₈ H ₂₆ N ₂ O ₆	366.10632		373.12258 (373.12288)	499.01187 (499.01190)		0.69 (1.49)	0.22 (0.28)				
ii	C ₁₇ H ₂₅ N ₃ O ₆	367.17434		374.19056 (374.19087)			0.58 (1.41)			374.19014 (374.19014)		0.55 (0.55)

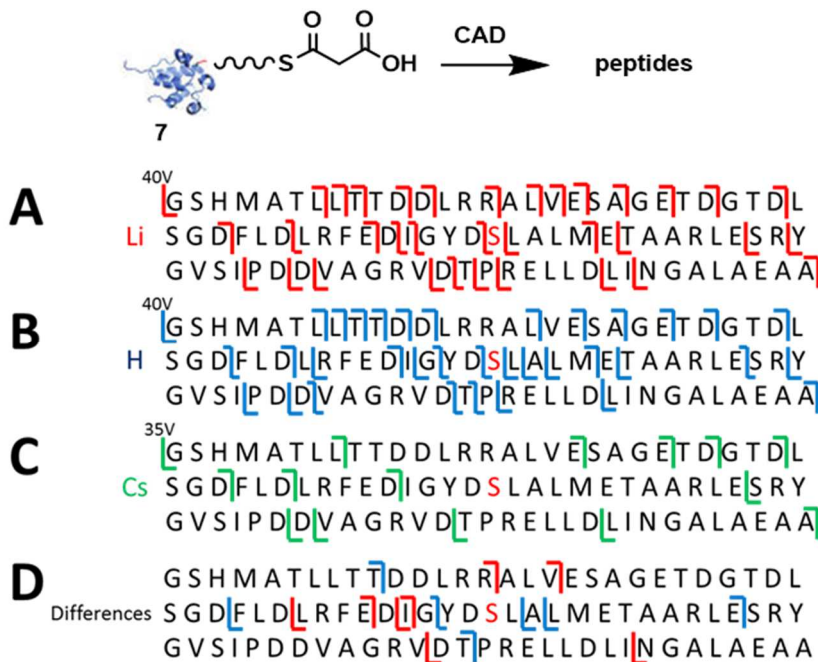
			EID						CAD			
			<i>m/z</i> detected (<i>m/z</i> before phasing)			Absolute Error (Error before phasing) (ppm)			<i>m/z</i> detected (<i>m/z</i> before phasing)		Absolute Error (Error before phasing) (ppm)	
	Predicted Formula	Theoretical Mass (Da)	Na	Li	Cs	Na	Li	Cs	Na	Li	Na	Li
	C ₁₇ H ₂₀ N ₂ O ₈	380.12197			513.02770 (513.02794)			0.56 (1.03)				
jj	C ₁₈ H ₂₆ N ₂ O ₇	382.17400			515.07981 (515.07941)			0.72 (0.06)				
	C ₂₂ H ₃₀ NO ₅	387.20457	388.21240 (388.21251)			1.43 (1.71)						
kk	C ₁₈ H ₂₃ N ₃ O ₇	393.15360		400.16992 (400.17014)	526.05963 (526.05967)		0.79 (1.34)	1.12 (1.20)				
ll	C ₁₇ H ₂₃ N ₃ O ₈	397.14852		404.16481 (404.16478)	530.05447 (530.05428)		0.71 (0.63)	0.96 (0.60)				
	C ₂₄ H ₃₄ NO ₄	399.24096	400.24873 (400.24873)			1.23 (1.23)						
mm	C ₁₉ H ₂₃ N ₃ O ₇	405.15360		412.17004 (412.17055)	538.05967 (538.05924)		1.06 (2.30)	1.17 (0.37)				
	C ₁₈ H ₂₃ N ₃ O	409.14852		416.16485 (416.16537)	542.05464 (542.05422)		0.78 (2.03)	1.25 (0.48)				
nn	C ₁₈ H ₂₅ N ₃ O ₈	411.16417		418.18062 (418.18044)	544.07015 (544.07020)		1.07 (0.64)	0.99 (1.08)				
	C ₂₄ H ₃₂ NO ₅	413.22022	414.22796 (414.22795)			1.12 (1.09)						
	C ₂₄ H ₃₀ O ₆	414.20424								421.21985 (421.21966)		0.94 (1.39)
	C ₁₉ H ₂₃ N ₃ O ₈	421.14852		428.16507 (428.16503)	554.05488 (554.05341)		1.28 (1.18)	1.66 (0.99)				
	C ₂₁ H ₂₆ O ₉	422.15768		429.17288 (429.17358)	555.06260 (555.06291)		1.87 (0.24)	0.94 (0.38)				
oo	C ₁₉ H ₂₅ N ₃ O ₈	423.16417		430.18080 (430.18136)	556.07025 (556.07031)		1.46 (2.76)	1.15 (1.26)		430.17995 (430.17980)		0.52 (0.87)

			EID						CAD			
			<i>m/z</i> detected (<i>m/z</i> before phasing)			Absolute Error (Error before phasing) (ppm)			<i>m/z</i> detected (<i>m/z</i> before phasing)		Absolute Error (Error before phasing) (ppm)	
	Predicted Formula	Theoretical Mass (Da)	Na	Li	Cs	Na	Li	Cs	Na	Li	Na	Li
pp	C ₂₂ H ₃₄ N ₂ O ₇	438.2366								445.25226 (445.25198)		0.77 (1.40)
qq	C ₂₂ H ₃₁ N ₃ O ₇	449.21620		456.23304 (456.23300)			1.83 (1.74)			456.23182 (456.23163)		0.84 (1.26)
	C ₂₂ H ₂₈ O ₁₀	452.16825		459.18356 (459.18437)	585.07350 (585.07358)		1.51 (0.25)	0.33 (0.19)				
	C ₂₃ H ₃₁ N ₃ O ₇	461.2162								468.23188 (468.23150)		0.69 (1.50)
	C ₂₃ H ₃₄ N ₂ O ₈	466.23152								473.24717 (473.24660)		0.75 (1.95)
rr	C ₂₃ H ₃₄ N ₃ O ₈	479.22677	480.23516 (480.23510)	486.24347 (486.24360)		2.32 (2.19)	1.43 (1.70)			486.24245 (486.24237)		0.67 (0.83)
ss	C ₂₃ H ₃₄ N ₂ O ₉	482.22643								489.24197 (489.24149)		0.95 (1.93)
tt	C ₂₃ H ₃₅ N ₃ O ₉	497.23733							520.22709 (520.22711)	504.25304 (504.25327)	0.02 (0.02)	0.58 (0.13)
	C ₂₂ H ₃₃ N ₃ O ₁₀	499.21659								506.23243 (506.23186)		0.32 (1.45)
uu	C ₂₂ H ₃₃ N ₃ O ₁₁	515.21151		516.21809 (516.21866)			1.35 (0.24)					
vv	C ₂₄ H ₃₃ N ₃ O ₁₀	523.21659		530.23370 (530.23384)			2.09 (0.24)					
M+	C ₂₄ H ₃₅ N ₃ O ₁₁	541.22716	564.21692 (564.21693)	548.24305 (548.24320)	674.13251 (674.13251)	0.02 (0.00)	0.21 (0.07)	0.13 (0.13)	564.21691 (564.21704)	548.24316 (548.24318)	0.04 (0.19)	0.01 (0.03)
Average Absolute Error (Average Absolute Error before phasing) (ppm) :						0.47 (0.53)	0.49 (0.57)	0.40 (0.40)			0.03 (0.24)	0.32 (0.56)

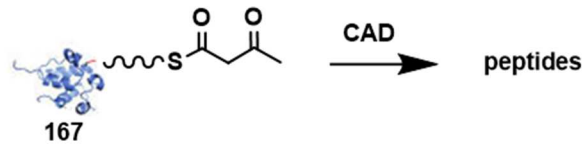
Appendix 70 Peak list – FTICR-MS electron induced dissociation (EID) or collisionally activated dissociation (CAD) of the nonhydrolysable photolabile carba(dethia) pantetheine **81** with sodium, lithium or caesium adduction. Those with a predicted structure have a designated letter that correlates with chapter 6.



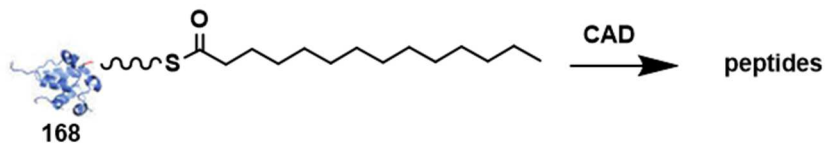
Appendix 71 Cleavage coverage maps showing *b* and *y* ions resulting from collisionally activated dissociation (35V and 25V) of acetyl-ACP **40** with (A, red) and without (B, blue) lithium adduction. The differences between the maps is shown (C).



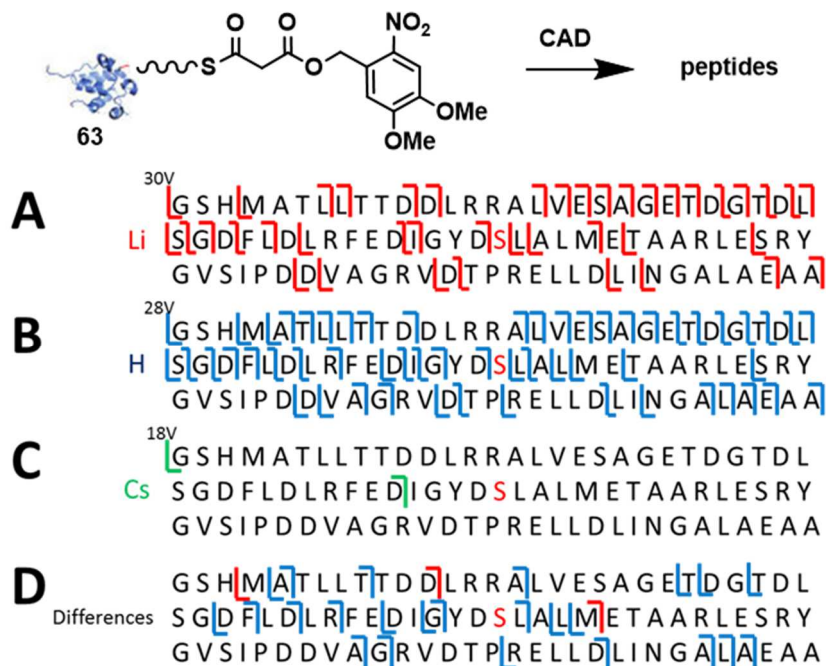
Appendix 72 Cleavage coverage maps showing *b* and *y* ions resulting from collisionally activated dissociation (40V and 35V) of malonyl-ACP **7** with lithium (A, red), with caesium (C, green) and without alkali (B, blue) adduction. The differences between the maps is shown (D).



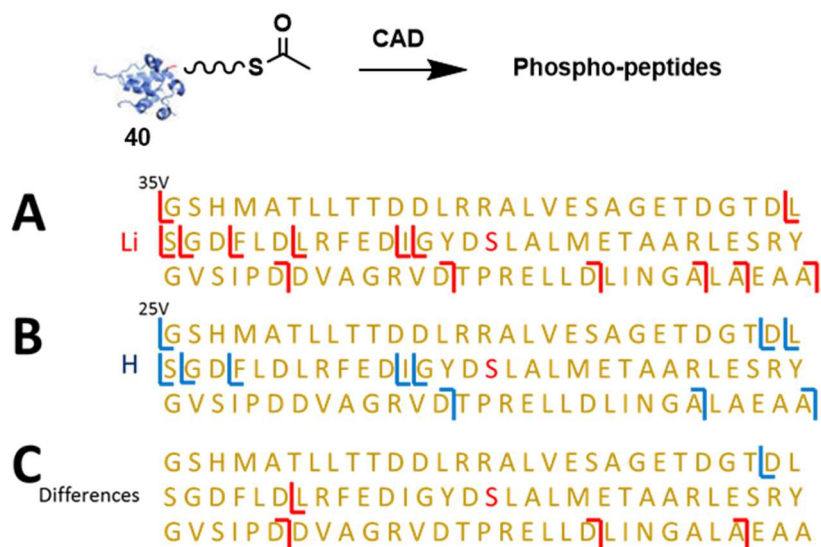
Appendix 73 Cleavage coverage maps showing *b* and *y* ions resulting from collisionally activated dissociation (40V and 30V) of acetoacetyl-ACP 167 with lithium (A, red), with caesium (C, green) and without alkali (B, blue) adduction. The differences between the maps is shown (D).



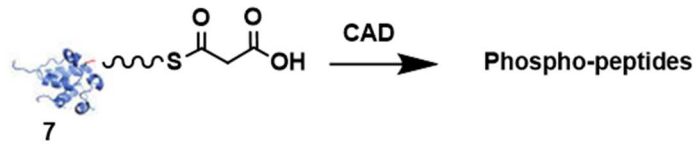
Appendix 74 Cleavage coverage maps showing *b* and *y* ions resulting from collisionally activated dissociation (35V and 25V) of myristoyl-ACP 168 with (A, red) and without (B, blue) lithium adduction. The differences between the maps is shown (C).



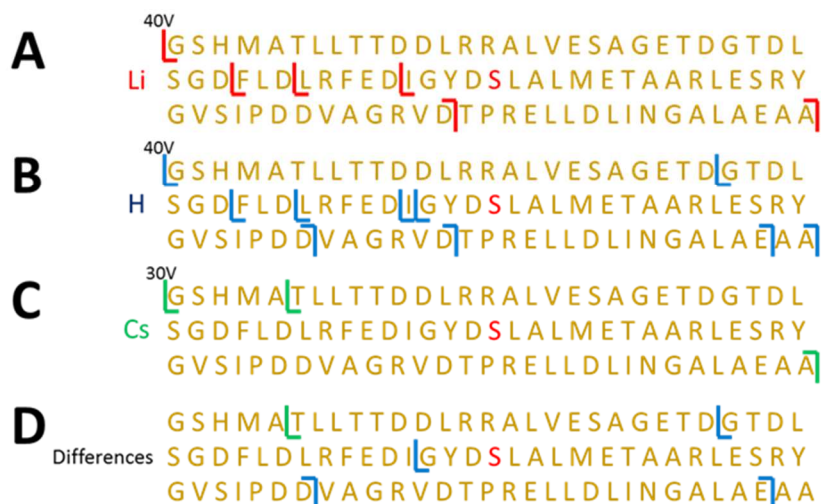
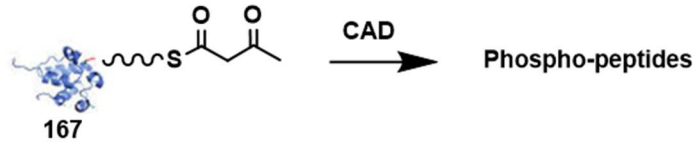
Appendix 75 Cleavage coverage maps showing *b* and *y* ions resulting from collisionally activated dissociation (30V, 28V and 18V) of nonhydrolysable photolabile malonyl carba(dethia) ACP analogue **63** with lithium (A, red), with caesium (C, green) and without alkali (B, blue) adduction. The differences between the maps is shown (D).



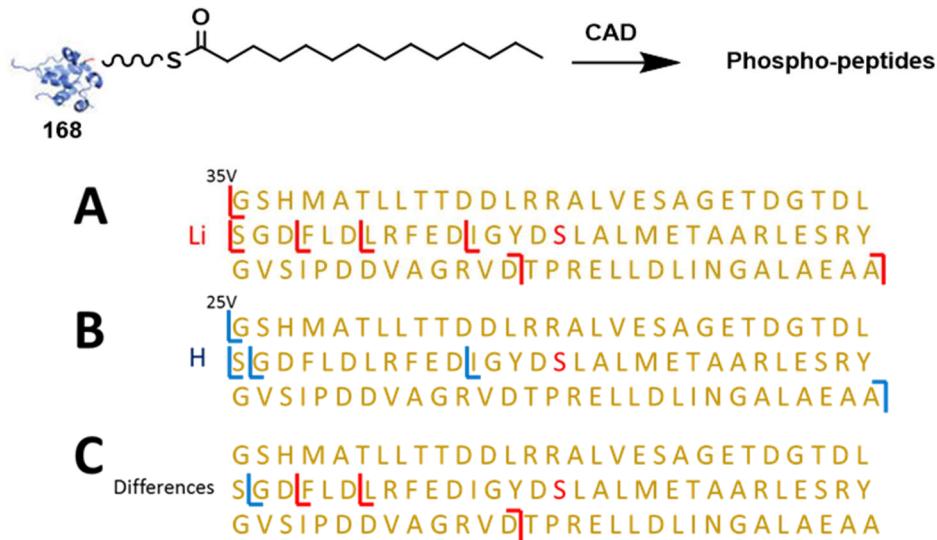
Appendix 76 Cleavage coverage maps only showing phosphorylated *b* and *y* ions resulting from collisionally activated dissociation (35V and 25V) of acetyl-ACP **40** with (A, red) and without (B, blue) lithium adduction. The differences between the maps is shown (C).



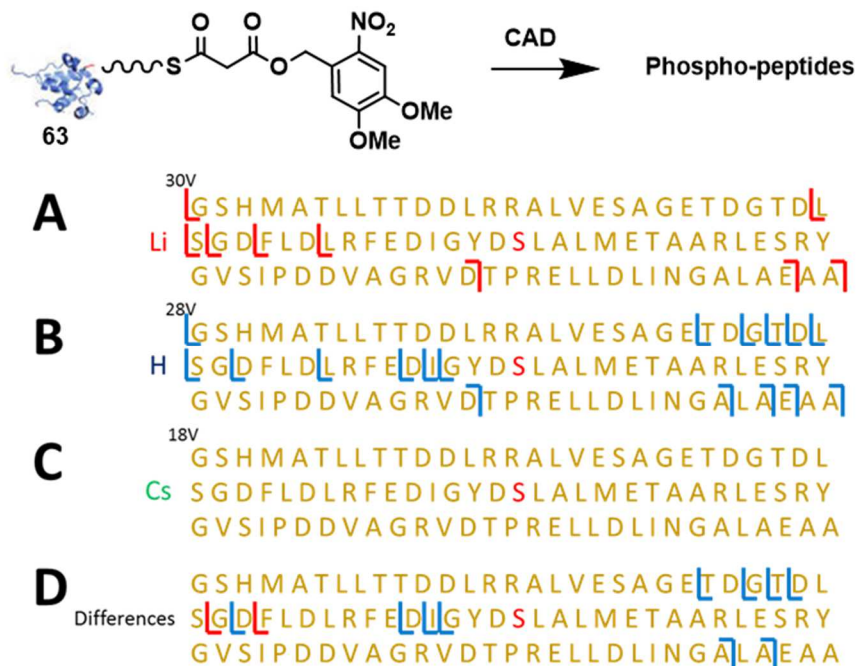
Appendix 77 Cleavage coverage maps only showing phosphorylated b and y ions resulting from collisionally activated dissociation (40V and 35V) of malonyl-ACP 7 with lithium (A, red), with caesium (C, green) (Note: none detected) and without alkali (B, blue) adduction. The differences between the maps is shown (D).



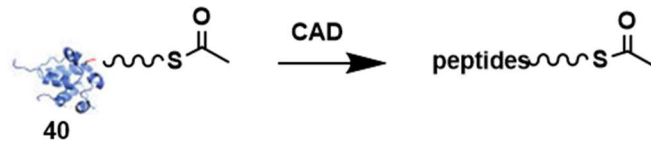
Appendix 78 Cleavage coverage maps only showing phosphorylated b and y ions resulting from collisionally activated dissociation (40V and 30V) of acetoacetyl-ACP 167 with lithium (A, red), with caesium (C, green) and without alkali (B, blue) adduction. The differences between the maps is shown (D).



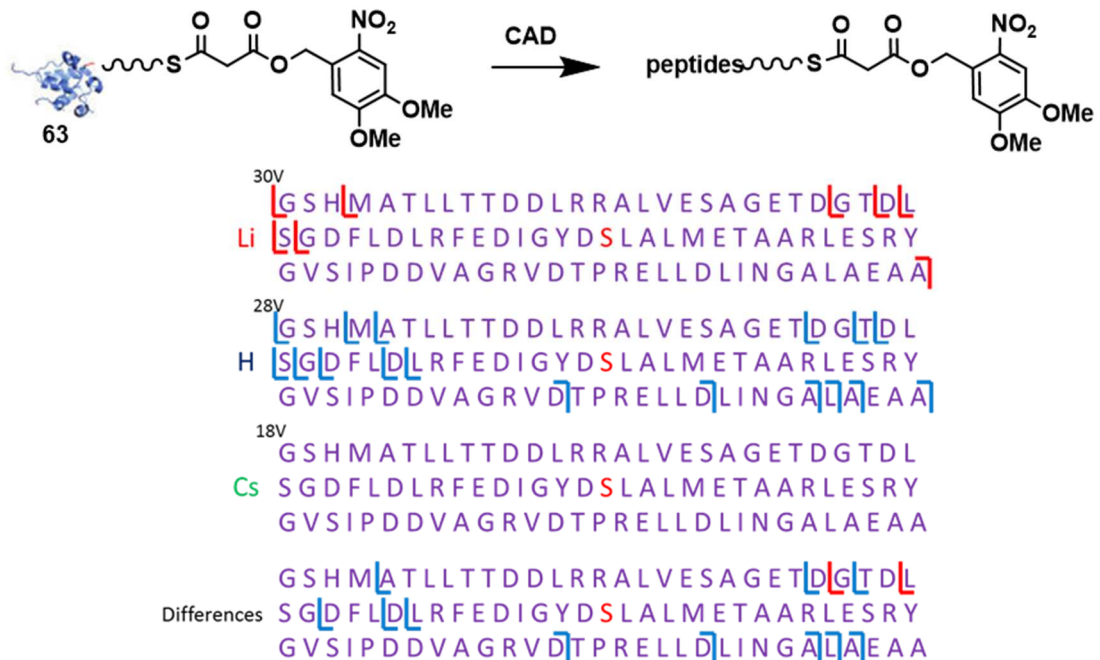
Appendix 79 Cleavage coverage maps only showing phosphorylated b and y ions resulting from collisionally activated dissociation (35V and 25V) of myristoyl-ACP **168** with (A, red) and without (B, blue) lithium adduction. The differences between the maps is shown (C).



Appendix 80 Cleavage coverage maps only showing phosphorylated b and y ions resulting from collisionally activated dissociation (30V, 28V and 18V) of nonhydrolysable photolabile malonyl carba(dethia) ACP analogue **63** with lithium (A, red), with caesium (C, green) (Note: none detected) and without alkali (B, blue) adduction. The differences between the maps is shown (D).



Appendix 81 Cleavage coverage maps only showing 'b' and 'y' ions with the acetyl-phosphopantetheinyl arm bound, resulting from collisionally activated dissociation (35V and 25V) of acetyl-ACP 40 with (A, red) and without (B, blue) lithium adduction. The differences between the maps is shown (C).



Appendix 82 Cleavage coverage maps only showing 'b' and 'y' ions with the nonhydrolysable photolabile malonyl carba(dethia)-phosphopantetheinyl arm bound, resulting from collisionally activated dissociation (30V, 28V and 18V) of nonhydrolysable photolabile malonyl carba(dethia) ACP analogue 63 with lithium (A, red), with caesium (C, green) (Note: none detected) and without alkali (B, blue) adduction. The differences between the maps is shown (D).